Journal of Applied Mechanics

(Contributions of the ASME Applied Mechanics Division)

Papers for Third U. S. National Congress of Applied Mechanics 163
Stress Distributions Around Hydrostatically Loaded Holes . . *A. J. Durelli and A. S. Kobayashi* 178
Casting of Metal Plates With High Explosive Charges . . . . . *W. E. Drummond* 184
New Method to "Lock-in" Elastic Effects . . . . . *J. W. Dally, A. J. Durelli, and W. F. Riley* 189
Torques on a Satellite Vehicle From Internal Moving Parts. . . . . *R. E. Roberson* 196
Initial and Subsequent Yield Surfaces in Plasticity . . *P. M. Naghdi, F. Essenburg, and W. Koff* 201
Effect of Finite Rotations on Gyroscopic Sensing Devices . . *L. E. Goodman and A. R. Robinson* 210
Torsion in Presence of Steady Creep. . . . . *S. A. Paul, B. Venkatraman, and P. G. Hodge, Jr.* 214
Calculation of Optimum Concentrated Damping for Continuous Systems . . . . *R. Plunkett* 219
Inertia Forces in Slider-Crank Mechanisms. . . . . *Ernst Meyer* 225
Redundant Trusses of Elastic-Strain-Hardening Material. . . . . *Hans Ziegler* 233
A Compressible Elastic, Perfectly Plastic Wedge . . . . . *D. R. Bland and P. M. Naghdi* 239
Stress Distribution in Rotating Disks and Cylinders . . . . . *A. M. Wahl* 243
Large-Deflection Analysis for Pressure and Heating . . . . . *M. L. Williams* 251
General Instability of Ring-Stiffened Shells . . . *G. D. Galletly, R. C. Slankard, and E. Wenk, Jr.* 259
Buckling of a Thin Plate Under Uniform Compression . . . . . *N. Yamaki* 267
Ring Damping of Free Surface Oscillations. . . . . *J. W. Miles* 274
On the Sloshing of Liquid in a Flexible Tank . . . . . *J. W. Miles* 277

Brief Notes

Criterion for Flow of a Bingham Plastic. . . . . *P. R. Pasley and A. Silber* 284
Static and Dynamic Deformation in Armco Iron . . . . . *H. P. Tardif and W. Erickson* 285
Torques on a Satellite Vehicle (Supplement) . . . . . *R. E. Roberson* 287
Pressure Losses in Noncircular Ducts . . . . . *T. F. Irvine, Jr., and E. R. G. Eckert* 288
Stresses in a Rotating Dumbbell-Shaped Disk . . . . . *B. B. Chatterjee* 290
Displacement Discontinuity Between Two Dissimilar Solids . . . . . *J. T. Frasier* 292
Second Acceleration in Four-Bar Mechanisms . . . . . *W. J. Carter* 293
Large Deflection of Cantilever Beams. . . . . *Kiichi Satō* 294
Heat Transfer in Swirling Laminar Pipe Flow . . . . . *R. Siegel and M. Perlmutter* 295
Levy-Type Solution for Rectangular Plate . . . . . *H. D. Conway* 297

Discussion of previously published papers by *G. W. Sutton; G. R. Brubs; Ching-Yang Nong; P. G. Hodge, Jr.; S. Mahalingam; A. A. Betser and M. M. Frocht; J. J. Bailey; S. H. Crandall; G. Gerard and A. C. Gilbert; A. Silber and P. R. Pasley; B. A. Boley and A. D. Barber; J. Duffy and R. D. Mindlin; D. C. Gazis and R. D. Mindlin; W. H. Hoppmann, II, and L. S. Magness; L. W. Lassiter; C. B. Atkinson; G. Hervey and K. L. Hansen; R. M. Cooper* 298
Book Reviews 319

JUNE, 1958

VOL. 25, NO. 2

Transactions of The American Society of Mechanical Engineers

Journal of Applied Mechanics

Papers Contributed to the Transactions by the ASME Applied Mechanics Division

EXECUTIVE COMMITTEE OF THE APPLIED MECHANICS DIVISION

W. Ramberg, *Chairman*
James M. Lemmlein, *Honorary Editor*
W. Prager, *Secretary*
D. C. Drucker and J. Kestin, *Technical Editors*

Published Quarterly by

The American Society of Mechanical Engineers

Publication Office, 20th and Northampton Streets, Easton, Pa.
Editorial Department at the Headquarters of the Society, 29 West Thirty-Ninth Street, New York 18, N. Y.
Papers should be forwarded to the Technical Editors, Journal of Applied Mechanics, ASME, Division of Engineering, Brown University, Providence 12, R. I.

OFFICERS OF THE SOCIETY

J. N. Landis, *President*
R. J. Kaiser, *Treasurer*
H. J. Bauer, *Assistant Treasurer*
O. B. Schier, II, *Secretary*

PUBLICATIONS COMMITTEE

Kemi Arrington, *Chairman*
Gordon A. Stetson, *Editor Emeritus*
H. K. Weber, *Production*
J. J. Jakosky, Jr., *Editor*
L. Burgert, *Consulting Editor*

By-Law: The Society shall not be responsible for statements or opinions advanced in papers or . . . printed in its publications (B13, Par. 4)

Published quarterly by The American Society of Mechanical Engineers. Publication office at 20th and Northampton Streets, Easton, Pa. The editorial department is located at the headquarters of the Society, 29 West Thirty-Ninth Street, New York 18, N. Y. Cable address, "Mechanec," New York. Price $1.50 a copy, $5.00 a year; to members $2.50 a year; single copy price to members, $1.00. Add 25c for postage to all countries outside the United States, Canada, and Pan-American Union. Changes of address must be received at Society headquarters seven weeks before they are to be effective on the mailing list. Please send old as well as new address. . . . By-Law: The Society shall not be responsible for statements or opinions advanced in papers or . . . printed in its publications (B13, Par. 4). . . . Second-class mail privileges authorized at Easton, Pa. . . . © Copyrighted, 1958, by The American Society of Mechanical Engineers. Reprints from this publication may be made on condition that full credit be given the JOURNAL OF APPLIED MECHANICS and the author, and that date of publication be stated.

ABSTRACTS OF PAPERS

Third U.S. National Congress of Applied Mechanics

Brown University, June 11-14, 1958

Appearing below are authors' abstracts of all papers which have been accepted for inclusion in the program. Papers presented at the Congress will be printed in full in the Proceedings of the Third U. S. National Congress of Applied Mechanics, to be published by The American Society of Mechanical Engineers.

The abstracts have been arranged so that the authors' names appear in alphabetical order within each of the five subject groupings. The affiliation of each author is shown; complete postal addresses will be given in the Proceedings. If necessary, authors may be reached through the Chairman of the Editorial Committee, Professor Robert M. Haythornthwaite, Box D, Brown University, Providence 12, R. I.

The Editorial Committee wishes to express its appreciation to the ASME Applied Mechanics Division and to the editors of the *Journal of Applied Mechanics* for their courtesy in publishing these abstracts.

General Lectures

Linear thermodynamics and the mechanics of solids. M. A. Biot, Shell Development Company and Cornell Aeronautical Laboratory.

The thermodynamics of linear irreversible processes is presented from a unified viewpoint. This provides a new and synthetic approach to the linear mechanics of deformation of solids, which includes as particular cases the classical theories of Elasticity, Thermoelasticity, and Viscoelasticity. The first two sections constitute an introduction to the general concepts and principles of linear thermodynamics as developed in the earlier work and presented in somewhat more detail. This is followed by the application of the general thermodynamic theory to Thermoelasticity. This combines the theories of Elasticity, Heat Transfer, and their coupled effects into a single treatment. Some immediate consequences are derived, such as the property of diffusion of entropy and certain fundamental relations with reference to thermal stresses. The introduction of inertia forces leads to a general formulation of thermoelastic dissipation of dynamical systems by Lagrangian methods. The second-order heat produced by the dissipation is evaluated. Linear Viscoelasticity and Relaxation Phenomena are also a particular case of the thermodynamic theory. The resulting stress-strain relations with heredity properties are discussed. The operational formulation of these relations leads naturally to a formal correspondence with the theory of Elasticity and to an operational-variational principle. The latter provides a generalization of Lagrange's equations in integrodifferential form to the dynamics and stress analysis of viscoelastic structures. Some specific applications of this principle are presented.

Some aspects of boundary-layer flow in subsonic and supersonic air streams. Hugh L. Dryden, National Advisory Committee for Aeronautics.

Boundary-layer flow remains an intensely active field of research in fluid mechanics. Theoretical workers are busy extending the theory of the two-dimensional incompressible laminar boundary layer to three-dimensional flow, to flows in which fluid is withdrawn or ejected through a porous wall, and to corresponding compressible flows. They are studying the stability of incompressible and compressible laminar boundary layers as a function of pressure distribution and heat transfer. Experimental workers, in much smaller numbers, are attempting to check the theoretical computations and to make the meaningful experiments which guide the assumptions involved in the several idealized models of the actual fluid flow. Some seek to establish a sound basis for the practical design of high-speed aircraft and missiles; others seek to know and understand more fully the fundamental processes. All are engaged in exploiting a field of research of outstanding importance in fluid mechanics.

The present lecture represents a review and comment on some aspects of recent boundary-layer research by one who, though once active in this field, is now only an interested bystander. He is impressed by the diligence of the mathematicians who still seek a sound basis for the original assumptions of Prandtl as well as better, more convenient, and more accurate methods of computation. He is intrigued by the similarities in the instability modes and details of transition in subsonic and supersonic boundary layers. He notes that, although turbulent motion is still the great mystery awaiting a simplifying concept, there is progress in revealing the shortcomings of assumptions formerly made.

No attempt is made to give a comprehensive review. The topics selected for discussion are those which it is hoped will interest a general audience as well as the lecturer and which contribute to an understanding of the flow and its effects.

On creep. Nicholas J. Hoff, Stanford University.

Although observed for the first time over a hundred years ago, creep attained some importance only in the early 1930's when it caused measurable deformations in the elements of heat-power generating equipment. The interest of engineers in creep was awakened a second time, and more intensely than before, when

GENERAL LECTURES

its effect on the reliability of nuclear power machines and hypersonic missiles had to be determined.

At the present time, practical metallurgists, theoretical physicists of the solid state, and engineers interested in applied mechanics hold widely different views regarding creep. The first group considers creep such a complex metallurgical phenomenon that it denies the feasibility of representing the creep process by mathematical formulas; applied mechanics men on the other hand want to predict structural behavior from creep laws and are even willing to invent them if they are not furnished by the experimental metallurgist. It is perhaps the privilege of the metal physicist to reconcile the two widely diverging standpoints through a better insight into the physical phenomena involved.

The paper reviews theoretical and experimental information available on creep. It presents various creep laws and the corresponding minimal principles. It shows how creep influences the distribution of stresses in structural and machine elements. It also explains how the time-dependent deformations lead to entirely new forms of structural instability in tension, bending, and compression.

The final item discussed is the philosophy of design in the presence of creep. It must include the concept of design for a finite lifetime, and it requires the determination of the probability of failure during the lifetime required.

Rotationally symmetric problems in shell theory. Eric Reissner, Massachusetts Institute of Technology.

General problems in the theory of thin elastic shells require the determination of stresses and deformations as a function of two space co-ordinates. Rotationally symmetric problems have the property that stresses and deformations depend on one space co-ordinate only. This means that, for time-independent problems, one is concerned with ordinary differential equations rather than with partial differential equations. The present lecture reviews a number of problems and solutions in the field of rotationally symmetric deformations of thin shells, not all of them dealing with shells of revolution which are the most natural source of such problems.

Consideration is given to linear and nonlinear problems of the statics of shells of revolution, with particular emphasis on asymptotic solutions and edge effects. The problem of bending of pressurized curved tubes is formulated in considerable generality.

Recent results on vibrations of shallow shells are surveyed. Relations between three-dimensional elasticity and thin shell theory are discussed for the case of rotational symmetry. Finally, an outline is given of recent developments concerning shells with helicoidal middle surface.

Dynamics, Vibrations, Elastic Waves

The solution of Duffing's equation for the softening spring system using the Ritz-Galerkin method with a three-term approximation. Cyril P. Atkinson, University of California; Charles P. Bourne, Stanford Research Institute.

This paper presents the results of an investigation of the solutions of the differential equation (Duffing's equation) $\ddot{q} + q - \frac{4}{3} q^3 = F \cos \omega t$ based on a three-term approximation to the solution $q(t)$. The assumed solution is of the form

$$q(t) = A \cos \omega t + B \cos 3\omega t + C \cos 5\omega t.$$

The method of solution used is known as the Ritz averaging method (or the Ritz-Galerkin method). The differential equation was solved for both free and forced oscillations. Solutions are presented in the form of amplitude versus frequency plots for the three components of the assumed solution. Resonance of the harmonics is indicated in certain regions of the amplitude versus frequency plane. In these regions the fundamental component alone is not adequate in describing the response of the system.

The response of elastic spherical shells to spherically symmetric internal blast loading. Wilfred E. Baker, Frank J. Allen, Aberdeen Proving Ground.

A general theory of the small-deformation elastic response of spherical shells of any thickness to spherically symmetric internal blast waves is developed. The theory is approximated for thin shells and compared with experiment.

On elastic impacts of spheres on long rods. Cliff S. Barton, Rensselaer Polytechnic Institute; Enrico G. Volterra, University of Texas.

This paper presents an experimental verification and a theoretical analysis for the longitudinal elastic impact of steel balls on an infinitely long cylindrical steel bar. Five balls of diameters ranging from 1 to 2 in. were dropped from heights ranging from 7.5 to 30 centimeters to impact longitudinally a 1-in-diam bar. Experimental results compare in table and graph form the pulse length, pulse amplitude, pulse shape, and time of peak amplitude as computed from the theoretical analysis. The electronic circuitry and equipment developed are described. The theoretical analysis indicates the validity of the Hertzian impact assumptions.

Vibration analysis by the root locus method. Robert H. Cannon, Jr., Massachusetts Institute of Technology.

The dynamics of complex mechanical systems may often be studied effectively by the "root locus" technique, which provides a plot of system characteristics as explicit functions of coupling strength, damping, or whatever parameter is desired. The method is explained using, as a model, a two-stage "shock mount" with heavy damping. The ready physical interpretation of root locus plots is demonstrated. (Quick graphical conversion to system frequency response is also shown.) Treatment of additional degrees of freedom is indicated. In a subsequent paper the method will be used to investigate stability for situations involving coupling of structural vibration modes into a control system.

Whirling of a heavy chain. T. K. Caughey, California Institute of Technology.

Approximate solutions are obtained for the nonlinear problem of the forced whirling of a heavy chain. It is shown that, for a given mode of whirling, triple-valued solutions are obtained for speeds of rotation above the linear critical speed for that mode. It is also shown that two of these solutions are stable while the third is unstable.

DYNAMICS, VIBRATIONS, ELASTIC WAVES

Energy dissipation in longitudinal vibration. C. S. Chang, University of Minnesota.

The problem of the longitudinal vibrations in a finite prismatic bar with a terminal viscous damper is solved. The complete boundary-value problem (forced vibration with arbitrary initial conditions) is first split into two parts according to the method developed by Mindlin and Goodman. One of these parts yields the steady-state solution and the other represents a free-vibration problem, which is then solved by the method of Boussinesq. Examples of the applications of the general solutions are given, and the amount of mechanical energy dissipated per cycle of steady-state vibration due to a sinusoidal exciting force is also computed.

Transient motion in mechanical wave-filters. Jerald N. Christiansen, Stanford University.

A general class of mechanical wave-filters is investigated. Examples include a chain of N oscillators, e.g., similar pendulums, with coupling. The case $N = 2$ is well known in connection with the phenomenon of beats in free motion when the coupling is slight. Existing steady-state solutions are reviewed, and to them is added a solution for the free motion with arbitrary initial conditions. It can be generalized to arbitrary forced motion by Duhamel integration.

Vibration of rectangular plates and plate systems. E. H. Dill, University of Washington; K. S. Pister, University of California.

A procedure for analyzing the steady-state free or forced vibration of single-span plates and continuous plates on nondeflecting supports is presented. The method is analogous to the slope-deflection method used in structural dynamics to analyze the vibration of continuous beams and frames. Natural frequencies of single-span plates for various boundary conditions are obtained as examples of the procedure. A seven-moment equation is formulated for plates continuous over nondeflecting supports. Application to three examples of continuous plates is included.

Electronic computer simulation of a system with a "trilinear" restoring function. M. Dost, C. P. Atkinson, University of California.

The differential equation, $\ddot{x} + c\dot{x} + f(x) = P \sin \Omega t$, has an odd, trilinear restoring function $f(x)$ that is alternately decreasing and increasing. Solutions were obtained by employing an electronic differential analyzer. Graphs, as produced by the computer, and response curves are presented for the resonance frequency ranges of the fundamental, second, and third harmonic. Two different kinds of jumps of the fundamental occurred: with negligible and with distinct phase change. Amplitude and phase jumps of superharmonics occurred simultaneously with smaller jumps of the fundamental. Two basically different configurations of the superharmonic components were found for the second and third harmonic.

Response of tall buildings to random earthquakes. A. Cemal Eringen, Purdue University.

A method of analysis is given for the calculation of mean square displacements and various correlation functions for a tall building having an arbitrary number of stories. The building is approximated by a series of masses and dashpots, and it is assumed that the mean square displacements of the earth movements are known. Mean square shearing forces and the energy present at each story are evaluated. It is indicated that Rice's formula may be used to calculate the number of times per unit time the random variable (e.g., displacements) will exceed a known, safe value. Computations concerning a ten-story building subject to purely random earthquake process were carried out on an electronic computer and are plotted.

Stresses in curved beams due to transverse impact. Werner Goldsmith, University of California; G. W. Norris, Jr., General Dynamics Corporation.

A sequence of photoelastic fringe patterns in curved and cantilever beams have been obtained by repeating the impact of a sphere on the free end of these bars and photographing the event at known time intervals. Some of the stress histories determined in this manner have been compared with corresponding strain gage results and analytical predictions. Static and dynamic values of the stress-optic coefficient and the modulus of elasticity are determined for CR-39, and the maximum values of the experimentally determined stresses for both static and dynamic loading conditions on a bent, a quarter circle, and a cantilever beam consisting of this material are compared.

Flexural vibrations of a thick-walled circular cylinder. Joshua E. Greenspon, The Martin Company.

This paper treats the flexural vibrations of a hollow circular cylinder of finite length, which is kept circular at its ends. The three-dimensional theory of elasticity is used and solutions to the equations of motion satisfying given boundary conditions are obtained. Curves of frequency parameter as a function of length ratio and thickness ratio are given.

Oscillations of a gas in an elastic cylindrical shell. H. V. Hahne, Lockheed Aircraft Corp.

The paper presents the analysis of the natural frequencies and modes of oscillation of a compressible gas contained in an elastic cylindrical shell. The mass and the elastic properties of the shell, as well as the coupling between the gas and the shell, are taken into consideration. First, the general case which includes all possible modes and their combinations is considered and the corresponding frequency equation is derived. This general frequency equation is then reduced to two special cases, that of purely circumferential and that of purely longitudinal modes. Numerical solutions of the frequency equation are obtained for the circumferential modes of a gas-filled steel shell of given dimensions.

Vibrations of a uniform, rotating beam with tip mass. George Handelman, William Boyce, Hirsh Cohen, Rensselaer Polytechnic Institute.

The effect of an added tip mass on the transverse vibrations of a uniform, cantilevered beam rotating with constant velocity about an axis through the clamped end is considered. Upper and lower bounds are established for the lowest frequency as a consequence of the minimum principle. It is shown that the tip mass tends to decrease the frequency as compared with the beam with free end. The first term in the asymptotic development for high modes is obtained.

Flexural vibration of orthogonally stiffened circular and elliptical plates. W. H. Hoppmann II, The Johns Hopkins University.

A study of the nodal patterns and frequencies of vibration of

DYNAMICS, VIBRATIONS, ELASTIC WAVES

stiffened circular and elliptical plates is presented in this paper. Some vibration results are also presented for unstiffened uniformly thin plates of aluminum. The differential equation of flexural vibration of a plate of orthotropic material is developed in polar co-ordinates. Results of determination of frequency of vibration of some of the plates by the Ritz method are given. The vibration experiments are described and sketches of the nodal patterns of both circular and elliptical plates, with and without stiffeners, are given.

Effect of rotatory inertia and shear on the vibration of beams treated by the approximate methods of Ritz and Galerkin. T. C. Huang, University of Florida.

Timoshenko's theory of lateral vibrations in an elastic beam takes into account both rotatory inertia and transverse shear deformation. Several techniques have been developed for the solution of equations according to the Timoshenko beam model. In this paper the methods of Ritz and Galerkin are presented. A solution with the Ritz method is illustrated for a beam with hinged ends. It is shown that the same results could be obtained from these two methods provided the same function is assumed for the approximate deflection curve.

Propagation of abrupt circular wave fronts in elastic sheets and plates. W. E. Jahsman, Lockheed Aircraft Corporation.

An in-plane or transverse ring load is suddenly applied to an elastic, homogeneous, isotropic sheet (plane stress) or plate (flexure). Abrupt wave fronts of stress and velocity or moment and velocity are produced, spreading outward and inward in concentric circles. The method of characteristics is used to determine the velocity of propagation and amplitude variation of these circular wave fronts before reflection. In the sheet, wave fronts propagating at the irrotational velocity c_1 and the equivoluminal velocity c_2 are produced. In the plate, wave fronts propagating at the plate velocity c_p and the velocities c_2 and k_2c_2 result. (k_2 is the shear correction factor used by Mindlin.) The amplitudes of all circular fronts vary inversely as the square root of the radius.

A simple mechanical method for measuring the reflected impulse of air blast waves. Orlando T. Johnson, Wendell C. Olson, James D. Patterson II, Aberdeen Proving Ground.

A mechanical method is described for measuring the impulse imparted to a flat rigid surface by the reflection (at normal incidence) of an air blast wave. The method consists of measuring the velocity at which a cylindrical plug of known mass is projected from a hole in a large rigid surface by a normally incident blast wave and computing the impulse from Newton's second law. Experimental results were obtained for spherical Pentolite explosive charges ranging in weight from $^1/_4$ to 2 lb and scaled distances from 0.5 to 2.5 ft/lb$^{1/3}$. Results are tabulated and presented graphically. In addition, a comparison is made with data obtained with piezoelectric gages.

Thermally induced elastic wave propagation in slender bars. J. E. Michaels, General Electric Company.

The solution is presented giving displacements and stresses for the propagation of thermally induced elastic waves in slender bars. Both semi-infinite and finite bars are treated. In each, the bar is considered to be disturbed from rest in its equilibrium position with ends stress-free. The temperature di tribution is an arbitrary function of time and one-dimensional space. Solutions are obtained by the method of integral transforms. As an example, a simple temperature distribution function is applied to the solution for the semi-infinite bar to illustrate the phenomenon. Results indicate that the phenomenon should be considered in investigations of the mechanism of structural failure due to thermal impact (extreme thermal shock).

On the use of approximate theories of an elastic rod in problems of longitudinal impact. Julius Miklowitz, California Institute of Technology.

Approximate solutions for the longitudinal impact and pressure shock problems in a semi-infinite circular rod, valid for large times, are derived in accord with the Mindlin-Herrmann theory. The solutions are shown to be equivalent. Further, they are in basic agreement with those that Skalak derived recently for the longitudinal impact problem from the linear equations of elasticity. It is shown that the differences lie in a wave front discontinuity and the adjustment of a correction factor, properties of the approximate theory solutions. Comparison of radial and axial strains with experiment is made and good agreement is found, particularly in the case of axial strain. Comparison is also made with related results from the Love and Bishop-Sutton approximate theories. Over-all properties considered, the Mindlin-Herrmann theory offers the best approximate theory representation of the rod disturbance for large times.

Vibrations of an infinite, elastic plate at its cut-off frequencies. R. D. Mindlin, Columbia University.

In addition to simple thickness vibrations, which are limiting forms of waves in a plate as the wave length approaches infinity, there are other limiting modes of vibration at infinite wave length. These modes have the same frequencies as those of the thickness modes, but their shapes are different. They degenerate to the thickness modes at certain values of Poisson's ratio.

Dynamic response of floating bridges to transient loads. J. P. Romualdi, E. D'Appolonia, T. E. Stelson, Carnegie Institute of Technology.

A dynamic analysis of floating bridges of one, two, three, and five floating supports is presented. The structures are studied to determine their response to moving loads, and the study is extended to a consideration of damping, mass of moving load, and virtual mass. The application of an electronic analog computor for the solution of problems of this type is discussed and solutions are worked out for each case. Virtual mass coefficients are obtained by an experimental procedure. The values thus obtained are checked by comparing calculated displacement-time relationships against experimental displacement-time relationships for model pontons subjected to known impulses.

Orbit changes and invariants in a Newtonian central force field V. G. Szebehely, General Electric Company.

This paper formulates the general aspects of variations of the orbit of a body moving in a Newtonian central force field. The problem solved in the paper might be formulated as follows: The velocity vector of the moving body is changed at a given point of the orbit; find the new orbit and its relation to the original orbit.

DYNAMICS, VIBRATIONS, ELASTIC WAVES

Interesting and important special cases are discussed, such as orbit changes with total energy preservation, with constant angular momentum, and with constant direction of the velocity vector. The invariants are found in the various cases and some general theorems are derived.

An engineering theory of longitudinal wave propagation in cylindrical elastic rods. E. C. Zachmanoglou, The University of California; E. Volterra, The University of Texas.

A one-dimensional theory of longitudinal wave propagation in cylindrical elastic rods is presented. This theory, which represents an improvement over a previous theory, both of which are based on the Method of Internal Constraints, takes into account second-order terms in the equation of constraints and brings to an engineering level the otherwise complicated numerical work involved in the exact theory. Numerical results obtained by the use of this theory are compared with those obtained by the exact theory.

Elasticity, Elastic Structures

Ellipsoidal shells subjected to lateral hydrostatic loading. J. H. Baltrukonis, The Ramo-Wooldridge Corporation.

The solution is obtained for the membrane stresses in a semi-ellipsoidal shell of revolution subjected to internal pressure varying linearly in a direction normal to the axis of revolution. This solution is applied to the calculation of the membrane stresses in the ellipsoidal head of a fluid-filled, horizontal, cylindrical tank. It is pointed out that circumferential compressive stresses exist over substantial portions of the head, thereby giving rise to the possibility of buckling in this region.

Lateral buckling of rimmed rotating discs. J. L. Bogdanoff, J. E. Goldberg, Purdue University; H. E. Helms, General Motors Corporation.

Two methods are presented for predicting whether or not a given radial temperature gradient will cause lateral buckling of a trimmed disc at a specified rotational speed. The web portion of the disc need not be uniform, but the assumptions of classical plate theory are used throughout the web. The first method assumes that classical plate theory is valid to the edge of the disc. The second method, applicable when the rim is thick, uses appropriate ring equations for the rim. The plate equations are written in a form which avoids the difficulties encountered in applying the usual equation to numerical integration of non-uniform disks.

Some observations on Saint Venant's principle. Bruno A. Boley, Columbia University.

Extensions of the von Mises-Sternberg statement of Saint Venant's principle to various boundary-value problems in elasticity theory and other fields are considered; a general form of the principle is then given as a property of elliptic differential equations. The possible applications to transient phenomena are discussed. An alternative formulation of the principle in terms of upper bounds rather than of orders of magnitude is outlined.

Elastic deformations of a shallow shell in the form of an elliptic paraboloid. T. F. Bridgland, Jr., William A. Nash, University of Florida.

The elastic deformations of a thin shallow shell in the form of an elliptic paraboloid are investigated by use of the Vlasov equations. The differential geometric characteristics of the middle surface of the shell are determined and the specialized form of the Vlasov equations for this shell are then presented. The two Vlasov equations are expressed in the form of a single equation of a complex variable, and this last equation is expressible in the form of a Volterra integral equation. This last form may be solved to determine the deformations and stresses in the shell.

Elastic theory of a weak-core sandwich panel, initially warped, simply supported and subjected to combined loadings. C. C. Chang, Bertrand T. Fang, Ibrahim K. Ebcioglu, University of Minnesota.

Based on small deflection theory, differential equations for the elastic bending and deflection of an orthotropic weak-core sandwich panel with small initial warping are derived by the variational energy method. The loads applied consist of arbitrarily distributed transverse loads and eccentrically applied edge loads and/or edge moments. Solutions of the differential equations for a simply supported rectangular panel with arbitrary initial warping and subjected to combined transverse loading and edge compression are obtained in the form of double Fourier series.

Stress singularities for a sharp-notched polarly orthotropic plate. R. L. Chapkis, M. L. Williams, California Institute of Technology.

Continuing a series of investigations into the character of possible bending or extensional stress singularities in the vicinity of angular or sharp-notched inclusions in thin plate of uniform thickness, the authors have now studied the effect of radial and circumferential orthotropy. Characteristic equations for all the usual boundary conditions are derived, and the qualitative effect of orthotropy upon the character of the stress is determined for the particular case of a cracked plate under free-free extension (or clamped-clamped bending). A stronger stress singularity is indicated if the shear rigidity exceeds the radial rigidity.

Solution of the equations of thermoelasticity. H. Deresiewicz, Columbia University.

Helmholtz's theorem on the resolution of a vector is applied to the displacement in the thermoelastic field equations, and the scalar potential expressed as a solution of equations of the type $(\nabla^2 + \delta^2)\,\varphi = 0$, where δ^2 is complex. The result is employed to study dilatational motion in an extended solid, longitudinal motion of an infinite circular cylinder, and thickness-stretch motion in an infinite slab.

Mean value theorems in the theory of elasticity. J. B. Diaz, L. E. Payne, University of Maryland.

Gauss's mean value theorem of potential theory states that the value of a harmonic function (harmonic on a sphere plus its interior) at the center of a sphere equals the arithmetic mean of the values of the function on the surface of the sphere. Are there similar "mean value theorems" in the theory of elasticity? In this paper, several of the possible mean value theorems of the theory of elasticity are obtained. The method of derivation

ELASTICITY, ELASTIC STRUCTURES

employed works simultaneously in the physically interesting cases of two and three dimensions as well as in higher dimensions.

Effect of imperfections on buckling of thin cylinders with fixed edges under external pressure. L. H. Donnell, Illinois Institute of Technology.

Buckling of thin fixed edge cylinders under all-around pressure is studied, using finite deflection theory and assuming imperfections of the type assumed in prior studies of other cases. No drop-off in resistance after buckling is found in this case, so that peak resistance is determined by the onset of yielding at highly stressed points. The relation between pressures producing yielding and the physical properties of the cylinders can be expressed by a single curve. Results found are consistent with tests and the range of imperfections found necessary to explain test results in other cases.

On elastic plates of variable thickness. F. Essenburg, P. M. Naghdi, University of Michigan.

This paper contains a derivation of *suitable* stress-strain relations for elastic isotropic plates of variable thickness which include the effects of transverse shear deformation and normal stress as well as the variation in thickness. The significance of the results is examined in the light of some simple examples where, in particular for torsion of plates whose thickness is such as to give rise to equilateral triangular and elliptic cross sections, exact agreement is obtained for the stress distribution with the corresponding results of Saint Venant's theory of torsion.

Thermal singularities for cylindrical shells. W. Flügge, Stanford University; D. A. Conrad, Bell Telephone Laboratories, Inc.

Singular solutions of the equations of the shallow cylindrical shell, or alternatively of the Donnell equations of the complete cylinder, are presented. It is shown that two of these solutions may be physically interpreted as thermal singularities; i.e., plane and bending hot spots. It is further shown that the concentrated force is not included among the solutions presented. Suggestions are made for applying the singularities to the solution of cylindrical shells with arbitrary temperature distribution.

A nondestructive method for three-dimensional photoelasticity. M. M. Frocht, L. S. Srinath, Illinois Institute of Technology.

The shear-difference method which has recently been extended to the solution of the general space problem required taking physical slices, or subslices, from models containing frozen stresses. It is shown in the present paper that the data required for the three-dimensional shear-difference method can be obtained by means of scattered light without slicing the model (and perhaps even without freezing), thereby providing a nondestructive method for three-dimensional photoelasticity. The necessary theory of scattered light is developed and experimental evidence provided showing the possible accuracy in the determination of the isoclinic parameters and birefringence. The possibilities of the method are further demonstrated by determining the stress distributions along critical lines in a diametrically compressed sphere and comparing the result with theory and previous experiments.

General instability of low buildings. John E. Goldberg, Purdue University.

A theory of general instability of one-story building structures is presented. The individual parallel, plane frames of the structure are assumed to be coupled by a bracing system which, in turn, is supported by elastic walls or frames. A lurching mode of general collapse is investigated. The prediction of stability or instability under a given set of loads is reduced to a small sequence of computationally simple problems.

Formulas for over-all thermoelastic deformation. J. N. Goodier, Stanford University.

When the linear thermoelastic problem of the isotropic homogeneous solid is taken in the form of the equivalent body and surface force problem, the Betti reciprocal theorem can be applied and leads to several useful results. The temperature distribution being arbitrary, it is shown that thermal stress gives zero total change of volume (above that of free thermal expansion). Formulas are found for the change of contained volume of thick-walled closed vessels and for over-all extensions, deflections, and rotations of flexural and torsional types, in bars of arbitrary section.

Thermal stresses in a sector prism. K. L. Hanson, G. Horvay, General Electric Company.

It is well known that a heat-generating circular cylinder of radius 1, with $\Theta = \Theta_M (1 - r^2)$ temperature distribution, incurs, far from the end faces, the maximum stress $E\alpha\Theta_M/(1 - \nu)$. It is shown in the present paper that sectioning the cylinder into six pie-shaped sectors, so as to provide more freedom for deformation but retaining the temperature distribution, reduces the maximum stress by about 30 per cent. In the Appendix it is demonstrated that the σ_z stress of a free cylindrical body of great length, far from the end faces, is $E\alpha T + \sigma_{zA}$, where σ_{zA} is the stress calculated for the plane strain case, and $T = T_0 + T_1x + T_2y$ is the linear component of $\Theta(x, y)$.

The stresses around a rectangular opening with rounded corners in a uniformly loaded plate. S. R. Heller, Jr., J. S. Brock, R. Bart, David Taylor Model Basin.

This paper presents a solution for the stresses around a rectangular opening with rounded corners in a uniformly loaded plate. The aspect ratio (length to width) and the radius of curvature of the corners are general. The complex-variable method of Muskhelishvili is used in conjunction with a conformal mapping technique to obtain a solution. Curves showing the tangential stress around the boundary of a typical family of rectangles are presented. In addition, curves are given which show the maximum values of the boundary stress as a function of both aspect ratio and corner radius. The numerical cases are sufficient to cover most openings found in engineering structures.

The infinite beam on equidistant supports and related problems. M. Hetényi, Northwestern University.

A method of systematic reduction is used in replacing the effect of continuity on the loaded span by two adjoining spans of proper flexural stiffness. The problems analyzed in this manner include: (*a*) the infinite beam on equidistant supports; (*b*) an infinite sequence of open continuous frames; and (*c*) an infinite sequence of closed frames supported at equal intervals. The procedure is analytical, and the results are "exact" within the limitations of the usual flexural theory of beams.

ELASTICITY, ELASTIC STRUCTURES

Nonlinear bending and buckling of circular plates. Herbert B. Keller, Edward L. Reiss, New York University.

Iterative solutions of finite difference approximations of the nonlinear von Karman plate equations are presented. Results are obtained for circular plates under a variety of boundary conditions subjected to either uniform lateral pressure or uniform edge thrust. The solution, carried out numerically on the AEC UNIVAC at New York University, yields a complete description of stresses and deflections for an apparently unlimited range of load parameters. In addition, boundary-layer phenomena are discussed. For computing purposes, this iterative method proves to be superior to the previously used power series method and may be applicable to other nonlinear problems.

An analysis of continuous beam-columns with uniformly distributed axial load. William M. Laird, Allan M. Bryson, University of Pittsburgh.

The theory of a single-span beam-column with uniformly distributed axial loading is extended to the case of a multispan member which is continuous over three or more supports. A three-moment equation is developed for cases where the axial-load distribution is a continuous function of span length and the uniform axial load is constant in each span. Formulas are given for the necessary three moment coefficients, and tabulations are presented for the case of zero concentrated end load. Some special cases are discussed and a numerical example is given.

Strain energy and equilibrium of a shell subjected to arbitrary temperature distribution. H. L. Langhaar, A. P. Boresi, University of Illinois.

A general theory of thermal stresses in shells is developed. The equations for small deflections of any shell are generalized to include the effects of a temperature distribution that is an arbitrary function of the curvilinear co-ordinates (x, y, z) of the shell. Additionally, the strain energy expression for any elastic isotropic shell is developed for an arbitrary temperature distribution. The analysis is based on the Kirchhoff assumption that normals to the middle surface remain straight and normal. Also, small-deflection approximations are used. Only elastic isotropic shells are considered, although a part of the theory is independent of the stress-strain relations.

A study of thick plates under tangential loads applied on the faces. C. W. Lee, L. H. Donnell, Illinois Institute of Technology.

The three-dimensional stresses and displacements in a thick plate under any tangential loads applied on both surfaces are obtained in the form of infinite series, whose first terms represent the classical thin-plate theory for antisymmetric loading and the plane-stress solution for symmetric loading. The general terms for these series solutions and also for the previously studied case of normal loads are included.

On the analysis of buckled plates. E. F. Masur, University of Michigan.

A new approach to the analysis of the postbuckling behavior of plates is presented. Based on the large deflection theory of von Karman, the middle-surface (membrane) stresses are shown to obey a minimum-energy principle. This principle, together with the employment of stress-function space, is utilized to develop a sequence of solutions, each of which can be made to approximate the correct solution to a closer degree than the previous one. An error estimate is provided at each stage through the establishment of upper and lower bound principles.

Flexibility analysis of piping systems formulated for digital computer solution. Robert H. Owens, University of New Hampshire.

The analysis is general within the framework of small deformation theory. In addition to a consideration of shear and tensile forces, a completely arbitrary distributed loading is imposed on the system. A general scheme for setting up the equations relating the loadings to the deformations is given for a system with any number of anchors and constraints. Formulas for the flexibility matrices and those matrices which govern the effect of the distributed loading on deformation are derived for straight sections and plane bends. All computations may be carried out easily on a digital computer.

On the torsion problem. H. Poritsky, C. E. Danforth, General Electric Company.

Several graphical, approximate numerical, and exact analytical methods of solving the torsion problems are examined. These are illustrated on cross sections of relatively small thickness such as characterize blades of compressors and turbines, and on an angle-iron cross section of small thickness. The methods covered include small-square "flux plotting," approximations by means of harmonic polynomials, conformal mapping on a unit circle, an approximation to the stress function which is parabolic in the distance n from the "mean line," and others.

Buckling of thin single and multilayer conical and cylindrical shells with rotationally symmetric stresses. P. P. Radkowski, Avco Manufacturing Corporation.

The buckling of simply supported, thin, single and multilayer conical shells under axially symmetrical loadings is analyzed in this paper. The results are presented in a compact manner so that they may be easily used for design and/or experimental purposes. The results are compared with known experimental values.

Pressure and thermal stress analysis of plate-type fuel subassemblies. N. C. Small, Westinghouse Electric Corporation.

In this paper finite difference equations are employed to determine a closed form solution for the redundant reactions in a plate-type fuel subassembly for a nuclear reactor. Both pressure and thermal loading are considered. The results are compared with a photoelastic analysis and with the values predicted by a simplified continuous elastic foundation theory.

Uniformly loaded square plate with no lateral or tangential edge displacements. F. J. Stanek, Oak Ridge National Laboratory.

The purpose of this paper is to present an analysis of a uniformly loaded square plate with no lateral or tangential displacements along the edges. It is assumed that these boundary conditions placed upon the displacements will be representative of the bottom of a bin or box which is supported by corner legs, such as a gravel bin. The Ritz energy method is used. The expressions for the displacements w, u, and v are assumed to be in the form of double trigonometric series. Three complete solutions were made, each time increasing the number of terms in the series, for various values of the dimensionless load (qa^4/Dh) up to approximately 100,000, which corresponds to a maximum lateral deflection w_0/h at the center of the plate of approximately 8.5. The results of the various solutions are then compared.

ELASTICITY, ELASTIC STRUCTURES

Thermal stresses in laminated, circular plates. Jack R. Vinson, General Electric Company.

Some multilayer structures which are subjected to heat inputs, such as portions of blunt forebodies and afterbodies of re-entry vehicles, can be approximated by considering a circular, laminated plate. It is desirable to determine the stress distribution and displacements in each lamina when the plate is subjected to an axisymmetric temperature distribution. In this paper, the governing general plate equations are derived for an isotropic thermoelastic plate composed of two laminae, subjected to an arbitrary axisymmetric temperature distribution, varying along the radius and through the thickness.

The conical disk spring. G. A. Wempner, University of Illinois.

This paper presents approximate formulas to describe the behavior of the conical disk spring. It is assumed that the shallow conical shell remains conical when subjected to the axially symmetric edge loads. The principle of stationary potential energy is used to derive the relations between load and deflection. Formulas relating the applied loads, stresses, and deflections are given for several types of edge constraint. The analysis is essentially a refinement and extension of the previous work of Almen and Laszlo (TRANS. ASME, vol. 58, 1936, pp. 305–314).

On the Donnell equations and Donnell type equations of thin cylindrical shells. Yi-Yuan Yu, Polytechnic Institute of Brooklyn.

The Donnell equations of thin cylindrical shells are characterized by being in a completely uncoupled form, but they also involve simplifying assumptions concerning the strain expressions. Equations of thin cylindrical shells in such uncoupled form are called Donnell type equations when no simplification of the strain expressions is involved in the derivation. A review of the previous results is first given on these equations, both static and dynamic, and either including or excluding the effects of transverse shear deformation and rotational inertia, together with their applications. A most complete set of Donnell type dynamic equations including the shear and rotation effects is then derived, which is shown to be reducible to the previous results. In particular, from this set of Donnell type dynamic equations is deduced a set of Donnell dynamic equations, also including the shear and rotation effects.

Plasticity, Viscoelastic Flow, Fracture

Normal incidence in the determination of large strain through the use of diffraction gratings. James F. Bell, The Johns Hopkins University.

In this paper the advantage of using normal incident light is discussed for the measurement of large strain by means of diffraction gratings. Exact expressions for both strain and surface angle are obtained and a direct method of over-all calibration is discussed, this latter permitting considerable improvement in accuracy over that previously reported for the method. Results are given for a 30,700 lines per in., 0.010-in-long diffraction grating gage on a specimen undergoing dynamic plastic strain from a constant velocity impact.

Stress wave propagation in lead. S. R. Bodner, H. Kolsky, Brown University.

The mechanical behavior of pure lead bars for sinusoidal vibrations and for stress pulse propagation was investigated. It was found that the damping in lead is approximately independent of frequency and is amplitude-dependent for large strains while the sound velocity increases slowly with frequency. The results of the vibration and pulse propagation methods were in good agreement and the latter results could therefore be predicted from vibration measurements.

A contour method for one-dimensional pulse propagation in elastic-plastic materials. Norman Davids, Sudhir Kumar, Pennsylvania State University.

This paper presents a method for solving graphically certain one-dimensional wave or pulse propagation problems of elastic-plastic waves. It makes use of contours of stress-strain and particle velocity superimposed on a space versus time diagram. A set of basic rules are stated that govern the relationships among the contours, with examples. Using a two-straight-line stress-strain relation, the solution of the problem of propagation of the trapezoidal pulse with peak pressure of somewhat more than twice the yield stress has been presented. The behavior of these contours in the permanently strained region, when interaction of waves by overtaking from the same side occurs, is one of the cases discussed in detail.

The plastic response of a simply supported beam to an impact load at the center. A. A. Ezra, The Martin Company.

A method is developed for determining the plastic response of the beam during impact, considering the material of the beam to be rigid-plastic, and including the effect of increased yield moment due to high rates of strain. The kinetic energy of impact is large compared to the strain energy the beam can store elastically, and its elastic behavior is not considered. The differential equations of motion are based on observed behavior and on the concept of moving plastic hinges. The theoretical values obtained by this method agree well with the experimental results of others.

Prediction of stress relaxation from creep tests of plastics. William N. Findley, Brown University.

Stress relaxation tests of a canvas laminate and a polyvinyl chloride plastic are presented together with recovery of polyvinyl chloride following relaxation. The results of the stress relaxation tests were compared with the prediction from the results of creep tests as expressed by the relation $\epsilon = \epsilon_0' \sinh \sigma/\sigma_s + m't^n \sinh \sigma/\sigma_m$. The agreement was excellent when this equation was assumed to apply to stress relaxation as well as creep. The prediction from strain-hardening and time-hardening theories was less satisfactory. Prediction of recovery following relaxation by means of the superposition principle was found to be reasonable but yielded a rate of recovery which was too high.

The mechanism of erosion of ductile metals. Iain Finnie, Shell Development Company.

The manner in which abrasive particles erode the surface of a

PLASTICITY, VISCOELASTIC FLOW, FRACTURE

ductile metal has been studied analytically and experimentally. By considering the behavior of a single abrasive grain impinging on the surface, equations have been derived which predict the weight loss by erosion. Experimental results for several metals show good agreement with the predicted variation of weight loss with particle velocity and direction relative to the surface. The material properties required for numerical weight loss prediction are shown to be compatible with those obtained from metal-cutting experiments.

Studies in photoplasticity. M. M. Frocht, R. A. Thomson, Illinois Institute of Technology.

This paper describes an extension of the "photoelastic" method to the plastic state. Using thin models of cellulose nitrate, factors of stress concentration and stress distributions were determined for several basic cases. The extension is made possible by the establishment of a suitable stress-optic law and the employment of the shear-difference method. The results obtained are in substantial agreement with theory and experiment. The method is at present limited to plane-stress problems in the elastoplastic state without unloading.

The load-carrying capacity of wide beams at finite deflection. R. M. Haythornthwaite, Brown University; W. E. Boyce, Rensselaer Polytechnic Institute.

Estimates of the post-yield carrying capacity of laterally loaded plates may be obtained conveniently from the velocity fields associated with either the limit load or the membrane solution. The latter can be used even when the limit load is not known. As an illustration, an approximate membrane solution is found for a centrally loaded rectangular plate, rigidly clamped along two opposite sides and free along the other two. The velocity field includes both a local circular symmetric deformation near the load and also a general beam bending mechanism. The rate of deflection is computed and the field is also used to obtain an upper bound to the limit load. Comparison is made with the results of tests of six steel beams of various widths.

Rotating disks—Insensitivity of design. Jacques Heyman, Brown University.

The plastic method of design of rotating disks leads to profiles very similar to those generated by conventional elastic methods. The minimum weight disk is investigated, and it is shown that a practical disk approximates very closely in its leading dimensions to the minimum weight disk. In particular, the axial length of a disk at its bore is insensitive to the precise form of profile, which makes an elastic trial-and-error method workable. This insensitivity is examined by using a plastic analysis.

Determination of the plastic stress-strain relations in tension of Nittany no. 2 brass under hydrostatic pressure. L. W. Hu, Pennsylvania State University.

This paper describes a new triaxial stress testing method for studying the plastic behavior of metals. Two-load tension tests were conducted on a Nittany No. 2 free machining brass under hydrostatic pressures up to 53,200 psi. Effects of hydrostatic compression on strain-hardening coefficient, strength coefficient, average true stress at rupture, and reduction in cross-sectional area at rupture are reported.

The plastic working ability test of sheet plastics by a deep-drawing process. Katsuhiko Ito, Brown University.

The plastic working ability of materials, especially the advisability of hot or cold working, is described on the basis of forming ability and retentivity. The deep-drawing process is applied to various sheet plastics, at both room and elevated temperatures, as a most suitable method of testing the plastic working ability of sheet materials. The relationships between the limiting drawing coefficients and working temperatures of several sheet plastics are examined. The influences of hot and cold punches in celluloid and also of fully cured and undercured phenol laminates on their plastic working ability are compared.

Overestimates of load for some two-dimensional forging operations. W. Johnson, University of Manchester.

The pressure to forge thick material with two dies of unequal width to cause the equal sideways displacement of material is derived using a slip-line field. The results are compared with those obtained using a discontinuous velocity field. Forging with two similar dies which cause unequal sideways material displacement is next examined. For thin material the forging pressure is determined using discontinuous velocity patterns for equal-width perfectly rough dies. Similarly, instances in which the die widths are unequal, where flashes are formed and where the dies are perfectly smooth, are examined. Finally, forgings in which material flows in four perpendicular directions are discussed.

On stress-strain relations based on slips. T. H. Lin, University of California.

Basic assumptions used in the slip polyaxial stress-strain relations of Batdorf and Budiansky are compared to those assumptions in the slip stress-strain relations proposed by the writer. The latter slip theory is modified to include the effect of latent hardening. A number of inelastic loadings have been calculated. For the cases calculated, the present theory gives better agreement with experimental data than the previous theories.

Yield failure of stiffened cylinders under hydrostatic pressure. M. E. Lunchick, David Taylor Model Basin.

Experimental results are presented of hydrostatic tests of stiffened cylinders. These results are compared with existing theories predicting the collapse pressure as well as a new method presented in the paper. This method is based on an elastic-plastic analysis of a stiffened cylinder comprised of an ideally plastic material. The test results agree best with theories using a Hencky-von Mises criterion of yielding and allowing for plastic reserve strength after the initiation of yielding.

Crack propagation under repeated loading. D. E. Martin, General Motors Corporation; G. M. Sinclair, University of Illinois.

Crack propagation data for axial load tests of sheet 24S-T3 aluminum alloy are presented for specimen lives ranging from 100,000 to 600,000 cycles. Cracks ranging from 0.004 in. to 1.5 in. in length were measured periodically up to one cycle prior to fracture. These data were analyzed to evaluate the influence of nominal stress and crack length on the cyclic rate of crack propagation and are compared with the analytical results of several investigations concerning crack growth. These investigations include the work of Head in Australia pertaining to fatigue crack propagation, and the works of Irwin and Bowie on the Griffith theory of crack growth.

PLASTICITY, VISCOELASTIC FLOW, FRACTURE

A method for analyzing primary creep data. K. R. Merckx, General Electric Company.

In this paper a general method for analyzing the strain rate $\dot{\epsilon}$ during primary creep as a function of the creep stress σ, testing temperature T, and the strain ϵ, is presented in form suitable for a graphical analysis. The mathematical model describing the creep rate has the form $\dot{\epsilon} = \epsilon^{-m} (\sigma/3G) \exp [k + d (\sigma/2G)]$, where G is the elastic shearing modulus and m, k, and d are parameters. An analysis of uranium creep data between 100–600°C is given. The method of generalizing the material model for use in problems where the stress condition is triaxial and the stresses vary with time is given. Also, some minor alterations of the material are included which facilitated the numerical evaluation of thermal stress problems.

On the infinite elastic, perfectly plastic wedge under uniform surface tractions. S. A. Murch, P. M. Naghdi, University of Michigan.

This paper is concerned with both plane strain and plane stress solutions of the infinite elastic, perfectly plastic wedge (of included angle $0 < \beta < 2\pi$) under uniform surface tractions, where Tresca's yield condition and its associated flow rules are employed. Following a detailed examination of the character of the initial yield, attention is confined to the class of problems where yielding occurs externally on one or both boundaries. Specifically, complete solutions are obtained for a wedge under uniform shear on one face in both states of plane strain and plane stress, in the light of which the symmetry of the stress tensor is also discussed.

On the steady creep of shells. E. T. Onat, H. Yüksel, Brown University.

A modified creep law which is particularly suitable for the investigation of rotationally symmetrical deformations of shells is discussed in detail. It is then applied to establish the creep behavior of cylindrical sandwich shells in terms of the stress resultants and deflection rates. The creep deflections of simply supported shells under the hydrostatic pressure is discussed as an example. Finite deflection of a solid circular membrane under uniform pressure is also discussed as a further example of the modified creep law.

Carrying capacity of elastic-plastic shells under hydrostatic pressure. B. Paul, Polytechnic Institute of Brooklyn; P. G. Hodge, Jr., Illinois Institute of Technology.

The limit load of a short rigid-plastic cylindrical shell, subjected to radial pressure only, represents a good approximation to the carrying capacity of the more realistic elastic-plastic shell. When axial loads are also present, the so-called beam column effect tends to reduce the carrying capacity of the elastic-plastic shell. In the present paper an approximate value of the carrying capacity is derived, including the beam column effect, for a completely plastic shell in a hydrostatic pressure field. In addition, a complete elastic-plastic solution, giving the deformations as the loading progresses, is presented in a particular numerical example. The approximate solution and the elastic-plastic solution predict the same carrying capacity in the example cited.

Strain-hardening solutions with generalized kinematic models. Nicholas Perrone, Polytechnic Institute of Brooklyn; P. G. Hodge, Jr., Illinois Institute of Technology.

Some general considerations for a theory of plastic strain hardening under biaxial stresses are discussed. It is shown that stresses which are forced to remain zero may still have an influence in the behavior of the material, but that zero strains may be eliminated. Further, it is shown that a suitable change in variable can always be made to give a simple relation between stress and strain in any direction. The results are illustrated in the solution of the bending of an I-beam with unequal flanges. The problem is treated, first, as a one-dimensional one in terms of the actual stresses, and then as a biaxial one in terms of the resultant moment and axial force. A comparison between the two treatments provides some suggestions for a general theory of biaxial hardening.

Creep buckling of a curved beam under lateral loading. T. H. H. Pian, Massachusetts Institute of Technology.

Variational theorem for creep is applied to the problem of creep deflection of a curved beam under lateral loading. The end of the beam is restrained from sliding motion; hence under a static load it is possible to buckle suddenly from one equilibrium condition to another. It is shown that this abrupt buckling may also occur under the action of creep deformation. Both viscoelastic and nonlinear creep properties are included in the analysis.

Chip formation during the turning operation in the presence of a built-up nose. Bernard W. Shaffer, New York University.

Chip formation in the turning operation, when some of the workpiece adheres to the base of the cutting tool forming a built-up nose, is analyzed as a plane strain problem of a perfectly plastic material. A slip-line field is presented which satisfies the stress and velocity boundary conditions of the problem. The results of this solution are then applied to provide expressions for the machining force and chip-thickness ratio. The solution for the turning operation is found to approach that for the orthogonal planing operation as the radius of the workpiece is increased.

Limit strength of thin-walled pressure vessels with an ASME standard torispherical head. R. T. Shield, D. C. Drucker, Brown University.

Results are presented for the maximum pressure which an unfired vessel with an ASME standard torispherical head can withstand before appreciable plastic deformation will occur. The effect of flanges on strength is considered. Although the procedures outlined permit variation of pressure in the axial direction to be taken into account fully, for convenience the calculations are based upon the assumption of uniform interior pressure. Work-hardening is not of much significance for thin-walled vessels of the usual steels and is ignored. A comparison is made with the ASME Code for Unfired Pressure Vessels. A real danger is pointed out which is especially important in connection with brittle fracture at low temperature.

On transient thermal stresses in linear viscoelasticity. Eli Sternberg, Brown University.

The principle of correspondence appropriate to the linear theories of elasticity and viscoelasticity is extended to account for the presence of a time-dependent temperature field, and is applied to the quasi-static determination of transient thermal stresses in a general, linear, homogeneous and isotropic, infinite viscoelastic medium with a spherical cavity. It is assumed that the body is free from loading and that the stress-inducing temperature distribution has polar symmetry about the center of the

PLASTICITY, VISCOELASTIC FLOW, FRACTURE

cavity. An exact solution to this problem is established in integral form on the assumption that all physical parameters are independent of the temperature. Closed explicit solutions, in terms of error functions, are deduced for the special instance in which the material is either a Maxwell or a Kelvin solid, if the temperature field obeys the heat-conduction equation and is generated by a suddenly applied, steadily maintained heating (or cooling) of the boundary.

A comparative study of elevated temperature creep in long rotating cylinders based on various flow criteria. A. M. Wahl, Westinghouse Electric Corporation.

Stress distributions under steady-state creep at elevated temperature are obtained for long rotating cylinders having axial bores, a problem of interest in turbine design. Comparison is made between stress distribution, peak stress, and creep deformation based on various flow criteria. Peak stresses found are considerably higher than average tangential stress, particularly for small ratios of inner to outer diameter. Creep deformations at the bore are higher, and those at the outside diameter lower, than those based on average stress. Curves are given for finding maximum stress for various diameter ratios and values of n in the power function stress-creep rate relation assumed.

Elastic-plastic stresses in rings under steady-state radial temperature variation. J. C. Wilhoit, Jr., The Rice Institute.

The plane stress case of a ring subject to a temperature gradient is considered. It is shown that a temperature gradient of sufficient magnitude causes initial yielding at the inner surface if the Tresca yield theory is employed. If the gradient is further increased it is shown that a second plastic region begins at the outer surface and moves inward but that an infinite thermal gradient would theoretically be required for the ring to become fully plastic.

Transient motion of a viscoelastic rectangular plate in fluid media. Gordon C. K. Yeh and Johann Martinek, Reed Research, Incorporated.

An equation of motion for the linear bending vibration of a thin plate of a viscoelastic material of Maxwell's type as derived previously by the authors is solved for transient motions of simply supported and clamped rectangular plates. The deflections can then be expressed as the linear combination of a set of time functions and a set of space functions. The time functions have the same forms for both cases and are in terms of the roots of a cubic algebraic equation for each mode. Damped oscillation is possible only when cubic equations have complex roots,

Fluid Flow, Aerodynamics, Heat Transfer

Determination of nitrogen temperatures by velocity-of-sound measurements. Vito D. Agosta, Polytechnic Institute of Brooklyn; H. Dean Baker, Columbia University.

For systems not in complete thermodynamic equilibrium, a pseudotemperature is defined as that temperature which prevails in the translational states. This assumes: (1) That the translational states are in thermal equilibrium among themselves; and (2) that the energy content of the gas, if all the other energy states were in equilibrium with the translational states, would not differ by a substantial amount from the actual energy content of the gas. It is shown that this defined temperature quantity can be determined from velocity-of-sound measurements in gases. For nitrogen in equilibrium in the range $530°R \leq T \leq 856°R$, temperatures calculated from velocity-of-sound measurements agreed to within 1 per cent of those measured by thermocouples.

Some compressibility and heat-transfer characteristics of the wall jet. Martin H. Bloom, Polytechnic Institute of Brooklyn; Martin H. Steiger, Sperry Gyroscope Co.

Compressibility and heat-transfer characteristics of a jet spreading out over a plane surface in a stationary ambient atmosphere (termed the "wall jet" by Glauert) are investigated. The major part of the paper deals with laminar flow, both planar and radial, over isothermal and nonisothermal surfaces, in regions away from the emission slot, and with the same jet and ambient gases, including dissociated gases in thermal equilibrium. Thermal solutions in similar form are obtained under the special conditions that the surface temperature is equal to the ambient temperature or that the enthalpy varies monotonically from the surface value to the ambient value. Asymptotic solutions are used to circumvent some lengthy computations. A procedure for treating different jet and ambient gases is indicated and a procedure for treating the turbulent case is discussed briefly.

A new interpretation of the free-space pressure field near a ship propeller. John P. Breslin, Stevens Institute of Technology.

The pressure fluctuations at a point in the vicinity of a propeller operating in a boundless incompressible fluid are found from the velocity potential function. This approach, which yields results in agreement with those obtained by different derivations, has the advantage of enabling one to interpret the character of the pressure field. It is shown that the linearized pressures are purely convective in nature and, hence, the pressure field acts as though it is a "static" distribution which moves with each blade. This result provides some conceptional gain in the application of the free-space field to the action expected on a flat plate. Some broad characteristics of the field are outlined. Detailed evaluation in terms of elliptic integrals is deferred to a later report.

Aerodynamic ablation of melting bodies. Theodore R. Goodman, Allied Research Associates, Inc.

A simple mathematical model has been derived to predict the aerodynamic ablations of melting bodies. The ablation on a flat plate with a constant heat input has been derived in detail. Also for this case, the ablation after heat shut-off has been derived. Another case that has been studied is the ablation after a thermal pulse. A simple experiment was performed which ablates water from a slab, and the results of this experiment substantiate the theory qualitatively (no quantitative data were obtained). Many other useful and interesting cases may be solved using the theory, and these have been pointed out.

Heat transfer in a power-producing porous solid. Leon Green, Jr., Aerojet-General Corporation.

The results of a one-dimensional analysis of the steady-state temperature distribution in a gas-cooled, heat-generating, po-

FLUID FLOW, AERODYNAMICS, HEAT TRANSFER

rous solid are presented. The analysis, which assumes the existence of a finite coefficient of heat transfer between the solid and gas phases, permits an average heat-transfer coefficient to be determined from experiments in which precise measurements of gas temperature at the entrance and exit faces of the solid are not required if the temperatures of the porous surfaces are known. In the limiting case of very high heat-transfer coefficients, the results are in agreement with those of a previous analysis in which the solid and gas temperatures within the porous structure were assumed to be substantially equal.

The forces acting on slender submerged bodies and body appendage combinations in oblique waves. Paul Kaplan, Pung Nien Hu, Stevens Institute of Technology.

The hydrodynamic forces and moments acting on a slender submerged body of revolution moving obliquely to the crests of regular waves are found by the application of slender-body theory, which utilized two-dimensional crossflow concepts. A comparison is made with an exact solution obtained by use of the circle theorem for a particular orientation, in order to judge the validity of the approximation utilized in the general case. The forces acting on body-appendage combinations are considered and solutions obtained for two different stern fin configurations.

On the similarity rules in diabatic flow. M. Z. v. Krzywoblocki, F. Y. Horiuchi, J. J. Voda, University of Illinois.

The diabatic flow is considered to be a flow of an inviscid, nonheat-conducting fluid with heat addition by means of sources, i.e., injection of heat. The governing fundamental equations for such a flow are: the first law of thermodynamics, Euler's equation of motion, and a pressure-density-entropy relation. In the first part the authors generalize the Prandtl-Glauert formula to diabatic, rotational flow; in the second part they derive a generalized similarity formula in the hodograph plane.

Creeping viscous flow through a two-dimensional channel of varying gap. William E. Langlois, E. I. du Pont de Nemours & Company.

The slow flow under pressure of a very viscous, incompressible, inelastic fluid through a two-dimensional channel of nonuniform gap is investigated theoretically. Three approximation methods are developed and compared. The flow from one uniform channel to another of smaller gap through a smooth constriction is considered in detail.

Wave generation by turbulent wind over a finite fetch. Owen M. Phillips, The Johns Hopkins University.

When a turbulent wind blows across the surface of an inviscid liquid (water), waves are generated by the interaction of the convected pressure fluctuations and the free surface. The rate of growth of each Fourier component of the wave field is the greatest when the convection velocity of the component of the pressure fluctuations is equal to the velocity of free surface waves of the same wave number. In this paper, the growth of waves over a finite fetch is studied, and an expression is derived for the mean square surface displacement $\bar{\xi}^2$ as a function of position in the wave field. For a semi-infinite sheet of water, $\bar{\xi}^2$ is proportional to the fetch, a relation in good agreement with experimental observations.

Study of the air flow between coaxial disks rotating with arbitrary velocities in an open or enclosed space. K. G. Picha, Georgia Institute of Technology; E. R. G. Eckert, University of Minnesota.

An experimental study of the flow of the main body of fluid between two rotating coaxial disks of equal diameter (outside the boundary layers at each disk) has been carried out. The disks rotated with equal and unequal angular velocities in the same and in opposite directions with Reynolds numbers between 2.6×10^5 and 11.9×10^5. The distance between the disks was varied from $^1/_{13}$ to $^7/_{13}$ of the disk diameter, and two boundary conditions on the cylindrical surface surrounding the disks were investigated. In one case the disks rotated in a large free space; in the second case the space between the disks was closed off by a stationary cylindrical shroud. The results of flow visualization studies, of velocity measurements, and of a boundary-layer calculation are reported.

Hypersonic stagnation-point heat transfer to surfaces having finite catalytic efficiency. Sinclaire M. Scala, General Electric Company.

The use of "noncatalytic" coatings has been suggested as a means of reducing the heat absorbed by a hypersonic vehicle by minimizing the catalytic recombination of atomic species. The theoretical merits of such coatings are investigated by solving the governing system of nonlinear differential equations subject to the appropriate conditions of velocity, temperature, pressure, and molar concentrations of reacting gaseous species, at the stagnation point of the body. The effects of homogeneous and heterogeneous atom recombination are included, and the results obtained yield the unique relationship between the catalytic efficiency of a surface and the heat transfer from the flowing dissociated gas which envelops the vehicle.

Thermal entrance region of a circular tube under transient heating conditions. E. M. Sparrow, R. Siegel, Lewis Flight Propulsion Laboratory.

An analysis is made for laminar forced-convection heat transfer in the thermal entrance region of a circular tube whose wall may take on arbitrary time variations of either surface temperature or surface heat flux. The time varying process may begin either from an already established steady-state heat-transfer situation, or from a situation where wall and fluid are at the same uniform temperature. The velocity profile is taken to be steady and fully developed (Poiseuille flow). The first step in the analysis determines the thermal response to a unit step change in wall temperature or wall heat flux by using the method of characteristics. Then, by a superposition technique, this solution is generalized to apply for arbitrary time variations. The final results are expressed in the form of integrals which may be easily evaluated for particular applications.

Exact solution of the Neumann problem. Calculation of noncirculatory plane and axially symmetric flows about or within arbitrary boundaries. A. M. O. Smith, Jesse Pierce, Douglas Aircraft Company.

An exact general method of solving the Neumann or second boundary-value problem has been developed and has been applied to the calculation of low-speed flows about or within bodies of almost any shape, provided the flow is either plane or axially symmetric. Solid-body, inlet, and purely internal flow problems can be solved. Because problems of interference can be treated

with ease, the method is capable of dealing with several bodies at once in the presence of one another. Boundaries need not be solid; that is, flows involving area suction can be calculated. With an IBM 704, calculations required from 3 minutes to 2 hours according to the complexity of the body.

Aerodynamics of wings and bodies at Mach number one. John R. Spreiter, Alberta Y. Alksne, Ames Aeronautical Laboratory.

A method is described for the approximate solution of the nonlinear equations of transonic flow theory for flows with free-stream Mach number one. Results in the form of pressure distributions are given for a number of specific applications involving airfoils, bodies of revolution, and slender bodies of arbitrary cross section. All results are compared either with existing theoretical solutions or with experimental data.

Finite cavity cascade flow. C. D. Sutherland, Hirsh Cohen, Rensselaer Polytechnic Institute.

Steady flow of an incompressible, nonviscous fluid past an infinite array of lifting foils under such conditions that fully developed cavities appear on the foil surfaces is considered. The foils are taken to be thin and at small angle of attack so that the linearized theory of Tulin may be applied. The linearized problem is solved for any stagger angle and any chord-foil spacing ratio in terms of the cavitation number, cavity length, exit angle, and exit velocity. The effect of changing chord-foil spacing ratio on cavitation number, exit angle, and lift coefficient is obtained as well as the relation between lift coefficient and cavitation number. Limiting cases of the solution, the isolated foil, and the cavity of infinite length agree with previous results.

Velocity measurements in the boundary layer and in the main flow between two coaxial disks rotating with equal velocities in air. William E. Welsh, Jr., General Electric Company; James P. Hartnett, University of Minnesota.

Velocity and pressure distributions were measured in subsonic air flow induced by the rotation of two coaxial disks moving with equal velocities. Disk rim Reynolds numbers varied from 2.35×10^5 to 6.19×10^5 and the spacing between the disks was varied from 4 to 8 inches. Particular emphasis is placed on the measured radial and tangential velocities within the boundary layer, and these results are compared with values reported for a single rotating disk.

On the flow of a stratified fluid. Chia-Shun Yih, University of Michigan.

This paper contains a discussion of the effect of inertia on steady stratified flows of an incompressible and inviscid fluid and an exact solution of the nonlinear partial differential equations governing such flows. The latter is a solution for the steady two-dimensional flow of a stratified fluid in a channel toward a line sink, with constant density gradient in the vertical direction at infinity.

THE PROCEEDINGS

of the Third U. S. National Congress of Applied Mechanics

will be published December, 1958

Price to members and nonmembers: $20 per volume

Send orders for copies to:
THE AMERICAN SOCIETY OF MECHANICAL ENGINEERS
29 West 39th St., New York 18, N. Y.

Stress Distributions Around Hydrostatically Loaded Circular Holes in the Neighborhood of Corners

By A. J. DURELLI[1] and A. S. KOBAYASHI,[2] CHICAGO, ILL.

The stress distributions around hydrostatically loaded circular holes in the neighborhood of corners was determined by using photoelasticity and brittle coatings. Photoelasticity (by means of a diffused-light polariscope) was used to determine the maximum shear lines (isochromatics), and brittle coatings were used to determine the directions of the principal stresses (isostatics). Tests were conducted for six plates with different ratios of hole radius to hole distance to the exterior boundary of plate (*R/L*). The results of these tests are presented in the form of curves. These curves show the distribution of the maximum shear stress along the diagonal of the plate, the maximum principal stress along the edges of the plate and of the hole, and the maximum shear stress along a perpendicular line to the exterior boundary drawn from the center of the hole. All these values are given as a function of *R/L*. Curves also are presented which compare the stresses on the diagonal of the plate at the boundary of the hole with the stresses computed using Lamé's equation for a thick-walled cylinder. Comparisons also are made with the results obtained by Jeffery for a semi-infinite plate with a circular hole subjected to a hydrostatic pressure. All results are given in dimensionless form with the applied pressure as reference. The results published in this paper are new, but the techniques used have been described previously in papers by researchers from the Armour Research Foundation.

Introduction

THE solution to the problem of the distribution of stresses around hydrostatically loaded circular holes in the neighborhood of corners can be approached numerically by determining arbitrary constants in an infinite series satisfying prescribed boundary conditions as done by Sekiya (1).[3] This procedure is very time-consuming since the convergence of this infinite series is slow and not accurate as can be seen by comparing the results in (1) and (3). The authors feel that the experimental approach to the problem is comparatively simple and justified and continue here a series of papers published on the subject (3, 4). In the present paper, a solution by means of photoelasticity and brittle coating is given. Six different plates were investigated, and the results are presented in the form of curves. Values are plotted in terms of a parameter R/L (representing the ratio of the hole radius to the distance from the exterior boundary). In each case the hole diameter was held to a fixed value in order to utilize the same loading jig, and the hole distance was varied to obtain the desired R/L ratio. The techniques used to conduct the tests have been described already by one of the authors (2, 3, 4, 5), and will only be summarized here.

Description of Test

A diffused-light polariscope (5) was used, and Columbia Resin CR-39 served as the model material. A special jig (2) was used to apply a uniform load to the interior boundary of the model, Fig. 1. The jig consists of two steel circular plates of $1^1/_2$-in. diam and a circular insert with a diameter of 1 in. and a thickness approximately equal to the thickness of the model; i.e., $^1/_4$ in. This insert was placed concentrically in between the two plates. Rubber tubing is placed inside the groove formed by the plates and the insert. When pressurized nitrogen gas is applied to the tube, the expansion of the tube produces hydrostatic loading on the model. As the plastic model deforms under the loading much more than the steel insert, the hole diameter of the plastic plate was made a few thousandths of an inch smaller than the diameter of the jig plates in such a way that the final diameter of the hole after loading was very close to the diameter of the jig.

The material was calibrated by using a calibration fixture which reproduced very closely the loading conditions on the model. This fixture, described in detail in the afore-mentioned papers, consists of a rectangular metal frame containing two sliding metal blocks. The bottom sliding block holds a rectangular piece of photoelastic material taken from the same sheet as the model. The rubber tubing is placed in a rectangular groove, and the rectangular piece is then adjusted to enter the groove to the same depth that the model enters the loading jig. A circular disk, cut from the same sheet of photoelastic material as the model, is placed between the two sliding blocks, and the upper block is adjusted to the disk size. As pressure is applied to the tubing a force is exerted through the insert to the block, and the disk is loaded in diametral compression. Knowing the line pressure in the rubber tubing, and the thickness of the rectangular insert, the effective pressure on the insert is determined from the calibration curve in reference (2). Similarly, the effective pressure is determined in the model.

The models, calibration disks, and calibration-fixture insert were machined from the same sheet of CR-39. All boundaries were roughed with a jig saw and finished with a router. All models were scribed to enable compensation readings to be made at fixed points. Light and dark field pictures were taken for each test.

Following the photoelastic tests, the models were sprayed with a brittle coating (Stresscoat). The coating was permitted to dry,

[1] Professor, Illinois Institute of Technology, and Supervisor, Armour Research Foundation. Assoc. Mem. ASME.

[2] Associate Engineer, Stress Analysis Section, Armour Research Foundation, Mechanical Engineering Research Department. Assoc. Mem. ASME.

[3] Numbers in parentheses refer to Bibliography at end of paper.

Contributed by the Applied Mechanics Division and presented at the Annual Meeting, New York, N. Y., December 1–6, 1957, of The American Society of Mechanical Engineers.

Discussion of this paper should be addressed to the Secretary, ASME, 29 West 39th Street, New York, N. Y., and will be accepted until July 10, 1958, for publication at a later date. Discussion received after the closing date will be returned.

Note: Statements and opinions advanced in papers are to be understood as individual expressions of their authors and not those of the Society. Manuscript received by ASME Applied Mechanics Division, November 15, 1956. Paper No. 57—A-4.

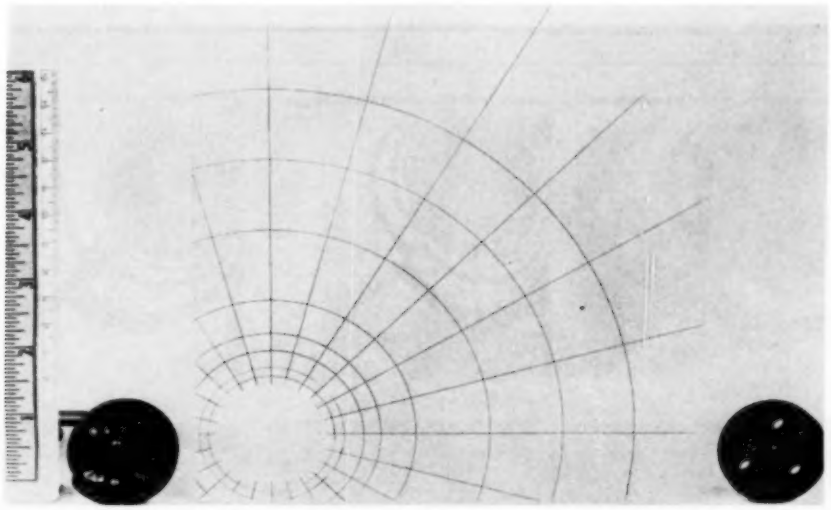

FIG. 1 LOADING JIG USED TO APPLY HYDROSTATIC PRESSURE ON HOLE BOUNDARY

and then the model was loaded as in the photoelastic tests. This load produced strains large enough to cause the coating to crack perpendicularly to the principal stress σ_1. Then the model was left under load for a couple of hours to allow the brittle coating to relax under the load. Upon quick unloading of the model, the brittle coating cracked perpendicularly to the principal stress σ_2. Thus the two families of principal stress directions were obtained from one brittle-coating test. When the field was not completely covered by cracks, refrigeration completed the isostatic pattern as explained in previous papers.

RESULTS AND CONCLUSIONS

Light and dark field photoelastic photographs and brittle-coating photographs are shown in Fig. 2. In the photoelastic photographs of $R/L = 0.91$ and 0.79, the inlet tube is shown along the diagonal of the plate and should not be confused with the isochromatic lines. Evaluation of the data, obtained in the tests, results in the curves shown in Figs. 3 to 10.

In Fig. 3 the maximum shear stress is plotted as a function of position along the diagonal line from the interior boundary to the exterior boundary. The highest value of maximum shear stress always occurs at the interior boundary. It is interesting to know that the maximum shear values become negative before approaching zero at the corner of the plate.

In Fig. 4 the maximum shear stress is plotted as a function of position along the diagonal line from the interior boundary to $4R$. Along this line the highest value of maximum shear stress also occurs at the interior boundary. As in the preceding figure, for larger R/L ratios the curves drop below zero for a short distance. Since the stresses in this region of the plate become very small and are of little practical importance, no special attempt was made to obtain a very precise distribution.

Fig. 5 shows the maximum shear stress along a line through the center of the hole perpendicular to the exterior boundary. It is interesting to note that for the larger R/L ratios the highest value of maximum shear stress exists at the outer boundary, while for the smaller R/L ratios it exists at the inner boundary. As the R/L ratio approaches zero the values obtained approach those computed using the Lamé thick-wall-cylinder equations.

Fig. 6 shows the distribution of stress along the exterior boundary of the plates. The maximum stress for large R/L ratios occurs near the point of intersection of a line drawn through the center of the hole perpendicular to the exterior boundary. As the R/L ratios decrease, the location of the peaks of the curves gradually move away from the corner of the plate. The curves drop below zero on both sides, indicating reversal of sign in the stresses.

Fig. 7 shows the stress distribution along the boundary of the hole. Also shown are the thick-wall-cylinder stresses for two R/L

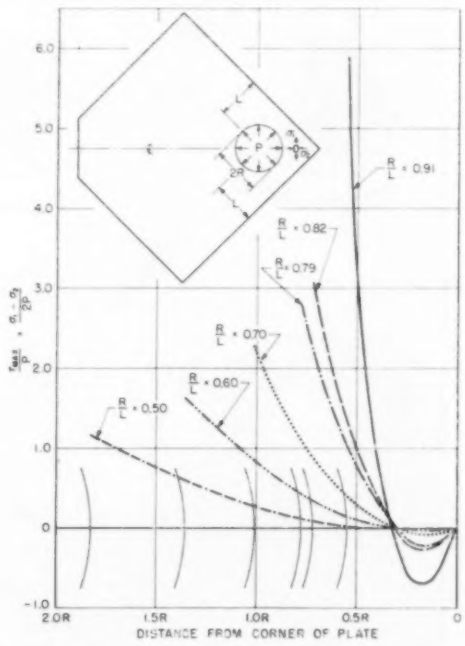

FIG. 3 HYDROSTATICALLY LOADED CIRCULAR HOLE IN THE NEIGHBORHOOD OF A CORNER

(Maximum shear stresses along diagonal, from hole boundary to corner of plate.)

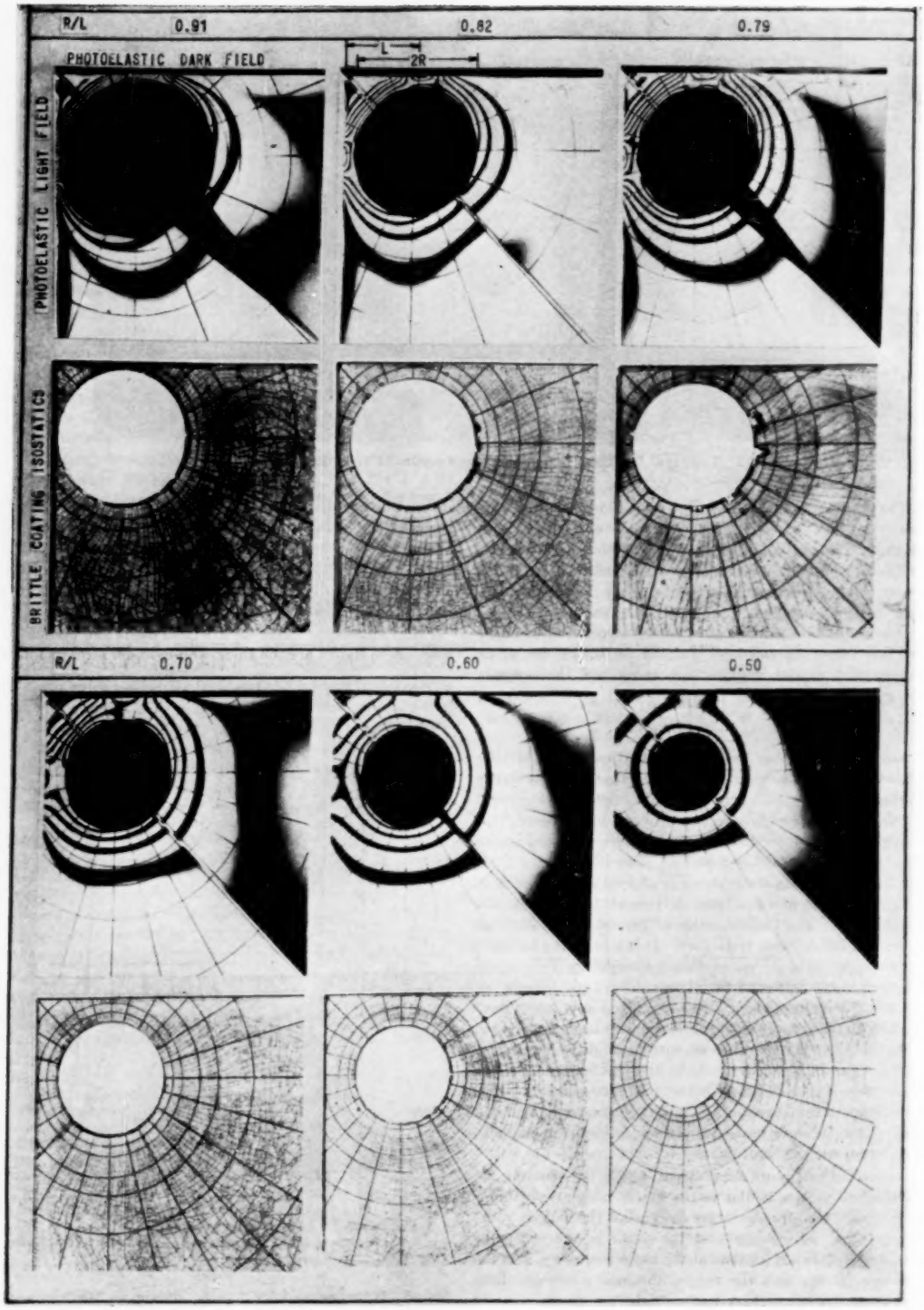

FIG. 2 STRESS DISTRIBUTIONS AROUND HYDROSTATICALLY LOADED CIRCULAR HOLES IN THE NEIGHBORHOOD OF CORNERS

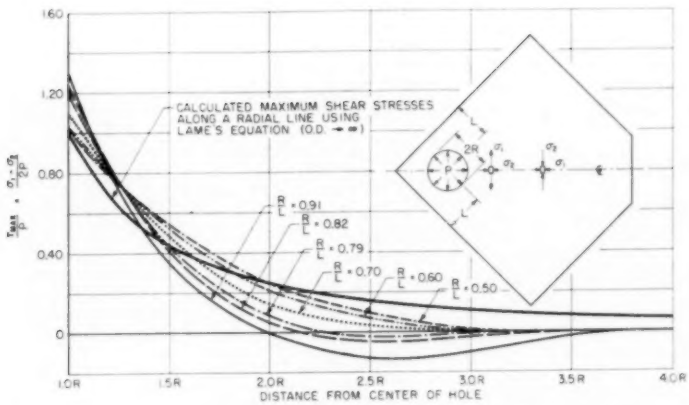

FIG. 4 HYDROSTATICALLY LOADED CIRCULAR HOLE IN THE NEIGHBORHOOD OF A CORNER
(Maximum shear stresses along diagonal, from hole boundary to 4.0*R*.)

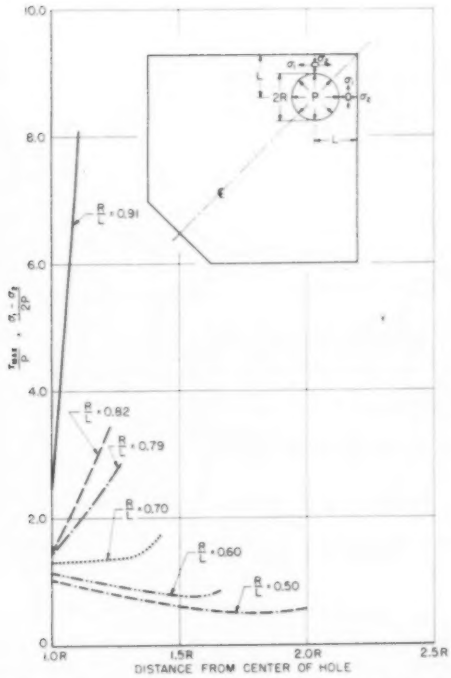

FIG. 5 HYDROSTATICALLY LOADED CIRCULAR HOLE IN THE NEIGHBORHOOD OF A CORNER
(Maximum shear stresses along the line through center of hole perpendicular to exterior boundary.)

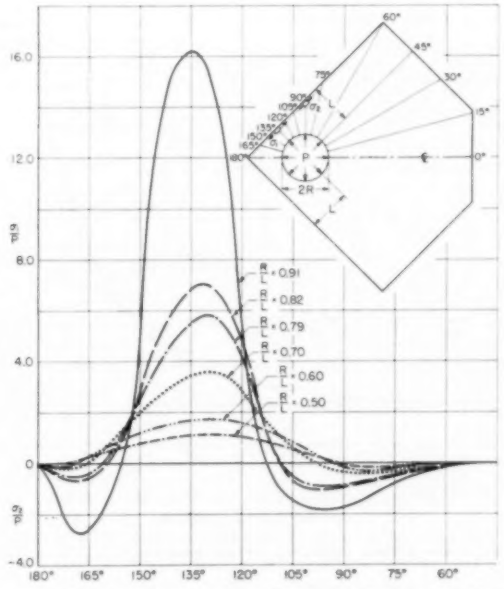

FIG. 6 HYDROSTATICALLY LOADED CIRCULAR HOLE IN THE NEIGHBORHOOD OF A CORNER
(Stress distribution along exterior boundary of plate.)

ratios computed using Lamé's equation. For all R/L ratios the curves approach Lamé's solution in the vicinity of the diagonal line from the hole to the corner of the plate. At other locations on the interior boundary, the curves deviate from Lamé's solution appreciably.

In Fig. 8 the stress (σ_1/P) is plotted for two points on the hole boundary, the point on the boundary at the intersection with the diagonal, and the point on the boundary at the intersection with a line drawn through the center perpendicular to the exterior boundary of the plate. These stresses are compared with similar stresses computed using Lamé's equation for thick-wall cylinders and Jeffery's formula for a semi-infinite plate with a circular hole subjected to hydrostatic pressure (6). Along the diagonal line the experimental curve follows the computed curves fairly closely but there is little agreement of stresses along the perpendicular line.

In Fig. 9 the stresses (σ_1/P) at the intersection of the perpendicular line with the exterior boundary are plotted against the R/L ratios. These stresses are compared with similar stresses computed using the afore-mentioned Lamé's and Jeffery's equations. It is interesting to notice that the experimental curve follows closely the curve obtained by Jeffery's equation but is farther away from the curve obtained by Lamé's equation.

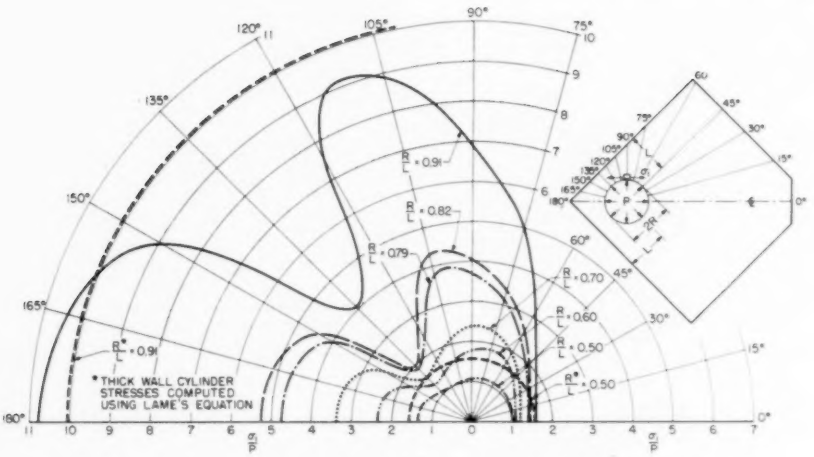

FIG. 7 HYDROSTATICALLY LOADED CIRCULAR HOLE IN THE NEIGHBORHOOD OF A CORNER
(Stress distribution along boundary of hole.)

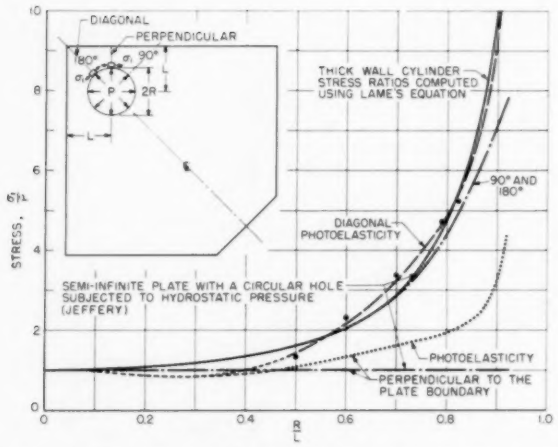

FIG. 8 HYDROSTATICALLY LOADED CIRCULAR HOLE IN THE NEIGHBORHOOD OF A CORNER
(Stresses at two points on the hole boundary, at intersection with the diagonal, and with a line perpendicular to plate boundary from hole center.)

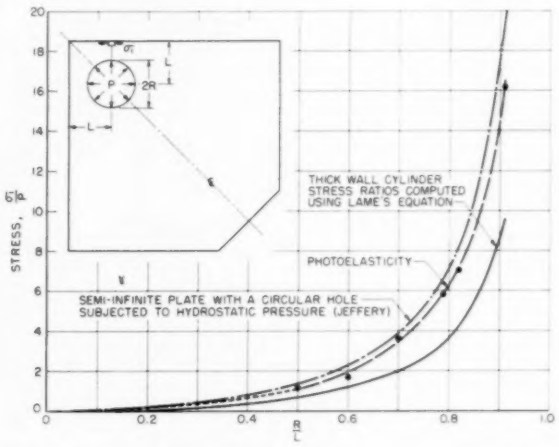
THICK WALL CYLINDER STRESS RATIOS COMPUTED USING LAME'S EQUATION
PHOTOELASTICITY
SEMI-INFINITE PLATE WITH A CIRCULAR HOLE SUBJECTED TO HYDROSTATIC PRESSURE (JEFFERY)
STRESS, σ/p
R/L

FIG. 9 HYDROSTATICALLY LOADED CIRCULAR HOLE IN THE NEIGHBORHOOD OF A CORNER
(Stresses at intersection of exterior boundary with the perpendicular line from the hole center to the exterior boundary.)

Fig. 10 shows a plot of maximum shear stresses on the boundaries for the various R/L ratios. From this set of curves it can be seen that, for ratios above 0.78, the maximum shear stress occurs on the outside boundary of the strip, while for the lower ratios the maximum occurs on the inside boundary. From the photoelastic photographs it can be seen that the points of maximum shear always occur on one of the boundaries. Hence, the accented portion of the curves can be used to determine the maximum shear stress in the plate for any R/L ratio.

With the stress distribution completely defined along the boundaries, Laplace's equation may be used to separate the stress inside the field using relaxation methods, or analogies with other experimental phenomena (electrolytic tank, membrane, and so on). It is also possible to separate the stresses by using the Lamé-Maxwell equation, using the information obtained from the photoelastic isochromatics and the brittle-coating isostatics, although the accuracy of this method of separating stresses is not high.

ACCURACY OF THE DETERMINATION

No direct check on the accuracy of the determination has been conducted for this series of tests. From previous experience with similar tests, it is estimated that the curves shown may be in error by 5 per cent of the maximum stresses.

Static equilibrium checks on the two lines perpendicular to the boundaries (drawn through the center) were conducted for $R/L = 0.91$, 0.79, and 0.70, assuming that σ_2 varies linearly from the interior boundary ($\sigma_2 = P$) to the exterior boundary ($\sigma_2 = 0$). This assumption is sufficiently accurate for thin cross sections since σ_2 is very small in comparison with σ_1. The total normal force across the perpendicular line checked within 3 per cent of the product of the internal pressure and the radius of hole for $R/L = 0.91$ and 0.79, and within 6 per cent for $R/L = 0.70$.

ACKNOWLEDGMENT

This research program was sponsored by the Armour Research

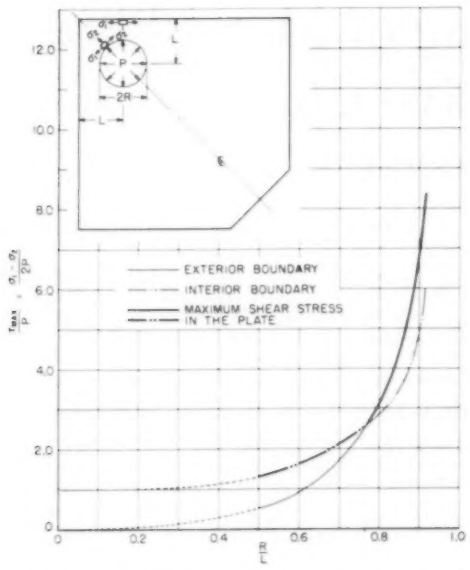

FIG. 10 HYDROSTATICALLY LOADED CIRCULAR HOLE IN THE NEIGHBORHOOD OF A CORNER
(Maximum shear stress in plate.)

Foundation. The authors are particularly indebted to Dr. G. A. Nothmann, Manager, Department of Mechanical Engineering Research, and Mr. K. W. Miller, Research Adviser for their support of this program. Credit is also given to Mr. W. F. Riley who made many valuable suggestions throughout the tests.

BIBLIOGRAPHY

1 "An Approximate Solution in the Problems of Elastic Plates With an Arbitrary External Form and a Circular Hole," by T. Sekiya, Proceedings of the 5th Japan National Congress for Applied Mechanics, 1955, pp. 95–98.

2 "Device for Applying Uniform Loading to Boundaries of Complicated Shape," by A. J. Durelli, R. L. Lake, and C. H. Tsao, Proceedings of the Society for Experimental Stress Analysis, vol. 11, no. 1, 1953, pp. 55–61.

3 "Stress Distribution in Square Plates With Hydrostatically Loaded Central Circular Holes," by A. J. Durelli and J. B. Barriage, JOURNAL OF APPLIED MECHANICS, Trans. ASME, vol. 77, 1955, pp. 539–544.

4 "Stress Distribution in Strips With Hydrostatically Loaded Central Circular Holes," by A. J. Durelli and W. R. Riley, Proceedings of the Mid-Western Conference on Solid Mechanics, October, 1955, pp. 81–93.

5 "Some Unorthodox Procedures in Photoelasticity," by A. J. Durelli and R. L. Lake, Proceedings of the Society for Experimental Stress Analysis, vol. 9, no. 1, 1951, pp. 97–122.

6 "Plane Stress and Plane Strain in Bipolar Co-Ordinates," by G. B. Jeffery, Philosophical Transactions of the Royal Society of London, series A, vol. 221, 1920, pp. 265–293.

Comments on the Cutting of Metal Plates With High Explosive Charges[1]

By W. E. DRUMMOND,[2] MENLO PARK, CALIF.

The problem of the cutting of metal plates with high explosive charges is analyzed by treating the metal hydrodynamically. The hydrodynamic problem is solved in the linearized approximation and it is assumed that the metal splits wherever the pressure becomes sufficiently negative. It is shown that such negative pressures occur where two rarefaction waves meet and the predicted location of these splits is in qualitative agreement with experiment.

Introduction

THIS paper is the result of some preliminary thinking on the problem of cutting metal plates with explosives and, as such, the conclusions reached should be regarded as tentative.

The problem[3] may be described as follows: A strip of explosive of height h, width w, and length l is placed on top of a large flat plate of metal of thickness y_0, Fig. 1. The explosive is detonated at B.

After the explosion, two cuts or cracks generally appear in the metal: a long cut down the middle and a cut across the end, Figs. 2(a) and 2(b).

The Method

In what follows we shall propose a hydrodynamic mechanism through which these phenomena can be understood qualitatively. In order to do this, however, we must first consider an idealized problem which can be more or less identified with the problem at hand. The approximate solution of this idealized problem will be seen to have certain properties which can be carried over to the solution of the real problem. It will be seen that these properties furnish a qualitative explanation of *most* of the observed phenomena.

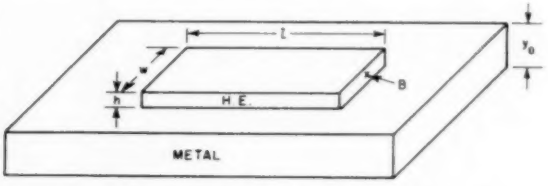

Fig. 1 Explosive metal configuration before detonation

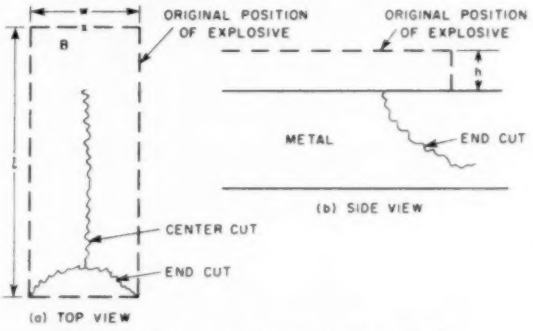

Fig. 2 Location of cuts in metal after explosion

The Idealized Problem

The first step in idealizing the problem is the following conjecture: The mechanism by which the end cut is formed is essentially the same as the mechanism by which the center cut is formed.

The basis for this conjecture can be seen by considering the position of the detonation front at successive instants of time. Viewed from the top, the line along which the detonation front meets the metal at successive instants of time is shown in Fig. 3.

An observer at P_1 at the edge of the explosive would see an oblique detonation front sweeping past. This is also just what an observer at P_2 would see, as long as P_2 is not on the center line of the explosive. To be sure, the angle the detonation front makes with the explosive edge is different in the two cases, but if the resulting flow is not a pathological function of this angle the two flows should be similar. We assume that this is the case; in fact, we assume that this is so even when the detonation front strikes the edge normally.

The question now arises: If these two mechanisms are the same, why do we not have two longitudinal cuts, one for each

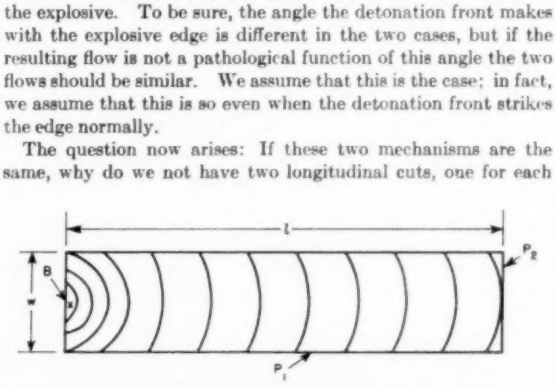

Fig. 3 Detonation front at successive instants of time

---

[1] This work was supported by the U. S. Army Corps of Engineers, Research and Development Laboratories, under Contract No. DA-44-009-ENG-2512.

[2] Physicist, Poulter Laboratories of Stanford Research Institute.

[3] "Behavior of Metals Under Impulsive Loads," by J. S. Rinehart and John Pearson, American Society for Metals, 1954, chapter 9.

"The Deformation of an Explosively Loaded Aluminum Single Crystal," by J. S. Rinehart, NAVORD Report 3504, June 6, 1955.

"Some Experimental Indications of the Stresses Produced in a Body by an Exploding Charge," by J. S. Rinehart, *Journal of Applied Physics*, vol. 22, no. 9, 1951, pp. 1178–1181.

"The Propagation of Shock Waves in Steel and Lead," by D. C. Pack, W. M. Evans, and H. J. James, Proceedings of the Physical Society, vol. 60, 1948, p. 1.

"Entropic Equations of State and Their Application to Shock Wave Phenomena in Solids," by G. E. Duvall and B. J. Zwolinski, *Journal of the Acoustical Society of America*, vol. 27, no. 6, 1955, pp. 1054–1058.

Contributed by the Applied Mechanics Division and presented at the Annual Meeting, New York, N. Y., December 1-6, 1957, of THE AMERICAN SOCIETY OF MECHANICAL ENGINEERS.

Discussion of this paper should be addressed to the Secretary, ASME, 29 West 39th Street, New York, N. Y., and will be accepted until July 10, 1958, for publication at a later date. Discussion received after the closing date will be returned.

NOTE: Statements and opinions advanced in papers are to be understood as individual expressions of their authors and not those of the Society. Manuscript received by ASME Applied Mechanics Division, February 6, 1957. Paper No. 57—A-89.

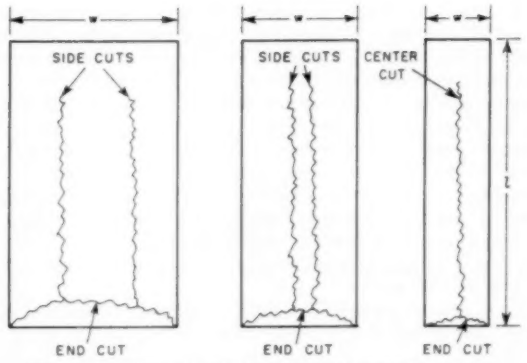

Fig. 4 Location of cuts for different explosive widths

side, rather than one cut down the center? The answer to this is that if the explosive is wide enough we do get two cuts experimentally—one on each side. As the explosive is reduced in width, these two cuts merge into the single center cut that is usually observed, Fig. 4.

Thus, if we believe this conjecture, the problem is reduced to that of finding a single mechanism.

Our next step is to idealize the problem of the end cut to such a point that we can reasonably hope to solve it. We do this by assuming that the explosive is infinitely wide and the distance from B to the other end of the explosive is infinitely long.

This reduces the problem to two space dimensions, and amounts to the earlier assumption that the flow resulting from the detonation wave reaching the edge of the explosive is not a strong function of the angle the detonation front makes with the boundary. Thus we consider the case of normal incidence and regard it as typical.

The idealized problem is pictured from the side in Fig. 5 at the time t_0 when the detonation front reaches the explosive boundary.

As pictured in Fig. 5, the problem is still too complicated to solve exactly. Thus we make one further approximation: We assume that the problem can be treated by the "linearized approximation."[4]

The simplifications introduced by the linearized theory are as follows:

1 The shock front in the metal is straight and carries a constant pressure at $t = t_0$.

2 The principle of superposition holds.

3 The flow is made up of two parts, one which is constant along the lines $y = \alpha x + B$ (called $C+$ characteristics) and one which is constant along the lines $y = -\alpha x + B$ (called $C-$ characteristics) where α is determined by the Mach number of the flow in front of the shock front.

[4] "Supersonic Flow and Shock Waves," by R. Courant and K. O. Friedrichs, Interscience Publishers, Inc., New York, N. Y., 1948, pp. 357–364.

"Linearized Theory of Steady High-Speed Flow," by G. N. Ward, Cambridge University Press, Cambridge, England, 1955.

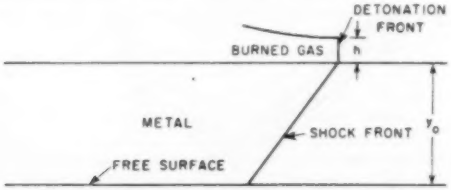

Fig. 5 Shock configuration in metal at $t = t_0$

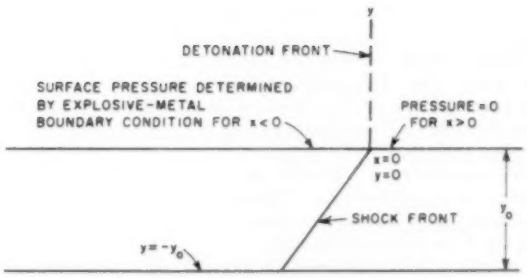

Fig. 6 Boundary conditions in metal at $t = t_0$

Along the metal surfaces $y = 0$ for $x > 0$, and $y = -y_0$ for all x, we have atmospheric pressure which for practical purposes we can set equal to zero. Thus at $t = t_0$ the situation is as follows (see Fig. 6).

The pressure and particle velocities behind the shock front are given by the sum of two functions, one of which is constant along the $C+$ characteristics and the other of which is constant along the $C-$ characteristics. The pressure along $y = 0$ for $x < 0$ is that value determined by the explosive-metal boundary conditions. We regard these values as initial conditions for the flow for $t > t_0$. We also have the boundary condition that the pressure is zero for $x > 0$ along $y = 0$, and along $y = -y_0$ for all x. Mathematically speaking, these conditions uniquely determine the flow for $t > 0$.

We first consider the boundary condition along $y = -y_0$. On the basis of the linearized theory, the effect of this free boundary is to reflect the shock front as a tension wave, with the wave front of the tension wave making the same angle with the normal to the free surface as the shock front makes with the free surface; i.e., the shock front is a $C+$ characteristic while the tension front is a $C-$ characteristic.[5] Thus as the shock sweeps along it is followed by a tension wave starting from the free surface,[6] Fig. 7.

Along the tension front the negative pressure due to the reflection is constant and equals $-p_0$ where p_0 is the pressure at the shock front. Thus at a point P along the tension front, the pressure is composed of two parts: (i) The pressure at the point on the explosive-metal interface which is connected to P by a $C+$ characteristic, p_i, and (ii) $-p_0$. Since p_0 is greater than all other pressures, the net pressure along the tension front is negative. Further, as we progress along the tension front away from the

[5] In the linearized theory we can have both compression and rarefaction shocks.

[6] "Deformation and Fractures Produced by Intense Stress Pulses in Steel," by W. M. Evans and Sir Geoffrey I. Taylor, *Research*, vol. 5, 1952, pp. 502–509.

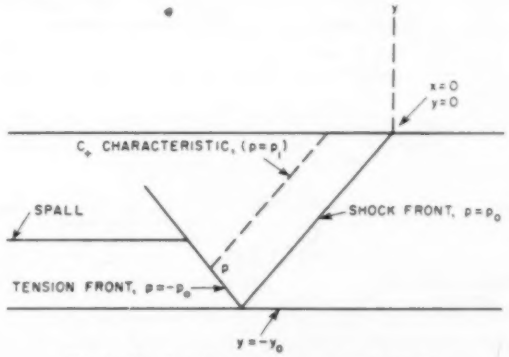

Fig. 7 Shock and reflected wave configuration

shock front, this tension increases monotonically. It may then happen that at some point along this line the tension exceeds the breaking strength of the metal. In this case the metal splits at this point. Since this point is sweeping along in the x-direction, the point split becomes a line at a constant distance from the bottom. This accounts for the long flat spall observed along the bottom of the metal.

We assume, for the present, that the tension never gets high enough for a spall to occur. This simplifies the discussion of the end split and, as we shall see later, the presence of the spall does not affect the end split materially.

In order to see the effect of the boundary condition along $y = 0$, $x > 0$, we construct a "pseudo-problem" which is mathematically equivalent to our idealized problem. This problem is pictured for $t = t_0$ in Fig. 8. The initial conditions for the lower half of the metal, i.e., for $y < 0$, are identical with the initial conditions for our idealized problem. The initial conditions in the upper half, i.e., for $y > 0$, are the negative of the initial conditions in the lower half: i.e., $p(x, y) = -p(x, -y)$. In order that these boundary conditions can be fulfilled, the metal is imagined to be split down the x-axis for $x < 0$.

From the initial condition we see that for $t > 0$ the pressure along $y = 0$ for $x > 0$ will always be zero. Thus as far as the lower half is concerned, the problem has the same initial conditions and boundary conditions as the idealized problem, and it follows that the solution for the two problems for $y < 0$ is identical. The advantage of the pseudo-problem is that the effect of the flow in the upper half on the flow in the lower half can be pictured in a familiar way and this is identical with the effect of the boundary condition along $y = 0$ for the real problem.

At a time $t > t_0$, the effect of the upper half is felt throughout a circle of radius $c(t - t_0)$ when c is the hydrodynamic sound velocity in the metal, Fig. 9.

We are now in a position to understand the end split. This is done by considering the flow at successive instants of time $t > t_0$. This is shown in Fig. 10(a, b, c, d).

At the point where the tension wave from the bottom and the rarefaction front from C first meet there is a local tension maximum. If this tension exceeds the breaking strength, the metal splits at that point. Note that this split starts in the interior of the metal and proceeds both ways. When the metal splits, the pressure goes to zero and hence, to satisfy this boundary condition at the breaking point, we must hypothesize a point source of negative pressure equal in magnitude to positive pressure at the front of the break. This negative pressure propagates with sound velocity. However, as shown in Fig. 10, the point of collision between R and T moves along R with a velocity larger than c and hence the metal breaks along the locus of intersection of R and T.[7] This locus is found by superimposing the different parts of Fig. 10 (see Fig. 11).

This is our picture of the basic processes involved in the end split. In practice there is always a long flat spall along the bot-

[7] This mechanism was first suggested by G. E. Duvall (private communication).

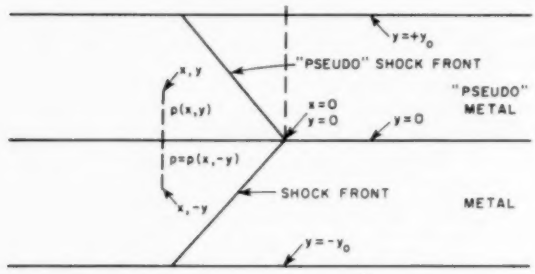

Fig. 8 Initial conditions for the "pseudo problem"

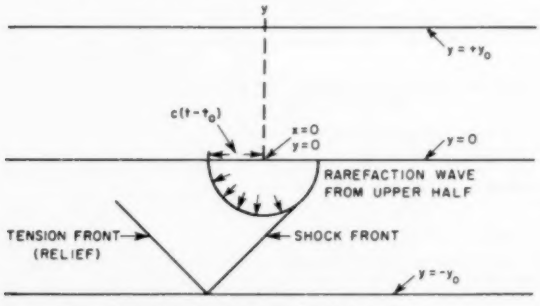

Fig. 9 Rarefaction configuration for $t > t_0$

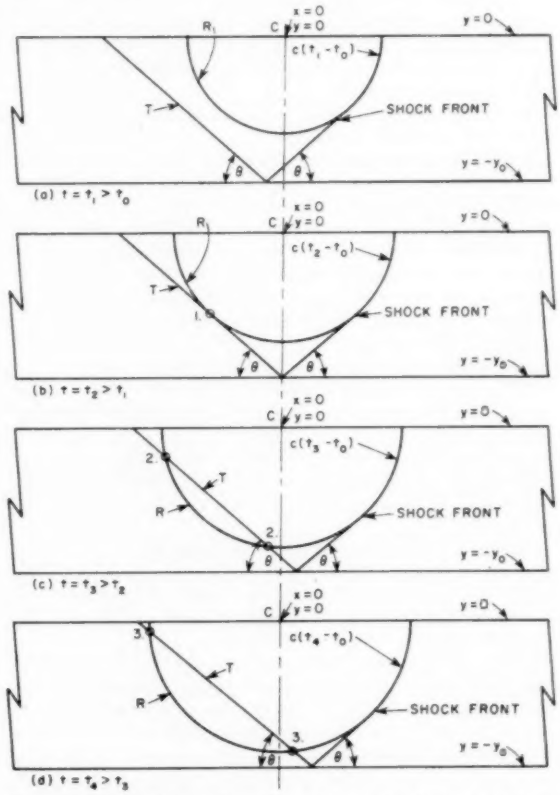

Fig. 10 Rarefaction configuration at successive instants of time

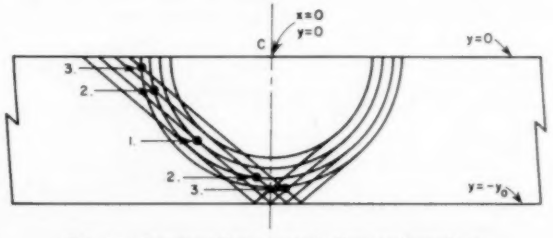

Fig. 11 Superposition of rarefaction configurations

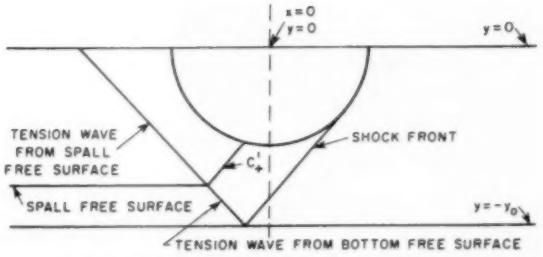

Fig. 12 Rarefaction configuration with bottom spall

tom of the plate. This, however, has only a small effect on the end split. As shown in Fig. 12, the effect of the spall is to introduce a new free surface a short distance from the bottom. The effect of this surface is to "reflect" not the entire shock wave but only that part of it behind the $C+$ characteristic $C'+$. If the pressure along $C'+$ is p_1 then the reflected wave will have a minimum pressure $-p_1$. Thus the net effect of the spall is to reduce the tension wave strength from $-p_0$ to $-p_1$. This in turn does not affect the mechanism of the end split.

If we now compare the observed end split with the predicted end split, we see a real similarity. Most striking is the qualitative similarity in curvature of the split. This curvature, however, should not be compared quantitatively since the detailed shape of the split is lost in going to the linearized approximation.

Nevertheless, we can make a semiquantitative comparison and experiment by noting the dependence of the position of the cut on the thickness of the metal, Fig. 13.

We observe that

$$r = y_0 \cos \theta$$

$$\sin \theta = \frac{U}{D}$$

where

U = shock velocity
D = detonation velocity

Thus we find

$$r = y_0 \left(1 - \frac{U^2}{D^2}\right)^{1/2}$$

Experimental values of r versus y_0 are shown in Fig. 14. The slope of r_0 versus y_0 is in the range of 0.7 to 0.8, depending on the estimates of U and D. Since the slope of the experimental curve is 0.75, we have semiquantitative agreement.

It should be emphasized that a great deal of physics is lost in going to the linearized approximation. For example, the phenomenon of attenuation is ignored and hence the dependence of the end split on explosive thickness is lost, as well as the detailed curvature of the split. Moreover, the "reflection" from the bottom and the effect of the bottom spall are oversimplified in the neighborhood of the spall by the linearized theory.

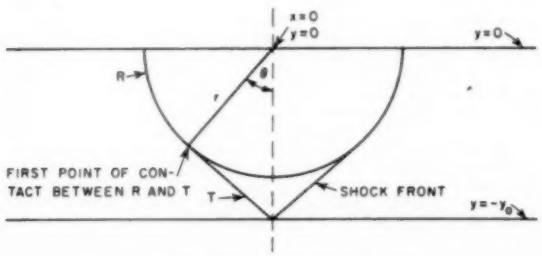

Fig. 13 First intersection of rarefaction waves

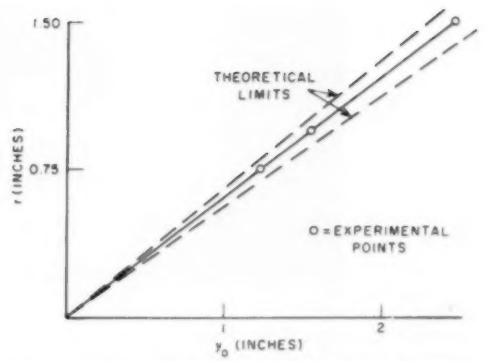

Fig. 14 Location of end split as a function of plate thickness

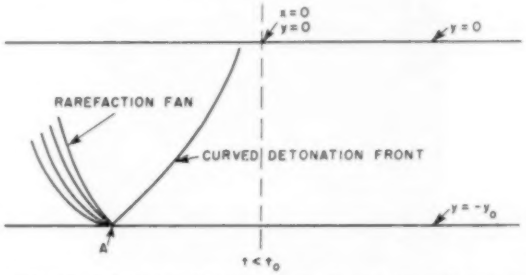

Fig. 15 Effect of nonlinearity on shock and reflected waves

Nevertheless, we can make qualitative estimates of the effect of the nonlinearity. Actually, for $t < t_0$ the shock front and the "reflected" tension wave are curved. Further, the pressure decreases continuously across the tension wave rather than suddenly; i.e., it is a rarefaction fan, Fig. 15. Moreover, the rarefaction wave starting at A will have a continuously varying pressure rather than a steep front.

The curvature of the shock front and of the rarefaction depends on the explosive thickness, the curvature increasing as the thickness is decreased. Qualitatively this means that the curvature of the end split increases as the explosive thickness decreases.

Conclusion

The general feeling at this writing is that the postulated mechanism gives a satisfactory description of the observed phenomena, explaining most of the observed effects. It should be mentioned that one effect still eludes explanation. It will be noted, Fig. 16, that the end split intersects the bottom spall and continues to meet the bottom free surface asymptotically; in the

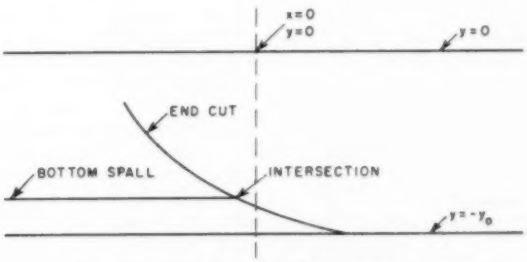

Fig. 16 Intersection of end cut and bottom spall

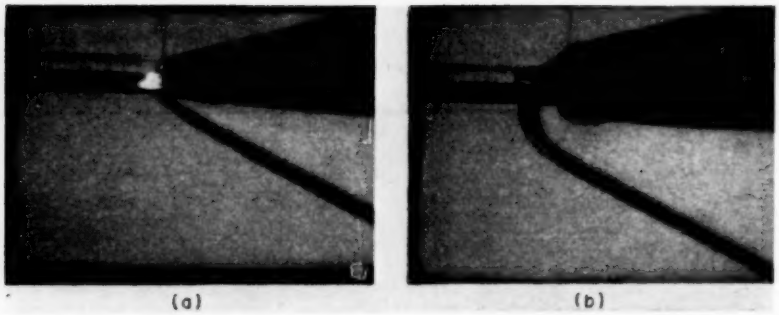

Fig. 17 (*a*) **Shock front when it reaches end of explosive. Note that this shock is moving to the left.** (*b*) **Shock front at a later time showing curvature introduced by rarefaction wave.**

Fig. 18 View showing both shock front and reflected rarefaction from bottom. This shock is moving to the right.

process the flat bottom spall is suppressed beyond the intersection with the end split. Experimentally, just the reverse is observed. The bottom spall continues, and the end split is suppressed beyond the intersection with the bottom spall. This contradiction, however, is not too surprising since it is in just this region that the nonlinear effect is important.

To see if the linearized picture of the propagation of the shock fronts bears some relation to reality, the same experiment was performed using lucite instead of metal. Since the lucite is transparent, the trajectories of the shock fronts can be followed with a high-speed framing camera. A sequence of such pictures is shown in Figs. 17 and 18. These photographs seem to bear out the general arguments given in the foregoing.

As a general rule, in problems of this type treated hydrodynamically, some sort of similarity theorem obtains. In particular, for explosive-induced shocks in metals, the following similarity theorem holds: If two initial explosive-metal arrangements are similar, i.e., the dimensions of explosive, metal, gaps, and so on, of one are larger than those of the other by a constant factor, then the resultant splits, cracks, spalls, etc., will be similar in the same sense.

Acknowledgments

The author wishes to thank Dr. George E. Duvall for discussions of the theory, and especially Mr. Sidney A. Moses who first noted this effect and who did all the experimental work.

A New Method to "Lock-in" Elastic Effects for Experimental Stress Analysis

By J. W. DALLY,[1] A. J. DURELLI,[2] AND W. F. RILEY,[3] CHICAGO, ILL.

A new method is described for "locking-in" an optical interference pattern and a mechanical distortion. The transparent model is cast from a modified epoxy resin with an embedded rubber-thread grid. The model is permitted partially to cure before it is loaded, then held under load while the plastic continues to cure. Upon removal of the load an isochromatic fringe pattern remains which is proportional to the elastic distribution of the maximum shearing stress. In addition, the permanently distorted grid has deformations which are proportional to the elastic distribution of strains. The method is applied to a disk under diametrical compression and a disk under gravitational loading. A comparison of experimental and theoretical results for these two cases shows, in general, good agreement. Most of the discrepancies between experimental and theoretical results are due to the large deformations in the neighborhood of the points of load application. An application of the method to the solution of a three-dimensional problem, namely, the gravitational stress distribution in a buttress-type dam, is discussed briefly.

Introduction

THE solution of a number of problems using methods of experimental stress analysis requires the locking-in of optical or mechanical effects produced by the stresses. The concept of locked-in fringes and the slicing of a model are the basis of the most commonly employed three-dimensional photoelasticity method. The locking-in of the optical and also of the mechanical effects can be employed advantageously in the solution of two-dimensional problems when the loading is of a form which interferes with the direct observation of the model. The problem of determining stresses in rotating disks is an example of this application. Other body-force problems fall into this class when use is made of a centrifuge to amplify the body forces, since the motion of the centrifuge makes the use of conventional photoelastic techniques difficult. Once the model distortions have been locked-in, the loading can be removed and the stresses determined provided the locked-in effects are representative of the elastic distribution of stresses present in the body at the time it was under load.

The most commonly used method of locking-in optical effects is the so-called "freezing" method. This method requires that the model be subjected to a heating cycle for an extended period of time while loaded. When the heating cycle is completed and the model has been returned to room temperature the loading is removed and the fringes are locked in the model. Slices are then cut from the model and observed. The fringe pattern is not disturbed if the machining operations are performed carefully.

An alternative to the freezing method was developed by one of the authors some years ago (1–4).[4] This alternative method was called the "creeping" method since it was based on the creep (or rather the retarded elasticity) properties of certain plastics such as the phenolformaldehydes. In the use of this method the distortions and the photoelastic effects are not locked in the model permanently, for after the load is removed they slowly creep out. However, the effects remain for a sufficient period of time to permit slicing and examination if the model geometry is relatively simple and only a few slices are needed.

A third method is presented in this paper. It is called the "curing" method since the locking-in of the model optical fringes and mechanical distortions is apparently produced by the curing of a young or semicured plastic under load. The effects are permanently locked in the model. As is the case in the creeping method, the curing method does not require any heating of the model for the plastic used is of the type which cures at room temperature. In the curing method as in the other two methods, the optical and mechanical effects represent the elastic stress distribution which was present in the model when it was under load.

The model material

The plastic material used in the development of this method was a clear epoxy resin manufactured by Ciba Company, Inc., Kimberton, Pa., known commercially as Araldite 502. The properties of this resin, particularly its modulus of elasticity can be varied over a very wide range by mixing it with a compatible plasticizer such as dibutyl phthalate. The composition used in this study was obtained by mixing 72 per cent resin with 20 per cent dibutyl phthalate and 8 per cent araldite hardener HN951. All of the constituents are liquid, and the manufacture of the plastic is accomplished simply by mixing the proper proportions of each and pouring the resultant mixture into a suitable mold.

In order to obtain a plastic in the semicured condition, the curing must be controlled quite carefully during the first few hours to obtain the desired properties. This is due to the fact that the reaction between the resin and the hardener is exothermic, and some provision must be made to carry away the heat which the reaction produces. This can be accomplished by using aluminum molds immersed in a cooling water bath. If smooth surfaces are desired, the aluminum mold can be lined with a thin film of cellulose acetate. The resin will not bond to this film and the model can be stripped from the mold with relative ease. If the cellulose-acetate layer is not used, then it is necessary to employ a release agent such as silicone grease to prevent the model from bonding to the mold. A plastic with the consistency of a hard-rubber eraser is obtained after curing for 12–16 hr in a water bath at 70 F.

The material can be cast to final form since it does not seem to have the layer of skin stresses which occurs in castings made from the commonly used plastics. This fact is advantageous when several models are needed (i.e., two and three-model

[1] Research Engineer, Stress Analysis Section, Armour Research Foundation of Illinois Institute of Technology. Assoc. Mem. ASME.

[2] Professor, Illinois Institute of Technology, and Supervisor, Armour Research Foundation. Assoc. Mem. ASME.

[3] Associate Research Engineer, Stress Analysis Section, Armour Research Foundation of Illinois Institute of Technology.

Contributed by the Applied Mechanics Division and presented at the Annual Meeting, New York, N. Y., December 1–6, 1957, of THE AMERICAN SOCIETY OF MECHANICAL ENGINEERS.

Discussion of this paper should be addressed to the Secretary, ASME, 29 West 39th Street, New York, N. Y., and will be accepted until July 10, 1958, for publication at a later date. Discussion received after the closing date will be returned.

NOTE: Statements and opinions advanced in papers are to be understood as individual expressions of their authors and not those of the Society. Manuscript received by ASME Applied Mechanics Division, March 15, 1957. Paper No. 57—A-71.

[4] Numbers in parentheses refer to the Bibliography at the end of the paper.

methods) or when the mold is easier to machine than the model (i.e., the case where the model contains a number of reentrant corners). Some preliminary tests also have indicated that a material of this type can be cast about rigid inclusions without producing excessive residual stresses in the neighborhood of the inclusion.

Material properties

To determine the optical and mechanical properties of the material, a circular disk under a diametrical compressive load was studied. The disk was machined from a sheet of the epoxy resin manufactured in the manner previously described. A rubber-thread grid network was embedded in the sheet of the material (5) to permit the simultaneous determination of the strains and of the isochromatics. The model was held under constant load for a period of 4 hr. During this period, the material deformed both elastically and permanently and became more rigid.

Photographic records were obtained of the isochromatic fringe pattern and of the grid before loading, and at various times after loading and after unloading of the model. In Fig. 1 a plot of fringe order versus position across the horizontal diameter of the disk shows that the isochromatic pattern changes with time; however, it is important to note that the pattern always represents the elastic distribution of stress in the disk while loaded. The three curves shown were obtained from photographs taken immediately after loading, 4 hr after loading (just prior to unloading), and 16 hr after unloading. Other photographs taken 20 hr after unloading and 64 hr after unloading showed no variation in the pattern from that obtained 16 hr after unloading. It was concluded therefore that the pattern obtained 16 hr after unloading is permanently cured in the model.

The difference between curves 1 and 2 is due to a combination of effects: (a) The creep, which is very pronounced, increases the fringe order at a particular point as a function of time. (*b*) The material very likely changes its chemical, mechanical, and optical properties as the curing progresses.

When the model is unloaded, deformations begin to creep out but the material continues to cure, and as it becomes more rigid it resists the relaxing effect. At some period of time after unloading, an equilibrium point is reached and the remaining distortions are locked in the material. For this particular composition of plastic this time period was less than 16 hr and the remaining fringe pattern is represented in curve 3. One of the primary factors which influences the position of curve 3 is the period of time the model is held under load. If, for instance, it were held under load until the curing of the plastic was complete, curve 3 would be very near curve 2. On the other hand, if the model was loaded for a short period of time, the position of curve 3 would be much lower than curve 1.

A plot showing the Cartesian components of strain along the horizontal diameter of the disk is illustrated in Fig. 2. This graph indicates that the distribution of ϵ_x and ϵ_y changes with time in a manner very similar to the fringe order. The strains due to creep are given by the difference between curves 1 and 2. When the load is relieved the strain creeps out until an equilibrium condition at curve 3 is reached. It should be noted that in Fig. 2 curve 3 indicates strains greater in absolute value than curve 1, whereas in Fig. 1 curve 3 indicates a fringe order less than curve 1. An explanation of this difference can be made by an examination of the strain-optic relation

$$n_{(t)} = \frac{E(t)}{2F(t)(1 + \nu(t))} [\epsilon_1(t) - \epsilon_2(t)]$$

where

$n_{(t)}$ = fringe order
$E(t)$ = modulus of elasticity
$F(t)$ = model fringe value (shear), $f(t)$ material fringe value (shear)
$\nu(t)$ = Poisson's ratio
$\epsilon_1(t), \epsilon_2(t)$ = principal strains
(t) = indicates quantities which are a function of time

Since E, F, and ν are all functions of time it is evident that if

$$\frac{E(t_1)}{2F(t_1)[1 + \nu(t_1)]} > \frac{E(t_3)}{2F(t_3)[1 + \nu(t_3)]}$$

the relative positions of curves 1 and 3 would be as shown in Fig. 2.

The material properties $E(t)$, $\nu(t)$, $f(t)$ were determined at the three following times:

t_1: immediately after loading
t_2: 4 hr after loading (just prior to unloading)
t_3: 16 hr after unloading (i.e., 20 hr after the load was applied)

The determination was made by computing the theoretical stresses at the $x/D = 0.40$ position on the horizontal axis of the disk in diametrical compression. The position $x/D = 0.40$ was selected rather than the position $x/D = 0.50$ because of the influence of the flattening of the disk at the points of load application on the stress distribution at $x/D = 0.50$. At points farther removed from the center than $x/D = 0.40$ the strains become smaller and are measured with less precision. The theoretical stresses were then equated to the experimentally determined strains through the well-known relations

$$\sigma_1 = \frac{E}{1 - \nu^2} [\epsilon_1 + \nu\epsilon_2]$$

$$\sigma_2 = \frac{E}{1 - \nu^2} [\epsilon_2 + \nu\epsilon_1]$$

These two equations were solved simultaneously for E and ν. The material fringe value f was determined at the same point by substitution of the theoretically determined stresses and the experimentally determined fringe order in the following equation

$$\sigma_1 - \sigma_2 = 2n \frac{f}{h}$$

where h is the thickness of the model.

The properties for the three particular times considered are shown in Table 1.

The elastic constants at t_3 are really fictitious quantities used to relate the stress when the model was under load to the strain left after the loading has been removed. The elastic constants at t_1 are the conventional instantaneous elastic constants. The elastic constants at t_2 have been computed using the total of both the elastic and nonelastic deformations accumulated during this period of time. Attention should be called to the fact that the strain-fringe value remained constant while the model was under load.

Verification of elastic interpretation of material effects

Using the values of E, ν, and f shown in Table 1 and grid measurements, the values of $\sigma_x - \sigma_y = \sigma_1 - \sigma_2$, σ_x, and σ_y were computed at 9 positions along the horizontal diameter of the disk. The points obtained from the test at t_1, t_2, and t_3 are plotted together with the theoretical distribution in Fig. 3. In all instances the experimental determinations checked well against the theoretical distributions. The maximum difference takes place in the central region of the disk where the influence of the flatten-

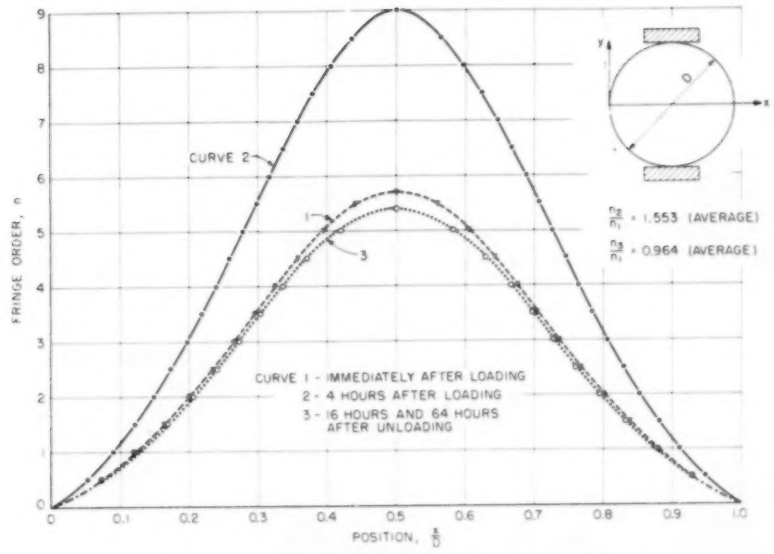

Fig. 1 Fringe order along horizontal diameter of disk with time as a parameter

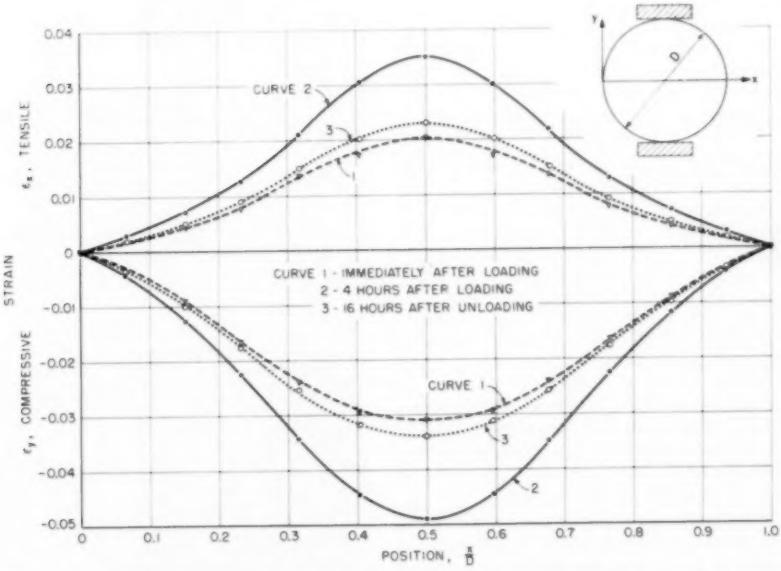

Fig. 2 Cartesian components of strain obtained from grid measurements along horizontal diameter of disk with time as a parameter

Table 1 Material properties

Time	Poisson's ratio, ν	Modulus of elasticity, E, psi	Material fringe value, f (shear), psi-in/fringe	Material fringe value, f (tension), psi-in/fringe	Fig. of merit, E/f (tension), fringe/in.	Strain fringe value $\left[\frac{1+\nu}{E}\right] f$ (tens)
t_1	0.366	993	1.22	2.44	406	0.00335
t_2	0.466	675	0.78	1.56	432	0.00338
t_3	0.405	926	1.28	2.56	362	0.00388

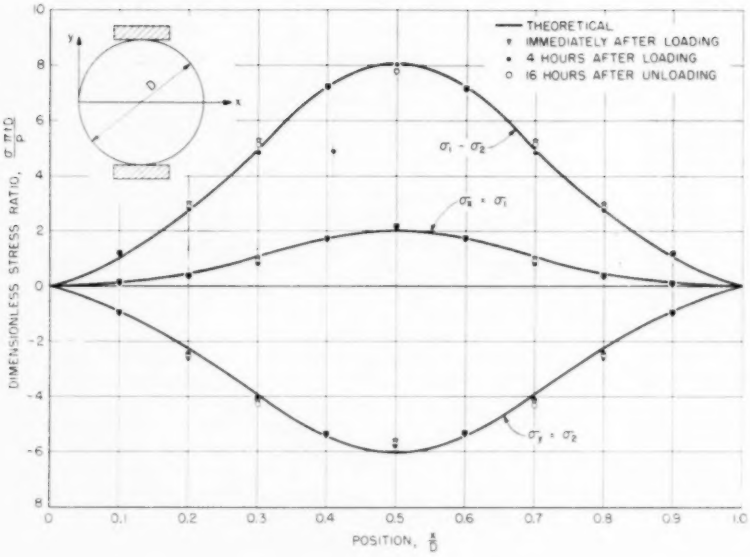

Fig. 3 Cartesian components of stress obtained from grid measurements along horizontal diameter of disk

ing of the boundary at point of load application is the greatest.

Isochromatic fringe patterns at a number of different times during the curing are shown in Fig. 4. It is observed that the time edge effect is not appreciable even on the saw-cut model which was photographed approximately 24 hr after machining the boundaries. The saw cut through about one half of the model shows that the fringe pattern is not disturbed by the machining process.

A comparison between curve 2 for fringes in Fig. 1 and a curve obtained using the theoretical solution of shear stresses in a disk under diametrical compressions shows a discrepancy between the two curves of less than 1 per cent of the maximum stress.

Records of the grid distortions at the four times under consideration are shown in Fig. 5. It is noted that changes in the grid network as a function of time in the region of the load application are noticeable to the naked eye.

Applications to body-force problems

The method of locking-in an optical pattern has an important application in the determination of stresses produced by gravitational loadings. This is especially true when a centrifuge is used to have a force field of sufficient intensity to produce a model response large enough to be measured with precision.

The recording of the stresses produced in the model by the centrifuge is a difficult problem. Direct visual observation is impossible unless the model is two-dimensional and a stroboscopic-type polariscope is employed. The conventional freezing technique is difficult to employ for the method requires a controlled heating cycle. If an oven is built about the entire centrifuge, the size of the oven is extremely large for a 6-in. model requires a 10-ft-diam centrifuge and a corresponding 10-ft-diam oven. If ovens are mounted on the centrifuge arms, their weight adds appreciably to the stresses at the hub of the centrifuge itself. In addition, the heating power and the temperature control power must be transmitted to the ovens through slip rings. Finally, the centrifuge would have to operate over an extended period of time The application of the creeping method for locking-in the stress pattern is not practical either because the force field required to produce sufficient model response is very high.

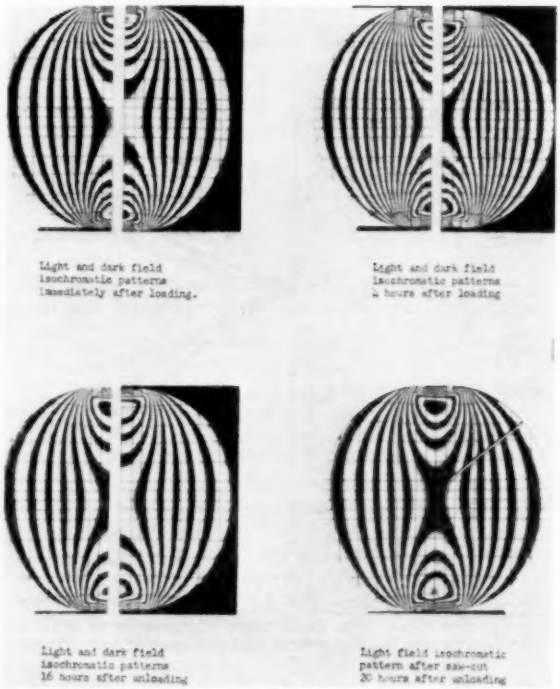

Fig. 4 Isochromatic patterns of disk at different times during curing period

The curing method provides a means of obtaining gravitational locked-in optical patterns more readily than the other methods for it requires no heating cycle and the material used is very sensitive. As an example, the locked-in fringe pattern for a heavy disk is shown in Fig. 6.

A theoretical fringe distribution was computed using the results of Mitchell (6) and compared with the experimental fringe dis-

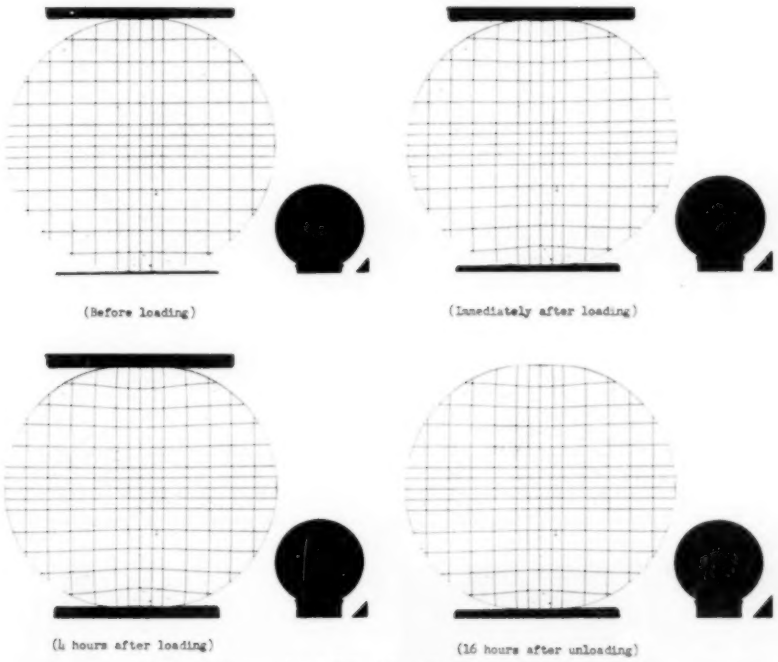

Fig. 5 Grid records of disk at four times during curing period

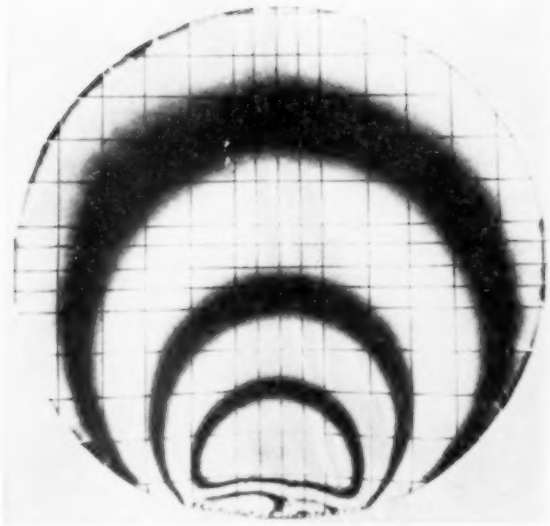

Fig. 6 Isochromatics (locked-in) associated with a heavy disk

tribution, Fig. 7. The comparison shows excellent agreement (using a fringe value $f = 3.52$) over the top half of the disk. The results diverge significantly, however, near the bottom of the disk. This difference is due to the large deformations at the bottom of the disk which permitted the load reaction to take place over an area at the base rather than on a line of contact.

The method has been employed in the solution of the three-dimensional stresses produced in a buttress-type dam under gravitational loading. This problem will not be dealt with at length in this section as it will be the subject of a forthcoming paper. However, it can be stated that results obtained using the new method were consistent and checked well with equilibrium relations. The three-dimensional model used in this investigation is shown in Fig. 8. The model was cast about a rubber-thread grid which was used to determine the stress distribution in the central plane of the model. A locked-in fringe pattern obtained by rotating the dam model in a 10-ft-diam centrifuge at about 300 rpm for 3 hr is shown in Fig. 9.

A limitation of the grid-distortion part of the method consists in the fact that the two photographs of the grid (before loading and after loading) have to be taken with the model at precisely the same position. If one of the photographs of the model does not have the same inclination in respect to the camera as the other one, a new distortion of the image takes place which confuses the distortion produced by the strain. No interpretable results could be obtained from the grid measurements of the heavy disk of Fig. 6 and it is believed that this is due to some warping of the plane of the disk, which took place during the testing in the centrifuge. This warping, however, did not affect the photoelastic results. It is believed that in general the heavy disk is a practical method of calibration for centrifuge tests.

Conclusions

The results presented in the preceding two sections indicate that the locked-in optical patterns represent an elastic distribution of the maximum shear stresses in the model and that the locked-in grid distortion represents the elastic distribution of strains. The maximum deviation of the experimental stress distribution from the theoretical occurs in regions where excessive deformations have influenced the results. This appears to be an inevitable consequence of the relatively low figure of merit of the material. This reported figure of merit however may not necessarily be associated with the method or even the material, for if the influencing parameters are varied (i.e., period of cure before

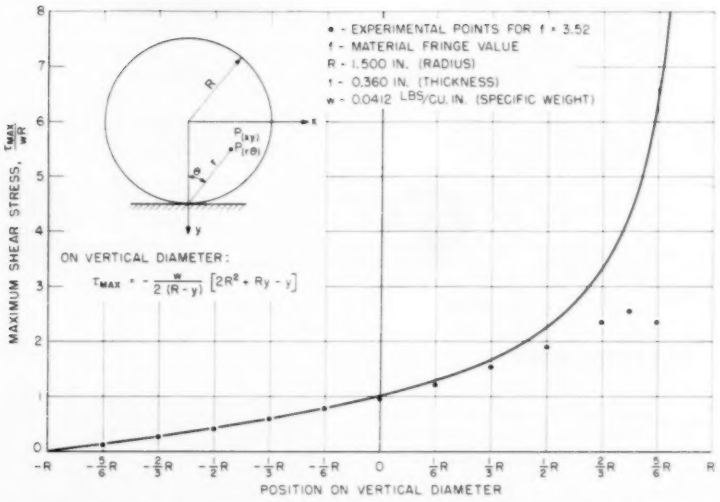

Fig. 7 Maximum shear-stress distribution in a heavy disk; theoretical and experimental

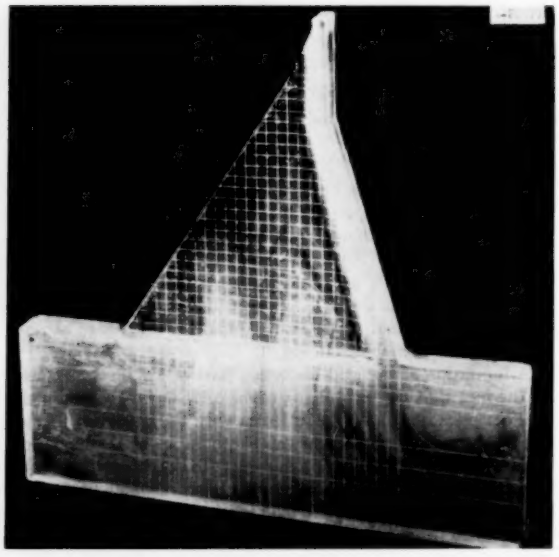

Fig. 8 Three-dimensional transparent model of a buttress-type dam with an embedded grid

Fig. 9 Locked-in fringe pattern associated with a gravitational loading of dam model. View was taken before slicing. Model was immerged in a tank with a liquid of approximately the same index of refraction as index of model material.

loading, duration of loading, percentage of plasticizer in composition, type of base epoxy, and so on), a higher figure of merit may be obtained unless the tests conducted herein were performed coincidentally at optimum conditions.

As reported, the method appears well suited for application to the solution of gravitational problems. It also seems well suited for the solution of problems in which a change in temperature changes the boundary conditions. As an example of this type of problem, consider the region defined in Fig. 10 as B which is bound by two rigid cylinders labeled A. Suppose that this system is subjected to the force P and a study is desired of the complicated stress distribution that is set up in region B. If the so-called freezing method is used, the material has to be heated and, unless both A and B have the same thermal coefficient of expansion, an extraneous thermal stress is imposed on B. These considerations apply also to inclusion problems.

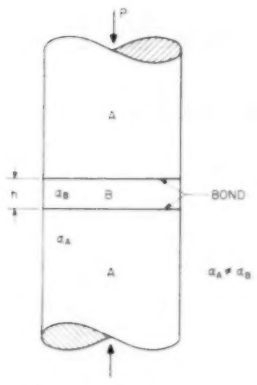

A - RIGID CONSTRAINING CYLINDERS
B - REGION OF INTEREST
P - AXIAL COMPRESSIVE LOADS
h - THICKNESS OF MATERIAL BETWEEN RIGID CYLINDERS
α - THERMAL COEFFICIENT OF EXPANSION

Fig. 10 Example of a problem in which changes in temperature influence boundary conditions

It should be pointed out that the newly developed material has a lower Poisson ratio than most commonly used three-dimensional photoelasticity materials. Therefore it may be possible, by means of grid analysis, to solve a three-dimensional problem completely without resorting to numerical integration.

Bibliography

1 "Some Unorthodox Procedures in Photoelasticity," by A. J. Durelli and R. L. Lake, Proceedings of the Society for Experimental Stress Analysis, vol. 9, no. 1, 1951, pp. 97–122.

2 "Simplified Procedures in Photoelasticity," by A. J. Durelli and R. L. Lake, *Machine Design*, vol. 21, no. 11, 1949, pp. 137–141.

3 "Three-Dimensional Photoelasticity," by A. J. Durelli and R. L. Lake, *Machine Design*, vol. 22, no. 12, 1950, pp. 122–125.

4 "Stresses in Rotating Parts," by R. L. Lake and A. J. Durelli, *Machine Design*, vol. 25, no. 7, 1953, pp. 128–131.

5 "Developments in the Grid Method of Experimental Stress Analysis," by A. J. Durelli and W. F. Riley, Proceedings of the Society for Experimental Stress Analysis, vol. 14, no. 2, 1957, pp. 91–100.

6 "A Treatise on the Mathematical Theory of Elasticity," by A. E. H. Love, Cambridge University Press, New York, N. Y., fourth edition, 1927, p. 219.

Torques on a Satellite Vehicle From Internal Moving Parts[1]

By R. E. ROBERSON,[2] DOWNEY, CALIF.

Many of the torques produced by the motion of parts within a body are negligibly small in most engineering applications. However, if the body is a satellite vehicle these small torques can be significant, even to playing a dominant role in the excitation of satellite attitude motions. This paper derives a complete expression for the attitude perturbation torque from this source, interpreting each of its terms. The atittude reference co-ordinate system is discussed. The nature of the torque is found for three simple cases.

Nomenclature

$\bar{a}_i$ = apparent acceleration of $\bar{\rho}_i$ as seen by an observer in $\mathfrak{B}_0$

$\bar{A}$ = apparent acceleration of $\bar{R}$ as seen by an observer in $\mathfrak{B}_0$

$\bar{E}$ = unit dyadic

$\bar{e}_X, \bar{e}_Y, \bar{e}_Z$ = unit vector in directions of XYZ-axes, respectively

$\bar{e}_p$ = unit vector along axis of rotation of wheel in Example 3

$\bar{e}_\epsilon$ = unit vector in direction of vibrational motion in Example 2

$\bar{e}_\xi, \bar{e}_\eta$ = unit vectors completing right-hand orthogonal set with $\bar{e}_p$ fixed in $\mathfrak{B}_0$

$\bar{H}$ = angular momentum of system

$\bar{I}_i (i = 0, 1, \ldots, N)$ = inertia dyadic of $\mathfrak{B}_i$, each calculated relative to axes parallel to $X_0Y_0Z_0$ passing through its own center of mass

I_p, I_d = polar and diametral moments of inertia of wheel in Example 3

I_X, I_Y, I_Z = diagonal components of $\bar{\Gamma}$ in XYZ-coordinate system

$\bar{J}_i (i = 1, 2, \ldots, N)$ = dyadic defined by Equation [5]

$\bar{J}_{10}$ = average value of $\bar{J}_1$ in Example 1

$\bar{K}$ = dyadic defined by Equation [6]

$\bar{L}$ = net external torque on system

$\bar{L}_P$ = perturbation torque from moving parts

L_{PX}, L_{PY}, L_{PZ} = components of $\bar{L}_P$ along XYZ-axes

m = total mass of system

$m_i (i = 0, 1, \ldots, N)$ = mass of body $\mathfrak{B}_i$

N = number of internal moving parts

$\bar{R}$ = vector locating center of mass of system relative to center of mass of $\mathfrak{B}_0$

$\bar{R}_0$ = average value of $\bar{R}$ in Example 1

$s(t)$ = relative variation of $\bar{\rho}_{10}$ in Example 1

t = time

$\bar{v}_i (i = 1, 2, \ldots, N)$ = time rate of change of $\bar{\rho}_i$ as seen by an observer in $\mathfrak{B}_0$

$\bar{V}$ = time rate of change of $\bar{R}$ as seen by an observer in $\mathfrak{B}_0$

XYZ = reference axes in the composite body (see section, "Choice of reference axes")

$X_0Y_0Z_0$ = basic co-ordinate axes in body $\mathfrak{B}_0$

$\bar{\epsilon}(t)$ = vector vibrational variation of $\bar{\rho}_2$ in Example 2

$\epsilon(t) = \epsilon_0 \sin \nu t$ = magnitude of $\bar{\epsilon}(t)$

$\bar{\gamma}(t)$ = variable part of dyadic given by Equation [9]

$\bar{\Gamma}$ = constant part of dyadic given by Equation [9]

$\bar{\rho}_i$ = vector locating center of mass of $\mathfrak{B}_i$ relative to center of mass of $\mathfrak{B}_0$

$\bar{\rho}_{10}$ = average value of $\bar{\rho}_1$ in Example 1

$\bar{\rho}_{20}$ = center of vibrational motion of $\bar{\rho}_2$ in Example 2

$\bar{\omega}_0$ = angular velocity of $\mathfrak{B}_0$ in inertial space

$\bar{\omega}_i (i = 1, 2, \ldots, N)$ = angular velocity of $\mathfrak{B}_i$ relative to $\mathfrak{B}_0$

$\omega_X, \omega_Y, \omega_Z$ = components of $\bar{\omega}_0$ along XYZ-axes

$\mathfrak{B}_i (i = 0, 1, \ldots, N)$ = designation of ith rigid body

Dots written above vector or dyadic bars denote total time derivatives

Dots written beneath vector or dyadic bars denote time derivatives of components as if base vectors were fixed in inertial space

Introduction

In considering the attitude motions of a satellite vehicle, one sees that a major source of attitude perturbation can be the effective torques arising from the motion of parts within the satellite.

Many small torques are produced by these internal parts which are discarded in conventional engineering problems involving structures carrying moving parts. Sometimes they are discarded because translation rather than rotation of the structure is of major interest. More often, it is because such effects as the gyroscopic coupling of the rotating parts with the rotation of the structure, and small shifts in center of mass, axes of inertia, and moments of inertia of the composite body produce torques which simply are too small to bother with compared to the substantial external torques on the structure.

The artificial satellite is quite a different case. External torques are extremely small by usual engineering standards, including the torques from the attitude coupling to the earth. Under these circumstances, the effective torque produced by the motion of external parts can be significantly large. Such effects as gyroscopic coupling and axis shifts which usually are negligible now play a central role in the dynamics of the problem.

This paper develops the effective attitude-excitation torques on a satellite vehicle which arise from the motion of internal parts. There are two basic restrictions on the analysis: (1) The parts have translations and rotations which are prescribed functions of time relative to the vehicle frame. The case in which there is a

---

[1] See Supplement to this paper in "Brief Notes" Section, this issue, p. 287.

[2] Staff Specialist, Guidance Engineering Department, Autonetics, Division of North American Aviation, Inc. Assoc. Mem. ASME.

Contributed by the Applied Mechanics Division and presented at the Annual Meeting, New York, N. Y., December 1–6, 1957, of THE AMERICAN SOCIETY OF MECHANICAL ENGINEERS.

Discussion of this paper should be addressed to the Secretary, ASME, 29 West 39th Street, New York, N. Y., and will be accepted until July 10, 1958, for publication at a later date. Discussion received after the closing date will be returned.

NOTE: Statements and opinions advanced in papers are to be understood as individual expressions of their authors and not those of the Society. Manuscript received by ASME Applied Mechanics Division, March 25, 1957. Paper No. 57—A-39.

kind of spring-damper coupling between a moving part and the body of the satellite will be treated elsewhere. (2) Only the rotational motion of the satellite about its center of mass is considered. This is not an important restriction, because the physical effects of the translatory motion generally are not of operational importance.[3]

Basic equations of motion

Consider that the satellite consists of a rigid main portion, body $\mathfrak{B}_0$ with mass m_0, and a number of moving (individually rigid) parts, bodies $\mathfrak{B}_i$ with masses m_i ($i = 1, 2, \ldots, N$). Let $X_0Y_0Z_0$ be a right-hand set of orthogonal axes rigidly imbedded in $\mathfrak{B}_0$, having its origin at the center of mass of this main body and an angular velocity $\bar{\omega}_0$ in inertial space. Let $\bar{\rho}_i$ denote the center of mass of $\mathfrak{B}_i$ relative to that of $\mathfrak{B}_0$, and $\bar{\omega}_i$ denote the angular velocity of $\mathfrak{B}_i$ relative to $\mathfrak{B}_0$. The geometry of the situation is shown in Fig. 1.[4] The motion of all subsidiary parts relative to the vehicle frame is completely specified by time functions $\bar{\rho}_i(t)$, $\bar{\omega}_i(t)$ ($i = 1, 2, \ldots, N$).

Next, denote by $\bar{I}_i (i = 0, 1, \ldots, N)$ the inertia dyadic of the various bodies, each calculated relative to axes parallel to $X_0Y_0Z_0$ passing through its own center of mass. Then the angular momentum $\bar{H}$ of the composite body about its common center of mass is[5]

$$\bar{H} = \bar{I}_0 \cdot \bar{\omega}_0 + \sum_{i=1}^{N} \bar{I}_i \cdot (\bar{\omega}_0 + \bar{\omega}_i) + m\bar{R} \times \dot{\bar{R}} - \bar{R} \times \sum_{i=1}^{N} m_i \dot{\bar{\rho}}_i - \sum_{i=1}^{N} m_i \bar{\rho}_i \times \dot{\bar{R}} + \sum_{i=1}^{N} m_i \bar{\rho}_i \times \dot{\bar{\rho}}_i \quad [1]$$

where

$$\bar{R} = \frac{1}{m} \sum_{i=1}^{N} m_i \bar{\rho}_i \quad [2]$$

and dots denote true time derivative as seen by an observer in inertial space.

Equation [1] can be simplified considerably using Equation [2] and the relation

$$\dot{\bar{\rho}}_i = \bar{v}_i + \bar{\omega}_0 \times \bar{\rho}_i \quad [3]$$

in which $\bar{v}_i$ is the time rate of change of $\bar{\rho}_i$ as seen by an observer in the $X_0Y_0Z_0$ co-ordinate system. The result is

$$\bar{H} = \left[\bar{I}_0 + \sum_{i=1}^{N} (\bar{I}_i + \bar{J}_i) - \bar{K} \right] \cdot \bar{\omega}_0 + \sum_{i=1}^{N} \bar{I}_i \cdot \bar{\omega}_i + \sum_{i=1}^{N} m_i \bar{\rho}_i \times \bar{v}_i - m\bar{R} \times \bar{\Gamma} \quad [4]$$

Here

$$\bar{J}_i = m_i(\bar{\rho}_i \cdot \bar{\rho}_i \bar{E} - \bar{\rho}_i \bar{\rho}_i) \quad [5]$$

$$\bar{K} = m(\bar{R} \cdot \bar{R} \bar{E} - \bar{R}\bar{R}) \quad [6]$$

[3] The possibility that the translatory motions excite rotational vibrations in moving parts is ruled out by the first assumption. Where small vibrations are excited which conceivably could affect stiffly mounted but very sensitive instrumentation, it is assumed that the vehicle acts as a force or velocity generator on the instrumentation, but that the latter does not have sensible motion which can influence gross vehicle motion.

[4] Note that the positioning of the $\bar{\omega}_i$ vector at center of mass CM_i does not mean to imply that the instantaneous axis of rotation is assumed to pass through CM_i.

[5] The Appendix summarizes the basic properties of dyadics used hereafter.

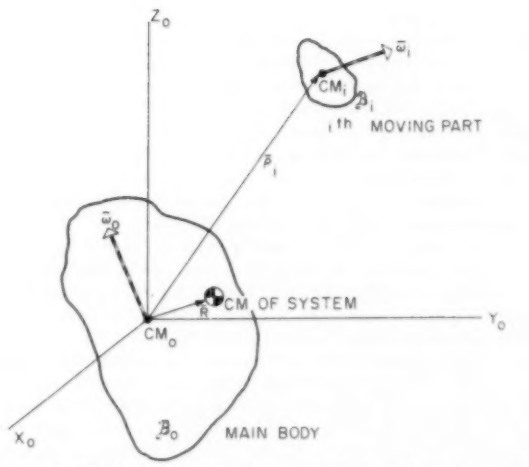

Fig. 1 Partitioning of satellite into main body and moving parts

$\bar{E}$ being the unit dyadic, and $\bar{\Gamma}$ is the apparent velocity of the center of mass of the composite body as seen by an observer in $\mathfrak{B}_0$. The dyadic $\bar{J}_i$ has the interpretation of the inertia dyadic of the ith part, calculated relative to the $X_0Y_0Z_0$-co-ordinate system, as if the part were a point mass situated at its center of mass. Also, $\bar{K}$ represents the inertia dyadic calculated relative to the $X_0Y_0Z_0$ system of a point having mass equal to the total mass of the composite body and situated at the center of mass of the composite body.

The rotational equations of motion, of course, are simply

$$\dot{\bar{H}} = \bar{L} \quad [7]$$

where L is the net external torque on the system.

If the vehicle were a single rigid body, Equation [7] would take the form

$$\frac{d}{dt}(\bar{\Gamma} \cdot \bar{\omega}_0) = \bar{L} \quad [8]$$

where $\bar{\Gamma}$ is the constant-coefficient inertia dyadic of the single body relative to its center of mass. (Note, however, that the time derivative of $\bar{\Gamma}$ generally is nonzero because of the rotation of the base vectors with respect to which $\bar{\Gamma}$ is resolved.) If $\bar{\Gamma}$ is diagonal when resolved in the $X_0Y_0Z_0$-co-ordinate system, the three scalar equations to which Equation [8] corresponds are in the form of the usual Euler equations.

This suggests splitting the inertia dyadic multiplying $\bar{\omega}_0$ in Equation [4] into two parts, a constant part $\bar{\bar{\Gamma}}$ and a time-variable part $\bar{\bar{\gamma}}(t)$. Explicitly, $\bar{\bar{\Gamma}}$ is the constant-coefficient and $\bar{\bar{\gamma}}$ is the variable-coefficient part of

$$\bar{I}_0 + \sum_{i=1}^{N} \bar{I}_i + \sum_{i=1}^{N} m_i(\bar{\rho}_i \cdot \bar{\rho}_i \bar{E} - \bar{\rho}_i \bar{\rho}_i) - m(\bar{R} \cdot \bar{R} \bar{E} - \bar{R}\bar{R}) \quad [9]$$

This partitioning is still ambiguous, of course, and further conditions must be added. Some obvious possibilities are:

1 Choose the constant coefficients as the means of the peak (maximum and minimum) excursions of the coefficients of the dyadic of Equation [9].

2 Choose the constant coefficients as large as possible such that the variable parts never become negative, and vary only through small positive values.

3 Choose the constant coefficients as the time average of the coefficients of the dyadic of Equation [9].

The advantage of the first is that the extreme values of the perturbation torques tend to be minimized by making their positive and negative peaks equal in magnitude. The second permits a simple and convenient visualization of the (always positive) residual variable moments and products of inertia. However, the third may have a commanding advantage in avoiding constant perturbation torques exciting the attitude motion. For example, if $\mathfrak{B}_0$ has a constant component of angular velocity about one of the co-ordinate axes, say ω_x, then constant perturbation-torque components arise from either a constant γ_{xz} or γ_{xy}.[6]

A firm decision as to just what is to be included in γ is not required at this point. It should be noted, though, that there are three sources contributing to $\bar{\bar{\gamma}}$. One of these is the variable projections onto the axes of $\mathfrak{B}_0$ of the inertia dyadics of the internal rotating parts, through the $\bar{\bar{I}}_i$ terms of Equation [9]. This contribution vanishes only if $\bar{\omega}_i$ coincides with an axis of rotational symmetry of $\mathfrak{B}_i$ and keeps a fixed orientation within $\mathfrak{B}_0$. Another is the translatory motion of the centers of mass of the moving parts, as if this motion caused no shift in the center of mass. The effect is expressed by the terms $m_i(\bar{\rho}_i \cdot \bar{\rho}_i \bar{\bar{E}} - \bar{\rho}_i \bar{\rho}_i)$ in Equation [9]. A situation in which these terms are the only source of variable inertia can be visualized by supposing that each part $\mathfrak{B}_i$ is actually two equal point masses, each with mass $\frac{1}{2}m_i$—a dumbbell, so to speak—situated diametrically opposite the composite center of mass, each pair of parts maintaining this symmetry as one of them undergoes motion described by $\bar{\rho}_i$. These terms do not contribute to γ when, for each motion of a part, there is an equivalent opposite motion by another part, producing a cancelling term. The third moment of inertia variation arises from center-of-mass shifts expressed in the term $m(\bar{R} \cdot \bar{R}\bar{\bar{E}} - \bar{R}\bar{R})$ of Equation [9]. The effect can be visualized as that of a point mass m moving with the composite center of mass of the vehicle, without regard for the motions of the individual bodies whose movement is causing $\bar{R}$ to shift.

In any case, Equation [7] can be rewritten after substituting Equation [4] as

$$\frac{d}{dt}(\Gamma \cdot \bar{\omega}_0) = \bar{L} - \frac{d}{dt}\left\{\bar{\bar{\gamma}} \cdot \bar{\omega}_0 + \sum_{i=1}^{N} \bar{\bar{I}}_i \cdot \bar{\omega}_i + \sum_{i=1}^{N} m_i \bar{\rho}_i x \bar{v}_i - m\bar{R} \times \bar{V}\right\} \quad \ldots\ldots [10]$$

The time-derivative expression on the right-hand side of Equation [10] can be interpreted as a torque on body $\mathfrak{B}_0$; moreover, a torque which vanishes if all of the subsidiary bodies are stationary relative to $\mathfrak{B}_0$. Therefore it is the attitude-perturbation torque arising from the motion of internal parts which we desired to find.

It is important to note that Equation [10] may be regarded as a vector differential equation of motion for the dependent quantity $\bar{\omega}_0$. However, some of the small terms which have been written on the right-hand side also involve $\bar{\omega}_0$. Therefore they do not all represent external perturbation torques on the vehicle. Those terms in $\bar{\omega}_0$ might more usually be carried to the left-hand side, whence their proper interpretation as parametric excitation terms appears. Normally it is not feasible to carry the analysis of the resulting motion very far except by a perturbation or iteration procedure or by numerical analysis. Often in an approximate analysis, the small parametric excitation terms may be left on the right-hand side, the $\bar{\omega}_0$ can be replaced by an approximating time function, and the term regarded as an externally applied torque. It is for this reason that the parametric excitation terms are written unconventionally as driving terms.

[6] Constant torques are particularly important because of the possibility that they tend to saturate any control system which is trying to maintain a prescribed attitude.

One further point of interest in this connection is brought out by Equation [10]. If $\bar{\bar{\gamma}}$ exists (i.e., has at least one nonzero coefficient varying with time) it is impossible to escape a parametric excitation of attitude motion (as expressed by $\bar{\omega}_0$) of $\mathfrak{B}_0$.

Perturbation torques

The perturbation-torque terms can be expanded as follows

$$\bar{L}_P = \frac{d}{dt}\left\{\gamma \cdot \bar{\omega}_0 + \sum_{i=1}^{N} \bar{\bar{I}}_i \cdot \bar{\omega}_i + \sum_{i=1}^{N} m_i \bar{\rho}_i \times \bar{v}_i - m\bar{R} \times \bar{V}\right\}$$
$$= \bar{\bar{\gamma}} \cdot \bar{\omega}_0 + \bar{\bar{\gamma}} \cdot \bar{\omega}_0 + \bar{\omega}_0 \times \bar{\bar{\gamma}} \cdot \bar{\omega}_0$$
$$+ \sum_{i=1}^{N} \{\dot{\bar{I}}_i \cdot \bar{\omega}_i + \bar{\bar{I}}_i \cdot (\bar{\omega}_0 \times \bar{\omega}_i) + \dot{\bar{I}}_i \cdot \bar{\omega}_i + (\bar{\omega}_0 + \bar{\omega}_i) \times \bar{\bar{I}}_i \cdot \bar{\omega}_i$$
$$- [\bar{\bar{I}}_i \times (\bar{\omega}_0 + \bar{\omega}_i)] \cdot \bar{\omega}_i + m_i \bar{\rho}_i \times \bar{a}_i + m_i \bar{\rho}_i \times (\bar{\omega}_0 \times \bar{v}_i)$$
$$+ m_i(\bar{\omega}_0 \times \bar{\rho}_i) \times \bar{v}_i\} - m\dot{\bar{R}} \times \bar{A} - m\bar{R} \times (\bar{\omega}_0 \times \bar{V})$$
$$- m(\bar{\omega}_0 \times \bar{R}) \times \bar{V} \quad \ldots\ldots [11]$$

where $\dot{\bar{\gamma}}, \dot{\bar{\omega}}_i, \dot{\bar{I}}_i$ represent time derivatives taken as if only the components were variable, while the base vectors were inertial; i.e., derivatives relative to an observer fixed in $\mathfrak{B}_0$. Also $\bar{a}_i$ and $\bar{A}$ are, respectively, the apparent accelerations of the centers of mass of $\mathfrak{B}_i$ and of the composite body as seen by a $\mathfrak{B}_0$-fixed observer.

It is possible to combine and simplify some of these terms. Specifically

$$\bar{\rho}_i \times (\bar{\omega}_0 \times \bar{v}_i) + (\bar{\omega}_0 \times \bar{\rho}_i) \times \bar{v}_i = \bar{\omega}_0 \times (\bar{\rho}_i \times \bar{v}_i)$$

and

$$\bar{R} \times (\bar{\omega}_0 \times \bar{V}) + (\bar{\omega}_0 \times \bar{R}) \times \bar{V} = \bar{\omega}_0 \times (\bar{R} \times \bar{V})$$

Also

$$\bar{\bar{I}}_i \cdot (\bar{\omega}_0 \times \bar{\omega}_i) - (\bar{\bar{I}} \times \bar{\omega}_0) \cdot \bar{\omega}_i = 0$$

and

$$(\bar{\bar{I}}_i \times \bar{\omega}_i) \cdot \bar{\omega}_i = 0$$

This leaves

$$\bar{L}_P = \bar{\bar{\gamma}} \cdot \dot{\bar{\omega}}_0 + \bar{\bar{\gamma}} \cdot \bar{\omega}_0 + \bar{\omega}_0 \times \bar{\bar{\gamma}} \cdot \bar{\omega}_0$$
$$+ \sum_{i=1}^{N} \{\dot{\bar{I}}_i \cdot \bar{\omega}_i + \bar{\bar{I}}_i \cdot \dot{\bar{\omega}}_i + (\bar{\omega}_0 + \bar{\omega}_i) \times \bar{\bar{I}}_i \cdot \bar{\omega}_i$$
$$+ m_i \bar{\rho}_i \times \bar{a}_i + m_i \dot{\bar{\omega}}_0 \times (\bar{\rho}_i \times \bar{v}_i)\}$$
$$- m\dot{\bar{R}} \times \bar{A} - m\bar{\omega}_0 \times (\bar{R} \times \bar{V}) \quad \ldots\ldots [12]$$

Let us consider these terms one by one:

(1) $\bar{\bar{\gamma}} \cdot \dot{\bar{\omega}}_0$. The inertial reaction torque which arises from the angular acceleration of $\mathfrak{B}_0$ acting on the instantaneous value of the residual (variable) inertia dyadic.

(2) $\dot{\bar{\gamma}} \cdot \bar{\omega}_0$. The apparent torque seen by an observer rotating with $\mathfrak{B}_0$ which arises from the time variation of the inertia dyadic (analogous to the apparent torque a twirling skater feels in moving his arms closer to or further from his body).

(3) $\bar{\omega}_0 \times \bar{\bar{\gamma}} \cdot \bar{\omega}_0$. A centrifugal torque which expresses the tendency of the residual part of the body to align itself with its "long" axis (in the sense of moments of inertia) along the angular velocity vector $\bar{\omega}_0$ (see also the interpretation of term (7), given later).

(4) $\bar{\bar{I}}_i \cdot \dot{\bar{\omega}}_i$. Inertial reaction torque from the angular acceleration of $\mathfrak{B}_i$ relative to $\mathfrak{B}_0$ as seen by an observer in $\mathfrak{B}_0$.

(5) $\dot{\bar{I}}_i \cdot \bar{\omega}_i$. Apparent torque arising from the changes in the inertia dyadic of part i, as seen by an observer rotating with $\mathfrak{B}_0$, these changes arising from changes in the projections of I_i on the axes of $\mathfrak{B}_0$.

(6) $\bar{\omega}_i \times \bar{I}_i \cdot \bar{\omega}_i$. A centrifugal torque expressing the tendency, seen by an observer in $\mathfrak{B}_0$, of $\mathfrak{B}_i$ to align itself with its "long" axis along the relative angular velocity vector $\bar{\omega}_0$.

(7) $\bar{\omega}_0 \times \bar{I}_i \cdot \bar{\omega}_i$. Inasmuch as $\bar{I}_i \cdot \bar{\omega}_i$ is the apparent angular momentum of $\mathfrak{B}_i$ from rotation about its center of mass, as seen by an observer in $\mathfrak{B}_0$, this quantity is the negative of the torque which would have to be supplied to make this angular momentum "keep up with" $\mathfrak{B}_0$ as the latter rotates.

(8) $m_i \bar{\rho}_i \times \bar{a}_i$. Inertial reaction torque on $\mathfrak{B}_0$ from the translational acceleration of $\mathfrak{B}_i$ relative to $\mathfrak{B}_0$.

(9) $m_i \bar{\omega}_0 \times (\bar{\rho}_i \times \bar{v}_i)$. Since $m_i \bar{\rho}_i \times \bar{v}_i$ is the apparent angular momentum of $\mathfrak{B}_i$ from translation of $\mathfrak{B}_i$ relative to $\mathfrak{B}_0$, an interpretation analogous to that of term (7) applies.

(10) $-m\bar{R} \times \bar{A} - m\bar{\omega}_0 \times (\bar{R} \times \bar{V})$. If the composite body is considered to be a particle of mass m moving with the center of mass of the composite body, these terms are analogous for the particle to terms (8) and (9) for $\mathfrak{B}_i$.

With respect to terms (8), (9), and (10) note that the origin of the reference system in $\mathfrak{B}_0$ could have been defined to coincide with the composite center of mass. Then terms (10) would vanish, their negatives appearing as additions to terms (8) and (9) as the index ranges over all bodies including $\mathfrak{B}_0$.

In review, the following procedure yields the perturbation torque:

1 Choose axes $X_0Y_0Z_0$ and find $\bar{I}_0$.

2 Describe the translation and rotation of $\mathfrak{B}_i$ and find $\bar{I}_i$, $\bar{J}_i$, and $\bar{K}$.

3 Form $\bar{I}_0 + \Sigma(\bar{I}_i + \bar{J}_i) - \bar{K}$ and decompose into $\bar{\Gamma} + \bar{\bar{\gamma}}$.

4 Evaluate terms (1–10).

In the next section, it also is shown that the process should be completed by the steps:

5 Find new reference axes XYZ which diagonalize $\bar{\Gamma}$.

6 Resolve L_P along these new axes.

Choice of reference axes

Equation [12] eventually must be put into scalar form by resolving it along a certain set of co-ordinate axes, XYZ. It is easy to put some general requirements on these axes. First, the orientation of $\mathfrak{B}_0$ should be given directly by the orientation of XYZ. If the latter are not rigidly embedded in $\mathfrak{B}_0$, at least there should be no rotation of this body relative to XYZ. This requirement reflects the fact that it is the main body whose attitude motions usually are of principal interest. Second, these axes should lie closely along the principal axes of the composite vehicle for convenience in treating the attitude motion. This requirement is made precise by defining XYZ so that the constant part $\bar{\Gamma}$ of the inertia dyadic is diagonalized when referred to these axes.

With this choice, Equation [10] takes the normal form for the Euler equations. If we assume the representations

$$\bar{\Gamma} = I_X \bar{e}_X \bar{e}_X + I_Y \bar{e}_Y \bar{e}_Y + I_Z \bar{e}_Z \bar{e}_Z \quad \ldots\ldots\ldots [13]$$

$$\bar{\omega}_0 = \omega_X \bar{e}_X + \omega_Y \bar{e}_Y + \omega_Z \bar{e}_Z \quad \ldots\ldots\ldots [14]$$

then Equation [10] becomes

$$\left.\begin{aligned} I_X\dot{\omega}_X + (I_Z - I_Y)\omega_Y\omega_Z &= L_X - L_{PX} \\ I_Y\dot{\omega}_Y + (I_X - I_Z)\omega_Z\omega_X &= L_Y - L_{PY} \\ I_Z\dot{\omega}_Z + (I_Y - I_X)\omega_X\omega_Y &= L_Z - L_{PZ} \end{aligned}\right\} \quad \ldots\ldots [15]$$

The orientation of $X_0Y_0Z_0$ in $\mathfrak{B}_0$ has not been specified heretofore. As far as the formal development is concerned, it can be chosen *ad libitum*. A convenient and natural choice is an orientation which diagonalizes $\bar{I}_0$. Suppose that this is made and $\bar{\Gamma}$ is found (generally nondiagonal relative to $X_0Y_0Z_0$). By equating $\bar{\Gamma}$ in its two alternate forms, one as in Equation [13] and the other in terms of $X_0Y_0Z_0$ base vectors with coefficients which now are known, one may take the scalar product of the equation by $\bar{e}_X$, $\bar{e}_Y$, and $\bar{e}_Z$ successively twice, thereby obtaining enough equations to permit a complete determination of I_X, I_Y, I_Z, and the direction cosines between the two sets of axes. If the bulk of the composite inertia is that of the main body $\mathfrak{B}_0$, the off-diagonal terms of $\bar{\Gamma}$ are relatively small and a simple small-angle transformation can be found between $X_0Y_0Z_0$ and XYZ.

The choice of an origin for XYZ is somewhat less obvious. Fortunately, it is not of great importance if our main concern is the attitude motion of the system, as it is here. For most purposes, it is a matter of indifference whether the origin of the reference axes is at one location or another within the body. However, there are some cases in which there is a preference for axes with origin at the composite center of mass, such as in calculating the gravitational and certain other torques on the body. Therefore for definiteness we assume that the origin of XYZ is at the composite center of mass. If $\bar{\rho}_i$ in Equation [12] is now considered to be referred to these new XYZ-axes, the terms (10) described in the foregoing disappear, and terms (8) and (9) are assumed to exist not only for $i = 1, \ldots, N$ but for $i = 0$ as well.

Examples

A number of practical examples could be considered, but only three will be given. The algebraic expressions become increasingly complex for more sophisticated cases, but no essentially new features are added. The derivation of the perturbation torque is relative to the $X_0Y_0Z_0$-axes. It should not be necessary here to illustrate the transformation into the XYZ-system.

Example 1. Consider a single point mass $\mathfrak{B}_1$ which translates relative to $\mathfrak{B}_0$ along a line through the composite center of mass. Measuring $\bar{\rho}_1$ from origin of $X_0Y_0Z_0$

$$\bar{\rho}_1 = [1 + s(t)]\bar{\rho}_{10}$$

where $\bar{\rho}_{10}$ is the average position of $\bar{\rho}_1$ over a long period of time.

Also $$\bar{R} = [1 + s(t)]\bar{R}_0$$

Although

$$\bar{I}_1 = 0, \bar{J}_1 = [1 + s(t)]^2 \bar{J}_{10}$$

and $$\bar{K} = [1 + s(t)]^2 \bar{K}_0$$

Also, in this special case of a single subsidiary body

$$\bar{J}_{10} - \bar{K}_0 = \frac{m_1 m_0}{m} (\bar{\rho}_{10} \cdot \bar{\rho}_{10} \bar{\bar{E}} - \bar{\rho}_{10}\bar{\rho}_{10})$$

Then

$$\bar{\Gamma} + \bar{\bar{\gamma}} = \bar{I}_0 + \frac{m_0}{m} \bar{J}_{10} + [2s(t) + s^2(t)] \frac{m_0}{m} \bar{J}_{10}$$

and

$$\bar{\bar{\gamma}} = \frac{m_0}{m} [2s(t) + s^2(t)] \bar{J}_{10}$$

Because the line of motion of $\mathfrak{B}_1$ passes through the composite center of mass as well as the center of mass of $\mathfrak{B}_0$ (in this special case), all of the terms (8–10) vanish.

Therefore the attitude-perturbation torque is

$$\bar{L}_P = \frac{m_0}{m} [2s(t) + s^2(t)] [\bar{J}_{10} \cdot \dot{\bar{\omega}}_0 + \bar{\omega}_0 \times \bar{J}_{10} \cdot \bar{\omega}_0]$$

$$+ \frac{2m_0}{m} \dot{s}(t)[1 + s(t)] \bar{J}_1 \cdot \bar{\omega} \quad \ldots\ldots [16]$$

At first thought, the fact that the line of motion of the part passes through the composite center of mass might indicate that attitude-perturbation torques are absent. Equation [16] shows that they are, indeed, present, arising from the interaction of the change in moment of inertia with the angular velocity of the $\mathfrak{B}_0$ reference frame.

Example 2. Consider a single point mass $\mathfrak{B}_2$ which undergoes translatory vibration through a small amplitude about a point fixed in $\mathfrak{B}_0$. Represent $\bar{\rho}_2$ as $\bar{\rho}_2 = \bar{\rho}_{20} + \bar{\epsilon}(t)$. Again $\bar{I}_0 = 0$ and $\bar{J}_2 - \bar{K} = \dfrac{m_0}{m}\bar{J}_2$, whence

$$\bar{\gamma} = \frac{m_0 m_2}{m}\left[(2\bar{\rho}_{20}\cdot\bar{\epsilon} + \bar{\epsilon}\cdot\bar{\epsilon})\bar{\bar{E}} - (\bar{\rho}_{20}\bar{\epsilon} + \bar{\epsilon}\bar{\rho}_{20} + \bar{\epsilon}\bar{\epsilon})\right] \quad [17]$$

Also, terms (8–10) combine to

$$\frac{m_0 m_2}{m}\left[\bar{\rho}_2 \times \bar{a}_2 + \bar{\omega}_0 \times (\bar{\rho}_2 \times \bar{v}_2)\right] \quad [18]$$

The basic question in this example is whether symmetrical oscillations rectify and cause a net effective torque on $\mathfrak{B}_0$.

If $\bar{\epsilon}(t) = \epsilon(t)\bar{e}_\epsilon$ with $\bar{e}_\epsilon$ is fixed in $\mathfrak{B}_0$ and $\epsilon(t) = \epsilon_0 \sin \nu t$, then it is easy to see that the terms in Equation [18] are oscillatory with zero time average, so that no average torque arises from these terms. On the other hand, $\bar{\omega}_0 \times \bar{\bar{\gamma}}\cdot\bar{\omega}_0$ contains a term $-\epsilon^2(t)(\bar{\omega}_0\cdot\bar{e}_\epsilon)(\bar{\omega}_0 \times \bar{e}_\epsilon)$. Thus even for a body rotating with constant velocity, a vibration along an axis which is neither parallel nor perpendicular to $\bar{\omega}_0$ induces an effective drift-producing torque on the body, this torque having a nonzero time-average value. It may be noted that the term $\bar{\bar{\gamma}}\cdot\dot{\bar{\omega}}_0$ also contains an ϵ^2 term.

Example 3. Consider a single rotating wheel $\mathfrak{B}_3$. Suppose that it rotates about its polar axis $\bar{e}_p$ which is constrained to remain fixed in $\mathfrak{B}_0$. Let this axis pass through the center of mass of the wheel, which also is assumed fixed in $\mathfrak{B}_0$. Under these circumstances, the projections of $\bar{I}_3$ onto the $X_0Y_0Z_0$-axes remain constant, although, of course, they are not zero. Both $\bar{J}_3$ and $\bar{K}$ are constant because $\bar{\rho}_3$ and $\bar{R}$ are constant. Thus $\bar{\bar{\gamma}} = 0$ and terms (8–10) vanish; that is, the only contributions arise from the $\bar{I}_3$ terms, terms (4–7). These have values as follows:

If I_p is the polar and I_d the diametral moments of the inertia of the wheel

$$\bar{I}_3 = I_p\bar{e}_p\bar{e}_p + I_d\bar{e}_\xi\bar{e}_\xi + I_d\bar{e}_\eta\bar{e}_\eta \quad [19]$$

where $\bar{e}_\xi$ and $\bar{e}_\eta$ are some unit vectors normal to $\bar{e}_p$ such that $\bar{e}_p$, $\bar{e}_\xi$, $\bar{e}_\eta$ is a right-hand orthogonal set. Now $\bar{\omega}_3 = \omega_3\bar{e}_p$ and $\dot{\bar{\omega}}_3 = \dot{\omega}_3\bar{e}_p$. Also $\dot{\bar{I}}_3 = 0$. Then from this source

$$\bar{L}_P = I_p\dot{\omega}_3\bar{e}_p + I_p\omega_3(\bar{\omega}_0 \times \bar{e}_p) \quad [20]$$

That is, there is a torque contribution about $\bar{e}_p$ if the wheel is accelerated relative to $\mathfrak{B}_0$. There is also a gyroscopic interaction between the spinning wheel and the rotating body $\mathfrak{B}_0$, equivalent to the torque required to precess the relative angular momentum of the spinning wheel at the angular rate of $\mathfrak{B}_0$.

APPENDIX

Note on dyadic products

A dyadic $\bar{\bar{D}}$ with the base vectors $\bar{e}_i (i = 1, 2, 3)$ is defined as the quadratic form

$$\bar{\bar{D}} = \sum_{i,j} d_{ij}\bar{e}_i\bar{e}_j$$

The d_{ij} are called the components of the dyadic. If

$$\bar{v} = \sum_i v_i\bar{e}_i$$

is any vector, we define products

$$\bar{\bar{D}}\cdot\bar{v} = \sum_{i,j} d_{ij}v_j\bar{e}_i$$

and

$$\bar{v}\cdot\bar{\bar{D}} = \sum_{i,j} v_i d_{ij}\bar{e}_j = \sum_{i,j} d_{ji}v_j\bar{e}_i$$

These products differ unless $\bar{\bar{D}}$ is symmetric; i.e., $d_{ij} = d_{ji}$. In a form like $\bar{v}_1\cdot\bar{\bar{D}} \times \bar{v}_2$, the product $v_1\cdot\bar{\bar{D}}$ is to be taken first to get a vector, and then vector multiplication is used in the normal way. Some dyadics are represented as the juxtaposition of two vectors (e.g., in Equations [5] and [6]), of the form $\bar{\bar{D}} = \bar{v}_1\bar{v}_2$. The latter product is to be interpreted as the dyadic whose ij-component is $v_{1i}v_{2j}$. It differs from $\bar{v}_2\bar{v}_1$ unless $v_{2i}v_{1j} \equiv v_{1i}v_{2j}$; that is, unless $\bar{v}_2$ is parallel to $\bar{v}_1$.

An Experimental Study of Initial and Subsequent Yield Surfaces in Plasticity[1]

By P. M. NAGHDI,[2] F. ESSENBURG,[3] AND W. KOFF,[4] ANN ARBOR, MICH.

Experimental results for twenty-five tubular specimens of a 24S-T-4 aluminum alloy, subjected to combined torsion-tension-reversed torsion, are reported in a study of the initial and two subsequent yield surfaces covering the first and the fourth quadrant of the axial stress-shear stress plane. Results are also given for two additional specimens subjected to tension followed by torsion, in order to compare the values of the initial shear modulus at the initiation of twist with the elastic shear modulus.

Introduction

IT IS well known that, under a uniaxial state of stress or a state of stress due to pure torsion, most materials exhibit the Bauschinger effect, i.e., possess a lower yield stress upon the reversal of the load, and, for example, following tension or torsion are said to be softer in compression or in reversed torsion, respectively. While under more general circumstances (such as a biaxial state of stress), no experimental evidence seems to be available with regard to the shape of subsequent yield surfaces (or loading functions) beyond the initial yield, sufficient information [see for example (1)[5]] is available to conclude that successive yield (or loading) surfaces are not merely blown-up versions of the original.

The incremental-strain theories of plasticity in general, and their stress-strain relations in particular, are dominated by the concept of a loading function which, corresponding to a given state of increments of stress, predicts the absence (during unloading and neutral loading) or presence (during loading) of additional increments of plastic strains. As plastic deformation is physically an anisotropic phenomenon in character, the loading function for a work-hardening material depends on the history of loading and exhibits Bauschinger effect as well as strain-hardening anisotropy, even if the material, in the unstrained state, is isotropic. In fact, as has been pointed out by Drucker (2), an isotropic work-hardening theory of plasticity cannot properly predict a Bauschinger effect during plastic deformation. It is relevant to mention here that loading functions which account for various degrees of initial and strain-hardening anisotropy as well as a Bauschinger effect have been considered by Drucker (3), Hill (4), and Edelman and Drucker (5), and that the difficulties of fitting mathematical theories of plasticity to experimental results are discussed by Stockton and Drucker (6).

The present paper contains experimental results for twenty-seven tubular specimens, made of a 24S-T-4 aluminum alloy, which were initially (reasonably) isotropic. Twenty-five specimens, subjected to combined torsion-tension-reversed torsion with variable loading paths, were employed in a study of the initial and two subsequent yield surfaces covering the first and the fourth quadrants of the axial stress-shear stress plane. The remaining specimens were subjected to tension alone followed by torsion (with various amounts of tension), and as in (7) enabled the determination of the initial shear modulus G_i at the initiation of twist. Although the latter type of experiment was performed on six specimens, the results for only two are reported here, since the character of the test data (except for loading paths) is the same as those described.

For the sake of clarity and for future reference it is well to call attention here to the fact that, while the specimens employed in previous investigations (7, 8) also were made of a 24S-T-4 aluminum alloy and were cut from a rolled thick plate stock possessing a rather severe initial anisotropy, the specimens employed in the present study were made of a round extruded stock, which at least by comparison (see Fig. 3) is reasonably isotropic.

Specimens and equipment

The thin-walled specimens employed were made of a round extruded 24S-T-4 aluminum-alloy stock, $1^1/_2$ in. diam (the stock has an age history of about 12 years). All specimens used had the nominal dimensions of 0.75-in. ID, 0.075-in. thickness, and tolerances were held to ± 0.001 in. in both eccentricity of bore and wall thickness; a detailed drawing of a typical specimen is given in (7). Initially, the specimens were reasonably isotropic as may be seen from a photomicrograph of the cross section of a typical specimen in Fig. 3 [compare with Fig. 4 in (7)]. As pointed out previously (7), it seems desirable to repeat here that the design requirements on wall thickness of the specimens were dictated by (*a*) elastic and plastic buckling in torsion; (*b*) dimensions of the extensometer; and (*c*) the available loading range of the machine.

The testing equipment employed in the present study is that used previously (7, 8) with some modifications, and only these modifications will be described in detail here.

The testing machine, a combin torsion-tension-reversed torsion machine, is powered by electric motors which drive the loading ram through variable-speed transmissions. In order to measure the axial force and torque to which the specimen is subjected, a load cell comprising a hollow steel circular cylinder coupled in series with the specimen has been introduced. The dimensions of the load cell are so selected that it will be subjected only to elastic deformation throughout the range of loads applied to the specimen. Two Wheatstone bridges, each consisting of eight SR-4 Type A-7 strain gages, are mounted on the surface of the cell. The tension-measuring bridge consists of gages aligned axially and circumferentially and the torque bridge consists of

[1] The results presented in this paper were obtained in the course of research sponsored by the Office of Ordnance Research (U. S. Army), under Contract DA-20-018-ORD-12099, with the University of Michigan.

[2] Professor of Engineering Mechanics, University of Michigan. Mem. ASME.

[3] Assistant Professor of Engineering Mechanics, University of Michigan. Assoc. Mem. ASME.

[4] Research Assistant, Department of Engineering Mechanics, University of Michigan.

[5] Numbers in parentheses refer to the Bibliography at the end of the paper.

Contributed by the Applied Mechanics Division and presented at the Annual Meeting, New York, N. Y., December 1–6, 1957, of THE AMERICAN SOCIETY OF MECHANICAL ENGINEERS.

Discussion of this paper should be addressed to the Secretary, ASME, 29 West 39th Street, New York, N. Y., and will be accepted until July 10, 1958, for publication at a later date. Discussion received after the closing date will be returned.

NOTE: Statements and opinions advanced in papers are to be understood as individual expressions of their authors and not those of the Society. Manuscript received by ASME Applied Mechanics Division, April 15, 1957. Paper No. 57—A-37.

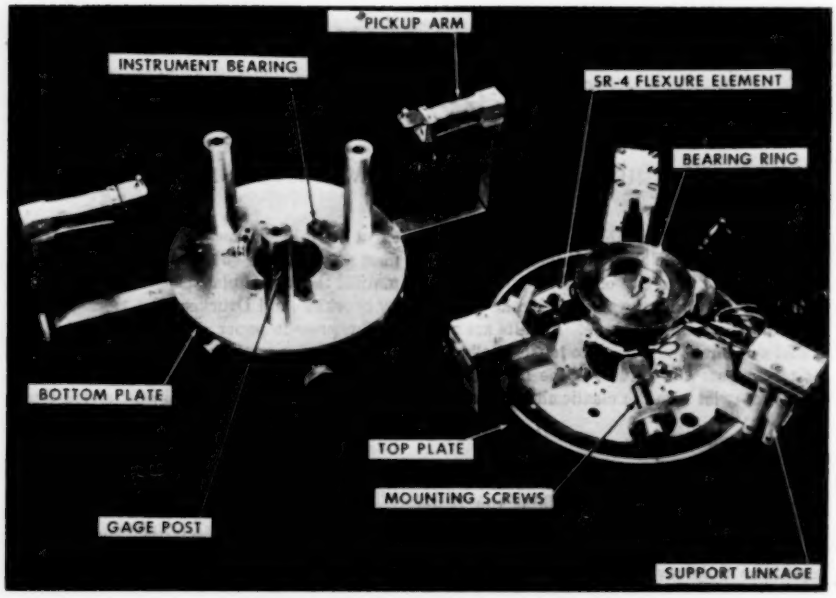

Fig. 1 Disassembled extensometer

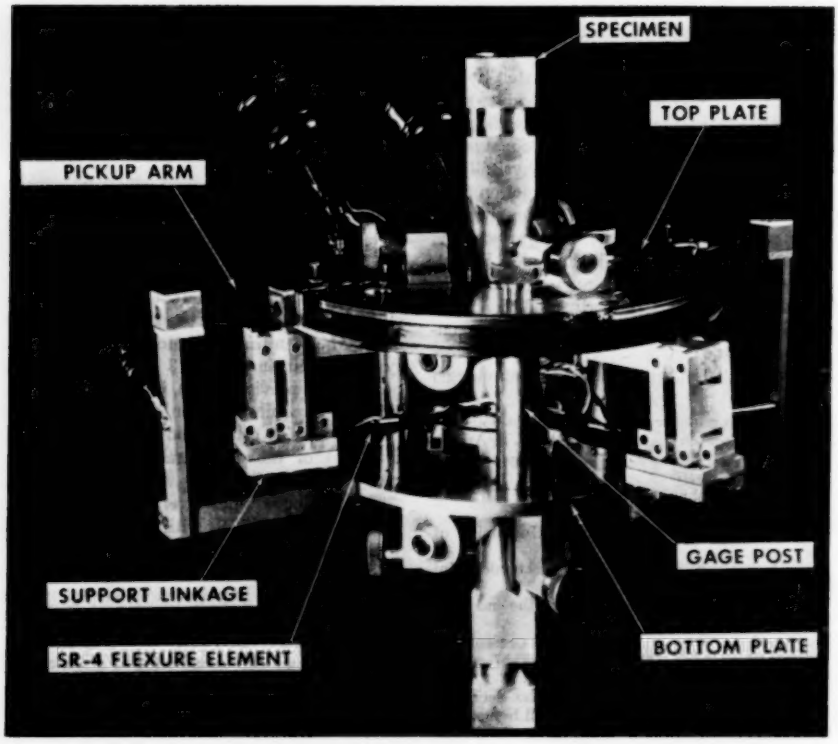

Fig. 2 Extensometer mounted on specimen

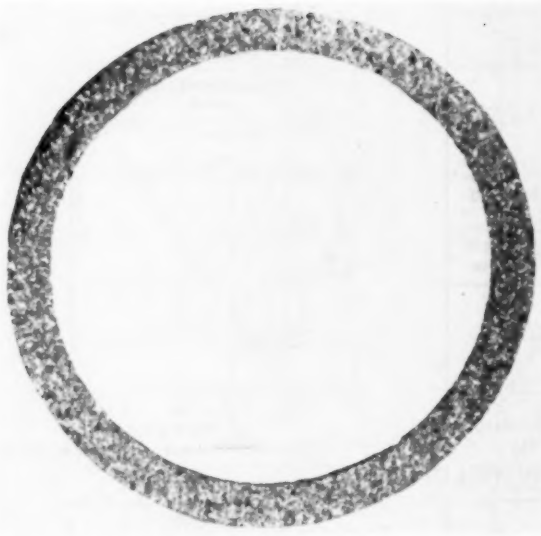

Fig. 3 Enlarged photomicrograph of specimen cross section

gages aligned at 45 deg to the axis of the cell. Pairs of gages comprising the various legs of the bridges are mounted at diametrically opposite positions on the cell so as to nullify any bending effects due to possible slight eccentricities which might result in the loading of the cell (the calibration of the load cell also indicated an independence of tension and torque measurements). In addition to the advantage of providing for the measurement of the load in reversed torsion, the present load cell improves the previously employed setup by coupling the cell directly in series with the specimen; all of the tension and torque in the specimen are transmitted to the load-recording means (the load cell of the present setup) whereas previously an unknown (although small) portion of the load was taken up by friction in the bearings.

In an effort to minimize the interaction of the angle of twist and the extension measurements [see Fig. 12(*c*) of (7)] of the previously employed extensometer, a substantial reconstruction of the extensometer shown in Figs. 1 and 2 was undertaken. The angle of twist-measuring mechanism was left intact but the means of measuring extension was substantially altered. The upper and lower plates, together with the steel bearing ring, were machined to closer tolerances, and the instrument bearings were replaced with precision roller bearings. To insure the parallelism of the upper and lower plates and to eliminate the possibility of a slight error introduced in the original design due to the utilization of removable gage blocks, three identical gage posts were added and rigidly attached to the lower plate. The gage posts are of such a length that when the upper plate is brought into contact with them (with the aid of thumb screws), the points of contact of the mounting screws are separated by precisely the gage length of the specimen (2.6250 in.). The four flexure arms were replaced by three straight flexure elements, each clamped to a support linkage. The support linkages provide each flexure element with a fixed end support and accommodate the radial displacement of the built-in end as extension takes place. As may be noted in Figs. 1 and 2, in redesigning the extensometer it was convenient to attach the bearing ring through the flexure elements and the support linkages to the top plate, and to mount the new precision roller bearings on the bottom plate; this is a reversal of the arrangement used previously [see Figs. 1 and 2 of (7)].

The recording equipment used in the present work is a Heiland Model 82-6 bridge balance unit, and a Heiland 712-B oscillograph employing Heiland galvanometers (No. 40-1000) having a sensitivity of 3.1 microamp/in. The sensitivities and resolutions of the four quantities measured are given in Table 1.

Table 1 Sensitivities and resolutions of quantities measured

	Sensitivity	Resolution
Axial strain, microin/in.	800	± 4
Shearing strain, microin/in.	830	± 4
Axial stress, psi/in.	4600	±23
Shearing stress, psi/in.	4200	±21

It also should be mentioned that, in view of the manner in which the test was conducted, it was highly beneficial to be able to monitor the path of loading. For this purpose two independent bridges mounted on the load cell were used to activate a Mosely Autograph (X-Y plotter). The resolutions and sensitivities of the torque and tensile-force measurements made by the monitoring agency were approximately one half of those recorded by the oscillograph.

Experimental results

Twenty-five specimens were employed in order to establish sixty-eight points on the initial, a first, and a second subsequent yield surfaces in the first and fourth quadrants of the axial-stress (σ_z) shear-stress ($\tau_{\theta z}$) plane. In many cases, with appropriate loading paths in combined torsion-tension-reversed torsion, a single specimen was utilized to obtain a single point on each of the three yield surfaces. The main steps in the history of a typical specimen, loaded in the first quadrant, will be described in detail as follows:

1 The specimen, in the virgin state, is subjected to the loading path shown in Fig. 4(*a*). In the course of this loading the specimen is initially subjected to tension alone, followed by a torsion with tension held essentially constant, all well within the elastic range. In approaching the region where the yield surface was anticipated to lie, the path of loading consists of a combination of both tension and torsion, thus enabling the crossing of the yield surface with a straight-line loading path which is oblique to the yield surface. The corresponding axial-stress axial-strain and shear-stress shear-strain curves are shown in Fig. 4(*b*, *c*). The time at which the inception of plastic strain is observed to occur, in Fig. 4(*b*, *c*)—the 114th second of the test—is also significantly marked on the plot of the path of loading (a reproduction of this plot is observed also by the operator during the running of the test on the X-Y plotter). Recalling that the testing machine is essentially a straining machine, it follows that for any given setting of the controls of the machine the loading path will be a straight line (not necessarily a radial path) so long as the deformation of the specimen is elastic. Since the load cell provides the specimen with an elastic support, at the inception of plastic strains (with the deformation rates held constant), an appreciable deviation from the straight-line loading path will be observed. Thus in summary, two methods of observing the inception of yield are available: The first, and most reliable, is the observation of the time of the inception of plastic strains on the stress-strain plots of Fig. 4(*b*, *c*), which is an *a posteriori* method since they are obtained from the developed oscillograph film.[6] The second method, which gives the same results as the first although less reliably, is the observation of a change in the direction of the loading path (with the deformation rates held constant) on both the oscillograph record and the monitoring agency. While, in

[6] Incidentally, this manner of determining the inception of yield (in the sense of being an *a posteriori* method) is similar to that employed by Taylor and Quinney, since in (9) the initial yield points were also obtained from the plots of reduced data after completion of an actual test.

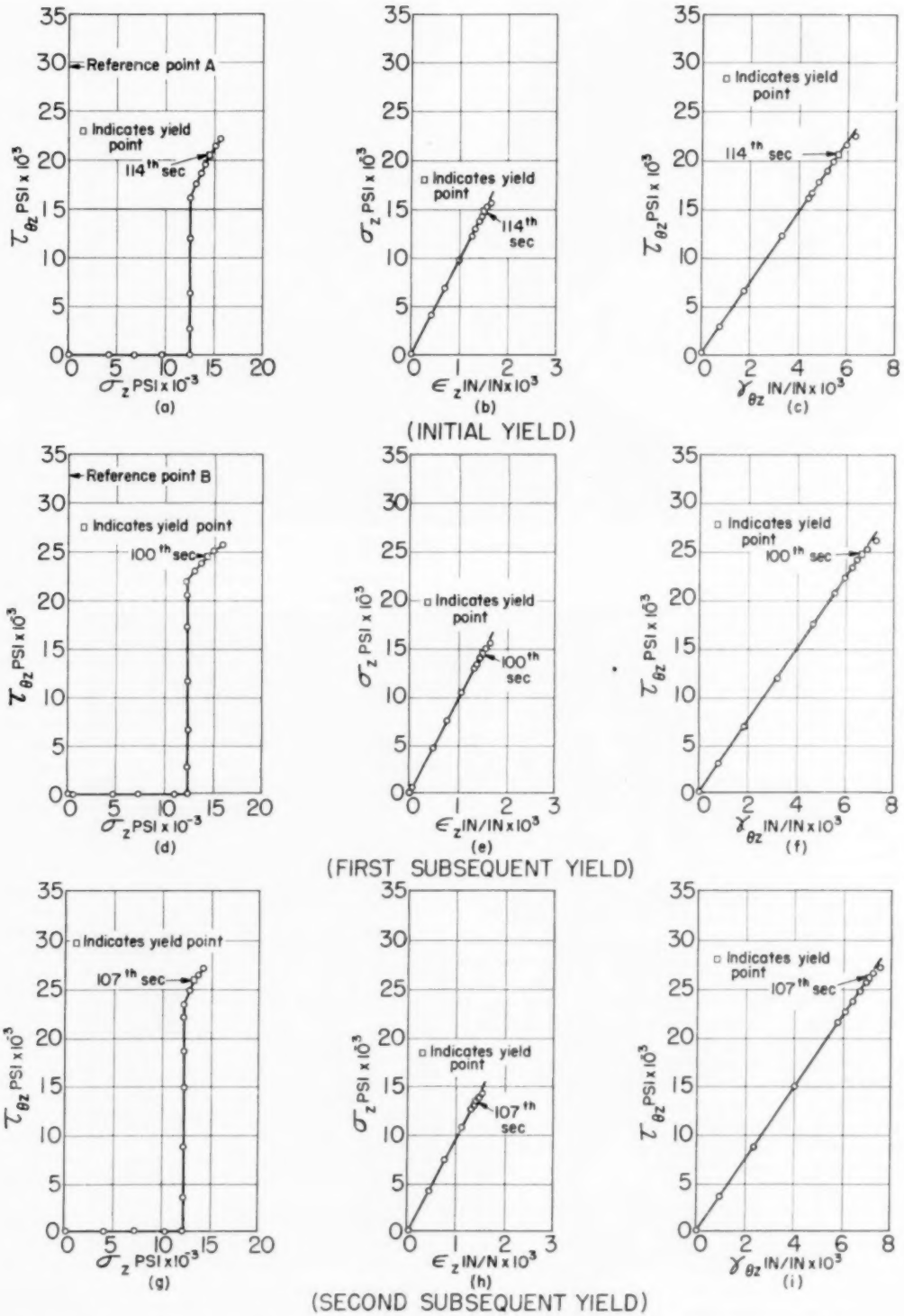

Fig. 4 Loading path and stress-strain curves for determination of initial and subsequent yield points of a typical specimen (No. 89) in the first quadrant

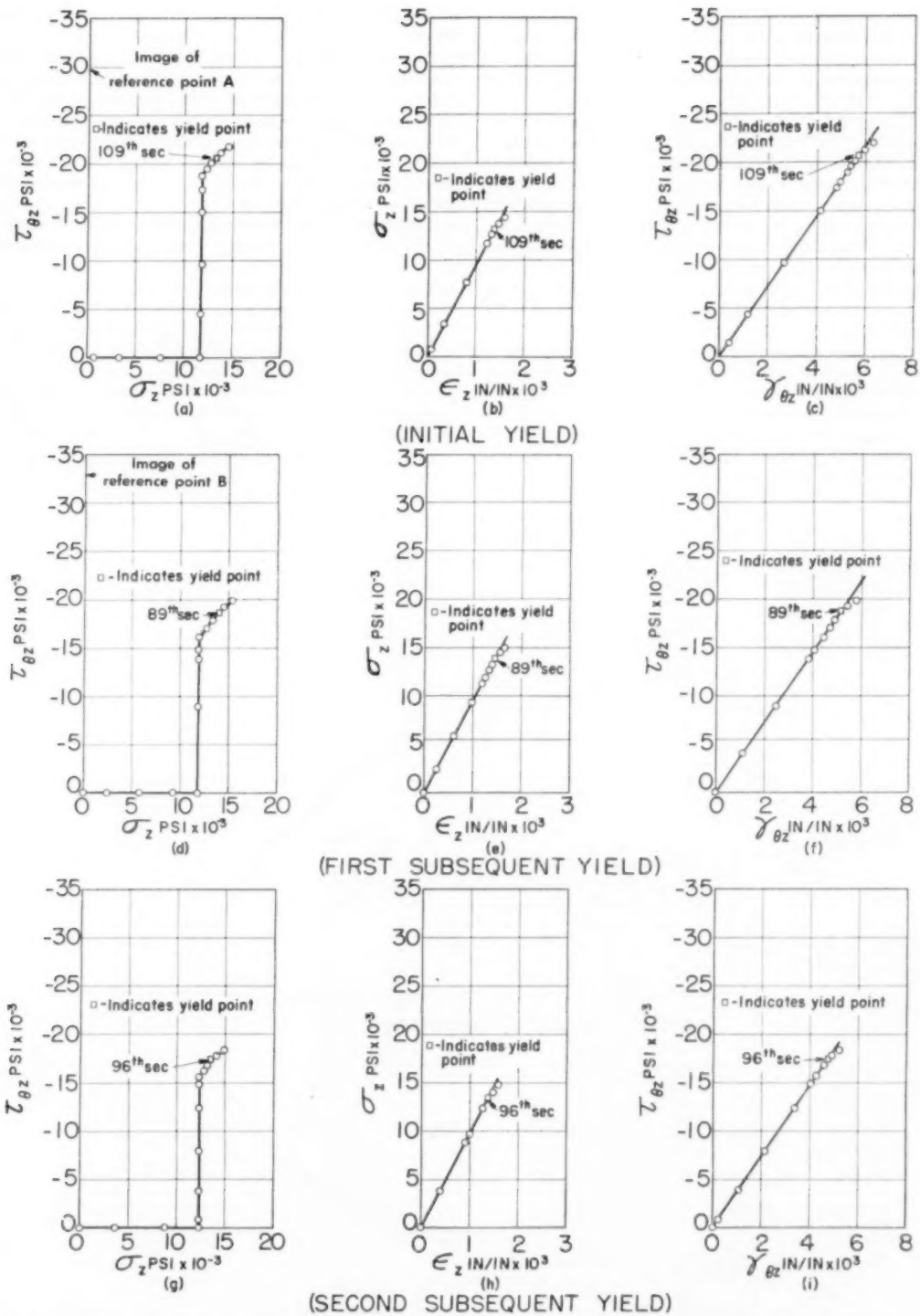

Fig. 5 Loading path and stress-strain curves for determination of initial and subsequent yield points of a typical specimen (No. 91) in the fourth quadrant

order to obtain a point on the initial yield surface it was necessary to "pierce" this surface slightly, it should be noted that the magnitude of the increments of plastic strain involved in this piercing are small compared with the plastic strains in the next step of the procedure.

2 As soon as the yield surface is reached the specimen is unloaded (elastically) to the state of zero stress, and next loaded in torsion alone to reference point A indicated in Fig. 4(*a*). As will be seen presently, this reference point plays a dominant role in establishing the first subsequent yield surface. After unloading, from reference point A, the specimen is then subjected to the loading path shown in Fig. 4(*d*) with corresponding axial-stress axial-strain and shear-stress shear-strain curves shown in Fig. 4(*e*, *f*), and the inception of the first subsequent yield surface is recognized in a manner similar to that used in the recognition of the initial yield surface.

3 The specimen is again unloaded to the state of zero stress and loaded in torsion to reference point B, which establishes the second subsequent yield surface. After unloading, the specimen is then subjected to the loading path shown in Fig. 4(*g*) with corresponding axial-stress axial-strain and shear-stress shear-strain curves shown in Fig. 4(*h*, *i*). The reaching of the second subsequent yield surface is again recognized by the technique described above.

The main steps in the history of another typical specimen, loaded in the fourth quadrant of the $\sigma_z - \tau_{\theta z}$ plane, including the loadings to reference points A and B, are similar to those described in the foregoing. The plots for such a typical specimen, similar to those of Fig. 4, are shown in Fig. 5, where for convenience of presentation the images of reference points A and B also are indicated. It should be emphasized, however, that the reference points A and B lie on the positive $\tau_{\theta z}$-axis and that all specimens are referred to these points irrespective of their loading paths. The experimentally determined initial and subsequent yield surfaces are shown in Fig. 6.

The role played by reference points A and B, in establishing the first and second subsequent yield surfaces, requires further elaboration: Prior to the use of any given specimen to determine a point on the first subsequent yield surface, it is first loaded to reference point A, and this loading is accompanied by a substantial amount of plastic deformation which is large in comparison with that resulting from the slight piercing of the initial yield surface mentioned previously. Thus prior to the time at which the specimens are used to determine points on the first

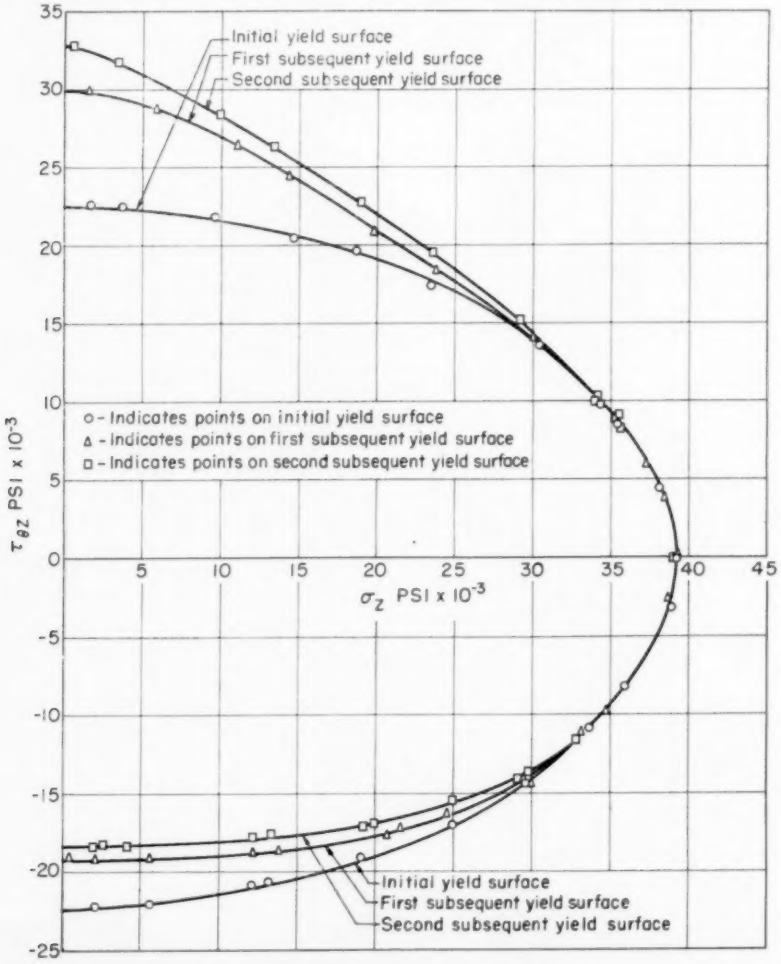

Fig. 6 Initial and subsequent yield surfaces

subsequent yield surface, all (except for possible slight differences in the piercing of initial yield) have had identical strain-hardening histories. In a similar manner, the loading of all specimens to reference point B establishes the second subsequent yield surface.

As noted earlier, in addition to the results shown in Fig. 6, six virgin specimens were subjected to tension well into the plastic range, followed by torsion with varying amounts of tension, primarily to determine the initial shear modulus G_i at the beginning of twist. The plots of experimental results for two typical specimens [arranged in a manner similar to those reported in (7)] are shown in Figs. 7 and 8, and should be regarded as significant only in so far as they afford a measure of the comparison of G_i with G_o together with the display of other relevant quantities.[7]

[7] Since the experiments reported in Figs. 7 and 8 were carried out more than a year after the remainder of the tests were completed, it is to be expected that by this time the accuracy of the calibration of the load cell undoubtedly will be affected by the change in the properties of the strain-gage bonding agent with time (although the reproducibility of the load-cell readings is in no way altered). As a matter of fact the oscillograph data for the experiments of Fig. 6 consistently gave values of $G_o = 3.75 \times 10^6$ psi, as may be seen in Figs. 4 and 5, while a slightly lower value is shown in Figs. 7(*b*) and 8(*b*). However, as the objective of these experiments resides in the comparison of G_i with G_o, it was deemed advisable to report these results despite the accuracy of the absolute values involved.

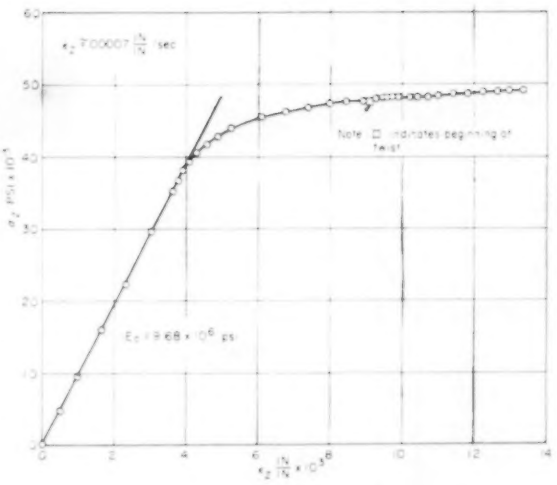

Fig. 7(*a*) Axial stress versus axial strain (Specimen No. 114)

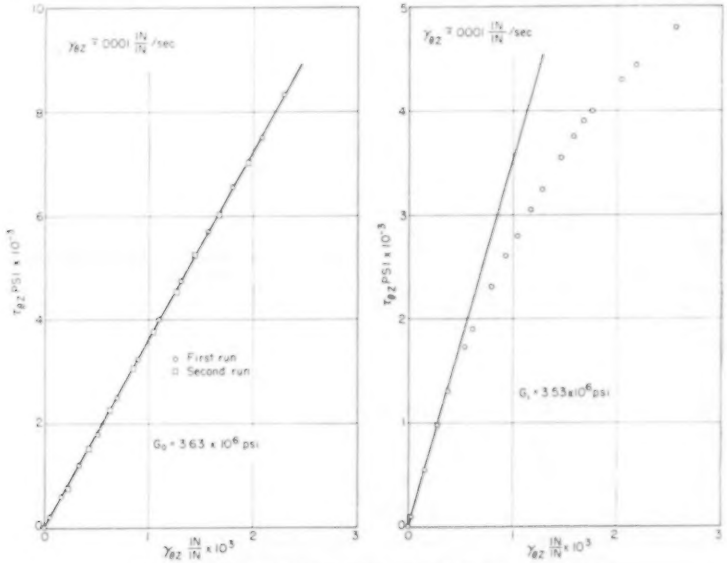

Fig. 7(*b*) Elastic and initial shear moduli (Specimen No. 114)

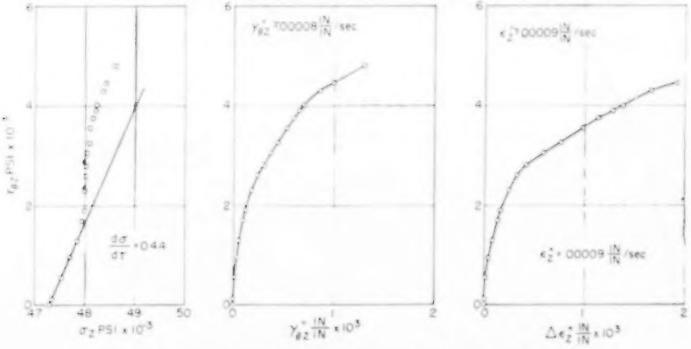

Fig. 7(*c*) Plastic strains and loading path (Specimen No. 114)

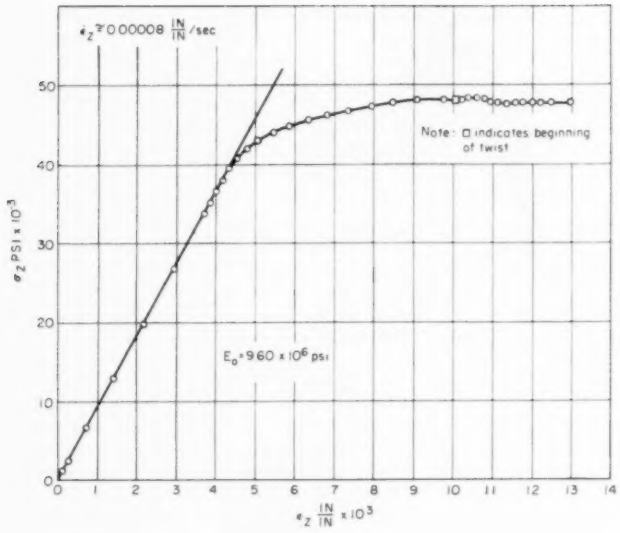

Fig. 8(*a*) Axial stress versus axial strain (Specimen No. 115)

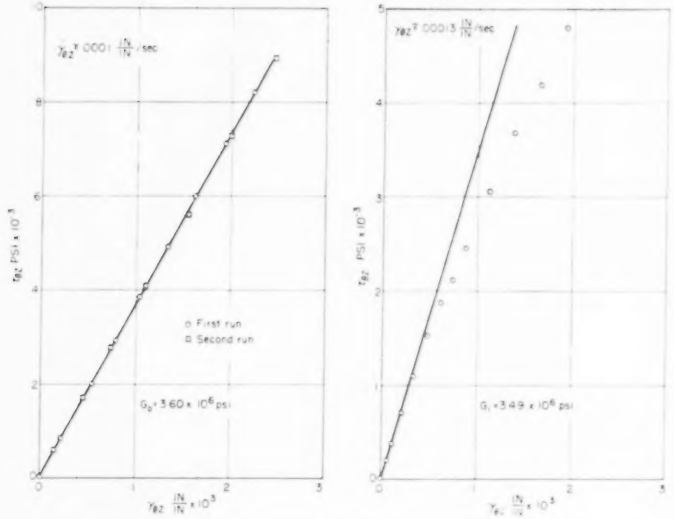
$\dot{\gamma}_{\theta z} = 0.0001$ IN/IN/sec
○ First run
□ Second run
$G_0 = 3.60 \times 10^6$ psi
$\dot{\gamma}_{\theta z} = 0.0013$ IN/IN/sec
$G_1 = 3.49 \times 10^6$ psi
$\tau_{\theta z}$ PSI x 10^3
$\gamma_{\theta z}$ IN/IN x 10^3

Fig. 8(*b*) Elastic and initial shear moduli (Specimen No. 115)

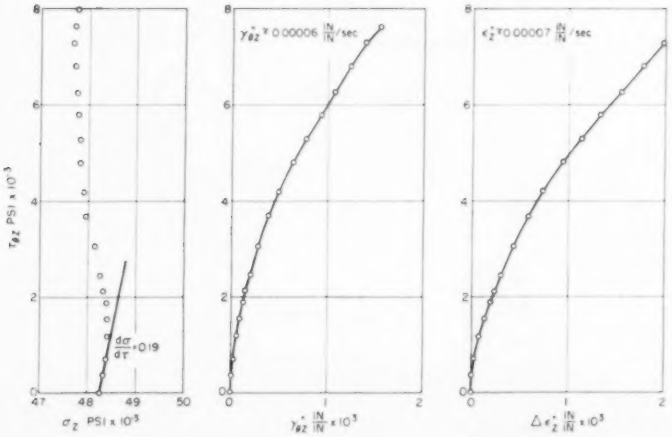
$\frac{d\sigma}{dt} = 0.19$
$\dot{\gamma}^*_{\theta z} = 0.00006$ IN/IN/sec
$\dot{\epsilon}^*_z = 0.00007$ IN/IN/sec
$\tau_{\theta z}$ PSI x 10^3
σ_z PSI x 10^3
$\gamma^*_{\theta z}$ IN/IN x 10^3
$\Delta\epsilon^*_z$ IN/IN x 10^3

Fig. 8(*c*) Plastic strains and loading path (Specimen No. 115)

Discussion of results

With reference to Fig. 6, it is observed that: (*a*) The initial as well as subsequent yield surfaces are convex; (*b*) the initial yield surface is essentially symmetric about the σ_z-axis; (*c*) while the yield stress in tension is unaltered (no cross effect), the first and second subsequent yield surfaces, in the neighborhood of $\tau_{\theta z}$-axis, display a pronounced Bauschinger effect which gradually vanishes as the curves approach the σ_z-axis; (*d*) the effect of work-hardening rapidly diminishes as the σ_z-axis is approached but evidently is accompanied by a gradual linearization of the subsequent yield surfaces in the first quadrant, producing a region of high curvature about the $\tau_{\theta z}$-axis. This latter is reminiscent of corners predicted by the slip theory of plasticity (10), which as pointed out in (11, 12), also may be viewed as a particular incremental theory based on an infinite set of plane loading surfaces; and (*e*) the initial yield surface, except for a slight deviation in the vicinity of the σ_z-axis, is almost identical with the Mises yield condition.

Although the initial yield surface may be well fitted by an isotropic stress theory of plasticity (where the loading function is dependent on the stress invariants only), to fit the initial and subsequent yield surfaces of the present study, the loading function of an anisotropic strain-hardening theory must be employed. Such a comparison with the mathematical theory of plasticity, though desirable, constitutes a formidable task and will not be attempted here.

As seen in Figs. 7 and 8, comparison of the elastic shear modulus (G_e) and the initial shear modulus at the initiation twist (G_i), reveal that they are essentially equal. In all cases (including the results of the four specimens not reported here), the percentage deviation between G_e and G_i is about 3 per cent or less. This result (i.e., $G_i = G_e$ during both loading and unloading), which is in agreement with that reported in (13, 14), supports the prediction of all initially isotropic incremental-strain theories of plasticity involving a smooth plastic potential. The difference in the values of G_i of the present paper and those given previously should be attributed to the character of the material employed in (7) which, as noted earlier, possessed a rather severe initial anisotropy.

Bibliography

1 "Über den Zusammenhang von Spannungen und Formaenderungen in Verfestigungsgebeit," by R. Schmidt, *Ingenieur-Archiv*, vol. 3, 1932, pp. 215–235.

2 "Relation of Experiments to Mathematical Theories of Plasticity," by D. C. Drucker, JOURNAL OF APPLIED MECHANICS, Trans. ASME, vol. 71, 1949, pp. 349–357.

3 "The Significance of the Criterion for Additional Plastic Deformation of Metals," by D. C. Drucker, *Journal of Colloid Science*, vol. 4, 1949, pp. 299–311.

4 "Mathematical Theory of Plasticity," by R. Hill, Clarendon Press, 1950.

5 "Some Extensions of Elementary Plasticity Theory," by F. Edelman and D. C. Drucker, *Journal of the Franklin Institute*, vol. 251, 1951, pp. 581–605.

6 "Fitting Mathematical Theories of Plasticity to Experimental Results," by F. D. Stockton and D. C. Drucker, *Journal of Colloid Science*, vol. 5, 1950, pp. 239–250.

7 "An Experimental Study of Biaxial Stress-Strain Relations in Plasticity," by P. M. Naghdi and J. C. Rowley, *Journal of the Mechanics and Physics of Solids*, vol. 3, 1954, pp. 63–80.

8 "Experiments Concerning the Yield Surface and the Assumption of Linearity in the Plastic Stress-Strain Relations," by P. M. Naghdi, J. C. Rowley, and C. W. Beadle, JOURNAL OF APPLIED MECHANICS, Trans. ASME, vol. 77, 1955, pp. 416–420.

9 "The Plastic Distortion of Metals," by G. I. Taylor and H. Quinney, Transactions of the Royal Society of London, series A, vol. 230, 1931, pp. 323–362.

10 "A Mathematical Theory of Plasticity Based on the Concept of Slip," by S. B. Batdorf and B. Budiansky, NACA TN 1871, 1949.

11 "Stress-Strain Relations, Uniqueness and Variational Theorems for Elastic-Plastic Materials With a Singular Yield Surface," by W. T. Koiter, *Quarterly of Applied Mathematics*, vol. 7, 1953, pp. 350–354.

12 "Plastic Stress-Strain Relations Based on Linear Loading Functions," by J. L. Sanders, Jr., Proceedings of the Second U. S. National Congress of Applied Mechanics, ASME, 1954, pp. 455–460.

13 "Experimental Studies of Polyaxial Stress-Strain Laws of Plasticity," by B. Budiansky, N. F. Dow, R. W. Peters, and R. P. Shepherd, Proceedings of the First U. S. National Congress of Applied Mechanics, ASME, 1951, pp. 503–512.

14 "An Experimental Investigation of Plastic Stress-Strain Relations," by J. L. Morrison and W. M. Shepherd, Proceedings of The Institution of Mechanical Engineers, vol. 163, 1950, pp. 1–9.

Effect of Finite Rotations on Gyroscopic Sensing Devices

By L. E. GOODMAN[1] AND A. R. ROBINSON,[2] MINNEAPOLIS, MINN.

The well-known noncommutativity of three-dimensional finite rotations has long been a curiosity in mechanics since, in actual solution of dynamical problems, the angular velocity, which is conveniently representable as a vector, plays a more natural role. In modern inertial guidance systems, however, the orientation of a body in space, i.e., a rotation, is of primary engineering interest. In this paper a simple method of determining orientation from the time history of three body components of angular velocity is developed by means of a new theorem in kinematics. As a special case of this theorem it is shown that a gyro subjected to a regime of rotations which returns it to the original space orientation will, in general, produce a residual signal. It will have experienced a nonzero and easily calculated mean angular velocity about its input axis. Some implications of the theorem for the design of inertial guidance systems and for the testing of gyros are discussed.

Introduction

THE modern gyroscope is a highly accurate means of sensing angular velocities. Its application in inertial guidance systems, where it is used to determine space orientations, imposes on the designer the necessity of insuring stability and sensitivity. In particular, translational motions such as linear vibration ought not induce any tendency for the axis of rotation (spin axis) of the instrument to change its spatial orientation. It was therefore a matter of interest when, during an investigation of the sources of vibration drift of single-degree-of-freedom integrating gyros,[3] it was noted that gyros mounted on the table of a commercial linear vibrator often exhibited abnormally high-drift rates at frequencies close to the resonances of the table supports. Even after a theory had been developed which correctly predicted the effect of the additional degrees of freedom arising from flexibility of the gyro parts, the abnormal drift rates at the frequencies just mentioned were not accounted for.

In an effort to bring these exceptional cases within the scope of a dynamical theory, the table motions were measured carefully. It was found that at the particular frequencies in question the table motion consisted of a slight wobble superposed on and co-periodic with the expected linear motion. The noncommutativity of finite rotations suggested that a three-dimensional rotational motion which returned a single-degree-of-freedom gyro to its original orientation might produce a residual signal, that is, an apparent drift. This, it developed, is the correct explanation. The anomalous drift is explained completely and its magnitude determined by means of a kinematical theorem developed in the next section. This effect is basically geometric and would be present even in a theoretically perfect instrument; it is, however, in practice, modified by the details of the way in which the motion of the outer case is transmitted to the gimbal. Since the effect of "conical motion," as this wobble has been termed, cannot be designed out of the instrument, it necessarily must be considered in the design of inertial guidance systems as well as in gyro testing. Some of these considerations are discussed in the last section of this paper.

A Kinematical Theorem

Consider a rigid body moving in any manner whatever. The motion may be specified by describing the motion of any point O, fixed in the body, and the rotations about O. In this paper, translational motions will not be of concern, so that one may think of the point O as fixed in space. We now restrict the motion, temporarily, by the following two conditions:

1 Some line OX, fixed in the body, returns at time T to the orientation it had at time zero. As a consequence, the cone generated by the line OX as time increases from zero to T intersects a fixed reference sphere of unit radius, centered on O, in a closed curve C.

2 The curve C is restricted to be a simple closed curve with continuously turning tangent.

Motions of this type will be termed "complete conical motions of OX." The theorem to be developed will first be proved for complete conical motions. Next, condition 2 will be weakened so that the theorem will be established for any physically realizable motion satisfying condition 1. Finally, the theorem will be extended so as to remove the necessity for the axis OX to return to its original orientation.

The position of a body after an axis OX has undergone a complete conical motion can be reached from its original position by at most a rotation of some amount Θ about OX. At any time t, the angular velocity vector $\omega(t)$ of the rigid body has a component ω_x along the instantaneous direction of OX. If A is the area on the sphere enclosed by the curve C, we assert that

$$\Theta = \int_0^T \omega_x dt + A \pm 2m\pi \quad \ldots\ldots\ldots\ldots [1]$$

where T, as defined above, is the total time for the complete conical motion, and m is an integer. The sense of rotation corresponding to the positive sign of Θ is to be given by the right-hand convention, with the thumb extending along the initial position of OX. The area A will be taken as positive if the orthogonal triad consisting of the outward normal to the sphere, the tangent to C in the direction of motion, and the normal to C directed toward the interior of A is right-handed. Actually, it is im-

[1] Professor of Mechanics, University of Minnesota. Mem. ASME.

[2] Assistant Professor, Department of Mechanics and Materials, University of Minnesota. Assoc. Mem. ASME.

[3] This investigation has been carried out in the Gyro Design and Development Section, Aeronautical Division, Minneapolis-Honeywell Regulator Company, under the supervision of J. W. Lower. The original suggestion which prompted the study of finite rotations described here, was made by S. L. Burgwin.

Contributed by the Applied Mechanics Division and presented at the Annual Meeting, New York, N. Y., December 1–6, 1957, of The American Society of Mechanical Engineers.

Discussion of this paper should be addressed to the Secretary, ASME, 29 West 39th Street, New York, N. Y., and will be accepted until July 10, 1958, for publication at a later date. Discussion received after the closing date will be returned.

Note: Statements and opinions advanced in papers are to be understood as individual expressions of their authors and not those of the Society. Manuscript received by ASME Applied Mechanics Division, January 11, 1957. Paper No. 57—A-30.

material which of the two areas separated by the curve C is considered as A, since they differ by a multiple of 2π, taking account of the foregoing sign convention.

The assertion embodied in Equation [1] may be proved as follows: Consider a point $B(t_1)$ on the path C; that is to say, OX passes through B at time t_1. In some short time dt, the arc BB' is traversed. At any point on the path C, the vector tangent to C, and thus tangent to the sphere as well, is parallel to some line OP lying in the plane perpendicular to OX. Let OY be another line in this plane, fixed with respect to the body as shown in Fig. 1. Take OP as that line in the plane perpendicular to OX which is parallel to the tangent to C at $B(t_1)$. At time $t_1 + dt$,

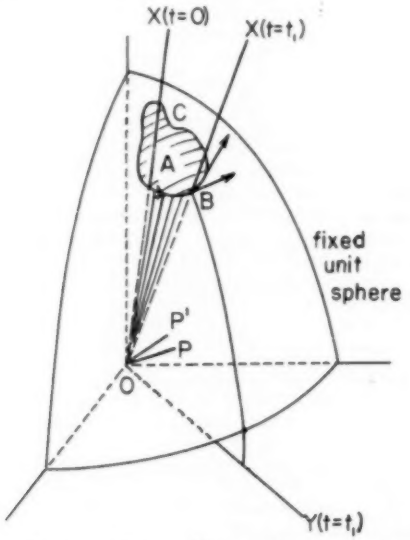

FIG. 1 COMPLETE CONICAL MOTION WITH RESPECT TO OX

the tangent vector at B' is parallel to OP' which lies in the plane of OP and OY. The line OY rotates through the angle $\omega_x dt$ with respect to OP in the time interval dt. But the tangent to C also changes direction in the interval dt by an amount equal to the angle between OP and OP'. This angle is equal to the angle between the great circle tangent to C at B and the great circle tangent at B', therefore equal to the geodesic curvature of C at some point on the arc BB' multiplied by the arc length ds. It can be seen then, that the line OY, fixed in the body, has rotated an amount $\omega_x dt - k_g ds$ with respect to the tangent to C, where k_g is the geodesic curvature of C. The infinitesimal rotation in question is the relative rotation of two lines. Such increments may be added algebraically since they represent rotations in a plane. Integrating over a complete cycle of motion, that is, from time zero to time T, one finds that a line fixed in the body and perpendicular to OX rotates an amount

$$\int_0^T \omega_x dt - \int_C k_g ds$$

relative to the tangent to C, drawn at the (moving) point where OX cuts the sphere. But, since the sphere and the curve C are fixed in space, the vector tangent to C has regained its initial orientation in space at the end of a complete conical motion. Therefore the angle Θ is given, up to a complete rotation, by the relative motion of OY and the tangent to C

$$\Theta = \int_0^T \omega_x dt - \int_C k_g ds \pm 2m'\pi \quad \ldots\ldots\ldots [2]$$

However, the line integral of the geodesic curvature around a simple closed curve with continuously turning tangent is related to the surface integral of the Gaussian curvature of the surface taken over the area A enclosed by the curve by means of the Gauss-Bonnet theorem (1)[4]

$$\int_C k_g ds + \int_A K\, d\sigma = 2\pi \quad \ldots\ldots\ldots\ldots [3]$$

where K is the Gaussian curvature, $+1$ for the present case of a unit sphere, and $d\sigma$ is an element of area on the sphere. Eliminating $\int_C k_g ds$ between Equations [2] and [3], we arrive at an expression for Θ

$$\Theta = \int_0^T \omega_x dt + A - 2\pi \pm 2m'\pi$$

which is equivalent to Equation [1]. This completes the proof of the restricted theorem.

The condition 2 given at the beginning of this section may be lightened first by allowing the simple closed curve C to have a finite number of corners, of exterior angle ψ_i, $i = 1, 2, \ldots j$. In the proof, Equation [2] must be modified to read

$$\Theta = \int_0^T \omega_x dt - \sum_{i=1}^{j} \int_{C_i} k_g ds - \sum_{i=1}^{j} \psi_i$$

where C_i is the smooth segment of C terminated by the ith corner. The Gauss-Bonnet theorem, however, must be altered in exactly the same way if C has corners; that is

$$\sum_{i=1}^{j} \int_{C_i} k_g ds + \sum_{i=1}^{j} \psi_i + \int_A K\, d\sigma = 2\pi$$

The expression for Θ in terms of the area is then unchanged. The theorem can be extended next to the case in which C is any rectifiable closed curve (with a finite number of corners) which intersects itself a finite number of times, instead of being a simple closed curve. If the circuit starts at some point E of the curve C, we proceed until the curve intersects the portion already traced out. At the point of intersection the axis OX has just undergone a complete conical motion. The area enclosed by the loop is found and then the loop is imagined to be erased. Upon the next intersection with the portion of C already traversed, we again have gone around a simple closed curve in one direction, and again can find the corresponding area. Continuing in this fashion, eventually we return to E, thereby completing another simple closed curve. The areas of the loops should be calculated with their correct signs and their sum used in Equation [1], in view of the discussion preceding Equation [2].

We may recapitulate the theorem as thus far developed as follows:

If a rigid body is rotated about a fixed point O in such a way that an axis OX returns to its original direction at time T, at that time the body has been rotated about OX through an angle given by the expression

$$\Theta_x = \int_0^T \omega_x dt + A_x \pm 2m\pi$$

where m is an integer, possibly zero, $\omega_x(t)$ is the component of angular velocity along OX, and A_x is the area intercepted on a fixed unit sphere centered on O by the cone which OX generates. The subscripts on Θ and A are inserted to prevent confusion when conical motions of more than one line in the same body are considered.

[4] Numbers in parentheses refer to the Bibliography at the end of the paper.

Extension of the result to the case in which OX does not return to its original orientation is effected by imagining added to the curve C, at any instant, a closure arc selected in a convenient way. The closure is by means of the circular arc (not in general a great circle) corresponding to that simple rotation about one axis which would return every line in the body to its primitive orientation. The existence of such a rotation is assured by Euler's theorem of kinematics. In this rotation, the components of angular velocity about any lines fixed in the body, say three orthogonal body axes, x, y, z, of which x is OX, remain in the same ratio. One then can speak meaningfully of the components of the simple rotation, for the time integrals of ω_x, ω_y, and ω_z will depend only on the total rotation and the direction cosines of the axis of rotation referred to the x, y, and z-axes, and not on the time history of the rotation.

The instantaneous orientation of the entire body can be reached from the position at time zero by a simple rotation with components $\varphi_x(t)$, $\varphi_y(t)$, $\varphi_z(t)$. If we imagine the curve C closed by the inverse of this rotation, we have from the theorem as stated previously

$$0 = \int_0^t \omega_x dt - \varphi_x + A_x \pm 2m\pi \ldots\ldots\ldots [4]$$

since $\Theta_x = 0$. Similar expressions hold with subscripts y and z. Here A_x is, of course, a function of time; the area in question is obtained by closing the curve in the manner specified. From Equation [4] we have immediately

$$\varphi_x = \int_0^t \omega_x dt + A_x \pm 2m\pi \ldots\ldots\ldots [5]$$

This completes the kinematical theorem.

It is interesting to note that if Equation [5] be differentiated with respect to time, we have

$$\frac{d\varphi_x}{dt} = \omega_x + \frac{dA_x}{dt} \ldots\ldots\ldots [6]$$

This expression may be compared with advantage to the corresponding form which arises when one computes the time rate of change of the angular momentum of a rigid body rotating about a point, as one does in a standard derivation of Euler's equation of motion (2). The unexpected areal velocity on the right-hand side of Equation [6] corresponds to the cross product of the angular velocity and the angular momentum in this analogy.

The generality of the foregoing theorem, referring as it does to any rotational motion of a rigid body, has led us to a search for precedents in the literature. The theorem is not to be found in the Koenigs' treatise on kinematics (3) or in the well-known treatises by Whittaker (4), by Klein and Sommerfeld (5), and by Appell (6). A restricted form, $\omega_z = 0$, C a closed curve, was known to Hamilton (7). His proof is quite different from the one given in this paper. Possibly owing to the special nature of the motion he postulated, or to the difficulty of extending his method of proof, this result seems not to have received very wide attention. Hamilton's special case is mentioned by Thomson and Tait (8) and by Lamb (9).

A very simple example may serve to illustrate the meaning of Equation [1]. Consider a rigid body rotating about an axis OZ. We concentrate our attention upon a line OX fixed in the body and making an angle β with OZ. As the body executes a complete rotation about OZ, the line OX traces out a circle on the fixed reference sphere. The quantity ω_z is simply $|\omega| \cos \beta$, since the angle β remains constant. In the complete conical motion of OX

$$\int_0^T \omega_z dt = 2\pi \cos \beta$$

But we recognize that every line in the body has returned to its original orientation after the complete rotation about OZ. In other words, $\Theta_z = 0$, or a multiple of 2π. The difference between Θ_z and

$$\int_0^T \omega_z dt$$

is exactly the area of the spherical cap on the reference sphere bounded by the circle which was swept out by OX.

$$A_z = 2\pi(1 - \cos \beta)$$

Small Angle Approximations

The major applications of the foregoing theorem will be to those cases in which the colatitude of any point on C, taking the original position of OX as the radius through the north pole of the reference sphere, is a small angle. If we denote the colatitude by β, and the azimuth angle from some reference meridian by θ, the proper element of area on the unit sphere is $\sin \beta \, d\beta \, d\theta$. For small β a simple approximation which gives the area with a relative error of the order of β^2 will prove to be extremely accurate as well as convenient to use.

As explained in the previous section, at any point B on the curve C there is a simple rotation with components φ_x, φ_y, φ_z such that the position of the body at point B can be reached from its initial position by means of this rotation. The magnitude of the rotation is

$$(\varphi_x^2 + \varphi_y^2 + \varphi_z^2)^{1/2} = \Phi$$

and the direction cosines of the axis of rotation are l, m, n, with respect to x, y, z-axes fixed in the body. The values of l, m, and n are given by φ_x/Φ, φ_y/Φ, and φ_z/Φ, respectively. We take the x-axis as OX.

It can be shown in a straightforward manner[5] that

$$\cos \beta = \cos \Phi + l^2(1 - \cos \Phi)$$

from which it follows that

$$\sin (\beta/2) = (m^2 + n^2)^{1/2} \sin (\Phi/2)$$

If β is approximated by

$$(m^2 + n^2)^{1/2} \Phi$$

which we will call γ, then β will be overestimated, with a relative error of the order of β^2. Instead of using $\sin \gamma \, d\gamma \, d\theta$ as the element of area, we use $\gamma \, d\gamma \, d\theta$, again entailing an overestimate with a relative error of the order of β^2. What has been done is simply to consider circular arcs to be straight lines, and the sphere to be a plane in the vicinity of the north pole.

The equation of the curve C may be written as $\gamma = \gamma(\theta)$, and the area A_z is then

$$\frac{1}{2} \int_{\theta_0}^{\theta(t)} \gamma^2 d\theta$$

By means of Green's theorem in the plane, one can obtain a more convenient expression in the form

$$A_z = \frac{1}{2} \int_{B_0}^{B(t)} (\varphi_y d\varphi_z - \varphi_z d\varphi_y) \ldots\ldots\ldots [7a]$$

or

$$A_z = \frac{1}{2} \int_0^t \left(\varphi_y \frac{d\varphi_z}{dt} - \varphi_z \frac{d\varphi_y}{dt} \right) dt \ldots\ldots\ldots [7b]$$

where the line integrals are taken along the curve C. Similar

[5] See, for instance, reference (4), p. 7.

expressions for A_y and A_z can be written by cyclically interchanging the subscripts. Equation [7a] can be combined with Equation [5] to give the final form of the approximation

$$\varphi_x = \int_0^t \omega_x dt + \frac{1}{2}\int_{B_0}^{B(t)} (\varphi_y d\varphi_z - \varphi_z d\varphi_y) \quad [8]$$

again with two similar expressions obtained by cyclic replacement of the subscripts.[6]

In particular, if the motion is a small wobble

$$\varphi_y = \alpha_y \sin(\lambda t - \delta), \quad \varphi_z = \alpha_z \sin(\lambda t)$$

the wobbling plane being perpendicular to OX, the area A_x (per cycle) is given by

$$A_x = \pi \alpha_y \alpha_z \sin \delta \quad [9]$$

Applications of the Theorem: Conclusions

In discussing the application of the kinematical theorem to the interpretation of gyro vibration tests, we consider first the single-degree-of-freedom "integrating" or "rate" gyro in conjunction with a tight servo loop which provides a restoring torque on the gimbal to keep it at rest relative to the case of the instrument. This torque is the output of the instrument. The essential reference axes of a single-degree-of-freedom gyro are the spin axis, the output axis, about which the gimbal can rotate, and the input axis perpendicular to these two. We identify the input axis with the line OX of the kinematical theorem, since it is the component of angular velocity along the input axis which is proportional to the output torque. Now suppose the gyro to be mounted on the table of a commercial vibrator which subjects it to a harmonic motion which is primarily a straight-line displacement in the plane of the input and spin axes. If, however, a slight wobble is superposed on the primary displacement, a conical motion of the input axis will ensue. In our observation this happens only at frequencies near the natural frequencies of the table supports. Since at the end of every cycle of motion all axes return to their original spatial orientations, $\Theta_x = 0$. But if the table rotations which comprise the wobble are out of phase, i.e., not a simple rocking, the area A_x will be different from zero and the gyro will record an ω_x necessary to satisfy Equation [1] with $m = 0$. That is, there will be an output torque corresponding to an apparent drift rate of A_x/T radians per second. For a perfect gyro this would be the only net drift observed. In practice, other vibrational effects, such as those due to compliance, are present. To obtain a proper measure of the performance of the gyro under vibration, the conical motion drift torque should be subtracted from the observed output torque. In test applications vibrators should be, as nearly as possible, free of conical motion.

Gyros are also used "open-loop"; that is, without a servo. In this application the restraining torque is provided by the medium which connects the gimbal to the case and some relative displacement must occur. In fact, this relative displacement is then the output of the gyro. If the interconnection is elastic, the instrument is said to be a rate gyro; if highly viscous it is an integrating gyro.

In interpreting open-loop vibration tests it must be remembered that the input axis is fixed in the gimbal and not in the case. The angular motions of the case being given, it is not difficult to compute those of the gimbal, although this computation will be different for different types of gyros. For high frequencies of vibration, the gimbal cannot rotate fast enough to follow the case, and the area A_x generally will be less than it would be in the closed-loop application.

One type of inertial guidance system employs three single-axis gyros with three mutually orthogonal input axes, all mounted on a platform. The platform can experience conical motion if that motion is faster than the response time of the system. The input axes of the roll, pitch, and yaw gyros can be considered the x, y, z-axes of the platform. If, as is common, the system is designed so as to restore

$$\int_0^t \omega_x dt, \quad \int_0^t \omega_y dt, \quad \text{and} \quad \int_0^t \omega_z dt$$

to zero, A_x, A_y, and A_z, in general, will not vanish at all time t. In view of Equation [5] this means that the guidance system will be deceived into changing the spatial orientation of the platform. For example, consider a vehicle in horizontal flight in an easterly direction. If the yaw axis undergoes uncorrected conical motion in the positive sense, the input axis of the yaw gyro sweeping out a circular cone whose half vertical angle is 10 milliradians, at the rate of 10 cps, the vehicle will veer northward at the rate of 0.18 deg/sec, according to Equation [9]. This rate of deviation is, of course, proportional to the square of the vertical angle and to the first power of the frequency. This effect can be mitigated somewhat by designing the platform shock mounts so as to isolate the platform from high-frequency conical motions.

[6] The Expression [8] appears in reference (10). In this reference, a second-order approximation is used from the start. The foregoing derivation shows that Equation [8] is, in fact, the correct third-order approximation (in β), since the area itself is second-order in β, and the relative error in the area is also second-order in β.

BIBLIOGRAPHY

1 "Differential Geometry," by D. J. Struik, Addison-Wesley, Cambridge, Mass., 1950, pp. 153–159.

2 "Principles of Mechanics," by J. L. Synge and B. A. Griffith, McGraw-Hill Book Company, Inc., New York, N. Y., second edition, 1949, pp. 351–352.

3 "Leçons de Cinématique," by G. X. P. Koenigs, A. Hermann, Paris, France, 1897.

4 "Analytical Dynamics," by E. T. Whittaker, Dover Publications, New York, N. Y., fourth edition, 1944.

5 "Über die Theorie des Kreisels," by F. Klein and A. Sommerfeld, Teubner, Leipzig, 1897–1910.

6 "Traité de Mécanique Rationelle," by P. Appell, Gauthier-Villars, Paris, France, sixth edition, vol. 2, 1953.

7 "Lectures on Quaternions," by W. R. Hamilton, Hodges & Smith, Dublin, Ireland, 1853, pp. 338–340.

8 "Treatise on Natural Philosophy," by Lord Kelvin (W. Thomson) and P. G. Tait, Cambridge University Press, Cambridge, England, Part I, 1896, p. 75.

9 "Higher Mechanics," by H. Lamb, Cambridge University Press, Cambridge, England, second edition, 1929, pp. 7–11.

10 "The Angular Displacement Vector," by M. B. Trageser, unpublished Document E-413, Massachusetts Institute of Technology, Instrumentation Laboratory, Cambridge, Mass., June, 1954.

Torsion of Cylindrical and Prismatic Bars in the Presence of Steady Creep[1]

By S. A. PATEL,[2] B. VENKATRAMAN,[3] AND P. G. HODGE, JR.,[4] BROOKLYN, N. Y.

This paper is concerned with the steady creep behavior of cylindrical and prismatic bars in which the deformations are caused by pure torsion. The creep problem is first reduced to one in nonlinear elasticity by means of the elastic analog. The elastic analysis is then carried out by means of the principles of minimum energies. These principles yield upper and lower bounds on the angle of twist. Closed-form solutions also are presented for some cross sections.

Introduction

IN A structure subject to creep, in general the strain is a function of time, stress, temperature, total deformation, and aftereffects. The experimental laws governing this relationship are far too complicated to lend themselves to easy analytical treatment of the creep problem in engineering structures. Moreover, a physical description of the phenomena which cause creep is many-sided. From a practical standpoint, it is too complex to be of much use at present. Finally, the creep properties of engineering materials are extremely sensitive to small changes in the temperature and the stresses, and creep experiments show considerable scatter.

A good portion of the creep data available relates to the secondary or steady phase (1)[5] and is based on tension tests at constant temperature and constant stress. Hoff (2) has shown that when creep strains of the order of magnitude of 1 or 2 per cent develop during the lifetime of a structure, it is often permissible to disregard the primary phase of the creep deformations. The tertiary phase may be due to changes in the material properties and often failure occurs when this phase is reached. Marin and Cuff (3) have investigated the creep characteristics of circular tubes subjected to torsion. Using the constants obtained in tension tests, they have shown that the theoretical predictions of steady creep in torsion are in good agreement with experimental results. Thus the assumption of steady creep may provide relatively simple analytical methods of predicting the deformations developed during the lifetime of engineering structures subjected to twisting moments. The velocity of deformation may be assumed to be independent of time if the elastic deformations and the primary creep deformations are considered negligible compared to the secondary creep deformations.

It was first observed by Hoff (2) that a steady creep problem is reduced to an analogous problem in nonlinear elasticity if the strain rates are replaced by strains. This will be reviewed briefly in the next section. This analog has been used previously in the analysis of trusses, rigid frames, and a thick-walled tube under internal pressure (4, 5, 6).

The elastic analog is used in the third section, and two approximate methods of solution are presented for the torsion of uniform bars of arbitrary cross sections. The methods are based on the principles of minimum potential energy and minimum complementary potential. In the succeeding section, the use of these methods is demonstrated in the solutions for cylindrical and prismatic bars having circular and triangular cross-sectional shapes and that of a regular polygon. Finally, the conclusions are summarized in the last section.

Elastic Analog for Steady Creep

The creep behavior of a specimen subjected to simple tension is assumed to be governed by the relation

$$\dot{\epsilon} = (\sigma/\lambda)^n \quad [1]$$

Here λ and n are material constants which depend upon the temperature, $\dot{\epsilon}$ is the strain rate, and σ the stress. It is further assumed that n is an odd integer, so that Equation [1] is valid for both tensile and compressive creep. As Hoff (2) first observed, Equation [1] is mathematically identical with the nonlinear stress-strain relation

$$\epsilon = (\sigma/\lambda)^n \quad [2]$$

where λ and n have the same values as in Equation [1], and ϵ and σ are the strain and stress, respectively. The solution of the creep problem and the elastic problem will be formally identical if the stress boundary conditions of the former are transferred to the latter, and the prescribed velocities are replaced by the numerically equal prescribed displacements. Once the elastic problem is solved, the stresses and strain rates of the creep problem are known immediately.

The present paper is concerned with the pure torsion of bars made of a material which is governed by Equation [1]. For the corresponding elastic problem, it is necessary to establish a stress-strain relation governing the general three-dimensional state of stress. Furthermore, to be consistent, this general relationship should reduce to Equation [2] in the uniaxial case. Based upon Prager's (7) general formulation, for an incompressible material the simplest such relation may be written

$$\epsilon_{ij} = CJ_2^m s_{ij} \quad [3a]$$

Here ϵ_{ij} is the strain tensor, and s_{ij} the stress-deviation tensor defined by[6]

---

[1] The results presented in this paper were obtained in the course of research sponsored by the Office of Naval Research.

[2] Research Assistant Professor of Aeronautical Engineering, Polytechnic Institute of Brooklyn.

[3] Research Associate, Polytechnic Institute of Brooklyn.

[4] Professor of Applied Mechanics, Polytechnic Institute of Brooklyn; now at Illinois Institute of Technology, Chicago, Ill. Mem. ASME.

[5] Numbers in parentheses refer to Bibliography at end of paper.

Contributed by the Applied Mechanics Division and presented at the Annual Meeting, New York, N. Y., December 1–6, 1957, of The American Society of Mechanical Engineers.

Discussion of this paper should be addressed to the Secretary, ASME, 29 West 39th Street, New York, N. Y., and will be accepted until July 10, 1958, for publication at a later date. Discussion received after the closing date will be returned.

Note: Statements and opinions advanced in papers are to be understood as individual expressions of their authors and not those of the Society. Manuscript received by ASME Applied Mechanics Division, March 8, 1957. Paper No. 57—A-27.

[6] Latin letters used as subscripts take on the values 1, 2, or 3. A repeated subscript is to be summed from 1 to 3. The Kronecker delta δ_{ij} is equal to 1 if $i = j$, 0 if $i \neq j$. Thus Equation [3b] stands for three relations of the type

$$s_{11} = \sigma_{11} - (1/3)(\sigma_{11} + \sigma_{22} + \sigma_{33}) = (1/3)(2\sigma_{11} - \sigma_{22} - \sigma_{33})$$

and six symmetric relations of the type $s_{12} = \sigma_{12}$.

$$s_{ij} = \sigma_{ij} - (1/3)\,\sigma_{kk}\hat{\delta}_{ij} \quad [3b]$$

J_2 is the second invariant of the stress-deviation tensor

$$J_2 = (1/2)s_{ij}s_{ij} \quad [3c]$$

and m and C are material constants. In the case of uniaxial tension in the x_1-direction Equations [3] reduce to

$$\epsilon_{11} = C(\sigma_{11}^2/3)^m(2\sigma_{11}/3) = (2C/3^{m+1})\,(\sigma_{11})^{2m+1} \quad [4]$$

A comparison of Equations [2] and [4] then shows that

$$\left.\begin{aligned} 2m &= (n-1) \\ 2C &= \frac{3^{(n+1/2)}}{\lambda^n} \end{aligned}\right\} \quad [5]$$

The solution of the nonlinear elastic problem of a structure obeying the stress-strain law of Equation [3] is identical to the solution of the steady creep problem of the same structure subject to the same forces obeying the law

$$\dot{\epsilon}_{ij} = CJ_2^m s_{ij} \quad [6]$$

where $\dot{\epsilon}_{ij}$ is the time rate of change of the strain tensor. Hence once the elastic problem is solved, the stresses and the velocities of deformation in the creep problem are known immediately. If, as will be assumed, the temperature and the applied forces do not vary with time, Equation [6] may be trivially integrated to obtain the creep strain as a linear function of time. The critical time at which any given displacement first reaches its maximum value may then be found.

With the elastic analog as basis, the remainder of the paper will discuss cylindrical and prismatic bars subject to pure torsion and obeying the nonlinear elastic law of Equation [3]. As in linear elasticity, the general form of the mathematical expressions for displacement or stress components, including arbitrary functions or parameters, is assumed. These are then determined by the use of the principles of minimum potential energy and minimum complementary potential. These principles are known to be valid for a nonlinear stress-strain law (8, 9, 10).

Energy Solutions

The mathematical analysis of a typical problem in the theory of elasticity leads to a system of partial differential equations for the stress or displacement components with appropriate boundary conditions. It is not always possible to solve these equations by a direct procedure. For instance, the stress-strain relations of Equation [3] in general would lead to a system of highly nonlinear differential equations not easy of solution. In such cases it is common practice to adopt an alternative analysis based on the minimum-energy principles and obtain approximate solutions. To this end it is necessary to know the energies stored in a unit volume of the material obeying the stress-strain law of Equation [3].

It follows from Equation [3] that the incremental strain energy dU_s and the incremental complementary energy dU_c per unit volume may be written

$$\left.\begin{aligned} dU_s \equiv \sigma_{ij}d\epsilon_{ij} &= s_{ij}d\epsilon_{ij} = C[J_2^m dJ_2 + 2J_2 dJ_2^m] \\ &= C(2m+1)J_2^m dJ_2 \\ dU_c \equiv \epsilon_{ij}d\sigma_{ij} &= \epsilon_{ij}ds_{ij} = CJ_2^m dJ_2 \end{aligned}\right\} \quad [7]$$

Integration of the incremental energies leads to the following total energies per unit volume in terms of either the stress invariant J_2 or the strain invariant

$$I_2 = (1/2)\,\epsilon_{ij}\epsilon_{ij} \quad [8]$$

$$\left.\begin{aligned} U_s &= C\,\frac{2m+1}{m+1}\,J_2^{m+1} = \frac{2m+1}{m+1}\,(I_2^{m+1}/C)^{1/(2m+1)} \\ U_c &= \frac{C}{m+1}\,J_2^{m+1} = \frac{1}{m+1}\,(I_2^{m+1}/C)^{1/(2m+1)} \end{aligned}\right\} \quad [9]$$

The total potential Π_s and total complementary potential Π_c are given by

$$\left.\begin{aligned} \Pi_s &= \int_V U_s dV - \int_{S_T} T_i u_i dS - \int_V f_i u_i dV \\ \Pi_c &= \int_V U_c dV - \int_{S_u} T_i u_i dS \end{aligned}\right\} \quad [10]$$

Here S_u represents that portion of the surface on which either the displacements u_i are prescribed or the corresponding tractions T_i are zero; S_T represents that portion over which either the tractions T_i are prescribed or the corresponding displacements u_i are zero, and f_i is the body force vector.

The principle of minimum potential energy then states that among all displacement fields u_i^* which satisfy the boundary conditions on displacement the actual one minimizes Π_s. Similarly, the principle of minimum complementary energy states that among all equilibrium stress fields σ_{ij}° which satisfy the boundary conditions on tractions the actual one minimizes Π_c. In other words, if Π_s^* and Π_c° are defined by

$$\left.\begin{aligned} \Pi_s^* &= \frac{2m+1}{m+1}\,\frac{1}{C^{1/(2m+1)}}\int_V (I_2^*)^{(m+1)/(2m+1)}dV \\ &\quad - \int_{S_T} T_i u_i^* dS - \int_V f_i u_i^* dV \\ \Pi_c^\circ &= [C/(m+1)]\int_V (J_2^\circ)^{m+1}dV - \int_{S_u} T_i^\circ u_i dS \end{aligned}\right\} \quad [11]$$

then

$$\Pi_s \le \Pi_s^*, \quad \Pi_c \le \Pi_c^\circ \quad [12]$$

Finally, for the actual state it is readily verified that

$$\Pi_s + \Pi_c = 0 \quad [13]$$

Therefore Equations [11] and [12] may be combined to yield upper and lower bounds on either of the total potentials

$$-\Pi_c^\circ \le -\Pi_c = \Pi_s \le \Pi_s^* \quad [14]$$

The expressions for the energies may now be used to obtain exact and approximate solutions of particular problems. In the case of Saint Venant torsion the foregoing equations may be considerably simplified. As in linear torsion it is assumed that the displacement field consists of a pure rotation about the axis plus a uniform warping. Thus if the z or x_3-axis is chosen parallel to the generators of the bar

$$u = u_1 = -\alpha zy, \quad v = u_2 = \alpha zx, \quad w = u_3 = \alpha\varphi(x, y) \quad [15]$$

where α is the angle of twist per unit length. It then follows from Equations [3] that all stress and strain components vanish except

$$\left.\begin{aligned} 2\epsilon_{13} = 2\epsilon_{31} &= \gamma_x = \alpha(\partial\varphi/\partial x - y) \\ 2\epsilon_{23} = 2\epsilon_{32} &= \gamma_y = \alpha(\partial\varphi/\partial y + x) \\ s_{13} = s_{31} &= \tau_x(x, y), \quad s_{23} = s_{32} = \tau_y(x, y) \end{aligned}\right\} \quad [16]$$

Two of the three equilibrium equations are satisfied identically while the remaining one is satisfied by the introduction of a stress function ψ defined by

$$\tau_x = \partial\psi/\partial y, \quad \tau_y = -\partial\psi/\partial x \quad [17]$$

The stress deviation and strain invariants then become

$$\left.\begin{aligned} J_2 &= \tau_x^2 + \tau_y^2 = (\partial\psi/\partial x)^2 + (\partial\psi/\partial y)^2 \\ I_2 &= (1/4)(\gamma_x^2 + \gamma_y^2) = (\alpha/2)^2\,[(\partial\varphi/\partial x - y)^2 \\ &\qquad + (\partial\varphi/\partial y + x)^2] \end{aligned}\right\} \quad \ldots [18]$$

Equations [11] for the energies may now be evaluated. The lateral surfaces of the cylinder are free from tractions, and there are no body forces. The end surfaces are of the type S_u, and the total work done is equal to $T\alpha L$ where T is the applied torque and L the length of the cylinder. Therefore

$$\left.\begin{aligned} \Pi_c^* &= \frac{2m+1}{m+1}\,\frac{L}{C^{1/(2m+1)}}\int_A (J_2^*)^{(m+1)/(2m+1)}dA \\ \Pi_c^\circ &= L\left\{[C/(m+1)]\int_A (J_2^\circ)^{m+1}dA - T^\circ\alpha\right\} \end{aligned}\right\} \quad \ldots [19]$$

where T° is defined by

$$T^\circ = 2\int_A \psi^\circ dA \quad \ldots [20]$$

The application of the principle of minimum complementary energy will be discussed first. Let ψ° be any fixed function which satisfies the boundary condition $\psi^\circ = 0$ on the boundary of the cross section, and consider the family of solutions $k\psi^\circ$. If $k = k^\circ$ is determined so as to minimize Π_c°, it is found that

$$k^\circ = \left[\frac{\alpha}{C}\,\frac{\int_A \psi^\circ dA}{\int_A (J_2^\circ)^{m+1}dA}\right]^{1/(2m+1)} \quad \ldots [21]$$

Substitution of Equation [21] into Equations [20] and [19] then yields

$$T^\circ = 2\left(\frac{\alpha}{C}\right)^{1/(2m+1)}\frac{[\int\psi^\circ dA]^{(2m+2)/(2m+1)}}{[\int (J_2^\circ)^{m+1}dA]^{1/(2m+1)}} \quad \ldots [22]$$

$$\Pi_c^\circ = -T^\circ L\alpha(2m+1)/(2m+2) \quad \ldots [23]$$

Equations [23] and [14] show that the torque for a given angle of twist computed for an arbitrary function ψ° is equal or less than the actual torque for the same angle of twist.

Equation [23] is a valid relationship for any function ψ°. In particular, it is valid for the actual stress function ψ. Therefore it follows from Equations [13] and [23] that the total potential energy is given by

$$\Pi_c = -\Pi_c = TL\alpha(2m+1)/(2m+2) \quad \ldots [24]$$

Equation [24] is now taken as the definition of the torque T^* to be associated with an arbitrary warping function φ^*

$$T^* = \frac{2m+2}{2m+1}\,\frac{\Pi_c^*}{L\alpha} = \left(\frac{\alpha}{2C}\right)^{1/(2m+1)} \int[(\partial\varphi^*/\partial x - y)^2 + (\partial\varphi^*/\partial y + x)^2]^{(m+1)/(2m+1)}dA \quad \ldots [25]$$

It then follows from Equation [14] that the torque for a given angle of twist computed from Equation [25] with an arbitrary function φ^* is equal to or greater than the actual torque for the same angle of twist.

The conclusions of the minimum principles are stated in terms of torque for a prescribed angle of twist. For application to the creep problem, it is more convenient to express them in terms of bounds on the angle of twist for an assumed torque. Now, Equations [22] and [25] define T° and T^* as increasing monotonic functions of α, and the actual torque T must be an increasing monotonic function of α located between these two. This situation is indicated schematically in Fig. 1. It is evident from Fig. 1 that, if the torque is prescribed, the corresponding angles of twist will satisfy

$$\alpha^* \leq \alpha \leq \alpha^\circ \quad \ldots [26]$$

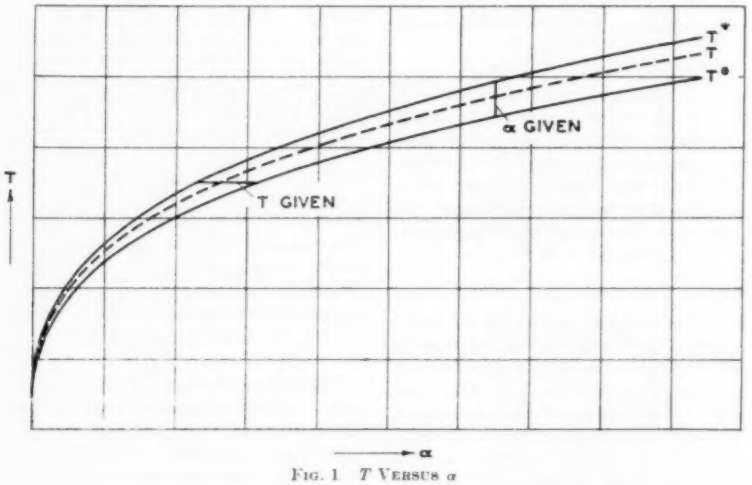

FIG. 1 T VERSUS α

where

$$\left.\begin{aligned} \alpha^* &= 2C\left\{T/\int[(\partial\varphi^*/\partial x - y)^2 + (\partial\varphi^*/\partial y + x)^2]^{(m+1)/(2m+1)}dA\right\}^{2m+1} \\ \alpha^\circ &= C(T/2)^{2m+1}\,\frac{\int[(\partial\psi/\partial x)^2 + (\partial\psi/\partial y)^2]^{m+1}dA}{[\int\psi dA]^{2m+2}} \end{aligned}\right\} \quad \ldots [27]$$

The application of these principles to circular and polygonal sections will be indicated in the next section.

EXAMPLES

The first example considered in this section is a circular cylindrical bar. Owing to the applied twisting moment, the generators of the cylinder will be deformed into helical curves. It is assumed, based on the known results of linear elasticity and rigid plasticity, that plane sections normal to the z-axis will remain

plane after deformation. Certainly this hypothesis can be used in conjunction with the principle of minimum potential energy, and it will be shown that it does, in fact, lead to the correct solution. In any event, if an approximate warping function is defined by

$$\varphi^* = 0 \quad [28]$$

it then follows from Equation [27] that the relation between the angle of twist and the applied torque is

$$\alpha^* = \frac{2C}{a}\left[\frac{3m+2}{3m+1}\frac{T}{\pi a^3}\right]^{2m+1} \quad [29]$$

It is readily seen that this result could be obtained directly.[7] Briefly, the resultant shear stress τ_r at a distance r from the center may be written

$$\tau_r = J_2^{1/2} = (\alpha r/2C)^{1/n} = 3^{-(n+1)/2n}\lambda(\alpha r)^{1/n} \quad [30]$$

where Equation [5] has been used to evaluate m and C. The torque is given by

$$T = 2\pi\int_0^a \tau_r r^2 dr \quad [31]$$

which leads to

$$\alpha = \frac{1}{a}\left[\frac{3^{(n+1)/2n}(3+1/n)T}{2\pi a^3\lambda}\right]^n \quad [32]$$

Evidently it follows from Equation [5] that $\alpha^\circ = \alpha$. Finally, the same solution may be obtained as an upper bound by considering

$$\psi^\circ = k^\circ[a^{1+1/n} - (x^2+y^2)^{(1+1/n)/2}] = k^\circ[a^{1+1/n} - r^{1+1/n}] \quad [33]$$

This satisfies the condition that $\psi^\circ = 0$ on the boundary. Substitution of Equation [33] into Equation [27] once again yields Equation [32] as the relation between the twist and the torque.

The "correct" choice of the warping or stress function did not prove difficult in the relatively trivial problem of the circular cylinder. However, such will not be the case with other types of cross section. Therefore it is desirable to find a reasonable basis for the choice of approximate functions. The behavior of a rigid plastic material provides one such basis. For n sufficiently large, it is known that the nonlinear stress-strain curve, Equation [2], differs arbitrarily little from that of a rigid plastic material (6). For this latter material, there is no warping of the cross section in the circular cylinder, and it was shown that this choice leads to the exact solution of the nonlinear elastic problem. The stress function for the same circular cylinder made of a rigid-plastic material is (11)

$$\psi^\circ = k[a - (x^2+y^2)^{1/2}] = k(a-r) \quad [34]$$

where k is the yield stress of the material. This stress function is now used in the nonlinear elastic problem. The value $k = k^\circ$ is chosen so as to make the complementary potential a minimum. It then follows from Equation [27] that

$$\alpha^\circ = (3C/a)\,(3T/2\pi a^3)^{2m+1} = (3/2a)\,[3^{(n+1)/(2n)}(3T/2\pi\lambda a^3)]^n \quad [35]$$

where the values of C and m have been used from Equation [5]. The ratio of this approximate solution to the exact solution, Equation [32], is

$$\alpha^\circ/\alpha = (3/2)(1+1/3n)^{-n} \quad [36]$$

which is greater than unity for all positive values of n. Whereas the potential energy analysis leads to the exact solution, the error in the complementary potential solution varies from 12.5 per cent for $n = 1$ to 7.5 per cent for $n \to \infty$.

The next example concerns prismatic bars whose cross sections are regular polygons of N sides (Fig. 2). The polygon may be considered to be made up of N identical isosceles triangles of the type OAB with length b and altitude $b/2 \tan(\pi/N)$; O being the centroid of the cross section. For the shaded half of the isosceles triangle, a rigid plastic bar has the displacement components

$$u = -\alpha xy, \quad v = \alpha xz, \quad w = \alpha\left(xy - y^2/\tan\frac{\pi}{N}\right) \quad [37]$$

Therefore the warping function for the same portion of the nonlinear elastic bar is assumed to be

$$\varphi^* = \left(xy - y^2/\tan\frac{\pi}{N}\right) \quad [38]$$

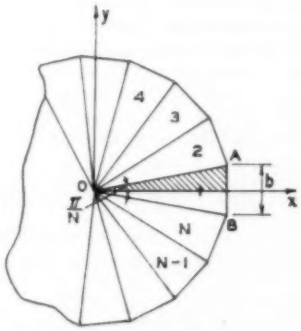

Fig. 2 Regular Polygon

The integral appearing in Equation [27] may be computed on the basis of this warping function. It will be $2N$ times the integral over half of one of the isosceles triangles. With this modification, Equation [27] yields the following potential-energy solution for the angle of twist

$$\alpha_N^* = (1/b)^{\frac{n+1}{2}}\,[12(1+1/2n)(1+1/3n)(T/N\lambda b^3)\tan^{2+1/n}(\pi/N)]^n \quad [39]$$

For the second approximate solution, the stress function for the shaded portion, Fig. 2, based on the rigid-plastic analysis, may be written

$$\psi^\circ = k^\circ\left(b/2\tan\frac{\pi}{N} - x\right) \quad [40]$$

The function ψ° satisfies the boundary conditions. It is used to compute the two integrals appearing in Equation [27] in a similar manner to that outlined for the potential-energy analysis. Thus Equation [27] yields the complementary potential solution

$$\alpha_N^\circ = (3/b)3^{\frac{n+1}{2}}\,[12(T/N\lambda b^3)\tan^{2+1/n}(\pi/N)]^n \quad [41]$$

The solutions for the particular cases of the square and equilateral triangular sections may be easily obtained from Equations [39] and [41] by putting $N = 4$ and $N = 3$, respectively.

The solutions α_N^* and α_N° represent lower and upper bounds, respectively, on the angle of twist for a given torque. The true value of α must lie between these two values. It is seen from Equations [39] and [41] that the ratio between these extreme values is

[7] See (3), where design curves of Equation [29] also are given.

$$\alpha_N^\circ/\alpha_N^* = 3/[(1 + 1/2n)(1 + 1/3n)]^n \quad \ldots\ldots [42]$$

Thus the potential-energy solution and the complementary potential solution differ from each other by 50 per cent for $n = 1$ and about 30 per cent for $n \to \infty$. These results will be commented upon in the final section.

As a final example, the triangular cross section of unequal sides shown in Fig. 3 is considered. The centroid of the triangle is at O. Each of the six triangles of the type OP_1R is considered separately. As for the case of the polygon, the warping function and the stress function for OP_1R may be written

$$\left.\begin{aligned} \varphi^* &= (xy - y^2/\tan\vartheta) \\ \psi^\circ &= k^\circ(p_R/\tan\vartheta - x) \end{aligned}\right\} \quad \ldots\ldots [43]$$

Similar functions may be chosen for the remainder of the six triangles with a proper rotation of the co-ordinate axes. These functions are used to compute the integrals appearing in Equations [27]. The integrals over the entire cross section will be the sum of the integrals over the six right triangles. Thus Equations [27] yield the following approximate solutions for the unit angle of twist

$$\left.\begin{aligned} \alpha^* &= (6C/p)\left\{\frac{T}{a^3}\,\frac{108(1 + 1/2n)(1 + 1/3n)}{[2(\xi^2 + \xi^2\eta^2 + \eta^2) - (1 + \xi^4 + \eta^4)]^{1+1/2n}[1 + 1/\xi^{1+1/n} + 1/\eta^{1+1/n}]}\right\}^n \\ \alpha^\circ &= (54C/p)\left\{\frac{T}{a_3}\,\frac{108}{[2(\xi^2 + \xi^2\eta^2 + \eta^2) - (1 + \xi^4 + \eta^4)]^{1+1/2n}\,[1 + 1/\xi + 1/\eta]^{1+1/n}}\right\}^n \end{aligned}\right\} \quad \ldots [44]$$

where $\xi = q/p$ and $\eta = r/p$. Equations [44] represent the extreme values of the angle of twist and their ratio is

$$\alpha^\circ/\alpha^* = 9\left[\frac{1 + 1/\xi^{1+1/n} + 1/\eta^{1+1/n}}{(1 + 1/\xi + 1/\eta)^{1+1/n}(1 + 1/2n)(1 + 1/3n)}\right]^n \quad \ldots\ldots [45]$$

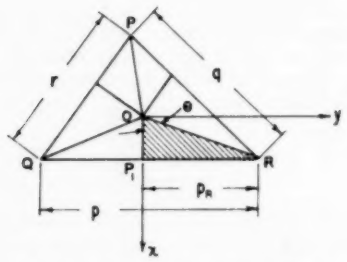

FIG. 3 TRIANGLE OF UNEQUAL SIDES

CONCLUSION

The present paper has been concerned with the steady creep analysis of cylindrical and prismatic bars. The methods presented can be used only when the final stress distribution prevails in good approximation during the lifetime of a structure. Before accepting the validity of the analysis outlined, it may prove useful to consider the limitations on the creep analyses of structures.

As was pointed out in the Introduction, the study of the creep phenomenon is still in its infancy. The expressions adopted for creep strains even from carefully controlled experiments are only approximate. An exact and painstaking analytical solution of the creep problem, based on these expressions, may differ considerably from experimental results. Consequently, in the solution of creep problems it would not be reasonable to expect an accuracy comparable to that in linear elasticity. However, creep has to be taken into account in many modern engineering problems, even if only to within an order of magnitude.

The choice of the warping and stress functions as in an ideally plastic prismatic bar yields bounds on the angle of twist which differ from each other by 30 per cent for $n \to \infty$ and 38 per cent for $n = 3$. Considering the scatter in experimental creep data, the accuracy may be considered reasonably good even for small values of n. It would, of course, be possible to find better approximate functions at the expense of introducing more arbitrary parameters. However, the resulting complicated analysis does not seem to be justifiable in our present state of knowledge of the creep phenomenon.

In conclusion, then, the paper offers to the practicing engineer a simple analytical method of solution to the problem of creep in torsion. The rigid-plastic analysis forms a reasonably sound basis in imposing limitations on the form of energy. Within the limitation of the creep-strain expressions adopted, the energy methods provide solutions of reasonable accuracy. Moreover, these solutions establish the bounds within which the true solution must lie, so that estimates of the error introduced can always be obtained.

BIBLIOGRAPHY

1 "On the Viscous Flow of Metals and Allied Phenomena," by E. N. da Andrade, Proceedings of the Royal Society, series A, vol. 84, No. A567, 1910, p. 1.

2 "Approximate Analysis of Structures in the Presence of Moderately Large Creep Deformations," by N. J. Hoff, *Quarterly of Applied Mathematics*, vol. 12, no. 1, 1955, pp. 49–55.

3 "Creep-Time Relations for Polystyrene Under Torsion, Bending and Torsion," by J. Marin and G. Cuff, Proc. ASTM, vol. 49, 1949, pp. 1158–1174.

4 "Analysis of Frameworks in the Presence of Steady Creep,"[8] by P. G. Hodge Jr. and B. Venkatraman, PIBAL Report No. 333, Polytechnic Institute of Brooklyn, Brooklyn, N. Y., 1955.

5 "Bending of Rigid Frames in the Presence of Steady Creep,"[8] by B. Venkatraman and P. G. Hodge, Jr., PIBAL Report No. 346, Polytechnic Institute of Brooklyn, Brooklyn, N. Y., 1956.

6 "Stress Distribution in the Presence of Steady Creep," by N. J. Hoff, Proceedings of the Conference on High Speed Aeronautics, Polytechnic Institute of Brooklyn, 1955, pp. 271–310.

7 "Strain Hardening Under Combined Stresses," by W. Prager, *Journal of Applied Physics*, vol. 16, no. 21, 1945, p. 837.

8 "New Horizons in the Mechanics of Solids," by R. Hill, *Journal of Mechanics and Physics of Solids*, vol. 5, no. 1, 1956, pp. 66–74.

9 "On the Variational Principles of Plasticity," by H. J. Greenberg, Brown University, ONR-NR-041-032, 1949.

10 "The Principles of Complementary Energy in Non-linear Elasticity Theory," by H. L. Langhaar, *Journal of the Franklin Institute*, vol. 256, no. 3, 1953, pp. 255–256.

11 "Theory of Perfectly Plastic Solids," by W. Prager and P. G. Hodge, Jr., John Wiley and Sons, Inc., New York, N. Y., 1951, pp. 62–86.

[8] The material contained in references (4) and (5) also appears in "Approximate Solutions of Some Problems in Steady Creep," by P. G. Hodge Jr., and B. Venkatraman in "Memorie Presentate al Symposium su la Plasticità nella Scienza della Costruzioni," Nicola Zanichelli, Bologna, Italy, 1956, pp. 138–165.

The Calculation of Optimum Concentrated Damping for Continuous Systems

By R. PLUNKETT,[1] SCHENECTADY, N. Y.

A method is presented for calculating the optimum concentrated damping for the vibration of continuous systems. It is applied to (*a*) a string damped near one end, (*b*) a cantilever beam driven at the center and damped at the free end, (*c*) a uniform blade with dovetail damping, and (*d*) the damped dynamic absorber. Aside from the specific results which are shown in the examples, there are some general conclusions. The vibration velocity and vibratory force are not necessarily in phase at maximum amplitude for optimum damping. The decay rate at optimum damping is not necessarily related to amplification at resonance, i.e.

$$\delta \neq \pi/Q$$

Nomenclature

The following nomenclature is used in the paper:

- a = mobilities, ratio of velocity to force
- A = constants
- b = mobilities
- C = damping constant
- d = distance
- f = frequency
- F = force
- i, j, k = indexes
- $j = \sqrt{-1}$
- L = length
- m = mass
- M = mobilities
- n = subscript for resonant frequencies
- q = dimensionless damping
- t = time
- u = velocity of sound
- v = velocity
- x = variable distance
- y = transverse displacement
- θ = phase angle
- ρ = radii in complex plane, or mass per unit length
- ω = circular frequency

Introduction

The analysis of damped continuous systems presents a number of practical difficulties. The decay rate of continuous beams with concentrated damping (5, 9)[2] or with certain kinds of continuous damping (6) has been considered. However, in general, the response of damped systems to vibratory forces is of more practical interest. Consider the case analyzed by Young: a cantilever beam with dashpot at the free end. If the beam is driven by a vibratory force at the same point as the dashpot, it is clear that the resonant amplitude for a unit vibratory force must decrease continuously with increasing dashpot constant, approaching zero as the constant approaches infinity. On the other hand, if the same beam is driven at its center it will reach infinite amplitude for zero dashpot constant, and infinite amplitude at resonance for infinite dashpot constant, since this represents complete support. Since there is some damping effect for all other values, there must be some optimum value which gives the least resonant amplitude. As Young has shown, there is also a damping value which gives maximum decay rate for each type of vibration. Since the decay rate is not dependent on the point of application of the vibratory force, it is clear that there can be no direct relationship between amplitude per unit force at resonance and decay rate. It also will be shown later that, unlike single-degree-of-freedom systems, multidegree and continuous systems need not have the vibratory velocity in phase with the force at that frequency which gives maximum response. In this paper, the problem of vibratory response of otherwise undamped systems with a single dashpot will be analyzed by impedance methods. This is a generalization of a method employed by Lewis (2) for torsional systems and by Den Hartog and Ormondroyd (1) for the dynamic vibration absorber.

It is our purpose in this paper to determine the minimum resonant amplitude for such a system and the value of dashpot constant which will give this minimum. We will consider both the case of known vibratory applied force and known vibratory applied motion.

Four examples have been worked out. In the first, it is shown that a taut wire damped near one end has a minimum resonant amplification of $2L/\pi d$, where d is the distance of the damper from one end. In the second example the forced-vibration solution of a classic problem of a cantilever beam is compared with the free-decay solution. The third case shows that dovetail damping of a uniform blade or bucket could be very effective, with amplification factors of two or less. In the fourth case this method is compared to the classical solution for the tuned dynamic absorber.

Analysis

The first case considered is that of the vibration velocity at one point of a linear vibratory system resulting from a vibratory force at another point (which includes a force at the same point). It is desired to find the effect of concentrated linear damping at still a third point. Let the force F_1 be applied at point 1 and the corresponding vibration velocity at the same point be v_1; let the damper (viscous or dashpot), with damping constant C, be applied across points with relative vibration velocity v_2 and result in a force $Cv_2 = -F_2$; and let the unknown vibration velocity at the third point be v_3. Any or all of these may be the same points. Since a linear system is assumed, superposition applies and the behavior of the system may be described in terms of influence coefficients. Thus

---

[1] Consulting Engineer, General Electric Company, General Engineering Laboratory. Mem. ASME.

[2] Numbers in parentheses refer to the Bibliography at the end of the paper.

Contributed by the Applied Mechanics Division and presented at the Annual Meeting, New York, N. Y., December 1–6, 1957, of THE AMERICAN SOCIETY OF MECHANICAL ENGINEERS.

Discussion of this paper should be addressed to the Secretary, ASME, 29 West 39th Street, New York, N. Y., and will be accepted until July 10, 1958, for publication at a later date. Discussion received after the closing date will be returned.

NOTE: Statements and opinions advanced in papers are to be understood as individual expressions of their authors and not those of the Society. Manuscript received by ASME Applied Mechanics Division, January 15, 1957. Paper No. 57—A-93.

$$\left.\begin{aligned} v_1 &= a_{11}F_1 + a_{12}F_2 \\ v_2 &= a_{21}F_1 + a_{22}F_2 \\ v_3 &= a_{31}F_1 + a_{32}F_2 \end{aligned}\right\} \quad \ldots\ldots\ldots\ldots\ldots [1]$$

Let the time variation of F_1 be given in complex notation by $F_1 e^{j\omega t}$. Then, since it has been assumed that there is no damping in the system when $C = 0$, all of the a are pure imaginary and are functions of ω and the stiffness and mass characteristics of the system only. By the mechanical equivalent of Foster's theorem it can be shown that they can be expressed in the form

$$a_{ij} = A_{ij}\,\omega^{\pm 1}\,\frac{\Pi\left(1 - \dfrac{\omega^2}{\omega_b^2}\right)}{\Pi\left(1 - \dfrac{\omega^2}{\omega_a^2}\right)}$$

where ω_a are the resonant frequencies (poles) of the undamped system and ω_b are the zero's (antiresonances) of point i with excitation at point j for the undamped system. This may be useful in the analysis but is not necessary in the further development.

Substituting

$$\left.\begin{aligned} F_2 &= -Cv_2 \\ v_2 &= a_{21}F_1 - a_{22}Cv_2 \end{aligned}\right\} \quad \ldots\ldots\ldots\ldots\ldots [2a]$$

or

$$v_2 = \frac{a_{21}F_1}{1 + a_{22}C}$$

thus

$$v_3 = a_{31}F_1 - a_{32}Cv_2$$

$$= a_{31}F_1 - \frac{a_{32}a_{21}C}{1 + a_{22}C}F_1$$

$$\frac{v_3}{F_1} = \frac{a_{31} + (a_{22}a_{31} - a_{32}a_{21})C}{1 + a_{22}C}$$

$$= jb_1\,\frac{1 + jb_2C}{1 + jb_3C};\quad jb_3 = a_{22} \quad \ldots\ldots\ldots\ldots [2b]$$

in which the b are pure real.

Let the ratio v_3/F_1 be denoted by the complex mobility M_{31}; the absolute value of $|M_{31}|^2$ is given by

$$|M_{31}|^2 = b_1^2\,\frac{1 + b_2^2C^2}{1 + b_3^2C^2} \quad \ldots\ldots\ldots\ldots\ldots [3]$$

For those values of ω for which $b_2^2/b_3^2 = 1$, $|M_{31}|$ is independent of C and these values of $|M_{31}|$ represent the lowest value that the maximum of $|M_{31}|$ may take over the frequency range of interest regardless of the value of C. As has been pointed out by Den Hartog and Ormondroyd (1) and by Lewis (2), the value of C that gives a zero slope for

$$\frac{\partial |M_{31}|}{\partial \omega}$$

at the invariant value of $|M_{31}|$ may be considered to be an optimum value for C.

Equation [2b] is a bilinear form in C and thus describes a semicircle in the complex mobility plane for positive values of C (7), Fig. 1. For

$$C = 0,\ M_{31} = jb_1$$

for

$$C = \infty,\ M_{31} = jb_1b_2/b_3$$

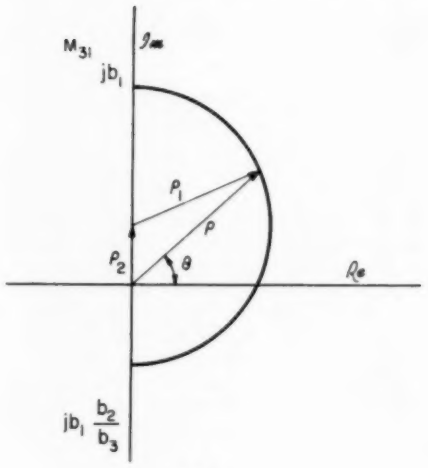

Fig. 1

which fixes both ends of the semicircle. From Fig. 1

$$\rho_1^2 = \rho^2 + \rho_2^2 - 2\rho\rho_2 \sin\theta$$

Differentiating with respect to ω

$$2\rho_1\rho_1' = 2\rho\rho' + 2\rho_2\rho_2' - 2\rho'\rho_2 \sin\theta - 2\rho\rho_2' \sin\theta - 2\rho\rho_2 \cos\theta\theta'$$

If

$$\frac{b_2}{b_3} = +1,\quad \rho_2 = \rho,\quad \text{and}\quad \rho_1 = 0$$

The foregoing condition requires only that $\theta = \pi/2$, which is obvious from Fig. 1. The physical interpretation is that point 2 is a null point for excitation either at points 1 or 3 (a_{32} or $a_{21} = 0$). We shall not consider further in this paper what are the requirements for C in this case.

If $b_2/b_3 = -1$, $\rho_2 = 0$, and $\rho_1 = \rho$; for a maximum of $|M_{31}|$, $\rho' = 0$

$$\rho_1' = -\rho_2' \sin\theta$$

Let jM_I be the value of M_{31} for $C = 0$ and jM_{II} be the value of M_{31} for $C = \infty$. Then

$$2\rho_2 = M_I + M_{II},\quad 2\rho_2' = M_I' + M_{II}'$$

$$2\rho_1 = M_I - M_{II},\quad 2\rho_1' = M_I' - M_{II}'$$

Thus

$$\sin\theta = -\frac{M_I' - M_{II}'}{M_I' + M_{II}'} \quad \ldots\ldots\ldots\ldots\ldots [3a]$$

Since there is no necessary reason for M_I' to equal M_{II}', $\sin\theta$ is not necessarily zero, which means that the force and velocity are not necessarily in phase for maximum M_{31}. This conclusion is valid whether or not the force is applied at the point of the measured velocity (points 1 and 3 identical). We note that $\partial|M_{31}|/\partial\omega$ may not equal zero for M_I' and M_{II}' of opposite sign, since $|\sin\theta| > 1$, which is impossible. This difficulty does not exist for point impedance M_{11}, since the derivatives are always positive. Thus Equation [3a] is a necessary condition for a maximum of M_{31} if $b_2/b_3 = -1$, and is both necessary and sufficient for M_{11}.

The value of C for $\partial|M_{21}|/\partial\omega = 0$ may be found from Equations [2b] and [3a]. It has been established already that

$$-b_2 = b_4 = ja_{22}$$

It is also clear from Equation [2b] that

$$\tan\theta = \frac{1 - b_2^2C^2}{2b_2C}$$

But

$$\tan^2\theta = \frac{\sin^2\theta}{1 - \sin^2\theta}$$

Substituting for $\sin\theta$ from Equation [3a], one gets

$$\frac{[1 - (b_2C)^2]^2}{4(b_2C)^2} = \frac{\left(1 - \dfrac{M_1'}{M_{11}'}\right)^2}{4\dfrac{M_1'}{M_{11}'}} \quad \ldots\ldots [3b]$$

or

$$b_2C = |a_{22}|C = \left(\frac{M_1'}{M_{11}'}\right)^{1/2}$$

so that C may be found from M_1', M_{11}', and a_{22}.

The values of ω for $b_2^2/b_3^2 = 1$ and the corresponding values of M_{21} may be found by considering the response curves (mobilities) of the system first with $C = 0$ and second with $C = \infty$ (v_2 forced to be zero or clamped). Since the points of interest are those in which $|M_{21}|$ is independent of C, the values of ω are given by the intersections of the two curves so found.

The second case of interest is the effect of C on the ratio of v_3 to v_1. By a similar process it may be shown that

$$\frac{v_3}{v_1} = \frac{a_{31}}{a_{11}}\frac{1 + jb_2C}{1 + jb_4C} \quad \ldots\ldots [4a]$$

or

$$\left|\frac{v_3}{v_1}\right|^2 = \left|\frac{a_{31}}{a_{11}}\right|^2\frac{1 + b_2^2C^2}{1 + b_4^2C^2} \quad \ldots\ldots [4b]$$

and the same argument for $b_2^2/b_4^2 = 1$ holds as was given before.

Examples

String. As an example, let us consider the case of a vibrating string of length L which is driven at one end with a lateral motion $v_1e^{j\omega t}$ and is damped near the fixed end by a dashpot which is fastened at a distance d from the fixed end, Fig. 2. It is desired to determine the maximum value of the ratio v_3/v_1, where v_3 is the velocity at $x = L/2$, as a function of C for values of ω near the first resonant frequency of the string. The differential equation of the string is given by (reference 1, Equation [93])

$$Tv_{xx} = \rho v_{tt} \quad \ldots\ldots [5]$$

where T is the tension and ρ the mass per unit length. The solution, for $C = 0$, that fits the left-hand boundary condition is

$$v = v_0\sin\frac{\omega x}{u} \quad \ldots\ldots [6]$$

where $u = (T/\rho)^{1/2}$ and is the velocity of wave propagation.

$$v_1 = v_0\sin\frac{\omega L}{u} \quad \ldots\ldots [7a]$$

$$v_3 = v_0\sin\frac{\omega L}{2u} \quad \ldots\ldots [7b]$$

or

$$\left(\frac{v_3}{v_1}\right)_0 = \frac{\sin\dfrac{\omega L}{2u}}{\sin\dfrac{\omega L}{u}} \quad \ldots\ldots [7c]$$

Likewise for $C = \infty$ (point 2 clamped)

$$\frac{v_3}{v_1} = \frac{\sin\dfrac{\omega\left(\dfrac{L}{2} - d\right)}{u}}{\sin\dfrac{\omega(L - d)}{u}} \quad \ldots\ldots [8]$$

Near the first resonant frequency, $\sin(\omega L/u)$ is very small and $v_3 \approx v_0$ for both cases. Letting

$$\left|\frac{v_3}{v_1}\right|_0^2 = \left|\frac{v_2}{v_1}\right|_\infty^2$$

then

$$\sin\frac{\omega L}{u} \approx -\sin\frac{\omega(L - d)}{u}$$

or

$$\frac{\omega L}{u} - \pi = \pi - \frac{\omega(L - d)}{u}$$

and

$$f_c = \frac{\omega_c}{2\pi} = \frac{u}{2L - d} \quad \ldots\ldots [9]$$

The value at f_c for $|v_3/v_1|$ may be found by substituting for ω from Equation [9] into Equation [7c], remembering that

$$\sin\frac{\omega L}{2u} \approx 1$$

and

$$\frac{\omega_c L}{u} = \frac{2\pi L}{2L - d} \approx \pi\left(1 + \frac{d}{2L}\right)$$

then

$$\left|\frac{v_3}{v_1}\right|_c \approx \left|\frac{1}{\sin\pi\left(1 + \dfrac{d}{2L}\right)}\right| \approx \frac{2L}{\pi d} \quad \ldots\ldots [10]$$

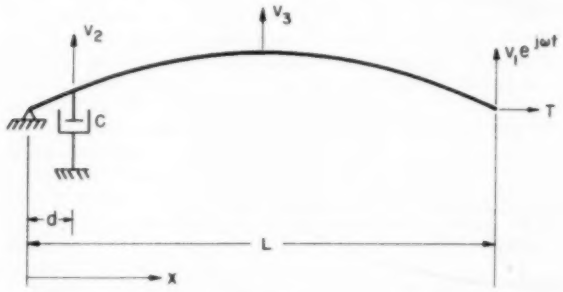

Fig. 2

Differentiation of Equations [7c] and [8] shows that

$$\left|\frac{v_3}{v_1}\right|_0' = \left|\frac{v_2}{v_1}\right|_\infty'$$

for the frequency given by Equation [9] or from Equation [3a], $\theta = 0$ for the optimum value of C. Thus, if d/L is sufficiently small, v_3 lags v_1 by 90 deg at these values of C and ω. From Equation [4a] this means that

$$b_2C = -b_4C = \pm 1$$

While there are several methods for determining b_2 or b_4, none of them is very simple. For example

$$b_2 = a_{22} - a_{32}a_{21}/a_{31}$$

and

$$b_4 = a_{22} - a_{12}a_{21}/a_{11}$$

Another way would be to use M_{21} for $C = \infty$, which is b_2/a_{22}, and multiply by a_{22}. Aside from the actual value of C, it is worth mentioning that the optimum value of C and the value of θ are usually different for v_3/v_1 than they are for M_{21}.

Since this configuration has no poles for the a of Equation [1] in the vicinity of ω_e ($a_{11} = 0$ for $\omega = \pi u/L$ is the resonant condition for $v_1 = 0$), an accurate value for a_{22} may be found using the usual approximations. Frequency ω_e of Equation [9] corresponds to a resonance of a string of length $L - d/2$. From Fig. 3 it may be seen that

$$y_2 \approx \frac{\pi d}{L}\, y$$

$$F_1 \approx -\frac{\pi y_0}{L}\, T$$

Since

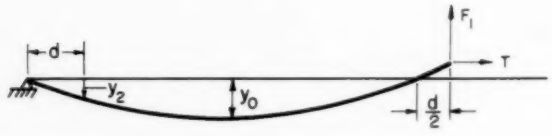

Fig. 3

$$v_2 = j\omega y_2 \text{ and } F_2 = 0$$

then

$$a_{21} = \frac{v_2}{F_1} = -j\frac{\omega d}{T} \qquad [11a]$$

Fig. 4, the condition for $C = \infty$, follows from Fig. 3 by symmetry. From Figs. 3 and 4 it is clear that $|M_{21}|_0 = |M_{21}|_\infty$. Since M_{21} is a bilinear form in C, the complex plane plot of M_{21} must degenerate to a point. Thus the phase relationship for v_2 and v_1 requires M_{11} to be pure real (negative) which by Equations [2b] and [3a] means that $|a_{22}C| = 1$. Needless to say, this is not the general condition for optimum C for this class of problem.

From Fig. 5 it may be seen that

$$F_1 \approx \frac{\pi y_0}{L}\, T \quad \text{and} \quad y_2 \approx -\frac{\pi y_0 d}{2L}$$

or

$$v_2 = -\frac{j\omega y_0 d}{2L} \qquad [11b]$$

thus

$$F_2 \approx \frac{\pi y_0 T}{L} - \frac{\pi y_0 T}{2L} = \frac{\pi y_0 T}{2L} \qquad [11c]$$

From the second of Equations [1]

$$v_2 = a_{21}F_1 + a_{22}F_2 \qquad [11d]$$

or

$$-j\frac{\omega \pi y_0 d}{2L} = -j\frac{\omega d}{T}\frac{\pi y_0 T}{L} + a_{22}\frac{\pi y_0 T}{2L} \qquad [11e]$$

so that

$$a_{22} = j\frac{\omega d}{T} \qquad [12a]$$

since

$$|a_{22}C| = 1, \quad C = \frac{T}{\omega d} \qquad [12b]$$

Fig. 4

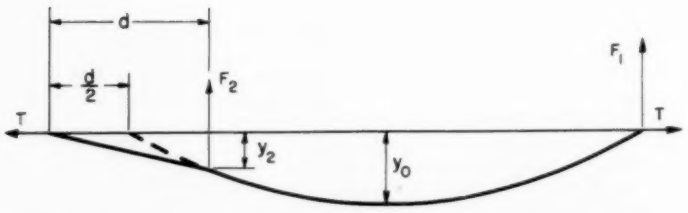

Fig. 5

but

$$\omega_c \approx \frac{\pi u}{L} = \frac{\pi}{L}\left(\frac{T}{\rho}\right)^{1/2}$$

or

$$C = \frac{(T\rho)^{1/2}}{\pi}\,\frac{L}{d} \qquad \text{[12c]}$$

This may be compared with the value for the input mobility at point 2 (a_{22}) found in the usual way (4) by computing the specific impedance from the effective mass at the point and dividing by the amplification factor. The effective mass of a string referred to its center is $\rho L/2$, and referred to point 2 is divided by the square of the velocity ratio or

$$m_{eff} = \frac{\rho L}{2}\,\frac{L^2}{\pi^2 d^2} \qquad \text{[13a]}$$

The specific impedance is found from ωm_{eff} and the amplification factor is $2L/(\pi d)$ (Equation [10]). Thus

$$C = \frac{\pi}{L}\left(\frac{T}{\rho}\right)^{1/2}\frac{\rho L}{2}\,\frac{L^2}{\pi^2 d^2}\,\frac{\pi d}{2L} = \frac{(T\rho)^{1/2}}{4}\,\frac{L}{d} \qquad \text{[13b]}$$

The difference between the values from Equations [13b] and [12c] is due to the fact that the development leading to Equation [13b] ignores all but the first mode of vibration; even so, it is sufficiently accurate for engineering purposes.

Cantilever With End Damping—Center Drive. Another example is the case of a uniform cantilever beam, driven at the center and with a dashpot fixed at the free end, Fig. 6.

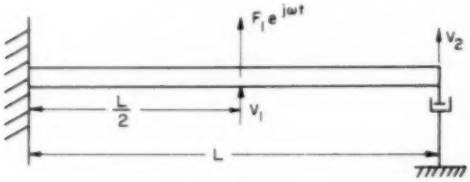

Fig. 6

In this case we shall determine the minimum resonance value for M_{11} and the corresponding value for C. The problem may be nondimensionalized in terms of the first resonant frequency and any appropriate size factor, such as the weight of the beam. M_{11} for $C = 0$ (clamped-free) and $C = \infty$ (clamped-supported) have been constructed by the methods of reference (4) for a beam weighing 1000 lb whose first resonant frequency is 100 cps, Fig. 7. An examination of this graph shows that the critical point occurs at a frequency of 540 cps and a mobility of 710 μin/lb sec. It is not difficult to show that slopes on a log-log plot may be used in place of the slopes used in Equation [3a] for finding $\sin\theta$ or in Equation [3b] for finding C. The logarithmic slopes $(\partial \log |M|)/(\partial \log f)$ for $M_{\rm I}$ and $M_{\rm II}$ are about 6.8 and 5.2 which gives $\sin\theta = -0.133$ or $a_{22}C = 1.14$.

From Fig. 8, $a_{22} = 780\ \mu$ in/lb sec at this frequency or $C = 1500$ lb/in/sec. To compare this with Young's values for the free-vibration case (5), we get dimensionless damping q, of 5.9 and dimensionless frequency of 5.5 as compared with his values of $q = 3$ and frequency 5.3.

Uniform Blade With Dovetail Damping. The case of a supported free beam, driven at the free end, and damped torsionally

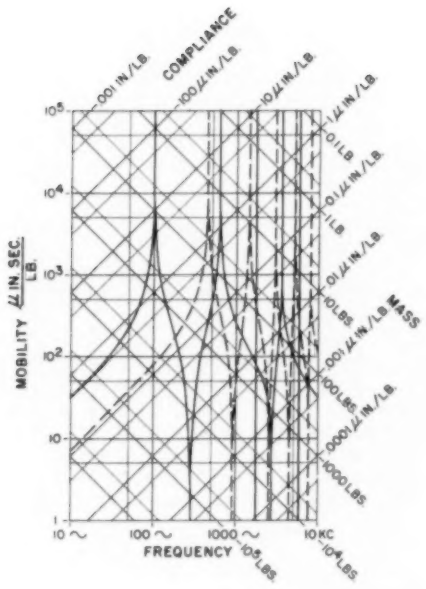

Fig. 7

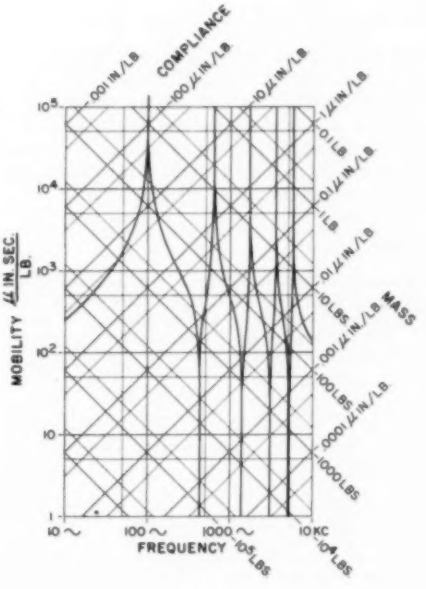

Fig. 8

at the supported end is shown in Figs. 9 and 10. This corresponds to the case of a uniform turbine bucket with dovetail damping. The major conclusion that can be drawn from Fig. 9 is that the amplification factor at resonance in terms of mobility (Yates, reference 8, shows velocity to correspond to stress) is less than 1 for the higher modes and is no more than 2 in terms of displacement for the first mode, for optimum damping. This indicates that great benefit may be derived from dovetail damping of proper magnitude. The magnitude of the equivalent

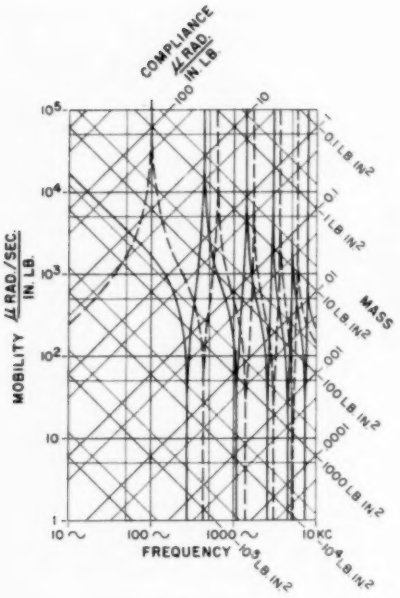

Fig. 9

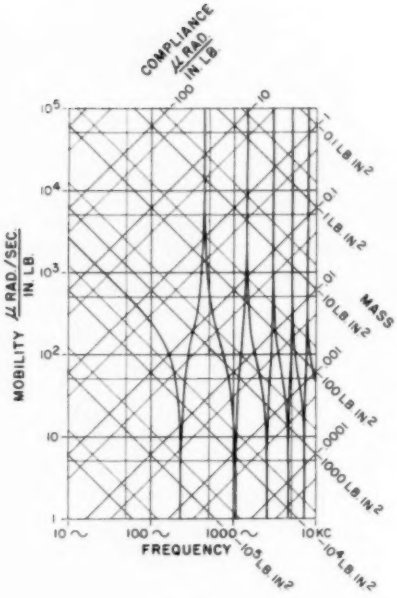

Fig. 10

damping from Fig. 10 may be of interest when reduced to friction factor.

Damped Dynamic Absorber. The case of the damped dynamic absorber of mass ratio $\mu = 0.05$ and tuned to the main system frequency also was calculated to compare the results with those of Den Hartog and Ormondroyd (reference 1, section 24). The dimensionless optimum damping D for the lower frequency is 0.15 and for the upper is 0.13. This may be compared with the average value (reference 1, Fig. 81*c*) of 0.145.

Bibliography

1 "Mechanical Vibrations," by J. P. Den Hartog, McGraw-Hill Book Company, Inc., New York, N. Y., third edition, 1947.

2 "The Extended Theory of the Viscous Vibration Damper," by F. M. Lewis, JOURNAL OF APPLIED MECHANICS, TRANS. ASME, vol. 77, 1955, p. 377.

3 "Communication Networks," by E. A. Gullemin, John Wiley & Sons, Inc., New York, N. Y., vol. 2, 1935, Chapters 5 and 10.

4 "Semi-Graphical Method for Plotting Vibration Response Curves," by R. Plunkett, Proceedings of the Second U. S. National Congress of Applied Mechanics, ASME, 1954, p. 21.

5 "Vibration of a Beam With Concentrated Mass, Spring and Dashpot," by D. Young, JOURNAL OF APPLIED MECHANICS, TRANS. ASME, vol. 70, 1948, p. 65.

6 "On Application of a Quasi-Static Variational Principle to a System With Damping," by M. Morduchow, JOURNAL OF APPLIED MECHANICS, TRANS. ASME, vol. 76, 1954, p. 8.

7 "Network Analysis and Feedback Amplifier Design," by H. W. Bode, D. Van Nostrand, Inc., New York, N. Y., 1945, Section 10.13, p. 233.

8 "Vibration Diagnosis in Marine Geared Turbines," by H. G. Yates, Transactions of the North East Coast Institution of Engineers and Shipbuilders, vol. 65, February, 1949, part 4, p. 225.

9 "The Free Lateral Vibrations of a Cantilever Beam With a Terminal Dashpot," by E. J. McBride, JOURNAL OF APPLIED MECHANICS, TRANS. ASME, vol. 65, 1943, p. A-168.

Unbalanced Inertia Forces in Slider-Crank Mechanisms of Large Eccentricity

By ERNST MEWES,[1] BRAUNSCHWEIG, GERMANY

An analysis of the various harmonic orders of the inertia forces in offset slider-crank mechanisms is presented. The formulas given here are valid for all practical values of eccentricity ratio (ratio of offset to length of connecting rod) and crank to connecting rod ratio. The influence of the latter ratio on the force components is evaluated with infinite series, whereas such is not the case for the eccentricity ratio. Rules for the full or partial balance of harmonic components of the first or any other single order are given.

Introduction

In reciprocating engines, the balance of the inertia forces of the mechanism depends on the number of pistons and the arrangement of cylinders and cranks.

If the cranks of an in-line engine with all cylinders similar, viewed in the direction of the shaft axis, divide 360 deg by n, then only those components of the inertia forces of order kn ($k = 1, 2, 3, \ldots$) remain free to act on the frame of the engine—all other orders being balanced. For example, in an in-line engine with 180-deg crank-angle spacing (four-stroke, 4-cylinder) the free inertia forces are of orders 2, 4, 6, ... In an engine with 120-deg crank spacing (four-stroke, 6-cylinder) the orders of the free forces would be 3, 6, ... (The odd orders 3, 9, ... would be present only in engines with offset cylinders, or in any eccentric slider-crank mechanism.) Hence it is desirable to know the relative magnitudes of the various orders of the mass forces.

The inertia force of a reciprocating mass m, for crank of radius R and instantaneous angular velocity $\dot{\Theta}$ and acceleration $\ddot{\Theta}$ of the shaft is

$$\left.\begin{aligned} P = mR[&\dot{\Theta}^2(\cos\Theta + A_1\sin\Theta + A_2\cos 2\Theta - A_3\sin 3\Theta \\ &- A_4\cos 4\Theta + + - - \ldots) + \ddot{\Theta}(\sin\Theta - B_1\cos\Theta \\ &+ B_2\sin 2\Theta + B_3\cos 3\Theta - B_4\sin 4\Theta - + \ldots)] \end{aligned}\right\} \quad \ldots[1]$$

where

$$B_n = \frac{1}{n}A_n \quad \ldots[2]$$

and the expressions for A_n are to be determined. The first-order component of the inertia force is

$$P_1 = mR[\dot{\Theta}^2(\cos\Theta + A_1\sin\Theta) + \ddot{\Theta}(\sin\Theta - A_1\cos\Theta)] \quad \ldots[3]$$

and the components of sequential orders are

$$P_2 = A_2 mR\left(\dot{\Theta}^2\cos 2\Theta + \frac{1}{2}\ddot{\Theta}\sin 2\Theta\right)$$

$$P_3 = A_3 mR\left(-\dot{\Theta}^2\sin 3\Theta + \frac{1}{3}\ddot{\Theta}\cos 3\Theta\right)$$

and so on.

Infinite series are obtained for the complete calculations of the quantities A_n which depend on the geometry of the slider crank. These series converge very rapidly for conventional reciprocating engines, where the offset (or eccentricity) is small or zero. In such cases only a few terms are required. It is desirable to know where these series may be terminated so that the accuracy of numerical results can be prescribed within definite limits. Furthermore it always should be possible to include as many terms as desired.

The following development has direct application to slider cranks of large eccentricity, such as those used in agricultural side mowers, separator sieves, and the like.

Development of formulas

We consider a slider-crank mechanism with a connecting rod whose center of gravity (cg) does not necessarily lie on the line connecting the bearing centers. In the general case, Fig. 1, the co-ordinates of the cg, if there is no play in the linkage, are given by

$$\left.\begin{aligned} \frac{X}{R} &= \cos\Theta + \frac{\xi}{\lambda}\cos\phi + \frac{\eta}{\lambda}\sin\phi \\ \frac{Y}{R} &= \sin\Theta - \frac{\xi}{\lambda}\sin\phi + \frac{\eta}{\lambda}\cos\phi \end{aligned}\right\} \quad \ldots[4]$$

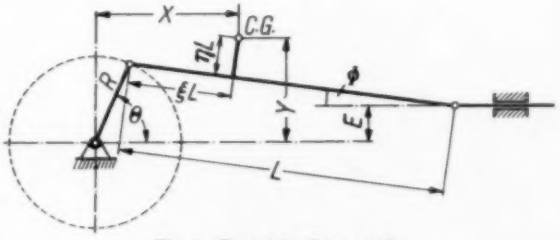

Fig. 1 Eccentric slider crank

The crank-rod ratio $\lambda = R/L$, and the eccentricity ratio $\epsilon = E/L$, are related to ϕ and Θ by

$$\sin\phi = \lambda\sin\Theta - \epsilon \quad \ldots[5]$$

from which

$$\begin{aligned} \cos\phi &= (1 - \sin^2\phi)^{1/2} \\ &= (1 - \epsilon^2 + 2\epsilon\lambda\sin\Theta - \lambda^2\sin^2\Theta)^{1/2} \\ &= (1 - \epsilon^2)^{1/2}\left[1 + \frac{2\epsilon\lambda}{1 - \epsilon^2}\sin\Theta\left(1 - \frac{\lambda}{2\epsilon}\sin\Theta\right)\right]^{1/2} \quad \ldots[6] \end{aligned}$$

Expansion of Equation [6] by the binomial theorem gives

---

[1] Dr.-Engineer, Institute for Fundamental Research in Agricultural Engineering, Forschungsanstalt für Landwirtschaft, Braunschweig-Voelkenrode.

Contributed by the Applied Mechanics Division and presented at the Annual Meeting, New York, N. Y., December 1–6, 1957, of The American Society of Mechanical Engineers.

Discussion of this paper should be addressed to the Secretary, ASME, 29 West 39th Street, New York, N. Y., and will be accepted until July 10, 1958, for publication at a later date. Discussion received after the closing date will be returned.

Note: Statements and opinions advanced in papers are to be understood as individual expressions of their authors and not those of the Society. Manuscript received by ASME Applied Mechanics Division, January 21, 1957. Paper No. 57—A-41.

$$\cos\phi = (1-\epsilon^2)^{1/2}(1 + a_1 \sin\Theta - a_2 \sin^2\Theta + a_3 \sin^3\Theta - + \ldots) \quad [7]$$

The calculation of the A_n is facilitated by introducing the auxiliary quantity

$$\mu = \frac{\lambda}{1-\epsilon^2} \quad [8]$$

such that

$$a_n = b_n \mu^n \quad [9]$$

$$b_1 = \epsilon$$

For $n > 1$ it can be shown that[2]

$$b_n = \frac{1}{n}\left[(2n-3)\epsilon b_{n-1} + (1-\epsilon^2)\frac{\partial b_{n-1}}{\partial \epsilon}\right] \quad [10]$$

The analysis can be simplified further by writing

$$b_n = c_n d_n \quad [11]$$

where, for $n = 1, 2, 3, \ldots$

$$c_{2n-1} = 2n\left|\binom{1/2}{n}\right|\epsilon \quad [12]$$

$$c_{2n} = \left|\binom{1/2}{n}\right| \quad [13]$$

and $\left|\binom{m}{n}\right|$ means the numerical value of the coefficient of the $(n+1)st$ term in the binomial expansion of $(1+x)^m$ for a general value of m. For example

$$\left|\binom{1/2}{4}\right| = \frac{1\cdot 1\cdot 3\cdot 5}{2\cdot 4\cdot 6\cdot 8}$$

The first values of d so obtained are

$$\left.\begin{aligned} d_1 &= d_2 = d_3 = 1 \\ d_4 &= 1 + 4\epsilon^2 \\ d_5 &= 1 + \frac{4}{3}\epsilon^2 \\ d_6 &= 1 + 12\epsilon^2 + 8\epsilon^4 \\ d_7 &= 1 + 4\epsilon^2 + \frac{8}{5}\epsilon^4 \end{aligned}\right\} \quad [14]$$

All of these values of b_n and d_n are unique and finite. Instead of using Equation [10] it is easier to determine the values of d_n for higher orders by means of the following scheme.

The coefficients of the highest power of ϵ in d_{2n} are

$$\frac{1}{2} \div \left|\binom{1/2}{n}\right|$$

Hence for

$$n = 1 \qquad \frac{1}{2}\cdot\frac{2}{1} = 1$$

$$n = 2 \qquad \frac{1}{2}\cdot\frac{2\cdot 4}{1\cdot 1} = \frac{4}{1}$$

$$n = 3 \qquad \frac{1}{2}\cdot\frac{2\cdot 4\cdot 6}{1\cdot 1\cdot 3} = \frac{4}{1}\cdot\frac{6}{3}$$

$$n = 4 \qquad \frac{4}{1}\cdot\frac{6}{3}\cdot\frac{8}{5}$$

and so on

Clearly, these values satisfy a recursive relation.

We now construct Table 1 which shows the ratios of coefficients of like powers of ϵ for successive even numbers of the sequence $d_6 - d_{14}$.

Table 1 Ratios of like powers of ϵ for successive even numbers of sequence $d_6 - d_{14}$

	ϵ^2	ϵ^4	ϵ^6	ϵ^8	ϵ^{10}
d_6	3				
d_8	2	6			
d_{10}	5/3	10/3	10		
d_{12}	3/2	5/2	5	15	
d_{14}	7/5	21/10	7/2	7	21

For example, the coefficient of ϵ^2 in d_8 is 12, while the corresponding coefficient in d_4 is 4, hence the ratio $12/4 = 3$ is entered opposite d_6 in the ϵ^2 column of Table 1.

Dividing the members of each column of Table 1 by the corresponding entries of the previous column, except the last members in each row, we obtain the values in the space beneath the stage line in Table 2. These have a simple sequence.

Table 2 Scheme of multipliers for coefficients of ϵ^{2m} in d_{2n}

	ϵ^2	ϵ^4	ϵ^6	ϵ^8	ϵ^{10}
d_4	4/1				
d_6	3/1	×6/3			
d_8	4/2	×3/1	×8/5		
d_{10}	5/3	×4/2	×3/1	×10/7	
d_{12}	6/4	×5/3	×4/2	×3/1	×12/9

and so on

For example, the entry for d_8 and ϵ^4 in Table 2 according to Table 1 is $6/2 = 3/1$; for d_{12} and ϵ^6 it is $5 \div 5/2 = 4/2$, and so on.

The ratios of the last terms of d_{2n+2} and d_{2n} are shown in Table 2 above the stage line, thus the coefficient of ϵ^2 in d_4 is 4/1 and the coefficient of ϵ^4 in d_6 is $6/3 \times 4/1 = 8$. The coefficient of ϵ^2 in d_6 $3/1 \times 4/1 = 12$, the coefficient of ϵ^2 in d_8 is $4/2 \times 3/1 \times 4/1 = 24$, the coefficient of ϵ^4 in d_8 is $3/1 \times 4/2 \times 6/3 \times 4/1 = 48$, etc.

All the expressions for d_{2n} can now be written down by starting with d_4; i.e.

$$d_4 = 1 + 4\epsilon^2$$

$$d_6 = 1 + 12\,\epsilon^2 + 8\,\epsilon^4$$

$$d_8 = 1 + 24\,\epsilon^2 + 48\,\epsilon^4 + \frac{64}{5}\,\epsilon^6$$

$$d_{10} = 1 + 40\,\epsilon^2 + 160\,\epsilon^4 + 128\,\epsilon^6 + \frac{128}{7}\,\epsilon^8$$

$$d_{12} = 1 + 60\,\epsilon^2 + 400\,\epsilon^4 + 640\,\epsilon^6 + \frac{1920}{7}\,\epsilon^8 + \frac{512}{21}\,\epsilon^{10}$$

$$d_{14} = 1 + 84\,\epsilon^2 + 840\,\epsilon^4 + 2240\,\epsilon^6 + 1920\,\epsilon^8 + 512\epsilon^{10} + \frac{1024}{33}\,\epsilon^{12}$$

and so on.

The coefficients of ϵ^{2n} in the odd d-values are obtained by dividing the coefficients in the previous even d-values by $(2n+1)$, so that the coefficients of ϵ^2 are divided by 3, those of ϵ^4 by 5, etc. Hence

[2] "Formeln für die Massenkraefte und kinematischen Zusammenhaenge bei geschraenkten Schubkurbelgetrieben," by E. Mewes, *Ingenieur-Archiv*, vol. 24, 1956, pp. 291–298.

Table 3 Binomial factorials $\binom{m}{n}$

m/n	1	2	3	4	5	6	7
2	2			$\binom{m}{m-n} = \binom{m}{n}$			
3	3						
4	4	6					
5	5	10					
6	6	15	20				
7	7	21	35				
8	8	28	56	70			
9	9	36	84	126			
10	10	45	120	210	252		
11	11	55	165	330	462		
12	12	66	220	495	792	924	
13	13	78	286	715	1287	1716	
14	14	91	364	1001	2002	3003	3432
15	15	105	455	1365	3003	5005	6435

and so on.

$$d_9 = 1 + 8\,\epsilon^2 + \frac{48}{5}\,\epsilon^4 + \frac{64}{35}\,\epsilon^6$$

$$d_{11} = 1 + \frac{40}{3}\,\epsilon^2 + 32\,\epsilon^4 + \frac{128}{7}\,\epsilon^6 + \frac{128}{63}\,\epsilon^8$$

$$d_{13} = 1 + 20\,\epsilon^2 + 80\,\epsilon^4 + \frac{640}{7}\,\epsilon^6 + \frac{640}{21}\,\epsilon^8 + \frac{512}{231}\,\epsilon^{10}$$

$$\approx 1 + 20\epsilon^2 + 80\epsilon^4 + 91.4\epsilon^6 + 30{,}5\epsilon^8 + 2\epsilon^{10}$$

and so on.

In converting the equation for $\cos\phi$ into a Fourier series we obtain

$$\cos\phi = (1-\epsilon^2)^{1/2}\left(-\frac{1}{2}\,e_0 + e_1\sin\Theta + e_2\cos 2\Theta - e_3\sin 3\Theta - e_4\cos 4\Theta + + - - \ldots\right) \quad \ldots\ldots [15]$$

with

$$\left.\begin{aligned} e_0 &= -2 + \frac{1}{2}\binom{2}{1}a_2 + \frac{1}{8}\binom{4}{2}a_4 + \ldots \\ e_1 &= a_1 + \frac{1}{4}\binom{3}{1}a_3 + \frac{1}{16}\binom{5}{2}a_5 + \ldots \\ e_2 &= \frac{1}{2}\,a_2 + \frac{1}{8}\binom{4}{1}a_4 + \ldots \\ e_3 &= \frac{1}{4}\,a_3 + \frac{1}{16}\binom{5}{1}a_5 + \ldots \end{aligned}\right\} \quad \ldots [16]$$

and so on. These values of $\binom{m}{n}$ are listed in Table 3.

For the components P_x, P_y of the resulting inertia force we obtain, if the mass of the connecting rod is m_r and the angular velocity of the crank is constant

$$\left.\begin{aligned} P_x/m_r R\dot{\Theta}^2 &= \cos\Theta + (\eta + \xi A_1)\sin\Theta + \xi(A_2\cos 2\Theta - A_3\sin 3\Theta - A_4\cos 4\Theta + + - - \ldots) \\ P_y/m_r R\dot{\Theta}^2 &= (1 - \xi + \eta A_1)\sin\Theta + \eta(A_2\cos 2\Theta - A_3\sin 3\Theta - A_4\cos 4\Theta + + - - \ldots) \end{aligned}\right\} \quad \ldots [17]$$

with

$$A_n = n^2(1-\epsilon^2)^{1/2}\,\frac{1}{\lambda}\,e_n = n^2(1-\epsilon^2)^{-1/2}\,\frac{1}{\mu}\,e_n$$

$$A_n = n^2\left(\frac{\mu}{2}\right)^{n-1}(1-\epsilon^2)^{-1/2}\left[b_n + b_{n+2}\binom{n+2}{1}\left(\frac{\mu}{2}\right)^2 + b_{n+4}\binom{n+4}{2}\left(\frac{\mu}{2}\right)^4 + \ldots\right] \quad \ldots\ldots [18]$$

From this, there results

$$\left.\begin{aligned} A_1 &= (1-\epsilon^2)^{-1/2}\left[2\,\frac{1}{2}\,\epsilon d_1 + 4\,\frac{1\cdot 1}{2\cdot 4}\,\epsilon d_3 3\left(\frac{\mu}{2}\right)^2 + 6\,\frac{1\cdot 1\cdot 3}{2\cdot 4\cdot 6}\,\epsilon d_5\,\frac{5\cdot 4}{1\cdot 2}\left(\frac{\mu}{2}\right)^4 + \ldots\right] \\ A_2 &= 4\,\frac{\mu}{2}\,(1-\epsilon^2)^{-1/2}\left[\frac{1}{2}\,d_2 + \frac{1\cdot 1}{2\cdot 4}\,d_4 4\left(\frac{\mu}{2}\right)^2 + \frac{1\cdot 1\cdot 3}{2\cdot 4\cdot 6}\,d_6\,\frac{6\cdot 5}{1\cdot 2}\left(\frac{\mu}{2}\right)^4 + \ldots\right] \\ A_3 &= 9\left(\frac{\mu}{2}\right)^2(1-\epsilon^2)^{-1/2}\left[4\,\frac{1\cdot 1}{2\cdot 4}\,\epsilon d_3 + 6\,\frac{1\cdot 1\cdot 3}{2\cdot 4\cdot 6}\,\epsilon d_5 5\left(\frac{\mu}{2}\right)^2 + 8\,\frac{1\cdot 1\cdot 3\cdot 5}{2\cdot 4\cdot 6\cdot 8}\,\epsilon d_7\,\frac{7\cdot 6}{1\cdot 2}\left(\frac{\mu}{2}\right)^4 + \ldots\right] \end{aligned}\right\} \quad \ldots [19]$$

and so on.

We write for $n = 1, 2, 3, \ldots$

$$A_n = C_n D_n \quad \ldots\ldots [20]$$

with

$$C_1 = \epsilon(1-\epsilon^2)^{-1/2};\quad C_2 = \mu(1-\epsilon^2)^{-1/2};$$

$$C_3 = \frac{9}{8}\,\mu^3\epsilon(1-\epsilon^2)^{-1/2};$$

$$C_4 = \frac{1}{4}\,\mu^3(1-\epsilon^2)^{-1/2};\quad C_5 = \frac{75}{128}\,\mu^4\epsilon(1-\epsilon^2)^{-1/2};$$

$$C_6 = \frac{9}{128}\,\mu^5(1-\epsilon^2)^{-1/2};\quad C_7 = \frac{245}{1024}\,\mu^6\epsilon(1-\epsilon^2)^{-1}\ :$$

$$C_8 = \frac{5}{256}\,\mu^7(1-\epsilon^2)^{-1/2}\ldots\ldots\ \ldots\ \ldots\ldots\ldots\ldots\ldots [21]$$

and

$$D_{2n-1} = d_{2n-1} + \frac{(2n-1)(2n+1)}{2n}\left(\frac{\mu}{2}\right)^2\left[d_{2n+1} + \frac{2n+3}{2}\left(\frac{\mu}{2}\right)^2\left\{d_{2n+3} + \frac{(2n+3)(2n+5)}{(2n+2)3}\left(\frac{\mu}{2}\right)^2\left\langle d_{2n+5} + \frac{(2n+5)(2n+7)}{(2n+3)4}\left(\frac{\mu}{2}\right)^2 d_{2n+7} + \ldots\right\rangle\right\}\right] \quad \ldots\ldots [22]$$

$$D_{2n} = d_{2n} + (2n-1)\left(\frac{\mu}{2}\right)^2\left[d_{2n+2} + \frac{(2n+1)(2n+3)}{(2n+2)2}\left(\frac{\mu}{2}\right)^2\left\{d_{2n+4} + \frac{2n+5}{3}\left(\frac{\mu}{2}\right)^2\left\langle d_{2n+6} + \frac{(2n+5)(2n+7)}{(2n+4)4}\left(\frac{\mu}{2}\right)^2 d_{2n+8} + \ldots\right\rangle\right\}\right] \quad \ldots\ldots [23]$$

Example

When $\epsilon = 0.3162$ then

$d_4 = 1.4$, $d_6 = 2.28$, $d_8 = 3.8928$, $d_{10} = 6.7298$

$d_{12} = 11.6677$, $d_{14} = 20.2372$, $d_{16} = 35.0966$, . . .

$d_5 = 1.1333$, $d_7 = 1.416$, $d_9 = 1.8978$, $d_{11} = 2.6718$

$d_{13} = 3.8945$, $d_{15} = 5.8219$, $d_{17} = 8.8692$, . . .

Further $\lambda = 0.36$ is given. The corresponding value of $\mu = 0.4$. The inertia force components up to the 6th order inclusive are calculated. They are

$C_1 = 0.333$ $\quad C_2 = 0.422$

$C_3 = 0.0600$ $\quad C_4 = 0.01686$

$C_5 = 0.00500$ $\quad C_6 = 0.000759$

. . .

Generally one obtains

$$\left.\begin{aligned}
D_1 &= 1 + \frac{3}{8}\mu^2\left(1 + \frac{5}{8}\mu^2\left[d_5 + \frac{35}{48}\mu^2\left\{d_7 + \frac{63}{80}\mu^2\left\langle d_9 + \frac{33}{40}\mu^2 d_{11} + \ldots\right\rangle\right\}\right]\right)\\
D_2 &= 1 + \frac{1}{4}\mu^2\left(d_4 + \frac{15}{32}\mu^2\left[d_6 + \frac{7}{12}\mu^2\left\{d_8 + \frac{21}{32}\mu^2\left\langle d_{10} + \frac{99}{140}\mu^2 d_{12} + \ldots\right\rangle\right\}\right]\right)\\
D_3 &= 1 + \frac{15}{16}\mu^2\left(d_5 + \frac{7}{8}\mu^2\left[d_7 + \frac{7}{8}\mu^2\left\{d_9 + \frac{99}{112}\mu^2\left\langle d_{11} + \frac{143}{160}\mu^2 d_{13} + \ldots\right\rangle\right\}\right]\right)\\
D_4 &= d_4 + \frac{3}{4}\mu^2\left(d_6 + \frac{35}{48}\mu^2\left[d_8 + \frac{9}{12}\mu^2\left\{d_{10} + \frac{99}{128}\mu^2\left\langle d_{12} + \frac{143}{180}\mu^2 d_{14} + \ldots\right\rangle\right\}\right]\right)\\
D_5 &= d_5 + \frac{35}{24}\mu^2\left(d_7 + \frac{9}{8}\mu^2\left[d_9 + \frac{33}{32}\mu^2\left\{d_{11} + \frac{143}{144}\mu^2\left\langle d_{13} + \frac{139}{40}\mu^2 d_{15} + \ldots\right\rangle\right\}\right]\right)\\
D_6 &= d_6 + \frac{5}{4}\mu^2\left(d_8 + \frac{63}{64}\mu^2\left[d_{10} + \frac{11}{12}\mu^2\left\{d_{12} + \frac{143}{160}\mu^2\left\langle d_{14} + \frac{39}{44}\mu^2 d_{16} + \ldots\right\rangle\right\}\right]\right)
\end{aligned}\right\} \ldots [24]$$

whence, for this example

$D_1 = 1 + 0.060 + 0.007 + 0.001 = 1.068$

$D_2 = 1 + 0.056 + 0.007 + 0.001 = 1.164$

$D_3 = 1 + 0.170 + 0.030 + 0.006 + 0.001 = 1.207$

$D_4 = 1.4 + 0.274 + 0.054 + 0.011 + 0.002 = 1.741$

$D_5 = 1.133 + 0.331 + 0.079 + 0.018 + 0.004 + 0.001 = 1.566$

$D_6 = 2.28 + 0.779 + 0.212 + 0.054 + 0.013 + 0.002 = 3.34$

and

$A_1 = 0.356$, $\quad A_2 = 0.449$, $\quad A_3 = 0.0724$, $\quad A_4 = 0.0294$

$A_5 = 0.00783$, $\quad A_6 = 0.00254$

For this example $\xi = 0.4$ and $\eta = 0.1$ are given. Then

$$P_x/m_r R\dot{\Theta}^2 = \cos\Theta + 0.242\sin\Theta + 0.180\cos 2\Theta - 0.0290\sin 3\Theta - 0.0118\cos 4\Theta + 0.00313\sin 5\Theta + 0.00102\cos 6\Theta - - + + \ldots$$

$$P_y/m_r R\dot{\Theta}^2 = 0.6356\sin\Theta + 0.0449\cos 2\Theta - 0.00724\sin 3\Theta - 0.00294\cos 4\Theta + 0.000783\sin 5\Theta + 0.000254\cos 6\,\Theta - - + + \ldots$$

Angular accelerations

Variable inertia force moments act around the cg of the rod as a result of its angular accelerations. The law for the angular accelerations may be established, if the variation of the sin (and cos) of the angle of direction of the part are given. From the always valuable relation

$$\frac{d^2\alpha}{dt^2} = \cos\alpha\,\frac{d^2\sin\alpha}{dt^2} - \sin\alpha\,\frac{d^2\cos\alpha}{dt^2} \quad \ldots\ldots [25]$$

applied to the connecting rod with the angle of direction ϕ we obtain

$$\ddot{\phi} = -\lambda\dot{\Theta}^2(1-\epsilon^2)^{1/2}\left[\left(-\frac{1}{2}e_0 + e_1\frac{\epsilon}{\lambda} + \frac{4-1}{2}e_2\right)\sin\Theta + \left(4e_2\frac{\epsilon}{\lambda} + \frac{9-1}{2}e_3\right)\cos 2\Theta - \left(\frac{4-1}{2}e_2 + 9e_3\frac{\epsilon}{\lambda} + \frac{16-1}{2}e_4\right)\sin 3\Theta - \left(\frac{9-1}{2}e_3 + 16e_4\frac{\epsilon}{\lambda} + \frac{25-1}{2}e_5\right)\cos 4\Theta + + - - \ldots\right] \quad \ldots\ldots [26]$$

with

$$A_0 = (1-\epsilon^2)^{1/2}e_0/\lambda \quad \ldots\ldots [27]$$

or

$$A_0 = (1-\epsilon^2)^{-1/2}\frac{1}{\mu}\left[-2 + \frac{1}{2}\binom{2}{1}\left|\binom{1/2}{1}\right|\mu^2 + \frac{1}{8}\binom{4}{2}\left|\binom{1/2}{2}\right| d_4\mu^4 + \ldots\right] \quad \ldots\ldots [28]$$

$$A_0 = -(1-\epsilon^2)^{-1/2}\frac{2}{\mu}\left[1 - \frac{1}{4}\mu^2\left\{1 + \frac{3}{16}\mu^2\left\langle d_4 + \frac{5}{12}\mu^2 d_6 + \ldots\right\rangle\right\}\right] \quad \ldots\ldots [29]$$

and

$$E_1 = -\frac{1}{2}A_0 + A_1\frac{\epsilon}{\lambda} + \frac{1-1/4}{2}A_2$$
$$E_2 = A_2\frac{\epsilon}{\lambda} + \frac{1-1/9}{2}A_3$$
$$E_3 = \frac{1-1/4}{2}A_2 + A_3\frac{\epsilon}{\lambda} + \frac{1-1/16}{2}A_4 \quad \ldots [30]$$

and so on, we obtain

$$\ddot{\phi} = -\lambda^2\dot{\Theta}^2(E_1\sin\Theta + E_2\cos 2\Theta - E_3\sin 3\Theta - E_4\cos 4\Theta + + - - \ldots) \ldots [31]$$

For the example given ($\lambda = 0.36$ and $\epsilon = 0.3162$) we obtain

$A_0 = -5.270\,(1 - 0.040 - 0.002) = -5.270 \times 0.958 = -5.05$

$E_1 = 2.525 + 0.313 + 0.0168 = 3.006, \quad \lambda^2E_1 = 0.389$

$E_2 = 0.395 + 0.032 = 0.427, \quad \lambda^2E_2 = 0.0553$

$E_3 = 0.1684 + 0.0635 + 0.0138 = 0.2457, \quad \lambda^2E_3 = 0.0318$

$E_4 = 0.0322 + 0.0258 + 0.0038 = 0.0618, \quad \lambda^2E_4 = 0.00800$

$E_5 = 0.01378 + 0.00688 + 0.00123 = 0.02189, \lambda^2E_5 = 0.00284$

Accuracy of numerical results

The variations of

$$P_x/m_rR\dot{\Theta}^2, \quad P_y/m_rR\dot{\Theta}^2 \quad \text{and} \quad -\ddot{\phi}/\dot{\Theta}^2$$

with Θ for the foregoing example are shown in Figs. 2, 3, 4. If these results are to be used with an accuracy of 1 per cent the following expressions are sufficient

$$P_x/m_rR\dot{\Theta}^2 = \cos\Theta + 0.24\sin\Theta + 0.18\cos 2\Theta - 0.03\sin 3\Theta - 0.01\cos 4\Theta$$

$$P_y/m_rR\dot{\Theta}^2 = 0.64\sin\Theta + 0.04\cos 2\Theta - 0.01\sin 3\Theta$$

$$-\ddot{\phi}/\dot{\Theta}^2 = 0.390\sin\Theta + 0.055\cos 2\Theta - 0.032\sin 3\Theta - 0.008\cos 4\Theta + 0.003\sin 5\Theta$$

For the desired accuracy of P_x (and P_y) the values $A_1 - A_4$ must be determined so that their absolute errors are less than 0.025. For this a calculation without d_8, d_7, and so on, can be used.

For $\eta = 0$ and $\xi = 1$ the inertia force acts in direction x, and $P_y = 0$

$$P/mR\dot{\Theta}^2 = \cos\Theta + A_1\sin\Theta + A_2\cos 2\Theta - A_3\sin 3\Theta - A_4\cos 4\Theta + + - - \ldots \ldots [32]$$

For an accuracy in this variation within 1 per cent, the values of A must be determined with errors less than 0.01. For the calculation of

$$P/mR\dot{\Theta}^2 = \cos\Theta + 0.36\sin\Theta + 0.45\cos 2\Theta - 0.07\sin 3\Theta - 0.03\cos 4\Theta + 0.01\sin 5\Theta$$

(for $\lambda = 0.36$; $\epsilon = 0.3162$) the values of d_7, d_8 may be omitted.

More interesting than the variation of the resultant of the forces (components)—except their maximum values—are the magnitudes of the individual orders of the inertia forces, as these components (orders) can give resonances.

If A_4 is to be calculated with an accuracy of 1 per cent, for this example d_8 still is needed; for an accuracy of 1 per mille for A_6, d_{16} still is necessary.

Effect of offset on the coefficients

Without offset ($E = 0$, whence $\epsilon = 0$)

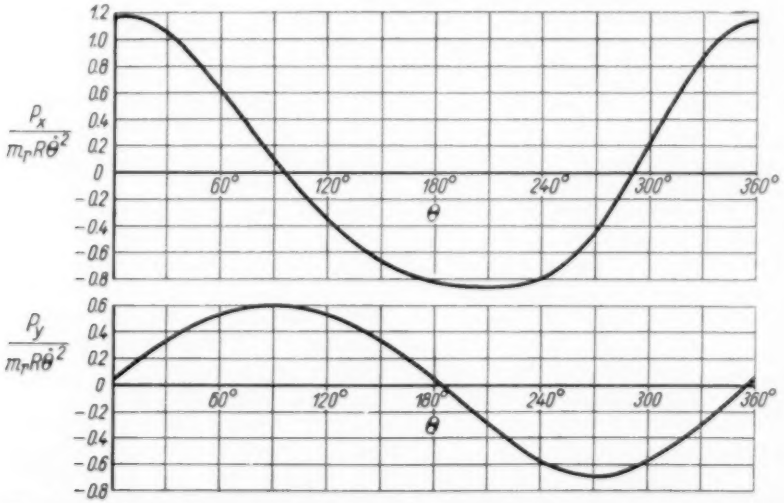

Figs. 2, 3 Variation of force components in X and Y-directions with crank-position angle for a given example with constant angular crankshaft velocity $\dot{\theta}$

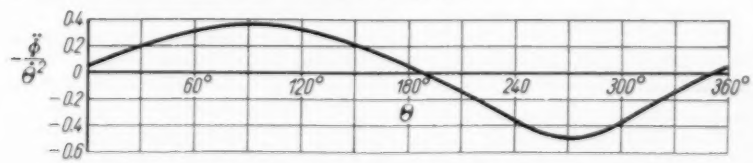

Fig. 4 Variation of angular acceleration of rod for given example

$$\left.\begin{aligned} a_{2n-1} &= 0 \\ a_{2n} &= \left|\binom{1/2}{n}\right| \lambda^{2n} \end{aligned}\right\} \quad n = 1, 2, 3 \ldots \ldots \ldots [33]$$

$$\cos\phi = 1 - \frac{1}{2}\lambda^2 \sin^2\Theta - \frac{1}{8}\lambda^4 \sin^4\Theta - \frac{1}{16}\lambda^6 \sin^6\Theta - \ldots \ldots [34]$$

For all the eccentricities of the slider crank, however

$$a_{2n-1} = 2n \left|\binom{1/2}{n}\right| \epsilon d_{2n-1} \left(\frac{\lambda}{1-\epsilon^2}\right)^{2n-1} \ldots \ldots [35]$$

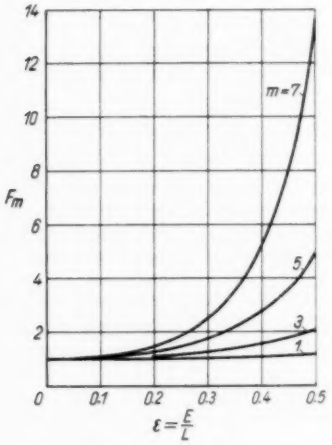

Fig. 5 Effect of eccentricity ratio on factors in some odd-order components of inertia force

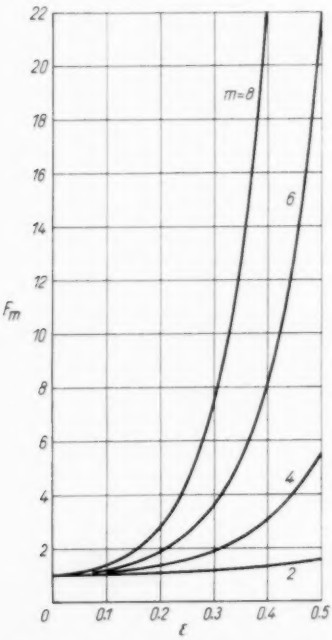

Fig. 6 Effect of eccentricity ratio on some even-order components

$$a_{2n} = \left|\binom{1/2}{n}\right| d_{2n} \left(\frac{\lambda}{1-\epsilon^2}\right)^{2n} \ldots \ldots \ldots [36]$$

The coefficients in cos ϕ become $a_n (1 - \epsilon^2)^{1/2}$ that may be called f_n. Then

$$\frac{a_{2n}(1-\epsilon^2)^{1/2}}{a_{2n(\epsilon=0)}} = \frac{f_{2n}}{\left|\binom{1/2}{n}\right| \lambda^{2n}} = F_{2n} = d_{2n}(1-\epsilon^2)^{1/2-2n} \ldots [37]$$

These factors as well as

$$\frac{f_{2n-1}}{2n\left|\binom{1/2}{n}\right| \epsilon\lambda^{2n-1}} = F_{2n-1} = d_{2n-1}(1-\epsilon^2)^{1/2-(2n-1)} \ldots [38]$$

$$F_m = d_m(1-\epsilon^2)^{1/2-m} \ldots \ldots \ldots \ldots \ldots [39]$$

are plotted against ϵ in Figs. 5 and 6 for

$$n = 1 - 4 (m = 1 - 8)$$

They show large increases for high eccentricities, especially with the factors F_{2n} for higher n. So, the magnitudes of the inertia forces, especially of higher orders, depend strongly on the eccentricities of the slider crank. That is

$$\left.\begin{aligned} A_0 &= -\frac{2}{\lambda} F_0 + \frac{1}{2}\left\langle \lambda F_2 + \frac{1\cdot3}{2\cdot2\cdot4}\left\{\lambda^3 F_4 + \frac{3\cdot5}{3\cdot3\cdot4}\left[\lambda^5 F_6 + \frac{5\cdot7}{4\cdot4\cdot4}(\lambda^7 F_8 + \ldots)\right]\right\}\right\rangle \\ A_2 &= \lambda F_2 + \frac{1\cdot3}{3\cdot1\cdot4}\left\{\lambda^3 F_4 + \frac{3\cdot5}{4\cdot2\cdot4}\left[\lambda^5 F_6 + \frac{5\cdot7}{5\cdot3\cdot4}(\lambda^7 F_8 + \ldots)\right]\right\} \\ A_4 &= \frac{1}{4}\left\{\lambda^3 F_4 + \frac{3\cdot5}{5\cdot1\cdot4}\left[\lambda^5 F_6 + \frac{5\cdot7}{6\cdot2\cdot4}(\lambda^7 F_8 + \ldots)\right]\right\} \end{aligned}\right\} \ldots [40]$$

and so on; and

$$\left.\begin{aligned} A_1 &= \epsilon\left\langle F_1 + \frac{1\cdot3}{2\cdot1\cdot4}\left\{\lambda^2 F_3 + \frac{3\cdot5}{3\cdot2\cdot4}\left[\lambda^4 F_5 + \frac{5\cdot7}{4\cdot3\cdot4}(\lambda^6 F_7 + \ldots)\right]\right\}\right\rangle \\ A_3 &= \frac{9}{8}\epsilon\left\{\lambda^2 F_3 + \frac{3\cdot5}{4\cdot1\cdot4}\left[\lambda^4 F_5 + \frac{5\cdot7}{5\cdot2\cdot4}(\lambda^6 F_7 + \ldots)\right]\right\} \end{aligned}\right\} \ldots [41]$$

and so on.

Special case for large L/R

In many agricultural machines such as vibrating sieves and similar devices, the proportion L/R is very large so that $\lambda \approx 0$; e.g., $L/R > 20$ for side mowers. For such proportions approximately

$$A_1 = \frac{\epsilon}{(1-\epsilon^2)^{1/2}} \ldots \ldots \ldots \ldots \ldots [42]$$

$$\left.\begin{aligned} P_x/m_rR\dot{\Theta}^2 &= \cos\Theta + \left[\eta + \xi\frac{\epsilon}{(1-\epsilon^2)^{1/2}}\right]\sin\Theta \\ P_y/m_rR\dot{\Theta}^2 &= \left[1 - \xi + \eta\frac{\epsilon}{(1-\epsilon^2)^{1/2}}\right]\sin\Theta \end{aligned}\right\} \quad \ldots [43]$$

while for a moment of inertia of the connecting member k^2L^2m, the moment around the cg is

$$M = -\frac{1}{(1-\epsilon^2)^{1/2}}k^2m_rRL\dot{\Theta}^2\sin\Theta \quad \ldots [44]$$

If a is the amplitude of the oscillation of $P_x/m_rR\dot{\Theta}^2$, then

$$a^2 = 1 + \left[\eta + \xi\frac{\epsilon}{(1-\epsilon^2)^{1/2}}\right]^2$$

$$= 1 + \eta^2 + 2\xi\eta\frac{\epsilon}{(1-\epsilon^2)^{1/2}} + \xi^2\frac{\epsilon^2}{1-\epsilon^2}$$

$$= \frac{1}{1-\epsilon^2}[(1+\eta^2)(1-\epsilon^2) + \xi^2\epsilon^2 + 2\xi\eta\epsilon(1-\epsilon^2)^{1/2}] \quad \ldots [45]$$

For $\eta = 0$

$$a = \left[\frac{1-\epsilon^2(1-\xi^2)}{1-\epsilon^2}\right]^{1/2} \quad \ldots [46]$$

For $\epsilon = 0.3$ and $\xi = 0.6$

$$a = \left(\frac{1 - 0.09 \times 0.64}{1 - 0.09}\right)^{1/2} = 1.018$$

For $\eta = 0$ and $\xi = 1$ is $P_y = 0$ and

$$P/mR\dot{\Theta}^2 = \cos\Theta + \frac{\epsilon}{(1-\epsilon^2)^{1/2}}\sin\Theta \quad \ldots [47]$$

$$a = \frac{1}{(1-\epsilon^2)^{1/2}} \quad \ldots [48]$$

This is the same factor as the proportion of the stroke to the crank diameter for large L/R. There is always available for this ratio the following infinite series which may be used for small values of λ

$$\frac{S}{2R} = \frac{1}{(1-\epsilon^2)^{1/2}}\left(1 + \frac{1}{2}\epsilon^2\mu^2 + \ldots\right) \quad \ldots [49]$$

$$= 1 + \frac{1}{2}\epsilon^2\frac{1}{1-\lambda^2} + \frac{1\cdot1}{2\cdot4}\epsilon^4\frac{3+\lambda^2}{(1-\lambda^2)^3}$$

$$+ \frac{1\cdot1\cdot3}{2\cdot4\cdot6}\epsilon^6\frac{5 + \binom{5}{3}\lambda^2 + \lambda^4}{(1-\lambda^2)^5} + \ldots \quad \ldots [50]$$

For $\eta = 0$, $\xi = 1$ and $\epsilon = 0.3$, $a = 1.048$

Further moments around shaft

Besides the moment around the cg of the connecting member the mass forces give moments around the shaft axis. Also, there are moments from the nonconstant velocity of revolution of shaft and flywheel. In all slider-crank mechanisms there are oscillating moments which act on the engine frame. These moments are independent of the magnitude of the flywheel and depend on the oscillating masses as well as on those of the connecting rod, further on the friction forces and mainly on the forces acting on the reciprocating parts (the pistons). So, these forces even when internal to the engine, influence the mass forces of the total mechanism.

Artificial balancing

The inertia forces and moments of each order can be balanced theoretically by shafts carrying eccentric masses and rotating in opposite directions with a different velocity for each order. For balancing the forces of the first order the masses may be fixed to the crankshaft and to a geared shaft rotating with the same velocity in the opposite direction.

With the arrangement of Fig. 7 we obtain from the eccentric masses rotating at constant velocity $\dot{\Theta}$ the components

$$\left.\begin{aligned} P_x' &= [-(m_1+m_3)\cos\Theta + (m_2+m_4)\sin\Theta]R\dot{\Theta}^2 \\ P_y' &= [-(m_2-m_4)\cos\Theta - (m_1-m_3)\sin\Theta]R\dot{\Theta}^2 \\ M_z' &= [(m_3Y_1 + m_4X_1)\cos\Theta \\ &\quad + (m_3X_1 - m_4Y_1)\sin\Theta]R\dot{\Theta}^2 \end{aligned}\right\} \quad \ldots [51]$$

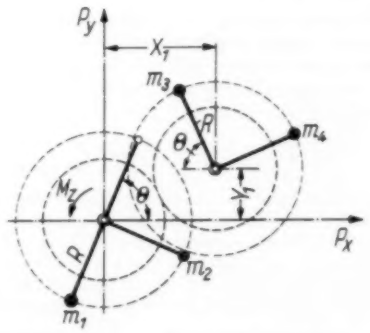

Fig. 7 Eccentric masses fixed to crankshaft and to a geared shaft rotating with same speed in opposite direction

The first-order harmonic components of the force components of the moving masses can be written in the form

$$\left.\begin{aligned} P_{x1} &= mR\dot{\Theta}^2(A_{x1}\cos\Theta + B_{x1}\sin\Theta) \\ P_{y1} &= mR\dot{\Theta}^2(A_{y1}\cos\Theta + B_{y1}\sin\Theta) \\ M_{z1} &= mR^2\dot{\Theta}^2(A_{z1}\cos\Theta + B_{z1}\sin\Theta) \end{aligned}\right\} \quad \ldots [52]$$

Then there are no resulting force components of the first order if

$$\frac{m_1}{m} = \frac{1}{2}(A_{x1} + B_{y1}) \quad \ldots [53]$$

$$\frac{m_2}{m} = -\frac{1}{2}(B_{x1} - A_{y1}) \quad \ldots [54]$$

$$\frac{m_3}{m} = \frac{1}{2}(A_{x1} - B_{y1}) \quad \ldots [55]$$

$$\frac{m_4}{m} = -\frac{1}{2}(B_{x1} + A_{y1}) \quad \ldots [56]$$

If we have no oppositely running shaft but only the crankshaft with the eccentric masses m_1 and m_2, then the resulting force in the first-order components is smallest for the Conditions [53] and [54]. We cannot say that this condition is always optimum because the forces often affect differently the strength of vibration in different directions. The diagram of the maximum resulting force as a function of m_1/m and m_2/m gives a cone with its apex at

$$P_{x0} = mR\dot{\Theta}^2(A_{x1}^2 + B_{x1}^2 + A_{y1}^2 + B_{y1}^2)^{1/2}$$

at $\qquad \frac{1}{2}(A_{x1} + B_{y1}), \quad -\frac{1}{2}(B_{x1} - A_{y1})$

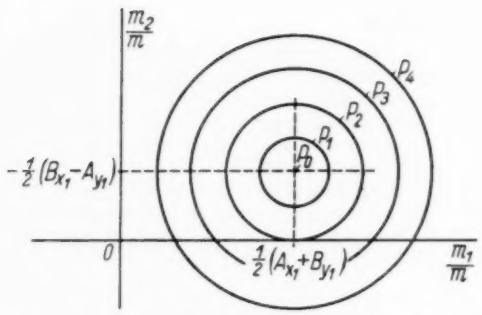

Fig. 8 Lines of equal resultant forces in first-order harmonic components of a slider crank with eccentric masses on rotating crankshaft

The lines of equal resulting forces are concentric circles in an $(m_1/m - m_2/m)$ diagram, Fig. 8.

Even if the force resultant vanishes (because of balancing by oppositely rotating shafts) it is still possible that a couple exists. This will vanish when

$$\frac{X_1}{R} = -\frac{A_{z1}m_4 + B_{z1}m_3}{m_3^2 + m_4^2}\, m \qquad [57]$$

$$\frac{Y_1}{R} = -\frac{A_{z1}m_3 - B_{z1}m_4}{m_3^2 + m_4^2}\, m \qquad [58]$$

For other positions of the oppositely rotating shaft there will remain couples whose greatest magnitude is proportional to the distance of the shaft from the point according to Equations [57], [58], Fig. 9.

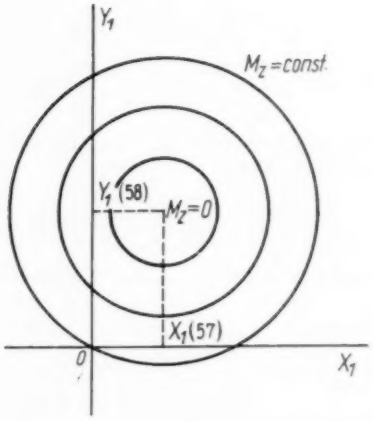

Fig. 9 Lines of equal magnitude of the remaining couples for different positions of oppositely rotating shaft with eccentric masses so that resulting force components of first harmonic order are balanced

The method of calculating balancing masses on rotating shafts for artificial balance of single-order harmonic components also may be used for other mechanisms.[3]

[3] "Massenausgleich an ebenen Kurbelgetrieben," by E. Mewes, *Zeitschrift fur angewandte Mathematik und Mechanik*, vol. 35, 1955, pp. 349–350, and vol. 36, 1956, p. 80.

Redundant Trusses of Elastic-Strain-Hardening Material[1]

By HANS ZIEGLER,[2] ZURICH, SWITZERLAND

W. Prager has given a geometric method for the determination of the load-carrying capacity of a redundant truss consisting of elastic, perfectly plastic bars. In the present paper this method is generalized for trusses consisting of elastic-strain-hardening bars with given limit loads in tension and compression.

Introduction

IDEAL trusses are subject to the following assumptions:

(*a*) Their elements are straight bars connected by smooth pins, the centers of which (the joints of the truss) lie on the center lines of the bars they connect.

(*b*) The weights of the bars are so small compared with the other loads that they may be neglected.

(*c*) The remainder of the external forces (loads and reactions) are acting at the joints.

These conditions insure that the bars are stressed in simple tension or compression.

If an ideal truss is statically determinate, the forces transmitted by the individual bars are entirely determined by the equilibrium of the joints and the bars, provided the deformations are so small that the geometry of the truss is not noticeably altered during the process of loading. Under this condition, the forces can be obtained, for instance, by means of a Maxwell diagram. They are independent of the rheological behavior of the materials employed, and likewise independent of the way the final state of loading has been reached. The design of the individual bars is, therefore, a straightforward process.

In a redundant truss, the situation is more complicated. Here, the distribution of the internal forces also depends on the deformations and thus on the dimensions of the elements as well as on their rheological response. Hence the stress analysis must be based on a tentative design of the members. Moreover, the final distribution under a given system of loads usually depends on the way in which these loads have been applied. A precise knowledge of this final distribution is obtained only by a careful study of the behavior of the truss during the various steps of the loading process.

In the case of a purely elastic truss, the necessity last mentioned does not yet arise. Here, the principle of Castigliano supplies the missing equations as soon as the dimensions of the members are given, and the internal forces are uniquely determined by the final loads.

The more complicated case of a truss consisting of elastic, perfectly plastic bars has been discussed recently by W. Prager.[3] His treatment is based on the fundamental idea of conceiving the state of stress in the truss as resulting from the superposition of more elementary states: A state of the first type for each parameter characterizing the system of loads, and a state of the second type for every degree of redundancy.

This elegant way of splitting up the state of stress is not only useful in the case of an elastic, ideally plastic truss. In this paper, a generalization for elastic-strain-hardening trusses with given limit loads for each member (fracture loads, buckling loads) is presented. The approach likewise is based on the assumption that the deformations are sufficiently small to maintain the original geometry of the truss. The treatment is essentially limited to the case of a simply redundant truss with a single load parameter.

Response of the members

Considering an arbitrary bar of the truss, we assume that its stress-strain diagram is of the elastic-strain-hardening type illustrated in Fig. 1. Here, ϵ denotes the strain and σ the stress. The yield stresses are $\sigma_t > 0$ in tension and $\sigma_c < 0$ in compression; E is the elastic modulus and C the modulus of strain-hardening. In a first loading OT and TA represent, respectively, the elastic and the plastic response. If the bar is unloaded from A, the load being subsequently reversed, AB represents the elastic unloading; BC illustrates the elastic loading in the reverse sense, and CD represents the subsequent plastic flow.

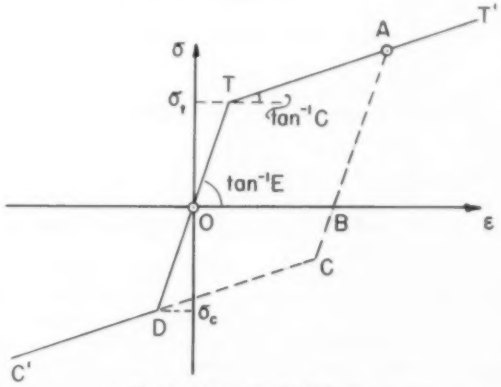

Fig. 1 Stress-strain diagram

The incremental stress-strain relations are

$$d\epsilon = \frac{1}{E}\, d\sigma \qquad [1]$$

in the elastic range, represented by all of the segments AC between the lines TT' and CC', and

$$d\epsilon = \frac{1}{C}\, d\sigma \qquad [2]$$

[1] The results presented in this paper were obtained in the course of research conducted under Contract Nonr 562(10) by the Office of Naval Research and Brown University.

[2] Professor of Mechanics, Eidg. Technische Hochschule; 1956/1957 Visiting Professor, Brown University, Providence, R. I.

Contributed by the Applied Mechanics Division and presented at the Annual Meeting, New York, N. Y., December 1–6, 1957, of The American Society of Mechanical Engineers.

Discussion of this paper should be addressed to the Secretary, ASME, 29 West 39th Street, New York, N. Y., and will be accepted until July 10, 1958, for publication at a later date. Discussion received after the closing date will be returned.

Note: Statements and opinions advanced in papers are to be understood as individual expressions of their authors and not those of the Society. Manuscript received by ASME Applied Mechanics Division, April 2, 1957. Paper No. 57—A-28.

[3] "Probleme der Plastizitätstheorie," by W. Prager, Birkhäuser, Basel and Stuttgart, 1955, p. 23.

in the plastic range, represented by the lines TT' and CC'.

We may assume that the bar in consideration has two limit stresses; namely, a limit stress σ_T in tension at which fracture is to be expected, and a limit stress σ_C in compression beyond which the danger of buckling arises. The corresponding points in the stress-strain diagram are denoted by T' and C', respectively.

The state of stress

Let the loads P_i acting on a truss depend on a load parameter μ. Thus they have the forms

$$P_i = \mu P_i', \quad (i = 1, 2, \ldots, q)$$

(where $q = 3$ in the special case illustrated in Fig. 2).

Unknown so far are the internal forces transmitted by the bars, which from now on will be referred to as stresses, and the external reactions. In a fixed-hinge support, two reactions are present; in a movable-hinge support, a single one. Let the stresses be denoted by $F_1, F_2, \ldots, F_n$ and the external reactions by $F_{n+1}, \ldots, F_s$. (In the case of Fig. 2, $n = 5$ and $s = 9$.)

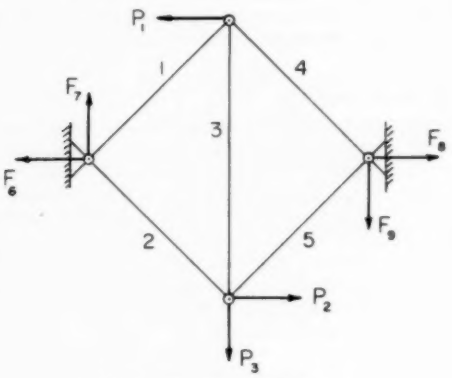

Fig. 2 Simply redundant truss

Formulating the equilibrium conditions for the joints, we obtain an inhomogeneous system of linear equations

$$\sum_{k=1}^{s} a_{ik}F_k = \mu b_i, \quad (i = 1, 2, \ldots, r) \ldots\ldots\ldots [3]$$

where $r/2$ is the number of joints, and the terms b_i are linear combinations of the loads P_i'.

In a statically determinate truss, the number r of linearly independent relations [3] is equal to the total number s of stresses and reactions. In this case, there exists exactly one solution.

If the truss is (externally or internally) simply redundant, the number of linearly independent relations [3] is $r = s - 1$. (In Fig. 2, for instance, $s = 9$ and $r = 8$.) The stress distribution (including reactions) is still a solution of the system

$$\sum_{k=1}^{s} a_{ik}F_k = \mu b_i, \quad (i = 1, 2, \ldots, s - 1) \ldots\ldots [4]$$

but not uniquely determined by it. The actual stress distribution, however, is included in the general solution of the system [4], which consists of a particular solution, and the general solution of the reduced system

$$\sum_{k=1}^{s} a_{ik}F_k = 0, \quad (i = 1, 2, \ldots, \quad - 1) \ldots\ldots [5]$$

It is obvious that a particular solution of the system [4] is given by $F_k = \mu F_k'$, where the F_k' represent an arbitrary elastic stress distribution in the nonprestrained truss under the loads P_i'. Such a distribution is easily obtained by current methods. As long as no plastic response has occurred, this is the real solution, since the solution of the system [5] in this case, on account of the fact that the unloaded truss is unstressed, is identically zero.

On the other hand, the general solution of the system [5] has the form $F_k = \nu F_k''$, where ν is an arbitrary parameter and the F_k'' represent an arbitrary stress distribution for which the members of the unloaded truss are in equilibrium. The distribution F_k'', likewise, is easily obtained by removing the loads and the constraints, assuming an arbitrary system of reactions in equilibrium, and calculating the stresses corresponding in the nonprestressed truss to these reactions by the methods used in a statically determinate truss.

Thus the actual stress distribution under the loads $P_i = \mu P_i'$ at any instant has the form

$$F_k = \mu F_k' + \nu F_k'', \quad (k = 1, 2, \ldots, s) \ldots\ldots\ldots [6]$$

It consists of two solutions, $\mu F_k'$ and $\nu F_k''$, which will be referred to as the solutions of the first and the second types. The first type solution represents the elastic stress distribution in the nonprestrained truss. The second type solution represents the influence of the plastic-strain history. It is not due, as the manner of calculating the F_k'' might imply, to a weakness in the constraints, but conversely to the fact that the truss with rigid constraints becomes prestrained in the course of its plastic response.

The only unknown quantity in Equations [6] is ν. As long as no plastic response has occurred, ν is zero, and the problem therefore is solved. After a plastic response, however, ν is usually different from zero, depending on the loading history. Thus the problem is reduced to the determination of the history parameter ν.

According to Equations [6] the instantaneous state of stress in the truss can be represented by a point P in a (μ, ν)-plane, Fig. 3. Its first co-ordinate, μ, is the load parameter; the other one, ν, is unknown *a priori*. When the load intensity is increased from zero, P travels along the μ-axis as long as the response of all bars is still elastic. When plastic response sets in, P leaves the μ-axis, and the determination of its path requires a careful study of the way in which the single bars respond to any further change of the load.

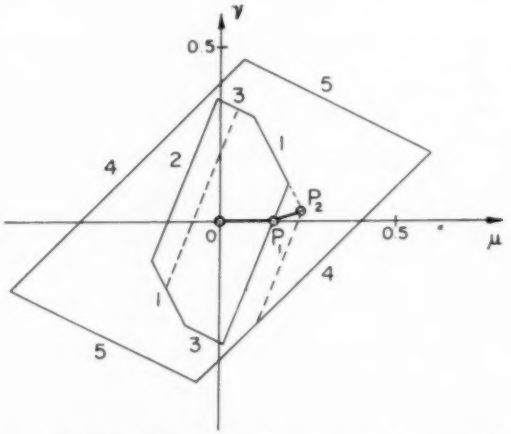

Fig. 3 Original yield polygon and yield polygon modified by the second step

In order to obtain the increment $d\nu$ corresponding to a given increment $d\mu$, we need one more relation to complete the system [4], and since the truss is redundant, this relation must represent a statement concerning the deformation. Let the elongations of the bars be denoted by λ_k, $(k = 1, 2, \ldots, n)$ and from now on referred to as strains. Since the stresses and reactions F_k'' are in equilibrium, their work in any virtual displacement is zero. The actual set of strains λ_k defines an admissible displacement, in which the reactions do no work. The missing condition is therefore

$$\Sigma F_k''\lambda_k = 0 \quad \ldots\ldots [7]$$

if from now on all sums without limits are extended over the bars alone $(k = 1, 2, \ldots, n)$.

As long as the truss has not undergone plastic deformations and the response of its members is purely elastic, the strains are given, according to Equation [1], by

$$\lambda_k = \alpha_k F_k, \quad (k = 1, 2, \ldots, n) \quad \ldots\ldots [8]$$

with

$$\alpha_k = \frac{l_k}{E_k A_k}, \quad (k = 1, 2, \ldots, n) \quad \ldots\ldots [9]$$

where l_k denotes the length of bar k, A_k its cross section, and E_k its elastic modulus. Hence, Equation [7] becomes, in terms of stresses

$$\Sigma \alpha_k F_k'' F_k = 0 \quad \ldots\ldots [10]$$

The unique solution of Equations [4] and [10] is the stress distribution of the first type. It follows that

$$\Sigma \alpha_k F_k'' F_k' = 0 \quad \ldots\ldots [11]$$

If a plastic response has occurred and a further change of the load intensity (for instance an infinitesimal unloading) represents a purely elastic process, we have, according to Equation [1]

$$d\lambda_k = \alpha_k dF_k, \quad (k = 1, 2, \ldots, n) \quad \ldots\ldots [12]$$

and thus, instead of Equations [4] and [10]

$$\sum_{k=1}^{s} a_{ik} dF_k = b_i d\mu, \quad (i = 1, 2, \ldots, s-1) \quad \ldots\ldots [13]$$

$$\Sigma \alpha_k F_k'' dF_k = 0 \quad \ldots\ldots [14]$$

Since this system follows from Equations [4] and [10] by replacing μ by $d\mu$, and F_k by dF_k, it has a unique solution, given by $dF_k = F_k' d\mu$. Comparing this result with the generally valid relation

$$dF_k = F_k' d\mu + F_k'' d\nu, \quad (k = 1, 2, \ldots, s) \quad \ldots\ldots [15]$$

following from Equations [6], we obtain $d\nu = 0$. Thus a purely elastic process (no matter whether preceded by any amount of plastic flow) is characterized by a straight path of P, parallel to the μ-axis.

If we finally consider a load increment for which the response of certain bars is plastic, we have to replace Equations [12], according to Equation [2], by

$$d\lambda_k = \alpha_k (E_k/C_k) dF_k \quad \ldots\ldots [16]$$

for these bars. Instead of Equation [14] we now have

$$\Sigma \alpha_k c_k dF_k = 0 \quad \ldots\ldots [17]$$

where

$$c_k = \begin{cases} F_k'' & \text{for elastic bars} \\ (E_k/C_k) F_k'' & \text{for plastic bars} \end{cases} \quad \ldots\ldots [18]$$

Equations [17] and [18] may be replaced by

$$\Sigma \alpha_k F_k'' dF_k + \Sigma' \alpha_k (E_k/C_k - 1) F_k'' dF_k = 0 \quad \ldots\ldots [19]$$

if here and in what follows the dash applied to the sum indicates a summation over the bars in plastic response alone. Inserting Equations [15] into [19], and making use of Equation [11], eventually we obtain the relation

$$d\mu \Sigma' \alpha_k (E_k/C_k - 1) F_k' F_k'' + d\nu [\Sigma \alpha_k F_k''^2 + \Sigma' \alpha_k (E_k/C_k - 1) F_k''^2] = 0 \quad \ldots\ldots [20]$$

between $d\mu$ and $d\nu$. It should be noted that Equation [20] is quite general, covering also the case of purely elastic response, where the dashed sums are empty and thus $d\nu = 0$.

The foregoing discussion can be generalized for trusses with M load parameters and N degrees of redundancy. Here, the stress distribution is a linear combination of M first type and N second type solutions. The geometrical representation, however, is cumbersome, since it requires a space of $M + N$ dimensions with M co-ordinate axes for $\mu_1, \mu_2, \ldots, \mu_M$, and N axes for $\nu_1, \nu_2, \ldots, \nu_N$. In a purely elastic process P travels in a subspace parallel to the axes $\mu_1, \mu_2, \ldots, \mu_N$, while in plastic response the path of P must be determined by a generalization of Equation [20]. If $M + N = 3$, i.e., for a simply redundant truss with two load parameters, or for a doubly redundant truss with a single load parameter, the representation is still comparatively simple since it only requires a three-dimensional space.

Response of the truss

The ensuing discussion will be limited to the simple case of two parameters μ and ν treated in detail in the foregoing section.

The bar k has two yield limits

$$F_{kt} = A_k \sigma_{kt} > 0$$

in tension and

$$F_{kc} = A_k \sigma_{kc} < 0$$

in compression. Provided its response so far has been elastic,

$$F_{kc} \leqq F_k \leqq F_{kt}$$

or, on account of Equation [6]

$$F_{kc} \leqq \mu F_k' + \nu F_k'' \leqq F_{kt}, \quad (k = 1, 2, \ldots, n) \quad \ldots\ldots [21]$$

In the (μ, ν)-plane (see Fig. 3 which corresponds to the truss of Fig. 2) the inequalities [21] are represented by n yield strips, bounded by the yield lines

$$\left.\begin{aligned} \mu F_k' + \nu F_k'' = F_{kc} < 0 \\ \mu F_k' + \nu F_k'' = F_{kt} > 0 \end{aligned}\right\} \quad (k = 1, 2, \ldots, n) \quad \ldots\ldots [22]$$

which are denoted by k in Fig. 3. Each of these yield strips contains the origin, and the response of the truss is elastic as long as the point P representing the state of stress lies inside all of the yield strips.

The region common to all yield strips is a convex polygon which will be called the original yield polygon. It may be bounded only by part of the yield lines (1, 2, 3 in Fig. 3) thus lying inside the remaining yield strips (4, 5). If the load intensity is increased from zero, P travels along the μ-axis, and the response of the truss is elastic as long as P lies inside the original yield polygon.

When P reaches the circumference of this polygon, hitting on one or more yield lines (2 in Fig. 3) the corresponding bars respond plastically to a further increase of the load. This implies the following consequences:

(*a*) According to the preceding section, a plastic response is

usually connected with a change of the parameter ν. This change must be calculated by Equation [20].

(*b*) According to the section "Response of the Members," a plastic flow modifies the yield limits of the bar in question. One of these yield limits is given by the actual stress, the other one differing from it by the constant amount $F_{k1} - F_{k0}$. Hence the yield lines passing through P are pushed along by P, retaining, however, their directions, and the corresponding yield strips take part in this translation. The yield polygon, likewise, is pushed along and is generally deformed at the same time.

As long as the same members respond plastically, the dashed sums in Equation [20] contain the same elements. Hence the path of P consists of straight segments, and the corners in the chain of these segments correspond to the values of the load parameter μ for which certain bars enter or leave the realm of plastic response. It is clear, therefore, that the response of the truss must be obtained in steps, each step corresponding to a straight segment.

Every one of these segments is given as soon as we know its starting point (which is the end point of the preceding segment) and the members responding plastically. The inclination is supplied by Equation [20]. If we use the notations

$$\beta_k = \alpha_k(E_k/C_k - 1) > 0, \qquad N = \Sigma\alpha_k F_k'^2 > 0 \ldots [23]$$

and

$$\Phi_k = -\beta_k F_k' F_k'', \quad \Psi_k = \beta_k F_k'^2 > 0 \ldots\ldots [24]$$

Equation [20] takes the form

$$-d\mu\Sigma'\Phi_k + d\nu(N + \Sigma'\Psi_k) = 0 \ldots\ldots [25]$$

Hence the segment has the inclination

$$v = \frac{\Sigma'\Phi_k}{N + \Sigma'\Psi_k} \ldots\ldots [26]$$

while the inclination of the yield line k, on account of Equations [22] and [24], is

$$u_k = \Phi_k/\Psi_k \ldots\ldots [27]$$

Thus the segment can be traced, its end point being the point of intersection with the next yield line which also determines the modified form of the yield polygon.

In Fig. 3, OP_1 corresponds to the elastic response under a monotonically increasing load parameter μ. As soon as P_1 is reached, bar 2 begins to flow. The inclination of the segment P_1P_2 follows from Equation [26] if the sums are limited to $k = 2$, and the end point P_2 is the point of intersection with yield line 1. The yield polygon for P_2 is indicated by dotted lines.

In this way, the response of the truss is obtained step by step, provided the bars responding plastically in every step are known. The yield strips enclosing the original yield polygon are in no way distinguished; the other yield strips usually begin to move as well after a few steps. Each step modifies the yield polygon, and if its new form is traced at the end of each step, unloading processes and reversals of the load can be treated in the same way if it is remembered that the path of μ inside the actual yield polygon is parallel to the μ-axis.

Figs. 4 through 7 illustrate the response of the truss of Fig. 2 to a further increase of the load. Apart from the sides of the yield polygon, these figures contain only the yield lines reached by P on its path. In the case illustrated here, P pushes along more and more yield lines, and finally the response of all bars is plastic.

In a truss where the ratios E_k/C_k are equal (E/C) for all bars, Φ_k, according to Equations [23] and [24], is given by

$$\Phi_k = -(E/C - 1)\alpha_k F_k' F_k'' \ldots\ldots [28]$$

If such a truss finally reaches a state where the response of all members is plastic, $d\nu$ becomes zero according to Equations [26] and [11]. Hence the path of P becomes parallel to the μ-axis. As a matter of fact, it is clear that such a truss responds to any further increase of the load like a (prestrained) truss with an elastic modulus C.

One point which still needs some consideration is the extent of the dashed sums in each step. In order to apply Equation [26], we must know which bars respond plastically. At the outset of an arbitrary step, at least one bar begins to flow which so far has responded elastically. It is possible, however, that other members, hitherto in plastic response, begin to unload elastically, particularly if certain ratios C_k/E_k are small, the corresponding bars thus being almost perfectly plastic.

According to a theorem by E. Melan[4] the response of the truss to an arbitrary increment $d\mu$ of the load parameter is unique. It follows that a segment, obtained for an arbitrary step under the assumption that certain bars respond plastically, represents the real solution if it lies outside the yield strips of the corresponding bars at the outset of the step (but inside the remaining yield strips).

In Figs. 3 through 7 the assumption that all bars with yield lines passing through P respond plastically supplies segments leaving all of the yield strips in question. These segments therefore represent the real solution.

Under the assumption that all of the bars in question flow, we will often hit on the correct solution. In cases where the segments obtained in this way lie inside certain yield strips, the calculation of v must be repeated under the assumption that the bars with least inclined yield lines respond elastically, until a consistent solution is found.

There are cases where the yield lines of several bars coincide. If this happens, the dashed sums in Equation [26] must be extended over all of these bars.

If we assume limit loads

$$F_{kT} = A_k\,\sigma_{kT} > 0 \text{ and } F_{kC} = A_k\sigma_{kC} < 0$$

for the bars, P must remain inside n limit strips bounded by limit lines. These limit strips are parallel to the corresponding yield strips, and the equations of the limit lines are given by [22], if on the right-hand sides the subscripts c and t are replaced by C and T, respectively. The limit strips enclose a limit polygon (similar to the yield polygon if the limit loads are proportional to the yield loads). As soon as P reaches the circumference of the limit polygon, one or more bars break or buckle.

In Fig. 7, $2'$ is the side of the limit polygon first reached by P in the position P_6. The original limit polygon (Fig. 8, drawn in a scale reduced in comparison with Figs. 3 through 7) is enclosed by the limit lines $1', 2', 3'$.

If P reaches the circumference of the original limit polygon on the limit lines of more than one bar, the load-carrying capacity of the truss is reached. It is represented by the abscissa of the last position of P.

If P reaches the limit line of a single bar i, its failure renders the truss statically determinate. A first consequence of this failure is a modification of the limit polygon, obtained by deleting the sides i. The second consequence is a jump of the parameter ν, which now assumes a value determined by

$$F_i = \mu F_i' + \nu F_i'' = 0 \ldots\ldots [29]$$

If the new position of P, calculated by means of Equation [29],

[4] "Zur Plastizität des räumlichen Kontinuums," by E. Melan, *Ingenieur-Archiv*, vol. 9, 1938, p. 116. See also, "The Mathematical Theory of Plasticity," by R. Hill, Oxford University Press, Oxford, England, 1950, p. 53

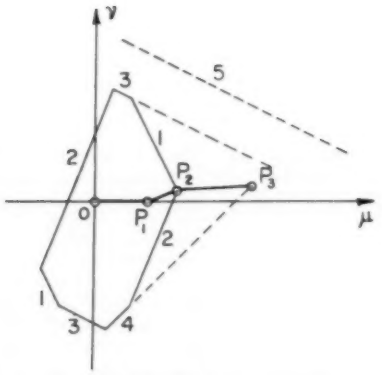

Fig. 4 Third step with initial yield polygon

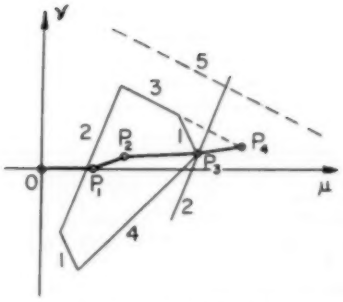

Fig. 5 Fourth step with initial yield polygon

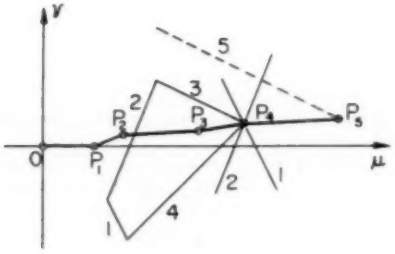

Fig. 6 Fifth step with initial yield polygon

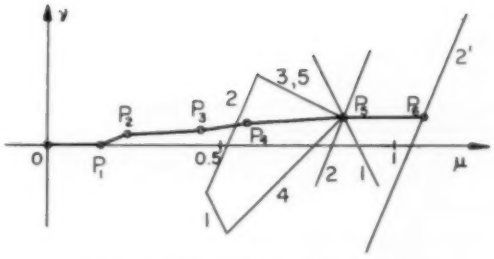

Fig. 7 Sixth step with initial yield polygon

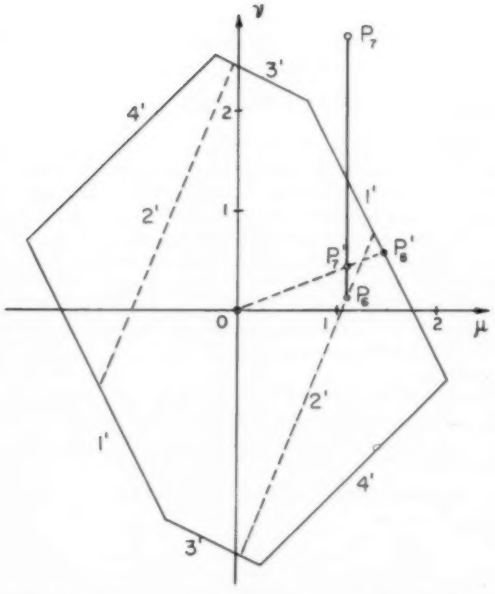

Fig. 8 Original and modified limit polygon. Last step: Failure of bar 2.

Table 1 Numerical values for illustrative example

bar	1	2	3	4	5
α_k	1	1	1	1	1
F_{kt}	1	.75	1	.8	1
F_{kc}	-1	-.75	-1	-.8	-1
F_{kT}	7	5.25	7	5.6	7
F_{kC}	-7	-5.25	-7	-5.6	-7
F_k'	-4	5	$\sqrt{2}$	2	-1
F_k''	-2	-2	$2\sqrt{2}$	-2	-2
E_k/C_k	2	2	2	2	2
$\beta_k=\alpha_k(E_k/C_k-1)$	1	1	1	1	1
$\Phi_k=-\beta_k F_k' F_k''$	-8	10	-4	4	-2
$\Psi_k=\beta_k F_k''^2$	4	4	8	4	4

lies outside the modified limit polygon or on its circumference, the load-carrying capacity is reached with the failure of the first bar.

This is the case in Fig. 8, where the modified limit polygon is enclosed by the limit lines 1′, 3′, 4′. The failure of bar 2 corresponds to a jump of P from P_6 to P_7 outside the modified limit polygon.

If the new position of P lies inside the modified limit polygon, a further increase of the load is possible. Since Equation [29] remains valid, a last step consists in a segment of a straight line passing through O, and its point of intersection with the circumference of the modified limit polygon finally defines the yield-carrying capacity.

This situation is exemplified in Fig. 8 by the segment $P_7'P_8'$. Here, the load-carrying capacity is given by the abscissa of P_8'.

It is worth while noting that the limit polygon of a truss in which bar i is absent from the start coincides with our modified limit polygon, and that Equation [29] is valid throughout the loading process. The failure of bar i therefore leads the point P back to the path it would have followed in the absence of this bar; bar i does not contribute to the load-carrying capacity of the truss. This result, limited to cases where a single bar fails and where the jump of P is restricted to the interior of the modified limit polygon, leads to the following conclusion:

If a simply redundant truss remains safe after failure of a bar, this bar does not contribute to the load-carrying capacity, although it modifies the strain history during the loading process. Hence it may be omitted from the start.

It should be noted, finally, that P travels on a straight line through O if the truss is unloaded after failure of a first bar.

An example

In the foregoing sections we have illustrated our general considerations by means of an example which now will be treated in detail. This treatment is facilitated by Table 1 containing the numerical values of the quantities needed (in given units of length and force). The first few lines contain the values of α_k, F_{k1}, F_{k2}, F_{k7}, F_{kC} for the five bars 1 through 5 of the truss in Fig. 2.

If we assume that the loads P_1, P_2, P_3 are equal, we may set

$$P_1' = P_2' = P_3' = 3\sqrt{2} \quad \ldots\ldots [30]$$

A simple calculation carried through for the elastic truss supplies the first type stresses F_k' in the next line of Table 1 together with the reactions

$$F_4' = \frac{1}{2}\sqrt{2}, \quad F_7' = \frac{9}{2}\sqrt{2}, \quad F_1' = \frac{1}{2}\sqrt{2}, \quad F_3' = \frac{3}{2}\sqrt{2} \quad \ldots\ldots [31]$$

A similar calculation for the unloaded (but prestrained) elastic truss supplies the second type stresses F_k'' in the following line and the corresponding reactions

$$F_4'' = -2\sqrt{2}, \quad F_7'' = 0, \quad F_3'' = -2\sqrt{2}, \quad F_3'' = 0 \ldots [32]$$

With the values obtained in this way, Equations [22] of the yield lines can be established and thus the original yield strips and the original yield polygon of Fig. 3 are obtained. If this process is repeated with the values of lines 4 and 5 instead of those of lines 2 and 3, we obtain the limit strips and the original limit polygon of Fig. 8.

The first step in the loading process is purely elastic. It is represented in Fig. 3 by the segment OP_1. From now on the truss responds plastically, and the calculation of the next steps is facilitated if the following lines in Table 1 are prepared, containing the ratios E_k/C_k and the values β_k, Φ_k, Ψ_k defined by Equations [23] and [24]. Besides, from [23] follows

$$N = 24 \quad \ldots\ldots [33]$$

At P_1 bar 2 begins to flow. From Equation [26], where the dashed sums are restricted to $k = 2$, follows, in connection with Equation [33] and the last two lines in Table 1, the inclination

$$v = \frac{5}{14} \quad \ldots\ldots [34]$$

of the next segment. This segment lies outside the yield strip 2, and its end point P_2 is the point of intersection with yield line 1. The dotted lines in Fig. 3 represent the yield polygon for P_2.

In Figs. 4 through 7 the next steps and their initial yield polygons are illustrated. The next bar responding plastically is 1, followed by 4, 3, and 5 in this order. The inclinations of the corresponding segments follow from Equation [26] where the dashed sums must be extended over more and more terms. Assuming that none of the bars is unloaded, we obtain

$$v = \frac{1}{16}, \frac{1}{6}, \frac{1}{22}, 0 \quad \ldots\ldots [35]$$

and since the corresponding segments do not lie inside the yield strips of the bars assumed in plastic response, these segments represent the real solution.

The first point lying on the circumference of the limit polygon is P_6 on limit line 2′. The failure of bar 2 renders the truss statically determinate, and P_7, Fig. 8, corresponds to the next value

$$v = \frac{5}{2}\mu \quad \ldots\ldots [36]$$

following from Equation [29] with $i = 2$ and from Table 1. Since P_7 lies outside the modified limit polygon, obtained by dropping limit lines 2′, the load-carrying capacity is given by the common abscissa

$$\mu = 1.08 \quad \ldots\ldots [37]$$

and P_6 and P_7.

Discussion

It should be noted that the concept of the load-carrying capacity as defined in the section "Response of the Truss," is limited to a monotonic loading process and thus has a more restricted meaning here than in an elastic-perfectly plastic truss where the load-carrying capacity is independent of the strain history. It is true that the process illustrated by Figs. 3 through 7, if modified by a temporary unloading, may end in the same point P_6. It is easy, however, to change the prescribed numerical values in such a way that, e.g., a loading process starting with a load reversal supplies another ultimate load than a straightforward process.

Thus in more involved loading processes only a step-by-step treatment supplies the actual value of the ultimate load.

Acknowledgment

The author is indebted to Prof. W. Prager for valuable suggestions.

A Compressible Elastic, Perfectly Plastic Wedge[1]

By D. R. BLAND[2] and P. M. NAGHDI[3]

This paper is concerned with a compressible elastic-plastic wedge of an included angle $\beta < \pi/2$ in the state of plane strain. The solution, deduced for an isotropic nonwork-hardening material, employs Tresca's yield criterion and the associated flow rules. By means of a numerical example the solution is compared with that of an incompressible elastic-plastic wedge in one case ($\beta = \pi/4$) for various positions of the elastic-plastic boundary.

Introduction

Available complete solutions to problems of plane elastic-plastic flow are few and, with the use of Prandtl-Reuss stress-strain relations, solutions in closed form have been possible only if the material is assumed to be incompressible in the elastic as well as in the plastic range. References to existing solutions of plane elastic, perfectly plastic strain may be found in (1)[4] where a complete solution in closed form is obtained for an acute elastic-plastic wedge in the state of plane strain. It should be mentioned, however, that a solution in closed form for a compressible elastic, perfectly plastic material of a thick-walled cylinder under internal pressure in the state of plane strain has been given by Koiter (2) where Tresca's singular yield condition and the associated flow rules are employed. Koiter's work has been extended in (3) to elastic-plastic work-hardening materials in the presence of temperature gradients.

The solution given in (1) for a wedge subjected to a uniform normal pressure on one boundary only is limited to wedge regions with an included angle $\beta < \pi/2$ and employs the stress-strain law of Prandtl-Reuss. For future purposes, it is expedient to record here some of the results obtained in (1). With reference to cylindrical polar co-ordinates (r, θ, z), the Mises yield condition for an incompressible material may be written as

$$s_\theta^2 + \sigma_{r\theta}^2 = k^2$$

or

$$\frac{1}{4}(\sigma_r - \sigma_\theta)^2 + \sigma_{r\theta}^2 = k^2 \quad \ldots\ldots [1]$$

where $\{\sigma_r, \sigma_\theta, \sigma_z, \sigma_{r\theta}\}$ are the components of the stress tensor, $\{s_r, s_\theta, s_z, \sigma_{r\theta}\}$ are the components of the stress deviation tensor, and k is the yield limit in simple shear. Yielding will begin simultaneously at the outside surfaces and on further plastic deformation, the elastic-plastic boundaries are the planes $\theta = \phi$ and $\theta = \beta - \phi$ as indicated in Fig. 1 (the z-axis is taken perpendicular to the plane of the cross section in Fig. 1). The plane components of stress in the elastic domain are of the form

$$\left.\begin{aligned} \sigma_r &= 2[(b + d\theta) - (a\cos 2\theta + c\sin 2\theta)] \\ \sigma_\theta &= 2[(b + d\theta) + (a\cos 2\theta + c\sin 2\theta)] \\ \sigma_{r\theta} &= -d + 2(a\sin 2\theta - c\cos 2\theta) \end{aligned}\right\};\ \phi \le \theta \le (\beta - \phi). \quad [2]$$

and the plane components of stress in the two plastic domains are

$$\left.\begin{aligned} \sigma_r &= -p + k(1 + \cos 2\theta) \\ \sigma_\theta &= -p + k(1 - \cos 2\theta) \\ \sigma_{r\theta} &= -k\sin 2\theta \end{aligned}\right\};\ 0 \le \theta \le \phi \ldots\ldots [3]$$

and

$$\left.\begin{aligned} \sigma_r &= -k[1 + \cos 2(\theta - \beta)] \\ \sigma_\theta &= -k[1 - \cos 2(\theta - \beta)] \\ \sigma_{r\theta} &= k\sin 2(\theta - \beta) \end{aligned}\right\};\ (\beta - \phi) \le \theta \le \beta \ldots [4]$$

where the coefficients a, b, c, d, and the relation between the lateral pressure p and the elastic-plastic boundary ϕ are given by

$$\left.\begin{aligned} a &= -\frac{k\sin\beta\cos 2\phi}{2\sin\alpha} = -\frac{(2k - p)}{4\alpha}\tan\beta\cos 2\phi \\ b &= -\frac{k}{2} + \frac{k(\beta - \phi)\cos\beta}{\sin\alpha} = \frac{\beta k - p(\beta - \phi)}{2\alpha} \\ c &= \frac{k\cos\beta\cos 2\phi}{2\sin\alpha} = \frac{2k - p}{4\alpha}\cos 2\phi \\ d &= -k\frac{\cos\beta}{\sin\alpha} = -\frac{2k - p}{2\alpha} \end{aligned}\right\} \ldots [5]$$

$$\frac{p}{2k} = \frac{1}{\tan\alpha}[\alpha\sin 2\phi(\tan\alpha + \tan\phi) + (\tan\alpha - \alpha)]$$
$$= 1 - \alpha\csc\alpha\cos\beta \ldots\ldots [6a]$$

where

$$\alpha = \beta - 2\phi \ldots\ldots [6b]$$

It may be noted here that the main features which rendered the foregoing solution possible are the facts that (a) the stresses in the elastic domain are independent of r, (b) the stresses in the plastic domains are statically determinate and also independent of r, and (c) one of the principal stresses, namely σ_z, is absent from Mises' yield condition for an incompressible material. In this connec-

[1] The work of one of the authors (P. M. Naghdi) presented in this paper was obtained in the course of research sponsored by the Office of Naval Research, under Contract Nonr-1224(01), Project NR-064-408, with the University of Michigan, and of the other author (D. R. Bland) while he was the holder of an I.C.I. Research Fellowship at King's College, London, England.

[2] Department of Mathematics, University of Manchester, Manchester, England.

[3] Professor of Engineering Mechanics, University of Michigan, Ann Arbor, Mich. Mem. ASME.

[4] Numbers in parentheses refer to Bibliography at end of paper.

Contributed by the Applied Mechanics Division and presented at the Annual Meeting, New York, N. Y., December 1–6, 1957, of The American Society of Mechanical Engineers.

Discussion of this paper should be addressed to the Secretary, ASME, 29 West 39th Street, New York, N. Y., and will be accepted until July 10, 1958, for publication at a later date. Discussion received after the closing date will be returned.

Note: Statements and opinions advanced in papers are to be understood as individual expressions of their authors and not those of the Society. Manuscript received by ASME Applied Mechanics Division, March 11, 1957. Paper No. 57—A-38.

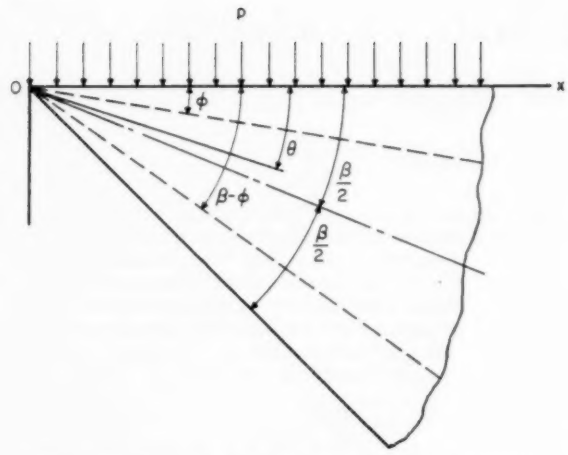

Fig. 1 Narrow wedge under a uniform lateral pressure

tion, we observe that for an incompressible material, Mises' and Tresca's yield conditions (when σ_z is the intermediate principal stress) are identical and that for problems of plane plastic flow of a compressible material, Tresca's yield condition is again given by Equation [1] as long as σ_z is the intermediate principal stress.

The present paper, employing Tresca's yield condition and the associated flow rules, is concerned with a compressible elastic, perfectly plastic wedge in the state of plane strain. The wedge region with an included angle[5] $0 < \beta < \pi/2$, as shown in Fig. 1, is subjected to a uniform normal pressure p (on one boundary only) which is assumed to be monotonically increasing with time. Since for an elastic body in the state of plane strain, the plane components of stress are independent of Poisson's ratio; and since for the compressible elastic-plastic wedge in question, (*a*) Tresca's yield condition (with σ_z as the intermediate principal stress) is identical with Equation [1], and (*b*) the state of stress in the plastic domain is statically determinate, it then follows that the plane components of stress given previously for an incompressible wedge (1), i.e., by Equations [2], [3], and [4], as well as the shape of the elastic-plastic boundary, hold also for the compressible wedge. In addition, as will be shown presently

$$\sigma_z = \nu(\sigma_r + \sigma_\theta); \quad 0 \leq \theta \leq \beta \ldots\ldots\ldots\ldots [7]$$

throughout the wedge, where ν is Poisson's ratio.

Determination of the displacements

We recall that the rate of plastic components of strain may be expressed in terms of a plastic potential f by expressions of the type[6]

$$\{\dot{\epsilon}_r'', \dot{\epsilon}_{r\theta}''\} = \frac{\partial f}{\partial\{\sigma_r, \sigma_{r\theta}\}}\dot{\lambda} \ldots\ldots\ldots\ldots [8]$$

where λ is a scalar function which depends on the co-ordinates as well as time t, prime and double primes refer, respectively, to the elastic and plastic components of strain, and dot denotes differentiation with respect to time. Thus when the plastic stress-strain relations are associated with Tresca's yield condition Equation [1], i.e., when

$$f = \frac{1}{2}\left\{\frac{1}{2}(\sigma_r - \sigma_\theta)^2 + \sigma_{r\theta}^2 + \sigma_{\theta r}^2\right\} - k^2$$

Equations [8] become

$$\left.\begin{aligned} \dot{\epsilon}_r'' &= -\dot{\epsilon}_\theta'' = \frac{1}{2}(\sigma_r - \sigma_\theta)\dot{\lambda} \\ \dot{\epsilon}_{r\theta}'' &= \sigma_{r\theta}\dot{\lambda} \\ \dot{\epsilon}_z'' &= 0 \end{aligned}\right\} \ldots\ldots\ldots [9]$$

We shall now proceed to determine the displacements in one of the two plastic regions; i.e., $0 \leq \theta \leq \phi$. Substitution of Equation [3] into Equation [9] followed by an integration with respect to time yields

$$\left.\begin{aligned} \epsilon_r'' &= -\epsilon_\theta'' = \lambda(k\cos 2\theta) \\ \epsilon_{r\theta}'' &= -\lambda(k\sin 2\theta) \\ \epsilon_z'' &= 0 \end{aligned}\right\}; \quad 0 \leq \theta \leq \phi \ldots\ldots [10]$$

where, since the strains are assumed independent of r, λ will be a function of θ and time only. Since in the state of plane strain

$$\epsilon_z = \epsilon_z' + \epsilon_z'' = 0$$

the last of Equation [10] requires the vanishing of the elastic component of the axial strain and hence by Hooke's law

$$\sigma_z = \nu(\sigma_r + \sigma_\theta)$$

also in the plastic region $0 \leq \theta \leq \phi$.

The nonvanishing elastic components of strains in the plastic region $0 \leq \theta \leq \phi$, obtained by substitution of Equation [3] and Equation [7] into the generalized Hooke's law, are given by

$$\left.\begin{aligned} \epsilon_r' &= \frac{k}{2G}\left[(1-2\nu)\left(1-\frac{p}{k}\right) + \cos 2\theta\right] \\ \epsilon_\theta' &= \frac{k}{2G}\left[(1-2\nu)\left(1-\frac{p}{k}\right) - \cos 2\theta\right] \\ \epsilon_{r\theta}' &= -\frac{k}{2G}\sin 2\theta \end{aligned}\right\}; \quad 0 \leq \theta \leq \phi \ldots [11]$$

where G is the shear modulus of elasticity. Substitution of Equations [10] and [11] into the strain-displacement relations

$$\left.\begin{aligned} \epsilon_r &= \frac{\partial u_r}{\partial r} \\ \epsilon_\theta &= \frac{u_r}{r} + \frac{1}{r}\frac{\partial u_\theta}{\partial \theta} \\ 2\epsilon_{r\theta} &= \frac{1}{r}\frac{\partial u_r}{\partial \theta} + \frac{\partial u_\theta}{\partial r} - \frac{u_\theta}{r} \end{aligned}\right\} \ldots\ldots [12]$$

yield three differential equations in the radial and tangential dis-

[5] As discussed in (1) this limitation is due to the character of the initial yield and the locus of the elastic-plastic boundary which depend on the loading as well as on the included wedge angle.

[6] It should be noted that as in (1) the components of strain and displacements are assumed to be infinitesimal so that in the stress-strain relations for the plastic range (resulting from the sum of the rates of elastic and plastic strains) the time derivative of stress following a point may be taken as equal to the partial derivative with respect to time at a fixed point of observation.

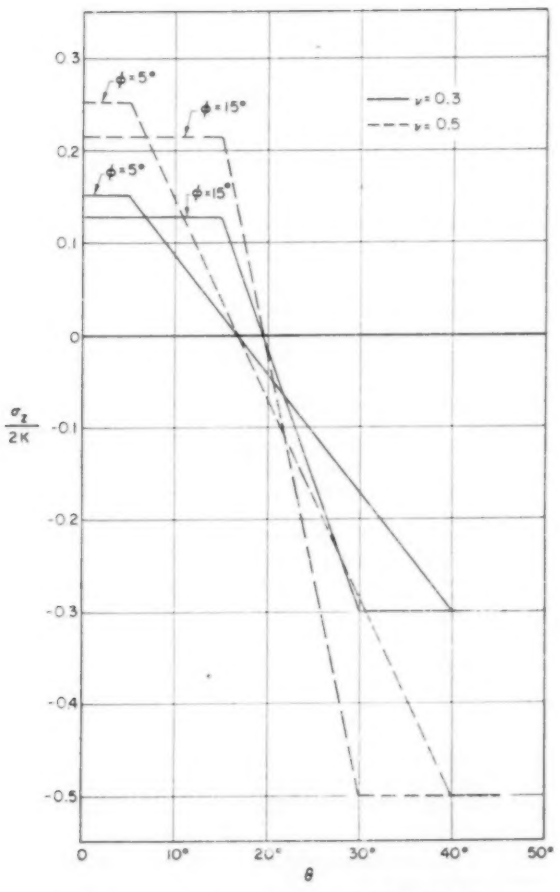

Fig. 2 Distribution of axial stress for both compressible and incompressible material

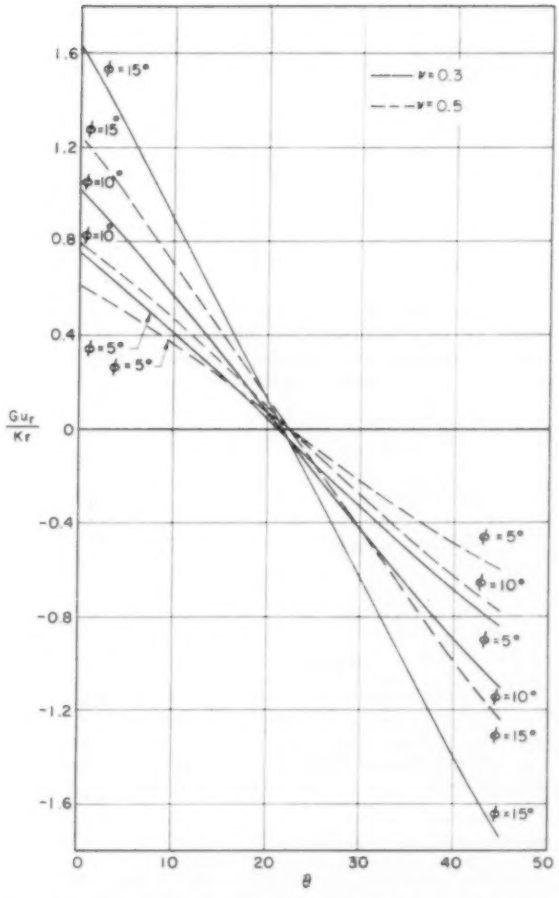

Fig. 3 Ratio of radial displacement to r (or radial strain) for both compressible and incompressible material

placements u_r and u_θ, the integration of the first two of which results in

$$\left.\begin{aligned} u_r &= r\left[\frac{(1-2\nu)}{2G}\,k\left(1-\frac{p}{k}\right) + \left(\frac{k}{2G}+\lambda\right)\cos 2\theta\right] \\ u_\theta &= -r\left[\left(\frac{k}{2G}+\lambda\right)\sin 2\theta + \int\frac{\partial\lambda}{\partial\theta}\sin 2\theta d\theta\right] + g(r,t) \end{aligned}\right\};\quad 0\le\theta\le\phi \quad \ldots[13]$$

where, on account of the vanishing of the displacements at the origin, the arbitrary function of θ and t arising due to integration of ϵ_r has been set equal to zero. The displacements as given by Equations [13] identically satisfy the third of Equation [12] provided that

$$\left.\begin{aligned} \lambda(\theta,t) &= B\log|\sec 2\theta+\tan 2\theta| + H \\ g(r,t) &= Cr - 2Br\log r \end{aligned}\right\} \quad \ldots[14]$$

where B, C, and H are functions of time. The displacements in the elastic domain, which with the aid of Equations [2] also may be obtained in a similar manner, are given by

$$\left.\begin{aligned} Gu_r &= r[(1-2\nu)(b+d\theta) - (a\cos 2\theta + c\sin 2\theta)] \\ Gu_\theta &= r[-2(1-\nu)d\log r + (a\sin 2\theta - c\cos 2\theta)] \end{aligned}\right\};\quad \phi\le\theta\le(\beta-\phi) \quad \ldots[15]$$

and the coefficient functions B, C, and H in Equations [14] are determined from the continuity requirements for u_r and u_θ at the elastic-plastic interface. Thus

$$\left.\begin{aligned} u_r &= r\{D+\cos 2\theta[A+B\log|\sec 2\theta + \tan 2\theta|]\} \\ u_\theta &= r\{-\sin 2\theta[A+B\log|\sec 2\theta + \tan 2\theta|] + B\log|\sec 2\theta| - 2B\log r + C\} \end{aligned}\right\};\quad 0\le\theta\le\phi \quad \ldots[16]$$

where

$$\left.\begin{aligned} D &= \frac{1-2\nu}{2G}(k-p), \quad B = \frac{1-\nu}{G}d \\ A &= \frac{k}{2G} + H, \\ H &= -\frac{1-\nu}{G}d\log|\sec 2\phi + \tan 2\phi| \\ C &= \frac{d}{2G}[1-2(1-\nu)\log|\sec 2\phi|] \end{aligned}\right\} ; \ 0 \le \theta \le \phi \quad [17]$$

The components of displacement for the region $(\beta - \phi) \le \theta \le \beta$, which may again be deduced in a similar manner, are of the same form as Equations [16] except that the argument θ is replaced by $(\theta - \beta)$ and the coefficient functions are

$$\left.\begin{aligned} D &= -\frac{1-2\nu}{2G}k, \quad B = \frac{1-\nu}{G}d \\ A &= -\frac{k}{2G} + H, \\ H &= -\frac{1-\nu}{G}d\log|\sec 2\phi - \tan 2\phi| \\ C &= \frac{d}{2G}[1-2(1-\nu)\log|\sec 2\phi|] \end{aligned}\right\} ; \ (\beta - \phi) \le \theta \le \beta \quad [18]$$

The displacements for an incompressible wedge, obtained from Equations [15], [16], [17], and [18] by putting $\nu = 1/2$, are identical with those given previously (1) since, as noted earlier, the yield conditions of Mises for an incompressible material, and Tresca's (with σ_z as the intermediate principal stress) are the same.

Numerical example—conclusion

Comparison of the displacements as well as the axial component of stress of the present paper with those of an incompressible material for the case $\beta = \pi/4$ are shown in Figs. 2, 3, and 4, and numerical values of the plane components of stress (since they are identical with those of an incompressible elastic-plastic wedge) for $\beta = \pi/4$ may be found elsewhere (1).

In view of the occurrence of a term proportional to $\log r$ in the expression for u_θ/r, it is seen that, as the deformation proceeds, the wedge does not maintain its straight edges. Consequently, the assumption that the components of stress and strain are independent of r remains valid so long as no appreciable error is introduced in the solution when the surface tractions are considered to act on the original shape of the wedge rather than on its current shape; this error is indeed negligible when the strains are infinitesimal. It should be mentioned, however, that the foregoing remark does not invalidate the corresponding solution of a wedge for a rigid, perfectly plastic material given in Prager and Hodge (4), as the manner of obtaining the displacements has to be modified when $G = \infty$.

Applications of the results given here may be found among the die blocks used in bending operations with rubber (e.g., Guerin process), where the die may be assumed to have a sharp edge and the pressure over the die face (exerted through a rubber pad) is essentially uniform. As an approximation, the solution also might lend itself to extrusion through a tapered die with a large circular opening, where the pressure near the die edge again may be assumed uniform and the displacements in the die approach plane strain conditions.

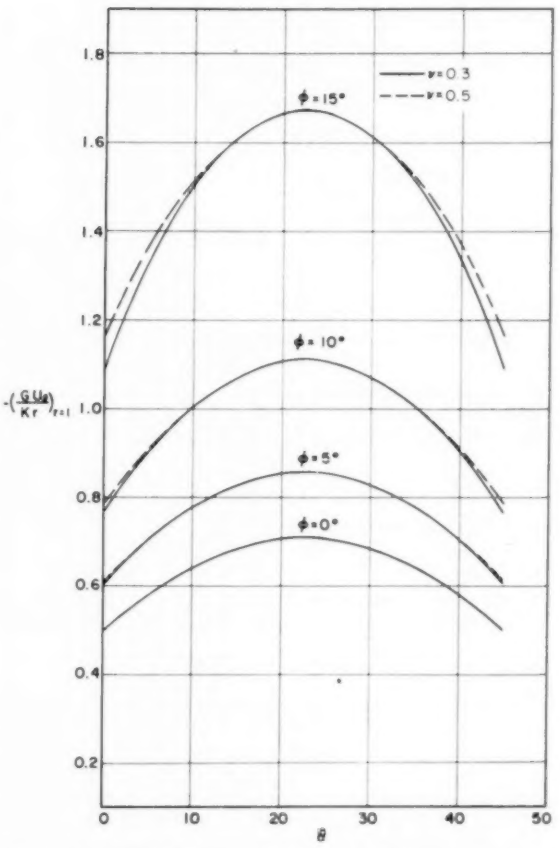

Fig. 4 Tangential displacement at $r = 1$ for both compressible and incompressible material

Finally, it may be mentioned that the inclusion of work-hardening in the elastic-plastic wedge considered here, introduces a further difficulty, as the state of stress in the plastic domain is no longer statically determinate and the yield stress k is dependent on the plastic components of strain.

Bibliography

1 "Stresses and Displacements in an Elastic-Plastic Wedge," by P. M. Naghdi, JOURNAL OF APPLIED MECHANICS, TRANS. ASME, vol. 79, March, 1957, pp. 98–104.

2 "On Partially Plastic Thick-Walled Tubes," by W. T. Koiter, Biezeno Anniversary Volume on Applied Mechanics, Haarlem, Holland, 1953, pp. 233–251.

3 "Elastoplastic Thick-Walled Tubes of Work-Hardening Material Subject to Internal and External Pressures and to Temperature Gradients," by D. R. Bland, *Journal of the Mechanics and Physics of Solids*, vol. 4, 1956, pp. 209–229.

4 "Theory of Perfectly Plastic Solids," by W. Prager and P. G. Hodge, Jr., John Wiley & Sons, Inc., New York, N. Y., 1951, chapter 5.

Further Studies of Stress Distribution in Rotating Disks and Cylinders Under Elevated-Temperature Creep Conditions

By A. M. WAHL,[1] PITTSBURGH, PA.

The analysis previously given for stress in rotating disks having central holes and under steady-state creep conditions is extended to cases where the radial and tangential stresses are equal over all or a portion of the disk, both constant and variable-thickness cases being considered. In addition, the solid rotating disk and the long rotating solid cylinder are treated, peak stresses above the elastic values being found under certain conditions. Charts are presented for determining ratios σ_{tm}/σ_{tav} between peak stress and average stress, for various diameter ratios, disk contours, and values of n in the power-function stress-creep rate relation. These indicate somewhat lower ratios of peak to average stress for the variable-thickness disks. Based on the theoretical results, curves of stress distribution are also worked out for several typical cases.

Nomenclature

The following nomenclature is used in the paper:

K', K_1, C = constants
$f(t)$ = function of time t
g = gravitational acceleration
h = thickness of disk at radius r (Fig. 1)
$K = \sigma_{tm}/\sigma_{tav}$ = ratio of peak to average stress. (This is similar to a stress-concentration factor.)
n, m = exponents
r = radius to any point of disk
r_o, r_i = outer and inner radii of disk with hole
w, w_i = radial deformation of disk at radius r, σ_i
$\dot{w}$, $\dot{w}_c$, $\dot{w}_i$ = radial deformation rates at radii x, x_c, x_i
$x = r/r_o$; $x_i = r_i/r_o$; $x_c = r_c/r_o$; $x_d = r_d/r_o$
$\alpha = (nm + n - 1)/n$
$\beta = \sigma_{tm}/\sigma_0$
γ = weight per unit volume of material
$\dot{\epsilon}_r$, $\dot{\epsilon}_t$, $\dot{\epsilon}_z$ = radial, tangential, axial strain rates
ν = Poisson's ratio
ω = angular velocity
σ_r, σ_t = radial and tangential stress at radius r
σ_{tm} = peak stress at $x = x_i$ or $x = 0$
σ_{tc}, σ_{td} = tangential stresses at x_c and x_d
σ_{r0}, σ_{rc} = radial stresses at r_o and r_c
σ_{tav} = average tangential stress across a diametral section of disk or rotor
$\sigma_0 = \gamma\omega^2 r_o^2/g$ = stress in freely rotating thin ring of radius r_o

Introduction

In a previous paper (1)[2] some formulas were derived for calculating stress distributions in rotating disks, both of constant and variable thickness, under steady-state creep at elevated temperatures. These formulas were based on the Tresca (maximum-shear) criterion and the associated flow rule as used in plasticity theory (2) and appear to give reasonable results when compared with test data (1, 3). However, the derivations in the previous papers were subject to the restriction that the radial stress was always less than the tangential stress ($\sigma_r < \sigma_t$). In the present paper this restriction is removed; also, the cases of the solid rotating disk and the long rotating cylinder are treated. As mentioned in (1), although our spin tests on 12 per cent chrome-steel disks at 1000 F appear to favor the use of the Tresca rather than the Mises criterion in so far as creep is concerned, further test results are necessary before definite conclusions may be drawn.

The formulas given in (1) also have been utilized to construct design charts of stress distribution under steady-state creep conditions for constant-thickness disks with various n-values and diameter ratios (4).

In all cases the disks or rotors are assumed to be subjected to a radial peripheral stress σ_{r0} to simulate the effect of blade loading, Fig. 1. Also as in previous paper (1), it is assumed here that a steady-state stress condition prevails and that the creep rate for constant stress can be expressed with sufficient accuracy for engineering work as a product of a power function of stress multiplied by a function of time.

Disk With Central Hole (Constant or Variable Thickness)

For the constant-thickness or variable-thickness disk with a central hole, three cases may be distinguished as follows:

Case 1. (Fig. 2*a*) $0 < \sigma_r < \sigma_t$ for $x_i < x < 1$.

Case 2. (Fig. 2*b*) $0 < \sigma_r < \sigma_t$ for $x_i < x < x_c$ and for $x_d < x < 1$; $\sigma_t = \sigma_r$ for $x_c \leqq x \leqq x_d$.

Case 3. (Fig. 2*c*) $0 < \sigma_r < \sigma_t$ for $x_i < x < x_c$ and $\sigma_r = \sigma_t$ for $x_c \leqq x \leqq 1$.

Case 1. For this case where $0 < \sigma_r < \sigma_t$ for $x_i < x < 1$, the analysis given in the previous paper (1) applies. The strain rates are taken as follows

$$\dot{\epsilon}_t = \frac{\dot{w}}{r_o x} = K'\sigma_t^n f(t) \quad [1]$$

$$\dot{\epsilon}_r = \frac{d\dot{w}}{r_o dx} = 0 \quad [2]$$

$$\dot{\epsilon}_z = -K'\sigma_t^n f(t) \quad [3]$$

---

[1] Advisory Engineer, Mechanics Department, Westinghouse Electric Corporation Research Laboratories. Fellow ASME.

Contributed by the Applied Mechanics Division and presented at the Annual Meeting, New York, N. Y., December 1–6, 1957, of THE AMERICAN SOCIETY OF MECHANICAL ENGINEERS.

Discussion of this paper should be addressed to the Secretary, ASME, 29 West 39th Street, New York, N. Y., and will be accepted until July 10, 1958, for publication at a later date. Discussion received after the closing date will be returned.

NOTE: Statements and opinions advanced in papers are to be understood as individual expressions of their authors and not those of the Society. Manuscript received by ASME Applied Mechanics Division, January 22, 1957. Paper No. 57–A-91.

[2] Numbers in parentheses refer to the Bibliography at the end of the paper. Additional references are given in (1) and (3).

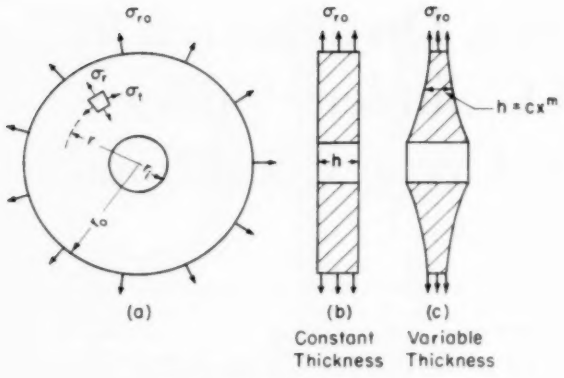

Fig. 1 Rotating disk with hole

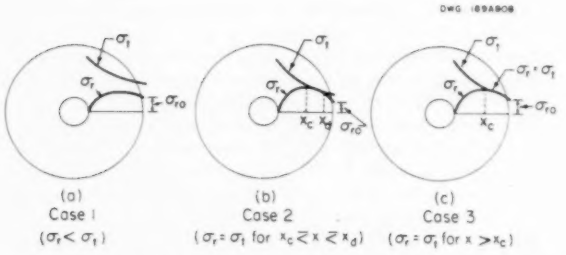

Fig. 2 Schematic stress distributions assumed for Case 1, Case 2, and Case 3

The known equilibrium equation for a rotating disk of variable thickness is

$$\frac{d}{dx}(xh\sigma_r) - h\sigma_t + \sigma_0 hx^2 = 0 \quad \ldots\ldots [4]$$

Using these expressions in conjunction with the boundary conditions ($\sigma_r = \sigma_{r0}$ at $x = 1$, $\sigma_r = 0$ at $x = x_i$) equations for σ_r and σ_t were derived in (1). Taking $x = r/r_o$, and $h = cx^m$ these may be expressed as follows

$$K = \frac{\sigma_{tm}}{\sigma_{tav}} = \frac{(1 - x_i^{m+1})\alpha}{(m+1)(1 - x_i^{\alpha})x_i^{1/n}} \quad \ldots\ldots [5]$$

$$\frac{\sigma_t}{\sigma_{tav}} = \frac{\sigma_{tm}}{\sigma_{tav}}\left(\frac{x_i}{x}\right)^{1/n} \quad \ldots\ldots [6]$$

$$\frac{\sigma_r}{\sigma_{tav}} = \frac{1}{x^{m+1}}\left[\frac{(x^{\alpha} - x_i^{\alpha})(1 - x_i^{m+1})}{(1 - x_i^{\alpha})(m+1)} - \frac{x^{3+m} - x_i^{3+m}}{(3+m)B}\right] \quad [7]$$

In this

$$B = \frac{\sigma_{tav}}{\sigma_0} = \left[\frac{\sigma_{r0}}{\sigma_0} + \frac{1 - x_i^{3+m}}{3+m}\right]\left(\frac{m+1}{1 - x_i^{m+1}}\right) \quad [8]$$

The constant-thickness case is obtained from these equations by taking $m = 0$.

Based on Equation [6] a typical plot of the ratio σ_t/σ_{tav} versus $x = r/r_o$ for $r_o/r_i = 6$, and for various n-values for the constant-thickness disk is shown in Fig. 3. (For plots of disks having other values of r_o/r_i, see reference 4.) It will be noted that the peak stress is at the inside diameter and that there is considerable nonuniformity in stress distribution, particularly

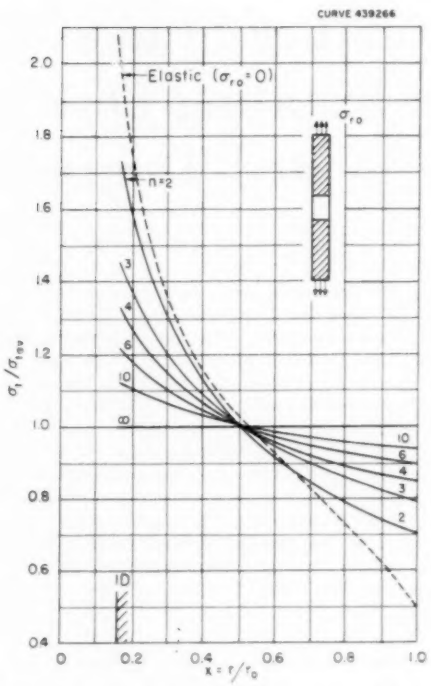

Fig. 3 Tangential stress distributions for rotating disk of constant thickness ($r_o/r_i = 6$)

for the lower n-values. (For comparison the elastic stress distribution for $\sigma_{r0} = 0$ and Poisson's ratio 0.3 is shown by the dashed curve.)

In Fig. 4 a plot of the values of $K = \sigma_{tm}/\sigma_{tav}$ for the constant-thickness disk ($m = 0$) based on Equation [5] is given for various n-values and various values of r_o/r_i. As will be shown later, the portions of the curves shown in full lines are sufficiently accurate for engineering purposes for values of r_o/r_i between 2 and 10, provided σ_{r0}/σ_0 is less than about 3, which includes most practical cases. The dashed portion of the curve for $n = 2$ also applies provided σ_{r0}/σ_0 does not exceed the values indicated on the curve in Fig. 5.

It is of interest to note that calculations made in (3) using the Mises criterion and a numerical integration method indicate values of σ_{tm}/σ_{tav} about 6 per cent less than those given in Fig. 4 for $r_o/r_i = 4.8$ and $n = 4 - 6$. For $n = 8$ the difference was about 5 per cent. However, the relative differences between the creep rates calculated using the two criteria are generally much larger than these percentage values would indicate since the rate is usually proportional to some rather large power of the stress.

To find out if the condition $0 < \sigma_r < \sigma_t$ holds for $x_i < x < 1$, Equation [7] may be divided by Equation [6], giving

$$\frac{\sigma_r}{\sigma_t} = \frac{1}{\alpha x^{\alpha}}\left[x^{\alpha} - x_i^{\alpha} - \frac{(m+1)(1 - x_i^{\alpha})(x^{3+m} - x_i^{3+m})}{(3+m)(1 - x_i^{m+1})B}\right] \quad [9]$$

By differentiating this expression with respect to x, the point at which σ_r/σ_t is a maximum may be found. In this way it is possible to determine whether or not the required condition $0 < \sigma_r < \sigma_t$ holds in the range $x_i < x < 1$. In this manner, for the constant thickness disk ($m = 0$), it can be shown that $\sigma_r < \sigma_t$ at all points of the disk (hence Equations [6], [7] are valid) for all values $r_o/r_i \leq 4$ provided $n > 2$, regardless of the value of σ_{r0}/σ_0.

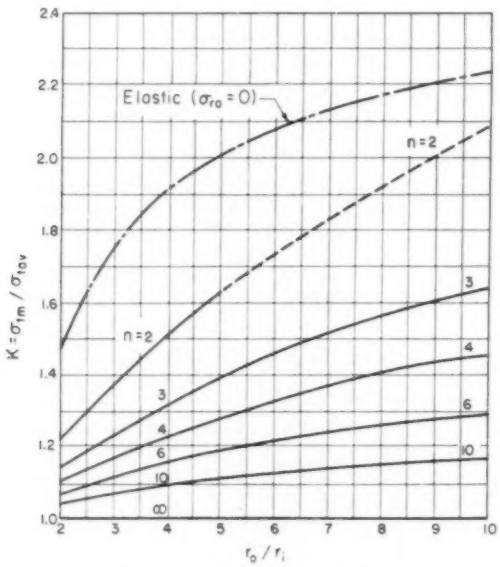

Fig. 4 Factors $K = \sigma_{1m}/\sigma_{1av}$ for rotating disks for various n and r_o/r_i values. Curves in full lines valid for $\sigma_{r0}/\sigma_0 \geq 3$. Dashed portion of curve for $n = 2$ is valid if σ_{r0}/σ_0 values are less than those given by Fig. 5.

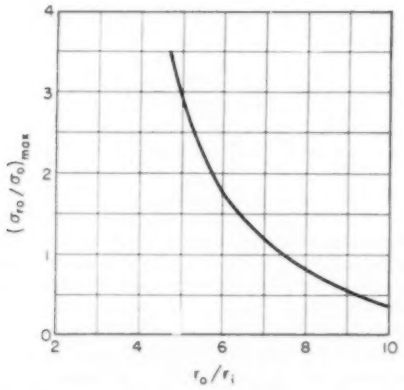

Fig. 5 Maximum values σ_{r0}/σ_0 for constant-thickness disk and $n = 2$. If σ_{r0}/σ_0 values are less than these, dashed portion of curve in Fig. 4 is valid.

For $r_o/r_i = 6$ and 10, it is found that Equations [6] and [7] are valid provided σ_{r0}/σ_0 does not exceed the values given in Table 1 for various values of n.

Table 1 Maximum values of σ_{r0}/σ_0

r_o/r_i	$n = 2$	$n = 3$	$n = 4$	$n = 6$	$n = 10$
6	1.81	5.07	∞	∞	∞
10	0.35	1.49	3.4	14	∞

Using Equation [9] it also may be shown that the dashed portion of the curve for $n = 2$, Fig. 4, is valid provided the σ_{r0}/σ_0 values are less than those shown on Fig. 5.

Where σ_{r0}/σ_0 exceeds the values given in Table 1 or Fig. 5, the stress distributions for σ_r and σ_t are as indicated in Fig. 2(*b*) or Fig. 2(*c*), and the more complicated analysis for Case 2 or 3 is

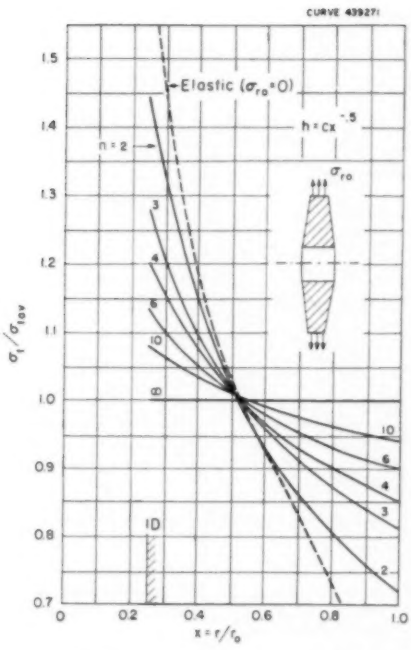

Fig. 6 Tangential stress distributions for rotating disk of variable thickness ($r_o/r_i = 4$, $m = -0.5$). Curves valid only if σ_{r0}/σ_0 values are less than those given in Fig. 7.

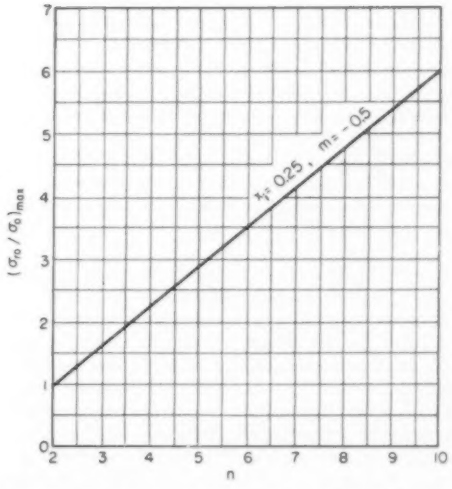

Fig. 7 Maximum values of σ_{r0}/σ_0 for variable-thickness disk. Values of σ_{r0}/σ_0 must be less than these for Fig. 6 to be valid.

necessary. However, the calculations which have been made so far indicate that even if these values of σ_{r0}/σ_0 are exceeded somewhat, the K-values given in Fig. 4 still may be reasonable approximations for the constant-thickness case.

A plot showing the distribution of σ_t/σ_{1av} as a function of x for a variable-thickness disk with $m = -0.5$ and $x_i = 0.25$ for various n-values, is shown in Fig. 6. This plot is based on Equation [6] and as shown in (4) these curves are valid for σ_{r0}/σ_0 values less than those given in Fig. 7. (The case where

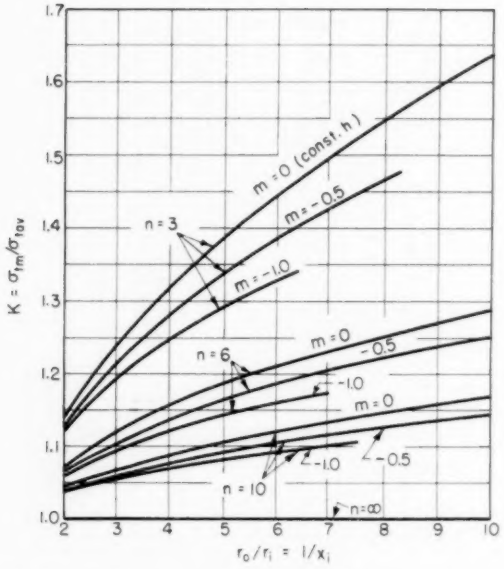

Fig. 8 Factors $K = \sigma_{1m}/\sigma_{1av}$ for variable-thickness rotating disks ($\sigma_r < \sigma_t$ assumed). Note: Curves apply if σ_{r0}/σ_0 values are less than those given in Figs. 7 and 9.

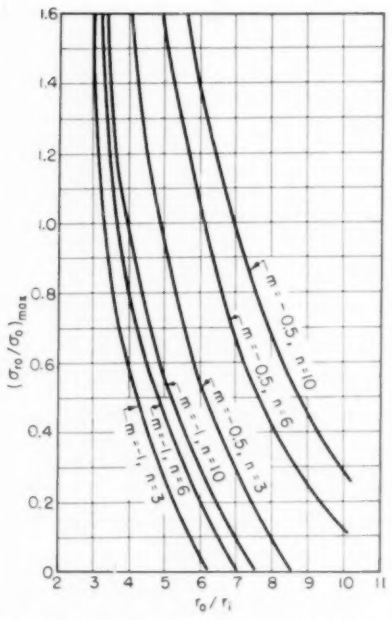

Fig. 9 Values of $(\sigma_{r0}/\sigma_0)_{max}$ below which Fig. 8 applies

σ_{r0}/σ_0 exceeds the values given in Fig. 7 will be discussed later under Case 3.)

A plot of values of $K = \sigma_{1m}/\sigma_{1av}$ for variable-thickness disks having $m = 0$, -0.5 and -1.0 corresponding to different disk contours is shown in Fig. 8. The upper group of curves is for $n = 3$, the middle for $n = 6$ and the lower for $n = 10$. These curves also are based on Equation [5] which requires that the condition $0 < \sigma_r < \sigma_t$ hold in the range $x_i < x < 1$. It may be shown using Equation [9] that this condition is satisfied provided that the σ_{r0}/σ_0 ratios are below the values indicated on the curves in Fig. 9 as functions of r_o/r_i for various values of n and m. Note that some of the curves in Fig. 8 are not extended beyond certain r_o/r_i values; the reason for this is that at such values the aforementioned condition $0 < \sigma_r < \sigma_t$ cannot be satisfied for values of $\sigma_{r0} > 0$.

Case 2 ($\sigma_r = \sigma_t$ for $x_c < x < x_d$). In this case, Fig. 2(*b*), the condition $0 < \sigma_r < \sigma_t$ is assumed in the range $x_i < x < x_c$ and $x_d < x \leqq 1$, and in these regions the expressions for strain rates $\dot{\epsilon}_t$ and $\dot{\epsilon}_r$ given by Equations [1], [2], [3] hold. In the range $x_c < x < x_d$, σ_r is taken equal to σ_t. Since in most cases it will be found that either Case 1 or Case 3 is valid, and since the treatment of Case 2 is rather lengthy, it will not be given here, particularly since the analysis is similar to that for Case 3.

Case 3 ($\sigma_r = \sigma_t$ for $x_c < x < 1$; $0 < \sigma_r < \sigma_t$ for $x_i < x < x_c$). In this case, Fig. 2(*b*), the condition $0 < \sigma_r < \sigma_t$ is assumed in the range $x_i < x < x_c$ and in this region, the expressions for strain rates $\dot{\epsilon}_t$ and $\dot{\epsilon}_r$ given by Equations [1] and [2] hold. In the range $x_c < x < 1$, σ_r is taken equal to σ_t. It would not be reasonable to assume $\sigma_r > \sigma_t$ in this range because this would require that $\dot{\epsilon}_t = \dot{w}/r = 0$ and hence $\dot{w} = 0$, based on the flow rule associated with the Tresca criterion; such could not be the case since for $x > x_c$

$$\dot{w} = \dot{w}_i + r_o \int_{x_c}^{x} \dot{\epsilon}_r dx$$

Since $\dot{\epsilon}_r$ cannot be negative for $\sigma_r > 0$, $\dot{w} \geqq \dot{w}_i$.

Taking $\sigma_r = \sigma_t$ in the range x_c to unity and following a similar method to that used by Prager (2) in plastic-flow problems, the strain rates in this range based on the Tresca criterion are expressed as follows

$$\dot{\epsilon}_t = \frac{\dot{w}}{r_o x} = \lambda K' \sigma_t^n f(t) \quad [10]$$

$$\dot{\epsilon}_r = \frac{d\dot{w}}{r_o dx} = (1 - \lambda) K' \sigma_t^n f(t) \quad [11]$$

$$\dot{\epsilon}_z = -K' \sigma_t^n f(t) \quad [12]$$

In these equations λ is a multiplier which is a function of x and which is taken to be unity at $x = x_c$; for x between x_c and unity the condition $0 < \lambda < 1$ is assumed to hold. (This assumption will be discussed later.)

Since $\sigma_r = \sigma_t$ for $x \geqq x_c$, the equilibrium Equation [4] may be integrated between x_c and x. Taking $\sigma_r = \sigma_{r0}$ at $x = 1$, the following expression for σ_t/σ_0 for $x_c \leqq x \leqq 1$ results

$$\frac{\sigma_t}{\sigma_0} = \frac{\sigma_r}{\sigma_0} = \frac{1}{x^m}\left[\frac{1 - x^{m+2}}{m + 2} + \frac{\sigma_{r0}}{\sigma_0}\right] \quad [13]$$

Also from Equation [1] for $x_i < x < x_c$

$$\frac{\sigma_t}{\sigma_0} = \left[\frac{\dot{w}_i}{K' r_0 f(t) \sigma_0^n x}\right]^{1/n} = B_1 x^{-1/n} \quad [14]$$

Equating the value of σ_t at $x = x_c$ from Equation [14] to that of σ_t at $x = x_c$ from Equation [13] we obtain

$$B_1 = \left[\frac{1 - x_c^{m+2}}{m + 2} + \frac{\sigma_{r0}}{\sigma_0}\right] x_c^{1-\alpha} \quad [15]$$

Using Equation [14] we may integrate Equation [4] between x_i and x_c. Taking $\sigma_r = \sigma_t$ at $x = x_c$ another expression for B_1 is obtained which can be equated to that given by Equation [15]. Solving the resulting equation for σ_{r0}/σ_0, we have

$$\frac{\sigma_{r0}}{\sigma_0} = \frac{\alpha[x_c^{m+3} - x_i^{m+3}]}{(m + 3)[x_c^{\alpha}(1 - \alpha) - x_i^{\alpha}]x_c^{1-\alpha}} - \frac{1 - x_c^{m+2}}{m + 2} \quad [16]$$

By utilizing this equation, values of σ_{r0}/σ_0 may be plotted as functions of x_c for certain values of the parameters m, x_i, and α. Using these values of σ_{r0}/σ_0 and x_c, the factor K becomes

$$K = \frac{\sigma_{tm}}{\sigma_{tav}} = \frac{B_1}{Bx_i^{1/n}} \quad [17]$$

where B_1 is determined from the given values of σ_{r0}/σ_0 and x_c using Equation [15], and B is given by Equation [8].

In the range $x_i \leqq x \leqq x_c$, Equation [6] holds, σ_{tm}/σ_{tav} being given by Equation [17]. In the same range

$$\frac{\sigma_r}{\sigma_{tav}} = \left(Kx_i^{1/n}\right)\left(\frac{x^\alpha - x_i^\alpha}{\alpha x^{m+1}}\right) - \frac{x^{m+3} - x_i^{m+3}}{B(m+3)x^{m+1}} \quad [18]$$

In the range $x_c \leqq x \leqq 1$

$$\frac{\sigma_t}{\sigma_{tav}} = \frac{\sigma_r}{\sigma_{tav}} = \frac{1}{x^m B}\left[\frac{1 - x^{m+2}}{m+2} + \frac{\sigma_{r0}}{\sigma_0}\right] \quad [19]$$

Having calculated the stresses for given values of x_c, α, and m, it is necessary to check on whether the parameter λ in Equations [11] and [12] lies within the required range $0 < \lambda < 1$ for x in the range between x_c and unity. Differentiating Equation [10] with respect to x and utilizing Equation [11], the following differential equation for λ is obtained

$$\frac{\lambda n}{\sigma_t}\left(\frac{d\sigma_t}{dx}\right) + \frac{d\lambda}{dx} + \frac{2\lambda}{x} - \frac{1}{x} = 0 \quad [20]$$

Integrating this equation and taking $\lambda = 1$ at $x = x_c$, the following expression is found

$$\lambda = \frac{1}{x^2\sigma_t^n}\int_{x_c}^{x} x\sigma_t^n dx + \frac{x_c^2\sigma_{tc}^n}{x^2\sigma_t^n} \quad [21]$$

In this, σ_t is given by Equation [19] and σ_{tc} is the value of σ_t at $x = x_c$. By a numerical evaluation of the integral in this equation it may be determined whether or not the condition $0 < \lambda < 1$ holds for $x_c < x < 1$. This usually will be the case, but if it is not, the more complicated analysis for Case 2 is required.

Using Equations [16] and [17] values of K for $n = 2$ and for various r_o/r_i and σ_{r0}/σ_0 values have been calculated for the constant-thickness disk, Fig. 10. Note that for small values of σ_{r0}/σ_0 these K-values equal those given by the curve in Fig. 4 for $n = 2$, while for larger values they are reduced somewhat. Typical curves of stress distribution versus radius based on Equations [14], [16], [18], and [19] are shown in Fig. 11 for the constant-thickness disk ($x_i = 0.125$, $n = 2$, $\sigma_{r0}/\sigma_0 = 2.35$) and in Fig. 12 for a variable-thickness disk ($x_i = 1/6$, $n = 3$, $m = -0.5$, $\sigma_{r0}/\sigma_0 = 0.97$). Checks made using Equation [21] show that the condition $0 < \lambda < 1$ holds for $x_c < x < 1$ in these cases.

As an example, Equations [16] and [19] have been applied to a case where $m = -0.5$, $n = 3$, $\alpha = 1/6$, and $x_i = 0.25$. This gives a disk having a contour as shown in Fig. 6, the rim thickness being half the bore thickness. The results of the calculation are given in Table 2.

Table 2 Results for disk with $m = -0.5$

x_c	1.0	0.9	0.8	0.751
σ_{r0}/σ_0	1.61	1.98	4.12	∞
K	1.28	1.28	1.26	1.19

From this table it may be seen that even for σ_{r0}/σ_0 values as high as 4.12 the K-factors differ only slightly from the value of 1.28 which is valid for small values of σ_{r0}/σ_0. A check made by approximate numerical integration of the integral in Equation [21] for λ indicates that the required condition $0 < \lambda < 1$ also holds in this case in the range from x_c to unity.

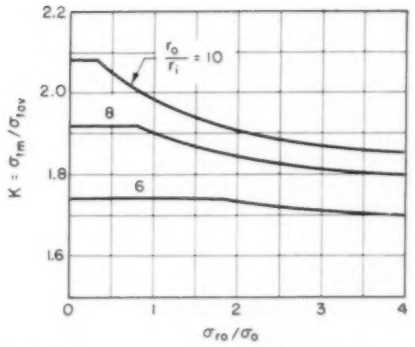

Fig. 10 Factors $K = \sigma_{tm}/\sigma_{tav}$ for various values of r_o/r_i, constant-thickness disk, $n = 2$

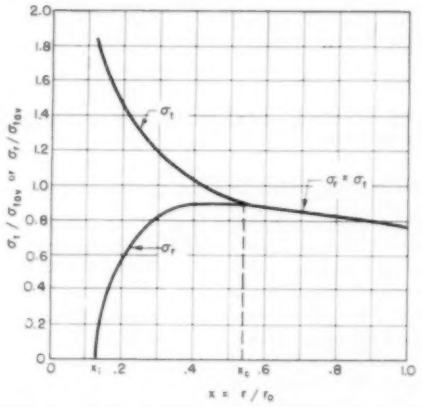

Fig. 11 Stress distributions in constant thickness disk with hole, $r_o/r_i = 8$, $n = 2$, $\sigma_{r0}/\sigma_0 = 2.35$

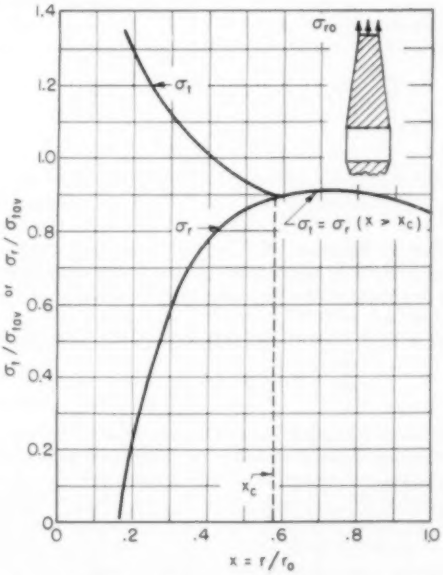

Fig. 12 Stress distributions in variable-thickness disk, $r_o/r_i = 6$, $m = 0.5$, $n = 3$, $\sigma_{r0}/\sigma_0 = 0.97$

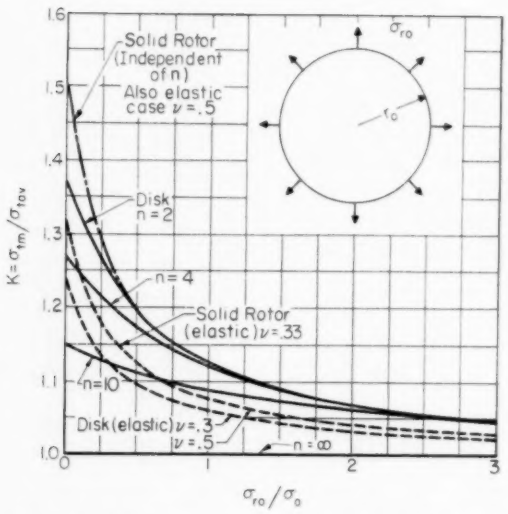

Fig. 13 Factors $K = \sigma_{im}/\sigma_{tav}$ versus σ_{r0}/σ_0 for solid disk or rotor for various n-values

Constant-Thickness Solid Disk

For calculating steady-state creep-stress distributions in the constant-thickness solid disk loaded by a peripheral radial stress σ_{r0}, Fig. 13, a method of approach, utilizing the Tresca criterion and the associated flow rule may be used as follows: Since $\sigma_r = \sigma_t$ at $x = 0$, it is assumed that for some range of x between zero and some point x_e, the condition $\sigma_r = \sigma_t$ holds. In this range, Equations [10] and [11] hold, provided that λ lies between zero and 1. At the center of the disk $\dot{\epsilon}_t = \dot{\epsilon}$, and hence $\lambda = 1/2$ for $x = 0$. At x_e, for certain values of σ_{r0}/σ_0, λ may become unity, and for $x > x_e$, $\sigma_r < \sigma_t$ and Equations [1] and [2] apply. It is also possible that λ may be less than unity for all values of x.

Assuming $\sigma_r = \sigma_t$ and h constant, the Equilibrium Equation [4] may be integrated taking $\sigma_t = \sigma_{im}$ at $x = 0$. Thus the following expressions for σ_r and σ_t are obtained for the range $0 \leqq x \leqq x_e$

$$\frac{\sigma_t}{\sigma_{tav}} = \frac{\sigma_r}{\sigma_{tav}} = \frac{\sigma_{im}}{\sigma_{tav}}\left(1 - \frac{x^2}{2\beta}\right) \quad [22]$$

where

$$\beta = \frac{\sigma_{im}}{\sigma_0} = K\frac{\sigma_{tav}}{\sigma_0} \quad [23]$$

Substituting Equation [22] into Equation [10], differentiating with respect to x, and equating the resulting expression for $d\dot{w}/dx$ to that given by Equation [11], we have

$$\frac{d\lambda}{dx} + \lambda\left[\frac{2 - \frac{x^2}{\beta}(1+n)}{\left(1 - \frac{x^2}{2\beta}\right)x}\right] = \frac{1}{x} \quad [24]$$

Integrating this and choosing the integration constant to give $\lambda = 1/2$ at $x = 0$, the expression for λ becomes

$$\lambda = \frac{1}{2x^2(n+1)}\left\{x^2 + 2\beta\left[\left(\frac{1}{1 - \frac{x^2}{2\beta}}\right)^n - 1\right]\right\} \quad [25]$$

It is found that for β greater than a certain value β_{cr}, $0 < \lambda < 1$ for $0 \leqq x \leqq 1$. In this case $\sigma_r = \sigma_t$ and Equation [22] will hold for all radii of the disk. This critical value β_{cr} is found by solving the following equation obtained by putting $x = 1$ and $\lambda = 1$ in Equation [25]

$$\frac{2n+1}{2\beta_{cr}} = \frac{1}{\left[1 - \frac{1}{2\beta_{cr}}\right]^n} - 1 \quad [26]$$

Values of β_{cr} calculated from this equation are tabulated in Table 3. Values of $(\sigma_{r0}/\sigma_0)_{cr} = \beta_{cr} - 0.5$ are also given.

Table 3 Values calculated from Equation [26]

n	2	3	4	6	10
β_{cr}	1.13	1.52	1.92	2.7	4.3
$(\sigma_{r0}/\sigma_0)_{cr}$	0.63	1.02	1.42	2.2	3.8

For values of σ_{r0}/σ_0 greater than the values given in this table the stresses become, using Equation [22]

$$\frac{\sigma_t}{\sigma_{tav}} = \frac{\sigma_r}{\sigma_{tav}} = K\left[1 - \frac{x^2}{2\frac{\sigma_{r0}}{\sigma_0} + 1}\right] \quad [27]$$

where

$$K = \frac{\sigma_{im}}{\sigma_{tav}} = \frac{\frac{\sigma_{r0}}{\sigma_0} + \frac{1}{2}}{\frac{\sigma_{r0}}{\sigma_0} + \frac{1}{3}} \quad [28]$$

Note that in this case the ratio of peak to average stress is independent of the exponent n.

If $\sigma_{r0}/\sigma_0 < (\sigma_{r0}/\sigma_0)_{cr}$ as given by Table 3, $\lambda = 1$ for some value $x = x_e$ between 0 and 1. To find this value, λ is taken as unity in Equation [25]. This gives

$$\left(\frac{1}{1 - \frac{x_e^2}{2\beta}}\right)^n = (1 + 2n)\frac{x_e^2}{2\beta} + 1 \quad [29]$$

Using Equations [1], [2], and [22] it may be shown that the stress σ_t for $x_e \leqq x \leqq 1$ is given by

$$\sigma_t = \sigma_{im}(1 - x_e^3/2\beta)(x_e/x)^{1/n} \quad [30]$$

By integrating Equation [4] between zero and unity, and utilizing Equations [22] and [30], we obtain

$$\frac{\sigma_{r0}}{\sigma_0} = \beta\left[\frac{x_e^{1/n} - x_e(1-\alpha)}{\alpha}\right] - \left[\frac{1}{3} - x_e^3\left(-\frac{1}{6} + \frac{1}{2\alpha}\right) + \frac{x_e^{2+1/n}}{2\alpha}\right] \quad [31]$$

For a given β, x_e is obtained from Equation [29] and σ_{r0}/σ_0 from Equation [31]. Using these values of β and σ_{r0}/σ_0, the factor K becomes

$$K = \frac{\sigma_{im}}{\sigma_{tav}} = \frac{\beta}{\frac{\sigma_{r0}}{\sigma_0} + 1/3} \quad [32]$$

This holds for $\sigma_{r0}/\sigma_0 < (\sigma_{r0}/\sigma_0)_{cr}$ (Table 3).

Integrating Equation [4] between x_e and x and using Equation [30], the value of σ_r becomes, for the range $x_e \leqq x \leqq 1$

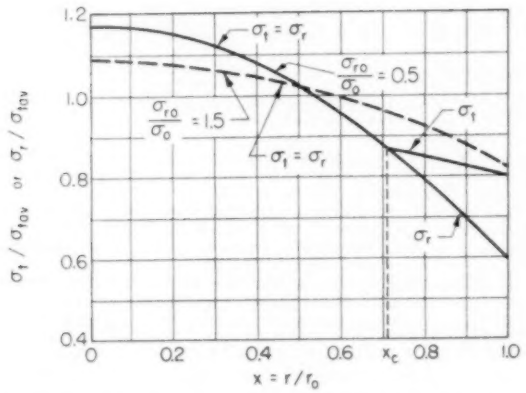

Fig. 14 Stress distributions in constant-thickness solid disk; $n = 4$

$$\frac{\sigma}{\sigma_{av}} = \frac{\sigma_{tm}}{\sigma_{tav}}\left(1 - \frac{x_c^2}{2\beta}\right)\left(\frac{x_c^{1/n}\, x^\alpha - x_c(1-\alpha)}{\alpha x}\right) - \frac{(x^2 - x_c^2)}{x\left(\frac{3\sigma_{r0}}{\sigma_0} + 1\right)} \quad [33]$$

Values of $K = \sigma_{tm}/\sigma_{tav}$ calculated for various n-values using Equation [28] for $\sigma_{r0}/\sigma_0 > (\sigma_{r0}/\sigma_0)_{cr}$ and using Equations [29], [31], and [32] for $\sigma_{r0}/\sigma_0 < (\sigma_{r0}/\sigma_0)_{cr}$ are plotted in Fig. 13. (The elastic curves for the disk taking Poisson's ratio equal to 0.3 and to 0.5 are shown dashed.) Contrary to what one might expect, these curves show that the peak stresses in the disk under creep conditions based on the Tresca criterion exceed the elastic values under certain conditions. Thus for $n = 4$, $\sigma_{r0} = 0$, $K = 1.26$ compared with a value of 1.24 for the elastic case where $\nu = 0.3$.

Incidentally, a calculation using the Mises criterion by the numerical integration method discussed in (3) for $n = 4$, $\sigma_{r0} = 0$ yields a value of $K = 1.18$ or somewhat below the elastic value. However, for $n = 2$, the K-value obtained using the Mises criterion probably also would be above the elastic value for $\sigma_{r0} = 0$.

Stress distributions obtained using these equations in a solid disk for $n = 4$ and $\sigma_{r0}/\sigma_0 = 0.5$ are shown by the solid line in Fig. 14. For $\sigma_{r0}/\sigma_0 = 1.5$ the dashed line is obtained and in this case $\sigma_r = \sigma_t$ for all values of x since $\sigma_{r0}/\sigma_0 > (\sigma_{r0}/\sigma_0)_{cr}$ as given by Table 3.

Solid Rotating Cylinder (Rotor)

A comparison of the steady-state creep-stress distribution in a long rotating cylinder with that found in the rotating disk is of interest. Away from the ends, it is reasonable to assume a condition of plane strain so that the strain rate $\dot{\epsilon}_z = -\dot{\epsilon}_0$ where $\dot{\epsilon}_0$ is positive and independent of the radius. Taking $\dot{\epsilon}_t = \dot{w}/r_o x$ and $\dot{\epsilon}_r = d\dot{w}/r_o dx$, using the constant-volume relation $\dot{\epsilon}_t + \dot{\epsilon}_r = \dot{\epsilon}_0$, and integrating, we obtain for a solid rotor[3]

$$\dot{w} = \frac{\dot{\epsilon}_0 r}{2} = \frac{\dot{\epsilon}_0 r_o x}{2} \quad [34]$$

This means that $\dot{\epsilon}_t = \dot{\epsilon}_r = \dot{\epsilon}_0/2$ for all values of x. At the center $\sigma_t = \sigma_r$ and it appears reasonable to take $\sigma_t = \sigma_r$ for all values of r to satisfy the condition $\dot{\epsilon}_t = \dot{\epsilon}_r$. Based on either the Tresca or Mises criterion, the strain rates are then given by

[3] Equation [34] is the same as that derived by Nadai (5) for the case of the solid rotating cylinder in the plastic state if $\dot{\epsilon}_0$ is taken as strain instead of strain rate.

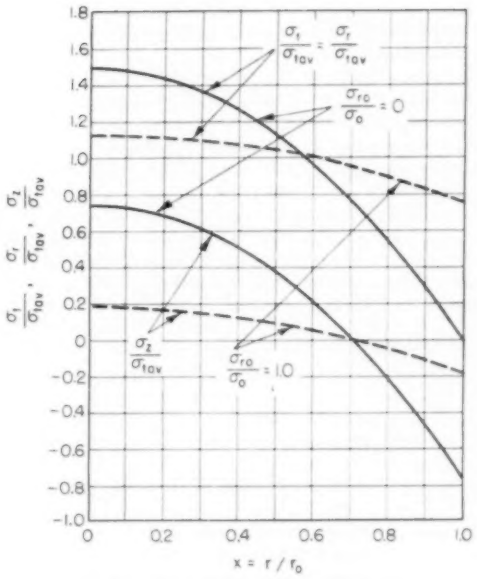

Fig. 15 Stress distribution in solid rotor

$$\dot{\epsilon}_t = \frac{\dot{w}}{r_o x} = \frac{1}{2} K' f(t)(\sigma_t - \sigma_z)^n \quad [35]$$

$$\dot{\epsilon}_r = \frac{d\dot{w}}{r_o dx} = \frac{1}{2} K' f(t)(\sigma_t - \sigma_z)^n \quad [36]$$

$$\dot{\epsilon}_z = -\dot{\epsilon}_0 = -K' f(t)(\sigma_t - \sigma_z)^n \quad [37]$$

Since $\sigma_r = \sigma_t$ at all points, these stresses are given by Equation [27], and the factor K by Equation [28].

From the condition that there is no resultant axial load on the cylinder, the following expression for σ_z is obtained

$$\frac{\sigma_z}{\sigma_{tav}} = \frac{\frac{1}{4}(1 - 2x^2)}{\frac{\sigma_{r0}}{\sigma_0} + \frac{1}{3}} \quad [38]$$

Curves showing the distribution of stresses σ_t, σ_r, and σ_z (which are independent of n) for a solid rotor based on Equations [27] and [38] are shown in Fig. 15. The solid lines are for $\sigma_{r0}/\sigma_0 = 0$ and the dashed lines for $\sigma_{r0}/\sigma_0 = 1$. Values of the factor K plotted versus σ_{r0}/σ_0 are shown by the dot-dash line in Fig. 13. (This is also the elastic curve for $\nu = 0.5$.) Note that these K-values are appreciably higher than the elastic value for a rotor with $\nu = 0.33$. Also, the K-values for the rotor are appreciably higher than those for the disk, particularly for $n > 3$ and $\sigma_{r0}/\sigma_0 < 0.5$.

Conclusions

The analysis of stress distribution for disks with holes indicates considerable nonuniformity of stress distribution under steady-state creep conditions particularly for lower n-values and higher ratios between outside and inside diameters. This would indicate that creep-rupture strengths of such disks subjected to long continued spin testing at elevated temperatures may be lower than would be expected on an average stress basis, particularly, for materials having limited ductility. However, actual long-time spin tests would be desirable to confirm this conclusion.

The K-values found for the variable-thickness disks are somewhat lower than for the constant-thickness disks, depending on the disk contour.

The analysis based on the Tresca criterion for the solid disks (without holes) also indicates appreciable nonuniformity of stress distribution under steady-state creep, particularly for the lower values of n and for the smaller ratios $\sigma_{r0}/\sigma_\theta$. Contrary to what one might expect, peak stress values somewhat above the elastic values are obtained under certain conditions. This is particularly true for disks having low values of n, and it may be true for values of n around 2 even if the Mises criterion is applied. This is also the case for the solid rotor even if the latter criterion is used. In the author's opinion, further spin tests at elevated temperature are needed as a check on these results.

Acknowledgment

The author is indebted to Mr. R. E. Peterson of the Westinghouse Research Laboratories for support and encouragement of this work, and to Dr. L. Schoenfeld for valuable comments.

Bibliography

1 "Analysis of Creep in Rotating Disks Based on the Tresca Criterion and Associated Flow Rule," by A. M. Wahl, JOURNAL OF APPLIED MECHANICS, TRANS. ASME, vol. 78, 1956, pp. 231–238.

2 "On the Use of Singular Yield Conditions and Associated Flow Rules," by William Prager, JOURNAL OF APPLIED MECHANICS, TRANS. ASME, vol. 75, 1953, pp. 317–320.

3 "Creep Tests of Rotating Disks at Elevated Temperature and Comparison With Theory," by A. M. Wahl, G. O. Sankey, M. J. Manjoine, and E. Shoemaker, JOURNAL OF APPLIED MECHANICS, TRANS. ASME, vol. 76, 1954, pp. 225–235.

4 "Stress Distribution in Rotating Disks Subjected to Creep Including Effects of Variable Thickness and Temperature," by A. M. Wahl, JOURNAL OF APPLIED MECHANICS, TRANS. ASME, vol. 79, 1957, pp. 299–305.

5 "Theory of Flow and Fracture of Solids," by A. Nadai, McGraw-Hill Book Company, Inc., New York, N. Y., 1950, p. 482.

Further Large-Deflection Analysis for a Plate Strip Subjected to Normal Pressure and Heating

By M. L. WILLIAMS,[1] PASADENA, CALIF.

In an earlier paper (1)[2] an analysis was carried out to determine the stresses and deflection in an infinite strip plate undergoing large deflections when the plate was subjected to a combined normal loading and uniform temperature rise through the thickness, both of which were permitted to vary across the plate width. This paper extends the analysis and design charts to the case where the temperature distribution through the thickness of the plate may have any desired distribution. If the usual plate assumptions regarding plane sections remaining plane are valid, then the arbitrary temperature distribution can be represented completely by the average temperature and the first moment of the temperature about the plate middle surface, as far as the engineering stresses and deflections are concerned. The convenient nondimensional design charts cover equilibrium positions in the buckling as well as nonbuckling range and show maximum stress and central deflection as a function of pressure, average temperature, and temperature moment for cases of both clamped and simply supported edges.

Introduction

THE extension of the previous work (1), which essentially covered the case wherein the temperature distribution through the thickness of the plate was an even function with respect to the plate middle surface, is again based upon the classical analysis of the large-deflection problem (2). This work was considered useful because there are cases, particularly in airplane and missile design, where the thin-plate nonlinear deflection regime is encountered. Furthermore, even considering that most structurally thin plates are also thermally thin, with respect to rate of heat transfer, cases of transient heating may occur wherein the distribution of the temperature rise through the plate thickness departs markedly from a constant value. For example, it is easily verified from a consideration of the steady-state heat-conduction equation, $\nabla^2 T(x, y, z) = 0$, that if the temperature is independent of the plate plane dimensions x and y, then the temperature distribution may be of the form $A + Bz$ and hence possess an antisymmetric as well as symmetric component with respect to the thickness direction z. Moreover, if nonsteady temperatures are introduced, even higher-order temperature variations enter.

In general, however, any resultant $T(z)$ can be separated into its even and odd components. It develops that, as usual, the customary engineering structural quantities of stress and deflection are completely prescribed by these two components as characterized by the average temperature (derived from the even component of $T[z]$) and the first moment of the temperature about the plate middle plane (derived from the odd component of $T[z]$).

As in the previous paper, the formulation has been based upon an energy approach to facilitate application to approximate solutions for related cases not included in this paper.

Formulation of Problem

For the strip of uniform thickness h, and width b, in the y-direction subjected to a normal pressure $p(y)$ and temperature rise $T(y, z)$, the normal deflection $w(y)$ and lateral displacement $v(y)$ are to be calculated assuming that the developed membrane or middle-plane stresses are to be accounted for. After a general formulation, the specific development is carried out assuming material properties independent of temperature.

In considering problems dealing with the deflections and stresses in heated thin plates from the potential energy formulation of the problem, the temperature effect amounts in the general case to the addition of a term (3)

$$W_T = \iiint \frac{E\alpha T(x, y, z)}{1 - 2\nu} [\bar{\epsilon}_x + \bar{\epsilon}_y + \bar{\epsilon}_z] dx dy dz \quad \ldots [1]$$

to the potential energy V, such that

$$V = U - W - W_T \quad \ldots [2]$$

where U and W are the strain energy and applied work contributions, respectively, in the absence of heating or cooling.

If the three-dimensional strains in the x, y, and z-directions, where z is normal to the (x, y)-plane of the plate, are $\bar{\epsilon}_x$, $\bar{\epsilon}_y$, $\bar{\epsilon}_z$, respectively, the plane-stress assumption for an isotropic homogeneous thin plate, $\sigma_z = 0$, leads to the relation

$$\sigma_z = \lambda(\bar{\epsilon}_x + \bar{\epsilon}_y + \bar{\epsilon}_z) + 2\mu\bar{\epsilon}_z = 0$$

or

$$\bar{\epsilon}_z = -\left(\frac{\lambda}{\lambda + 2\mu}\right)(\bar{\epsilon}_x + \bar{\epsilon}_y) \quad \ldots [3]$$

where λ and μ are the Lamé constants. Following the usual procedure for small bending of the thin plates[3] wherein the deflec-

[1] Associate Professor, Guggenheim Aeronautical Laboratory, California Institute of Technology; also, Consultant, Douglas Aircraft Company, Long Beach Division.

[2] Numbers in parentheses refer to the Bibliography at the end of the paper.

Contributed by the Applied Mechanics Division and presented at the Annual Meeting, New York, N. Y., December 1–6, 1957, of The American Society of Mechanical Engineers.

Discussion of this paper should be addressed to the Secretary, ASME, 29 West 39th Street, New York, N. Y., and will be accepted until July 10, 1958, for publication at a later date. Discussion received after the closing date will be returned.

Note: Statements and opinions advanced in papers are to be understood as individual expressions of their authors and not those of the Society. Manuscript received by ASME Applied Mechanics Division, February 4, 1957. Paper No. 57—A-14.

[3] For the thin plates contemplated to be covered by this analysis, the effects of the nonlinear bending-stress distribution through the plate thickness due to the arbitrary temperature distribution will be confined to the boundaries and will contribute local Saint Venant disturbances which will not affect the gross quantities of usual interest for engineering purposes. See a similar example in "Theory of Elasticity," by S. Timoshenko and J. N. Goodier, McGraw-Hill Book Company, Inc., New York, N. Y., second edition, 1951, p. 99.

tions are not too large, the strains are composed of both average extensional strains, e_x and e_y, and plane-section bending strains through the plate thickness, $z(\partial^2 w/\partial x^2)$ and $z(\partial^2 w/\partial y^2)$,

$$\bar{e}_x = e_x - z(\partial^2 w/\partial x^2) \quad [4]$$

$$\bar{e}_y = e_y - z(\partial^2 w/\partial y^2) \quad [5]$$

thus

$$\bar{e}_z = -\frac{\nu}{1-\nu}[e_x + e_y - z\nabla^2 w(x, y)] \quad [6]$$

and upon substituting into Equation [1], the thermal contribution to the potential energy becomes

$$W_T = \iiint \frac{E\alpha T(x, y, z)}{1-\nu}[(e_x + e_y) - z\nabla^2 w]dxdydz \quad [7]$$

or upon separating the integration through the thickness assuming now for convenience in this case that the material properties are independent of the temperature distribution through the plate thickness

$$W_T = \iint \frac{E\alpha}{1-\nu}(e_x + e_y)\left\{\int_{-h(x,y)/2}^{h(x,y)/2} T(x, y, z)dz\right\} dxdy \quad [7a]$$

$$- \iint \frac{E\alpha}{1-\nu}\nabla^2 w(x, y)\left\{\int_{-h(x,y)/2}^{h(x,y)/2} zT(x, y, z)dz\right\} dxdy$$

where the bracketed terms in the first and second integrals are, respectively, the average temperature $h\bar{T}(x, y)$ and first moment of the temperature distribution about the plate middle plane, $kh^2(x, y)T^{(1)}(x, y)$, where k is a numerical factor depending upon the distribution,[4] and $T^{(1)}(x, y)$ is the temperature of the top $(z = h/2)$ surface above average; i.e.

$$T^{(1)}(x, y) = T(x, y, h/2) - \bar{T}(x, y)$$

Inasmuch as for the case of an infinite strip, where conditions are to be considered identical at every section along the x-direction, variations in the lateral displacement u and any other quantities with respect to x can be neglected, Equation [7] becomes independent of x. The other contributions to the total potential energy V are made up of

$$U_m = \int_{-b/2}^{b/2} \frac{Eh}{2(1-\nu^2)}\left[\left(\frac{dv}{dy}\right)^2 + \frac{dv}{dy}\left(\frac{dw}{dy}\right)^2 + \frac{1}{4}\left(\frac{dw}{dy}\right)^4\right] dy \quad [8]$$

$$U_b = \int_{-b/2}^{b/2} \frac{D}{2}\left(\frac{d^2 w}{dy^2}\right)^2 dy \quad [9]$$

$$W_p = \int_{-b/2}^{b/2} p(y)w(y)dy \quad [10]$$

the subscripts indicating middle surface, bending, and loading, respectively. Upon combining Equations [8]–[10] with [7a] independent of x, the potential energy Equation [2] becomes

$$V = \int_{-b/2}^{b/2}\left\{\frac{Eh}{2(1-\nu^2)}\left[v'^2 + v'w'^2 + \frac{1}{4}w'^4\right] + \frac{D}{2}w''^2 - pw - \frac{Eh\alpha\bar{T}(y)}{1-\nu}\left[v' + \frac{1}{2}w'^2\right] + \frac{kEh^3\alpha T^{(1)}(y)}{1-\nu}w''\right\} dy \quad [11]$$

[4] If, for example, $T(x, y, z) = 100\,[5 + 2(2z/h) - (2z/h)^2 + (2z/h)^3]$, then by evaluating the appropriate integrals, $h\bar{T} = 100h(14/3)$ and $kh^2T^{(1)} = 100h^2(13/30)$. With $T^{(1)} \equiv T(h/2) - \bar{T} = 100\,(7) - 100\,(14/3) = 100\,(7/3)$, $k = 100\,(13/30) \div 100\,(7/3) = 13/70$.

where the primes indicate differentiation with respect to y. Paralleling the previous work, dimensionless forms are introduced

$$\left.\begin{array}{llll} \eta = 2y/b & p(\eta) = p_0 g(\eta) & \bar{T}(\eta) = \bar{T}_0 f(\eta) & \\ \bar{v} = v/b & E(\eta) = E_0 s(\eta) & T^{(1)}(\eta) = T_0^{(1)} r(\eta) & \\ \bar{w} = w/b & & & \end{array}\right\} \quad [12]$$

and the potential energy written as

$$V = \frac{b}{2}\int_{-1}^{1}\left\{\frac{2hE_0 s(\eta)}{1-\nu^2}[\bar{v}'^2 + 2\bar{v}'\bar{w}'^2 + \bar{w}'^4] - \frac{2E_0 h^3 s(\eta)}{3(1-\nu^2)b^2}\bar{w}''^2 - p_0 b g(\eta)\bar{w} - \frac{2E_0 h\alpha\bar{T}_0}{1-\nu}s(\eta)f(\eta)[\bar{v}' + \bar{w}'^2] + \frac{4kEh^3\alpha T_0^{(1)} r(\eta)}{(1-\nu)b}\bar{w}''\right\} d\eta \quad [13]$$

where the primes now indicate differentiation with respect to η.

Upon carrying out the variations upon $\bar{v}$ and $\bar{w}$ in the usual fashion, there result the two differential equations

$$\frac{d}{d\eta}\left\{\frac{4E_0 h}{1-\nu^2}s(\eta)[\bar{v}' + \bar{w}'^2] - \frac{2E_0 h\alpha\bar{T}_0}{1-\nu}f(\eta)s(\eta)\right\} = 0 \quad [14]$$

$$\frac{d^2}{d\eta^2}\left\{\frac{4E_0 h^3}{3(1-\nu^2)b^2}s(\eta)\bar{w}''\right\} - \frac{d}{d\eta}\left\{\left[\frac{8E_0 h}{1-\nu^2}s(\eta)[\bar{v} + \bar{w}'^2] - \frac{4E_0 h\alpha\bar{T}_0}{1-\nu}s(\eta)f(\eta)\right]\frac{d\bar{w}}{d\eta}\right\} - p_0 b g(\eta) + \frac{4kE_0 h^3\alpha T_0^{(1)}}{(1-\nu)b}s(\eta)\frac{d^2 r}{d\eta^2} = 0 \quad [15]$$

and the natural boundary conditions on the moment and shear. Thus considering also the possible boundary conditions which may be prescribed on the deflection itself, the four possible boundary conditions at $\eta = \eta^*$, two of which must be selected, are

$$\text{Deflection} = w(\eta^*) \quad [16]$$

$$\text{Slope} = w'(\eta^*) \quad [17]$$

$$\text{Moment} = -\frac{b}{4}\left\{\frac{2E_0 h^3 s(\eta^*)}{3(1-\nu^2)b^2}2\bar{w}''(\eta^*) + \frac{4kE_0 h^3\alpha T_0^{(1)}}{(1-\nu)b}r(\eta^*)\right\} \quad [18]$$

$$\text{Shear} = \frac{1}{2}\left\{4N\bar{w}'(\eta^*) + \frac{d}{d\eta}[\text{Moment}]\right\}_{\eta=\eta^*} \quad [19]$$

For clamped edges one would have the usual conditions of zero deflection, Equation [16], and slope, Equation [17]

$$\bar{w}(\pm 1) = 0 \quad [20]$$

$$\bar{w}'(\pm 1) = 0 \quad [21]$$

whereas for simply supported edges the deflection [16] and moment [18] must vanish giving

$$\bar{w}(\pm 1) = 0 \quad [22]$$

$$\bar{w}''(\pm 1) = 8\frac{h}{b}\frac{r(\pm 1)}{s(\pm 1)}\left[\frac{3(1+\nu)}{8}\left(\frac{b}{h}\right)^2\alpha T_0^{(1)}(-k)\right] \quad [23]$$

Note in Equation [23] that if there is no antisymmetric temperature variation, $\bar{w}''(\pm 1) = 0$.

Returning now to the integration of the differential Equations [14] and [15], the first of these may be integrated directly to give

$$\frac{4E_0h}{1-\nu^2}\,s(\eta)\,[\bar{v}' + \bar{w}'^2] - \frac{2E_0h\alpha T_0}{1-\nu}\,f(\eta)s(\eta) = 2N \quad \ldots [24]$$

where the unknown constant of integration N can be physically identified with the average middle-plane load per unit plate length. Then upon substituting Equation [24] into [15] there results

$$\frac{d^2}{d\eta^2}\left[\frac{4E_0h^3}{3(1-\nu^2)b^2}\,s(\eta)\,\frac{d^2\bar{w}}{d\eta^2}\right] - \frac{4N}{b}\,\frac{d^2\bar{w}}{d\eta^2} = p_0 g(\eta) - \frac{4kE_0\alpha}{1-\nu}\left(\frac{h}{b}\right)^2 T_0^{(1)}\,\frac{d^2r}{d\eta^2} \quad \ldots [25]$$

Equations [24] and [25] therefore apply to the strip-plate case for any distributed normal pressure and for any temperature increment distribution which varies across the plate width and/or through the plate thickness.

It is thus observed that the addition to the problem of a temperature which varies through the thickness of the plate has two effects. The first is that the previous results for a temperature which remained constant through the thickness of the plate may be formally generalized by remarking that if the temperature distribution is symmetrical about the plate middle surface, thus implying symmetrical temperature boundary conditions, all the previous results (1) may be used by replacing the constant value of the temperature by its average value through the plate thickness.

Secondly, if the temperature distribution is antisymmetric, there is a change of the plate normal loading such that the new equivalent pressure is increased by a term proportional to the square of the thickness-to-width ratio. The calculation of the local bending moment and shear is also modified as indicated in Equations [18] and [19].

Note that, as indicated earlier, there are many practical cases where the plate is sufficiently wide to imply a predominantly one-dimensional heat flow through the thickness alone, $T = T(z)$; the only steady-state temperature change which can exist is therefore a constant temperature rise plus a superimposed linear variation. This is evident by specializing $\nabla^2 T(x, y, z) = 0$. Other one-dimensional temperature distributions of course can exist if nonsteady heating is present such that $T = T(z, t)$.[4]

In order to attack certain specific problems define the following nondimensional quantities assuming uniform plate thickness

Average membrane stress

$$\Lambda^2 \equiv 6\left(\frac{b}{h}\right)^2 \frac{N(1-\nu^2)}{2E_0h} = \left(\frac{b}{2}\right)^2 \frac{N}{D} \quad \ldots [26]$$

Normal pressure

$$\Pi \equiv \frac{3(1-\nu^2)}{64}\,\frac{p_0b^4}{E_0h^4} = \frac{1}{256}\,\frac{p_0b^4}{Dh} \quad \ldots [27]$$

Average temperature (zero temperature moment)

$$\Theta \equiv \frac{3(1+\nu)}{8}\left(\frac{b}{h}\right)^2 \alpha T_0 \quad \ldots [28]$$

First temperature moment

$$\Theta_1 \equiv \frac{3(1+\nu)}{8}\left(\frac{b}{h}\right)^2 \alpha T_0^{(1)}(-k) \quad \ldots [29]$$

[4] It has been shown by many authors that thermal stresses computed from time-varying temperatures can be considered as pseudo-static for all normal situations.

Upon integrating twice, the equilibrium equation normal to the plate becomes

$$s(\eta)\,\frac{d^2\bar{w}}{d\eta^2} - \Lambda^2\bar{w} = 8\,\frac{h}{b}\,\Theta_1 r(\eta) + 16\,\frac{h}{b}\,\Pi \int\int g(\eta)d\eta d\eta \quad \ldots [30]$$

The complete integration of course would yield four constants to be determined by the two deflection boundary conditions at $\eta = \pm 1$.

The other differential equation for displacement, $\bar{v}(\eta)$, is Equation [14] which yields two integration constants, one of which is N if the alternate form, Equation [24], is used. These two constants are determined by the conditions placed upon $\bar{v}(\eta)$ at $\eta = \pm 1$, usually $\bar{v}(\pm 1) = 0$ for fixed edges.

Having formulated the problem it remains to consider some specific examples which are thought to have the widest application. Thus in the ensuing computations, the applied normal pressure is taken as constant and the temperature has been restricted to be an arbitrary function of thickness only, and hence independent of temperature variation at different positions along the plate width. Cases for two combinations of boundary conditions have been carried out.

Special Case of Simply Supported Edges

For the case of two simply supported edges, using boundary conditions [22] and [23], and $g(\eta) = r(\eta) = s(\eta) = 1$, the deflection is found upon integration of Equation [30] as

$$\bar{w}(\eta) = \frac{8}{\Lambda^2}\,\frac{h}{b}\left\{\Pi\left[1 - \eta^2 - \frac{2}{\Lambda^2}\left(1 - \frac{\cosh \Lambda\eta}{\cosh \Lambda}\right)\right] - \Theta_1\left[1 - \frac{\cosh \Lambda\eta}{\cosh \Lambda}\right]\right\} \quad \ldots [31]$$

and the displacement in the plane of the plate is

$$\frac{3}{4}\left(\frac{b}{h}\right)^3 \bar{v}(\eta) = \left[\frac{8\Pi}{\Lambda^2}\right]^2 \left\{\frac{\Theta + (\Lambda^2/8)}{(8\Pi/\Lambda^2)^2}\,\eta - \eta^3 + \frac{3}{\Lambda\cosh\Lambda}\,\frac{(2\Pi/\Lambda^2) + \Theta_1}{\Pi}\,[\Lambda\eta\cosh\Lambda\eta - \sinh\Lambda\eta] - \frac{3\Lambda}{16\cosh^2\Lambda}\left[\frac{(2\Pi/\Lambda^2) + \Theta_1}{\Pi}\right]^2 [\sinh 2\Lambda\eta - 2\Lambda\eta]\right\} \quad \ldots [32]$$

Upon requiring $\bar{v}(\pm 1) = 0$, there results the determining equation for Λ, the normalized membrane stress

$$\Theta + \frac{1}{8}\Lambda^2 = \left[\frac{8\Pi}{\Lambda^2}\right]^2 F^2(\Lambda) + \frac{96}{\Lambda^4}\,\Pi\Theta_1 F_1^2(\Lambda) + \frac{24}{\Lambda^2}\,\Theta_1^2 F_2^2(\Lambda) \quad \ldots [33]$$

where $$F^2(\Lambda) = 1 - \frac{6}{\Lambda^2} + \frac{15}{2}\,\frac{\tanh\Lambda}{\Lambda^3} - \frac{3}{2}\,\frac{\operatorname{sech}^2\Lambda}{\Lambda^2} \quad \ldots [34]$$

$$F_1^2(\Lambda) = (3/\Lambda)\tanh\Lambda - 2 - \operatorname{sech}^2\Lambda \quad \ldots [35]$$

$$F_2^2(\Lambda) = (1/\Lambda)\tanh\Lambda - \operatorname{sech}^2\Lambda \quad \ldots [36]$$

It may be observed that if there is no antisymmetric heating, $\Theta_1 = 0$, then there results the equation obtained earlier (1). Further it may be noted that when there is no pressure on the plate

$$\Theta + \frac{1}{8}\Lambda^2 - \frac{24}{\Lambda^2}\,\Theta_1^2\left[\frac{\tanh\Lambda}{\Lambda} - \operatorname{sech}^2\Lambda\right] = 0 \quad \ldots [37]$$

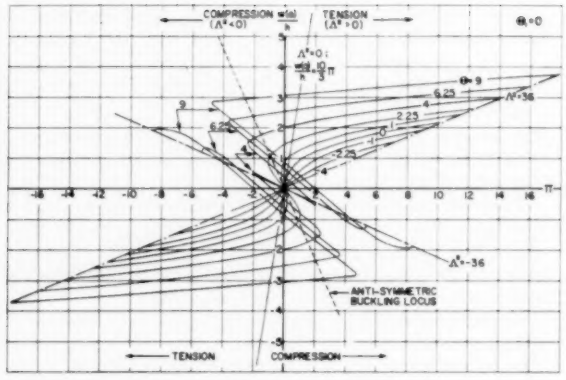

(a)

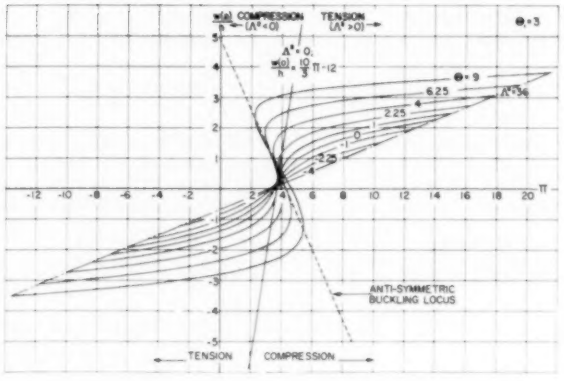

(d)

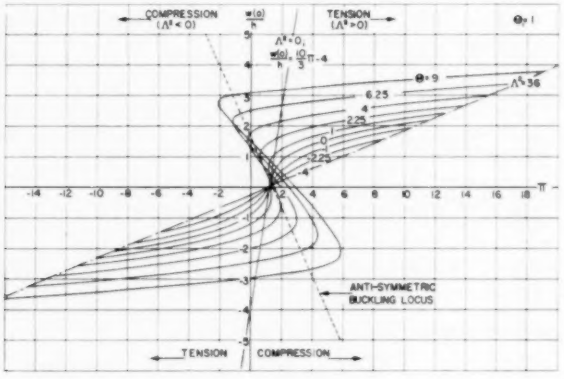

(b)

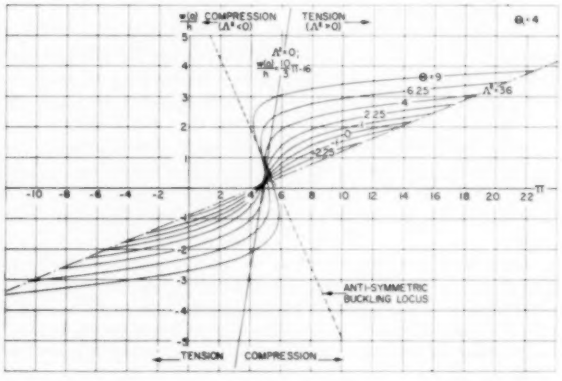

(e)

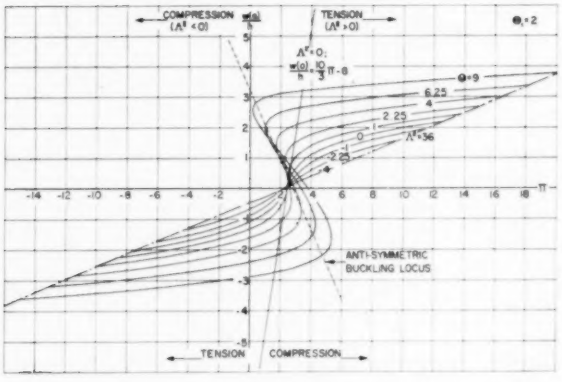

(c)

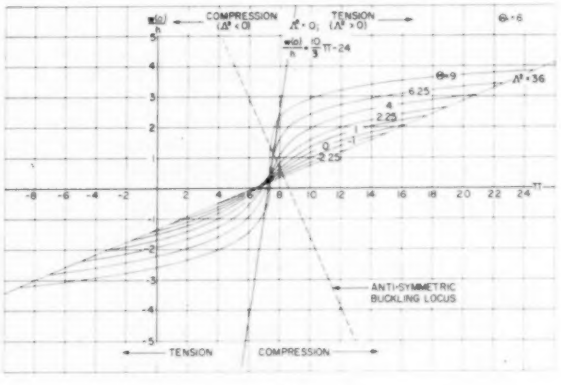

(f)

FIG. 1 CENTRAL DEFLECTION, SIMPLY SUPPORTED EDGES, FOR TEMPERATURE MOMENTS OF $\Theta_1 = 0, 1, 2, 3, 4, 6, 8,$ AND 10, RESPECTIVELY

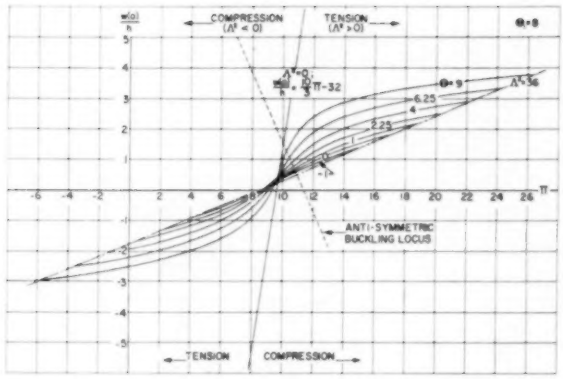

(*g*)

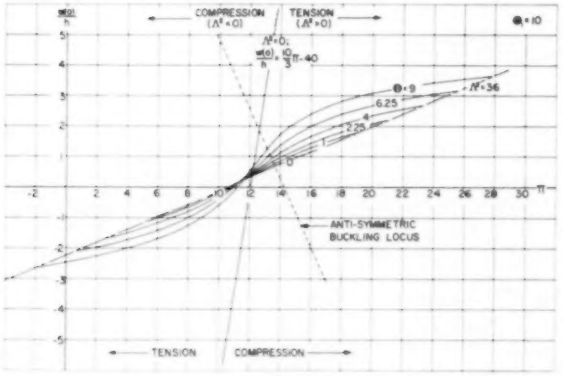

(*h*)

FIG. 1 (*Continued*)

from which the middle-plane stress during thermal loading only may be found.

When the middle-plane stress becomes compressive, i.e., N is replaced by $-N$ in Equation [25], the character of the solution changes from hyperbolic to trigonometric functions, which results can be obtained formally throughout by replacing Λ by $i\Lambda$, using $i = \sqrt{-1}$, or Λ^2 by $-\Lambda^2$.

The necessary calculations have been carried out; $F^2(\Lambda)$, $F_1^2(\Lambda)$, and $F_2^2(\Lambda)$ are given in Table 1.[6] Using these data, Equation [33] was used to determine the middle-plane stress as a function of Π and Θ for various steps in the antisymmetric temperature moment Θ_1. The results are plotted in Fig. 2.[7] (The locus shown is a line of symmetry in the sense that the increment of pressure to a given Θ value on either side of the locus is the same.) The central deflection was then evaluated from Equation [31] at $\eta = 0$ and also plotted as a function of the pertinent variables in Fig. 1. Some of the higher mode, and usually less interesting, central buckling deflections have been omitted so as not to confuse the figures.

Inasmuch as it is also convenient to have values of the bending

[6] Certain errors in the latter significant figures for the corresponding tables in reference (1) have been corrected by the more accurate automatic digital programming used in the current calculations.

[7] Deflections and stresses for negative values of Θ_1 can be obtained from the figures using symmetry conditions. For example, see Equation [33] where $\Theta_1 < 0$ and $\Pi > 0$ is equivalent to $\Theta_1 > 0$ and $\Pi < 0$ for the same membrane stress and average temperature.

TABLE 1(*a*) SIMPLY SUPPORTED EDGES—TENSION RANGE

Λ	$F^2(\Lambda)$	$F_1^2(\Lambda)$	$F_2^2(\Lambda)$
0	0	0	0
0.25	0.000599861	−0.000990935	0.0396598
0.50	0.00834274	−0.0137448	0.137787
0.75	0.0339747	−0.0559900	0.250279
1.00	0.0819946	−0.135192	0.341620
1.25	0.148211	−0.244534	0.398212
1.50	0.224303	−0.370410	0.422726
1.75	0.302448	−0.500025	0.424117
2.00	0.377282	−0.624609	0.411363
2.25	0.445904	−0.739430	0.391213
2.50	0.507193	−0.842655	0.368053
3.00	0.608093	−1.014811	0.321819
3.5	0.684367	−1.148060	0.281553
4.0	0.741983	−1.251844	0.248491
4.5	0.785951	−1.333991	0.221674
5.0	0.819984	−1.400236	0.199800
5.5	0.846727	−1.454631	0.181745
6.0	0.868054	−1.500031	0.166640

TABLE 1(*b*) SIMPLY SUPPORTED EDGES—COMPRESSION RANGE

Λ	$F^2(i\Lambda)$	$F_1^2(i\Lambda)$	$F_2^2(i\Lambda)$
0	0	0	0
0.25	0.000667617	−0.00109649	−0.0438318
0.50	0.0125291	−0.0206315	−0.205841
0.75	0.0859437	−0.141486	−0.625743
1.00	0.457720	−0.753296	−1.86811
1.20	1.93611	−3.18559	−5.47250
1.25	2.93846	−4.83454	−7.64985
1.40	14.7057	−24.1914	−30.4741
1.50	105.564	−173.647	−190.449
$\pi/2$	∞	− ∞	− ∞
1.60	753.252	−1239.05	−1194.26
1.75	26.1006	−42.9381	−34.6291
1.80	17.3326	−28.5158	−21.7533
2.00	6.71387	−11.0520	−6.86692
2.25	3.75162	−6.18570	−3.08470
2.50	2.69250	−4.45447	−1.85685
2.70	2.25492	−3.74872	−1.39856
3.00	1.87632	−3.16287	−1.06784
3.20	1.71954	−2.94860	−.985146
3.50	1.56390	−2.81924	−1.03329
3.75	1.48602	−2.92794	−1.29944
4.00	1.45874	−3.47218	−2.05109
4.2	1.51395	−4.89066	−3.73722
4.3	1.61388	−6.63032	−5.69351
4.4	1.85759	−10.4761	−9.88351
4.5	2.58165	−21.4133	−21.4743
4.6	6.23668	−75.7244	−77.5766
4.7	437.872	−6466.02	−6498.36
$3\pi/2$	∞	− ∞	− ∞
4.75	50.1453	−726.037	−712.847
4.80	10.5361	−139.731	−132.987
4.90	3.38160	−33.9715	−29.8215
5.00	2.18850	−16.4562	−13.1040
5.30	1.46298	−6.10360	−3.53708
5.50	1.34196	−4.53423	−2.17220
5.70	1.27765	−3.78247	−1.55099
6.00	1.22197	−3.23019	−1.13319

stress readily available, Equation [18] was employed in the form [$s(\eta) = r(\eta) = 1$]

$$-M(\eta) = D\left\{\frac{4}{b}\bar{w}''(\eta) - \frac{32}{b}\frac{h}{b}\Theta_1\right\} \quad \ldots\ldots [38]$$

which for the simply supported edge case, using Equation [31], gives

$$M_{ss}(\eta) = \frac{32Dh}{b^2}\left\{\frac{2\Pi}{\Lambda^2} + \Theta_1\right\}\left\{1 - \frac{\cosh \Lambda\eta}{\cosh \Lambda}\right\} \quad \ldots. [39]$$

The bending stress σ_b is related to the moment through the usual plate relation $\sigma_b = 6M/h^2$ and thus one also can write

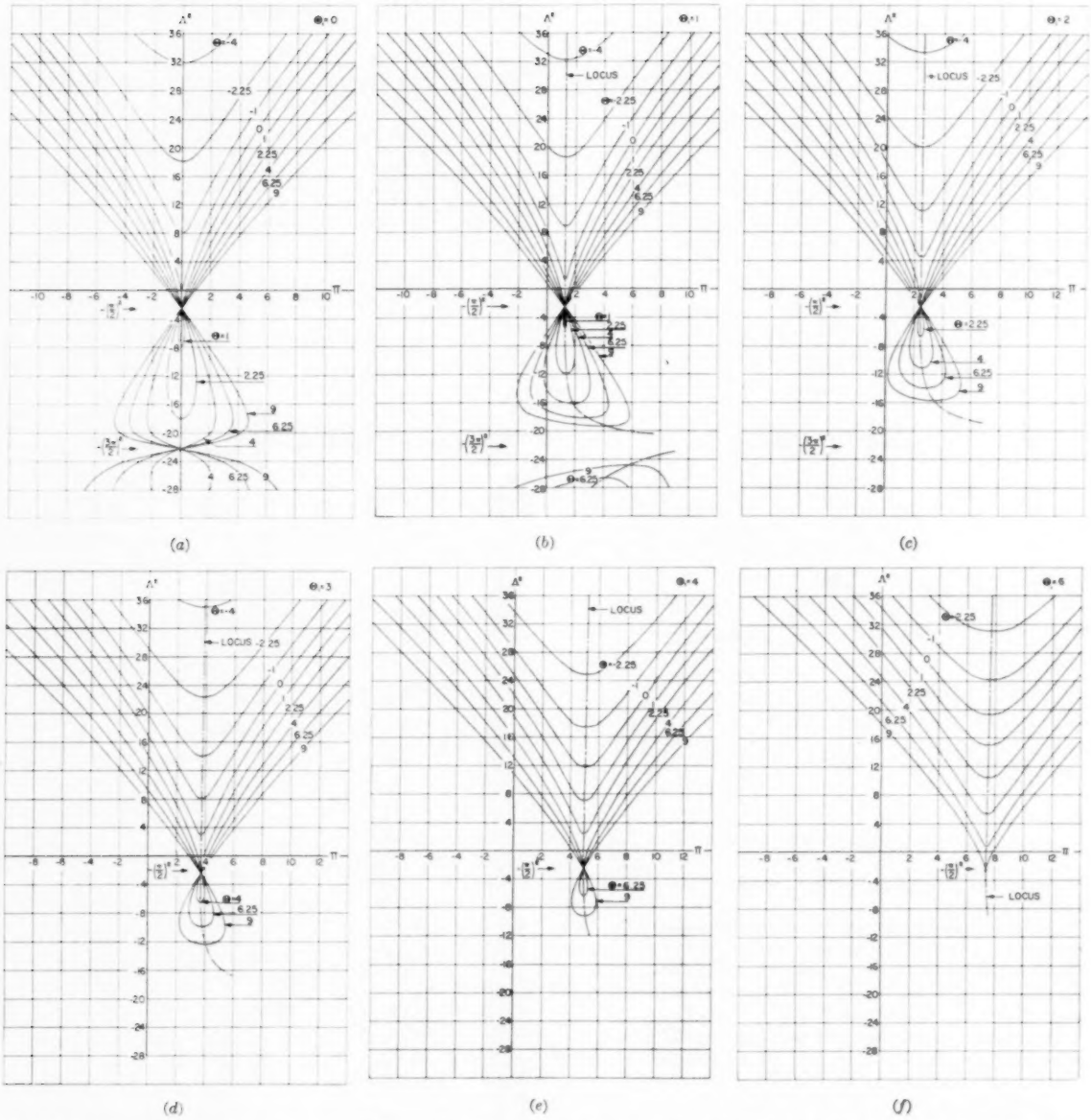

FIG. 2 MEMBRANE STRESS, SIMPLY SUPPORTED EDGES, FOR TEMPERATURE MOMENTS OF $\Theta_1 = 0, 1, 2, 3, 4, 6, 8,$ AND 10, RESPECTIVELY

$$\frac{b^2h}{4D}\,\sigma_{bss} = 48\left[\frac{2\Pi}{\Lambda^2} + \Theta_1\right]\left[1 - \frac{\cosh \Lambda\eta}{\cosh \Lambda}\right] \quad \ldots\ldots [40]$$

which can be evaluated easily for its maximum value at $\eta = 0$, or, if desired, graphed for design use (5).

Then inasmuch as the average middle-plane stress, $\sigma_m = N/h$, can be expressed in the form

$$\frac{b^2h}{4D}\,\sigma_{mss} = \Lambda^2 \quad \ldots\ldots [41]$$

the addition of Equations [40] and [41] gives the nondimensional combined surface stresses

$$\frac{b^2h}{4D}\,\sigma_{ss} = \Lambda^2 \pm 48\left[\frac{2\Pi}{\Lambda^2} + \Theta_1\right]\left[1 - \frac{\cosh \Lambda\eta}{\cosh \Lambda}\right] \quad \ldots [42]$$

SPECIAL CASE OF CLAMPED EDGES

When both edges of the strip plate are clamped, the analysis for plates with antisymmetric heating becomes somewhat simpler because then the boundary conditions and differential equations depend solely upon the displacements. (The derived force quantities such as the moment and shear do of course depend

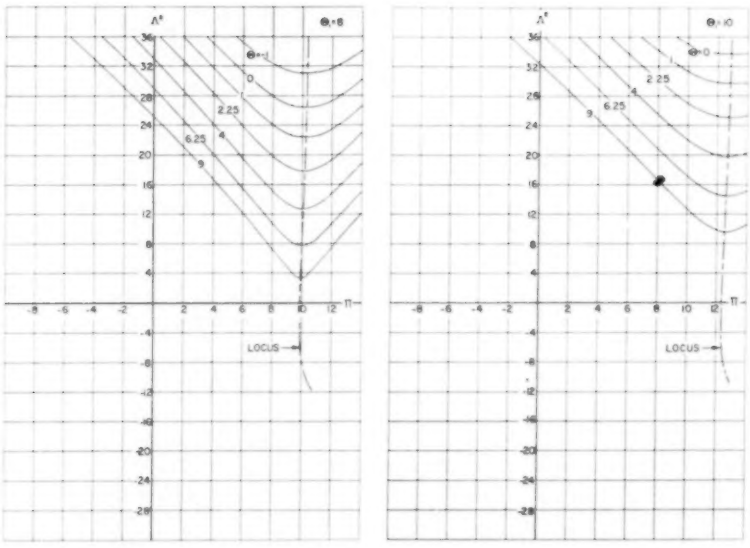

(g) (h)

FIG. 2 (*Continued*)

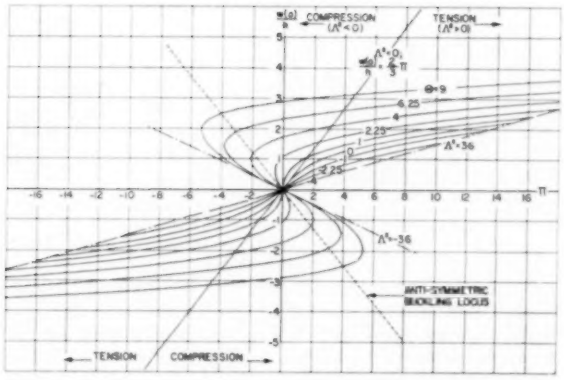

FIG. 3 CENTRAL DEFLECTION, CLAMPED EDGES, FOR ANY TEMPERATURE MOMENT Θ_1

upon the temperature moment.) It may be verified readily therefore that the solutions for the deflection and displacement will be formally the same as in the case $\Theta_1 = 0$. The results of reference (1) may be used in their entirety and are repeated here for completeness

$$w(\eta) = \frac{8\Pi}{\Lambda^2}\frac{h}{b}\left[1 - \frac{2}{\Lambda}\coth\Lambda - \eta^2 + \frac{2}{\Lambda\sinh\Lambda}\cosh\Lambda\eta\right] \quad \ldots\ldots[43]$$

$$\frac{3}{4}\left(\frac{b}{h}\right)^2\theta(\eta) = \left[\frac{8\Pi}{\Lambda^2}\right]^2\left\{1 - \eta^2 - (1-\eta)F_c^2(\Lambda) + \frac{3\,\mathrm{csch}^2\Lambda}{4\Lambda}\left[\sinh 2\Lambda - \sinh 2\Lambda\eta - 2\Lambda(1-\eta)\right] - \frac{6\,\mathrm{csch}\,\Lambda}{\Lambda^2}\left[\Lambda\cosh\Lambda - \Lambda\eta\cosh\Lambda\eta + \sinh\Lambda\eta - \sinh\Lambda\right]\right\} \quad \ldots\ldots[44]$$

TABLE 2 CLAMPED EDGES

Λ	$F_c^2(\Lambda)$	Λ	$F_c^2(i\Lambda)$
0.5	0.00037787	1.0	0.007806
1.0	0.0052493	1.5	0.053602
1.5	0.021447	2.0	0.28444
2.0	0.052011	2.5	1.83252
2.5	0.094615	2.6	2.88004
3.00	0.14427	2.7	4.86376
3.5	0.19535	2.8	9.081031
4.0	0.24724	2.9	20.19523
4.5	0.29532	3.0	63.12526
5.0	0.33965	π	∞
5.5	0.38004	3.2	464.67028
6.00	0.41663	3.3	69.26236
		3.4	28.45890
		3.5	16.13379
		3.7	7.99366
		4.0	4.21558
		4.5	2.48911
		5.0	2.12504
		5.5	2.99313
		5.7	4.56483
		6.0	17.46910
		2π	∞

NOTE: The values in the first two columns are based on the tabulation by Shaw, Pohle, and Perrone (4)

$$\Theta + \frac{1}{8}\Lambda^2 = \left[\frac{8\Pi}{\Lambda^2}\right]^2 F_c^2(\Lambda) \quad \ldots\ldots[45]$$

where $$F_c^2(\Lambda) = \left\{1 + \frac{6}{\Lambda^2} - \frac{9\coth\Lambda}{2\Lambda} - \frac{3\,\mathrm{csch}^2\Lambda}{2}\right\} \quad \ldots\ldots[46]$$

$F_c^2(\Lambda)$ for this clamped case is given in Table 2; the middle-plane stress as a function of pressure and average temperature (note the independence upon Θ_1) in Fig. 4; and the maximum deflection, $w(0)/h$, in Fig. 3.

Again it is convenient to have the bending stresses, which do depend upon the thermal moment, readily available. Using Equation [18] or the equivalent form Equation [38] specialized for the case of clamped edges, the bending moment

$$M_{el} = \frac{32Dh}{b^2}\left\{\frac{2\Pi}{\Lambda^2}\left[1 - \frac{\Lambda\cosh\Lambda\eta}{\sinh\Lambda}\right] + \Theta_1\right\} \quad \ldots\ldots[47]$$

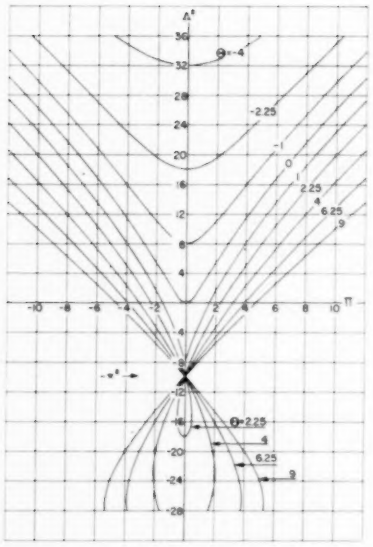

FIG. 4 MEMBRANE STRESS, CLAMPED EDGES, FOR ANY TEMPERATURE MOMENT Θ_1

when transformed into the dimensionless surface stress becomes

$$\frac{b^2h}{4D}\sigma_{bcl} = 48\left\{\frac{2\Pi}{\Lambda^2}\left[1 - \frac{\Lambda\cosh\Lambda\eta}{\sinh\Lambda}\right] + \Theta_1\right\} \quad [48]$$

Inasmuch as the bending stress usually has two positions of interest, viz., the central ($\eta = 0$) and edge ($\eta = \pm 1$) values, values for both normally would be evaluated for design purposes.

In a manner similar to the previous case, the middle-plane and bending stresses can be combined to give, for clamped edges

$$\frac{b^2h}{4D}\sigma_{bcl} = \Lambda^2 \pm 48\left\{\frac{2\Pi}{\Lambda^2}\left[1 - \frac{\Lambda\cosh\Lambda\eta}{\sinh\Lambda}\right] + \Theta_1\right\} \quad [49]$$

ANTISYMMETRIC DEFLECTION SHAPES

In the previous paper it was shown that, as might be expected, more than one equilibrium mode shape might exist if the middle-plane stress were compressive, i.e., Λ replaced by $i\Lambda$. Indeed if a multiplicity of modes of the trigonometric functions are admitted, antisymmetric as well as symmetric deflections can occur. While the stability question will not be discussed at this time it is useful to construct the possible equilibrium antisymmetric mode shapes for the two boundary conditions treated in this paper:

1 As the deflections for the clamped-edge case have been shown to be independent of the thermal moment, the previous results will again apply if Λ^2 is read as the average middle-plane stress. The stresses at which the antisymmetric deflection shapes can occur are given by the eigenvalues of

$$\Lambda^* \cot \Lambda^* = 1 \quad [50]$$

which upon using Equation [43] with Λ replaced by $i\Lambda^*$ gives the central deflection

$$\frac{w(0)}{h} = -\frac{8\Pi}{\Lambda^2}\left[1 + \frac{2}{\Lambda^{*2}} - \frac{2}{\Lambda^*\sin\Lambda^*}\right] \quad [51]$$

The locus for these possible antisymmetric buckling modes is indicated in Fig. 4.

2 The eigenvalues for the simply supported antisymmetric buckling case are calculated as before from

$$\sin\Lambda^* = 0 \quad [52]$$

or $\Lambda^* = n\pi$ where $n = 1, 2, 3 \ldots$ The central deflection is then obtained from Equation [31] again replacing, for the compressive range, Λ by $i\Lambda^* = in\pi$ to obtain

$$\frac{w(0)}{h} = -\frac{8\Pi}{(n\pi)^2}\left\{1 + \frac{2[1-(-1)^n]}{(n\pi)^2}\right\} + \frac{8\Theta_1}{(n\pi)^2}[1-(-1)^n] \quad [53]$$

These loci for the various amounts of thermal moment are indicated in Fig. 2.

Perhaps it should be pointed out that while the central deflection is the same for either mode at the bifurcation condition, i.e., either a symmetric or antisymmetric mode at the eigenvalue Λ^*, $w(0)/h$ will not be the maximum deflection if the mode is antisymmetric. For example, as discussed more fully in the previous paper, the lowest mode antisymmetric maximum deflection occurs at the quarter-span point.

CONCLUSION

As a final remark it may be stated that it is impractical to present calculations and curves covering too wide a variation of parameters. The effort in this paper has been concentrated upon those combinations of parameters falling in the region between thick-plate and membrane solutions; i.e., $1 \leq w(0)/h \leq 4$. While the computations of course could be extended, it is believed that outside this region satisfactory results can be achieved for most purposes by using the limit-case solutions.

ACKNOWLEDGMENT

The author is greatly indebted to R. M. Edmiston, of the Strength and Dynamic Stability Section, Douglas Aircraft Company, for his care, patience, and co-operation in carrying out the substantial data reduction and preparing the presentation of the design curves in this paper.

BIBLIOGRAPHY

1 "Large Deflection Analysis for a Plate Strip Subjected to Normal Pressure and Heating," by M. L. Williams, JOURNAL OF APPLIED MECHANICS, Trans. ASME, vol. 77, 1955, pp. 458–464.

2 "Theory of Plates and Shells," by S. Timoshenko, McGraw-Hill Book Company, Inc., New York, N. Y., 1940, pp. 1–33.

3 "Fundamental Principles and Methods of Thermo-Elasticity," by W. S. Hemp, *Aircraft Engineering*, vol. 26, April, 1954, p. 126; also, *Aeronautical Quarterly*, August, 1956.

4 "The Non-Linear Deflection of Infinite Strip Plates," by F. S. Shaw, F. Pohle, and N. Perrone, Polytechnic Institute of Brooklyn, Brooklyn, N. Y., PIBAL Report No. 225, June, 1953.

5 "Large Deflection and Stress Analysis for Thin Plates—I," by M. L. Williams and R. M. Edmiston, Technical Report LB-25419, Douglas Aircraft Co., Long Beach Division, September, 1957.

General Instability of Ring-Stiffened Cylindrical Shells Subject to External Hydrostatic Pressure—A Comparison of Theory and Experiment

By G. D. GALLETLY,[1] R. C. SLANKARD,[2] AND E. WENK, JR.[3]

Tests are described of a number of machined-stiffened cylinders subjected to external hydrostatic pressure, and the observed general instability strengths compared with predictions from theories of Kendrick and Nash. Agreement with Kendrick was found rather good. Results also are presented from electrical strain gages which show in detail the growth of embryonic lobes and nonlinear characteristics of deformation at the threshold of buckling. Weakening effects of imperfect circularity are discussed.

Introduction

IN THE strength design of ring-stiffened cylinders under external pressure, consideration must be given to all possible modes of yielding and instability failures. One such mode is that of general instability, in which both the stiffeners and shell plating undergo extensive deformation from end to end with serious loss in load-carrying capacity. Resistance to such failure requires provision of rings of adequate size and spacing, and, if properly chosen, the material may be loaded up to its yield point, which is probably an optimum condition for minimum weight.

Although the spacing of ring stiffeners on cylindrical shells can be determined readily from existing analyses to insure adequate shell strength under external pressure, the question of stiffener size to insure adequate general instability strength has not been as well resolved. Tokugawa (1)[4] was the first to recognize this mode of collapse, and his theoretical results found wide application in submarine design, using arbitrary factors of safety. Furthermore, experimental analyses by Trilling (2) as well as Tokugawa have been interpreted broadly as confirming the theory.

Around 1950, renewed investigation of the general instability problem at the David Taylor Model Basin revealed a number of serious shortcomings in both mathematical and experimental treatment such that additional research in both areas was considered necessary, especially if certain empiricisms in the use of Tokugawa's work were to be overcome. For the first time, attention was directed to the fact that the rational proportioning of stiffeners involved two types of solutions; namely (*a*) for perfectly circular shells, and (*b*) for those with initially imperfect shape associated with normal processes of fabrication. This separation of the problem assumed particular significance when it was realized that the theories available or being developed were for perfect structures, whereas the models employed for confirmation were imperfect. As one important consequence, a program of tests was developed to check theory using models as nearly circular as could be fabricated by careful machining. A second step was to extend the theory to include effects of initial out-of-roundness.

The background and details of an experimental program with machined models are described in this paper, together with an evaluation of observed buckling pressures, particularly in terms of the more recent theories of Kendrick (3) and Nash (4). Results from electrical strain gages are presented which include plots of embryonic lobe formation and the nonlinear characteristics of deformation at the threshold of the buckling process.

Background

The concept of using ring stiffeners to increase the strength of cylindrical shells under external pressure was confirmed when von Mises discovered that the buckling strength of cylinders varied in some manner inversely with unsupported length. Such stiffeners induce local bending and shear effects which disturb the otherwise uniform membrane deformations in the shell. Since the rings are loaded radially by the shell through mutual interaction, there is the possibility that the rings could buckle at some critical value of the applied pressure. If the stiffened cylinder were sufficiently long, all the rings would buckle simultaneously in a general instability mode; the strength could be determined by isolating one such typical stiffener and applying the well-known ring-buckling analysis of Lévy (5), using radial loads given by von Sanden and Günther (6). This method which predicts the general instability pressure for an infinite stiffened cylinder has been used to approximate ring strength, although experimental verification was lacking.

For relatively short stiffened cylinders, support at the boundaries propagates toward the center so as to invalidate application of the simple ring analysis. Tokugawa was the first to recognize the significance of finite-cylinder length, but his analysis has since been found to be in error. It is understood that Fernández (7) also arrived at similar results, but his solution has not been

[1] Shell Development Company, Emeryville, Calif. Assoc. Mem. ASME.

[2] Department of Air Force, Washington, D. C.

[3] Chairman, Department of Engineering Mechanics, Southwest Research Institute, San Antonio, Texas.

[4] Numbers in parentheses refer to the Bibliography at the end of the paper.

Contributed by the Applied Mechanics Division and presented at the Annual Meeting, New York, N. Y., December 1–6, 1957, of THE AMERICAN SOCIETY OF MECHANICAL ENGINEERS.

Discussion of this paper should be addressed to the Secretary, ASME, 29 West 39th Street, New York, N. Y., and will be accepted until July 10, 1958, for publication at a later date. Discussion received after the closing date will be returned.

NOTE: Statements and opinions advanced in papers are to be understood as individual expressions of their authors and not those of the Society. Manuscript received by ASME Applied Mechanics Division, January 2, 1957. Paper No 57—A-73.

evaluated. About the same time, Flügge (8) indicated methods of solution in which the stiffened cylinder was treated as an orthotropic shell but did not extend results for engineering application.

Salerno and Levine (9) attempted a more rational analysis with Rayleigh-Ritz energy methods, involving buckling configurations similar in form to those used by von Mises for shell instability. Kendrick (3) and Nash (4) working independently, however, discovered errors in that derivation and subsequently have published correct solutions; Kaminsky (10) also has extended Kendrick's work for different end conditions. Implications of these various theories are discussed elsewhere in this paper. It should be noted that, in all these cases, the solutions were confined to the range of small deflection and to perfectly circular structures.

Despite these many contributions to the theory, the experimental analysis of general instability appears to have been neglected. Tokugawa's models were machined but made of brass with nonelastic properties; Trilling's were welded and so short that the influence of end conditions was undesirably large. Both sets of tests were in a limited range of geometries, without benefit of instrumentation or measurements of initial circularity. Similar deficiencies are noted in the results of Pelluz (11).

To correct this deficiency, the program described herein was undertaken to test a series of carefully machined models designed to fail by general instability; results were thus anticipated over a range of stiffener size, stiffener spacing, cylinder length, and ratios of cylinder thickness to diameter which could be employed to check both existing theories and future refinements for perfect structures. The first series in this program, with variation in stiffener sizes, is described herein. Apart from simple observation of the buckling pressures, the tests also were planned with sufficient instrumentation to permit examination of the buckling phenomena in finer detail.

Description of models

The primary requirements in designing these models were freedom from initial imperfections and residual stress, proportions such that failure would occur in a general instability mode, selection of geometries in a range of general interest, and selection of size of models that would facilitate test procedures.

To satisfy these prerequisites, it was decided to use models machined from thick stress-relieved tubes, the rings being monolithic with the shell. This fabrication procedure would insure circular and stress-free models, and, by employing high-strength steels, a general instability mode of failure could be achieved without prior yielding.

The models were roughly 8-in. diam. As shown in Fig. 1, bolting rings at both ends were machined integrally with the stiffened cylinder for attachment to a closure plate and to the pressure tank. The arrangement for applying external pressure is shown in Fig. 2. Of particular note is the access to the interior of the model both for instrumentation and for visual inspection while the model is under pressure. The tank diameter was selected so that the volume of pressure fluid and its associated energy content when compressed would be minimized to reduce the extent of model damage at the time of collapse.

The model geometries were chosen for several series, in each of which only one parameter would be varied at a time. For these tests, the thickness, the diameter, and length of cylinder and the stiffener spacing were fixed, and the size of the stiffeners was varied through a range of depths in the ratio 1:2:3:4. Duplicate tests in two cases were conducted to check the repeatability of results with identical models.

When planning tests, the selection of geometries was refined further by using the theoretical analysis of Kendrick as a guide to determine whether the ring sizes were small enough to insure a general instability collapse. Calculations for other less pertinent modes of failure also were made as a precaution against their intervening at lower pressures.

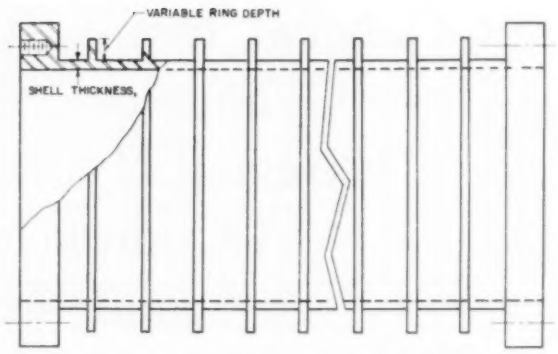

Fig. 1 Schematic diagram of machined models

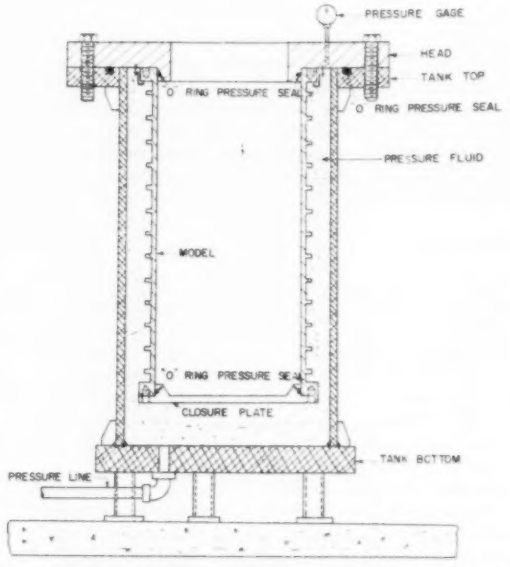

Fig. 2 Schematic diagram showing model in pressure tank

Except for Model 3, electrical strain gages were installed on the inner surface of the shell around the circumference and opposite the centermost stiffening ring. These were installed in sets of 24, with gages every 15 deg apart to detect any nonaxisymmetric behavior which, from prior tests reported by Wenk, Slankard, and Nash (12), was expected to occur even in the machined models.

Experimental results

All models failed in the desired general instability mode, as is illustrated by the photographs taken after collapse and shown in Fig. 3. Repeatability of test results is demonstrated by agreement between Models 1 and 2, and 5 and 6.

The collapse pressures P_f are compared with pressures P_{cr} predicted by various theories in Table 1 in terms of nondimensional ratios P_{cr}/P_f; these also are shown graphically in Fig. 4. The observed number of buckling lobes is compared with predictions from Kendrick's theory, part I, in Table 1. The variation of strength with stiffener size is plotted in Fig 5.

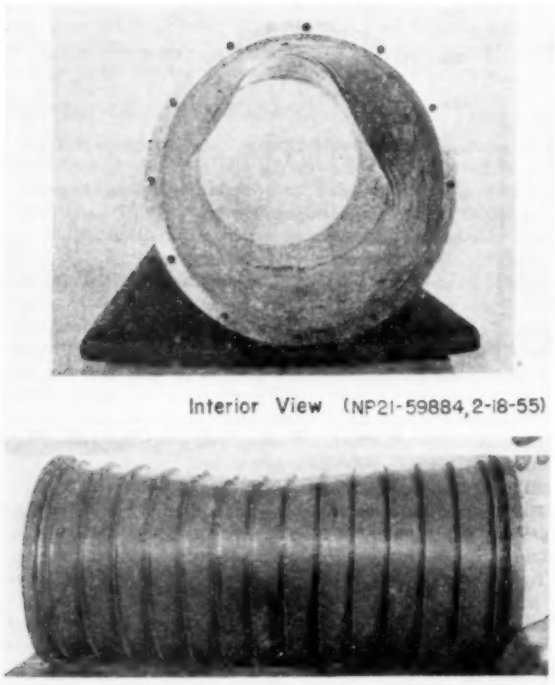

Fig. 3 View showing Model 6 after failure

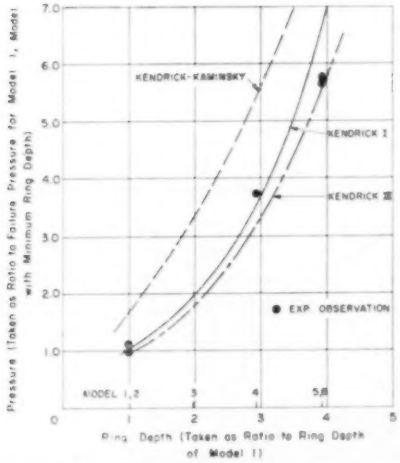

Fig. 4 Comparison of theoretical and observed collapse pressures

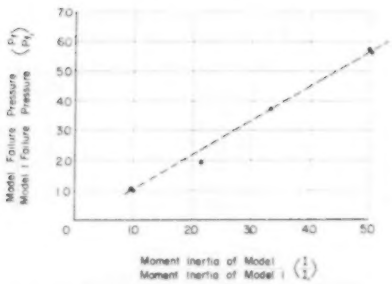

Fig. 5 Plot showing relationship of ratio of experimental pressures (P_f) to failure pressure of Model 1 (P_{f1}) with ratio of moment of inertia for rings of models (I) to moment of inertia of Model 1 (I_1)

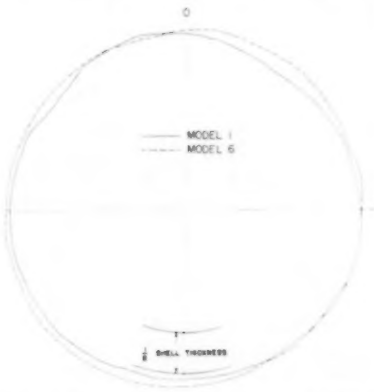

Fig. 6 Initial circularity contours of centermost ring for Models 1 and 6

Notwithstanding the machine process of fabricating, measurements of circularity were made prior to the tests because of indications that even small imperfections may influence strength seriously. All measurements were taken by means of an Ames dial micrometer at the rings where strain gages subsequently were installed; typical circularity charts are given in Fig. 6. In lieu of harmonic analyses of the circularity measurements, two simplified methods were selected for expressing the initial out-of-roundness. These are described in the Appendix. Results are summarized in Table 2. It can be seen that the maximum departures from circularity were 6 to 9 per cent of the shell thickness, which, considering the absolute value of the irregularity, is very small indeed—but still finite.

Two interesting phenomena associated with these imperfections as observed from the strain data were (*a*) localized bending effects with consequent departure from axial symmetry, and (*b*) nonlinear elastic variation of strain with pressure. As shown in Figs. 7, 8 and 9, these data suggest that embryonic lobes de-

Table 1 Ratio of theoretical collapse pressures (P_{cr}) to pressures at which the machined models failed (P_f)

	General instability				Axisymmetric yielding				
					Shell			Frame	
Model No.	Kendrick I	Kendrick III	Kendrick-Kaminsky	Nash	Shell instability von Mises	v. Sanden Günther	Salerno Pulos	v. Sanden Günther	Salerno Pulos
1(4)*	1.012(4)†	0.976	1.637	1.595	11.417	5.714	6.160	6.113	8.387
2(4)	0.989(4)	0.937	1.607	1.570	11.080	5.517	5.950	5.897	8.052
3(3)	0.994(3)	0.920	1.714	1.705	5.686	2.538	2.670	3.046	4.908
4(3)	0.960(3)	0.842	1.534	1.355	3.085	1.888	2.060	2.336	2.902
5(3)	1.200(3)	0.997	1.589	1.513	2.040	1.259	1.365	1.665	2.313
6(3)	1.160(3)	0.967	1.542	1.474	1.997	1.237	1.329	1.621	2.254

* Observed no. lobes. † Computed no. lobes.

Table 2 Initial out-of-roundness as determined by methods A and B for machined models

Model No.	Eccentricity-shell thickness ratio (e/h) Method A	Method B
1	0.0398	0.0398
2	0.0556	0.0376
3	0.0865	0.0645
4	0.0318	0.0198
5	0.0258	0.0258
6	0.0316	0.0257

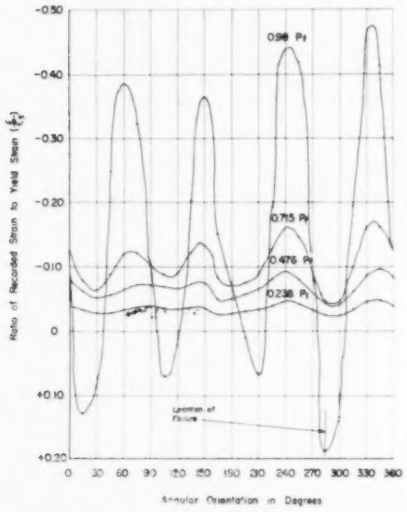

Fig. 7 Circumferential strains recorded directly under ring No. 7 (sta. 13) at various pressures for Model 1

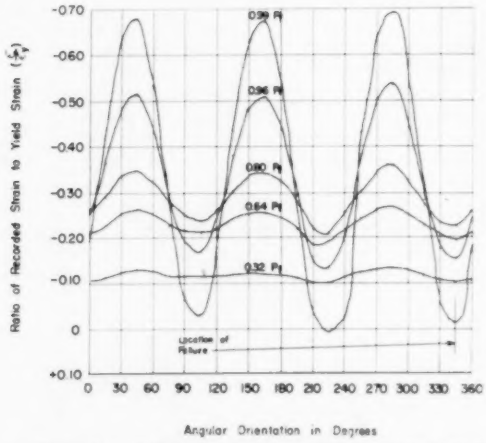

Fig. 8 Circumferential strains recorded directly under ring No. 7 (sta. 13) at various pressures for Model 4

veloped in all models at pressures considerably below failure, with the number of lobes equal to the number into which a perfectly circular model would collapse. The ordinates of these curves, incidentally, are the nondimensional ratios ϵ/ϵ_y where ϵ is the observed strain and ϵ_y is that at which uniaxial yielding would take place; i.e., σ_y/E. The periodicity of the strain variation around the circumference is certainly striking. In all probability, collapse occurred when one of these lobes grew explosively, since the

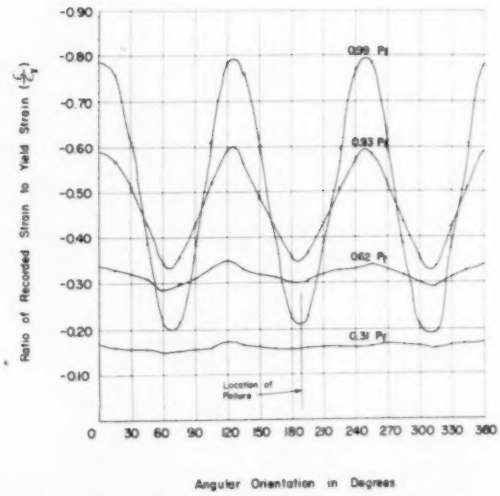

Fig. 9 Circumferential strains recorded directly under ring No. 7 (sta. 13) at various pressures for Model 6

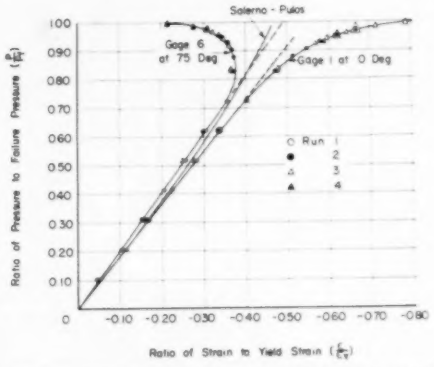

Fig. 10 Circumferential strain at inner fiber of ring No. 7 for Model 6

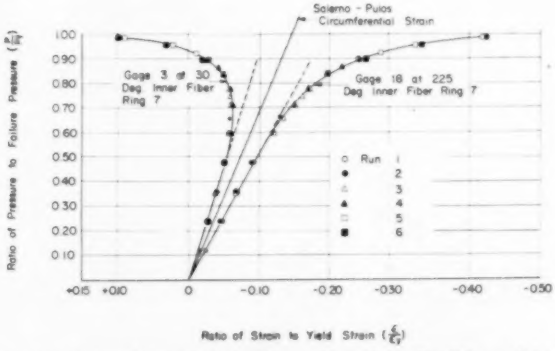

Fig. 11 Circumferential strain at inner fiber of ring No. 7 for model 1

location of failure coincided with the largest incipient inward lobe.

In Figs. 10 and 11 are plotted the observations of strain as a function of applied pressure, both in nondimensional terms. Of particular note is the nonlinear behavior which was confirmed by repeated loading and unloading to be fully elastic. Also shown on

the curves are the theoretical strains calculated from the analysis by Salerno-Pulos (13) for axisymmetric deformation associated with perfectly circular stiffened cylinders.

Evaluation of strain measurements

By averaging the strain observations from all 24 gages in a circumferential set, a good indication can be obtained of the membrane deformation of the ring, independent of the bending component. This has been done for all models except No. 3 which was not so completely instrumented; results are plotted in Figs. 12, 13, and 14. For comparison, the experimental data are shown with the theoretical predictions of Salerno-Pulos and von Sanden-Günther. It will be recalled that the Salerno-Pulos analysis of stress in a stiffened cylinder includes consideration of the nonlinear beam-column effect due to end pressure that von Sanden-Günther had neglected. The difference in results for these particular geometries, however, is seen from the graphs to be relatively small, and the nonlinear effect is practically insignificant. Test results agreed slightly better with the more refined analysis.

The fact that the behavior was completely elastic is supported by both the repeatability of results without permanent set and the recognition, as shown in Table 3, that the maximum recorded strain, even near the collapse pressure P_f, was always less than the yield strain ϵ_y. It is possible, of course, that higher strains existed at positions other than where strain gages were located, particularly on the outside surface of the ring. Nevertheless, the observed level of strain, always well below ϵ_y, is consistent with other observations of purely elastic behavior. These results may prove useful in the future for evaluating the validity of an out-of-roundness analysis.

The nonlinear elastic characteristics also lend themselves to another valuable application for predicting nondestructively the

Table 3 Comparison of maximum recorded circumferential strain at inner fiber of ring bordering central bay with strain necessary to cause yielding in ring

Model	$\epsilon_{max}/\epsilon_y$	P^*/P_f
1	0.476	0.982
2	0.290	0.990
3	...	...
4	0.696	0.991
5	0.807	0.995
6	0.784	0.990

NOTE:
P^* is pressure at which ϵ_{max} was recorded.
P_f is pressure at which model failed.

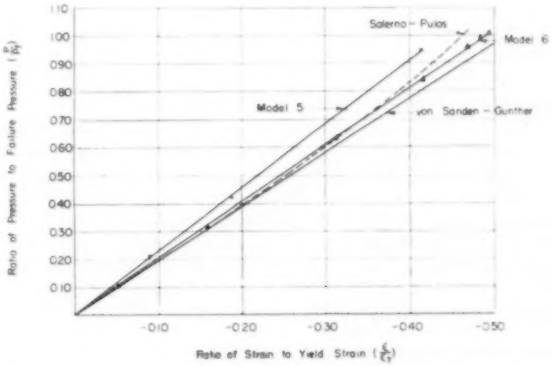
Salerno - Pulos
Model 6
Model 5
von Sanden - Gunther
Ratio of Pressure to Failure Pressure ($\frac{P}{P_f}$)
Ratio of Strain to Yield Strain ($\frac{\epsilon}{\epsilon_y}$)

Fig. 12 Comparison of theoretical and average experimental strain at inner fiber of ring No. 7 for identical Models 5 and 6

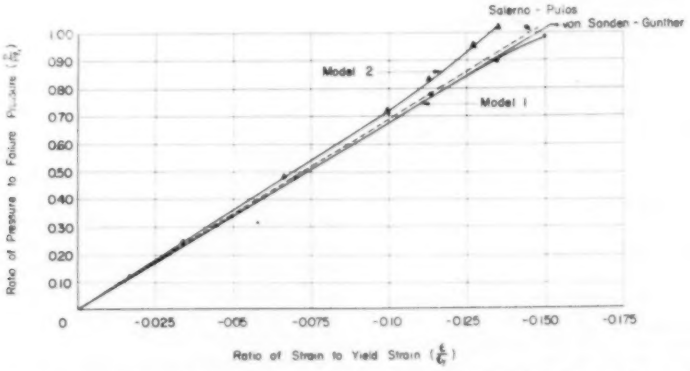
Salerno - Pulos
von Sanden - Gunther
Model 2
Model 1
Ratio of Pressure to Failure Pressure ($\frac{P}{P_f}$)
Ratio of Strain to Yield Strain ($\frac{\epsilon}{\epsilon_y}$)

Fig. 13 Comparison of theoretical and average experimental strain at inner fiber of ring No. 7 for identical Models 1 and 2

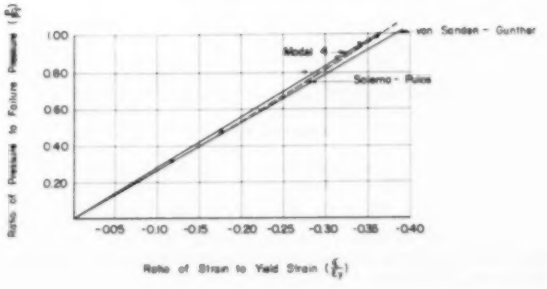
von Sanden - Gunther
Model 4
Salerno - Pulos
Ratio of Pressure to Failure Pressure ($\frac{P}{P_f}$)
Ratio of Strain to Yield Strain ($\frac{\epsilon}{\epsilon_y}$)

Fig. 14 Comparison of theoretical and average experimental strain at inner fiber of ring No. 7 for Model 4

collapse pressures for perfect cylinders. Using only the strain data, and by a simple extension of Southwell's methods described by Galletly and Reynolds (14), the general instabilitys trengths of all the models have been predicted. These are the pressures at which the bending strains would become infinite according to the amplifying term $1/(1-P/P_{cr})$, so that the strength can be estimated from the asymptotic trend of the strain in Figs. 10 and 11.

Table 4 Ratio of theoretical pressure as determined by Southwell's method for a perfect cylinder (P_{cr}) with pressure at which machined models failed (p_f)

Model	P_{cr}/P_f
1	1.040
2	1.010
3	...
4	1.035
5	1.040
6	1.020

The Southwell results are given in Table 4 as a ratio to the observed collapse pressures. In all cases, the correlation is closer than 5 per cent. This agreement suggests that, if the principles underlying the Southwell technique are valid, the observed buckling pressures are very close indeed to those which would be developed if the specimens were absolutely perfect. It may be concluded that the buckling pressures were but slightly affected by out-of-roundness and legitimately may be calculated from theories developed for perfect specimens.

Comparison of observed and computed buckling pressures

Before proceeding with an evaluation of the observed buckling pressures, the reader may be assisted by amplification of certain details of theory. Attention is directed first to the matter of assumed buckling configurations and of related boundary conditions. Kendrick (3) and Nash (4) both take buckling patterns which represent the formation of harmonic circumferential lobes. In this (Part I) study, however, Kendrick assumed a longitudinal displacement pattern which conforms to a simple sine curve, a condition which signifies zero restraint to rotation of the generator at the ends. In a refinement, Part III, Kendrick (15) recognizes additional between-stiffener deformation of the type that occurs in shell or interbay buckling. These alternate hypothetical modes of failure are represented in Fig. 15.

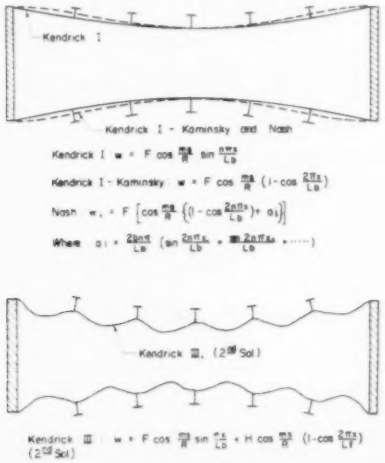
Kendrick I
Kendrick I - Kaminsky and Nash
Kendrick I $w = F\cos\frac{n\theta}{R}\sin\frac{n\pi x}{Lb}$
Kendrick I - Kaminsky $w = F\cos\frac{n\theta}{R}\left(1-\cos\frac{2\pi x}{Lb}\right)$
Nash $w_1 = F\left[\cos\frac{n\theta}{R}\left\{\left(1-\cos\frac{2n\pi x}{Lb}\right)+a_1\right\}\right]$
Where $a_1 = \frac{2n\pi}{Lb}\left(\sin\frac{2n\pi A_1}{Lb}+\frac{m}{n}\sin\frac{2n\pi A_2}{Lb}+\cdots\right)$
Kendrick III (2nd Sol)
Kendrick III (2nd Sol) $w = F\cos\frac{n\theta}{R}\sin\frac{\pi x}{Lb}+H\cos\frac{n\theta}{R}\left(1-\cos\frac{2\pi x}{Lr}\right)$

Fig. 15 Comparison of assumed buckling shapes used by Kendrick, Nash, and Kaminsky

Nash, in addition to including numerous terms in his strain-energy expressions for ring twisting and bending which Kendrick neglected, took as his buckled shape one which corresponds to clamped ends. Kaminsky's extension of Kendrick's work assumes the same end condition, and his tabulated results show, without question, that the buckling pattern and associated boundary conditions have considerable influence on the strength.

The comparison of observed collapse pressures with various theories is shown in Table 1. Most striking is the close correlation with Kendrick, with not much difference on the average between results of his Part I and Part III. Correlation with Nash and Kaminsky is poor. There is thus the temptation to conclude immediately that these experimental results validate Kendrick's theory, and at that with better success than either experimental or theoretical analysts have a right to expect. There are, however, a number of factors which suggest that the closeness of this agreement could be fortuitous.

Firstly, there are various assumptions and simplifications in Kendrick's Part III theory which render it so approximate that complete agreement with test results cannot be expected:

(*a*) Out-of-plane bending, torsional, and warping terms were omitted when strain energy in the ring stiffeners was evaluated. Inclusion of these items probably would decrease P_{cr}. The errors introduced by this simplification can be estimated from comparison of Nash's analysis, which includes these terms, with Kaminsky-Kendrick's, which does not; from Table 1, these differences are on the order of 5 to 10 per cent.

(*b*) The prebuckling deformations were considered uniform so that the discontinuity effects imposed by the stiffeners were neglected. Von Sanden-Tölke (16) have shown that the use of the correct prebuckling conditions which involve variation in stress resultants along the length induced by the stiffeners can increase the shell-buckling pressures. While this feature has not been investigated in the case of general instability, some similar consequence, although of unknown degree, can be expected.

(*c*) Kendrick's analyses assume that all bays are of equal length, although in these tests the end bays were shortened. (Nash's theory, however, accommodates this variation.) Again, the effects on P_{cr} are unknown but in this case they are believed to be insignificant.

(*d*) The use of an energy method requires an assumption of buckling configurations which are arbitrary and selected on a judgment basis only. Despite numerous attempts in these and other tests, no exact postbuckling shape ever has been observed while the model is completely elastic. That is, all inspections and measurements have been made after collapse has occurred and deformation has always been sufficiently intense to cause the material to yield and the lobes to remain in the model after removal of pressure, as shown in Fig. 3. The use of more elaborate assumed buckling patterns to investigate this feature theoretically has involved such laborious calculation so far as to defeat the attempt. Nevertheless, it is known that the use of any but the correct buckling shape, in effect, introduces an artificial restraint that raises the P_{cr}. Thus it is quite possible that the predictions from Kendrick's theory as well as from all the other energy solutions are too high. As will be noted later, this matter of lobe shape may be the most significant factor requiring further investigation.

There also are several conditions which may represent actual differences between the structure treated by theory and that under test:

(*a*) Of considerable importance is the relationship of the assumed lobe shape and the implied boundary condition to the boundary conditions actually present in the tests. The experi-

ment was designed with the intention that the attachments to the tank and to the closure plate would introduce end restraint corresponding to a fully clamped condition. There have been no measurements to confirm this test arrangement. However, on the basis of the good correlation of observed buckling pressures with those of Kendrick's theory and the poor correlation with Kaminsky and Nash, it is easy for the notion to arise that the boundary conditions must be identical with Kendrick's; i.e., that the test conditions represent simple support! The authors, however, tentatively have rejected this conclusion.

Considering the care and control exercised in conducting these tests, could this agreement have been coincidental? For example, could two effects have been present that were compensating—such as fixed or partially fixed end conditions in the models which would raise the buckling strength above Kendrick's predictions with simple support, coupled with decrease in strength due to imperfections in the models which in combination would lower the test pressures enough to coincide with the prediction?

(*b*) It is certainly true that the models, while machined, were still imperfect—as in fact all physical structures are likely to be. No attempt is made here to apply available theory for evaluating loss in strength due to out-of-roundness, but that its effects were present is clearly demonstrated by the nonsymmetric and nonlinear elastic strain data discussed heretofore. Tests with such imperfect models always should give $P_f < P_{cr}$ where the P_{cr} corresponds to the collapse pressure predicted by theory for perfect models. (Observations were slightly the other way.) Yet the Southwell results, which represent strengths of perfect structures, differ only slightly from observations, thus suggesting that there was very little weakening effect of out-of-roundness. The Southwell method, incidentally, is believed valid in this case because the prebuckling deformations in the imperfect structure follow the pattern of buckling in a perfect one; the plots of strain in Figs. 12, 13, and 14 are believed to constitute ample demonstration of that relationship.

Discussion and conclusions

Apart from all the uncertainties in the theories just described, there is the additional question whether the small-deflection type of analysis is sufficiently accurate or whether a satisfatory evaluation of general instability strength must await a large-deflection analysis. True, the buckling pressure for a perfect stiffened cylinder given by the small-deflection theories would coincide with that from the more complete analysis, but it is known in other instances of shell structures that the presence of even minute imperfections might prevent that value from ever being achieved. In fact, with externally loaded spherical shells, both large-deflection theory and tests suggest that buckling occurs by snap-through at something less than half the classical small-deflection pressure (17). Moreover, recent tests (18) and analyses (19, 20) show a similar snap-through phenomenon for unstiffened cylindrical shells under external pressure, although the weakening effects of out-of-roundness in that case do not appear too serious. The situation for stiffened cylinders is completely unexplored. Axisymmetric components of initial deformations have been shown to have possibly significant effects on the large deflection-load deflection characteristics (21, 22).

Apart from the matter of circularity, some explanation is required for the fact that the Southwell predictions for a perfect structure agreed so well with Kendrick's theories notwithstanding the probable disparity between assumed and actual boundary conditions. One possible explanation lies in the area of assumed buckling displacements and the importance of boundary conditions. Kendrick expressed the view that the analysis with simple support would represent adequately even conditions of clamped support because, as he reasoned, the edge effects in shells decay so rapidly that the buckling process would develop quite independently of the boundary condition. While this phenomenon of decay exists for the equilibrium problem by actually introducing one arbitrary condition representing fixed ends, Kaminsky has clearly shown the concept inapplicable for buckling.

There now develops a serious question as to whether the $(1 - \cos 2\pi x/L_s)$ form of buckling configuration assumed by Kaminsky and by Nash for fixed ends is correct. It is conceivable, at least, that some other postbuckling pattern, $f(x)$, actually exists involving less energy of deformation but which has a sharp curvature at the ends compatible with a condition of no rotation of the generator, and which in the middle corresponds in shape to that for simple support. If this pattern is the real one, the P_{cr} calculated by Kaminsky would be too high, so that the actual differences between clamped and simple support might not be so great after all. This possibility can only be illuminated from future theoretical analyses in which other buckling configurations satisfying clamped end boundary conditions are tried, or by actual measurement of lobe shape while test specimens are buckled so little as not to pass the elastic limit.

The final question remains as to how these results should be interpreted for engineering application. Standard practice for shell instability has been to apply theories such as von Mises for a perfect structure, with empirical factors selected to accommodate unknowns of imperfect shape and edge conditions. Numerous tests have verified that this procedure is sufficiently precise for many pressure-vessel applications. Attempts are now being made to consider the weakening effects of out-of-roundness in a rational manner (23) such that the empiricism can be minimized.

A similar process is suggested for the case of general instability. For perfect structures, the tests described herein, although decidedly limited in number, agree with Kendrick's theories. Even though a full understanding of the problem is lacking, the correlation thus suggests the conclusion that such analysis could be used with confidence, if adequate factors of safety could be chosen to accommodate imperfect shape.

Later refinements in theory, when verified by test, may improve rigor of treatment of the usual less-than-perfect structures. They would be useful for computing both the strength of such stiffened cylinders and the nonlinear elastic behavior which occurs before buckling.

Acknowledgments

The tests and analyses described in this paper were carried out by the authors at the David Taylor Model Basin, Navy Department, Washington, D. C., while they were members of the staff.

Sponsorship of this research by the Bureau of Ships, guidance by Mr. Frank Dunham of that activity, and the support of this program by the Model Basin are gratefully acknowledged.

Bibliography

1 "Model Experiments on the Elastic Stability of Closed and Cross-Stiffened Circular Cylinders under Uniform External Pressure," by T. Tokugawa, Proceedings of the World Engineering Congress, Tokyo, Japan, vol. 29, 1929, p. 249.

2 "The Influence of Stiffening Rings on the Strength of Thin Cylindrical Shells under External Pressure," by C. Trilling, David Taylor Model Basin Report 396, February, 1935.

3 "The Buckling under External Pressure of Circular Cylindrical Shells with Evenly Spaced Equal Strength Circular Ring Frames, Part I," by S. Kendrick, Naval Construction Research Establishment Report R.211, February, 1953.

4 "General Instability of Ring Reinforced Shells Subject to Hydrostatic Pressure," by W. A. Nash, Proceedings of the Second U. S. National Congress of Applied Mechanics, Ann Arbor, Mich., June, 1954.

5 "Mémoire sur un nouveau cas intégrable du problème de l'élastique et l'une de ses applications," by M. Lévy, *Journal de Math., pure et appliquée* (Liouville), series 3 to 10, 1884, pp. 5–42.

6 "Über das Festigkeitsproblem quersteifter Hohlzylinder unter allseitig gleichmassigem Aussendruck," by K. von Sanden and K. Günther, *Werft und Reederei*, vol. 1, 1920, Nos. 8, 9 and 10, and vol. 2, 1921, No. 17. (Also David Taylor Model Basin Translation No. 38, March, 1952).

7 "Sobre la organización y calculo de la estructura resistente de un submarino," by A. Fernández Avila, Congress de Ingeniería Naval, 1932.

8 "Die Stabilität der Kreiszylinderschale," by W. Flügge, *Ingenieur Archiv*, vol. 3, no. 5, December, 1932, p. 463.

9 "General Instability of Reinforced Shells under Hydrostatic Pressure," by V. L. Salerno and B. Levine, Polytechnic Institute of Brooklyn Report 189, September, 1951.

10 "General Instability of Ring-Stiffened Cylinders with Clamped Ends under External Pressure by Kendrick's Method," by E. L. Kaminsky, David Taylor Model Basin Report 855, July, 1954.

11 "Experiencias con modelos de casos resistentes de submarinos," by A. Arevalo Pelluz, *Ingeniería Naval*, vol. 16, 1948, p. 772.

12 "Experimental Analysis of the Buckling of Cylindrical Shells Subjected to External Hydrostatic Pressure," by E. Wenk, Jr., R. C. Slankard, and W. A. Nash, Proceedings of the Society for Experimental Stress Analysis, vol. 12, no. 1, 1954, p. 178.

13 "Stress Distribution in a Circular Cylindrical Shell under Hydrostatic Pressure Supported by Equally Spaced Circular Ring Frames," by V. L. Salerno and J. G. Pulos, Polytechnic Institute of Brooklyn Report 171-A, 1951.

14 "A Simple Extension of Southwell's Method for Determining the Elastic General Instability Pressure of Ring-Stiffened Cylinders Subject to External Hydrostatic Pressure," by G. D. Galletly and T. E. Reynolds, Proceedings of the Society for Experimental Stress Analysis, vol. 13, no. 2, 1956, p. 141.

15 "The Buckling under External Pressure of Circular Cylindrical Shells with Evenly Spaced Equal Strength Circular Ring Frames, Part III," by S. Kendrick, Naval Construction Research Establishment Report R.244, September, 1953.

16 "Über Stabilitätsprobleme dünner, Kreizylindrischer Schalen," by K. von Sanden and F. Tölke, *Ingenieur-Archiv*, vol. 3, 1932, pp. 24–66. (Also David Taylor Model Basin Translation No. 33, December, 1949).

17 By Th. von Karman, Forschungsarbeiten No. 81, Berlin, Germany, 1910.

18 "Observations of Snap-Through Action in Thin Cylindrical Shells Under External Pressure," by A. F. Kirstein and E. Wenk, Jr., David Taylor Model Basin Report 1062, November, 1956.

19 "Effect of Imperfections on Buckling of Thin Shells under External Pressure," by L. H. Donnell, Final Report on First Phase, Contract Nonr-1406(01), Illinois Institute of Technology, Chicago, Ill., June, 1955.

20 "Buckling and Post-Buckling Behavior of Cylindrical Shells Subjected to External Pressure," by H. L. Langhaar and A. P. Boresi, presented at Ninth International Congress of Applied Mechanics, Brussels, Belgium, September, 1956.

21 "Recent Results in the Theory of Large Deflection of Cylindrical Shells," by J. Kempner, Ninth International Congress of Applied Mechanics, Brussels, Belgium, September, 1956.

22 "The Effects of Initial Deflections of the Shell Between Frames on Deformations of Stiffened Cylinders Under Uniform External Pressure," by M. E. Luńchick and R. D. Short, Jr., unpublished report of David Taylor Model Basin.

23 "The Effects of Boundary Conditions and Initial Out-of-Roundness on the Strength of Thin Walled Cylinders Subject to External Hydrostatic Pressure," by G. D. Galletly and R. Bart, JOURNAL OF APPLIED MECHANICS, TRANS. ASME, vol. 78, 1956, pp. 351–358.

APPENDIX

Methods of determining initial out-of-roundness

Method A. The centroid and area of the circularity contours were first determined and the radius of the mean circle R_m whose area was equal to that of the circularity contour was calculated. With the centroid as a center, a circle of radius R_m was then described. The initial out-of-roundness was then taken as the maximum radial distance between the mean circle and the circularity contour.

Method B. The centroid and radius R_m were determined as for Method A. Then the number of lobes, n, into which the perfect stiffened cylinder would collapse was determined from Kendrick's Part I theory. An arc of length $\pi R/n$ was then drawn on transparent paper. This arc was rotated around the entire periphery of the circularity contour, with the end points of the arc always remaining in contact with the contour. The initial out-of-roundness was then taken as the maximum radial distance between the arc and the circularity contour.

Buckling of a Thin Annular Plate Under Uniform Compression

By N. YAMAKI,[1] SENDAI, JAPAN

This paper deals with the elastic stability of a circular annular plate under uniform compressive forces applied at its edges. By integrating the equilibrium equation of the buckled plate, the problem is solved in its most general form for twelve different combinations of the boundary conditions of the edges. For each case cited the lowest critical loads are calculated with the ratio of its radii as the parameter. It is clarified that the assumption of symmetrical buckling, which has been made by several researchers, often leads to the overestimate for the stability of the plate. Discussions for the limiting cases of the circular plate and infinite strip also are included.

Introduction

THE ELASTIC stability of a circular annular plate has been treated by several researchers under various loading conditions. For example, Dean (1)[2] investigated the case of shearing forces distributed along the edges, and Meissner (2) and Way (3) studied the cases where uniform compressive forces are applied along one of the edges. Further, Willers (4) discussed the case where the plate is subjected to the bending moment caused by initial stresses. Some of these problems also have been extended to the plate with variable thickness (5, 6, 7, 8).

The stability of a thin annular plate under uniform compressive forces applied at both edges, the subject of this paper, also was treated by Olsson (9) and Schubert (10) for several boundary conditions, but in these investigations the deflection surface was assumed to be symmetrical with respect to the center. Here it should be noted that, in the study of the buckling problem, only the lowest critical load is of practical significance and that the assumption of symmetrical buckling does not necessarily lead to this desired one. From this point of view, the generalization of these works is attempted in this paper.

In what follows, the fundamental equations are first derived by integrating the differential equation for the buckled plate. Using these results, the general stability conditions are obtained for various boundary conditions, from which the least critical loads are determined with the ratio of radii as the parameter. Discussions for the limiting cases also are given.

Basic Equations

Assume that a thin annular plate, Fig. 1, is compressed in its middle plane by forces uniformly distributed along the edges, $r = a$ and $r = b$. Denoting by p the intensity of the force and by w the deflection of the plate, the equilibrium equation for the buckled plate becomes

$$D\nabla^4 w + p\nabla^2 w = 0 \quad \ldots\ldots [1]$$

where

$$D = \frac{Eh^3}{12(1-\nu^2)}, \quad \nabla^2 = \frac{\partial^2}{\partial r^2} + \frac{1}{r}\frac{\partial}{\partial r} + \frac{1}{r^2}\frac{\partial^2}{\partial \theta^2}$$

Here D is the flexural rigidity of the plate, h is the plate thickness, and E and ν are Young's modulus, and Poisson's ratio, respectively.

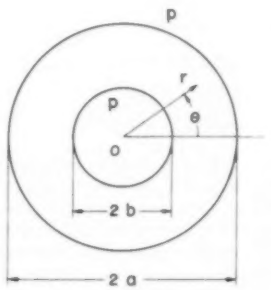

Fig. 1

To simplify the expression, we introduce the following notations

$$\rho = r/a, \quad \beta = b/a, \quad k^2 = pa^2/D \quad \ldots\ldots [2]$$

$\rho = 1$ and $\rho = \beta$ now represent the outer and inner edges, respectively. Further, we assume the deflection surface as

$$w = u_n(\rho)\cos n\theta, \quad (n = 0, 1, 2\ldots) \quad \ldots\ldots [3]$$

where $u_n(\rho)$ is a function of ρ alone and n is the number of nodal diameters. It will be noted that $n = 0$ corresponds to the symmetrical deflection surface.

Substituting Equation [3] into [1] and using the foregoing notations, we obtain the following ordinary differential equation

$$\nabla_n^4 u_n + k^2\nabla_n^2 u_n = 0 \quad \ldots\ldots [4]$$

where

$$\nabla_n^2 = \frac{d^2}{d\rho^2} + \frac{1}{\rho}\frac{d}{d\rho} - \frac{n^2}{\rho^2}$$

The solution of Equation [4] can be expressed as

$$\left.\begin{aligned} u_0 &= A_0 J_0(k\rho) + B_0 Y_0(k\rho) + C_0 + D_0 \ln\rho, \quad (n = 0) \\ u_n &= A_n J_n(k\rho) + B_n Y_n(k\rho) + C_n\rho^n \\ &\quad + D_n\rho^{-n}, \quad (n = 1, 2\ldots) \end{aligned}\right\} \quad \ldots [5]$$

---

[1] Assistant Professor at Institute of High Speed Mechanics, Tōhoku University.

[2] Numbers in parentheses refer to the Bibliography at the end of the paper.

Contributed by the Applied Mechanics Division and presented at the Annual Meeting, New York, N. Y., December 1–16, 1957, of The American Society of Mechanical Engineers.

Discussion of this paper should be addressed to the Secretary, ASME, 29 West 39th Street, New York, N. Y., and will be accepted until July 10, 1958, for publication at a later date. Discussion received after the closing date will be returned.

Note: Statements and opinions advanced in papers are to be understood as individual expressions of their authors and not those of the Society. Manuscript received by ASME Applied Mechanics Division, February 27, 1957. Paper No. 57—A-11.

where $A_n, B_n, \ldots$ are constants of integration, and J_n and Y_n are the Bessel functions of the first and second kinds, respectively. Equation [3] together with Equations [5] represent the general expression for the deflection of the plate.

Now the boundary conditions for typical cases are expressed as follows:

1 Clamped edge

$$w = 0, \quad \partial w/\partial\rho = 0 \qquad [6]$$

2 Simply supported edge

$$w = 0, \quad \frac{\partial^2 w}{\partial\rho^2} + \frac{\nu}{\rho}\left(\frac{\partial w}{\partial\rho} + \frac{1}{\rho}\frac{\partial^2 w}{\partial\theta^2}\right) = 0 \qquad [7]$$

3 Free edge subjected to the uniform compressive force p

$$\left.\begin{aligned} &\frac{\partial^2 w}{\partial\rho^2} + \frac{\nu}{\rho}\left(\frac{\partial w}{\partial\rho} + \frac{1}{\rho}\frac{\partial^2 w}{\partial\theta^2}\right) = 0 \\ &\frac{\partial}{\partial\rho}\left(\frac{\partial^2 w}{\partial\rho^2} + \frac{1}{\rho}\frac{\partial w}{\partial\rho} + \frac{1}{\rho^2}\frac{\partial^2 w}{\partial\theta^2}\right) \\ &\quad + \frac{1-\nu}{\rho}\frac{\partial}{\partial\theta}\left[\frac{\partial}{\partial\rho}\left(\frac{1}{\rho}\frac{\partial w}{\partial\theta}\right)\right] + k^2\frac{\partial w}{\partial\rho} = 0 \end{aligned}\right\} \qquad [8]$$

4 Movable edge (we denote the edge which can deflect freely but cannot rotate as "movable")[3]

$$\left.\begin{aligned} &\partial w/\partial\rho = 0 \\ &\frac{\partial}{\partial\rho}\left(\frac{\partial^2 w}{\partial\rho^2} + \frac{1}{\rho}\frac{\partial w}{\partial\rho} + \frac{1}{\rho^2}\frac{\partial^2 w}{\partial\theta^2}\right) \\ &\quad + \frac{1-\nu}{\rho}\frac{\partial}{\partial\theta}\left[\frac{\partial}{\partial\rho}\left(\frac{1}{\rho}\frac{\partial w}{\partial\theta}\right)\right] = 0 \end{aligned}\right\} \qquad [9]$$

We note that the first of Equations [8] and the second of Equations [9] mean the vanishing of the bending moment and shearing force, respectively, and the second of Equations [8] stands for the condition that the shearing force at the edge should be equal to the normal component of the applied load. On substituting the general expression for w obtained in the foregoing, each condition in Equations [6] through [9] can be expressed as follows:

(a) $w = 0$ at $\rho = \rho_0$

$$\left.\begin{aligned} &A_0 J_0(k\rho_0) + B_0 Y_0(k\rho_0) + C_0 + D_0 \ln\rho_0 = 0, \quad (n = 0) \\ &A_n J_n(k\rho_0) + B_n Y_n(k\rho_0) + C_n\rho_0^n \\ &\qquad + D_n\rho_0^{-n} = 0, \quad (n \neq 0) \end{aligned}\right\} \qquad [10]$$

(b) $\partial w/\partial\rho = 0$ at $\rho = \rho_0$

$$\left.\begin{aligned} &A_0 k\rho_0 J_1(k\rho_0) + B_0 k\rho_0 Y_1(k\rho_0) - D_0 = 0, \quad (n = 0) \\ &A_n[nJ_n(k\rho_0) - k\rho_0 J_{n+1}(k\rho_0)] + B_n[nY_n(k\rho_0) \\ &\quad - k\rho_0 Y_{n+1}(k\rho_0)] + nC_n\rho_0^n - nD_n\rho_0^{-n} = 0, \quad (n \neq 0) \end{aligned}\right\} \qquad [11]$$

(c) Bending moment vanishes at $\rho = \rho_0$

$$\left.\begin{aligned} &A_0 k\rho_0[k\rho_0 J_0(k\rho_0) - (1-\nu)J_1(k\rho_0)] \\ &\quad + B_0 k\rho_0[k\rho_0 Y_0(k\rho_0) - (1-\nu)Y_1(k\rho_0)] \\ &\qquad + (1-\nu)D_0 = 0, \quad (n = 0) \\ &A_n\{[n(n-1) - (1-\nu)^{-1}k^2\rho_0^2]J_n(k\rho_0) \\ &\quad + k\rho_0 J_{n+1}(k\rho_0)\} + B_n\{[n(n-1) \\ &\quad - (1-\nu)^{-1}k^2\rho_0^2]Y_n(k\rho_0) + k\rho_0 Y_{n+1}(k\rho_0)\} \\ &\quad + n(n-1)C_n\rho_0^n + n(n+1)D_n\rho_0^{-n} = 0, \quad (n \neq 0) \end{aligned}\right\} \qquad [12]$$

[3] This is the generalization of the boundary condition considered in the paper by Olsson (9).

(d) Shearing force is equal to the normal component of the applied load at $\rho = \rho_0$

$$\left.\begin{aligned} &D_0 = 0, \quad (n = 0) \\ &A_n[(n-1)J_n(k\rho_0) - k\rho_0 J_{n+1}(k\rho_0)] \\ &\quad + B_n[(n-1)Y_n(k\rho_0) - k\rho_0 Y_{n+1}(k\rho_0)] \\ &\quad + C_n\left[n - 1 - \frac{k^2\rho_0^2}{n(1-\nu)}\right]\rho_0^n \\ &\quad - D_n\left[n + 1 - \frac{k^2\rho_0^2}{n(1-\nu)}\right]\rho_0^{-n} = 0, \quad (n \neq 0) \end{aligned}\right\} \qquad [13]$$

(e) Shearing force vanishes at $\rho = \rho_0$

$$\left.\begin{aligned} &A_0 J_1(k\rho_0) + B_0 Y_1(k\rho_0) = 0, \quad (n = 0) \\ &A_n\{n[n(n-1)(1-\nu) + k^2\rho_0^2]J_n(k\rho_0) \\ &\quad - k\rho_0[n^2(1-\nu) + k^2\rho_0^2]J_{n+1}(k\rho_0)\} \\ &\quad + B_n\{n[n(n-1)(1-\nu) + k^2\rho_0^2]Y_n(k\rho_0) \\ &\quad - k\rho_0[n^2(1-\nu) + k^2\rho_0^2]Y_{n+1}(k\rho_0)\} \\ &\qquad + n^2(n-1)(1-\nu)C_n\rho_0^n \\ &\qquad - n^2(n+1)(1-\nu)D_n\rho_0^{-n} = 0, \quad (n \neq 0) \end{aligned}\right\} \qquad [14]$$

Thus, when the dimensions of the plate and the boundary conditions at its edges are given, we obtain, for each value of n, four homogeneous linear equations in A_n, B_n, C_n, and D_n. To have nontrivial solutions, the determinant of these equations should vanish, from which the eigenvalue k can be determined. It will be noted that only the least value of k thus obtained is of physical significance and that the corresponding value of n gives the favorite type of distortion of the plate. The critical value of the compressive force is obviously given by

$$p = k^2 D/a^2 \qquad [15]$$

Stability Conditions for Specific Cases

Now we will derive the stability conditions for the following twelve cases, which include all the practical combinations of the standard boundary conditions at the edges.

Case 1. Both Edges Clamped. Let us first assume that the deflection surface is symmetrical with respect to the center; i.e., $n = 0$. Then, taking into account the results in the preceding section, we have the following equations from the given boundary conditions

$$\begin{aligned} &A_0 J_0(k) + B_0 Y_0(k) + C_0 = 0 \\ &A_0 k J_1(k) + B_0 k Y_1(k) - D_0 = 0 \\ &A_0 J_0(k\beta) + B_0 Y_0(k\beta) + C_0 + D_0 \ln\beta = 0 \\ &A_0 k\beta J_1(k\beta) + B_0 k\beta Y_1(k\beta) - D_0 = 0 \end{aligned}$$

The critical value of the compressive force is now determined by equating to zero the determinant of these equations, which gives

$$\begin{aligned} &J_1(k)Y_0(k) - J_0(k)Y_1(k) + \beta[J_1(k\beta)Y_0(k\beta) - J_0(k\beta)Y_1(k\beta)] \\ &\quad - k\beta\ln\beta[J_1(k)Y_1(k\beta) - J_1(k\beta)Y_1(k)] \\ &\quad + \beta[J_0(k)Y_1(k\beta) - J_1(k\beta)Y_0(k)] \\ &\quad - [J_1(k)Y_0(k\beta) - J_0(k\beta)Y_1(k)] = 0 \end{aligned} \qquad [16]$$

Recalling Lommel's formula

$$J_{n+1}(x)Y_n(x) - J_n(x)Y_{n+1}(x) = 2/\pi x \qquad [17]$$

and introducing the following notations

$$\left.\begin{aligned}\Phi_n(k,\beta) &= J_n(k)Y_n(k\beta) - J_n(k\beta)Y_n(k)\\ \Psi_n(k,\beta) &= J_n(k)Y_{n+1}(k\beta) - J_{n+1}(k\beta)Y_n(k)\\ \theta_n(k,\beta) &= J_{n+1}(k)Y_n(k\beta) - J_n(k\beta)Y_{n+1}(k)\end{aligned}\right\}\ldots[18]$$

the foregoing condition simplifies to

$$(4/\pi k) - k\beta \ln \beta\Phi_1 + \beta\Psi_0 - \theta_0 = 0, \quad (n = 0)\ldots[19]$$

By a similar procedure, the following stability condition will be obtained for values of n different from zero

$$(8n/\pi k) - k\beta(\beta^n - \beta^{-n})\Phi_{n+1} + 2n\beta^{n+1}\Psi_n - 2n\beta^{-n}\theta_n = 0, \quad (n \neq 0)\ldots[20]$$

Now we will examine the two limiting cases where $\beta \to 0$ and $\beta \to 1$. In the case where β tends to zero, we obtain, on making use of the expansions of the Bessel functions, the following equations from the foregoing conditions

$$\left.\begin{aligned}4 - 2J_0(k) - 2k[\gamma + \ln(k/2)]J_1(k)\\ + \pi kY_1(k) = 0, \quad (n = 0),\\ J_{n+1}(k) = 0, \quad (n \neq 0)\end{aligned}\right\}\ldots[21]$$

where $\gamma = 0.577216\ldots$. These give the stability conditions for a clamped circular plate under uniform edge compression, when the deflection at its center is constrained.

In the case where $\beta \to 1$, or $\epsilon \equiv 1 - \beta \to 0$,[4] it will be observed that the value of k increases indefinitely being proportional to $1/\epsilon$. Noting that $J_\mu(x)$ and $Y_\mu(x)$, where μ has any assigned value and x is large, can be expressed approximately as (11)

$$J_\mu(x) = \left(\frac{2}{\pi x}\right)^{1/2}\cos\left(x - \frac{2\mu+1}{4}\pi\right),$$
$$Y_\mu(x) = \left(\frac{2}{\pi x}\right)^{1/2}\sin\left(x - \frac{2\mu+1}{4}\pi\right)\ldots[22]$$

both Equations [19] and [20] reduce to $1 - \cos k\epsilon = 0$, from which we have

$$\beta \to 1: \quad k \to 2\pi/(1-\beta), \quad (n = 0, 1, 2\ldots)\ldots[23]$$

Here we notice, from actual calculations, that the value of n corresponding to the least value of k increases indefinitely as $\beta \to 1$, while the ratio n/k is less than unity for any value of n. Now we remember the following approximate formulas (12)

$$\left.\begin{aligned}J_\nu(\nu\sec\alpha) &= \left(\frac{1}{2}\nu\pi\tan\alpha\right)^{-\frac{1}{2}}\cos\left[\nu(\tan\alpha - \alpha) - \frac{1}{4}\pi\right]\\ Y_\nu(\nu\sec\alpha) &= \left(\frac{1}{2}\nu\pi\tan\alpha\right)^{-\frac{1}{2}}\sin\left[\nu(\tan\alpha - \alpha) - \frac{1}{4}\pi\right]\end{aligned}\right\}\ldots[24]$$

where α is a fixed positive acute angle and ν is large. Using these relations and keeping in mind that

$$\lim_{\substack{\beta\to 1-0\\ n\to\infty}}\beta^n = \lim_{\substack{\epsilon\to 0\\ n\epsilon = 0(1)}}(1-\epsilon)^{n\epsilon/\epsilon} = \exp(-n\epsilon)\ldots[25]$$

Equation [20] yields

$$2N(K^2 - N^2)^{1/2} + (2N^2 - K^2)\sinh N \sin(K^2 - N^2)^{1/2} - 2N(K^2 - N^2)^{1/2}\cosh N\cos(K^2 - N^2)^{1/2} = 0\ldots[26]$$

where $N = n\epsilon$ and $K = k\epsilon$. This equation gives the least value of K as 6.089 when $N = 2.40$; hence we have

$$\beta \to 1: \quad k \to 6.089/(1-\beta), \quad n \to 2.40/(1-\beta)\ldots[27]$$

These values are precisely equivalent to the least critical load and the corresponding number of half-waves of a clamped infinite strip subjected to uniform compression (see Equations [63] in the Appendix).

Case 2. Outer Edge Clamped, Inner Edge Simply Supported. In this case, the boundary conditions at $\rho = 1$ are given by Equations [6] and those at $\rho = \beta$ by Equations [7]. Proceeding as before, we obtain the following stability conditions

$$\left.\begin{aligned}&[4(1-\nu)/\pi k] - k\beta^2\Phi_0 - (1-\nu)\beta(k\ln\beta\Phi_1 - \Psi_0)\\ &\quad + (k^2\beta^2\ln\beta - 1 + \nu)\theta_0 = 0, \quad (n = 0)\\ &(8n/\pi k) - 2n(1-\nu)^{-1}k\beta^{n+2}\Phi_n - k\beta(\beta^n - \beta^{-n})\Phi_{n+1}\\ &\quad + 2n\beta^{n+1}\Psi_n + [(1-\nu)^{-1}k^2\beta^2(\beta^n - \beta^{-n})\\ &\quad - 2n\beta^{-n}]\theta_n = 0, \quad (n \neq 0)\end{aligned}\right\}\ldots[28]$$

These conditions reduce to Equations [21] when β tends to zero. By using Equations [22], both Equations [28] lead to $\sin k\epsilon - k\epsilon\cos k\epsilon = 0$ as $\beta \to 1$, from which we have

$$\beta \to 1: \quad k \to 4.493/(1-\beta), \quad (n = 0, 1, 2\ldots)\ldots[29]$$

This value of k just corresponds to the buckling load of the infinite strip with one edge clamped and the other edge simply supported (see Appendix). Calculations show that for values of β near to 1, the smallest value of k is given by taking $n = 0$; hence we need not consider the case where n is large.

Case 3. Outer Edge Clamped, Inner Edge Free. The stability conditions in this case become

$$\left.\begin{aligned}&(1-\nu)\Phi_1 - k\beta\theta_0 = 0, \quad (n = 0)\\ &(8/\pi k)(n^2 - 1 - n\eta_n)\\ &\quad - 2(1-\nu)^{-1}k\beta^{n+2}(2n - 2 - \eta_n)\Phi_n\\ &- (k\beta/n)[(n^2 - 1 - \eta_n)\beta^n - (n^2 - 1 + \eta_n)\beta^{-n}]\Phi_{n+1}\\ &\quad + 2\beta^{n+1}(n^2 - 1 - \eta_n)\Psi_n + \{\eta_n(2n - 2 - \eta_n)\beta^n\\ &\quad - [\eta_n^2 + 2(n^2 - 1 - n\eta_n)]\beta^{-n}\}\theta_n = 0, \quad (n \neq 0)\end{aligned}\right\}\ldots[30]$$

where we have introduced the abbreviation

$$\eta_n = k^2\beta^2/n(1-\nu)\ldots[31]$$

When $\beta \to 0$, these conditions reduce to

$$J_{n+1}(k) = 0, \quad (n = 0, 1, 2\ldots)\ldots[32]$$

which agrees with the result obtained by Nadai for a clamped circular plate subjected to uniform edge compression (13).

When $\beta \to 1$, on making use of Equations [22], both the foregoing equations lead to $\cos k\epsilon = 0$, from which we have

$$\beta \to 1: \quad k \to \frac{\pi}{2}\Big/(1-\beta), \quad (n = 0, 1, 2\ldots)\ldots[33]$$

This is equivalent to the buckling load of the infinite strip with one edge clamped and the other edge free (see Appendix).

Case 4. Outer Edge Clamped, Inner Edge Movable. In this case, we obtain the following conditions

[4] From the assumption of a "thin" annular plate, it is implied that $a - b = a\epsilon$ is always much greater than the thickness h, i.e., when h is fixed, we must take a so large as to satisfy this condition even when $\epsilon \to 0$.

$$\left.\begin{aligned} &\Phi_1 = 0, \quad (n = 0) \\ &(8/\pi k) - 2(1-\nu)^{-1}k\beta^{n+2}\Phi_n - (k\beta/n)[(1+\eta_n)\beta^n \\ &\quad - (1-\eta_n)\beta^{-n}]\Phi_{n+1} + 2(1+\eta_n)\beta^{n+1}\Psi_n \\ &\quad + [(\beta^n + \beta^{-n})\eta_n - 2\beta^{-n}]\theta_n = 0, \quad (n \neq 0) \end{aligned}\right\} \quad \ldots [34]$$

When $\beta \to 0$, these equations lead to the same results as in Case 3, while when $\beta \to 1$, the foregoing equations lead to $\sin k\epsilon = 0$ for finite values of n, from which we have

$$\beta \to 1: \quad k \to \pi/(1-\beta), \quad (n = 0, 1, 2 \ldots) \ldots\ldots [35]$$

In this case, calculations show that the value of n which gives the least value of k increases indefinitely as $\beta \to 1$. Accordingly, recalling Relations [24] and [25], we obtain from the second of Equations [34]

$$N \tanh N + (K^2 - N^2)^{1/2} \tan (K^2 - N^2)^{1/2} = 0 \ldots [36]$$

from which the least value of k and its corresponding value of n are given as

$$\beta \to 1: \quad k \to 3.045/(1-\beta), \quad n \to 1.20/(1-\beta) \ldots [37]$$

It is easy to see that these are exactly equivalent to the buckling load and the wave length of the infinite strip with one edge clamped and the other edge movable (see Equations [67] in the Appendix).

Case 5. Outer Edge Simply Supported, Inner Edge Clamped. In this case, the stability conditions are

$$\left.\begin{aligned} &[4(1-\nu)/\pi k] + k\Phi_0 - (1-\nu)(k\beta \ln \beta\, \Phi_1 + \theta_0) \\ &\quad + \beta(k^2 \ln \beta + 1 - \nu)\Psi_0 = 0, \quad (n = 0) \\ &(8n/\pi k) + 2n(1-\nu)^{-1}k\beta^{-n}\Phi_n - k\beta(\beta^n - \beta^{-n})\Phi_{n+1} \\ &\quad + \beta[(1-\nu)^{-1}k^2(\beta^n - \beta^{-n}) \\ &\quad + 2n\beta^{-n}]\Psi_n - 2n\beta^{-n}\theta_n = 0, \quad (n \neq 0) \end{aligned}\right\} \quad \ldots [38]$$

When $\beta \to 0$, these equations become as follows

$$\left.\begin{aligned} &2(1-\nu)[2 - J_0(k)] + 2k[\gamma + \ln(k/2)][kJ_0(k) \\ &\quad - (1-\nu)J_1(k)] - \pi k[kY_0(k) \\ &\quad - (1-\nu)Y_1(k)] = 0, \quad (n = 0) \\ &kJ_n(k) - (1-\nu)J_{n+1}(k) = 0, \quad (n \neq 0) \end{aligned}\right\} \quad \ldots [39]$$

In the case where $\beta \to 1$, we obtain the same results as in Case 2.

Case 6. Both Edges Simply Supported. The stability conditions in this case are

$$\left.\begin{aligned} &[4(1-\nu)/\pi k] - k[(1-\nu)^{-1}k^2\beta^2 \ln \beta + \beta^2 - 1]\Phi_0 \\ &\quad - (1-\nu)k\beta \ln \beta\, \Phi_1 + \beta(k^2 \ln \beta + 1 - \nu)\Psi_0 \\ &\quad + (k^2\beta^2 \ln \beta - 1 + \nu)\theta_0 = 0, \quad (n = 0) \\ &(8/\pi k) - (1-\nu)^{-1}k[(2+\xi_n)\beta^{n+2} - (2+\eta_n)\beta^{-n}]\Phi_n \\ &- (k\beta/n)(\beta^n - \beta^{-n})\Phi_{n+1} + \beta[\xi_n(\beta^n - \beta^{-n}) + 2\beta^n]\Psi_n \\ &\quad + [\eta_n(\beta^n - \beta^{-n}) - 2\beta^{-n}]\theta_n = 0, \quad (n \neq 0) \end{aligned}\right\} \quad \ldots [40]$$

where we have introduced a new symbol

$$\xi_n = k^2/n(1-\nu) \ldots\ldots [41]$$

When $\beta \to 0$, these equations reduce to Equations [39] as in Case 5, while when $\beta \to 1$, they lead to $\sin k\epsilon = 0$ for finite values of n, from which we have

$$\beta \to 1: \quad k \to \pi/(1-\beta), \quad (n = 0, 1, 2 \ldots) \ldots [42]$$

This is equivalent to the buckling load of the infinite strip with simply supported edges (see Appendix).

Case 7. Outer Edge Simply Supported, Inner Edge Free. The stability conditions in this case are

$$\left.\begin{aligned} &k^2\beta\Phi_0 + (1-\nu)^2\Phi_1 - \\ &\quad k(1-\nu)(\Psi_0 + \beta\theta_0) = 0, \quad (n = 0) \\ &(8/\pi k)(n^2 - 1 - n\eta_n) - (1-\nu)^{-1}k \\ &\quad \{(2+\xi_n)(2n-2-\eta_n)\beta^{n+2} \\ &\quad - [\eta_n^2 + 2(n^2 - 1 - n\eta_n)]\beta^{-n}\}\Phi_n \\ &- (k\beta/n)[(n^2 - 1 - \eta_n)\beta^n - (n^2 - 1 + \eta_n)\beta^{-n}]\Phi_{n+1} \\ &\quad + \beta[(2+\xi_n)(n^2 - 1 - \eta_n)\beta^n \\ &- \xi_n(n^2 - 1 + \eta_n)\beta^{-n}]\Psi_n + \{\eta_n(2n-2-\eta_n)\beta^n \\ &\quad - [\eta_n^2 + 2(n^2 - 1 - n\eta_n)]\beta^{-n}\}\theta_n = 0, \quad (n \neq 0) \end{aligned}\right\} \quad \ldots [43]$$

In the case where $\beta \to 0$, these conditions reduce to

$$kJ_n(k) - (1-\nu)J_{n+1}(k) = 0, \quad (n = 0, 1, 2 \ldots) \ldots [44]$$

which agrees with the result obtained by Nadai for a simply supported circular plate subjected to uniform edge compression (13).

In this case, we see that the value of k remains finite as $\beta \to 1$. Noting that $\epsilon \equiv 1 - \beta \to 0$ and expanding the Bessel functions with argument $k\beta$ in the Taylor series, the foregoing equations yield

$$\beta \to 1: \quad k = [(1-\nu)(2n^2 + 1 + \nu)]^{1/2}, \quad (n = 0, 1, 2 \ldots) \ldots\ldots [45]$$

These are not equivalent to the corresponding values of the infinite strip, which seems to be due to the differences in the shape of the buckled surface (see Equations [69] in the Appendix).

Case 8. Outer Edge Simply Supported, Inner Edge Movable. In this case we have the following stability conditions

$$\left.\begin{aligned} &(1-\nu)\Phi_1 - k\Psi_0 = 0, \quad (n = 0) \\ &(8/\pi k) - (1-\nu)^{-1}k[(2+\xi_n)\beta^{n+2} - (2-\eta_n)\beta^{-n}]\Phi_n \\ &\quad - (k\beta/n)[(1+\eta_n)\beta^n - (1-\eta_n)\beta^{-n}]\Phi_{n+1} \\ &\quad + \beta[(2+\xi_n)(1+\eta_n)\beta^n - \xi_n(1-\eta_n)\beta^{-n}]\Psi_n \\ &\quad + [\eta_n(\beta^n + \beta^{-n}) - 2\beta^{-n}]\theta_n = 0, \quad (n \neq 0) \end{aligned}\right\} \quad \ldots [46]$$

When $\beta \to 0$, these equations lead to the same result as in Case 7, while when $\beta \to 1$, they reduce to $\cos k\epsilon = 0$ for finite values of n, from which we have

$$\beta \to 1: \quad k \to \frac{\pi}{2}\Big/(1-\beta), \quad (n = 0, 1, 2 \ldots) \ldots [47]$$

This is equivalent to the buckling load of the infinite strip with one edge simply supported and the other edge movable (see Appendix).

Case 9. Outer Edge Free, Inner Edge Clamped. The stability conditions in this case are

$$\left.\begin{aligned} &(1-\nu)\Phi_1 - k\Psi_0 = 0, \quad (n = 0) \\ &(8/\pi k)(n^2 - 1 - n\xi_n) \\ &\quad + 2(1-\nu)^{-1}k(2n-2-\xi_n)\beta^{-n}\Phi_n \\ &- (k\beta/n)[(n^2 - 1 + \xi_n)\beta^n - (n^2 - 1 - \xi_n)\beta^{-n}]\Phi_{n+1} \\ &\quad + \beta\{[\xi_n^2 + 2(n^2 - 1 - n\xi_n)]\beta^n \\ &\quad - \xi_n(2n-2-\xi_n)\beta^{-n}\}\Psi_n \\ &\quad - 2(n^2 - 1 - \xi_n)\beta^{-n}\theta_n = 0, \quad (n \neq 0) \end{aligned}\right\} \quad \ldots [48]$$

When $\beta \to 0$, these equations reduce to

$$k^2[kJ_n(k) - (1-\nu)J_{n+1}(k)] - n(n-1)(1-\nu)[2kJ_n(k) - (n+1)(1-\nu)J_{n+1}(k)] = 0, \quad (n = 0, 1, 2 \ldots) \ldots\ldots [49]$$

while when $\beta \to 1$, we obtain the same results as in Case 3.

Case 10. Outer Edge Free, Inner Edge Simply Supported. The stability conditions in this case are

$$\left.\begin{aligned}
&k^2\beta\Phi_0 + (1-\nu)^2\Phi_1 \\
&\qquad - k(1-\nu)(\Psi_0 + \beta\theta_0) = 0, \quad (n=0) \\
&(8/\pi k)(n^2 - 1 - n\xi_n) - (1-\nu)^{-1}k \\
&\qquad \{[\xi_n^2 + 2(n^2 - 1 - n\xi_n)]\beta^{n+2} \\
&\qquad - (2n - 2 - \xi_n)(2 + \eta_n)\beta^{-n}\}\Phi_n \\
&- (k\beta/n)[(n^2 - 1 + \xi_n)\beta^n - (n^2 - 1 - \xi_n)\beta^{-n}]\,\Phi_{n+1} \\
&\qquad + \beta\{[\xi_n^2 + 2(n^2 - 1 - n\xi_n)]\beta^n \\
&- \xi_n(2n - 2 - \xi_n)\beta^{-n}\}\Psi_n + [\xi_n(n^2 - 1 + \xi_n)\beta^{n+2} \\
&\qquad - (n^2 - 1 - \xi_n)(2 + \eta_n)\beta^{-n}]\theta_n = 0, \quad (n \neq 0)
\end{aligned}\right\} \quad \ldots [50]$$

In the limiting cases where $\beta \to 0$ and $\beta \to 1$, the foregoing conditions lead to the same results as in Cases 9 and 7, respectively.

Case 11. Outer Edge Movable, Inner Edge Clamped. In this case, we have the following conditions

$$\left.\begin{aligned}
&\Phi_1 = 0, \quad (n=0) \\
&(8/\pi k) + 2(1-\nu)^{-1}k\beta^{-n}\Phi_n - (k\beta/n)[(1-\xi_n)\beta^n \\
&- (1+\xi_n)\beta^{-n}]\Phi_{n+1} + \beta[2\beta^n - \xi_n(\beta^n + \beta^{-n})]\Psi_n \\
&\qquad - 2(1+\xi_n)\beta^{-n}\theta_n = 0, \quad (n \neq 0)
\end{aligned}\right\} \quad \ldots [51]$$

When $\beta \to 0$, the foregoing equations reduce to

$$k^2 J_{n+1}(k) - n[kJ_n(k) - (1-\nu)J_{n+1}(k)] = 0, \qquad (n = 0, 1, 2 \ldots) \quad \ldots [52]$$

while when $\beta \to 1$, we have the same results as in Case 4.

Case 12. Outer Edge Movable, Inner Edge Simply Supported. The stability conditions in this case are

$$\left.\begin{aligned}
&(1-\nu)\Phi_1 - k\beta\theta_0 = 0, \quad (n=0) \\
&(8/\pi k) - (1-\nu)^{-1}k[(2-\xi_n)\beta^{n+2} - (2+\eta_n)\beta^{-n}]\Phi_n \\
&\qquad - (k\beta/n)[(1-\xi_n)\beta^n - (1+\xi_n)\beta^{-n}]\Phi_{n+1} \\
&\qquad + \beta[(2-\xi_n)\beta^n - \xi_n\beta^{-n}]\Psi_n + [\eta_n(1-\xi_n)\beta^n \\
&\qquad - (2+\eta_n)(1+\xi_n)\beta^{-n}]\theta_n = 0, \quad (n \neq 0)
\end{aligned}\right\} \quad \ldots [53]$$

In the limiting cases given by $\beta \to 0$ and $\beta \to 1$, we obtain from these conditions the same results as in Cases 11 and 8, respectively.

Here it should be noted that, in so far as the symmetrical buckling is concerned, the stability conditions for Cases 3, 4, 7, and 8, respectively, are identical with those for Cases 12, 11, 10, and 9.

Numerical Results

For each case treated in the foregoing, the values of k satisfying the stability conditions are calculated for various values of β by taking $n = 0, 1, 2 \ldots$. The least values of k and the corresponding values of n thus obtained are listed in Table 1 and the same values also are represented in Fig. 2. The value of 0.3 has been adopted for the Poisson's ratio ν.

It will be easy to see that in Cases 1, 4, and 11, the number of nodal diameters of the buckled surface increases as the hole of the plate becomes large, while in Cases 3, 7, and 8, the plate always buckles in a symmetrical form. In the remaining cases with the exception of Case 9, the plate first buckles in the shape with one nodal diameter, and later in a symmetrical form, as the ratio of radii β increases from zero. The behavior of the plate in Case 9 is almost similar to the foregoing cases, but for the values of β ranging from 0.25 to 0.42, it buckles in the shape with two nodal diameters.

Based on the assumption of symmetrical buckling, the critical values of the load have been calculated by Schubert for Cases 1, 2, 5, 6, 9, and 10, and by Olsson for Cases 4 and 11. The results here obtained for $n = 0$ are ascertained to be consistent with those previously obtained. Further, it is obvious that this assumption is not valid, since it often gives exaggerated values for the buckling load.

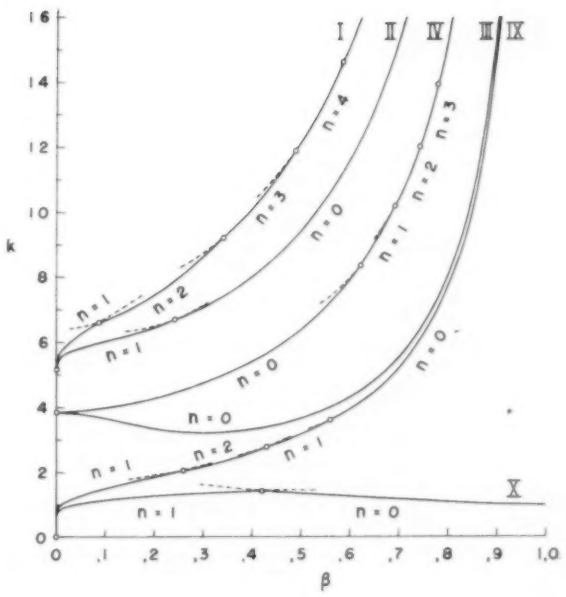

(a)

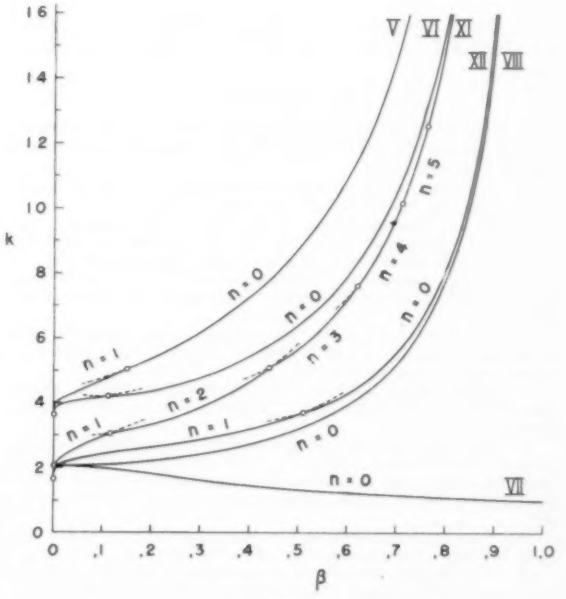

(b)

Fig. 2 Values of k for Various Values of β; $\nu = 0.3$
(Roman numerals show classification of cases used in the paper.)

TABLE 1 LEAST VALUES OF k AND CORRESPONDING NUMBERS OF n; $\nu = 0.3$

	β	0	0.02	0.05	0.1	0.2	0.3	0.4	0.5	0.6	0.7	0.8	0.9	1.0
Case 1	k	5.135	5.90	6.25	6.68	7.43	8.63	10.10	12.15	15.20	20.27	(30.45)[a]	(60.89)	–
	n	1	1	1	2	2	2	3	4	5	7	(12)	(24)	–
Case 2	k	5.135	5.65	5.80	6.02	6.43	7.06	8.00	9.42	11.60	15.31	22.76	45.20	–
	n	1	1	1	1	1	0	0	0	0	0	0	0	–
Case 3	k	3.832	3.83	3.78	3.62	3.30	3.19	3.30	3.65	4.29	5.52	8.09	15.89	–
	n	0	0	0	0	0	0	0	0	0	0	0	0	–
Case 4	k	3.832	3.83	3.86	3.94	4.24	4.71	5.39	6.39	7.93	10.49	15.56	(30.45)	–
	n	0	0	0	0	0	0	0	0	0	2	4	(12)	–
Case 5	k	3.625	4.15	4.32	4.71	5.36	6.16	7.23	8.73	10.98	14.73	22.22	44.69	–
	n	1	1	1	1	0	0	0	0	0	0	0	0	–
Case 6	k	3.625	3.98	4.07	4.20	4.34	4.75	5.41	6.40	7.93	10.52	15.74	31.43	–
	n	1	1	1	1	0	0	0	0	0	0	0	0	–
Case 7	k	2.049	2.04	2.03	1.98	1.80	1.61	1.45	1.32	1.22	1.14	1.07	1.01	0.954
	n	0	0	0	0	0	0	0	0	0	0	0	0	0
Case 8	k	2.049	2.05	2.06	2.09	2.20	2.40	2.71	3.18	3.92	5.19	7.78	15.61	–
	n	0	0	0	0	0	0	0	0	0	0	0	0	–
Case 9	k	0	1.09	1.28	1.49	1.84	2.18	2.60	3.14	3.92	5.19	7.78	15.61	–
	n	1	1	1	1	1	2	2	1	0	0	0	0	–
Case 10	k	0	0.926	1.02	1.12	1.25	1.34	1.40	1.32	1.22	1.14	1.07	1.01	0.954
	n	1	1	1	1	1	1	1	0	0	0	0	0	0
Case 11	k	1.675	2.38	2.61	2.94	3.31	3.84	4.64	5.69	7.22	9.79	14.88	(30.45)	
	n	1	1	1	1	2	2	2	3	3	4	6	(12)	
Case 12	k	1.675	2.18	2.29	2.42	2.63	2.87	3.19	3.64	4.29	5.52	8.09	15.89	
	n	1	1	1	1	1	1	1	1	0	0	0	0	

[a] Values in parentheses are obtained approximately by the corresponding asymptotic formulas.

ACKNOWLEDGMENT

The author wishes to express his thanks to Prof. Emeritus Seiichi Higuchi and Prof. Fukusaburo Numachi, Tohoku University, for their invaluable advice during the course of the present work.

BIBLIOGRAPHY

1 "The Elastic Stability of an Annular Plate," by W. R. Dean, Proceedings of the Royal Society of London, England, series A, vol. 106, 1924, pp. 268–284.

2 "Über das Knicken kreisringförmiger Scheiben," by E. Meissner, *Schweizerche Bauzeitung*, vol. 101, 1933, pp. 87–89.

3 Private communication of S. Way to Timoshenko. See "Theory of Plates and Shells," by S. Timoshenko, McGraw-Hill Book Company, Inc., New York and London, 1940, pp. 324–325.

4 "Die Stabilität von Kreisringplatten," by Fr. A. Willers, *Zeitschrift für angewandte Mathematik und Mechanik*, vol. 23, 1943, pp. 252–258.

5 "Knickung der auf Scherung beanspruchten Kreisringplatte mit veränderlicher Dicke," by K. Federhofer and H. Egger, *Ingenieur-Archiv*, vol. 14, 1943, pp.155–166.

6 "Knickung der Kreisplatte und Kreisringplatte mit veränderlicher Dicke," by K. Federhofer, *Ingenieur-Archiv*, vol. 11, 1940, pp. 224–238.

7 "Über die Knickung der Kreisringplatte von veränderlicher Dicke," by R. G. Olsson, *Ingenieur-Archiv*, vol. 12, 1941, pp. 123–132.

8 "Knickung der Kreisplatte und Kreisringplatte mit veränderlicher Dicke," by H. Egger, *Ingenieur-Archiv*, vol. 12, 1941, pp. 190–200.

9 "Über axialsymmetrische Knickung dünner Kreisringplatten," by R. G. Olsson, *Ingenieur-Archiv*, vol. 8, 1937, pp. 449–452.

10 "Die Beullast dünner Kreisringplatten, die am Aussen- und Innenrand gleichmässigen Druck erfahren," by A. Schubert, *Zeitschrift für angewandte Mathematik und Mechanik*, vol. 25/27, 1947, pp. 123–124.

11 "A Treatise on the Theory of Bessel Functions," by G. N. Watson, Cambridge University Press, 1922, p. 199.

12 Ibid., p. 234.

13 "Über das Ausbeulen von kreisförmigen Platten," by A. Nadai, *Zeitschrift des Vereines Deutscher Ingenieure*, vol. 59, 1915, p. 222.

Appendix

Buckling of Rectangular Plates Uniformly Compressed in Two Perpendicular Directions With Two Opposite Edges Simply Supported. Consider a rectangular plate with its length L and width l, subjected to uniform compressive forces p along its all edges, Fig. 3. The equation for the deflected plate is

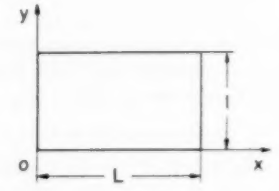

FIG. 3

$$D\nabla_e^4 w + p\nabla_e^2 w = 0 \quad \text{.....[54]}$$

where $\nabla_e^2 = \partial^2/\partial x^2 + \partial^2/\partial y^2$. Assuming that the edges $x = 0$ and $x = L$ are simply supported, the general expression for w can be represented in the form

$$w = \left\{ A_m \sinh \frac{m\pi}{\alpha l} y + B_m \cosh \frac{m\pi}{\alpha l} y + C_m \sin \left[\lambda^2 - \left(\frac{m\pi}{\alpha} \right)^2 \right]^{1/2} \frac{y}{l} + D_m \cos \left[\lambda^2 - \left(\frac{m\pi}{\alpha} \right)^2 \right]^{1/2} \frac{y}{l} \right\} \sin \frac{m\pi}{\alpha l} x, \quad (m = 1, 2, 3 \ldots)$$

.....[55]

where

$$\alpha = L/l, \quad \lambda^2 = pl^2/D \text{.....} [56]$$

m is the number of half-waves in the x-direction.

The boundary conditions for the edge parallel to the x-axis are expressed as follows

1 Clamped edge

$$w = \partial w/\partial y = 0 \text{.....} [57]$$

2 Simply supported edge

$$w = \partial^2 w/\partial y^2 = 0 \quad \ldots\ldots [58]$$

3 Free edge subjected to the compressive force p

$$\frac{\partial^2 w}{\partial y^2} + \nu \frac{\partial^2 w}{\partial x^2} = 0, \quad \frac{\partial^3 w}{\partial y^3} + (2 - \nu) \frac{\partial^3 w}{\partial x^2 \partial y} + \frac{p}{D} \frac{\partial w}{\partial y} = 0 \quad \ldots\ldots [59]$$

4 Movable edge

$$\frac{\partial w}{\partial y} = 0, \quad \frac{\partial^3 w}{\partial y^3} + (2 - \nu) \frac{\partial^3 w}{\partial x^2 \partial y} = 0 \quad \ldots\ldots [60]$$

If the boundary conditions for the edges $y = 0$ and $y = l$ are given, we can obtain the stability condition in the same manner as before. Now we will consider the specific cases.

(a) Both Edges Clamped. The stability condition in this case becomes

$$(\varphi_m^2 - \psi_m^2) \sinh \varphi_m \sin \psi_m + 2\varphi_m \psi_m (1 - \cosh \varphi_m \cos \psi_m) = 0 \quad \ldots\ldots [61]$$

where

$$\varphi_m = m\pi/\alpha, \quad \psi_m = [\lambda^2 - (m\pi/\alpha)^2]^{1/2} \quad \ldots\ldots [62]$$

For the infinite strip, i.e., $\alpha \to \infty$, the foregoing condition gives the least value of λ and its corresponding value of m as

$$\lambda = 6.089, \quad m = 2.40\alpha/\pi \quad \ldots\ldots [63]$$

Considering the differences in symbols, it will be easily recognized that these values are precisely equivalent to Equations [27] in Case 1.

(b) One Edge Clamped, the Other Edge Simply Supported. The stability condition is

$$\varphi_m \tan \psi_m - \psi_m \tanh \varphi_m = 0 \quad \ldots\ldots [64]$$

When $\alpha \to \infty$, this condition gives the least value of λ as 4.493 for the case $m = 1$, which is equivalent to Equation [29] in Case 2.

(c) One Edge Clamped, the Other Edge Free. The stability condition is

$$2(1 - \nu)\varphi_m^2 \psi_m (\nu\varphi_m^2 + \psi_m^2) + [(\nu\varphi_m^2 + \psi_m^2)^2 + (1 - \nu)^2 \varphi_m^4] \psi_m \cosh \varphi_m \cos \psi_m - [(\nu\varphi_m^2 + \psi_m^2)^2 - (1 - \nu)^2 \varphi_m^2 \psi_m^2] \varphi_m \sinh \varphi_m \sin \psi_m = 0 \quad \ldots\ldots [65]$$

When $\alpha \to \infty$, we have $\lambda = \pi/2$ for $m = 1$, which is equivalent to Equation [33] in Case 3.

(d) One Edge Clamped, the Other Edge Movable. The stability condition is

$$\varphi_m \tanh \varphi_m + \psi_m \tan \psi_m = 0 \quad \ldots\ldots [66]$$

When $\alpha \to \infty$, the least value of λ and its corresponding value of m are given as

$$\lambda = 3.045, \quad m = 1.20\alpha/\pi \quad \ldots\ldots [67]$$

These are equivalent to Equations [37] in Case 4.

(e) Both Edges Simply Supported. The stability condition is $\sin \psi_m = 0$, from which we have $\lambda = \pi$ and $m = 1$ as $\alpha \to \infty$. This is equivalent to Equation [42] in Case 6.

(f) One Edge Simply Supported, the Other Edge Free. The stability condition is

$$(1 - \nu)^2 \varphi_m^3 \psi_m \tanh \varphi_m - (\nu\varphi_m^2 + \psi_m^2)^2 \tan \psi_m = 0 \quad \ldots [68]$$

When $\alpha \to \infty$, this condition gives for finite values of m

$$\lambda = [2(1 - \nu)]^{1/2} m\pi/\alpha, \quad (m = 1, 2, 3 \ldots) \quad \ldots\ldots [69]$$

As stated previously, these are not equivalent to Equations [45], but it will be observed that the differences between the corresponding values become smaller as m increases.

(g) One Edge Simply Supported, the Other Edge Movable. The stability condition is $\cos \psi_m = 0$, from which we have $\lambda = \pi/2$ and $m = 1$ as $\alpha \to \infty$. This is equivalent to Equation [47] in Case 8.

Ring Damping of Free Surface Oscillations in a Circular Tank

By J. W. MILES,[1] LOS ANGELES, CALIF.

A rough analysis of the effect of an annular ring on the sloshing oscillations of liquid in a cylindrical tank is carried out. The damping per cycle (logarithmic decrement) for moderate amplitudes is predicted as proportional to the square root of the amplitude and the three-halves power of the ring area. The corresponding force on the ring also is calculated.

Introduction

WE CONSIDER a cylindrical tank of radius a containing fluid to a depth h and an annular ring of area $\alpha\pi a^2$ attached to the inner wall a distance d below the free surface, as shown in Fig. 1. We assume:

(a) Radial width, $\alpha a/2$, is small compared with the radius of the tank, i.e., $\alpha \ll 1$.

(b) Local flow in the neighborhood of the ring is unaffected by the presence of either the free surface or the bottom of the tank.

(c) Dominant mode of sloshing corresponds to that of linearized potential flow except in a small neighborhood of the ring.

Assumption (a) is in accord with practical design requirements. Assumption (b) may be rather crude, especially if the amplitude is so large that the ring breaks the free surface, but further analytical refinement probably is not justified (see third section). Assumption (c) is thought quite adequate for moderate amplitudes, as indicated by the agreement between theoretical and observed values for the period of the dominant mode.

Equations of motion

The displacement of the free surface for the dominant mode of oscillation of a liquid in a circular cylinder is given by[2]

$$\zeta(r, \theta, t) = \zeta_1 \frac{J_1(kr)}{J_1(ka)} \cos\theta \cos(\omega t) \quad [1]$$

$$\omega^2 = kg \tanh(kh) \text{ and } ka = 1.84 \quad [2a, b]$$

where r and θ are polar co-ordinates, a the radius of the cylinder, h the depth of the liquid, Fig. 1, J_1 a Bessel function, and ζ_1 the maximum amplitude of sloshing during any one cycle. We assume that damping has only a small effect over one cycle of motion and can be taken into account *a posteriori* (relative to the potential flow) by allowing ζ_1 to be a slowly varying function of time. The corresponding fluid velocity in the immediate neighborhood of the wall ($r \sim a$) has the vertical component

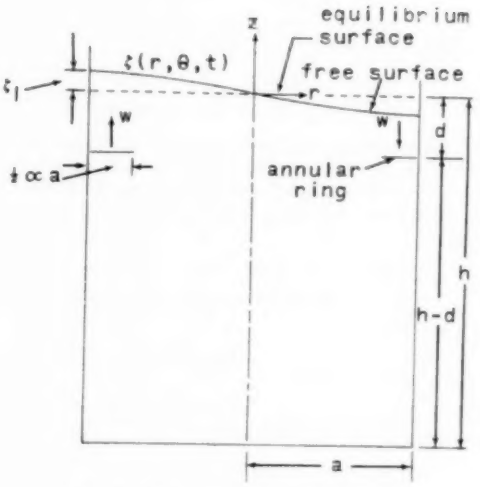

Fig. 1 Cross section of circular tank

$$w = -\omega\zeta_1 f(z) \cos\theta \sin(\omega t) \quad [3]$$

where

$$f(z) = \frac{\sinh[k(z+h)]}{\sinh(kh)} \quad [4]$$

the free surface is (approximately) at $z = 0$ and the bottom at $z = -h$. There is, in addition, a circumferential component

$$u = \omega\zeta_1 \left\{\frac{\cosh[k(z+h)]}{ka \sinh(kh)}\right\} \sin\theta \sin(\omega t) \quad [5]$$

but we shall neglect its effect in the following analysis, noting that $u = 0$ at those points ($\theta = 0, \pi$) where $|w|$ is a maximum and that the local dissipation rate varies roughly as $|w|^2$ (cf. Equation [7]). The total energy of the motion is found to be

$$E = \frac{1}{4}\rho g S[1 - (ka)^{-2}]\zeta_1^2 \quad [6]$$

where S denotes the cross-sectional area (πa^2).

We now consider the motion of Equation [3] to be obstructed by the annular ring of area αS [inner and outer radii of $a(1 - \alpha/2)$ and a, $\alpha \ll 1$] at $z = -d$, Fig. 1. A wake then will form on the downstream side of this ring (i.e., locally downstream; note that at any instant downstream is above the ring over one half of the annulus and below over the other half), in consequence of which it will be subjected to a pressure of $(\rho w^2/2)C_D$, where C_D is the local drag coefficient.

The mean rate of energy dissipation over a cycle of duration $2\pi\omega^{-1}$ is given by

$$\overline{\frac{dE}{dt}} = -\frac{\omega}{2\pi}\int_0^{2\pi/\omega} dt \iint_{\alpha S}\left(\frac{1}{2}\rho w^2 C_D\right)|w| dS \quad [7]$$

---

[1] Professor of Engineering, University of California; Consultant, The Ramo-Wooldridge Corporation.

[2] "Hydrodynamics," by H. Lamb, Dover Publications, New York, N. Y., sixth edition, 1945, p. 285.

Contributed by the Applied Mechanics Division and presented at the Annual Meeting, New York, N. Y., December 1–6, 1957, of The American Society of Mechanical Engineers.

Discussion of this paper should be addressed to the Secretary, ASME, 29 West 39th Street, New York, N. Y., and will be accepted until July 10, 1958, for publication at a later date. Discussion received after the closing date will be returned.

Note: Statements and opinions advanced in papers are to be understood as individual expressions of their authors and not those of the Society. Manuscript received by ASME Applied Mechanics Division, March 18, 1957. Paper No. 57—A-31.

Substituting w from Equation [3] and assuming C_D to be constant in carrying out the integrations[3] over θ and t (neglecting the slow variation of ζ_1 in the latter integration) yields

$$\frac{d\overline{E}}{dt} = -\frac{1}{2}\rho\alpha S C_D[\omega\zeta_1 f(-d)]^3\left(\frac{4}{3\pi}\right)^2 \quad [8]$$

The factor $(4/3\pi)^2$ may be subject to some correction if C_D is not constant over the ring, but this is likely to be negligible compared with other uncertainties; e.g., if C_D varies as $(\cos\theta)^{-1/2}$, as in the next section, Equation [8] requires to be increased by only $7^1/_2$ per cent.

The damping ratio (logarithmic decrement divided by 2π) is given by

$$\gamma = -\frac{d}{d(\omega t)}\log\zeta_1(t) \quad [9a]$$

$$= -\frac{1}{2}\frac{d}{d(\omega t)}\log\overline{E(t)} \quad [9b]$$

$$= -(2\omega E)^{-1}\overline{(dE/dt)} \quad [9c]$$

Substituting Equations [6] and [8] in [9c] and eliminating ω through Equation [2], we obtain

$$\gamma = \phi(ka, kd, kh)\alpha(\zeta_1/a)C_D \quad [10]$$

where

$$\phi = \frac{(4/3\pi)^2 f^3(-d)ka\tanh(kh)}{[1-(1/ka)^2]} \quad [11a]$$

Taking $ka = 1.84$, assuming $h > a$ so that the hyperbolic tangent may be approximated by unity and $f(-d)$ by $\exp(-kd)$, and rounding off the result we have

$$\phi \doteq 0.5e^{-5.52(d/a)}, \quad h > a \quad [11b]$$

The drag coefficient

The mean drag coefficient, assumed constant in the preceding section, must in general have the form

$$C_D = C_D(\mathrm{Re}, d/a, h/a, \alpha, \zeta_1/a) \quad [12]$$

where Re is an appropriately defined Reynolds number. We shall neglect the explicit dependence of C_D on α (which—in so far as it is small—must be significant only through its role in Re) and h/a (which could be important only if the bottom were sufficiently close to the ring to affect the wake). It is quite likely, on the other hand, that the wake above the ring would be appreciably modified by the proximity of the free surface, especially as d/a must be small for effective damping, and we therefore retain the dependence of C_D on d/a.

We consider first the possible importance of the Reynolds number Re, which we refer to the mean absolute velocity over the ring,

$$\bar{w} = \frac{4}{\pi^2}\zeta_1[kg\tanh(kh)]^{1/2}f(-d) \quad [13]$$

and to the effective width αa (doubling the actual width to allow for the image effect of the wall), whence

$$\mathrm{Re} = 0.55\alpha[\tanh(1.84h/a)]^{1/2}\left\{\frac{\sinh[1.84(h-d)/a]}{\sinh(h/a)}\right\}(ga)^{1/2}\frac{\zeta_1}{\nu} \quad [14]$$

where ν denotes the kinematic viscosity. Assuming $h > a$, $g = 980$ cm sec^{-2}, and $\nu = 10^{-2}$ stokes (as for water at room temperature) we have

$$\mathrm{Re} = 1720\alpha\sqrt{a}\zeta_1 e^{-1.84d/a} \text{ (cgs units)} \quad [15]$$

The drag coefficient on a flat plate in an oscillating fluid has been measured by Keulegan and Carpenter.[4] Their results appear to be relatively independent of (or at least uncorrelated with) Reynolds number in the range $5\cdot10^2 < \mathrm{Re} < 14\cdot10^3$. A less reliable criterion is the critical Reynolds number above which the flow is fully turbulent and C_D constant in steady flow. This is found to be roughly 10^3 (Eisner[5]) and would be achieved for a sloshing amplitude of less than 2 in. in a 10-ft-diam tank with a ring area of only 1 per cent ($\alpha = 0.01$) near the free surface ($d \ll a$). It appears, therefore, that the dependence of C_D on Re is not likely to be important.

Keulegan and Carpenter did find, on the other hand, that C_D depended strongly on the "period-parameter" U_mT/D, where U_m denotes the timewise maximum velocity, T the period, and D the plate width; in the present notation

$$\frac{U_mT}{D} = \frac{[\omega\zeta_1 f(-d)\cos\theta](2\pi/\omega)}{\alpha a} = \frac{2\pi f(-d)}{\alpha}\left(\frac{\zeta_1}{a}\right)\cos\theta \quad [16]$$

Within the limits of experimental and/or Reynolds number scatter, their data may be fitted to the empirical relation[6]

$$C_D = 15(U_mT/D)^{-1/2}, \quad 2 \le U_mT/D \le 20 \quad [17a]$$

Their data also indicate

$$C_D = 2, \quad U_mT/D \ge 100 \quad [17b]$$

in agreement with the steady flow result.[5]

If Equations [16] and [17a, b] are substituted in Equation [10] on the basis of the approximation for $h > a$ and correction factors introduced to allow for additional variations of C_D and also for small errors in the integrations over θ (we equate θ to zero in calculating C_D) and t, we obtain

$$\gamma = 3\alpha^{3/2}e^{-4.60(d/a)}F_a(\mathrm{Re}, d/a, h/a, \alpha, \zeta_1/a)(\zeta_1/a)^{1/2} \quad [18a]$$

and

$$\gamma = \alpha e^{-5.52(d/a)}F_b(\mathrm{Re}, d/a, h/a, \alpha, \zeta_1/a)(\zeta_1/a) \quad [18b]$$

The results, Equations [18a] and [18b], should be suitable, with values of F_a and F_b approximating unity in order of magnitude, for the amplitude ranges indicated by Equations [17a] and [17b], respectively. Of these two possibilities, the first would appear to be both more accurate and more valuable for design purposes. It seems likely, on the other hand, that amplitudes sufficiently large to yield the very large values of the period parameter on which Equations [17b] and [18b] rest might produce splashing (either by the ring breaking the free surface or by wave breaking), in which event very much larger values of the damping ratio would be expected.

Force on the ring

The force per unit area on the ring is given by

$$Z(\theta, t) = C_D\frac{1}{2}\rho w^2 \quad [19a]$$

[3] $\frac{1}{2\pi}\int_0^{2\pi}|\cos x|^3\,dx = \frac{4}{3\pi}$

[4] "Forces on Cylinders and Plates in an Oscillating Fluid," by G. H. Keulegan and L. H. Carpenter, National Bureau of Standards Report 4821, Washington, D. C., September 5, 1956.

[5] "Das Widerstandsproblem," by F. Eisner, Third International Applied Mechanics Congress, Stockholm, Sweden, 1930.

[6] We are indebted to Professor Garrett Birkhoff for this suggestion, as well as for bringing the work of Keulegan and Carpenter to our attention.

$$= \frac{\rho}{2}\omega^3 f^2(-d)\zeta_1^2 C_D \cos^2\theta \sin^2(\omega t) \ldots [19b]$$

It is advisable to design for the maximum value of this force, especially in consequence of the tendency of the angular sloshing node to rotate. We find it convenient to express this maximum as an equivalent head of the liquid; viz.

$$H = Z_{max}/\rho g \ldots [20a]$$

$$= \frac{1}{2} ka \tanh(kh) f^2(-d)(C_D)_{max}(\zeta_1^2/a) \ldots [20b]$$

where ω^2 has been substituted from Equation [2]. Substituting C_D from Equations [17*a*, *b*], assuming $h > a$, and applying the correction functions F_a and F_b,[7] we obtain

$$H \doteq 5.5\alpha^{1/2} e^{-2.7\delta(d/a)} F_a(\mathrm{Re}, d/a, h/a, \alpha, \zeta_1/a)(\zeta_1/a)^{1/2}\zeta_1 \ldots [21a]$$

and

$$H \doteq 1.9 e^{-3.6\delta(d/a)} F_b(\mathrm{Re}, d/a, h/a, \alpha, \zeta_1/a)(\zeta_1^2/a) \ldots [21b]$$

Experimental confirmation

Howell and Ehler[8] have measured the damping coefficients of each of three baffles (of the type considered here) for which $\alpha = 0.140$, 0.290, and 0.546 in a tank of approximately 1 ft diam. Their data for damping ratio versus amplitude exhibit considerable scatter, but it appears to be more consistent with Equation [18*a*] than [18*b*] for $\alpha = 0.140$; for $\alpha = 0.290$ and 0.546 the consistency with Equation [18*a*] is rather less satisfactory, but the latter values of α almost certainly are not "small" in the sense of the foregoing analysis. The mean value of F_a inferred from their data for $\alpha = 0.140$ and values of ζ_1/a between 0.08 and 0.13 is 1.5; a point at $\zeta_1/a \doteq 0.2$ yielded $F_a = 1.8$. An attempt to correlate these data with Equation [18*b*], on the other hand, yielded $F_b \doteq 5$. (We assume that the proximity of either F_a or F_b to unity indicates to some extent the validity of the respective approximations.)

On the basis of these comparisons, it appears that Equation [18*a*] should provide a satisfactory estimate of damping for sufficiently small values of α (say $\alpha < 0.15$) with $F_a \doteq 1.5$, but more accurate experimental data would be desirable.

Numerical example

Let $a = 60$ in., $\alpha = 0.2$ (6-in-wide ring), and $d = 2$ in. The amplitude at which $\gamma = 0.03$ then is found to be 0.45 in. on the basis of Equation [18*a*] with $F_a = 1.5$. The corresponding ($\theta = 0$) value of the period parameter is approximately 8. The corresponding maximum head on the ring would be 0.14 in.

Conclusions

We conclude that the damping ratio of an annular ring of area $\alpha\pi a^2$ at a depth d below the free surface of a liquid in a circular tank of radius a is approximately $4.5\alpha^{3/2} \exp(-4.6d/a)(\zeta_1/a)^{1/2}$ for sloshing oscillations of amplitude ζ_1, assuming $\alpha \ll 1$ and $\zeta_1 \ll a$.

Additional experimental confirmation would be desirable, both in order to establish the limits on α and ζ_1/a and to determine a more accurate value of the constant multiplier.

[7] Strictly speaking, the dependence of F_a and F_b on h must be somewhat different for H; also, there will be minor differences associated with the correction for the angular integration in the calculation of γ.

[8] "Experimental Investigation of the Influence of Mechanical Baffles on the Fundamental Sloshing Mode of Water in a Cylindrical Tank," Ramo-Wooldridge Corporation Report No. GM-TR-69, Los Angeles, Calif., July 6, 1956.

On the Sloshing of Liquid in a Flexible Tank[1]

By J. W. MILES,[2] LOS ANGELES, CALIF.

The kinetic and potential energies of an incompressible fluid having a free surface in a cylindrical tank subjected to translation, rotation, and simple bending are derived in the forms

$$\frac{1}{2}\sum_i\sum_j m_{ij}\dot{q}_i\dot{q}_j \quad \text{and} \quad \frac{1}{2}\sum_i\sum_j k_{ij}q_iq_j$$

where the $q_i(t)$ are generalized co-ordinates. The results are illustrated by a calculation of the frequency equation for coupled bending and free-surface motions. It is found that if the mass of the empty tank is small compared with that of the liquid and the depth of the liquid is equal to the tank diameter the presence of the free surface increases the bending frequency (relative to that calculated with a plane cap that coincides with the liquid surface and is normal to the axis of the cylinder) by about 5 per cent for cantilever bending oscillations and 27 per cent for free-free bending oscillations.

Introduction

WE SHALL consider here the motion of a liquid having a free surface and otherwise enclosed in a flexible cylinder of circular cross section, the walls of which have an arbitrarily prescribed motion.

The motion of a free surface (sloshing) in a stationary, rigid tank was treated originally by Poisson (1828) and Rayleigh (1876); their results are presented by Lamb (1).[3] The sloshing associated with translation and rotation of a rigid tank of rectangular section has been treated by Graham (2), who represented each sloshing mode by an equivalent pendulum. Graham's work was extended by Kachigan (3) to translation and by Gleghorn to both translation and rotation of a circular tank [a problem treated earlier, but not without error, by Lorell (4)].

Graham's pendulum analogy may be extended to cover arbitrary wall motions, but the results then would be sufficiently complex to make the analogy of questionable advantage. We shall proceed by formulating the kinetic and potential energies of the fluid motion; these may be incorporated in a more general, dynamical analysis through the over-all Lagrangian of the system containing the tank. We remark that this approach requires the imposition on the fluid of only kinematic boundary conditions; the dynamical boundary condition of constant pressure at the free surface will follow as a consequence of Lagrange's equations.[4]

Formulation

Let $q_i(t)$, $i = 1, 2, 3, \ldots$, denote generalized co-ordinates corresponding to the following displacements (Fig. 1):[5]

1 $q_1(t)$, a translation along $\theta = 0$.

2 $q_2(t)$, a rotation about the centroidal axis $|\theta| = \pi/2$.

3 $q_3(t)f(z)$, a simple bending displacement along $\theta = 0$ (in accordance with the usual beam assumptions, bending implies that plane sections remain plane and that the neutral axis is not extended).

4 $q_i(t)\psi^{(i)}(r, \theta)$, $i \geq 4$, sloshing displacements of the free surface relative to the displaced surface that would have resulted from rotation, translation, and bending (as if the cylinder had been capped by a plane normal to its generators and coinciding with the liquid surface).

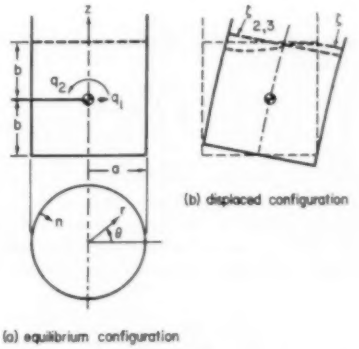

FIG. 1 CROSS SECTION AND ELEVATION OF TANK

We seek expressions for the corresponding potential and kinetic energies in the forms

$$V = \frac{1}{2}\sum_i\sum_j k_{ij}q_iq_j \quad \ldots\ldots [1]$$

$$T = \frac{1}{2}\sum_i\sum_j m_{ij}\dot{q}_i\dot{q}_j \quad \ldots\ldots [2]$$

The potential energy will be composed of two parts, corre-

---

[1] This paper is a revised version of Ramo-Wooldridge Report AM No. 6-16, September 28, 1956.

[2] Professor of Engineering, University of California; Consultant, The Ramo-Wooldridge Corporation.

[3] Numbers in parentheses refer to the Bibliography at the end of the paper.

Contributed by the Applied Mechanics Division and presented at the Annual Meeting, New York, N. Y., December 1-6, 1957, of THE AMERICAN SOCIETY OF MECHANICAL ENGINEERS.

Discussion of this paper should be addressed to the Secretary, ASME, 29 West 39th Street, New York, N. Y., and will be accepted until July 10, 1958, for publication at a later date. Discussion received after the closing date will be returned.

NOTE: Statements and opinions advanced in papers are to be understood as individual expressions of their authors and not those of the Society. Manuscript received by ASME Applied Mechanics Division, April 13, 1957. Paper No. 57—A-12.

[4] This follows from the fact that Euler's equation for the fluid motion may be deduced from Hamilton's principle.

[5] We remark that the end results may be applied to any three-dimensional, small motions of the tank, since the motions of translation along $\theta = \pi/2$ and rotation about the centroidal axis $\theta = 0, \pi$ are identical with but independent of those considered; translation along the z-axis gives only an $Mv^2/2$ contribution to the kinetic energy, and rotation about the z-axis has no effect by virtue of the assumed absence of viscosity.

sponding to the respective elevations of the liquid center of gravity resulting from the bending and sloshing displacements (translation and rotation will, by themselves, have no effect on the potential energy).[6] We remark that both of these elevations will be of the order of the square of the respective displacements in so far as the latter are, as assumed, small. Let $q_3^2 e_3$ denote the center of gravity elevation due to bending and ζ and $\zeta_{2,3}$ the total and rotation-bending elevations of the free surface, so that

$$\zeta = \zeta_{2,3} + \sum_{i=4}^{\infty} q_i \psi^{(i)} \quad [3]$$

We then have for the potential energy

$$V = Mgq_3^2 e_3 + \frac{1}{2}\rho g \iint_A (\zeta^2 - \zeta_{2,3}^2) dA \quad [4]$$

where M denotes the total mass of the liquid, ρ its density, g the acceleration of gravity (or, more generally, the total acceleration along the z-axis), and A the area of the free surface. Substituting Equation [3] in Equation [4] and comparing the result to Equation [1] yields (where $\zeta_{2,3} = \zeta_2 + \zeta_3$)

$$k_{33} = 2Mge_3 \quad [5a]$$

$$k_{ij} = \rho g \iint_A \psi^{(i)}\psi^{(j)} dA, \quad i, j \geq 4 \quad [5b]$$

$$k_{ij} = \rho g \iint_A (\zeta_i/q_i)\psi^{(j)} dA, \quad i = 2, 3, \quad j \geq 4 \quad [5c]$$

The kinetic energy of the fluid motion may be calculated from the well-known formula (5)

$$T = -\frac{\rho}{2} \iint_S \phi \phi_n dS \quad [6]$$

where S denotes the complete boundary of the fluid (including the free surface), n the inwardly directed normal to this boundary, and ϕ the velocity potential; we assume frictionless, irrotational flow, so that ϕ satisfies Laplace's equation. We may, by virtue of the assumption of small displacements, pose the linear expansion

$$\phi = \sum_i q_i(t)\phi^{(i)} \quad [7]$$

where the $\phi^{(i)}$ are time-independent. Substituting Equation [7] in [6] and comparing the result to Equation [2] yields

$$m_{ij} = -\rho \iint_S \phi^{(i)}\phi_n{}^{(j)} dS = -\rho \iint_S \phi_n{}^{(i)}\phi^{(j)} dS \quad [8]$$

where the identity of the alternative expressions follows from Green's theorem.

Boundary-Value Problems

We have now to determine the potentials $\phi^{(i)}$ from Laplace's equation, which in cylindrical polar co-ordinates reads

$$\phi_{rr} + \frac{1}{r}\phi_r + \frac{1}{r^2}\phi_{\theta\theta} + \phi_{zz} = 0 \quad [9]$$

We place the origin of co-ordinates at the centroid of the tank and define the equilibrium boundaries as $z = -b$ (bottom), $r = a$ (lateral wall), and $z = b$ (free surface), as shown in Fig. 1.

We may pose the boundary conditions corresponding to the motions enumerated in the preceding section at the equilibrium positions by virtue of the assumption of small displacements, whence

$$\phi_z|_{z=b} = \dot{\zeta} = \dot{q}_2(t) rc_\theta - \dot{q}_3(t) f'(b) rc_\theta + \sum_{i=4}^{\infty} \dot{q}_i(t)\psi^{(i)}(r, \theta) \quad [10a]$$

$$\phi_z|_{z=-b} = \dot{q}_2(t) rc_\theta - \dot{q}_3(t) f'(-b) rc_\theta \quad [10b]$$

$$\phi_r|_{r=a} = [\dot{q}_1(t) - \dot{q}_2(t) z + \dot{q}_3(t) f(z)] c_\theta \quad [10c]$$

where $\cos\theta$ is abbreviated as c_θ. Substituting the expansion [7] in Equations [10a,b,c] and equating coefficients of the q_i, we arrive at the following schedule of boundary conditions

$i =$	1	2	3	4
$\phi_z^{(i)}\|_{z=b}$	0	rc_θ	$-f'(b)rc_\theta$	$\psi^{(i)}$
$\phi_z^{(i)}\|_{z=-b}$	0	rc_θ	$-f'(-b)rc_\theta$	0
$\phi_r^{(i)}\|_{r=a}$	c_θ	$-zc_\theta$	$f(z)c_\theta$	0

[11]

We require solutions to Equation [9] satisfying the sets of boundary conditions delineated in the columns of this schedule.

The translational potential $\phi^{(1)}$ is provided by the elementary solution

$$\phi^{(1)} = rc_\theta \quad [12]$$

as may be verified by direct substitution.

The boundary conditions on the rotational potential, $\phi^{(2)}$, may be satisfied at $z = \pm b$ or $r = a$ by the elementary solutions zrc_θ or $-zrc_\theta$, respectively, but expansions in cylindrical harmonics are necessary to complete the solutions. We have the alternative forms

$$\phi^{(2)} = zrc_\theta + c_\theta \sum_{s=0}^{\infty} A_s J_1[(2s+1)(\pi r/2b)] \cdot \sin[(2s+1)(\pi z/2b)] \quad [13a]$$

$$= -zrc_\theta + c_\theta \sum_{s=1}^{\infty} B_s J_1(\beta_s r/a) \sinh(\beta_s z/a) \quad [13b]$$

where the β_s are the roots of the transcendental equation

$$J_1'(\beta_s) = 0, \quad s = 1, 2, \ldots \quad [14a]$$

which yields

$$\beta_1 = 1.84, \quad \beta_2 = 5.34, \quad \beta_3 = 8.54, \quad \beta_4 = 11.71, \ldots \quad [14b]$$

Imposing the boundary conditions at $r = a$ and $z = \pm b$, respectively, and utilizing the known properties of Fourier and Fourier-Bessel series, we find

$$A_s = 32(-)^{s+1} b^2 \{(2s+1)^2 \pi^2 J_1'[(2s+1)(\pi a/2b)]\}^{-1} \quad [15a]$$

$$B_s = 4a^2 \{\beta_s(\beta_s^2 - 1) J_1(\beta_s) \cosh(\beta_s b/a)\}^{-1} \quad [15b]$$

We seek a solution for $\phi^{(3)}$ in the form

$$\phi^{(3)} = C_0 rc_\theta + c_\theta \sum_{s=1}^{\infty} C_s I_1(s\pi r/2b) \cos[s\pi(z+b)/2b] + c_\theta \sum_{s=1}^{\infty} D_s J_1(\beta_s r/a) \{f'(b) \cosh[\beta_s(z+b)/a] - f'(-b) \cosh[\beta_s(z-b)/a]\} \quad [16]$$

[6] Vertical translation, of course, would contribute to the potential energy. Lateral translation also could contribute if there were a lateral component of the static acceleration field, but then the free surface no longer would be normal to the generators of the cylinder in its equilibrium position, and the boundary-value problem posed by the fluid motion would be considerably more difficult.

Imposing the boundary conditions at $r = a$ and $z = \pm b$, we obtain

$$C_s = 2bF_s\{\pi s I_1'(\pi sa/2b)\}^{-1}, \quad C_0 = F_0 \ldots\ldots [17a]$$

$$D_s = -2a^2\{\beta_s(\beta_s^2 - 1)J_1(\beta_s)\sinh(2\beta_s b/a)\}^{-1} \ldots [17b]$$

where the F_s are the Fourier coefficients of $f(z)$, viz.

$$F_s = \left(\frac{2 - \hat{\delta}_s^0}{2b}\right)\int_{-b}^{b} f(z)\cos[s\pi(z + b)/2b]dz \ldots [18]$$

and $\hat{\delta}_j^i$ is the Kronecker delta ($\hat{\delta}_j^i = 1$ if $i = j$; $= 0$ if $i \neq j$).

The sloshing potentials are identical with those for a rigid tank, for which the $\psi^{(i)}$ are known to be proportional to $J_1(\beta_s r/a)c_\theta$, where the β_s are given by Equation [14]. The normalization of these modes is arbitrary, depending on the definitions of the corresponding q_i; we choose

$$\psi^{(s+3)}(r, \theta) = c_\theta J_1(\beta_s r/a)/J_1(\beta_s), \quad s = 1, 2, \ldots\ldots [19]$$

which has the practical advantage of rendering q_4 the (spatial) maximum displacement of the dominant mode of sloshing. We then have for the sloshing potentials

$$\phi^{(s+3)} = a\psi^{(s+3)}(r, \theta)\beta_s^{-1}\operatorname{csch}(2\beta_s b/a)\cosh[\beta_s(z + b)/a] \ldots [20]$$

as may be verified by substitution in Equations [9] and [11].

Inertia Coefficients

We shall consider the inertia coefficients m_{ij} in turn, using Equations [8], [11], and [12]–[20] with a minimum of connecting text. We find it convenient to factor out the total mass of the liquid, viz.

$$M = 2\pi\rho a^2 b \ldots\ldots [21]$$

from each of these coefficients, but it should be noted that those coefficients having the subscript 2 (rotation) do not have the dimensions of mass alone.

$$m_{11} = -\rho\int\int_{r=a}\phi^{(1)}\phi_n^{(1)}dS \ldots\ldots [22a]$$

$$= M \ldots\ldots [22b]$$

This result is, of course, obvious *a priori*.

$$m_{12} = 0 \ldots\ldots [23]$$

$$m_{13} = -\rho\int\int_S \phi^{(1)}\phi_n^{(3)}dS \ldots\ldots [24a]$$

$$= M\{F_0 - (a^2/8b)[f'(b) - f'(-b)]\} \ldots [24b]$$

$$m_{1,s+3} = -\rho\int\int_{z=b}\phi^{(1)}\phi_n^{(s+3)}dS \ldots\ldots [25a]$$

$$= \frac{1}{2}Mab^{-1}\beta_s^{-2} \ldots\ldots [25b]$$

$$m_{22} = -\rho\int\int_S \phi^{(2)}\phi_n^{(2)}dS \ldots\ldots [26a]$$

$$= -\rho\int\int_S (zrc_\theta)(zrc_\theta)_n dS - \rho\int\int_S [\phi^{(2)}\phi_n^{(2)} - (zrc_\theta)(zrc_\theta)_n]dS \ldots [26b]$$

$$= \rho\int\int\int_V (z^2 + r^2c_\theta^2)dV - \rho\int\int_S [\phi^{(2)} \mp zrc_\theta][\phi^{(2)} \pm zrc_\theta]_n dS \ldots [26c]$$

where Green's theorem has been used to convert the first integral of Equation [26b] to the first integral of Equation [26c] and ensures the reciprocal cancellation of the cross products in the second integral. We may identify the first integral of Equation [26c] as the moment of inertia the fluid would have if rigid, viz.

$$I_R = M\left(\frac{1}{4}a^2 + \frac{1}{3}b^2\right) \ldots\ldots [27]$$

If we make the top choice of signs in the second integral and substitute $\phi^{(2)}$ from Equation [13a], we obtain (where the integral is to be taken over both $z = +b$ and $z = -b$)

$$m_{22} = I_R - \rho\int\int_{z=\pm b}(\phi^{(2)} - zrc_\theta)(\mp 2rc_\theta)dS \ldots\ldots [28a]$$

$$= I_R - 128\pi^{-4}Mb^2\sum_{s=0}^{\infty}(2s + 1)^{-4}(1 - \psi_{2s+1}) \ldots\ldots [28b]$$

$$= M\left(\frac{1}{4}a^2 - b^2\right) + 128\pi^{-4}Mb^2\sum_{s=0}^{\infty}(2s + 1)^{-4}\psi_{2s+1} \ldots [28c]$$

where ψ_s is defined by

$$\psi_s = \psi(s\pi a/2b) \ldots\ldots [29a]$$

$$\psi(x) = [xI_1'(x)]^{-1}I_1(x) = [xI_0(x) - I_1(x)]^{-1}I_1(x) = 1 - [I_2(x)/I_1'(x)] \ldots\ldots [29b]$$

$$\psi(0) = 1 \ldots\ldots [29c]$$

and is plotted in Fig. 2.

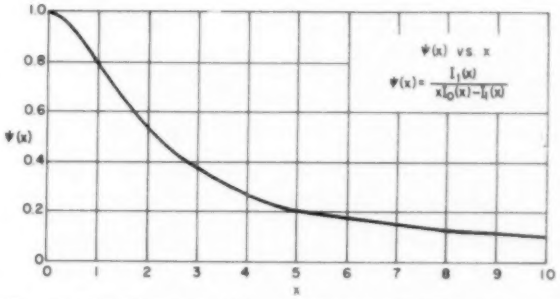

Fig. 2 The Function $\psi(x)$, as Defined by Equations [29]

Alternatively, substituting $\phi^{(3)}$ from Equation [13b] and making the lower choice of signs in Equation [26c], we obtain

$$m_{22} = I_R - \rho\int\int_{r=a}(\phi^{(2)} + zrc_\theta)(-2zc_\theta)dS \ldots\ldots [30a]$$

$$= I_R - 8Ma^2\sum_{s=0}^{\infty}\beta_s^{-2}(\beta_s^2 - 1)^{-1}[1 - (\beta_s b/a)^{-1}\tanh(\beta_s b/a)] \ldots [30b]$$

$$= M\left(\frac{1}{3}b^2 - \frac{3}{4}a^2\right) + 8Ma^2b^{-1}\sum_{s=1}^{\infty}\beta_s^{-3}(\beta_s^2 - 1)^{-1}\tanh(\beta_s b/a) \ldots [30c]$$

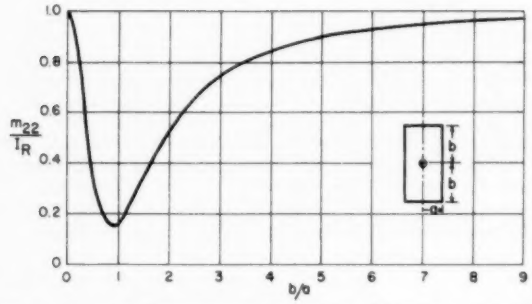

FIG. 3 RATIO OF EFFECTIVE TO RIGID BODY MOMENT OF INERTIA FOR CYLINDRICAL TANK ROTATING ABOUT TRANSVERSE, CENTROIDAL AXIS

The results of Equations [28b] and [30b] agree with those obtained by G. J. Gleghorn (unpublished), who presented the graph shown in Fig. 3.

$$m_{22} = -\rho \iint_S \phi^{(2)}\phi_n^{(2)} dS \quad [31a]$$

$$= M\left\{\frac{1}{2b}\int_{-b}^{b} zf(z)\,dz + \frac{8b}{\pi^2}\sum_{s=0}^{\infty}(2s+1)^{-2}\psi_{2s+1}F_{2s+1} + [f'(b)+f'(-b)]\left[\frac{1}{3}b^2 - \frac{1}{8}a^2 + \frac{32b^2}{\pi^4}\sum_{s=0}^{\infty}(2s+1)^{-4}\psi_{2s+1}\right]\right\} \quad [31b]$$

$$m_{2,s+2} = -\rho \iint_{z=b} \phi^{(2)}\phi_n^{(s+2)} dS \quad [32a]$$

$$= \frac{1}{2} Ma\beta_s^{-2}[2(\beta_s b/a)^{-1}\tanh(\beta_s b/a) - 1] \quad [32b]$$

$$m_{22} = \rho \iint_{r=a} \phi^{(2)} f(z) c_\theta dS - \rho f'(b) \iint_{z=b} \phi^{(2)} r c_\theta dS + \rho f'(-b) \iint_{z=-b} \phi^{(2)} r c_\theta dS \quad [33a]$$

$$= MF_0^2 + \frac{1}{2}M\sum_{s=1}^{\infty}\psi_s F_s^2 - Ma^2b^{-1}\sum_{s=1}^{\infty}(\beta_s^2-1)^{-1}[f'(b)\chi_s(b) - f'(-b)\chi_s(-b)] + \frac{1}{8}Ma^2b^{-1}[f'(-b)-f'(b)]F_0 + 2\pi^{-2}Mb\sum_{s=1}^{\infty}s^{-2}(1-\psi_s)[(-)^{s+1}f'(b)+f'(-b)]F_s + Ma^2b^{-1}\sum_{s=0}^{\infty}\beta_s^{-2}(\beta_s^2-1)^{-1}\operatorname{csch}(2\beta_s b/a)\times\{[f'^2(b)+f'^2(-b)]\cosh(2\beta_s b/a) - 2f'(b)f'(-b)\} \quad [33b]$$

where we have introduced the integral

$$\chi_s(b) = (\beta_s a)^{-1}\operatorname{csch}(2\beta_s b/a)\int_{-b}^{b} f(z)\cosh[\beta_s(z+b)/a]dz \quad [34a]$$

$$= \sum_{p=0}^{\infty}(-)^p[\beta_s^2 + (p\pi a/2b)^2]^{-1}F_p \quad [34b]$$

and where Equation [34b] follows from Equation [34a] after a Fourier expansion of the hyperbolic function and comparison to Equation [18]

$$m_{2,s+2} = -\rho \iint_{z=b} \phi^{(2)}\phi_n^{(s+2)} dS \quad [35a]$$

$$= \frac{1}{2}Mab^{-1}\chi_s(b) - \frac{1}{2}Ma^2b^{-1}\beta_s^{-2}\operatorname{csch}(2\beta_s b/a)[f'(b)\cosh(2\beta_s b/a) - f'(-b)] \quad [35b]$$

We remark that the $m_{2,s+2}$ and $m_{2,s+2}$ may be either positive or negative or may vanish.

$$m_{s+2,s+2} = -\rho \iint_{z=b} \phi^{(2)}\phi_n^{(2)} dS \quad [36a]$$

$$= \frac{1}{4}Mab^{-1}\beta_s^{-2}(\beta_s^2-1)\coth(2\beta_s b/a) \quad [36b]$$

POTENTIAL-ENERGY COEFFICIENTS

We consider first the elevation of the liquid center of gravity associated with bending. Under the usual (simple-beam) assumption that plane sections of the distorted tank remain plane, a cylindrical element of height dz that originally had its centroid at z is distorted into an element of trapezoidal cross section in the plane of bending, as shown in Fig. 4; moreover, the original centroid of this cross section is depressed in consequence of the

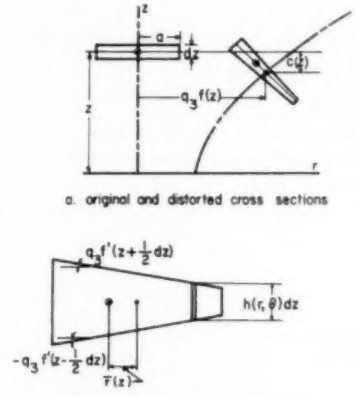

FIG. 4 DISPLACEMENT OF CROSS-SECTION CENTROID

requirement that the neutral axis remain unextended. The amount of this depression, say $c(z)$, may be deduced by equating the length of the bent axis to its original length; in so doing, we may assume, without loss of generality, that the prescribed bending mode is such that at least one point on the neutral axis, say z_0, experiences no vertical displacement.[7] We then have

$$\int_{z_0}^{z-c(z,t)} [1 + q_3^2(t)f'^2(z_1)]^{1/2}\,dz_1 = z - z_0 \quad [37]$$

which, in first approximation, yields

$$c(z,t) = \frac{1}{2}q_3^2(t)\int_{z_0}^{z} f'^2(z_1)dz_1 \quad [38]$$

[7] The prescription of the depression at one point of course must be included as a part of the specification of the bending mode.

We have next to calculate the displacement from the neutral axis of the center of gravity of the distorted element, which coincides with the geometrical centroid by virtue of the assumed incompressibility of the liquid (we remark that the center of gravity of the corresponding element of an elastic solid filling the tank would have remained at the centroid of the undistorted section). The depth at any point of the distorted section, Fig. 4*b*, is given by

$$h(r, \theta, t) = dz - q_s \left[f'\left(z + \frac{1}{2}\,dz\right) - f'\left(z - \frac{1}{2}\,dz\right)\right] rc_\theta \ldots\ldots [39a]$$

$$= dz\,[1 - q_s f''(z) r c_\theta] \ldots\ldots [39b]$$

The volume of this element then is

$$dV = \int_0^a \int_0^{2\pi} h(r, \theta) r\,dr\,d\theta = \pi a^2 dz \ldots\ldots [40]$$

i.e., the volume remains constant, as otherwise follows directly from the assumption that plane sections remain plane. The centroidal displacement toward the undisturbed axis ($r = 0$) is given by

$$\bar{r}(z) = \frac{1}{dV} \int_0^a \int_0^{2\pi} (-rc_\theta) h(r, \theta) r\,dr\,d\theta \ldots\ldots [41a]$$

$$= \frac{1}{4}\, a^2 q_s(t) f''(z) \ldots\ldots [41b]$$

Finally, we have for the center-of-gravity elevation of the distorted cylinder

$$\bar{z} = \frac{1}{V} \int_{-b}^{b} [z - c + \bar{r} q_s f'] dV \ldots\ldots [42a]$$

$$= \frac{1}{2b} \int_{-b}^{b} \left[z - \frac{1}{2}\, q_s^2 \int_{z_0}^{z} f'^2(z_1) dz_1 + \frac{1}{4}\, a^2 q_s^2 f'(z) f''(z) \right] dz \ldots\ldots [42b]$$

$$= -\frac{1}{4}\, q_s^2 \left[\int_{z_0}^{b} f'^2(z) dz - \int_{-b}^{z_0} f'^2(z) dz - \frac{1}{b} \int_{-b}^{b} z f'^2(z) dz \right] + \frac{1}{16}\, a^2 b^{-1} q_s^2 [f'^2(b) - f'^2(-b)] \ldots\ldots [42c]$$

Equating $\bar{z}$ to the displacement $q_s^2 e_2$ of Equations [4] and [5], we have

$$k_{22} = Mg \left\{ \frac{a^2}{8b} [f'^2(b) - f'^2(-b)] + \frac{1}{2b} \int_{-b}^{b} z f'^2(z) dz - \frac{1}{2} \int_{z_0}^{b} f'^2(z) dz + \frac{1}{2} \int_{-b}^{z_0} f'^2(z) dz \right\} \ldots\ldots [43]$$

Turning to the potential energy of the sloshing motions, substituting Equation [19] in [5*b*,*c*] and carrying out the integrations yields

$$k_{ij} = \frac{1}{4}\, Mgb^{-1} \beta_s^{-2} (\beta_s^2 - 1) \delta_j^i, \quad i = s + 3 \ldots\ldots [44]$$

$$k_{2i} = \frac{1}{2}\, Mg(a/b) \beta_s^{-2}, \quad i = s + 3 \ldots\ldots [45]$$

$$k_{i2} = -k_{2i} f'(b), \quad i = s + 3 \ldots\ldots [46]$$

Examples

We consider in this section the application of the foregoing results to a stationary tank of liquid. If M_e denotes the mass of the empty tank and ω_e the circular frequency of its dominant bending mode, which for the motion $q_2(t) f(z)$ will have the generalized mass $M_e \bar{f}^2$, the total energies of the oscillating tank when full[8] are

$$T = \frac{1}{2}\, M_e \bar{f}^2 \dot{q}_2^2 + \frac{1}{2}\, m_{22} \dot{q}_2^2 + \dot{q}_2 \sum_1^\infty m_{2,s+2} \dot{q}_{s+2} + \frac{1}{2} \sum_1^\infty m_{s+2,s+2} \dot{q}_{s+2}^2 \ldots\ldots [47a]$$

$$V = \frac{1}{2}\, M_e \bar{f}^2 \omega_e^2 q_2^2 + \frac{1}{2}\, k_{22} q_2^2 + \frac{1}{2} \sum_{s=1}^\infty k_{s+2,s+2} q_{s+2}^2 + q_2 \sum_{s=1}^\infty k_{2,s+2} q_{s+2} \ldots\ldots [47b]$$

Substituting T and V in Lagrange's equations, dividing the resulting equations of motion through by the total liquid mass M, introducing the normalized inertia coefficient

$$\bar{m}_e = M_e \bar{f}^2 / M \ldots\ldots [48]$$

and the uncoupled frequencies[9]

$$\omega_2^2 = (\bar{m}_e + \bar{m}_{22})^{-1} (\bar{m}_e \omega_e^2 + k_{22}) \ldots\ldots [49a]$$

$$\omega_{s+2}^2 = \bar{m}_{s+2,s+2}^{-1} k_{s+2,s+2} = (\beta_s g/a) \tanh (2\beta_s h/a) \ldots\ldots [49b]$$

we obtain

$$(\bar{m}_e + \bar{m}_{22})(\ddot{q}_2 + \omega_2^2 q_2) + \sum_1^\infty (\bar{m}_{2,s+2} \ddot{q}_{s+2} + k_{2,s+2} q_{s+2}) = 0 \ldots\ldots [50a]$$

$$\bar{m}_{2,s+2} \ddot{q}_2 + k_{2,s+2} q_2 + m_{s+2,s+2} (\ddot{q}_{s+2} + \omega_{s+2}^2 q_{s+2}) = 0, \quad s = 1, 2, \ldots\ldots [50b]$$

The frequency determinant of Equations [50] is

$$\Delta = \begin{vmatrix} (\bar{m}_e + \bar{m}_{22})(\omega_2^2 - \omega^2) & k_{2,s+2} - \bar{m}_{2,s+2}\omega^2 \\ k_{2,s+2} - \bar{m}_{2,s+2}\omega^2 & \bar{m}_{s+2,s+2}(\omega_{s+2}^2 - \omega^2) \end{vmatrix} \ldots [51]$$

where the partitioning lines separate the first row and column from the remainder of the determinant, with the implication that the remaining, nondiagonal terms are all zeros. Equating Δ to zero, eliminating the ith term in the first row by subtracting out the ith row premultiplied by

$$(k_{2,i+2} - \bar{m}_{2,i+2}\omega^2)/\bar{m}_{i+2,i+2}(\omega_{i+2}^2 - \omega^2)$$

and introducing the coupling coefficients

$$\alpha_{2s} = \bar{m}_{2,s+2}^2 \bar{m}_{s+2,s+2}^{-1} (\bar{m}_{22} + \bar{m}_e)^{-1} \ldots\ldots [52a]$$

$$\Omega_{2s} = k_{2,s+2}/\bar{m}_{2,s+2} \ldots\ldots [52b]$$

we obtain the frequency equation

$$\omega^2 - \omega_2^2 - \sum_{s=1}^\infty \alpha_{2s} (\omega^2 - \Omega_{2s})^2 (\omega^2 - \omega_{s+2}^2)^{-1} = 0 \ldots [53]$$

[8] We remark that the tank can be "full" and still not lose liquid when sloshing by virtue of our assumption of small displacements. Even were the tank not full, however, it usually would suffice to neglect the tank wall above the equilibrium free surface in consequence of its relatively small inertia.

[9] The effects of small amounts of damping in the liquid or tank walls could be included by making ω_2 and ω_{s+2} or ω_2 alone, respectively, complex.

In many problems of practical interest the first few sloshing frequencies (ω_4, ω_5, . . .) and $(\Omega_{2s})^{1/2}$ will be small compared with ω_3, while the α_{2s} for large s will be quite small (being of order β_s^{-3}). We then have

$$\omega^2 \doteq \omega_3^2 \left[1 - \sum_{s=1}^{\infty} \alpha_{3s} \right]^{-1} \quad [54]$$

as an approximation to the coupled bending frequency.[10] We emphasize that this is not the lowest frequency, but it does correspond to the most important mode from the standpoint of dynamic stresses in the tank walls.

In order to illustrate the numerical orders of magnitude to be expected in such problems, we assume the tank to be constrained such that it will bend as a cantilever. We also assume that the deflection function may be approximated by

$$f(z) = \left(\frac{z+b}{2b} \right)^2, \quad -b \leqq z \leqq b \quad [55a]$$

$$= \frac{1}{3} + 4\pi^{-2} \sum_{s=1}^{\infty} (-)^s s^{-2} \cos [s\pi(z+b)/2b] \quad [55b]$$

It should be remarked specifically that this approximation to the deflection function is not intended to be used in the determination of the elastic energy, which is implicitly represented by ω_3. We find for the corresponding inertia coefficients[11]

$$\bar{m}_{33} = \frac{1}{45} - \frac{1}{6}\left(\frac{a}{b}\right)^2 - \frac{7}{384}\left(\frac{a}{b}\right)^4 + \frac{16}{\pi^4} \sum_{s=1}^{\infty} s^{-4} \psi(s\pi a/2b) + 2\left(\frac{a}{b}\right)^2 \sum_{s=1}^{\infty} \beta_s^{-3}(\beta_s^2 - 1)^{-1} \coth (2\beta_s b/a) \quad [56]$$

$$\bar{m}_{3,s+3} = \frac{1}{2}\left(\frac{a}{b}\right)\beta_s^{-2} - \left(\frac{a}{b}\right)^2 \beta_s^{-3} \coth (2\beta_s b/a) + \frac{1}{4}\left(\frac{a}{b}\right)^2 \beta_s^{-4} \quad [57]$$

$$\bar{k}_{33} = \frac{1}{2} gb^{-1} \left(\frac{1}{4} a^2 b^{-2} - \frac{1}{3} \right) \quad [58]$$

$$\bar{k}_{3,s+3} = -\frac{1}{2} gab^{-2}\beta_s^{-2} \quad [59]$$

We obtain the following numerical values (slide-rule accuracy) for a tank having equal depth and diameter ($a = b$)[12]

$$\left.\begin{aligned} \bar{m}_{33} &= 0.079 \\ \bar{m}_{34} &= 0.0089, \qquad \bar{m}_{35} = 0.0114 \\ \bar{m}_{44} &= 0.0960, \qquad \bar{m}_{55} = 0.0453 \\ \alpha_{34} &= 0.0103, \qquad \alpha_{35} = 0.0358 \\ \bar{k}_{33} &= -0.0416\ (g/a) \\ \omega_4^2 &= 1.84(g/a), \qquad \omega_5^2 = 5.34(g/a) \\ \Omega_{34} &= -16.6(g/a), \qquad \Omega_{35} = -1.54(g/a) \end{aligned}\right\} \quad [60]$$

Assuming the tank wall to be of uniform density ρ_1 and thickness t, we find for the relative mass coefficient

$$\bar{m}_e = \frac{4\pi abt\rho_1 f^2}{2\pi a^2 b\rho} = 2\left(\frac{\rho_1 t}{\rho a}\right)\bar{f}^2 = \frac{2}{5}\left(\frac{\rho_1 t}{\rho a}\right) \quad [61]$$

while the frequency of the empty tank (based on the true deflection function for a cantilever beam) is (6)

$$\omega_e = \left(\frac{0.600\pi}{2b}\right)^2 \left(\frac{Ea^2}{2\rho_1}\right)^{1/2} \quad [62]$$

If we neglect $\bar{k}_{33}$ relative to $\bar{m}_e\omega_e^2$ and $\bar{m}_e$ relative to $\bar{m}_{33}$ in Equation [49a], i.e., assume all of the kinetic energy of the primitive bending mode to be in the liquid and all of the potential energy in the wall, we obtain[13]

$$\omega_3^2 = \bar{m}_{33}^{-1}\bar{m}_e\omega_e^2 = 2.0(Et/\rho a^3) \quad [63]$$

This almost certainly would be much larger than either $|\Omega_{34}|$ or ω_5^2, and we conclude that the effect of the first two sloshing modes is to increase the frequency of the primitive bending mode (i.e., the mode that would have resulted if the free surface had been replaced by a plane cap) approximately by the fraction $\alpha_{34} + \alpha_{35}$; viz., about 5 per cent.

We consider, as a second example, a free tank, such as might be approximated by a vertically rising rocket that carries liquid fuel. The bending mode in this case must be subjected to the constraints of vanishing transverse and angular momentum. The total transverse momentum of the liquid and empty tank is given by

$$\mathfrak{M}_x = \rho \iiint_V \left(\phi_{,r\theta} - \frac{1}{r}\phi_{,\theta s\theta} \right) r\, dr\, d\theta\, dz + \frac{M_e}{2b}\int_{-b}^{b} \dot{q}_3 f dz \quad [64a]$$

$$= \rho \int_{-b}^{b}\int_0^a \int_0^{2\pi} (r\phi)_{,r} \cos\theta\, d\theta\, dr\, dz + M_e F_0 \dot{q}_3 \quad [64b]$$

$$= \pi\rho a \int_{-b}^{b} (\sec\theta\phi)_{r=a}\, dz + M_e F_0 \dot{q}_3 \quad [64c]$$

$$= M\dot{q}_3 \left\{ [1 + (M_e/M)]F_0 + \frac{1}{8} a^2 b^{-1}[f'(-b) - f'(b)] \right\} \quad [64d]$$

We shall assume the symmetric (so that vanishing transverse momentum implies vanishing angular momentum) deflection function

[10] This approximation, which amounts to neglecting the potential energy of the liquid relative to the elastic energy, also may be obtained directly from Equations [50] by setting $\omega_{s+3}^2 = \bar{k}_{3,s+3} = 0$ therein.

[11] We have used the summations

$$\sum_1^{\infty} s^{-4} = (\pi^4/90), \quad \sum_1^{\infty} \beta_s^{-2}(\beta_s^2 - 1)^{-1} = 1/8$$

and

$$\sum_1^{\infty} \beta_s^{-4}(\beta_s^2 - 1)^{-1} = 7/192$$

to simplify this result.

[12] We have included the second sloshing mode because $\alpha_{35} > \alpha_{34}$ for $a = b$.

[13] If the fluid had been regarded as solid we would have obtained $\omega_3^2 = 0.79(Et/\rho a^3)$, which is more than 60 per cent too low!

$$f(z) = 1 - 3\mu(z/b)^2 \quad [65a]$$

$$= (1 - \mu) - 12\pi^{-2}\mu \sum_{s=1}^{\infty} s^{-2} \cos [s\pi(z + b)/b] \quad [65b]$$

Substituting Equation [65a] in [64d] and imposing $\overline{m}_s = 0$ on the result yields

$$\mu = \left\{1 - \frac{3}{2}(a/b)^2[1 + (M_s/M)]^{-1}\right\}^{-1} \quad [66]$$

We find for the inertia coefficients

$$\overline{m}_{33} = (1 - \mu)^2 - \frac{4}{5}\mu^2 + 3\mu(1 - 2\mu)(a/b)^2 - \frac{21}{8}\mu^2(a/b)^4 + 144\pi^{-4}\mu^2 \sum_{s=1}^{\infty} s^{-4}\psi(s\pi a/b) + 144\mu^2(a/b)^2 \sum_{s=1}^{\infty} \beta_s^{-3}(\beta_s^2 - 1)^{-1} \coth(\beta_s b/a) \quad [67]$$

$$\overline{m}_{3,s+3} = \frac{1}{2}(1 - 3\mu)(a/b)\beta_s^{-2} + 6\mu(a/b)^2\beta_s^{-3} \coth(\beta_s b/a) - 3\mu(a/b)^2\beta_s^{-4} \quad [68]$$

Assuming $a = b$ and neglecting M_s relative to M, we find $\mu = -2$ and

$$\overline{m}_{33} = 8.39, \quad \overline{m}_{34} = -0.469, \quad \alpha_{34} = 0.273, \quad \Omega_{34} = 3.78(g/a) \quad [69]$$

while $\overline{k}_{33} = 0$ from symmetry. The approximations $\overline{m}_s \ll \overline{m}_{33}$ and $\omega_3^2 \gg \omega_4^2$ also are likely to be valid here, so we may conclude that the presence of a free surface increases the free-free oscillation frequency of a tank of liquid having equal depth and diameter by about 27 per cent (as compared with 5 per cent for cantilever oscillations).

BIBLIOGRAPHY

1 "Hydrodynamics," by H. Lamb, Dover Publications, New York, N. Y., sixth edition, 1945, sections 191 and 157.

2 "The Characteristics of Fuel Motion Which Affect Airplane Dynamics," by E. W. Graham, Douglas Aircraft Company, Santa Monica, Calif., Report SM 14212, 1951.

3 "Forced Oscillations of a Fluid in a Cylindrical Tank," by K. Kachigan, Convair Report ZU-7-046, San Diego, Calif., 1955.

4 "Forces Produced by Fuel Oscillations," by J. Lorell, Jet Propulsion Laboratory Progress Report 20-149, 1956.

5 Reference (1), section 136.

6 "Mathematical Methods in Engineering," by Th. von Karman and M. A. Biot, McGraw-Hill Book Company, Inc., New York, N. Y., 1940, p. 289.

Brief Notes*

On the recommendations of the Executive Committee of the ASME Applied Mechanics Division, it has been decided to initiate a section devoted to brief notes on technical matters in mechanics. These notes must not be longer than 750 words (about 2½ double-spaced typewritten pages, including figures) and will be subject to the usual review procedure prior to publication. After approval such notes will be published as soon as possible, normally in the next issue of the Journal. The notes should be submitted to the Technical Editors of the *Journal of Applied Mechanics*.

Criterion for Flow of a Bingham Plastic Between Two Cylinders Loaded by Torque and Pressure Gradient

By P. R. PASLAY[1] and A. SLIBAR[2]

The criterion for the initiation of flow of a Bingham material between two concentric circular cylinders is considered. An external torque and an axial pressure gradient are acting on the plastic. For three values of the ratio of outer to inner radii of the cylinders the solutions are presented graphically.

Introduction

The material under consideration does not deform unless the quadratic invariant of the reduced stress tensor J_2 exceeds a critical value τ_0[3]. The stress-deformation rate relations are such that, when flow occurs, the shear stresses at every point have the same sign as the corresponding shear-deformation rates.

This analysis gives the combination of external torque and axial pressure gradient necessary to start flow between two concentric cylinders, Fig. 1. The right circular cylinders are assumed to be long enough so that end effects may be neglected.

This problem finds application in oil-field drilling operations where the drilling mud can be approximated as a Bingham plastic.

The equations governing three-dimensional flow of Bingham plastics have been proposed by W. Prager and K. Hohenemser[3]

$$d_{ij} = 0 \qquad |J_2^{1/2}| \leq \tau_0$$

$$d_{ij} = \frac{1}{2\mu}\left(\frac{|J_2^{1/2}| - \tau_0}{|J_2^{1/2}|}\right) S_{ij} \qquad |J_2^{1/2}| \geq \tau_0$$

where

d_{ij} = component of deformation-rate tensor

$S_{ij} = \sigma_{ij} - \delta_{ij}\frac{1}{3}\sum_K \sigma_{KK}$ = component of reduced stress tensor

δ_{ij} = Kronecker delta

$J_2 = \frac{1}{2}\sum_{ij} S_{ij}S_{ji}$ = quadratic invariant of reduced stress tensor

τ_0 = critical shear stress

μ = viscosity coefficient for Bingham plastic

σ_{ij} = component of stress tensor

Solution. Taking advantage of symmetry and neglecting end effects the stress field is given in cylindrical co-ordinates (r, z, θ) by

$$\sigma_{rr} = \sigma_{\theta\theta} = \sigma_{zz} = Kz + p_0$$

$$\sigma_{z\theta} = 0$$

$$\sigma_{r\theta} = \frac{T}{2\pi r^2}$$

$$\sigma_{rz} = \frac{C}{r} - \frac{1}{2}Kr$$

and

$$J_2 = \sigma_{rz}^2 + \sigma_{r\theta}^2$$

where

K = applied axial pressure gradient
T = external torque per unit axial length
C = constant
p_0 = pressure at $z = 0$

Two separate physical situations must be anticipated since (*a*) under the action of an external torque[4] flow is initiated only at $r = r_i$, Fig. 1; and (*b*), while under the action of a pressure gradient alone[5] flow is initiated simultaneously at $r = r_i$ and $r = r_0$.

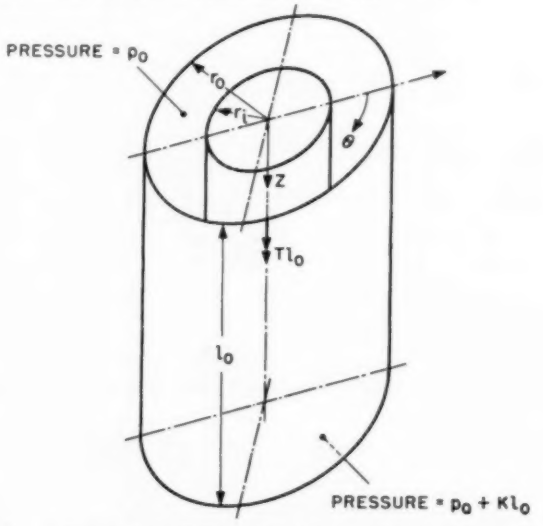

Fig. 1 Concentric cylinders showing co-ordinate system and loading

[1] General Electric Company, Schenectady, N. Y. Mem. ASME.

[2] Professor, Technische Hochschule, Stuttgart, Germany.

[3] W. Prager and K. Hohenemser, "Über die Ansätze der Mechanik der Kontinua," *Zeitschrift für Angewandte Mathematik und Mechanik*, vol. 12, 1932, p. 216.

[4] P. R. Paslay and A. Slibar, "Die Fliessbedingung und das Verformungsgesetz viskoser plastischer Stoffe," *Oesterreichisches Ingenieur-Archiv*, vol. 10, 1956, p. 328.

[5] A. Slibar and P. R. Paslay, "Die axiale Strömung von Bingham Plastiken in konzentrischen Rohren," *Zeitschrift für Angewandte Mathematik und Mechanik*, vol. 37, 1957, p 441.

* Discussion of papers in Brief Notes should be addressed to the Secretary, ASME, 29 West 39th Street, New York, N. Y., and will be accepted until July 10, 1958, for publication at a later date. Discussion received after the closing date will be returned.

Note: Statements and opinions advanced in papers are to be understood as individual expressions of their authors and not those of the Society. Manuscript received by ASME Applied Mechanics Division, September 27, 1957.

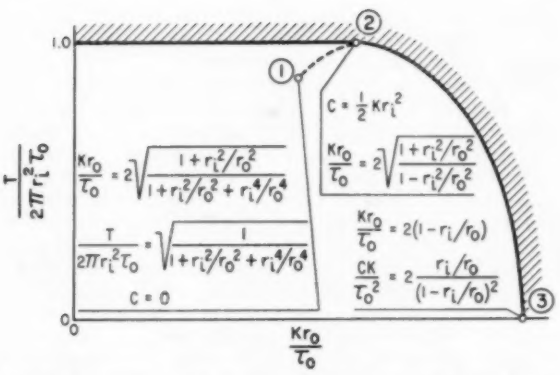
1.0
0
0
C = ½ Kr_i²
C = 0
Kr_0/τ_0 = 2√((1 + r_i²/r_0²)/(1 + r_i²/r_0² + r_i⁴/r_0⁴))
Kr_0/τ_0 = 2√((1 + r_i²/r_0²)/(1 − r_i²/r_0²))
T/(2πr_i²τ_0) = √(1/(1 + r_i²/r_0² + r_i⁴/r_0⁴))
Kr_0/τ_0 = 2(1 − r_i/r_0)
CK/τ_0² = 2 r_i/r_0 / (1 − r_i/r_0)²
T/(2πr_i²τ_0)
Kr_0/τ_0

Fig. 2 Schematic sketch of interrelation of external torque T and pressure gradient K necessary for the initiation of flow. Flow will occur in the cross-hatched region.

Physically, this is because the shear stresses have the same sign as the shear-deformation rates and the velocity fields must be continuous.

For combined load it must be noted that, in order to have flow start simultaneously at $r = r_i$ and $r = r_0$, two requirements must be satisfied; (1) $J_2^{1/2} = \tau_0$ must hold for $r = r_i$ and $r = r_0$, and (2) the sign of σ_{rz} for $r = r_i$ and $r = r_0$ must be opposite so that a continuous flow field can be associated with the stress field. That is, assuming K to be positive, then C must be positive and, therefore, for this case $C/r_i > 1/2(Kr_i)$ and $C/r_0 < 1/2(Kr_0)$ must hold.

In cases where K is sufficiently small the flow will initiate at $r = r_i$. Compatibility for the flow field demands that at the outset of this type of flow $\sigma_{rz} = 0$ at $r = r_i$; i.e., the constant C must take the value

$$C = \frac{1}{2} K r_i^2$$

and $\sigma_{r\theta} = \tau_0$ for $r = r_i$ so that $T/(2\pi r_i^3 \tau_0) = 1$ holds.

For larger values of K flow begins simultaneously for $r = r_i$ and $r = r_0$ so that

$$J_2|_{r=r_0} = J_2|_{r=r_i} = \tau_0^2$$

Substituting the stress field into the foregoing equations and requiring C to be positive in accordance with the second requirement for the case mentioned yields

$$\frac{C}{r_i \tau_0} = \left[\frac{K^2 r_0^2}{4\tau_0^2} - \frac{T^2}{4\pi^2 r_i^4 \tau_0^2}\left(1 + \frac{r_i^2}{r_0^2}\right)\right]^{1/2}$$

$$\frac{\tau_0^2}{K^2 r_0^2} = \frac{1}{4}\left(1 + \frac{r_i^2}{r_0^2}\right) - \frac{T^2}{4\pi^2 r_i^4 \tau_0^2}\frac{\tau_0^2}{K^2 r_0^2}\left(\frac{r_i}{r_0}\right)^2 - \frac{r_i}{r_0}\left[\frac{1}{4} - \frac{T^2}{4\pi^2 r_i^4 \tau_0^2}\frac{\tau_0^2}{K^2 r_0^2}\left(1 + \frac{r_i^2}{r_0^2}\right)\right]^{1/2}$$

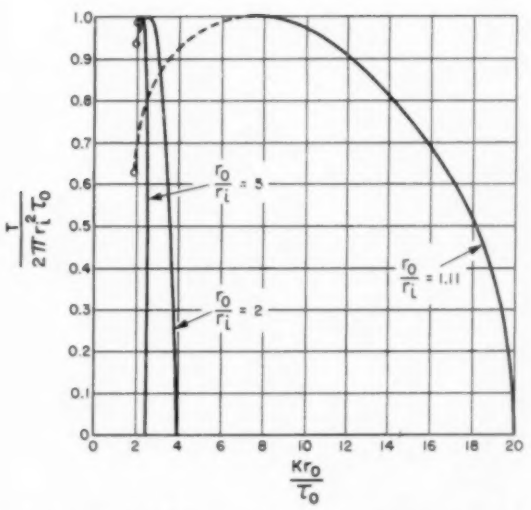

Fig. 3 Interrelation of external torque T and pressure gradient K for initiation of flow for several values of the ratio of cylinder radii, r_0/r_i

Fig. 2 shows the general shape of the foregoing relations between the torque T and pressure gradient K for outset of flow. The curve marked by ②②① terminates at ① since the resulting stress field is not real beyond this point. Although no formal proof is presented here, physical considerations lead to the conclusion that there is no compatible flow field to be associated with the resulting stress field along the dotted curve ①②.

In Fig. 3, solutions are presented graphically for $r_0/r_i = 1.11$, 2, and 5.

Strain-Aging, Work-Hardening, and Inhomogeneous Deformation in Armco Iron After Static and Dynamic Deformation

By H. P. TARDIF[1] and W. ERICKSON,[1] QUEBEC, CANADA

During the course of an investigation on the mechanical properties of metals at high rates of strain a few experiments were carried out to determine the mechanical properties of the material after static and dynamic deformation.

Harris and White[2] had reported previously that plastic straining by impact caused greater hardening than did straining by an equal amount of static strain. They used tensile deformation by longitudinal impact on an annealed mild steel at a velocity of 50 fps, and static deformation at a rate of 0.02 ipm, the amount of deformation being 5.5 per cent in the two cases. The results were 123.7, 162.4, and 212.0 VHN, respectively, for the unstrained, the statically strained, and the dynamically strained specimen.

Later on, Campbell and Duby[3] reported completely different results than the foregoing in that static straining in this case work-hardened the metal to a greater extent than dynamic strain-

[1] Canadian Armament Research and Development Establishment, Quebec, Quebec, Canada.

[2] D. B. Harris and M. P. White, "Comparison of the Hardening Produced in a Yield-Point Steel by Uniaxial Loading Under Static and Under Dynamic Conditions," Journal of Applied Mechanics, vol. 21, Trans. ASME, vol. 76, 1954, p. 194.

Manuscript received by ASME Applied Mechanics Division, January 20, 1958.

[3] J. D. Campbell and J. Duby, "The Yield Behaviour of Mild Steel in Dynamic Compression," *Proceedings of the Royal Society of London*, vol. 236A, 1956, p. 24.

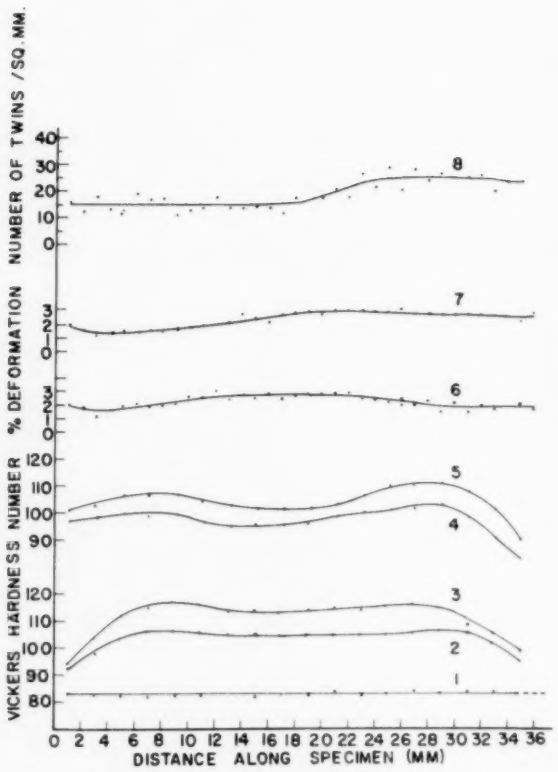

Curve 1: Hardness of original material
2: Hardness of specimen statically deformed 2.6 per cent
3: Same as 2, but aged 20 min at 100 C
4: Hardness of specimen dynamically deformed 2.5 per cent
5: Same as 4, but aged 20 min at 100 C
6: Percentage deformation along specimen given an over-all static deformation of 2.6 per cent
7: Percentage deformation along specimen given an over-all dynamic deformation of 2.5 per cent
8: Number of twins per sq mm along dynamically deformed specimen

Fig. 1

ing did. They reported values of 102, 113, and 126 Brinell, respectively, for unstrained, dynamically strained, and statically strained specimens. However, the specimens were strained by compression impact instead of tensile impact and were deformed by 4.1 per cent at an average rate of $480s^{-1}$.

It was thought that perhaps this discrepancy could be due to inhomogeneous deformation in the compression impact specimens or to strain-aging effects after dynamic and static deformation. To investigate these effects small compression specimens 0.75 in. diam and 1.5 in. long were machined with flat, parallel, and smoothly ground end faces and tested both under static and dynamic conditions. The dynamic test was carried out in a drop tester where a weight of 6.2 lb was dropped from a height of 15 ft to impact on the specimen at a velocity of 31 fps, which should give a maximum stress of about 55,000 psi on the specimen according to existing formulas.[4] The over-all deformation of the specimens in the described conditions was found to be 2.5 per cent. Other specimens were then deformed by the same amount in a compression machine at a rate of 0.06 ipm.

After deformation, the specimens were immersed immediately in a bath at −20 F, cut in two along the longitudinal axis, and polished on the cut faces while being kept at low temperature. One half of each specimen was reheated to room temperatures and hardness-tested. Three rows of indentations 2 mm apart were made from one end to the other of the specimens, the indentations also being 2 mm apart. The average of the three surveys was obtained and used to plot graphs. The other half of each specimen was aged at 100 C for 20 min and hardness-tested at room temperature in the same manner as just described.

A few other specimens were scribed every 2 mm on their circumferences and the distance between these lines determined after deformation to give an idea of the variation in amount of strain along the specimens.

Finally, one of the impacted specimens was polished and etched along its longitudinal axis and a survey made of the number of mechanical twins observed. The twins were counted at distances of every 2 mm on an area 2 sq mm in size.

The results shown in Fig. 1 are typical of others obtained in many specimens. The original hardness of the Armco iron used was very uniform. The changes in hardness after the various tests are given in Table 1.

Table 1 Changes in hardness values

Condition of specimen	Vickers hardness no.
Annealed	83
Dynamically deformed 2.6 per cent	95
Statically deformed 2.5 per cent	105
Dynamically deformed 2.6 per cent and aged	102
Statically deformed 2.5 per cent and aged	114

Similarly deformed cylinders were then machined down to small tensile specimens and tested after the aging treatment. The results show the same trend observed in the hardness results. The values given in Table 2 are the average values obtained on four specimens.

Table 2 Tensile-test results

Condition of specimen	0.2 per cent PS, psi	UTS, psi
Annealed	19400	46100
Statically deformed 2.35 per cent and aged	32400	52500
Statically deformed 2.62 per cent and aged	32600	52080
Dynamically deformed 2.4 per cent and aged	29900	50500

Discussion of Tests Results

The conclusions derived from the foregoing results will now be presented. First, the hardness is not uniform throughout the length of the specimens. Under static conditions the hardness is lower at both ends of the specimens and appreciably higher away from the ends with a slight drop in the center portion of the specimens. Under dynamic conditions the hardness shows the same pattern but not in a perfectly symmetrical manner as the curve is higher at the impacted end of the specimen. The hardness-test results obtained before aging show that the work-hardening produced for a given amount of deformation is smaller for dynamic conditions than it is for the static condition. After aging under the same treatment the statically deformed specimens appear to age by a slightly greater amount than the dynamically deformed

[4] M. P. White, "On the Impact Behavior of a Material With a Yield Point," JOURNAL OF APPLIED MECHANICS, vol. 16, TRANS. ASME, vol. 71, 1949, pp. 39–52.

specimens. The hardness results quoted were taken halfway through the length of the specimens. This is an important point to note for, although the hardness curves after aging show approximately the same pattern as before the aging treatment, the increase in hardness is, however, not exactly the same along the length of the specimens and is much lower, for example, at both ends of the statically deformed specimens.

It was hoped that measurements of percentage deformation and number of twins along the specimens would help elucidate some of the observations. The percentage deformation curves follow about the same pattern as that of hardness curves, except for the drop at the ends. The impact specimens show slightly more deformation at the impacted end. Curves of the number of twins along the specimens show some scatter as compared to hardness curves, but a definite trend to high number of twins toward the impacted end can readily be observed.

It would thus appear that under compression impact the work-hardening produced in Armco iron is less than that produced by the same amount of statically applied strain. This applies for the center portion of the specimens. Effects such as strain-aging and inhomogeneous deformation at the ends of the specimens can change the magnitude of the phenomenon by an appreciable amount.

Work is continuing on this problem to investigate the effects of amount and type of deformation on the relative work-hardening under static and dynamic deformation.

Torques on a Satellite Vehicle From Internal Moving Parts (Supplement)

By R. E. ROBERSON,[1] DOWNEY, CALIF.

Previous results on attitude perturbation torques on a satellite from internal moving parts are supplemented. The torque is expressed explicitly in terms of attitude external driving torques. Reference axes in the main body of the satellite are related to the wandering principal axes.

Nomenclature

THE nomenclature of this note is that of a previous paper,[2] with the following additions:

$\bar{H}$ = apparent angular momentum of internal moving parts as seen by observer in XYZ frame

$X^*Y^*Z^*$ = principal axes of inertia of satellite and its moving parts

$\tilde{\theta}$ = vector attitude deviation, assumed small

Dots under bars mean time derivative of components only, as if base vectors were constant.

Introduction

Perturbation torques on a satellite from internal moving parts have been derived[2] using as dependent variable the angular velocity $\tilde{\omega}_0$ of the main body in inertial space. Components were resolved along body-fixed axes XYZ which diagonalize the constant part $\bar{I}$ of the inertia dyadic. In this note, perturbation torques are obtained in attitude deviation angles of body-fixed XYZ-axes from orientation reference axes xyz, using $\tilde{\omega}_0$ components in terms of these angles obtained elsewhere.[3] The relationship between XYZ and the principal axes of inertia $X^*Y^*Z^*$ of the composite vehicle also is found.

Perturbation Torques

Let xyz be a set of attitude reference axes with angular velocity $\tilde{\omega}$ in inertial space, and define attitude deviation angles θ_1, θ_2, θ_3 between xyz and the satellite body axes XYZ as shown in Fig. 1.

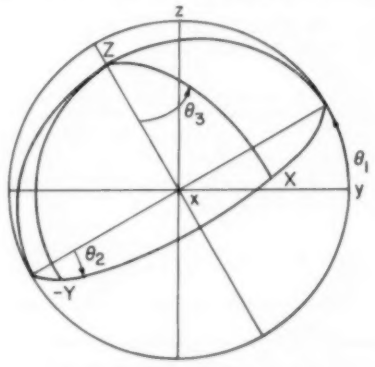

Fig. 1 Attitude deviation angles

Denote by $\tilde{\omega}_0$ the angular velocity of XYZ and define a vector $\tilde{\theta}$ by $\tilde{\theta} = \theta_1\tilde{e}_X + \theta_2\tilde{e}_Y + \theta_3\tilde{e}_Z$. Discussion is limited to small angles. To first order in small angles, $\tilde{\omega}_0 = \dot{\tilde{\theta}} + \tilde{\omega} \times \tilde{\theta} + \tilde{\omega}$ which is given as Equation (19)[3] in component form.

An expression for perturbation torque from moving parts is given by Equation (12).[2] The only terms which can depend on $\tilde{\theta}$ and its rates are those which contain $\tilde{\omega}_0$,

$$\bar{\bar{\gamma}}\cdot\dot{\tilde{\omega}}_0 + \dot{\bar{\bar{\gamma}}}\cdot\tilde{\omega}_0 + \tilde{\omega}_0 \times \bar{\bar{\gamma}}\cdot\tilde{\omega}_0 + \tilde{\omega}_0 \times \bar{H} \qquad (1)$$

Here $\bar{H} = \sum_{i=1}^{N} \bar{I}_i\cdot\tilde{\omega}_i$ is the apparent angular momentum of the moving parts as seen in XYZ. Denote the remaining terms of Equation (12),[2] purely time functions, by $\bar{D}_0(t)$.

Putting the expression for $\tilde{\omega}_0$ in (1), the portion of perturbation torque containing θ_1, θ_2, θ_3 becomes

$$D(t) + \{\bar{\bar{\gamma}}\cdot\dot{\tilde{\theta}} + (\dot{\bar{\bar{\gamma}}} + 2\bar{\bar{\gamma}} \times \tilde{\omega} + \bar{\bar{E}} \times \bar{H})\cdot\tilde{\theta} + [\dot{\bar{\bar{\gamma}}} \times \tilde{\omega} + \bar{\bar{\gamma}} \times \dot{\tilde{\omega}} + (\bar{\bar{\gamma}} \times \tilde{\omega}) \times \tilde{\omega} + (\tilde{\omega}\cdot\bar{H}\bar{\bar{E}} - \tilde{\omega}\bar{H})]\cdot\theta\} \qquad (2)$$

where

$$D(t) = \bar{\bar{\gamma}}\cdot\dot{\tilde{\omega}} + \dot{\bar{\bar{\gamma}}}\cdot\tilde{\omega} + \tilde{\omega} \times \bar{\bar{\gamma}}\cdot\tilde{\omega} + \tilde{\omega} \times \bar{H} \qquad (3)$$

depends only on the motion of xyz and the internal parts, not on the satellite itself, and $\bar{\bar{E}}$ is the unit dyadic. In obtaining (2), only first-order terms in $\tilde{\theta}$ and $\dot{\tilde{\theta}}$ are kept. The bracketed quantity in (2), denoted by $\bar{P}(\tilde{\theta}, t)$, is the complete first order θ-dependent portion of the perturbation torque; that is, the parametric excitation torque. The total perturbation torque is $\bar{L}_P = \bar{D}_0(t) + \bar{D}_1(t) + \bar{P}(\tilde{\theta}, t)$. Thus the parametric excitation terms have been separated from the effective external excitation; the explicit forms have been obtained for each.

---

[1] Advanced Engineering Department, Autonetics Division of North American Aviation, Inc. Assoc. Mem. ASME.

[2] R. E. Roberson, "Torques on a Satellite Vehicle From Internal Moving Parts," appearing in this issue of the JOURNAL OF APPLIED MECHANICS, pp. 208–213.

Manuscript received by ASME Applied Mechanics Division, June 21, 1957.

[3] R. E. Roberson, "Attitude Control of a Satellite Vehicle—An Outline of the Problems," presented at the 8th International Congress of Astronautics, Barcelona, Spain, October 7–12, 1957.

Principal Axes

The principal axes $X^*Y^*Z^*$ diagonalize $\bar{\Gamma} + \bar{\gamma}$, with $\bar{\Gamma}$ diagonalized with respect to the XYZ-axes; that is, $\bar{\Gamma} = I_1 \bar{e}_X \bar{e}_X + I_2 \bar{e}_Y \bar{e}_Y + I_3 \bar{e}_Z \bar{e}_Z$. The problem is to find a rotation of XYZ into $X^*Y^*Z^*$ which carries $\bar{\Gamma} + \bar{\gamma}$ into the diagonal form

$$\vartheta_1 \bar{e}_{X^*} \bar{e}_{X^*} + \vartheta_2 \bar{e}_{Y^*} \bar{e}_{Y^*} + \vartheta_3 \bar{e}_{Z^*} \bar{e}_{Z^*}$$

and to find the principal moments $\vartheta_1, \vartheta_2, \vartheta_3$. This is a well-known problem for which general solutions are available. One special case is easy to solve explicitly.

Let

$$\bar{\gamma} = \gamma_{11} \bar{e}_X \bar{e}_X + \gamma_{12} \bar{e}_X \bar{e}_Y + \gamma_{13} \bar{e}_X \bar{e}_Z + \gamma_{21} \bar{e}_Y \bar{e}_X + \ldots \quad (\gamma_{ij} = \gamma_{ji})$$

Assume $\gamma_{12}, \gamma_{23}, \gamma_{31}$ are small quantities relative to the differences $I_1 - I_2, I_2 - I_3, I_3 - I_1$, respectively. In this case the angles ψ_i between principal and body axes are small, with values $\psi_1 = \gamma_{23}/(I_2 - I_3)$ (ψ_2, ψ_3 by cyclic permutation) to within second-order terms in such small ratios. Also

$$\vartheta_1 = I_1 + \gamma_{11} + 2\left[\frac{\gamma_{12}^2}{I_1 - I_2} + \frac{\gamma_{13}^2}{I_1 - I_3}\right] \qquad (4)$$

(ϑ_2, ϑ_3 by cyclic permutation of indexes)

This development has two principal applications. First, the ψ-angles permit the off-diagonal γ-components to be interpreted in terms of axes of inertia shifts, which is important in obtaining a physical picture of the situation. Second, Equation (4) permits the reduction to the basis of this paper of other torques which act on the vehicle, especially gravitational torques which involve not I_1, I_2, and I_3, but ϑ_1, ϑ_2, and ϑ_3.

It is seen that the parametric excitation terms provide intermode coupling between θ_1, θ_2, and θ_3-motions because all three angles of their derivatives generally appear in each component of $\bar{P}(\bar{\theta}; t)$. The direct coupling of the $\theta_1 - \theta_3$ modes has been discussed,[3] but θ_2 is an independent mode except for the effect here. If $\gamma_{12} = \gamma_{23} = H_X = H_Z = 0$, the component $P_Y(\bar{\theta}; t)$ depends only on θ_2, suggesting possible design conditions to insure that θ_1 and θ_3 disturbances are not propagated into θ_2-motion.

With respect to the driving torque $\bar{D}_1(t)$, the following points stand out: First, the existence of a net $\bar{H}$ (with nonvanishing components) necessarily creates forced oscillations of the attitude equations. However, these perhaps can be minimized by keeping H_X and H_Z very small by suitable rotating $\bar{H}$ within the vehicle, inasmuch as these components are multiplied by ω_y which is large relative to the ω_x and ω_z which multiply H_Y. Second, it can be shown by writing $\bar{D}_1(t)$ in component form and discarding products of small terms that $\bar{\gamma}$-components principally effective in producing external torques are γ_{12} and γ_{23} and their derivatives (the same culprits as in the θ_2-coupling with θ_1 and θ_3 mentioned previously). Having these components vanish means that the shift in axes of inertia caused by internal moving parts is constrained to take place about the Y-axis.

Comparison of Experimental Information and Analytical Prediction for Laminar Entrance Pressure Drop in Ducts With Rectangular and Triangular Cross Sections[1]

By T. F. IRVINE, JR.,[2] and E. R. G. ECKERT,[3]
MINNEAPOLIS, MINN.

Prediction of Pressure Drop

This note is concerned with the calculation of the pressure drop for laminar flow through ducts with a length L which is larger than the entrance length but not so large that entrance losses can be neglected. The following relation can be used.

$$\frac{P_0 - P_L}{\rho \frac{\bar{w}^2}{2}} = f \frac{L}{d_h} + K$$

where f is the friction factor for developed flow, $\bar{w}$ the average velocity, d_h the hydraulic diameter, and K a measure of the excess pressure drop occurring in the entrance region. Fig. 1 indicates the location at which the static pressures P are measured. The term K has to account for the momentum change occurring in the entrance region since the fluid is at rest at the pressure P_0, but possesses a certain velocity field at the end of the entrance region. The K-factor also includes a pressure-loss term due to the larger wall shear in the entrance region than in developed flow. This second contribution to K, however, is small compared to the first one in laminar flow. By considering both the momentum and additional wall-shear contributions for laminar flow through a duct with circular cross section, Schiller [1][4] obtained a value $K = 2.16$ and Goldstein [2], by a more rigorous treatment, $K = 2.41$. The momentum term alone for this case results in a value $K = 2$.

For ducts with noncircular cross section, the momentum term can be calculated in a simple way when the velocity field in the developed region is known. The skin-friction term can only be obtained by a tedious calculation of the velocity field in the whole entrance region. It has, therefore, been recommended in reference [3] to calculate the pressure drop with an accuracy which is sufficient for most engineering purposes by including the momentum term only in the parameter K. K-values obtained in this way for various cross sections were presented in the same publication. In this note, these parameters will be compared with experimental data for two duct cross sections; i.e., a rectangle with an aspect ratio of 3:1 and a 23-deg isosceles triangle.

[4] Numbers in brackets designate References at end of paper.

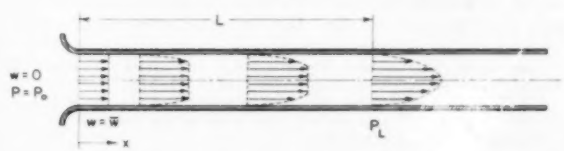

Fig. 1 Sketch of flow development in entrance region of duct

---

[1] Publication of the Heat Transfer Laboratory, Universtiy of Minnesota; Research sponsored by the Aeronautical Research Laboratory, Wright Air Development Center, Ohio.

[2] Assistant Professor of Mechanical Engineering, Institute of Technology, University of Minnesota.

[3] Professor of Mechanical Engineering, University of Minnesota. Mem. ASME.

Manuscript received by ASME Applied Mechanics Division, October 10, 1957.

Measured Pressure Drop

The data used in this note were obtained on the experimental apparatus described in detail in reference [3]. Only a brief description will be given here.

Under the influence of a blower located downstream, air from the room was drawn through a series of cloth settling screens, past a well-rounded entrance section and into the noncircular duct. After leaving the duct in which the measurements were performed, the air traveled through a transition section wherein the cross section gradually changed from a noncircular shape into a circular one. It then passed through a honeycomb flow straightener, a flow-rate meter, and was returned to the room through the blower.

Measurements were made with a rectangular and a triangular duct. Table 1 summarizes the important dimensions of both.

Fig. 2(*a*) shows the data for the 23-deg isosceles-triangle duct. The K-values are plotted against duct Reynolds number. At Reynolds numbers below 715, the theoretical value of $f \cdot \mathrm{Re} = 53$ was used for the friction correction. At higher Reynolds numbers, the fully developed pressure drop as determined by measurements was used. This was necessary since for such a duct a departure from the theoretical friction curve is already apparent [3]. An analytically determined K-value was obtained for a circular sector having the same apex angle as outlined in the first section. The developed velocity field is contained in [5]. Fig. 2(*a*) shows that the experimental and theoretical values of K agree remarkably well. Individual deviations as large as 20 per cent are present, but the average value of the data is practically identical with the calculated value $K = 2.50$.

Fig. 2(*b*) shows the same type of data as described in the foregoing for the rectangle with the 3:1 aspect ratio. In this case, the developed friction was calculated with the theoretical value of $f \cdot \mathrm{Re} = 69$. The fully developed velocity field was taken from [6]. As seen in the figure, the experimental values of K are on the average 15 per cent higher than the calculated value of 2.0. Such a deviation is still within the limits discussed previously.

Table 1 Inside Dimensions of Ducts Used in Experiments

Type of duct	Over-all length, ft	Hydraulic diameter, in.	Cross-section dimensions	Length in hydraulic diameters
Isosceles triangle	5.0	0.305	Base: 0.380 in. Apex angle: 23 deg	197
Rectangle	11.5	0.747	Sides: $a = 1.503$ in. $b = 0.498$ in.	185

Pressure measurements were made through wall pressure-tap holes 0.0180-in. diam. The pressure differences were measured with either a commercial micromanometer (Meriam Type A-750) when the pressure difference was greater than 0.05 in. of water, or with the laboratory micromanometer described in reference [4] when greater sensitivity was needed. For Reynolds-number calculations, the air temperature was measured with a shielded precision mercury glass thermometer and the room pressure level with a Fortin Type 2-380 barometer. Air flows were measured by either a rotometer or a thin-plate orifice.

The difference between the total pressure ahead of the entrance and of the static pressure at a location sufficiently far down the duct, where previous measuremnts had shown the flow to be fully developed, was measured. A subtraction of the fully developed friction, which was considered to act over the entire duct, then gave the experimental K-value for the particular cross section under consideration. The results of the measurements are illustrated in Figs. 2(*a*), (*b*).

Summary

It appears from these comparisons that pressure drop in ducts including the entrance region can be predicted with an accuracy of approximately 20 per cent when the flow is laminar and when flow separation at the entrance cross section does not occur. For turbulent flow, the entrance momentum pressure drop is usually only moderately larger than $\rho(\bar{u}^2/2)$.

Acknowledgment

The authors wish to acknowledge the assistance of Mr. Roger Schmidt who made the experimental measurements.

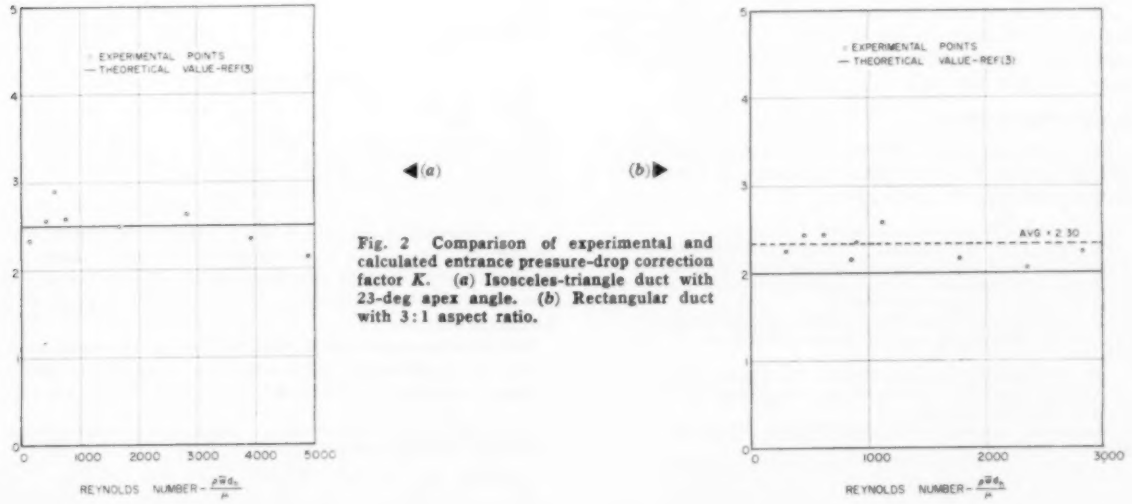

Fig. 2 Comparison of experimental and calculated entrance pressure-drop correction factor K. (*a*) Isosceles-triangle duct with 23-deg apex angle. (*b*) Rectangular duct with 3:1 aspect ratio.

References

1 L. Schiller, "Über den Strömungswiderstand von Rohren Verschiedenen Querschitts und Rauhigkeitsgrades," *Zeitschrift für Angewandte Mathematik und Mechanik*, vol. 3, 1923, p. 2.

2 S. Goldstein, "Modern Developments in Fluid Mechanics," Clarendon Press, Oxford, vol. 1, 1938, pp. 299–310.

3 E. R. G. Eckert and T. F. Irvine, Jr., "Incompressible Friction Factor, Transition, and Hydrodynamic Entrance Length Studies of Ducts with Triangular and Rectangular Cross Sections," Proceedings of Fourth Midwest Conference of Fluid Mechanics, April, 1957.

4 R. Eichhorn and T. F. Irvine, Jr., "Description of a Sensitive Micromanometer," Paper 57—SA-63, presented at the Semi-Annual Meeting of The American Society of Mechanical Engineers, June, 1957.

5 E. R. G. Eckert and T. F. Irvine, Jr., "Flow in Corners of Passages with Noncircular Cross Sections," Trans. ASME, vol. 78, 1956, pp. 709–718.

6 H. F. P. Purday, "An Introduction to the Mechanics of Viscous Flow," Dover Publications, Inc., New York, N. Y., 1949.

Stresses in a Dumbbell-Shaped Disk Rotating About an Axis Lying in Its Middle Plane

By B. B. CHATTERJEE,[1] WEST BENGAL, INDIA

This paper is concerned with the determination of stresses in a dumbbell-shaped disk rotating about an axis perpendicular to the axis of symmetry in its middle plane. The peripheral stress also is calculated.

Nomenclature

The following nomenclature is used in this note:

σ_x, σ_y, τ_{xy} = components of stress in Cartesian co-ordinates
κ = angular velocity of rotation
η = Poisson's ratio
$\gamma = 2(1 - \eta)$
$\Theta = \sigma_x + \sigma_y$
$\Phi = \sigma_x - \sigma_y + 2i\tau_{xy}$
$z = x + iy$
$\bar{z} = x - iy$
$\Omega(z)$, $\omega(z)$ = complex potentials

Introduction

In this paper, an attempt is made to find stresses in a dumbbell-shaped disk rotating about an axis perpendicular to the axis of symmetry in its middle plane. The problem is dealt with as one of generalized plane stress in which body forces are present. The reversed mass accelerations in steady rotation are treated as body forces. The case of semicircular and semielliptical disks have been discussed by Sen (1937).[2] Hodge (1956)[3] has somewhat extended the same problem. He has applied the Mises yield criterion to obtain the maximum speed at which the plate can rotate and remain wholly elastic. The cases of thin blades bounded by a parabola or a lemniscate have been discussed recently by Chatterjee (1956).[4]

Fundamental Equations

Let us take the middle plane of the disk as the plane $Z = 0$, and the axis of Y as the axis of rotation. The equations of motion satisfied by the mean stresses are

$$\frac{\partial \sigma_x}{\partial x} + \frac{\partial \tau_{xy}}{\partial y} = -\rho\kappa^2 x, \quad \frac{\partial \tau_{xy}}{\partial x} + \frac{\partial \sigma_y}{\partial y} = 0 \tag{1}$$

where κ is the angular velocity of rotation. The stress components can therefore be expressed in terms of the stress function χ by the formulas

$$\sigma_x = \frac{\partial^2 \chi}{\partial y^2} - \frac{1}{2}\rho\kappa^2 x^2$$
$$\sigma_y = \frac{\partial^2 \chi}{\partial x^2} - \frac{1}{2}\rho\kappa^2 x^2, \quad \tau_{xy} = -\frac{\partial^2 \chi}{\partial x \partial y} \tag{2}$$

The method of solution given by Stevenson (1943)[5] will be employed. His solutions for the stresses in terms of two complex potentials $\Omega(z)$ and $\omega(z)$ are

$$2\Theta = 2(\sigma_x + \sigma_y) = \Omega'(z) + \overline{\Omega}'(\bar{z}) + (4 - \gamma)\rho \frac{\partial W}{\partial z}$$
$$-2\Phi = -2(\sigma_x - \sigma_y + 2i\tau_{xy}) = z\overline{\Omega}''(\bar{z}) + \bar{\omega}''(\bar{z}) - \gamma\rho \frac{\partial W}{\partial \bar{z}} \tag{3}$$

where $\gamma = 2(1 - \eta)$, η is Poisson's ratio, and $U = \partial W/\partial z$ is the body-force potential function.

The boundary condition for an unstressed boundary is

$$\frac{\delta}{\delta s}\{\Omega(z) + z\overline{\Omega}'(\bar{z}) + \bar{\omega}'(\bar{z}) - \gamma\rho W\} = -4\rho \frac{\partial W}{\partial z} \cdot \frac{\partial z}{\partial s} \tag{4}$$

In this case

$$U = \partial W/\partial z = -\frac{1}{8}\kappa^2(z + \bar{z})^2$$

or

$$W = -(\kappa^2/24)(z^3 + 3z^2\bar{z} + 3z\bar{z}^2) \tag{5}$$

Solution

Transformation $z = c\sigma(1 + \lambda\sigma^n)$ where n is integral and greater than zero, and c, λ are real positive constants, maps the interior of a curvilinear polygon on the interior of a unit circle in a complex σ-plane, and is everywhere conformal if $z'(\sigma) \neq 0$ within the unit circle.

The transformation is of particular interest in two cases, when $n = 2$, the curvilinear polygon resembles a dumbbell, and when n is large we have an approximation to a cogwheel. In the first

[1] Lecturer in Mathematics, Jadavpur University.

[2] B. Sen, "Die Spannungen in Dünnen Halbreiskförmigen und Halbelliptieschen Scheiben, die um den sie Begrenzenden Durchmesser Rotieren," *Zeitschrift für Angewandte Mathematik und Mechanik*, band 17, heft 3, 1937, pp. 181–183.

[3] P. G. Hodge, Jr., "Stress Functions for Rotating Plates," Journal of Applied Mechanics, vol. 23, Trans. ASME, vol. 78, 1956, pp. 273–276.

[4] B. B. Chatterjee," Stress in Certain Thin Blades Rotating About an Axis Lying in Their Middle Plane," *Sonderdruck aus der Zamm*, band 36, heft 5/6, 1956, pp. 1–2.

Manuscript received by ASME Applied Mechanics Division, May 20, 1957.

[5] A. C. Stevenson, "Some Boundary Problems of Two-Dimensional Elasticity," *Philosophical Magazine*, vol. 34, 1943, pp. 766–793.

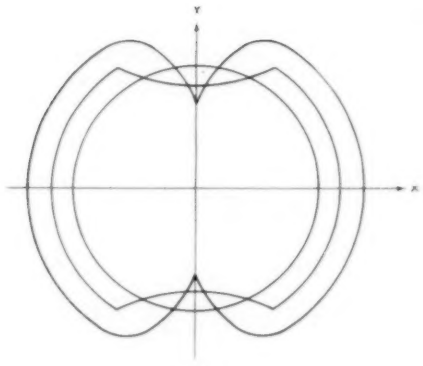

Fig. 1

case, varying λ from $^1/_3$ to zero results in a succession of shapes ranging from a two-cusped epicycloid to a circle. Fig. 1.

The boundary condition (4) becomes on the boundary $\sigma\bar{\sigma} = 1$

$$\begin{aligned}
\bar{z}'(\sigma)\Omega_0(\sigma) + z(\sigma)\overline{\Omega}_0'(\sigma) + \bar{\omega}_0'(\sigma) = \frac{1}{2}\rho\kappa^2 c^4\Bigg[&\frac{1+\eta}{6}\lambda^3\sigma^3 \\
&+ \frac{1+\eta}{2}(\lambda^2+\lambda^4)\sigma^2 + \Big\{\frac{5(1+\eta)+\lambda(7+5\eta)}{10} \\
&+ \frac{3(1+\eta)}{2}\lambda^3\Big\}\sigma^3 + \Big\{\frac{(1+\eta)+2\lambda(5+3\eta)+3\lambda^3(7+\eta)}{6} \\
&+ \frac{15(1+\eta)+3\lambda(7+5\eta)}{10}\lambda^2\Big\}\sigma^2 \\
&+ \sigma\Big\{\frac{(3+\eta)+\lambda(5+\eta)+2\lambda^2(7+\eta)}{2} \\
&+ \frac{(1+\eta)+2\lambda(5+3\eta)+3\lambda^3(7+\eta)}{2}\lambda\Big\} \\
&+ \Big\{-\frac{(3-\eta)+\lambda(5-\eta)+2\lambda^2(9-\eta)}{2} \\
&+ \frac{3(3+\eta)+3\lambda(5+\eta)+6\lambda^2(7+\eta)}{2}\lambda\Big\}\sigma^{-1} \\
&+ \Big\{-\frac{2(5-3\eta)+3\lambda^2(3-\eta)}{6}\lambda \\
&- \frac{3(3-\eta)+3\lambda(5-\eta)+6\lambda^2(9-\eta)}{2}\lambda\Big\}\sigma^{-3} \\
&+ \Big\{-\frac{7-5\eta}{10}\lambda^2 - \frac{2(5-3\eta)+3\lambda^2(3-\eta)}{2}\lambda^2\Big\}\sigma^{-5} \\
&+ \Big\{-\frac{3(7-5\eta)}{10}\lambda^3\Big\}\sigma^{-7}\Bigg]
\end{aligned}$$

Let us choose the complex potentials

$$\Omega_0(\sigma) = c^3[A\sigma + B\sigma^3 + C\sigma^5 + D\sigma^7 + E\sigma^9]$$

$$\omega_0(\sigma) = c^4[F\sigma^2 + G\sigma^4 + H\sigma^6 + K\sigma^8]$$

These make

$$\begin{aligned}
\bar{z}'(\sigma)\Omega_0(\sigma) + z(\sigma)\Omega_0'(\sigma) + \bar{\omega}_0'(\sigma) &= c^4[E\sigma^9 + (D+3\lambda E)\sigma^7 + (C+3\lambda D)\sigma^6 \\
&+ (B+3\lambda C+\lambda A)\sigma^3 + (2A+6\lambda B)\sigma \\
&+ (3\lambda A + 3B + 5\lambda C + 2F)\sigma^{-1} + (5C+7\lambda D+4G)\sigma^{-3} \\
&+ (7D+9\lambda E+6H)\sigma^{-5} + (9E+8K)\sigma^{-7}]
\end{aligned}$$

Comparing coefficients, we have

$$E = \frac{1}{12}\rho\kappa^2(1+\eta)\lambda^2$$

$$D + 3\lambda E = \frac{1}{4}\rho\kappa^2(1+\eta)\lambda^2 + \frac{1}{4}\rho\kappa^2(1+\eta)\lambda^4,$$

$$C + 3\lambda D = \frac{1}{2}\rho\kappa^2\Bigg[\frac{5(1+\eta)+\lambda(7+5\eta)}{10}\lambda + \frac{3(1+\eta)}{2}\lambda^3\Bigg],$$

$$\begin{aligned}
B + 3\lambda C + \lambda A &= \frac{1}{2}\rho\kappa^2\Bigg[\frac{(1+\eta)+2\lambda(5+3\eta)+3\lambda^2(7+\eta)}{6} \\
&\quad + \frac{15(1+\eta)+3\lambda(7+5\eta)}{10}\lambda^2\Bigg],
\end{aligned}$$

$$2A + 6\lambda B = \frac{1}{2}\rho\kappa^2\Bigg[\frac{(3+\eta)+\lambda(5+\eta)+2\lambda^2(7+\eta)}{2} + \frac{(1+\eta)+2\lambda(5+3\eta)+3\lambda^3(7+\eta)}{2}\lambda\Bigg],$$

$$\begin{aligned}
3\lambda A + 3B + 5\lambda C + 2F &= \frac{1}{2}\rho\kappa^2\Bigg[-\frac{(3-\eta)+\lambda(5-\eta)+2\lambda^2(9-\eta)}{2} \\
&\quad + \frac{3(3+\eta)+3\lambda(5+\eta)+6\lambda^2(7+\eta)}{2}\lambda\Bigg],
\end{aligned}$$

$$5C + 7\lambda D + 4G = \frac{1}{2}\rho\kappa^2\Bigg[-\frac{2(5-3\eta)+3\lambda^2(3-\eta)}{6}\lambda - \frac{3(3-\eta)+3\lambda(5-\eta)+6\lambda^2(9-\eta)}{2}\lambda\Bigg],$$

$$7D + 9\lambda E + 6H = \frac{1}{2}\rho\kappa^2\Bigg[-\frac{7-5\eta}{10}\lambda^2 - \frac{2(5-3\eta)+3\lambda^2(3-\eta)}{2}\lambda^2\Bigg],$$

$$9E + 8K = \frac{1}{2}\rho\kappa^2\Bigg[-\frac{3(7-5\eta)}{10}\lambda^3\Bigg].$$

We thus get

$$A = \frac{1}{8}\rho\kappa^2\Bigg[\frac{3\lambda^4(7+\eta) - 4\lambda^2(1-\eta) - 4\lambda - (3+\eta)}{3\lambda^2-1}\Bigg],$$

$$B = \frac{1}{24}\rho\kappa^2\Bigg[\frac{9\lambda^5(7+\eta) + 6\lambda^3(5+3\eta) + 6\lambda^2(3+\eta) - \lambda(11+9\eta) - 2(1+\eta)}{3\lambda^2-1}\Bigg],$$

$$C = \frac{1}{2}\rho\kappa^2\Bigg[\frac{5(1+\eta)+\lambda(7+5\eta)}{10}\Bigg]\lambda,$$

$$D = \frac{1}{4}\rho\kappa^2(1+\eta)\lambda^2,$$

$$E = \frac{1}{12}\rho\kappa^2(1+\eta)\lambda^3,$$

$$F = -\frac{1}{4}\rho\kappa^2[2 + \lambda(3+\eta) + 4\lambda^2 + (\eta-7)\lambda^3].$$

$$G = -\frac{1}{24}\rho\kappa^2\lambda[96\lambda^2 + 3(11+\eta)\lambda + 26],$$

$$H = -\frac{1}{30}\rho\kappa^2\lambda^2[23 + 15\lambda^2],$$

$$K = -\frac{9}{40}\rho\kappa^2\lambda^2.$$

The peripheral stress is given by

$$P = \frac{1}{2}\left[\Omega'(z) + \overline{\Omega}'(\bar{z}) - \frac{1}{4}(1+\eta)\rho\kappa^2(z+\bar{z})^2\right]_{z=e^{i\theta},\ \bar{z}=e^{-i\theta}}$$

$$= \frac{1}{2}\rho\kappa^2c^2\left[\frac{1}{4}\left\{\frac{3\lambda^4(7+\eta) - 4\lambda^2(1-\eta) - 4\lambda - (3+\eta)}{3\lambda^2 - 1}\right\}\right.$$

$$\times\left\{\frac{1 + 3\lambda\cos 2\theta}{1 + 6\lambda\cos 2\theta + 9\lambda^2}\right\}$$

$$+\frac{1}{4}\left\{\frac{9\lambda^3(7+\eta) + 6\lambda^2(5+3\eta) + 6\lambda^2(3+\eta) - \lambda(11+9\eta) - 2(1+\eta)}{3\lambda^2 - 1}\right\}$$

$$\times\left\{\frac{3\lambda + \cos 2\theta}{1 + 6\lambda\cos 2\theta + 9\lambda^2}\right\}$$

$$+\frac{1}{2}\left\{\frac{5(1+\eta) + \lambda(7+5\eta)}{1 + 6\lambda\cos 2\theta + 9\lambda^2}\right\}\lambda\{\cos 4\theta + 3\lambda\cos 2\theta\}$$

$$+\frac{7}{2}(1+\eta)\lambda^2\left\{\frac{\cos 6\theta + 3\lambda\cos 4\theta}{1 + 6\lambda\cos 2\theta + 9\lambda^2}\right\}$$

$$+\frac{3}{2}(1+\eta)\lambda^3\left\{\frac{\cos 8\theta + 3\lambda\cos 6\theta}{1 + 6\lambda\cos 2\theta + 9\lambda^2}\right\}$$

$$-\frac{1}{4}(1+\eta)\{2(1+\lambda^2) + 2(1+2\lambda)\cos 2\theta + 4\lambda\cos 4\theta + 2\lambda^2\cos 6\theta\}\Big]$$

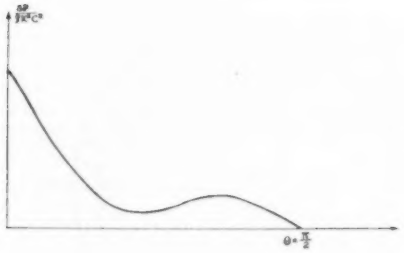

Fig. 2

A graph has been drawn showing the variation of the peripheral stress with the values of θ for the particular case when $\lambda = 1/3$. The value of η has been taken as $1/4$. $\lambda = 0$ gives the case of the circular disk. Fig. 2.

Displacement Discontinuity on the Interface of Two Joined Dissimilar Semi-Infinite Elastic Solids

By J. T. FRASIER,[1] UNIVERSITY PARK, PA.

The Papkovitch functions are given for a displacement discontinuity over a portion of the interface of two dissimilar isotropic semi-infinite elastic solids joined across a plane.

RONGVED[2] has given the general solution for an arbitrary dislocation over a plane area in an infinite isotropic elastic solid. This solution can be extended to that for a dislocation over a plane area on the interface of two dissimilar semi-infinite isotropic media joined across a plane boundary. The means of this extension and its results are presented here. Practical application of the results could be of use in investigations regarding displacement incompatibilities over grain boundaries.

The solution presented by Rongved is in terms of the Papkovitch functions[3] B_i and β which are related to the displacement u_i in an isotropic elastic solid by

$$u_i = B_i - \frac{1}{4(1-\nu)}(x_jB_j + \beta)_{,i} \qquad (1)$$

In the absence of body forces, as is the case for the problems under discussion, the Papkovitch functions are harmonic. The solution was obtained by considering the infinite solid as being composed of two elastically similar semi-infinite solids joined across a plane interface (the plane $z = 0$) containing an arbitrary area A over which a displacement discontinuity exists. Rongved's solution deals with two separate cases: (a) for a discontinuity normal to the area A, and (b) for a discontinuity tangential to the area A in the direction of the x-axis. A plane dislocation of general nature can be obtained by superposition of these solutions. The boundary conditions over the plane interface $z = 0$ are that the traction be continuous through this plane, and that the displacements be continuous everywhere except over A where the incompatible component must involve a term defining the dislocation. When Rongved wrote out these boundary conditions in terms of the Papkovitch functions B_i and β for the half-space in $z \geq 0$, and B_i' and β' for the half-space occupying $z \leq 0$, he considered the case where both solids have the same shear modulus μ and Poisson's ratio ν. The problem can be extended by assuming that the medium in $z \geq 0$ has the elastic constants μ and ν, and that in $z \leq 0$ the constants μ' and ν'.

By writing the afore-mentioned boundary conditions with this consideration, a solution can be obtained by employing the procedure used in the case for the single set of constants. This solution has been carried out and is that for two dissimilar semi-infinite solids joined across a plane interface containing a dislocation. The results are presented in the following. The primed constants and functions are related to the half-space $z \leq 0$. The functions $\bar{u}_x$ and $\bar{u}_z$ define the discontinuities over A in the x and z-directions, respectively, and are zero over the remainder of $z = 0$.

---

[1] Graduate Assistant in Engineering Mechanics, The Pennsylvania State University.

[2] L. Rongved, "Dislocation Over a Bounded Plane Area in an Infinite Solid," JOURNAL OF APPLIED MECHANICS, vol. 24, TRANS. ASME, vol. 79, 1957, pp. 252–254.

[3] P. Papkovitch, "Solution générale des équations differentielles fondamentales d'élasticité exprimée par trois fonctiones harmoniques," *Comptes Rendus*, vol. 195, 1932, pp. 513–515; "Expressions générales des composantes des tensions, ne renfermant comme fonction arbitraires que des fonction harmoniques," *Comptes Rendus*, vol. 195, 1932, pp. 754–756.

Manuscript received by ASME Applied Mechanics Division, November 29, 1957.

The Papkovitch functions for a discontinuity $\bar{u}_z$ in the component of displacement normal to A are

$$B_x = B_x' = B_y = B_y' = 0 \tag{2}$$

$$B_z = (-C_2/2\pi)\frac{\partial}{\partial z}\int_A \frac{\bar{u}_z}{r_0}\,ds \tag{3}$$

$$\beta = (-C_2/2\pi)\int_A \frac{\bar{u}_z}{r_0}\,ds \tag{4}$$

$$B_z'(x, y, -z) = (C_1/C_2)B_z(x, y, z) \tag{5}$$

$$\beta'(x, y, -z) = [(1 - \nu')/(1 - \nu)]\beta(x, y, z) \tag{6}$$

where

$$ds = d\xi d\eta$$

$$r_0 = [(x - \xi)^2 + (y - \eta)^2 + z^2]^{1/2}$$

$$C_1 = 4(1 - \nu')\mu/[\mu' + (3 - 4\nu')\mu]$$

$$C_2 = -4(1 - \nu)\mu'/[\mu + (3 - 4\nu)\mu']$$

$$C_3 = -8\mu\mu'(1 - \nu)[(1 - 2\nu)(1 - \nu') + (1 - 2\nu')(1 - \nu)]/[\mu + (3 - 4\nu)\mu'][\mu' + (3 - 4\nu')\mu]$$

Those for a tangential discontinuity $\bar{u}_x$ in the x-component of displacement over A are

$$B_x = -\frac{\mu'}{(\mu + \mu')}\frac{\partial I}{\partial z} \tag{7}$$

$$B_y = 0 = B_y' \tag{8}$$

$$B_z = -C_4\frac{\partial I}{\partial z} \tag{9}$$

$$\beta = C_5\left[x\frac{\partial I}{\partial z} - z\frac{\partial I}{\partial x}\right] + C_6\frac{\partial}{\partial x}\int^z I(x, y, \alpha)d\alpha \tag{10}$$

$$B_x'(x, y, -z) = -(\mu/\mu')B_x(x, y, z) \tag{11}$$

$$B_z'(x, y, -z) = C_7 B_z(x, y, z) + C_8\frac{\partial I(x, y, z)}{\partial x} \tag{12}$$

$$\beta'(x, y, -z) = C_9\left[x\frac{\partial I(x, y, z)}{\partial z} - z\frac{\partial I(x, y, z)}{\partial x}\right] + \frac{(1 - \nu')}{(1 - \nu)}\beta(x, y, z) \tag{13}$$

where

$$C_4 = \frac{\mu'[\mu' + (3 - 4\nu)\mu]}{(\mu + \mu')[\mu + (3 - 4\nu)\mu']}$$

$$C_5 = \frac{\mu'}{\mu + \mu'}$$

$$C_6 = -\frac{\mu\mu'\{(\mu - \mu')(1 - 2\nu')[(3 - 4\nu)^2 - 1] + 8(\mu + \mu')(1 - \nu)(\nu' - \nu)\}}{(\mu + \mu')[\mu + (3 - 4\nu)\mu'][\mu' + (3 - 4\nu')\mu]}$$

$$C_7 = \frac{(1 - \nu')[\mu + (3 - 4\nu)\mu']}{(1 - \nu)[\mu' + (3 - 4\nu')\mu]}$$

$$C_8 = -\frac{(\mu - \mu')[\mu'(1 - \nu') + \mu(1 - \nu)]}{(\mu + \mu')(1 - \nu)[\mu' + (3 - 4\nu')\mu]}$$

$$C_9 = -\frac{(1 - \nu')}{(\mu + \mu')}\left[\frac{\mu'}{(1 - \nu)} + \frac{\mu}{(1 - \nu')}\right]$$

$$I = -\frac{1}{2\pi}\int_A \frac{\bar{u}_z}{r_0}\,ds$$

Second Acceleration in Four-Bar Mechanisms as Related to Rotopole Motion

By W. J. CARTER,[1] AUSTIN, TEXAS

The second acceleration of the driven crank in a four-bar mechanism may be determined by an extension of the acceleration analysis given by Koenig.

Nomenclature

The following nomenclature is used in the paper:

- a, b, c, d = links of four-bar mechanism
- 1, 4 = fixed centers of four-bar mechanism
- 2, 3 = moving centers of four-bar mechanism
- P_{bd} = rotopole common to links b and d
- P_{ac} = rotopole common to links a and c
- ω = angular velocity of link, with lower-case-letter subscripts to indicate link
- α = angular acceleration of link, with lower-case-letter subscripts to indicate link
- $\beta = d\alpha/dt$ of link (second acceleration) with lower-case-letter subscripts to indicate link

Angular Accelerations by Method of L. R. Koenig[2]

Fig. 1 shows a four-bar mechanism with fixed link (d), crank (a), lever (c), and connecting link (b). The intersections of these links or their extensions define the rotopoles P_{ac} and P_{bd}. The rotopoles are points common to the links having the same velocity in each link. The common velocity of links (a) and (c) at their rotopole is v_{ac}. It may be seen that

$$v_{ac} = e\omega_a = f\omega_c$$

from which

$$\omega_c = \omega_a\frac{e}{f} \tag{1}$$

[1] Associate Professor of Mechanical Engineering, The University of Texas. Mem. ASME.

[2] L. R. Koenig, "A Uniform Method for Determining Angular Accelerations," Journal of Applied Mechanics, vol. 13, Trans. ASME, vol. 68, 1946, p. A-41.

Manuscript received by ASME Applied Mechanics Division, January 27, 1958.

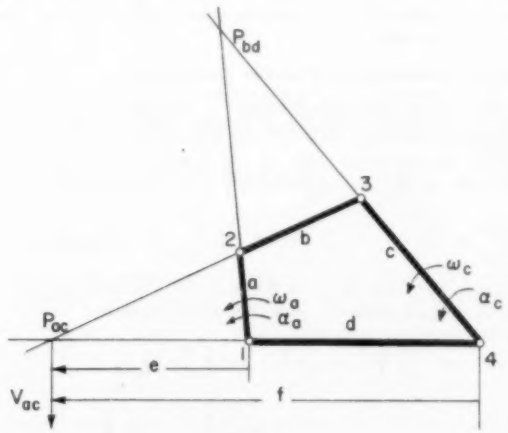

Fig. 1

where e and f are the distances from the fixed centers 1 and 4 to the rotopole.

Equation (1) may be differentiated with respect to time, giving

$$\alpha_c = \omega_a \left(\frac{1}{f} \frac{de}{dt} - \frac{e}{f^2} \frac{df}{dt} \right) + \frac{e}{f} \alpha_a \tag{2}$$

The quantities de/dt and df/dt are both equal in magnitude to the velocity of the rotopole along the pole line p_{cb} and in this case have the same algebraic sign. Thus

$$\alpha_c = \omega_a \frac{de}{dt} \left(\frac{1}{f} - \frac{e}{f^2} \right) + \frac{e}{f} \alpha_a \tag{3}$$

When this equation is used it is necessary that proper regard be given to the signs of the terms. Specifically, de/dt is considered positive when e and f are increasing; and ω_a, ω_c, α_a, and α_c are positive when they are counterclockwise.

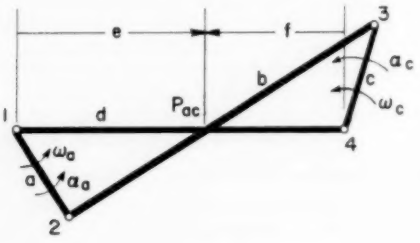

Fig. 2

When the rotopole P_{ac} is between the fixed centers, as shown in Fig. 2, crank and lever turn in opposite directions, with the result that

$$\omega_c = -\omega_a \frac{e}{f} \tag{4}$$

which leads to

$$\alpha_c = -\omega_a \frac{de}{dt} \left(\frac{1}{f} + \frac{e}{f^2} \right) - \frac{e}{f} \alpha_a \tag{5}$$

As before, the signs of ω_a, ω_c, α_a, and α_c are taken as positive when counterclockwise.

In the use of Equations (3) and (6) for the determination of angular accelerations, the rotopole velocity de/dt is usually found by graphical methods.

Second Acceleration of Four-Bar Mechanism

For the case where the rotopole P_{ac} is outside the fixed centers, we may differentiate Equation (3) with respect to time to yield

$$\beta_c = \omega_a \frac{d^2e}{dt^2} \left(\frac{1}{f} - \frac{e}{f^2} \right) + 2\omega_a \left(\frac{de}{dt} \right)^2 \left(\frac{e}{f^3} - \frac{1}{f^2} \right) + 2\alpha_a \frac{de}{dt} \left(\frac{1}{f} - \frac{e}{f^2} \right) + \beta_a \frac{e}{f} \tag{6}$$

When the rotopole P_{ac} is between the fixed centers, the corresponding equation for the second acceleration is

$$\beta_c = -\omega_a \frac{d^2e}{dt^2} \left(\frac{1}{f} - \frac{e}{f^2} \right) - 2\omega_a \left(\frac{de}{dt} \right) \left(\frac{1}{f^2} + \frac{e}{f^3} \right) - 2\alpha_a \frac{de}{dt} \left(\frac{1}{f} + \frac{e}{f^2} \right) - \frac{e}{f} \beta_a \tag{7}$$

The term d^2e/dt^2 in Equations (6) and (7) is the acceleration of the rotopole. This may be determined in a straightforward manner using Coriolis' law. The same regard for signs of the various quantities as indicated for Equations (3) and (5) applies here. Term d^2e/dt^2 is taken as positive when in the direction of positive de/dt.

This method of determining the second acceleration requires somewhat less labor than purely vector methods. By inverting the mechanism to consider link a fixed, this method may be used to determine the second acceleration of link b.

Large Deflection of Thin Circular Cantilever Beams

By KIICHI SATO,[1] SENDAI, JAPAN

This note treats of a problem similar to Conway's work,[2] except that the direction of the applied force P is reversed so as to cause the inflection of elastica as shown in Fig. 1. In the present work, the deflection of the beam is treated in two stages, the first and second; namely, in the first stage the magnitude of the force P is relatively small and the curvatures at all points on the strained beam take the same signs as the initial ones, while in the second stage the strained beam has one point of inflection of the elastic line, Fig. 1.

The solution to the first stage will be obtained by effecting some slight alterations on Conway's results as follows: P, α, and the term $(\sin \alpha - \sin \phi)^{1/2}$ in Equation [24] and in that of $R\beta$ shown in Conway's paper should take the negative sign. Also Equation [25] should be of the form

$$1 - \sin \phi = 2k^2 \sin^2\theta = (1 - \sin \alpha) \sin^2 \theta$$

With these modifications we obtain the equations in which the imaginary unit i is multiplied on the right-hand sides of Equations [26], [27], and on the left of Equation [28]. In our equations, however, i is virtually canceled because $a[=(P/D)^{1/2}]$ in those equations is replaced with ai.

For the second stage it will be convenient to follow the same

[1] Assistant of Mechanical Engineering, Tōhoku University.

[2] H. D. Conway, "The Nonlinear Bending of Thin Circular Rods," Journal of Applied Mechanics, vol. 23, Trans. ASME, vol. 78, 1956, pp. 7–10.

Manuscript received by ASME Applied Mechanics Division, April 26, 1957.

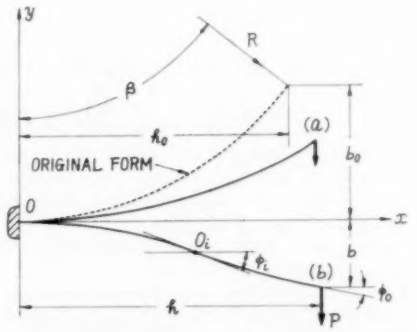

Fig. 1 Loaded beam: (a) In the first stage; (b) in the second stage

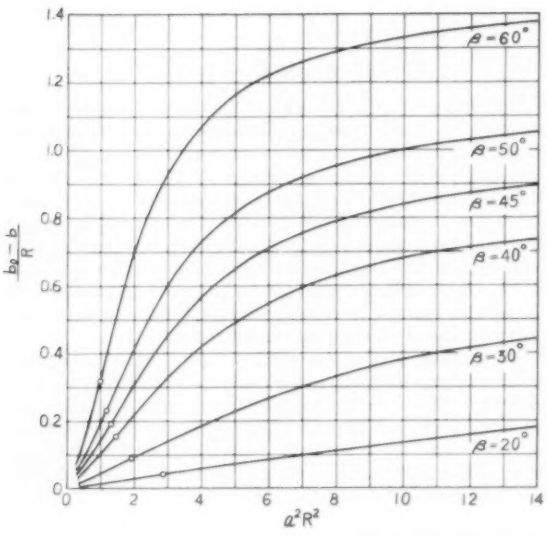

Fig. 2 Vertical deflection ratio at free end of beam versus nondimensional quantity

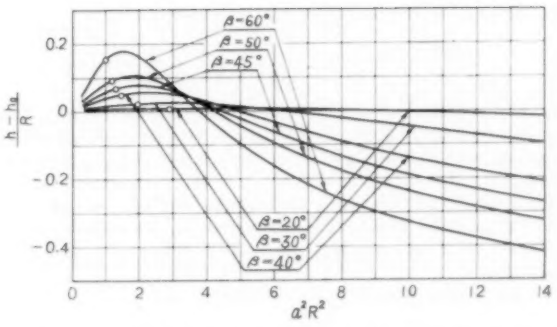

Fig. 3 Horizontal deflection ratio at free end of beam versus nondimensional quantity

method as Hymans[2] adopted. Following this method, a circular cantilever beam can be reduced to an initially straight cantilever with a couple applied at its free end. The strained beam due to a force P applied at its free end can be treated as two loaded straight cantilevers by cutting it at the point of inflection O_i. In this case the clamped and free ends of the original beam are considered as the clamped ends of each separated cantilever, and only a force P is applied at the free end O_i of each beam. The solution to this stage can be obtained in the same way as in the first stage. Then it may be shown that the equations of deflection will be of the same form as those of K. E. Bisshopp and D. C. Drucker,[4] or H. J. Barten,[5] except that the slope at one clamped end (the free end of the original beam) is not zero. From the fact that the slope at each free end (the point of inflection O_i of the original beam) of two cantilevers is one and the same, the deflection of the original beam in this stage can be computed easily.

By the use of the notations of Conway's paper,[2] the deflection ratios $(b_0 - b)/R$ and $(h - h_0)/R$ are plotted versus the nondimensional quantity $a^2R^2 = PR^2/D$ in Figs. 2 and 3 of this note, respectively. The marks o on the curves of Figs. 2 and 3 show the transition points from the first stage to the second stage. The strained beam giving the deflection at the transition point has the point of inflection of the elastic line at its clamped end.

It must be noted that small value of a^2R^2 cannot be computed in this analysis as follows: Replacing α and a^2 in Equation [23] of Conway's paper by $-\alpha$ and $-a^2$, respectively, we obtain

$$\sin \alpha = \frac{1}{2a^2R^2} - \sin \phi_0$$

From this equation, it may be inferred that a^2R^2 cannot be less than $1/2(1 + \sin \phi_0)$, in which ϕ_0 is slightly less than β. For practical purposes, however, since a^2R^2 should increase continuously from zero, the small values of a^2R^2 and of the deflection for it will be computed by some other ways; e.g., elementary theory.

In conclusion, the author offers his hearty thanks to Professor Emeritus S. Higuchi of Tōhoku University for his advice.

Heat Transfer in Swirling Laminar Pipe Flow

By R. SIEGEL[1] and M. PERLMUTTER,[2]
CLEVELAND, OHIO

The fluid motion resulting from a tangential swirl superimposed on Poiseuille flow entering a straight round pipe has been treated by Talbot.[3] The object of this note is to determine the effect of the decaying swirl on the heat transfer for a uniform heat flux applied at the pipe wall. For comparison, the thermal-entry region for Poiseuille flow without swirl has been recalculated using the present numerical method. The geometry considered is shown in Fig. 1.

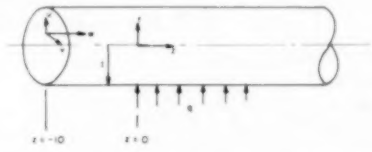

Fig. 1

In Talbot's solution the axial velocity w and the radial velocity u are determined using an integral method. The solution does not apply near the entrance of the pipe where the swirl is initiated ($z = -10$, Fig. 1). Therefore the start of the heated section was placed downstream at $z = 0$ where the fluid-flow configuration was better defined.

Basic Equations

If we assume constant fluid properties and neglect axial heat conduction in comparison with that in the radial direction, the

[2] F. Hymans, "Flat Spring With Large Deflections," Journal of Applied Mechanics, vol. 13, Trans. ASME, vol. 68, 1946, pp. 223–230.

[4] K. E. Bisshopp and D. C. Drucker, "Large Deflection of Cantilever Beams," *Quarterly of Applied Mathematics*, vol. 3, 1945, pp. 272–275.

[5] H. J. Barten, "On the Deflection of a Cantilever Beam," *Quarterly of Applied Mathematics*, vol. 2, 1944, pp. 168–171; vol. 3, 1945, pp. 275–276.

[1] NACA Lewis Flight Propulsion Laboratory. Assoc. Mem. ASME.

[2] NACA Lewis Flight Propulsion Laboratory.

[3] L. Talbot, "Laminar Swirling Pipe Flow," Journal of Applied Mechanics, vol. 21, Trans. ASME, vol. 76, 1954, pp. 1–7.

Manuscript received by ASME Applied Mechanics Division, September 3, 1957.

energy equation can be written in dimensionless form as

$$u\frac{\partial\theta}{\partial r}+w\frac{\partial\theta}{\partial z}=\frac{1}{\text{Re Pr}}\left(\frac{\partial^2\theta}{\partial r^2}+\frac{1}{r}\frac{\partial\theta}{\partial r}\right) \tag{1}$$

In this equation all velocities have been divided by W_m, the maximum velocity of the axial Poiseuille velocity profile entering the pipe, and all length dimensions have been divided by the tube radius a. $\theta=(Tk)/(qa)$, where T is the temperature, k the thermal conductivity, and q the uniform heat flux per unit area at the pipe wall. Pr is the Prandtl number, and Re is the Reynolds number based on a and W_m. From Talbot[3] the axial velocity is given by

$$w(r,z)=1-r^2+w_m'(z)[1-6r^2+5r^3] \tag{2}$$

and from the continuity equation the radial velocity is then found as

$$u(r,z)=7.693u_m(z)\left[\frac{r}{2}-\frac{3}{2}r^3+r^4\right] \tag{3}$$

w_m' is the value, at the tube center line, of the axial velocity perturbation which is added to the Poiseuille flow, and u_m is the maximum radial velocity. The values of $w_m'(z)$ and $u_m(z)$ are given by Talbot[3] for the numerical example considered here. It is noted that the tangential velocity does not appear in the energy equation. Thus the heat transfer would be unaffected by a swirl which did not change in the axial direction since in this case the radial velocity would be zero and the axial velocity would have a Poiseuille distribution.

Numerical Solution

Equation (1) can be expressed in finite-difference form as

$$\begin{aligned}\theta(r,z+\Delta z)=\;&\theta(r+\Delta r,z)\frac{1}{w(r,z)}\left(\frac{\Delta z}{\Delta r}\right)\left[-\frac{u(r,z)}{2}+\frac{1}{\text{Re Pr}}\left(\frac{1}{\Delta r}+\frac{1}{2r}\right)\right]\\&+\theta(r,z)\left[1-\frac{2}{\text{Re Pr}}\frac{\Delta z}{(\Delta r)^2}\frac{1}{w(r,z)}\right]\\&+\theta(r-\Delta r,z)\frac{1}{w(r,z)}\left(\frac{\Delta z}{\Delta r}\right)\left[\frac{u(r,z)}{2}+\frac{1}{\text{Re Pr}}\left(\frac{1}{\Delta r}-\frac{1}{2r}\right)\right]\end{aligned} \tag{4}$$

At the center line ($r=0$) this reduces to

$$\begin{aligned}\theta(0,z+\Delta z)=\;&\theta(\Delta r,z)\frac{2}{w(0,z)}\frac{\Delta z}{(\Delta r)^2}\frac{1}{\text{Re Pr}}\\&+\theta(0,z)\left[1-\frac{2}{\text{Re Pr}}\frac{\Delta z}{(\Delta r)^2}\frac{1}{w(0,z)}\right]\end{aligned} \tag{5}$$

At the wall ($r=1$) the uniform heat-flux boundary condition yields

$$\theta(1,z)=\Delta r+\theta(1-\Delta r,z) \tag{6}$$

The local heat-transfer coefficient is found from the definition

$$h=\frac{q}{T_w-T_m}$$

where T_w is the wall temperature, and T_m is the mixed mean fluid temperature. This can be expressed as a local Nusselt number

$$\text{Nu}=\frac{h2a}{k}=\frac{2}{\theta(1,z)-\dfrac{4z}{\text{Re Pr}}} \tag{7}$$

The specific example considered here is for Re = 1000, Pr = 0.7, and the tangential velocity

$$v(r,z)=0.8J_1[(\text{Re}\bar{\beta}_1)^{1/2}r]e^{-\beta_1(z+10)}$$

The expression for $v(r,z)$ arises as the first term of an approximate Bessel series solution to the equation of motion for the tangential velocity. The reader is referred to Talbot[3] for definition of terms in v and for the numerical values of w_m' and u_m which have been evaluated for this particular tangential-velocity distribution. The maximum tangential velocity at the beginning of the swirl is comparable in magnitude with the mean entering axial velocity. Before reaching the beginning of the heated section the tangential swirl has decayed by about 20 per cent. It was felt that this was a reasonable example to indicate whether a decaying swirl could have a significant effect on the heat transfer.

The problem was programmed for an IBM 650 computer using increment sizes, $\Delta r=0.04$ and $\Delta z=0.04$ [this kept the coefficient of $\theta(r,z)$ in Equation (4) always positive]. The calculation was performed from $z=0$ to $z=70$ giving a final Graetz number of $2\text{Re Pr}/z=20$. At $z=0$ the boundary condition was taken as $\theta=0$ for all r, except at $r=1$ where θ was taken as 0.02 to account for the wall heat flux.

Results and Discussion

The calculation was performed for flow both with and without swirl. The latter is simply the thermal-entry situation for uniform heat flux with a parabolic velocity distribution, and a similar numerical computation has already been performed by Kays.[4] However, in the discussion of Kays' paper, Lipkis indicates that, for the uniform-wall-temperature case, Kays' calculation is about 8 per cent too high near the tube inlet. Since the present calculation employs smaller increment sizes it was felt that the nonswirl case should be recomputed so a direct comparison could be made with the swirl computation. An indication of the accuracy of the finite-difference computations can be obtained by comparing the results for the nonswirl case with the exact solution.[5] Numerical values are listed in Table 1 and a plot of the present results is shown in Fig. 2.

Table 1 Comparison of Results

$\frac{2\text{Re Pr}}{z}$	Local Nusselt number, Without swirl: Kays[4]	Without swirl: Exact[5]	Without swirl: Present	With swirl
1400	....	....	14.07	16.31
800	13.81	11.6	11.7	13.5
400	10.40	9.29	9.42	10.8
200	8.06	7.49	7.62	8.58
133.3	7.05	6.66	6.78	7.53
100	6.56	6.15	6.27	6.86
66.7	5.76	5.55	5.67	6.07
50	5.37	5.20	5.33	5.60
33.3	4.95	4.82	4.95	5.09
25	4.74	4.62	4.77	4.84
20	4.59	4.51	4.68	4.71

Fig. 3 gives the ratio of local Nusselt number with swirl to that without swirl. It is seen that, in this example, at about 40 diameters from the beginning of the swirl the effect on the heat transfer has decreased to less than 1 per cent. The increase in heat transfer in the region where the swirl is fairly large is about 15 per cent. A consideration of the pressure drop as given by Talbot[3] in his equation

[4] W. M. Kays, "Numerical Solutions for Laminar-Flow Heat Transfer in Circular Tubes," TRANS. ASME, vol. 77, 1955, pp. 1265–1272.

[5] R. Siegel, E. M. Sparrow, and T. M. Hallman, "Steady Laminar Heat Transfer in a Circular Tube With Prescribed Wall Heat Flux," to be published in *Applied Scientific Research*.

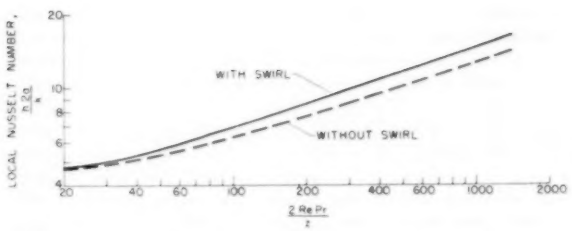

Fig. 2 Local Nusselt number for laminar swirling flow (for curve with swirl, Re = 1000, Pr = 0.7, and ratio of maximum tangential to maximum axial velocity at start of heating ≈ 0.45)

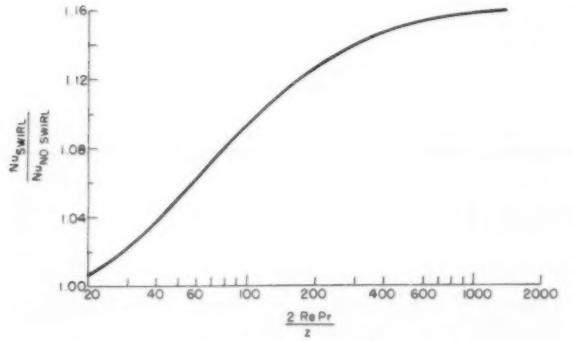

Fig. 3 Ratio of local Nusselt number with swirl to that without swirl

$$\frac{\partial p}{\partial z} \approx \frac{\partial}{\partial z} \int_0^r \frac{v^2}{r}\, dr - \frac{4}{\mathrm{Re}}$$

indicates that the increase in pressure drop is larger than the improvement in heat transfer.

A Levy-Type Solution for a Rectangular Plate of Variable Thickness

By H. D. CONWAY,[1] ITHACA, N. Y.

A solution is given for the bending of a uniformly loaded rectangular plate, simply supported on two opposite edges and having arbitrary boundary conditions on the others. The thickness variation is taken as exponential in order to make the solution tractable, and thus closely approximates to uniform taper if the latter is small.

A RECTANGULAR plate simply supported on its vertical edges is shown in Fig. 1. For thickness variations which are functions only of y, the differential equation for linear small-deflections neglecting stretching of the middle surface is[2]

$$D\Delta\Delta W + 2\frac{\partial D}{\partial y}\frac{\partial}{\partial y}\Delta W + \frac{\partial^2 D}{\partial y^2}\Delta W - (1-\nu)\frac{\partial^2 D}{\partial y^2}\frac{\partial^2 W}{\partial x^2} = q \quad (1)$$

with the usual notation. Writing the flexural rigidity D in the form $D = D_0 e^{cy}$ where D_0 and c are arbitrary constants, gives

$$\Delta\Delta W + 2c\frac{\partial}{\partial y}\Delta W + c^2\frac{\partial^2 W}{\partial y^2} + c^2\nu\frac{\partial^2 W}{\partial x^2} = \frac{q}{D_0}e^{-cy} \quad (2)$$

Solutions of this equation for a semi-infinite plate loaded only on its longer edges ($q = 0$) have recently been given by the writer.[3]

To solve the present problem, the complementary solution is written in the form

$$W_1 = \sum_{n=1,3,5}^{\infty} F(y)\cos\gamma_n x; \quad \gamma_n = \frac{n\pi}{2a} \quad (3)$$

this solution giving simple support on the two vertical edges. Substituting (3) in (2) with $q = 0$ gives

$$F^{\mathrm{IV}} + 2cF^{\mathrm{III}} + (c^2 - 2\gamma_n^2)F^{\mathrm{II}} - 2c\gamma_n^2 F^{\mathrm{I}} + (\gamma_n^4 - \nu c^2\gamma_n^2)F = 0 \quad (4)$$

For solutions of the form $F = Ae^{\lambda y}$, the characteristic equation is

$$\lambda^4 + 2c\lambda^3 + (c^2 - 2\gamma_n^2)\lambda^2 - 2c\gamma_n^2\lambda + (\gamma_n^4 - \nu c^2\gamma_n^2) = 0 \quad (5)$$

the roots of which are found by writing the foregoing in the form

$$(\lambda + \alpha + \beta_1)(\lambda + \alpha - \beta_1)(\lambda + \alpha + \beta_2)(\lambda + \alpha - \beta_2) = 0 \quad (6)$$

and are

$$\lambda_{1,2} = -\frac{c}{2} \pm \frac{1}{2}(c^2 + 4\gamma_n^2 + 4c\gamma_n\sqrt{\nu})^{1/2}$$

$$\lambda_{3,4} = -\frac{c}{2} \pm \frac{1}{2}(c^2 + 4\gamma_n^2 - 4c\gamma_n\sqrt{\nu})^{1/2} \quad (7)$$

We now require a particular solution of Equation (1) also giving simple support on $x = \pm a$. To find this we expand unity in a Fourier series of $\cos\gamma_n x$ in the interval $x = \pm a$ and write the loading intensity q as

$$q = \frac{4q}{\pi}\sum_{n=1,3,5}^{\infty}\frac{1}{n}(-1)^{(n-1)/2}\cos\gamma_n x, \ \gamma_n = \frac{n\pi}{2a} \quad (8)$$

The appropriate particular solution can then be written as

$$W_2 = e^{-cy}\sum_{n=1,3,5}^{\infty} F_n\cos\gamma_n x \quad (9)$$

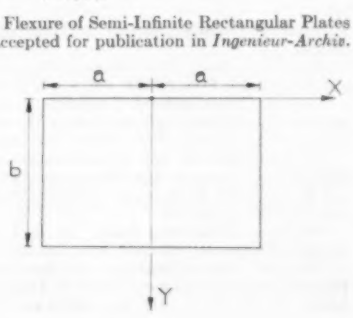

Fig. 1 Rectangular plate simply supported on $x = \pm a$ and having flexural rigidity $D = D_0 e^{cy}$

[1] Professor of Mechanics, Department of Engineering Mechanics and Materials, College of Engineering, Cornell University.

[2] S. Timoshenko, "Theory of Plates and Shells," McGraw-Hill Book Co. Inc., New York, N. Y., 1940, p. 195.

Manuscript received by ASME Applied Mechanics Division, November 7, 1957.

[3] H. D. Conway, "The Flexure of Semi-Infinite Rectangular Plates of Varying Thickness," accepted for publication in *Ingenieur-Archiv*.

where F_n is found by substitution in (1) and hence we obtain

$$W_2 = \frac{4qe^{-cy}}{\pi D_0} \sum_{n=1,3,5}^{\infty} \frac{(-1)^{(n-1)/2}}{n(\gamma_n^4 - \gamma_n^2 c^2 y)} \cos \gamma_n x \qquad (10)$$

Thus the complete solution is

$$W = \frac{4q}{\pi D_0} \sum_{n=1,3,5}^{\infty} \left(Ae^{\lambda_1 y} + Be^{\lambda_2 y} + Ce^{\lambda_3 y} + De^{\lambda_4 y} + \frac{(-1)^{(n-1)/2} e^{-cy}}{n(\gamma_n^4 - \gamma_n^2 c^2 y)} \right) \cos \gamma_n x \qquad (11)$$

where the λ are given by Equations (7) and the constants are obtained from the conditions on $y = 0, b$. The particular case of a uniform thickness plate can, of course, be obtained by writing $c = 0$. Noting that Equations (7) then give two sets of equal roots $\pm\gamma_n$, the solution for uniform thickness is the well-known

$$W = \frac{4q}{\pi D} \sum_{n=1,3,5}^{\infty} \left(Ae^{\gamma_n y} + Be^{-\gamma_n y} + Cye^{\gamma_n y} + Dye^{-\gamma_n y} + \frac{(-1)^{(n-1)/2}}{n\gamma_n^4} \right) \cos \gamma_n x \qquad (12)$$

The summations of (11) for specific boundary conditions will involve considerable labor and since they must be repeated for each side ratio a/b and c value, they will not be made here.

Discussion

A Photoelastic Study of Strain Waves Caused by Cavitation[1]

A. J. Durelli.[2] The author emphasizes the advantages of the use in photoelasticity of the material-strain fringe value in respect to the material-stress fringe value. This is particularly true in viscoelastic materials. Substantiation of the usefulness of this approach can be found in papers published by the writer and several of his associates, dealing with various phases of the properties of phenolformaldehydes,[3] of Columbia Resin CR-39,[4] and of epoxy resins.[5]

In some of these papers it is pointed out that it is actually possible to take advantage of the fact that birefringence can be present in a plastic, without a stress. The "crept-in" photoelastic effect can be used a long time after the loads have been removed from the specimen.[6]

More recently it also has been shown that transversal displacements in Marblette plates can be measured a long time after the loads have been removed, to determine the sum of the principal stresses.[7] However, only in a few instances has the writer computed the value of the strain fringe values. Strains have to be measured precisely for this purpose. Poisson's ratio values given by the author are remarkably accurate.

The results published by the author in Fig. 2 seem very important to the writer because they indicate the limit of application of his method of working with CR-39.

The writer has difficulty in following the evaluation of the photoelasticity tests reported by the author. It doesn't seem to be proved that the displacement of the residual fringes in thin pieces of Columbia resin is as sensitive and as accurate a means of measurement as the author claims. The conclusions obtained from Formula [21] seem to be premature. The formula depends in a very sensitive way on the value of Poisson's ratio, on the value of the diameter of the strained area, and on the fringe order. The author postulates the diameter of the strained area without giving experimental evidence and uses a value of 0.25 as fringe order which again does not seem substantiated by his tests.

Author's Closure

The author wishes to thank Professor Durelli for his many fine comments. His results concerning the strain-optic coefficient of cast epoxy resins are not inconsistent with the present study. Whether or not this is advantageous depends upon the application.

With regard to the accuracy of the strain measurements, the strain gages on the specimen were calibrated with Huggenberger extensometers against time.[8] The Huggenberger gages had been calibrated by means of monochromatic light interference patterns. Thus the creep strains measurements were accurate to 1 per cent. The precision of Poisson's ratio is indicated in Fig. 4.

For the dynamic experiments (see Fig. 13), no direct strain gage calibration was possible. However, the following indirect calibration was used:

Two A-8 strain gages were glued onto the impact specimen, one on each side. Directly on top of each gage, another A-8 gage was cemented. A comparison of the change in resistance during impact between the inboard set and the outboard set revealed

[1] By G. W. Sutton, published in the September, 1957, issue of the JOURNAL OF APPLIED MECHANICS, TRANS. ASME, vol. 79, pp. 340–348.

[2] Professor, Illinois Institute of Technology, Chicago, Ill. Mem. ASME.

[3] Some Unorthodox Procedures in Photoelasticity," by A. J. Durelli and R. L. Lake, *Proc. SESA*, vol. 9, no. 1, 1951, pp. 97–122.

[4] "Stress Concentrations Produced by Semi-Circular Notches in Infinite Plates Under Uniaxial State of Stress," by A. J. Durelli, R. L. Lake, and E. Phillips, *Proc. SESA*, vol. 10, no. 1, pp. 53–64.

[5] "Experiments for the Determination of Transient Stress and Strain Distributions in Two-Dimensional Problems," by A. J. Durelli and W. F. Riley, JOURNAL OF APPLIED MECHANICS, TRANS. ASME, vol. 79, 1957, pp. 69–76.

[6] "Stresses in Rotating Parts," by R. L. Lake and A. J. Durelli, *Machine Design*, vol. 25, no. 7, 1953, pp. 128–131.

[7] "Use of Creep to Determine the Sum of the Principal Stresses in Two-Dimensional Problems," by A. J. Durelli and W. F. Riley, *Proc. SESA*, vol. 14, no. 2, 1957, pp. 109–116.

[8] "A Study of the Application of Photoelasticity to the Investigation of Stress Waves," by G. W. Sutton, PhD thesis, California Institute of Technology, Pasadena, Calif., 1955.

that the difference was within the manufacturer's stated calibration accuracy. This was evidence that the gages cemented to the bar read the true strain within a few per cent.

Fig. 2 shows the viscoelastic behavior of CR-39 during long-time creep tests. Since the author was mostly concerned with high-speed response, the results presented in Figs. 7, 8, and 9 are the ones which are applicable, while Fig. 2 indicates the limitation of CR-39 for static experiments.

The motion pictures of cavitation were used to obtain the sequence of events leading to the stress pulse, not the magnitude of the fringe order. No accuracy was claimed for the motion picture photoelastic experiment; see page 347 of the paper. The fringe order of 0.25 is reported on the bottom of page 346, and was measured by means of a photomultiplier with 5461Å light; see Fig. 15. The fringe order was determined as follows:

The quarter wave plate and analyzer were mounted such that they could be rotated at 30 rev/sec. The positions of the polaroids and quarter wave plates were interchanged, and the analyzer was then rotated, with the X sweep of the photomultiplier oscilloscope in operation. The height of the trace on the oscillogram then corresponded to $^1/_2$ fringe order. After reassembly of the apparatus, the cavitation experiment with the photomultiplier was then performed. The amplitude of the spike (Fig. 15) was then measured. Its maximum height corresponds to $^1/_2$ the calibration height ± 10 per cent; thus the fringe order is 0.25 ± 10 per cent.

The diameter of the stressed area is postulated to be the same as that of the small pit, reported at the top of page 347. These individual pits are clearly visible in Fig. 16 (top), surrounding the main pit. The variation of the diameter of the pit was less than 20 per cent.

The author hopes that the foregoing description of the calibration, while somewhat lengthy, may be of help to the casual reader who may not be acquainted with some of the ultra high-speed techniques which have been developed at the California Institute of Technology.

The value of 2×10^5 psi cavitation stress should not be surprising to Professor Durelli, in view of other published data which indirectly indicate the order of magnitude of the stress level.[9] In fact, the apparent high level of stress led to the reported investigation in order to obtain a more quantitative estimate of the cavitation stress level.

Analysis of Stresses and Strains Near the End of a Crack Traversing a Plate[1]

F. A. McClintock.[2] It is interesting to note how high the applied stresses can be and still satisfy the author's condition that the radius of the plastic zone be small compared to the crack length; i.e., $r_p/a \leqslant r/a < 0.1$. The solid line in Fig. 1 of this discussion shows the distribution of strain in front of a crack in a biaxial tensile field, as given by Equations [3] and [5]. As indicated by the dotted line, plastic yielding will extend at least as far as the radius at which the stress is the yield stress of the material, and actually equilibrium of the y component of force across the x-axis will require that it extend farther. Triaxiality would only inhibit yielding significantly if the thickness of the sheet were greater than about r_p. In the case of a crack subjected to shear, the plastic zone extends twice as far as would be calculated from the theory of elasticity.[3] Taking the radius of the plastic zone to be twice the radius at which $\sigma = Y$ according to elasticity theory, we find

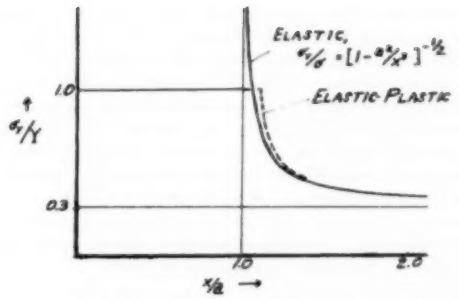

Fig. 1 Stress distributions ahead of crack under biaxial tension, for $\sigma/Y = 0.3$

$$r_p/a = 2[(\sigma/Y)^2/2] < 0.1 \quad \text{or } \sigma/Y < 0.3$$

Hence the nominal applied stress must be well below the yield stress if the radius of the zone of plastic deformation is to be small compared to the crack length. And perhaps one also should require that the zone of plastic deformation should be small compared to an elastic region which is itself small compared to the crack length. This would limit the applied stress even further.

Where the plate thickness is enough greater than r_p so that a plane-strain condition exists at the elastic-plastic boundary, there is a surprising amount of elastic constraint. For, from Equations [2] and [3], except at the very tip of the crack, $\sigma_x = \sigma_y$ and hence for plane strain

$$\epsilon_z = 0 = \sigma_z/E - 2\nu\sigma_x/E \quad \text{or} \quad \sigma_z = 2\nu\sigma_x$$

Thus the maximum difference between the principal stresses, which approximately governs yielding, is

$$Y = \sigma_x - \sigma_z = \sigma_x(1 - 2\nu)$$

For $\nu = 1/3$, the value of σ_x at which yielding occurs would be 3 times that for an unnotched specimen. Thus the author's presentation has made it easy to recognize that important constraints may arise in elastic as well as plastic stress distributions around notches.

It also may be noted that the plastic zone really consists of two regions, one caused by general yielding over macroscopic regions, and the other associated with the ductile fracture required to join cleavage fractures in neighboring grains. It is this latter region, whose radius is of the order of the grain size r_g, which is truly local to the surfaces of the crack. To insure that the general plastic deformation be negligible, it is necessary that

$$r_p = a\left(\frac{\sigma}{Y}\right)^2 < r_g \quad \text{or} \quad \sigma/Y < r_g/a$$

For macroscopic cracks in material with ordinary grain sizes, this condition would be satisfied only for very low values of the

[9] "On the Mechanism of Cavitation Damage," by M. S. Plesset and A. T. Ellis, TRANS. ASME, vol. 77, October, 1955, pp. 1055–1064.

[1] By G. R. Irwin, published in the September, 1957, issue of the JOURNAL OF APPLIED MECHANICS, TRANS. ASME, vol. 79, pp. 361–364.

[2] Associate Professor, Department of Mechanical Engineering, Massachusetts Institute of Technology, Cambridge, Mass. Mem. ASME.

[3] "Elastic-Plastic Stress and Strain Distributions Around Sharp Notches Under Repeated Shear," by J. A. H. Hult and F. A. McClintock, Proceedings of the Ninth International Congress for Applied Mechanics, Brussels, Belgium, 1956.

applied stress. Where the general plastic zone is not negligible, it would seem that an understanding of the energy absorbed in plastic deformation around the crack, supplied by $\mathcal{G}$, would require an analysis based on the theory of plasticity. This analysis might involve not only the material, but also the size of the crack, the previous history of loading, and, as noted in reference (7) of the paper and elsewhere,[4] the thickness of the sheet. This limitation on our understanding of the energy absorbed in plastic deformation makes the correlation obtained from the concept of crack extension force seem somewhat fortuitous, but of course does not negate the practical utility of the resulting equations in those cases where they correlate experimental data.

F. R. Steinbacher.[5] It is of interest to note that the author's solution, although applying Westergaard's (author's reference 11) method differently, agrees with certain phases of those obtained by Williams[6] recently. For example, both show that for a symmetrically loaded crack the energy density is not a maximum along the crack direction but at an angle of approximately ± 70 deg. However, it would be of interest to obtain experimental verification of this from strain gages located near the crack in a pattern similar to the one suggested in Fig. 2 of the paper. It is of interest to note that Liu and Carpenter,[7] in plotting the energy distribution on the surface of a steel plate containing a symmetrically loaded central crack, did obtain patterns of equal energy lines which agree reasonably well with the author's energy distribution as a function of r and θ.

The use of the symbol $\mathcal{G}$ as a force tending to cause crack extension instead of dW/dA, the strain-energy rate, appears to change Equation [12] from the one quoted in the author's earlier work only symbolically; namely

$$S_y = \left[\frac{E\,dW/dA}{\pi 2x}\right]^{1/2} \quad \ldots\ldots\ldots\ldots\ldots [1]$$

Attempts to evaluate either $\mathcal{G}$ or dW/dA experimentally has shown that either value is very susceptible to material and to the configurations of the specimen. As a matter of fact, Kies[8] and more recently Frisch[9] have shown that for some materials values for $\mathcal{G}$ may vary as much as 3 to 1. Our experience has shown that such variations can be reduced somewhat by using $(E\mathcal{G}/\pi)^{1/2}$. Nevertheless, since neither term is too satisfactory for predicting crack propagation characteristics in aircraft fail-safe design, reliable modifications and corrections for either Equation [12] or [17] must be found.

It is quite possible, of course, that much of this variation could be due to the differences which exist between the characteristics of a stationary crack and those of a rapidly moving crack. There is sure to be as much difference as there is in the characteristics of starting friction and sliding friction. Even a better illustration may be that of the removal of metal from a specimen, as with a lathe. In each case the force needed to start the action is always greater than that required to keep it going. Lockheed is presently investigating this phase of crack propagation.

M. L. Williams.[10] The author has presented another of his illuminating papers on the subject of stress fields around a crack. To extend his results, an additional interpretation of his quantity $\mathcal{G}$, "the strain-energy-loss rate associated with extension of the fracture accompanied only by plastic strains local to the crack surfaces" may be suggested. Also the subsequent relation draws attention to another characteristic dimensional quantity, namely, the radius of curvature at the base of the crack during deformation which at fracture may perhaps be associated with a critical "notch radii" or "base particle width."[11]

The first term in the displacement variation normal to the crack for the particular case discussed by the author, or the more general series expansion,[6] shows that locally the free edges of the crack deform according to the positive square root of the distance from the base of the crack, i.e.

$$v(x, 0) = Kx^{1/2} + \ldots$$

from which the local radius of curvature R at the base of the crack is found to be finite and equal to $R = (1/2)K^2$ and thus

$$v(x, 0) = (2R)^{1/2}x^{1/2}$$

comparing the author's expression

$$v(x, 0) = \frac{2}{E}\left(\frac{E\mathcal{G}}{\pi}\right)^{1/2}(2x)^{1/2}$$

there is the association

$$\mathcal{G} = \frac{\pi E}{4}R$$

which may be of additional assistance in physical interpretation, and perhaps related to Neuber's work on equivalent particle size from which effective stress-concentration factors are deduced.

In the latter part of the paper, the apparent dissimilarity with other results[6] as to the circumferential location of the maximum normal stress, σ_y —73.4 or 60 deg—is quickly resolved by noting that the maximum stresses were evaluated holding y and r constant, respectively.

Author's closure

The author wishes to thank those who submitted discussions for their suggestions and for their interest in his paper. In this reply the discussion by Williams is considered first, since those by McClintock and by Steinbacher refer to experimental matters, whereas the paper dealt primarily with theoretical viewpoints.

By Williams' method[6] for developing the stress distribution at the base of a stationary crack, one may obtain the stresses associated with a shear-type displacement of the crack surfaces along with the stresses associated with separation-type crack-surface displacements. Only stresses of the latter type were discussed by the writer. The stress relations for a crack opening subjected to shear are, however, easily represented in terms of the stress function method of the writer's paper. For example, if one assumes the Airy stress function is

$$F = -y\,\mathrm{Re}\bar{Z}$$

---

[4] "Some Design Considerations for Tear-Resistant Airplane Structures," by A. Sorensen, Institute of the Aeronautical Sciences Preprint No. 618, Jan., 1956.

[5] Group Engineer, Structural Development Group, Lockheed Aircraft Corporation, Burbank, Calif.

[6] "On the Stress Distribution at the Base of a Stationary Crack," by M. L. Williams, JOURNAL OF APPLIED MECHANICS, TRANS. ASME, vol, 79, 1957, pp. 109–114.

[7] A Study of Plastic Deformation and Fracturing by Strain Energy Distribution," by S. I. Liu and S. T. Carpenter, Ship Structure Committee, Bureau of Ships, Report SSC-38, December 20, 1950.

[8] "The Resistance of Materials to Fracture Propagation and Gun Fire Damage," by J. A. Kies, Naval Research Laboratory Memo Report 594, May, 1956.

[9] "Comparison of Semi-Empirical Solutions for Crack Propagation with Experiments," by J. Frisch, TRANS. ASME, vol. 80, 1958, pp. 921–928.

[10] Associate Professor, California Institute of Technology, Pasadena, Calif.

[11] "Theory of Notch Stresses," by H. Neuber, Edward Bros., Inc., Ann Arbor, Mich., 1946.

then the five stress functions Z of the examples in the paper provide the solution to five specific problems of cracks subjected to shearing forces. The crack-extension force associated with each of these stress fields tends to produce extension of the crack as a shear dislocation.

Williams' discussion suggests that the crack-extension force $\mathcal{G}$ may be related to Neuber's plastic particle hypothesis. The relationship of this hypothesis to the Griffith equation was discussed by Orowan.[12]

The general relationship of $\mathcal{G}$ to notch stress theory can be stated concisely as follows. Assume the stress intensity factor represented by the symbol $\mathcal{K}$ where

for plane strain

$$\mathcal{K}^2 = \frac{E\mathcal{G}}{(1 - \nu^2)\pi}$$

and for plane stress

$$\mathcal{K}^2 = \frac{E\mathcal{G}}{\pi}$$

with E and ν being Young's modulus and Poisson's ratio. Then for any notch, internal or external, and having nearly zero flank angle

$$\mathcal{K} = \underset{R \to 0}{Lim} \frac{1}{2} \sigma_m \sqrt{R}$$

where σ_m is the maximum tensile stress at the root of the notch and R is the notch root radius of curvature.

In terms of Neuber's plastic particle hypothesis

$$\mathcal{K} = \sigma_p \sqrt{\frac{\epsilon}{2}}$$

where σ_p is the average tensile stress across a small segment of length ϵ beyond the end of the crack. Since fracture strength experiments do not determine critical values of σ_p and $\sqrt{\epsilon}$ separately but only a critical value of their product, those using the Neuber hypothesis must assume a value of σ_p, usually the ultimate tensile strength, in order to obtain an experimental value for a critical plastic particle size ϵ.

By substituting "empirical" for "fortuitous" in his final sentence the author can agree with all of McClintock's remarks. However, readers should not confuse a theoretical estimate of the limits of applicability of brittle fracture theory with what appears to be the actual situation practically. Fracture strengths, $\mathcal{G}_c$, measured with flat sheets in uniform tension have shown no significant error due to local plastic yielding when the net section stress was less than the yield stress. For the nonuniform stress field of a spinning disk with the crack in the central region of greatest stress, Winne and Wundt[13] found that plastic yielding influenced the measured values of $\mathcal{G}_c$ only when the average net section stress exceeded 65 per cent of the yield stress. Thus the suggested crack-extension force analysis is applicable when, as in common engineering practice, the net section stress has been made substantially less than the yield stress.

Difficulties with variations in $\mathcal{G}_c$ or dW/dA for the same material have been experienced at the author's laboratory as well as by Steinbacher and his associates. These difficulties are of two kinds: (*a*) The stress distribution actually present in the test specimen may differ from that assumed in the calculation of $\mathcal{G}_c$. For example, a thin sheet in uniaxial tension with a central starting crack may buckle across the span of the crack unless supported by face plates whereas the equation used for calculation of $\mathcal{G}_c$ assumes the sheet is flat; (*b*) under conditions of plane strain (thick sections) $\mathcal{G}_c$ is much less than for conditions of plane stress (thin sections). In general, whether due to triaxiality, temperature, or strain rate, changes which cause an increase of yield stress cause a decrease of $\mathcal{G}_c$.

Different values of $\mathcal{G}_c$ or dW/dA for the same material due to (*b*) are to be expected from the physical nature of the property and the variability itself is of definite interest. Inconsistent results due to (*a*) can be eliminated with growth in testing experience.

[12] "Energy Criteria of Fracture," by E. Orowan, *The Welding Journal Research Supplement*, March, 1955.

[13] "Application of the Griffith-Irwin Theory of Crack Propagation to the Bursting Behavior of Disks," by D. H. Winne and B. M. Wundt, ASME Paper No. 57—A-249.

A Direct Method for Determining Airy Polynomial Stress Functions[1]

J. N. Goodier.[2] Problems of the kind illustrated in this paper by the two examples worked out are not completely determinate boundary-value problems in the theory of elasticity because the loadings, or reactions, or both, are specified only as resultants. The distribution of traction forming the resultant is not specified. It follows that there is no unique solution. The method proposed appears to lead to a unique solution, and this means that one solution has somehow been singled out. Examination of Equations [11] and [16] shows that they do not demand $C_{mn} = 0$ as the text following Equation [17] would have it. They merely allow such a solution out of an infinity of solutions. Thus an arbitrary choice has occurred here. Being the choice of the simplest solution, it has led to the well-known solution usually obtained by seeking the polynomial stress function of lowest degree which meets the required resultant conditions. A similar comment applies to the second example, and in general.

It also may be of interest to point out that polynomial stress functions can be written down at once, avoiding the necessity of obtaining relations between coefficients as in Equation [8]. The function of the nth degree (only) is obtained from the form

$$\phi = \mathrm{Re}[\bar{z}\psi(z) + \chi(z)], \qquad z = x + iy$$

by taking

$$\psi(z) = (a_n + ib_n)z^{n-1}, \qquad \chi(z) = (c_n + id_n)z^n$$

where a_n, b_n, c_n, d_n are arbitrary real constants.

G. Horvay.[3] The author furnishes a new method of solution to the old problem of finding the biharmonic polynomial which properly represents the effects of prescribed tractions applied to the boundary of a rectangle. It may be mentioned that Donnell on one hand,[4] Boley and Tolins[5] on the other, also tackled the

[1] By Ching-Yuan Neou, published in the September, 1957, issue of the JOURNAL OF APPLIED MECHANICS, TRANS. ASME, vol. 79, pp. 387–390.

[2] Professor of Engineering Mechanics, Stanford University, Stanford, Calif. Mem. ASME.

[3] General Electric Research Laboratory, Schenectady, N. Y. Mem. ASME.

[4] "Bending of Rectangular Beams," by L. H. Donnell, JOURNAL OF APPLIED MECHANICS, TRANS. ASME, vol. 74, 1952, p. 123.

[5] "On the Stresses and Deflections of Rectangular Beams," by B. A. Boley and I. S. Tolins, JOURNAL OF APPLIED MECHANICS, TRANS. ASME, vol. 78, 1956, pp. 339–342.

problem, but in a different manner, using the method of progressive approximations by biharmonic polynomials.[6] This algorithm automatically breaks off when the applied tractions are polynomials. The DBT approach appears preferable to the Neou method, at least in principle, because the calculations may be terminated whenever the improvement produced by the successive polynomials is judged to be negligible. (In the author's method one has to complete the calculations before the solution is usable.) In practice the author's method may very well lead more quickly to the goal. This has not been checked.

The present comments aim to re-emphasize the oft-forgotten fact that the biharmonic-polynomials approach is inapplicable to rectangles which are nearly squares. In Fig. 1(*a*) we show a square, subject to the traction

$$\sigma_y(x, \pm 1) = P_2(x) = \frac{3x^2 - 1}{2} \quad \ldots\ldots\ldots\ldots [a]$$

on top and bottom; P_k denotes the kth Legendre polynomial. Writing the harmonic polynomials[7]

$$V_n = \mathcal{J}(z^n), \qquad U_n = \mathcal{R}(z^n)$$

i.e.

$$V_1 = y \qquad U_2 = x^2 - y^2$$

$$V_3 = 3x^2y - y^3 \qquad U_4 = x^4 - 6x^2y^2 + y^4$$

$$V_5 = 5x^4y - 10x^2y^3 + y^5 \qquad U_6 = x^6 - 15x^4y^2 + 15x^2y^4 - y^6$$

. . . . . .

one verifies that

$$\Phi_a = \frac{1}{8} U_4 - \frac{1}{4} U_2 + \frac{1}{4} yV_3 \quad \ldots\ldots\ldots\ldots [a]$$

is the biharmonic polynomial which produces the prescribed $\sigma_y(x, \pm 1)$ traction, but creates, at the same time, an equally large

$$\sigma_x(\pm 1, y) = -\frac{3y^2 - 1}{2} \quad [\tau(\pm 1, y) = 0] \ldots\ldots [a]$$

stress on the left and right edges. In this case therefore the best one can do is to write

$$\Phi_{\text{approx}} = \frac{1}{2} \Phi_a$$

That leaves residuals

$$\sigma_y(x, \pm 1) = \frac{3x^2 - 1}{4}, \qquad \sigma_x(\pm 1, y) = -\frac{3y^2 - 1}{4}$$

on the four edges; these residuals no longer can be reduced by the biharmonic-polynomial approach, but must be removed by an eigenfunction method.[8,9]

The cases shown in Figs. 1(*b*, *c*) of this discussion illustrate the same fact. When self-equilibrating tractions, such as

$$\tau(x, \pm 1) = \pm \tilde{P}_1(x) \equiv \pm \int_{-1}^{x} P_2(\xi) d\xi = \pm \frac{x^2 - x}{2} \ldots [b]$$

or

$$\sigma_y(x, \pm 1) = P_4(x) = \frac{35x^4 - 30x^2 + 3}{8} \quad \ldots\ldots\ldots [c]$$

act on the horizontal edges of the square, the polynomial biharmonic functions

$$\Phi_b = \frac{1}{16} U_4 + y \left[-\frac{1}{80} V_5 + \frac{1}{12} V_3 + \frac{19}{240} V_1 \right] \ldots\ldots [b]$$

$$\Phi_c = \frac{7}{48} U_6 - \frac{15}{16} U_4 - 2U_2 + y \left[\frac{7}{16} V_5 + \frac{5}{6} V_3 - \frac{7}{12} V_1 \right] \ldots\ldots [c]$$

create stresses along the vertical edges, to wit

$$\sigma_x(\pm 1, y) = -\frac{3}{35} P_4(y) + \frac{13}{21} P_2(y);$$

$$\tau(\pm 1, y) = \mp 2\tilde{P}_2(y) \ldots\ldots [b]$$

$$\sigma_x(\pm 1, y) = 2P_4(y) - \frac{65}{3} P_2(y);$$

$$\tau(\pm 1, y) = \pm 35\tilde{P}_2(y) \ldots\ldots [c]$$

[6] There are still further types of approaches floating around in the literature.

[7] $\mathcal{R}$, $\mathcal{J}$ denote real and imaginary parts.

[8] "The Use of Self-Equilibrating Functions in Solution of Beam Problems," by G. Horvay and J. S. Born, Proc. Second U. S. Congress of Applied Mechanics, ASME, 1954, pp. 267–276.

[9] "Saint Venant's Principle: A Biharmonic Eigenvalue Problem," JOURNAL OF APPLIED MECHANICS, TRANS. ASME, vol. 79, 1957, pp. 381–386.

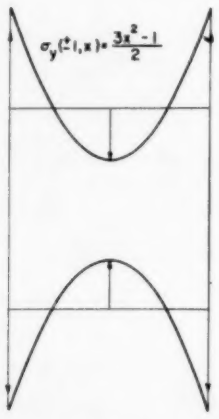

Fig. 1(*a*)

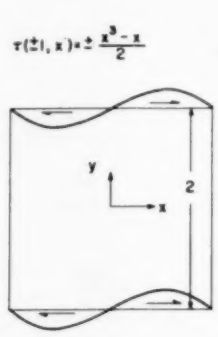

Fig. 1(*b*)

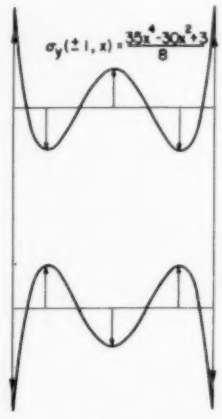

Fig. 1(*c*)

which again cannot be eliminated by biharmonic polynomials without restoring the tractions that produced them.

When the rectangle is narrow like a beam, then the story is the same, but the ending is different. Figs. 4(*a*) and 5(*a*) of Horvay and Born[8] illustrate the case of a rectangle with x, y-dimensions 2/5 and 2, respectively. A traction

$$\sigma_x\left(\frac{1}{5}, y\right) = 4(3y^2 - 1)$$

is applied; the three other edges are free. The maximum residual left by the biharmonic-polynomial solution on the short edges is found to be

$$\sigma_y\left(-\frac{1}{5}, \pm 1\right) = -1.73$$

as contrasted with the maximum stress in the rectangle

$$\sigma_y(1, 0) = -38.5$$

As in the previous cases, the self-equilibrating residuals cannot be eliminated by biharmonic polynomials (only an eigenfunction approach can eliminate them), but they may now be neglected in a first approximation. (In the reference, however, they are not neglected but are eliminated by means of a variationally determined eigenfunction expansion. The results so obtained are then compared with the results of a calculation where the variational method replaces the biharmonic-polynomial method from the outset and automatically suppresses the residuals along the edges; the second phase of the problem is thereby eliminated. The agreement of the results by the two methods is found to be very good.)

A. L. Ross,[10] **H. A. Eagle.**[11] In reading the author's solution for finding the coefficients $C_{mn} = 0$, it is indicated that it results from a unique solution of Equations [11], [16], [12], and [17]. However, an examination of, say, Equations [11] and [16] for a specific value of m, shows that there are n unknown coefficients C_{mn} and only two equations for their solution, which of course means that a unique solution cannot be determined from these equations alone. Of course, an examination of the results of the first example shows that for this problem the trivial solution, for $m > 2$, is indeed the unique and correct one. It therefore appears that a more detailed discussion of the method used in proving that these coefficients actually are zero is in order. The Recursion Relationship [8] and the two pairs of Equations [11], [16], [12], and [17] will be used to determine the coefficients of the three sections of the matrix shown as Fig. 2 of this discussion. The coefficients in the three regions will be determined by three distinct patterns of solution. For a matrix of $M \times N$ size the coefficients of Region I can be shown to be zero by the use of the Recursion Relationships [8] since all coefficients outside of the region, i.e., for $n > N$ or $m > M$ are assumed to be identically zero. In determining the coefficients of Region II, one makes use of Equations [11] and [16] to find the second and fourth columns and uses Equations [12] and [17] to find the first and third columns of this region. The coefficients of Region III are shown to be zero by a pattern along diagonals (Region III*a*) and four column rows (Region III*b*) and then progressing upward. Coefficients of Regions III*a* can be shown to be identically zero by the use of the Recursion Equation [8] as was done for Region I. The coefficients of Region III*b* can then be shown to be identically

[10] Principal Engineer, Aircraft Nuclear Propulsion Department, General Electric Company, Cincinnati, Ohio.

[11] Technical Engineer, Aircraft Nuclear Propulsion Department, General Electric Company.

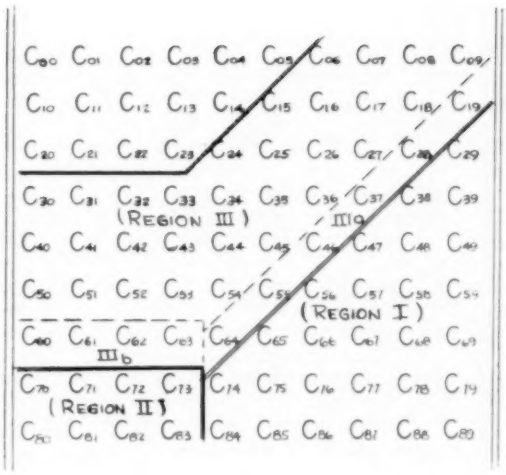

Fig. 2

zero in the same manner as was used for Region II. Proceeding in this manner, the coefficients in Regions I, II, III of the matrix can be shown to be identically zero. The remaining coefficients are then determined as outlined in a clear manner by the author.

C. J. Thorne.[12] It is well known that the real and imaginary parts of $f(z)$, $f(\bar{z})$, $\bar{z}f(z)$, and $zf(\bar{z})$ with $z = x + iy$ are biharmonic functions. With $f(z) = z^n/n!$ we have a unique set of biharmonic polynomials convenient under differentiation. It may be of interest to know that these polynomials have been tabulated for many values over the unit square.[13]

Author's Closure

The author wishes to thank Drs. Goodier, Horvay, Ross, Eagle, and Thorne for their helpful discussions. Besides, he wishes to point out that the sentence following Equation [17] on page 388 should read: "Equations [11] for $m \geqslant 3$ and [16]. . ." instead of "Equation [17] for $m \geqslant 3$ and [16]. . .".

The question of taking $C_{mn} = 0$ for $m \geqslant 3$ as unique solutions to the Equations [11], [16], [12], and [17] might well be answered by the Ross-Eagle proof, if we could only establish the fact that the matrix is finite and all the C_{mn} outside of the region of $n > N$ or $m > M$ are assumed to be identically zero. In fact, the matrix is finite and the question is where to draw the lines in our infinite matrix. Many investigators use a polynomial stress function up to $m + n = 5$, without giving any reasons for leaving out the terms of higher power which might be important.

Equations [11] for $m \geqslant 3$ and [16] for a particular value of m can be satisfied either by $C_{mn} = 0$ or by an infinite number of sets of solutions which correspond to an infinite number of combinations of boundary conditions. Although an alternative boundary condition of $\sigma_x = 0$ at the free end in Example 1 may be used to replace the self-equilibrating conditions, the number of combinations of boundary conditions is certainly not infinite. Moreover, although there are more than two unknowns in the two simultaneous Equations [11] and [16], the indeterminacy, however, can be removed if we take into account all the Equations

[12] U. S. Naval Ordnance Test Station, China Lake, Calif.

[13] "A Table of Harmonic and Biharmonic Polynomials and Their Derivatives," by C. J. Thorne, Supplement to Bulletin No. 39 of the Utah Engineering Experiment Station, University of Utah, November, 1949.

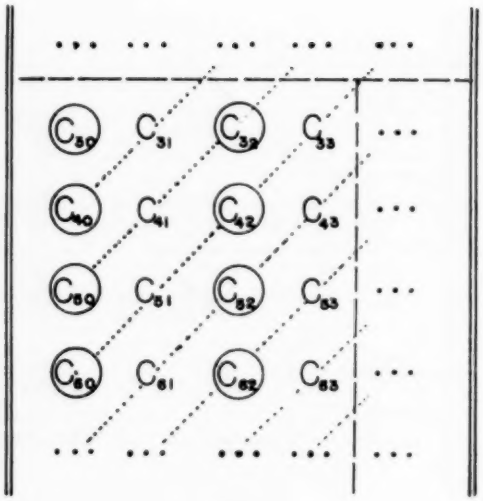

Fig. 3

[11] and [16] for $m = 3, 4, 5 \ldots, M$ (where M is a very large number or infinite) and the interdependence of the various C_{mn}. By successive substitutions from the recursion Equation [8], it is possible to express C_{mn} for $n \geqslant 4$ in terms of the two C_{mn} at the lower ends of the diagonals in the Matrix [4]. For example

$$C_{24} = -15C_{60} - 2C_{42},$$

and

$$C_{06} = 2C_{60} + \frac{1}{5} C_{42}.$$

Now, for $M - 2$ rows (below the dotted line in Fig. 3 of the discussion), we have $M - 2$ Equations [11] and [16], respectively, for $M - 2$ unknowns C_{m0} and C_{m2} respectively (shown by O in Fig. 3), i.e., the number of independent unknowns is now equal to the number of independent equations. The solution is thus

$$C_{m0} = C_{m2} = 0 \quad \text{for } m = 3, 4, 5 \ldots$$

unless the determinant of C_{m0} and C_{m2} of the powers of $x^m y^n$ in the $2(M - 2)$ equations is zero which is most unlikely. The same reasoning can be used to obtain $C_{mn} = 0$ in Equations [12] for $m \geqslant 3$ and [17].

Further support for $C_{mn} = 0$ for $m \geqslant 3$ and $n =$ even number can be rallied from the obvious fact that because of the asymmetric loadings at $y = \pm a$, the polynomial terms even in y must be excluded and, by virtue of Equation [16] or [8], C_{m0} for $m \geqslant 3$ must all be zero.

The author fully realizes the existence of many excellent methods other than the biharmonic polynomial approach, such as the method of complex potentials, the Donnell-Boley-Tolins method of successive approximation, variational principle, etc., as mentioned by various discussers. The complex stress function,

$$\phi = \text{Re} \sum_{n=2}^{N} [\bar{Z}(a_n + ib_n)Z^{n-1} + (c_n + id_n)Z^n],$$

($N = \infty$, theoretically) is an elegant, but more complex, way for representing a polynomial stress function of Equation [3]. Although it enjoys the advantage of being no longer subjected to the compatibility Equation [8], the expansion of, for instance, $\text{Re}[\bar{Z}(a_5 + ib_5)Z^4 + (c_5 + id_5)Z^5]$ into

$$(a_5 + c_5)x^5 - (3b_5 + 5d_5)x^4y - (2a_5 + 10c_5)x^3y^2 - (2b_5 - 10d_5)x^2y^3 - (3a_5 - 5c_5)xy^4 + (b_5 - d_5)y$$

is no simpler than the use of Equation [3] subjected to the restriction of Equation [8], which, for most of the time, is used to set one C_{mn} to zero by inspection when the other two coefficients in the Equation [8] are zero. Besides, to obtain σ_x, σ_y, and τ_{xy} from:

$$\sigma_x + \sigma_y = 4\text{Re}\psi'(Z)$$

and

$$\sigma_y - \sigma_x + 2i\tau_{xy} = 2[\bar{Z}\psi''(Z) + \chi''(Z)]$$

is certainly more tedious than to obtain Equation [5], [6], and [7] from Equation [3].

Since it is clearly indicated in the paper that the present method applies only to a long narrow rectangular beam under continuous loadings, we must rule out the case of a square plate or a rectangular strip having a small length-to-depth ratio; otherwise the influences of the extraneous end tractions could hardly get a chance to fade out, as are clearly illustrated in Dr. Horvay's discussion, and consequently the results would find little or no place to be held, by virtue of Saint Venant's principle as good approximations to the exact stress conditions in the beam.

Interaction Curves for Shear and Bending of Plastic Beams[1]

E. T. Onat.[2] The static analysis of perfectly plastic beams shows that bending usually predominates so that the concept of simple plastic hinges is sufficient for most cases. As the author's results indicate once more, the shearing action is of importance only for extremely short beams. Therefore it might seem at first that the establishment of approximate interaction curves for bending and shear of plastic beams is hardly justified since the structures in question cannot any longer be labeled as beams. However, the analysis of the plastic behavior of the beams under impulsive loading[3] indicates that shear action may be important even for technical beams at the initial stage of loading. Therefore any attempt to include the shear action into the analysis in an approximate manner (such as the author's) may be of great help for a better understanding of the dynamic behavior of beams. However, the author's approach to establish interaction curves for shear and bending is open to some objections.

The author states at the outset that the derivation of the interaction curve is first approached from the view of statically admissible stress fields. It is difficult to see that statically admissible fields are indeed used since no effort is made to extend the field beyond the critical section considered. Moreover, it is seen from Equations [4] and [1] that the stress-boundary conditions are violated at $y = \pm h$ since τ_{xy} is not zero there.

On the other hand, the assumption that the deformation in the critical section of the beam is the composite of a pure bending and uniform shear does not necessarily result in a kinematically admissible velocity field that leads to the rate of energy dissipa-

[1] By P. G. Hodge, Jr., published in the September, 1957, issue of the JOURNAL OF APPLIED MECHANICS, TRANS. ASME, vol. 79, pp. 453–456.

[2] Associate Professor of Engineering, Brown University, Providence, R. I.

[3] "Impact of Finite Beams of Ductile Metal," by P. S. Symonds and C. F. A. Leth, *Journal of the Mechanics and Physics of Solids*, vol. 2, 1954, p. 92.

tion given by Equation [16]. It is easily seen that, if no effort is made to extend the strain-rate field of Equation [15] beyond the critical cross section considered, no claim should be made that this strain-rate field is kinematically admissible. As a matter of fact, the success of the interaction curves for bending and stretching of plastic beams[4] is related to the fact that physically significant kinematically admissible velocity fields may be found which can be associated with the desired rates of curvature and extension at the critical cross section under consideration. Even the simple plastic hinge does not correspond to a discontinuity which acts within the section but it spreads out over a distance equal to the depth of the beam.[5,6] It can be stated in conclusion that the introduction of generalized stresses and strains and associated strain rates cannot alone constitute a basis for approximate analysis.

Two-dimensional stress and velocity fields must be considered in order to obtain a realistic inclusion of shear effects.

Author's Closure

The author wishes to thank Professor Onat for his illuminating comments on the possible effect of shear in dynamic plasticity problems. Certainly, it was not the author's intention to imply that the approximate treatment in the paper was a completely accurate answer to the problem. Naturally, two-dimensional stress and velocity fields would be preferable, if they could be found. In fact, to be strictly accurate, three-dimensional fields must be constructed.

However, the author cannot agree with the rather discouraging picture painted by Professor Onat. Just as a simple bending theory is sufficiently accurate for many beam problems, so may the theory presented in the paper be useful in cases for which shear is of some importance. In view of the fact that very few two-dimensional solutions are available, it would seem worth while to at least consider the proposed approximate theory. Certainly, it would be desirable to compare the results of the approximate theory with a more exact theory and with experiments in both static and dynamic problems. Until this has been done, it is difficult to make a final assessment of the value of the approximate theory.

Forced Vibration of Systems With Nonlinear, Nonsymmetrical Characteristics[1]

F. R. Arnold.[2] Contrary to the author's statement, his method does not yield an exact solution for the free-vibration case ($P = 0$) of the nonlinear problem. Even for this case for which the exact range and period of oscillation may be determined by ordinary methods, the exact solution is not a pure harmonic as is assumed, and the amplitude of the harmonic is only approximate in that it is one half the range of oscillation. At best, this free-vibration "solution" is characterized by a range of oscillation equal in magnitude to the exact one and a period equal to the exact period. The details of the exact motion are not there. It is entirely possible that another method would come closer to the details of the motion and be slightly off in amplitude for any selected frequency of vibration.

The author may be interested in papers by K. Klotter and others on the Ritz method as listed in the bibliography of the paper by the writer in the JOURNAL OF APPLIED MECHANICS, December, 1955.

The author's method requires that the free-vibration solution be known first. This is often quite a trick to obtain. The Ritz method needs nothing but the differential equation as the starting point.

The method as presented is, however, another interesting approach to approximate solutions of nonlinear problems which well deserve all the methods that can be devised.

Author's Closure

The author wishes to thank Professor Arnold for his comments. In the expression $F(a) = \omega_a{}^2 a$ given in the paper, a is half the range of free vibration and ω_a the corresponding frequency. In the case of a bilinear characteristic or a characteristic of the form $f(x) = \alpha x + \beta x^3$, the relationship between a and ω_a can be determined exactly by direct methods. It is then assumed that a is the amplitude of the one-term approximation for free vibrations. The graphical construction then yields an approximate value for one half the range of forced vibration. In the special case $P = 0$, however, the method gives an exact value for the magnitude of one half the range of oscillation. It was in this sense that the term "exact solution" was used in the paper. As Professor Arnold states, the method does not give any indication regarding the details of the motion. The method has been put forward as an improvement of the Martienssen method and, as such, it has the usual limitations of one-term approximate solutions.

A Photoelastic Study of Maximum Tensile Stresses in Simply Supported Short Beams Under Central Transverse Impact[1]

A. J. Durelli.[2] This paper is a new contribution in the field of wave propagation, a field which is being explored very intensively at present in many laboratories in many countries. The particular experience of the authors will certainly be found useful by other investigators.

A few comments, basic in nature, seem appropriate:

1 The authors give 154 psi as a fringe value for the Castolite they used. This is considerably less than the average value 215 psi given by Flynn (reference of the paper) for Castolite. Although the authors do not give any details about the way the fringe value was determined, they mentioned that SR-4 strain gages were used for the purpose of calibration. The basic question to be raised is the interpretation of the readings of the SR-4 gage cemented to a plastic model. The authors are referred to the

[4] "The Influence of Axial Forces on the Collapse Load of Frames," by E. T. Onat and W. Prager, Proceedings First Midwest Conference on Solid Mechanics, University of Illinois, Urbana, Ill., 1953, pp. 40–42.

[5] "The Effect of Shear on the Plastic Bending of Beams," by D. C. Drucker, JOURNAL OF APPLIED MECHANICS, TRANS. ASME, vol. 78, 1956, pp. 509–514.

[6] "Plane Plasticity," by B. B. Hundy, Paper MW/B/54 of the Solid Mechanics Group of the Mechanical Working Division, British Iron & Steel Research Association.

[1] By S. Mahalingam, published in the September, 1957, issue of the JOURNAL OF APPLIED MECHANICS, TRANS. ASME, vol. 79, pp. 435–439.

[2] Associate Professor of Mechanical Engineering, Stanford University, Stanford, Calif.

[1] By A. A. Betser and M. M. Frocht, published in the December, 1957, issue of the JOURNAL OF APPLIED MECHANICS, TRANS. ASME, vol 79, pp. 509–514.

[2] Supervisor, Armour Research Foundation, and Professor, Illinois Institute of Technology, Chicago, Ill. Mem. ASME.

work of A. B. J. Clark[3] who reports that electrical strain gages exhibit only about 75 per cent of the resistance change one would calculate using the gage factor specified by the manufacturer, when the gages are cemented on CR-39 bars. According to Clark this difference may be attributed to the greater stiffness of the gage wire grid compared to the plastic. It is possible that a similar phenomenon took place in the calibration conducted by the authors. If this is true, their fringe value should be raised accordingly and the fringe value so obtained will be very close to Flynn's.

2 The authors make some considerations on the presence of isotropic points and to substantiate them they refer the reader to Fig. 2 in the paper. This figure appears to be a light-field photograph, although this is not mentioned specifically in the paper. If this is true, no conclusions about the isotropic points can be made from the photograph since isotropic points are shown only in dark-field photographs. The only statement that can be made about the white bands preceding the $^1/_2$-order dark fringe in the light-field photograph is that the maximum shear stress at the points of the white bands is less than $^1/_2$ the fringe value.

3 In Fig. 6 the straight lines have been extrapolated by the authors to intersect the axis of the abscissa. If this procedure is correct, it would indicate that for the $(Ld)^{-1/2}$, corresponding to the points of intersection, the beams under the impact show no stress. It seems more reasonable that all the curves should pass through the origin.

4 No consideration has been given by the authors to the fact that the beam supports used in the test may restrain the free movement of the beam ends. This restriction may have an important influence on the maximum stresses in the beam.

5 The two lowest points corresponding to beams $L = 3.4$ in. and $L = 5.0$ in. in Fig. 6 have not been plotted by the authors in Fig. 5. If this had been done, the end of the curves corresponding to $L = 5.0$ in. and $L = 3.4$ in. in Fig. 5 would have had a different shape.

6 The authors do not explain why they selected photoelasticity as the approach to the research program reported in the paper. Since the authors calibrated using an electrical resistance-wire strain gage and since they reported values of stress occurring only at one point, it appears that the whole research could have been conducted using one strain gage cemented at this point. This approach probably would have been simpler and more accurate than photoelasticity and in addition it would have permitted the authors to use materials other than plastics.

Author's Closure[4]

After this paper was submitted for publication, we found that good agreement between the experimental and the theoretical results could be obtained by modifying the theory so that $W = P\delta/2$ instead of $W = P\delta$, and $2f = 215$ psi (Flynn's value) instead of $2f = 154$ psi (Betser's value). This observation was made in our laboratory and independently arrived at by Dr. P. D. Flynn who also suggested the possibility that the gage effect reported by Clark and referred to by Dr. Durelli could perhaps resolve the conflict between the two different fringe values.

These observations, and a good many more, were presented at the Berkeley meeting, June 1957, by the writer, in a rather complete discussion of the problems still to be solved in connection with the dynamic fringe value and a suitable theory for beams under impact. A complete discussion of these topics must be deferred for a separate paper, since they are not only lengthy but also involve new experimental work which is still incomplete. At this time we merely wish to point out that Clark's conclusions do not provide an adequate explanation. We have gone into the question of gage factors for strain gages mounted on plastics in some detail and our findings are reported in a paper before the SESA.[5]

This, we believe, answers the only essential point in Dr. Durelli's discussion, unless it be to add that, if he has difficulties determining an isotropic point from a photograph with a bright background, there is nothing to prevent him from examining the negative.

[3] "Static and Dynamic Calibration of Photoelastic Model Material, CR-39," by A. B. J. Clark, *Proceedings of the Society for Experimental Stress Analysis*, vol. 14, 1956, p. 195.

[4] Dr. Betser is now in Israel and the closure was written by Dr. Frocht.

[5] The paper, "On the Effect of Current on Gage Factor," by M. M. Frocht, D. Landsberg, and B. C. Wang, was presented at the Spring Meeting of the SESA, May, 1958, in Cleveland, Ohio.

A Type of Flame-Excited Oscillation in a Tube[1]

By A. A. Putnam.[2] The author is to be congratulated on a fine addition to the literature concerning fundamental studies of combustion acoustics. He has advanced a quite reasonable explanation of the production of sound by a flat flame above a grid. It is believed, however, that the type of flat flame described in the paper has been observed earlier and reported by Putnam and Dennis.[3] The oscillation induced by a cellular flame in the author's equipment is believed to be similar to that reported by Markstein and Squire,[4] even though they did not use a grid.

In the foregoing work reported,[3] the equipment was much more squat than the author's, being about 8 in. diam by 18 in. long, and was effectively closed at both ends. The observed ranges of oscillation agreed with those that would have occurred in the Rijke gauze-tone type of experiment, as do the ranges of data which the author reports. For this reason, the flame was treated by Putnam and Dennis[3] as a diffuse heat source supplying heat to the grid, and the rate of loss of heat from the grid was analyzed. It was found that, with the proper choice of time lag, the oscillations could be explained. In the author's treatment, a time lag of the necessary magnitude is inserted automatically in the assumptions leading to Equation [2]. These results emphasize an important factor; many combustion acoustic phenomena can be explained in a variety of ways if a time-lag term of the proper magnitude is included. Thus it is often difficult to prove a theory correct, or to choose between two alternative theories. In any case, it has been shown again that in low-velocity systems a "rough" calculation based on the Rayleigh criterion does an excellent job of explaining the observable phenomenon.

The author comes to an interesting conclusion in that "the least stable frequency is always one such that the flame is positioned within the second quarter wave length from the downstream end of the tube." However, it is difficult to visualize physically the reason for this conclusion. Further comment on this point would be appreciated. For instance, this statement could be interpreted

[1] By J. J. Bailey, published in the September, 1957, issue of the JOURNAL OF APPLIED MECHANICS, vol. 24, TRANS. ASME, vol. 79, pp. 333–339.

[2] Assistant Chief, Aeronautics and Thermodynamics Division, Battelle Memorial Institute, Columbus, Ohio. Mem. ASME.

[3] "Burner Oscillations of the Gauze-Tone Type," by A. A. Putnam and W. R. Dennis, *Journal of the Acoustical Society of America*, vol. 26, 1954, p. 716.

[4] "On the Stability of a Plane Flame Front in Oscillating Flow," by G. H. Markstein and W. Squire, *Journal of the Acoustical Society of America*, vol. 27, 1955, p. 416.

to mean that, for a grid in the upstream quarter of the combustor, the fundamental mode of oscillation is preferred to all higher modes in all instances.

Author's Closure

The author wishes to thank Dr. Putnam for his discussion.

It was not intended to do more than mention the occurrence of the cellular instability as it was not investigated in any detail. It is, perhaps, quite possible that the theory of Markstein and Squire[4] might apply.

The flat-flame phenomenon described seems very likely to be essentially the same as that reported by Putnam and Dennis.[3] However, the explanation proposed by Putnam and Dennis does not apply. Attempts to excite oscillations by means of a heated gauze screen showed that, for comparable screen temperatures, the driving of the flame is of quite a different order of magnitude from the Rijke-type driving; and in the author's experiment the Rijke-type action of the heated gauze was quite inadequate to produce the results reported.

Dr. Putnam is correct in pointing out that a time lag is inserted in the assumptions of Equation [2], and indeed the time lag does seem to be of the correct order of magnitude. The assumptions, however, are suggested as at least very plausible in that they are based on what is observed in the case of steady flows. More detailed information, though doubtless desirable, was not available.

In general, the least stable frequency is the one such that the flame is positioned within the second quarter wave length from the downstream end of the tube. This is so because most of the losses are by acoustic radiation and increase rapidly with frequency. Therefore, in general, the lowest mode excited is the one heard. This does mean that the fundamental is the most unstable frequency with the holder in the upstream half of the tube. Observations of the fundamental were not made, however, because oscillations of this type always built up extremely rapidly, leading almost immediately to flash-back. Nevertheless the frequency initially heard under those conditions was apparently the fundamental as predicted.

Negative Group Velocities in Continuous Structures[1]

Miguel C. Junger.[2] The author introduces his analysis of negative group velocities by stating that they ". . . apparently have not been noticed in continuous media before." Actually Tolstoy and Usdin[3] discuss their existence in elastic plates, and Oliver[4] reports this phenomenon in cylindrical rods, also on theoretical grounds. Furthermore, the former paper gives three references to analyses of crystal vibrations by Mindlin, going back to 1951, which imply the existence of group and phase velocities of opposite sign.

The physical interpretation proposed by Tolstoy and Usdin[3] is that there exist ". . .slow wave packets in which the wave troughs and crests will be traveling, at a rather high speed, . . . toward the source." The packets themselves travel, of course, away from the source. This interpretation agrees with Crandall's discussion of steady-state conditions.

The expression "negative group velocities" is misleading, as it suggests that energy is moving toward the source. It is clearer, even though clumsy, to speak of a "group velocity of sign opposite to that of the phase velocity."

Author's Closure

The author wishes to thank Dr. Junger for pointing out the prior publication of Tolstoy and Usdin.[5] He agrees that "group velocity of sign opposite to that of the phase velocity" is a more precise appellation than either "negative group velocity" or "negative phase velocity" which was favored by Tolstoy and Usdin.[3]

It is interesting that in uniform plates and rods this phenomenon apparently occurs only in the second and certain of the higher modes, whereas in the systems with a massless elastic foundation treated in the paper[5] the anomaly occurs in the fundamental mode.

Photothermoelasticity: An Exploratory Study[1]

M. L. Williams.[2] The authors are to be commended for introducing a new application of a standard technique. In the field of aeronautical engineering especially, the subject of thermal-stress analysis of necessity has been receiving an increasing amount of attention and therefore an additional mode of attack is most welcome.

At the risk of emphasizing the obvious, it is perhaps worth stressing the fact that, within the elastic range and over the range of constant material properties, the principal thermal-stress difference may be determined in the specimen without specific knowledge of the internal temperature distribution. From the plane-stress relations

$$\sigma_1 = [E/(1 - \nu^2)][e_1 + \nu e_2 - (1 + \nu)\alpha\Delta T]$$

$$\sigma_2 = [E/(1 - \nu^2)][e_2 + \nu e_1 - (1 + \nu)\alpha\Delta T]$$

one easily finds upon computing $\sigma_1 - \sigma_2$, the quantity proportional to the number of isochromatic fringes, that

$$n = (t/f)(\sigma_1 - \sigma_2) = [E/(1 + \nu)][e_1 - e_2]$$

which is seen to be independent of the temperature-rise distribution. It is this fact, namely, that the respective thermal expansions or strains without stress identically disappear, which distinguishes the simplicity of the photothermoelastic approach from that of more conventional methods, and leads directly to a rapid evaluation of the (usually critical) boundary thermal stresses.

Authors' Closure

We greatly appreciate Professor Williams' interest in our paper and the fact that he has explicitly indicated a rather unique aspect of the photothermoelastic technique.

---

[1] By S. H. Crandall, published in the December, 1957, issue of the JOURNAL OF APPLIED MECHANICS, TRANS. ASME, vol. 79, pp. 622–623.

[2] Partner, Cambridge Acoustical Associates, Cambridge 38, Mass.

[3] "Wave Propagation in Elastic Plates: Low and High Mode Dispersion," by I. Tolstoy and E. Usdin, *Journal of the Acoustical Society of America*, vol. 29, 1957, pp. 37–42.

[4] "Elastic Wave Dispersion in a Cylindrical Rod by a Wide-Band Short-Duration Pulse Technique" by Jack Oliver, *Journal of the Acoustical Society of America*, vol. 29, 1957, pp. 189–194.

[5] See also, "The Timoshenko Beam on an Elastic Foundation," by Stephen H. Crandall, Third Midwestern Conference on Solid Mechanics, University of Michigan Press, Ann Arbor, Mich., 1957, pp. 146–159.

[1] By G. Gerard and A. C. Gilbert, published in the September, 1957, issue of the JOURNAL OF APPLIED MECHANICS, TRANS. ASME, vol. 79, pp. 355–360.

[2] Associate Professor, California Institute of Technology, Pasadena, Calif.

The Forced Lateral Oscillations of Trailers[1]

L. Segel.[2] The authors are to be complimented on their comprehensive derivation of the equations of motion of the single-pivot towed trailer. The writer would like to point out, however, that if linearizing assumptions are made immediately, by virtue of restricting the lateral velocity of the trailer to be small relative to the forward velocity, it becomes feasible to handle trailer dynamic problems which possess more than one degree of freedom. For example, stability studies have been made at the writer's laboratory, in connection with an Army research and development contract, which treated not only the motions of a four-wheeled trailer but the motions of the towing vehicle as well. The resulting equations were sixth-order and represented a four-degree-of-freedom system.

When high-order multidegree-of-freedom systems are examined for stability or the degree of stability, it is generally sufficient to determine the frequency and damping of the resulting modes of motion. For the case which has been treated in the paper, it is apparent that the one-degree-of-freedom trailer, with lateral oscillation of the hitch point, is always stable. More complicated systems can be unstable, however.

The writer also would like to point out that the authors' observation that the damping is inversely proportional to the forward velocity is a general truth which applies to the lateral motions of all vehicles guided by forces arising from the pneumatic tire. Physically this can be seen by noting that a rolling tire moving with a lateral velocity v is operating at a slip angle α where

$$\tan \alpha = \frac{v}{V}$$

and V = forward velocity of the tire. Thus a tire side force is produced which opposes the lateral velocity, and this basically constitutes the origin of the damping forces that appear in the equations of motion. Since the opposing force is a function of slip angle α, this force decreases linearly with increasing forward velocity per unit value of lateral velocity v. A more complete exposition of this point has been reported elsewhere.[3,4]

H. Ziegler.[5] In the introduction to their paper the authors state: "The first attempts to solve this problem were made by Williams and Ziegler, both making special assumptions about the forces transmitted from the road to the wheel. Both of these solutions state that the response of the trailer (i.e., snaking) does not depend upon the forward velocity of the trailer, a result not in agreement with observations."

As far as the writer is concerned, this statement is based on a section of his textbook on Mechanics[6] where he treats an extremely simplified version of the problem as an example for the well-known stability criteria of Routh and Hurwitz. At the end of this section the writer states that the actual problem of snaking is more complicated and that lateral oscillations actually only occur beyond a critical speed.

The last remark is not a conjecture but has been established in a detailed investigation[7] followed by a supplement,[8] both published in 1938. These papers are not referred to in the writer's textbook, and thus they escaped the notice of the authors.

Fundamentally, the treatment of the writer (which, incidentally, also includes trailers with two axles) differs in two respects from the treatment of the authors:

(a) In both cases the side force on the wheel is assumed to be proportional to the slip angle. The authors, starting from more recent experimental results and using a first approximation, treat this force as independent of the driving velocity, while the writer assumed this force proportional to the magnitude of the slip velocity. This is a minor difference, and it is evident that the qualitative character of the results is not affected by it.

(b) The authors state, "the resulting motion depends on both the towing vehicle and the trailer. If snaking of the trailer occurs, both elements of the system take part in the motion." Afterward, and in spite of this statement, they prescribe the lateral motion of the towing point in the form of a harmonic oscillation with given amplitude and a frequency proportional to the forward velocity of the towing vehicle. Here lies the essential difference between the authors' and the writer's treatments. As follows the authors' own statement, the oscillation of the towing point depends on the trailer as well as on the towing vehicle. Hence this oscillation cannot be prescribed without replacing the snaking problem by an entirely different one. Also, the assumption that the frequency of this oscillation is proportional to the speed of the towing vehicle is arbitrary. Since the towing vehicle is part of the oscillating system, influenced by the motion of the trailer, the actual problem consists in an investigation of the free oscillations of the system consisting of towing vehicle and trailer under the influence of the forces at the wheels. This is the method the writer adopted in his treatment.

On the authors' assumptions, one winds up with a resonance phenomenon. There is snaking for all values of the forward velocity, accentuated more or less under the speed corresponding to resonance. This speed, however, remains unpredictable in view of the arbitrary assumptions made concerning the excitation.

On the basis of the writer, one obtains a stability problem with self-excited oscillations appearing beyond a critical forward speed. This critical speed depends on the data of the system, and there are many ways of improving the stability by modifying these data.

Since the results of either investigation are entirely different in character, it should be a simple matter to decide between them on the basis of practical observations or experiments. The writer's results were in good agreement with experiments[9] which preceded and actually suggested his investigation.

Authors' Closure

The authors wish to thank Professor Ziegler and Mr. Segel for their interesting discussions.

Both authors cite work which has been carried out to study the stability of the combined towing vehicle and trailer. The solu-

---

[1] By A. Slibar and P. R. Paslay, published in the December, 1957, issue of the JOURNAL OF APPLIED MECHANICS, TRANS. ASME, vol. 79, pp. 515–519.

[2] Cornell Aeronautical Laboratory, Inc., of Cornell University, Buffalo, N Y.

[3] "Research in the Fundamentals of Automobile Control and Stability," by L. Segel, *Transactions of the Society of Automotive Engineers*, vol. 65, 1957 pp. 527–540.

[4] "Research in Automobile Stability and Control and in Tire Performance," five papers presented to The Institution of Mechanical Engineers on November 13, 1956, by W. F. Milliken, Jr., D. W. Whitcomb, L. Segel, W. Close, C. L. Muzzey, and A. G. Fonda.

[5] Professor of Applied Mechanics, Swiss Federal Institute of Technology (ETH), Zurich.

[6] "Mechanik," by H. Ziegler, Birkhäuser, Basel, second edition, vol. 3, 1956, p. 132.

[7] Die Querschwingungen von Kraftwagenanhängern," by H. Ziegler, *Ingenieur Archiv*, vol. 9, 1938, pp. 96–108.

[8] "Der Einfluss von Bremsung und Steigung auf die Querschwingungen von Kraftwagenanhängern," by H. Ziegler, *Ingenieur-Archiv*, vol. 9, 1938, pp. 241–243.

[9] Carried out by the Forschungsinstitut für Kraftfahrwesen und Fahrzeugmotoren (Prof. Kamm) at Stuttgart.

tion to this problem is of considerable importance in the proper design of vehicles. While the papers referred to lead to a better understanding of the problem, the most severe handicap at present in solutions of this type is that the effects of steering of the towing vehicle are not taken into account.

There does not appear to be much known regarding the human elements of steering. One might, for example, assume the driver attempts to maintain the motion of the towing vehicle in a straight line and then, for prescribed external excitation (possibly wind gusts), solve for the steering necessary to fulfill that requirement. This steering will, in turn, influence the motion of the tow point and, if a trailer is attached, influence the motion of the trailer. In the authors' opinion, it is necessary to establish some criteria before solutions regarding the combined motion of towing vehicle and trailer can be expected to predict actual performance.

Clearly, the treatment of the latter problem becomes quite complex and any means of simplifying the analysis would be worth while. It is for this reason that our investigation was carried out. The results of the authors' analysis give the displacement amplitude at any point on the trailer due to amplitude excitation at the tow point of the trailer and the resulting force system at the tow point. This means that for any problem which involves constant forward velocity motion of a towing vehicle, with known properties on which are superposed perturbation motions, the effect of attaching a trailer can be determined since the trailer properties at the tow point are known from our analysis. In this way, for example, cases where the trailer behaves as a vibration absorber can be predicted. In fact, when the towing vehicle characteristics are properly prescribed, the case where no steering occurs should yield the solutions referred to by the discussers for constant forward velocity.

The method of analysis outlined above has the further advantage that the properties of the towing vehicle and trailers are known separately, and the relative merits of attaching different trailer models to a specified towing vehicle can be evaluated rapidly.

A further point concerning the presence of a system instability is that the problem considered here is always stable so that the excitation that causes instability must originate in the towing vehicle, and the effects of this instability will appear in the forces which are applied by the towing vehicle to the trailer tow point.

Two instabilities that occur for a trailer of the type considered are not included in our analysis; although the first is important for design, they occur where (*a*) the towing vehicle is being severely braked, and (*b*) the towing vehicle is backed up. In each case the trailer and towing vehicle "jackknife."

Dynamic Response of Beams and Plates to Rapid Heating[1]

M. A. Brull.[2] The results presented in this paper are most interesting since they indicate the conditions under which inertia forces become important in the thermoelastic analysis of beams and plates. There is apparently, however, a small discrepancy in the statement of the boundary conditions for a simply supported plate subjected to a "thermal moment." In Equations 8[*a*] the authors state that the boundary conditions are

$$\frac{\partial^2 v}{\partial x^2}(0, z, t) = \frac{\partial^2 v}{\partial x^2}(a, z, t) = \frac{\partial^2 v}{\partial z^2}(x, 0, t) = \frac{\partial^2 v}{\partial z^2}(x, b, t) = 0$$

If the stress couples are defined as

$$M_x = -\int_{-h/2}^{h/L} \sigma_x y dy, \quad M_z = -\int_{-h/2}^{h/2} \sigma_z y dy \quad \text{and} \quad M_{xz} = -M_{zx} = -\int_{-h/2}^{h/2} \sigma_{xz} y dy$$

the appropriate stress-strain relations are

$$M_x = D\left[\frac{\partial^2 v}{\partial x^2} + \nu \frac{\partial^2 v}{\partial z^2}\right] + (1 + \nu)M_T$$

$$M_z = D\left[\frac{\partial^2 v}{\partial z^2} + \nu \frac{\partial^2 v}{\partial x^2}\right] + (1 + \nu)M_T$$

$$M_{xz} = D(1 - \nu)\frac{\partial^2 v}{\partial x \partial z}$$

where

$$M_T = \alpha E \int_{-h/2}^{h/2} T y dy$$

It is then clear that for a simply supported edge at $x = 0$ the traction-free condition requires $M_x = 0$ or

$$D\frac{\partial^2 v}{\partial x^2} = -(1 + \nu)M_T$$

Thus a proper statement of the boundary condition is

$$D\frac{\partial^2 v}{\partial x^2}(0, z, t) = -(1 + \nu)M_T(0, z, t)$$

$$D\frac{\partial^2 v}{\partial x^2}(a, z, t) = -(1 + \nu)M_T(a, z, t)$$

$$D\frac{\partial^2 v}{\partial z^2}(x, 0, t) = -(1 + \nu)M_T(x, 0, t)$$

$$D\frac{\partial^2 v}{\partial z^2}(x, b, t) = -(1 + \nu)M_T(x, b, t)$$

In connection with plate problems with such time-dependent boundary conditions, the very useful general technique of solution proposed by Berry and Naghdi[3] should not be overlooked.

E. L. McDowell.[4] The condensed nature of the paper makes it difficult to assess the true value of the results presented. That there are instances of rapid heating of beams and plates for which inertia effects must be considered is not to be doubted. However, the precise magnitude of the inertia effect indicated in the paper is subject to question.

Since a beam may be considered as a degenerate case of a rectangular plate, the writer will restrict his comments to the analysis of the plate problem formulated by the authors. Consider a simply supported rectangular plate, under a uniform heat input suddenly applied over one face. This uniform heat input gives rise to a uniform thermal moment M_T, and one is led to consider the motion of a rectangular plate subjected to uniform moments M_T, distributed along the edges and otherwise free from load.

The static solution, disregarding inertia effects and initial con-

[1] By B. A. Boley and A. D. Barber, published in the September, 1957, issue of the JOURNAL OF APPLIED MECHANICS, TRANS. ASME, vol. 79, pp. 413–416.

[2] Associate Professor of Applied Mechanics, University of Pennsylvania, Philadelphia, Pa.

[3] "On the Vibration of Elastic Bodies Having Time-Dependent Boundary Conditions," by J. G. Berry and P. M. Naghdi, *Quarterly of Applied Mathematics*, vol. 14, April, 1956, pp. 43–50.

[4] Senior Research Engineer, Armour Research Foundation, Chicago, Ill. Mem. ASME.

ditions, is readily constructed from the known solution[5] of a rectangular plate, simply supported along the edges and bent by uniform moments along two opposite edges. In view of this known solution, the center static deflection for the present problem is

$$(v_{st})_{max} = M_T \frac{2a^2}{\pi^3 D} \sum_{m=1,3,5}^{\infty} (-1)^{\frac{m-1}{2}} \frac{1}{m^3} \left[\frac{\alpha_m \tanh \alpha_m}{\cosh \alpha_m} + \frac{b^2}{a^2} \frac{\beta_m \tanh \beta_m}{\cosh \beta_m} \right]$$

where

$$\alpha_m = \frac{m\pi b}{2a}, \qquad \beta_m = \frac{m\pi a}{2b}$$

The static deflection just given bears little resemblance to the static deflection presented in Equation [9] of the paper. As a matter of fact, for the case of a square plate, the foregoing deflection is about three fourths of the deflection found by the authors.

From the form of Equation [9] of the paper, it appears that the procedure of derivation used by the authors was to assume a double Fourier expansion of both the thermal moment and the deflection, i.e.

$$M_T = \sum_{n=1}^{\infty} \sum_{m=1}^{\infty} c_{nm} \sin \frac{n\pi x}{a} \sin \frac{m\pi z}{b}$$

$$v_{st} = \sum_{n=1}^{\infty} \sum_{m=1}^{\infty} d_{mn} \sin \frac{n\pi x}{a} \sin \frac{m\pi z}{b}$$

The coefficients c_{nm} are readily determined, and direct substitution in the equilibrium Equation [7] immediately determines the coefficients d_{nm}. Evaluation of the resulting series for v_{st} at the center of the plate leads to Equation [9] of the paper. Observe, however, that this assumed form of the solution violates the stated boundary conditions of the problem in that the edges are now free from moments.

Since it appears that the static solution presented by the authors violates the stated boundary conditions one may presume that their dynamic solution also will suffer this defect. It seems that the ratio of these "solutions" can yield only a very doubtful appraisal of the effect of inertia under rapid heating.

It also should be pointed out that Equations [7], [7*a*], [8*a*], [8*b*] should be multiplied on the right-hand side by

$$(1 - \nu), \quad \left(\frac{1+\nu}{2}\right), \quad (-1/D), \quad \text{and} \quad \left(\frac{1+\nu}{2}\right)$$

respectively, to obtain a formulation of the problem consistent with their reference (5).[6]

Authors' Closure

The authors wish to thank the discussers for bringing to their attention some errors in Equations [7] and [8] of the paper; in checking back to their original work, they fortunately found that the calculations were indeed performed on the basis of the correct equations, and that therefore these errors are merely typographical. Aside from this, the doubts raised by the second discusser are unfounded.

The static solution of the plate problem was obtained by Maulbetsch's method.[7] The deflection can be easily expressed either in terms of circular trigonometric functions along one Cartesian co-ordinate direction in the plane of the plate and hyperbolic in the other, or in terms of circular functions in both directions; the latter method was adopted in the paper. It should be noted that, contrary to the second discusser's suggestion, there is no contradiction between the use of a double sine series (whose second derivations ostensibly are zero at $x = 0, a$ and $y = 0, b$) and a nonzero moment (which would require nonzero values for these derivatives). The sine series (for example, for the edge $x = a$) converges in fact to the correct value at $x = a - 0$, though it converges, at $x = a$ itself, to the average (i.e., zero) of the values at $x = a - 0$ and $x = a + 0$. The behavior of Fourier series in the neighborhood of such discontinuities is well known;[8] the present approach was adequate for the purposes of the computations, required for the paper, pertaining to the interior of the plate.

It was pointed out, at the time of the oral presentation of this paper, by the chairman of the session, Dr. R. Plunkett, that both the static and dynamic solutions may be constructed with the aid of isothermal solutions corresponding to prescribed edge moments. Such moments must be applied over all four edges and not, as the second discussion seems to imply, over two opposite edges only.

[5] "Theory of Plates and Shells," by S. Timoshenko, McGraw-Hill Book Company, Inc., New York, N. Y., 1940, pp. 199–202.

[6] "Similarity Laws for Stressing Heated Wings," by H-S. Tsien, *Journal of the Aeronautical Sciences*, vol. 20, January, 1953, pp. 1–11.

[7] See "Theory of Plates and Shells," by S. Timoshenko, McGraw-Hill Book Co., Inc., New York, N. Y., 1940, p. 176ff.

[8] See, for example, "Fourier Series and Boundary Value Problems," by R. V. Churchill, McGraw-Hill Book Co., Inc., New York, N. Y., 1941.

Stress-Strain Relations and Vibration of a Granular Medium[1]

C. W. Thurston.[2] It may be of interest to extend the derivation of the differential stress-strain relations given by the authors to the case in which the array of spheres is subjected to an arbitrary initial state of stress. This may be done by the following method suggested to the writer by the authors: The unit cube (authors' Fig. 1) is taken to be in a sequence of states of strain in each of which only one component, in turn, is different from zero. For each state, the relations between all the components (zero and nonzero) of strain and the corresponding components of relative displacement between centers of contiguous spheres are then written in accordance with the expressions immediately preceding the authors' Equations [16] and [17]. This gives, in each case, six equations in terms of the 18 (unknown) components of displacement. Three more equations are obtained from the conditions for the equilibrium of moments (authors' Equations [10]) in which the authors' Equations [12] are inserted. The final nine equations are the conditions of compatibility of the relative displacements (authors' Equations [11]). The solution of each set of 18 equations (12 of which are common to each set) yields the components of relative displacement in terms of the different nonzero strain components; hence the sum of the solutions of the 6 sets yields the relations between each component of displacement and all the components of strain.

The stress and strain may now be related by substituting the expressions found in the foregoing into the authors' Equations [12] and the result, in turn, into the authors' Equations [9]. The final expressions, referred to the principal axes of the unit cube, are of the form appropriate to a triclinic crystal

$$d\sigma_m = c_{mn} d\epsilon_n \qquad m, n = 1, 2, \ldots, 6$$

[1] By J. Duffy and R. D. Mindlin, published in the December, 1957, issue of the JOURNAL OF APPLIED MECHANICS, TRANS. ASME, vol. 79, pp. 585–593.

[2] Instructor in Civil Engineering, Columbia University, New York, N. Y.

where c_{mn} represents the symmetric array ($c_{mn} = c_{nm}$) of 21 independent coefficients whose elements are

$$4\sqrt{2}Rc_{11} = c_{xx} + c_{xy} + s_{xx} + s_{xy} - 2(\bar{s}_{xx}{}^2\Lambda_{xx} + \bar{s}_{xy}{}^2\Lambda_{xy} - 2\bar{s}_{xx}\bar{s}_{xy}\Lambda_{yz})/\Delta$$

$$4\sqrt{2}Rc_{12} = c_{xy} - s_{xy} + 2(\bar{s}_{xy}{}^2\Lambda_{xy} + \bar{s}_{yz}\bar{s}_{zx}\Lambda_{xy} - \bar{s}_{xx}\bar{s}_{xy}\Lambda_{yz} - \bar{s}_{xy}\bar{s}_{yz}\Lambda_{zx})/\Delta$$

$$4\sqrt{2}Rc_{14} = 2(\bar{s}_{yy}\bar{s}_{xy}\Lambda_{xy} - \bar{s}_{yy}\bar{s}_{zx}\Lambda_{yz})/\Delta + 2(s_{yy} + s_{yz})(\bar{s}_{zx}\Lambda_{xy} - \bar{s}_{xy}\Lambda_{zx})/\Delta$$

$$4\sqrt{2}Rc_{15} = \bar{c}_{xx} - \bar{s}_{xx} + 2(\bar{s}_{xx}\bar{s}_{xy}\Lambda_{xz} - \bar{s}_{xx}\bar{s}_{zx}\Lambda_{xy})/\Delta + 2(s_{zz} + s_{xz})(\bar{s}_{zx}\Lambda_{xz} - \bar{s}_{xy}\Lambda_{yz})/\Delta$$

$$4\sqrt{2}Rc_{16} = \bar{c}_{xy} + \bar{s}_{xy} - 2[\bar{s}_{xx}\bar{s}_{zx}\Lambda_{xz} + (s_{xz} + s_{xy})\bar{s}_{xy}\Lambda_{xy}]/\Delta + 2(s_{xx}\bar{s}_{zx} + \bar{s}_{xx}s_{xy} + \bar{s}_{xx}\bar{s}_{xy})\Lambda_{yz}/\Delta$$

$$4\sqrt{2}Rc_{44} = c_{yz} + s_{yz} + 2s_{yy} - 2[\bar{s}_{yy}{}^2\Lambda_{xy} + (s_{yy} + s_{yz})^2\Lambda_{yz} - 2(s_{yy} + s_{yz})\bar{s}_{yy}\Lambda_{xz}]/\Delta$$

$$4\sqrt{2}Rc_{45} = 2[(s_{yy} + s_{yz})\bar{s}_{zx}\Lambda_{yz} + (s_{zz} + s_{zx})\bar{s}_{yy}\Lambda_{yz}]/\Delta - 2[\bar{s}_{yy}\bar{s}_{zx}\Lambda_{zx} + (s_{yy} + s_{yz})(s_{zz} + s_{zx})\Lambda_{xy}]/\Delta$$

where

$$\Lambda_{ij} = s_{ii}s_{jj} + s_{jj}s_{kk} + s_{kk}s_{ii} + s_{kk}{}^2 - \bar{s}_{kk}{}^2 + 2(s_{ii} + s_{jj})s_{jk} + 2(s_{jj} + s_{kk})s_{ij} + 4s_{jk}s_{ki}$$

$$\Lambda_{ij} = \bar{s}_{ii}\bar{s}_{jj} + \bar{s}_{kk}(s_{ii} + s_{jj} + 2s_{ij})$$

$$\Delta = 8s_{jk}s_{ki}s_{ij} + 2(s_{ii}s_{jj}s_{kk} - \bar{s}_{ii}\bar{s}_{jj}\bar{s}_{kk}) + (s_{ii}{}^2 - s_{jj}{}^2)(s_{jj} + s_{kk} + 2s_{jk}) + 4s_{ii}(s_{ij}s_{jk} + s_{jk}s_{ki}) + (s_{jj}{}^2 - s_{kk}{}^2)(s_{kk} + s_{ii} + 2s_{ki}) + 4s_{jj}(s_{jk}s_{ki} + s_{ki}s_{ij}) + (s_{kk}{}^2 - s_{ii}{}^2)(s_{ii} + s_{jj} + 2s_{ij}) + 4s_{kk}(s_{ki}s_{ij} + s_{ij}s_{jk}) + 2(s_{ii}s_{jj} + s_{jj}s_{kk} + s_{kk}s_{ii})(s_{jk} + s_{ki} + s_{ij})$$

and

$$c_{ij} = 1/C_{ij} + 1/C_{ij}' \qquad \bar{c}_{ij} = 1/C_{ij} - 1/C_{ij}'$$

$$s_{ij} = 1/S_{ij} + 1/S_{ij}' \qquad \bar{s}_{ij} = 1/S_{ij} - 1/S_{ij}'$$

$$s_{ii} = 1/S_{ii} + 1/S_{ii}' \qquad \bar{s}_{ii} = 1/S_{ii} - 1/S_{ii}'$$

The remaining coefficients may be written by cyclical interchange of subscripts, as follows

$c_{11} \rightarrow c_{22} \rightarrow c_{33}$ $\quad$ $c_{12} \rightarrow c_{23} \rightarrow c_{31}$

$c_{14} \rightarrow c_{25} \rightarrow c_{36}$ $\quad$ $c_{15} \rightarrow c_{26} \rightarrow c_{34}$

$c_{16} \rightarrow c_{24} \rightarrow c_{35}$ $\quad$ $c_{44} \rightarrow c_{55} \rightarrow c_{66}$

$c_{45} \rightarrow c_{56} \rightarrow c_{64}$

Influence of Width on Velocities of Long Waves in Plates[1]

E. Volterra.[2] In a recent report (1),[3] E. C. Zachmanoglou and the writer developed a second approximation of the method of internal constraints by taking into account second-order terms in the equation of constraints and satisfying the requirement that normal stresses vanish on the surface of the bar or of the plate under consideration. This approach has the main advantage that,

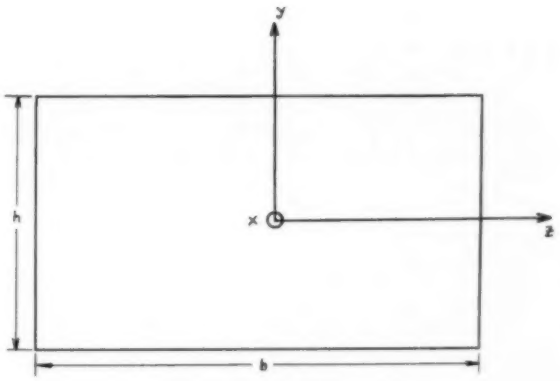

Fig. 1

while the degree of accuracy of the general method is increased, the equations of motion and corresponding boundary conditions, which univocally define the unknown functions of the problem, maintain the same simple mathematical form as in the cases in which only linear terms of the equations of constraint are taken into consideration (which cases were discussed in previously published papers (2–8)).

This method gives, in the case of a bar of rectangular cross section, Fig. 1 of this discussion, the following dispersion equation for longitudinal waves

$$\left(\frac{h}{L}\right)^4\pi^4\beta^2\left[\left(\frac{c}{c_0}\right)^2 - \frac{(1-\sigma)}{(1+\sigma)(1-2\sigma)}\left(1 - \frac{4}{3}\frac{\sigma^2}{(1-\sigma)}\right)\right]\left[\left(\frac{c}{c_0}\right)^2 - \frac{k}{2(1+\sigma)}\right]^2 - \left(\frac{h}{L}\right)^2\pi^2(1+\beta^2)\frac{(1-\sigma)}{(1+\sigma)(1-2\sigma)}\left[\left(\frac{c}{c_0}\right)^2 - \frac{k}{2(1+\sigma)}\right]\left[\left(\frac{c}{c_0}\right)^2 - \frac{1}{(1-\sigma^2)}\left(1 - \frac{2}{3}\sigma^2\right)\right] + \frac{\left(\frac{c}{c_0}\right)^2 - 1}{(1+\sigma)^2(1-2\sigma)} = 0 \qquad \ldots [1]$$

In Equation [1] σ is Poisson's ratio, $\beta = b/h$, L the wave length, h and b the dimensions of the rectangular cross section of the bar, k has the same significance as Timoshenko's shear coefficient, c is the phase velocity, and $c_0 = (E/\rho)^{1/2}$ the bar velocity. The dispersion equation for longitudinal waves in the case of plane stress is obtained from Equation [1] by letting $\beta \rightarrow 0$ and is given by

$$\left(\frac{h}{L}\right)^2 = \frac{1}{\pi^2}\frac{1}{(1-\sigma)^2}\frac{\left(\frac{c}{c_0}\right)^2 - 1}{\left[\left(\frac{c}{c_0}\right)^2 - \frac{k}{2(1+\sigma)}\right]\left[\left(\frac{c}{c_0}\right)^2 - \frac{1}{(1-\sigma^2)}\left(1 - \frac{2}{3}\sigma^2\right)\right]} \qquad \ldots [2]$$

In the plane-strain case the theory based on the method of internal constraints gives the following dispersion equation for longitudinal waves

[1] By D. C. Gazis and R. D. Mindlin, published in the December, 1957, issue of the JOURNAL OF APPLIED MECHANICS, TRANS. ASME, vol. 79, pp. 541–546.

[2] Professor of Engineering Mechanics, University of Texas, Austin, Texas. Mem. ASME.

[3] Numbers in parentheses refer to the Bibliography at the end of this discussion.

$$\left(\frac{h}{L}\right)^2 = \frac{1}{\pi^2}\frac{(1-\sigma)}{(1+\sigma)(1-2\sigma)}\frac{\left(\frac{c}{c_0}\right)^2 - \frac{1}{(1-\sigma^2)}}{\left[\left(\frac{c}{c_0}\right)^2 - \frac{k}{2(1+\sigma)}\right]\left[\left(\frac{c}{c_0}\right)^2 - \frac{(1-\sigma)}{(1+\sigma)(1-2\sigma)}\left(1 - \frac{2}{3}\frac{\sigma^2}{(1-\sigma)^2}\right)\right]} \quad \ldots\ldots\ldots [3]$$

In the case of a bar of rectangular cross section the theory based on the second approximation of the method of internal constraints gives the following dispersion equation for flexural waves

$$(r_{z/L})^2 = \frac{1}{4\pi^2}\frac{k}{2(1+\sigma)}\frac{\left(\frac{c}{c_t}\right)^2}{\left[\left(\frac{c}{c_0}\right)^2 - \frac{k}{2(1+\sigma)}\right]\left[\left(\frac{c}{c_0}\right)^2 - (1+\epsilon)\right]} \quad \ldots\ldots [4]$$

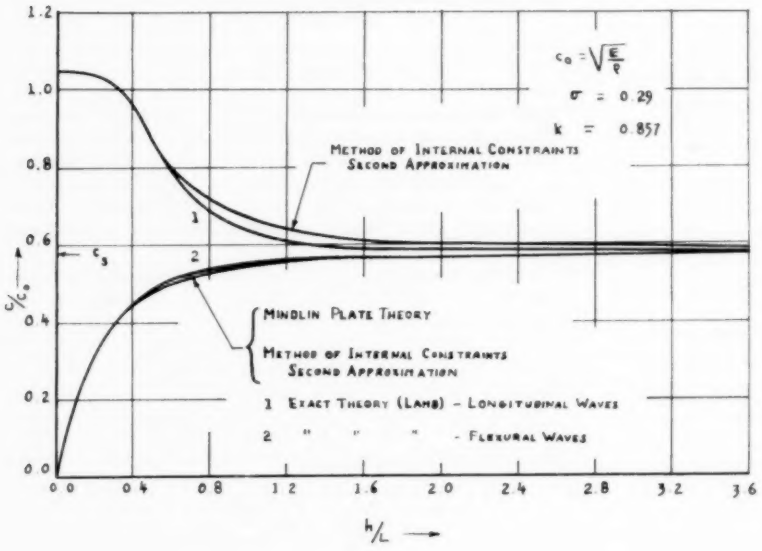
$c_0 = \sqrt{\frac{E}{\rho}}$
σ = 0.29
k = 0.857
METHOD OF INTERNAL CONSTRAINTS SECOND APPROXIMATION
1
2
c_s
MINDLIN PLATE THEORY
METHOD OF INTERNAL CONSTRAINTS SECOND APPROXIMATION
1 EXACT THEORY (LAMB) - LONGITUDINAL WAVES
2 " " " - FLEXURAL WAVES
c/c₀
h/L
0.0 0.4 0.8 1.2 1.6 2.0 2.4 2.8 3.2 3.6
0.0 0.2 0.4 0.6 0.8 1.0 1.2

Fig. 2 Phase velocity of flexural and longitudinal waves in plane strain

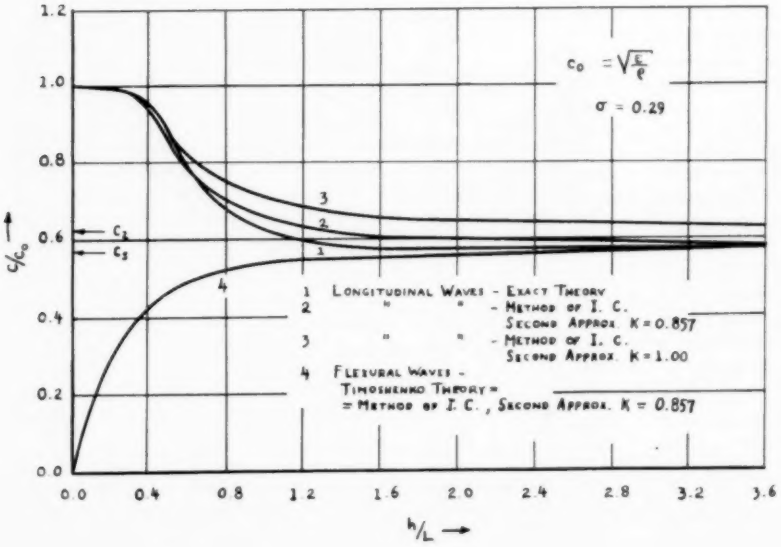
$c_0 = \sqrt{\frac{E}{\rho}}$
σ = 0.29
c_1
c_2
1 LONGITUDINAL WAVES - EXACT THEORY
2 " " - METHOD OF I. C. SECOND APPROX. K = 0.857
3 " " - METHOD OF I. C. SECOND APPROX. K = 1.00
4 FLEXURAL WAVES - TIMOSHENKO THEORY = = METHOD OF I. C., SECOND APPROX. K = 0.857
c/c₀
h/L
0.0 0.4 0.8 1.2 1.6 2.0 2.4 2.8 3.2 3.6
0.0 0.2 0.4 0.6 0.8 1.0 1.2

Fig. 3 Phase velocity of longitudinal and flexural waves in plane stress

The quantity

$$\epsilon = k \frac{\sigma^2}{2(1+\sigma)} \frac{I_y}{I_z}$$

is the correction of the Timoshenko theory taking into account the effects of the dimensions of the bar in the z-direction. r_z is the radius of gyration of the cross section with respect to the z-axis. The dispersion equation for flexural waves in the case of plane stress is obtained from Equation [4] by letting $\epsilon \to 0$ and is given by

$$(r_{z/L})^2 = \frac{1}{4\pi^2} \frac{k}{2(1+\sigma)} \frac{\left(\frac{c}{c_0}\right)^2}{\left[\left(\frac{c}{c_0}\right)^2 - \frac{k}{2(1+\sigma)}\right]\left[\left(\frac{c}{c_0}\right)^2 - 1\right]} \quad \ldots\ldots [5]$$

Equation [5] is the same dispersion equation of the classical Timoshenko Theory (9).

In the plane-strain case the theory based on the method of internal constraints gives the following dispersion equation for flexural waves

$$\left(\frac{h}{L}\right)^2 = \frac{3}{\pi^2} \frac{k}{2(1+\sigma)} \frac{\left(\frac{c}{c_0}\right)^2}{\left[\left(\frac{c}{c_0}\right)^2 - \frac{k}{2(1+\sigma)}\right]\left[\left(\frac{c}{c_0}\right)^2 - \frac{1}{(1-\sigma^2)}\right]} \quad \ldots\ldots [6]$$

Equation [6] coincides with the dispersion equation obtained by Mindlin (10).

In Figs. 2 and 3, herewith, the results given by the method of internal constraints from Equations [2], [3], [5], and [6] in the case of plane strain and plane stress are compared with the exact theory given by Lamb (11). The value for k was taken equal to 0.857 which value is the ratio of the velocities of the Rayleigh surface waves to the distortional waves in an infinite medium.

Bibliography

1 "A Second Approximation of the Method of Internal Constraints as Applied to Dynamic Problems," by E. C. Zachmanoglou and E. Volterra, OOR Technical Report No. 6, May 20, 1957, Contract No. DA-30-155-ORD-709, Project No. 454.13, Rensselaer Polytechnic Institute, Troy, N. Y.

2 "The Equations of Motion for Curved Elastic Bars Deduced by the Use of the Method of Internal Constraints," by E. Volterra, *Ingenieur-Archiv*, 23 Band, 6 Heft, 1955, pp. 402–409.

3 "A One-Dimensional Theory of Wave-Propagation in Elastic Rods Based on the Method of Internal Constraints," by E. Volterra, *Ingenieur-Archiv*, 23 Band, 6 Heft, 1955, pp. 410–420.

4 "Some Applications of the Method of Internal Constraints to Dynamic Problems," by E. Volterra, Proceedings of the September, 1955, Madrid Colloquium of the International Union of Theoretical and Applied Mechanics on Deformation and Flow of Solids, Springer-Verlag, 1956, pp. 236–250.

5 "The Equations of Motion for Elastic Plates and Cylindrical Shells Deduced by the Use of the Method of Internal Constraints," by E. Volterra, OOR Technical Report No. 3, February 20, 1956, Contract No. DA-30-115-ORD-709, Project No. 454.13, Rensselaer Polytechnic Institute, Troy, N. Y.

6 "Eigenvibrations of Curved Elastic Bars According to the Method of Internal Constraints," by E. Volterra, *Ingenieur-Archiv*, 24 Band, 5 Heft, 1956, pp. 317–329.

7 "The Equations of Motion for Curved and Twisted Elastic Bars Deduced by the Use of the Method of Internal Constraints," by E. Volterra, *Ingenieur-Archiv*, 24 Band, 6 Heft, 1956, pp. 392–400.

8 "Free and Forced Vibrations of Straight Elastic Bars According to the Method of Internal Constraints," by E. Volterra and E. C. Zachmanoglou, *Ingenieur-Archiv*, 25 Band, 6 Heft, 1957, pp. 424–436.

9 "On the Correction for Shear of the Differential Equations for Transverse Vibrations of Prismatic Bars," by S. P. Timoshenko, *The Philosophical Magazine*, vol. 91, Sixth Series, 1921, pp. 742–746.

10 "Influence of Rotatory Inertia and Shear on Flexural Motions of Isotropic, Elastic Plates," by R. D. Mindlin, JOURNAL OF APPLIED MECHANICS, TRANS. ASME, vol. 73, 1951, pp. 31–38.

11 "On Waves in an Elastic Plate," by H. Lamb, *Proceedings of the Royal Society of London*, series A, vol. 93, 1917, pp. 114–118.

Nodal Patterns of the Free Flexural Vibrations of Stiffened Plates[1]

G. B. Warburton.[2] The authors have presented some very interesting results correlating theory and experiment for the natural frequencies and nodal patterns for flexural vibrations of stiffened plates. However, the writer considers that in the section of the paper on "Compounded Normal Modes of Flexural Vibrations," the authors have confused two phenomena. These are:

(*a*) *The combining or compounding of normal modes.* When two normal modes of vibration of a plate have natural frequencies which are approximately equal, these two modes can be excited simultaneously by a suitable driving frequency, that is, a driving frequency nearly equal to the two natural frequencies, applied at a suitable point in the plate; i.e., a point which does not coincide with the nodal lines of either nodal pattern. In theory, an infinite number of different compounded nodal patterns can be obtained, and the resulting pattern will depend on the exact value of the exciting frequency and on the location of the point of excitation. In Fig. 4, the authors obtain such a pattern for a stiffened plate.

(*b*) *Normal modes with nonparallel nodal patterns.* The writer here refers to those normal modes of isotropic, square plates for which the nodal pattern does not approximate to lines parallel to the edges. Unlike the compounded normal modes of (*a*), there is a unique nodal pattern for each mode of type (*b*). Chladni gave examples of these modes for a square plate with free edges, and many later writers have reported theoretical and experimental investigations of these modes. Such normal modes may occur for isotropic square or almost square plates when the boundary conditions in the X and Y-directions are identical, e.g., all edges free, or all edges fixed, or two adjacent edges fixed and the others free, with the exception that the modes do not exist in isotropic plates with all edges simply supported.

The authors' method of treating the vibrations of an orthogonally stiffened plate is to replace it by an equivalent orthotropic plate of uniform thickness. The writer considers that, unless a plate is isotropic as well as having identical boundary conditions in the X and Y-directions, normal modes of nonparallel form cannot exist; thus such modes cannot exist for an orthogonally stiffened plate irrespective of the boundary conditions.

The authors state that the writer in an earlier paper[3] indicated that the combining phenomenon did not occur in isotropic square plates with simply supported edges. The writer considers that the authors have misinterpreted his views; his paper considered approximate methods of obtaining the natural frequencies of flexural vibration of isotropic, rectangular plates with various

[1] By W. H. Hoppmann, II, and L. S. Magness, published in the December, 1957, issue of the JOURNAL OF APPLIED MECHANICS, TRANS. ASME, vol. 79, pp. 526–530.

[2] Head, Postgraduate School of Applied Dynamics, Department of Engineering, University of Edinburgh, Edinburgh, Scotland.

[3] "The Vibration of Rectangular Plates," by G. B. Warburton, Proceedings of The Institution of Mechanical Engineers, vol. 168, 1954, pp. 371–381.

boundary conditions for normal modes, including those with nonparallel nodal patterns. The possibility of compounded normal modes occurring in practice was only mentioned briefly. The statement that the nodal lines of simply supported square plates were always parallel to the edges of the plate was contained in sections of the paper discussing the existence of nonparallel normal modes of type (*b*) and was not intended to infer that normal modes could not be compounded for this boundary condition.

For an isotropic square plate with simply supported edges the natural frequencies of the modes $m|n$ and $n|m$ would be identical. In practice, because of imperfections in the plate, these frequencies would be nearly equal. A small lack of uniformity in the lengths of the sides could be investigated theoretically, i.e., $a/b = 1 + \delta$, where $0 < \delta \ll 1$, but a small lack of uniformity of (*a*) the elastic properties in the principal directions, (*b*) the thickness, or (*c*) the supports, would have a similar effect. For excitation of the type used in the authors' experiments, compounded nodal patterns could be predicted for an exciting frequency in the neighborhood of the two natural frequencies, provided that the point of excitation did not coincide with a nodal line of either normal mode.

Authors' Closure

The authors wish to express their appreciation for the discussion of their paper by Professor Warburton. However, they must take exception to two points in his remarks. Reference to a confusion is a purely subjective matter and may be argued, but the use of the word "misinterpretation" can rightly be questioned in terms of what Professor Warburton said in his paper, at least the portion that is germane to the problem of simply supported rectangular plates, and what is contained in the paper of the authors. In meeting these issues the authors are not questioning the general remarks either in the writer's discussion or in his papers. They do wish, however, to emphasize the fact that their paper deals theoretically with a rectangular simply supported plate and experimentally only with a square plate with simple supports. As the writer agrees in his discussion, the experimental results agree with the theory. To investigate this relationship was one of the prime objectives of the paper.

The authors would welcome results of a theoretical or experimental study of the effects of "a small lack of uniformity of (*a*) the elastic properties in the principal directions, (*b*) the thickness, or (*c*) the supports."

Again we thank Professor Warburton and take this opportunity to acknowledge the very interesting work he has done in his study of plates.

Turbulence in Small Air Jets at Exit Velocities up to 705 Feet per Second[1]

Mark V. Morkovin.[2] At the time when the investigations reported in the paper were in progress there existed no rigorous method for interpretation of unsteady hot-wire data at subsonic speeds. Recent analysis,[3] based on calibrations of Spangenberg,[4] indicates that considerable errors may be incurred if the "incompressible" sensitivity laws for longitudinal fluctuations u' are used beyond a Mach number of 0.2–0.3. The sensitivity formulas[3] which take compressibility into account (and which have been tested at supersonic speeds) show that the Mach-number range 0.5–1.2 is indeed most difficult to probe with a hot-wire anemometer.

The original paper did not disclose sufficient information (e.g., sensitivity formulas used, wire overheat, stagnation temperature of the jets, and the temperature in the surrounding air, and so on) which would enable us to assess the foregoing errors in the different velocity regions (potential core, transition region, fully developed flow). We present instead, Figs. 1(*a*) and 1(*b*), the relative variations with Mach number and overheat of the nondimensional electrical sensitivities[5] with respect to vorticity fluctuation (turbulence), $\Delta e_\tau/\bar{e}$, with respect to entropy fluctuation (temperature-density spottiness), $\Delta e_\sigma/\bar{e}$, and with respect to sound, $\Delta e_\pi/\bar{e}$. The ratios of the sensitivities do not depend on the particular circuit constants (not given) but are functions of the wire material and Reynolds number. Figs. 1(*a*) and 1(*b*) were computed with the author's wire in mind; namely, 0.0003 in. platinum −20 per cent iridium wire, $^1/_{16}$ in. long. The temperature coefficients of resistivity were taken as $\alpha_r = 0.00085$ per deg C, $\beta_r = 0$, and the nonlinearity of King's law with overheat was disregarded.

At a given flow and overheat position of the hot wire, the total response consists of superposition of the separate responses in which, however, the correlation between the three modes of fluctuations must be taken into account. In flows, where entropy fluctuations arise as a result of compressibility effects in a shear layer, the correlation of the vorticity and entropy fluctuations is generally high. The correlation between sound and the other two fluctuation modes is usually negligible because of the difference in their propagation rates. As a matter of fact, the smallness[6] of $\Delta e_\pi/\Delta e_\sigma$ in Fig. 1(*b*) indicates, that inside the shear flow, the contribution of the sound to the total signal is generally negligible.

There are likely to be three sources of temperature spottiness[7] in the author's experiments: (*a*) The spottiness carried by the "free stream" from the settling chamber, which bears the imprint of the entropy history of the air supply and is here unknown. (*b*) The boundary layer in the wooden nozzle brings about a temperature stratum with

$$\Delta T \sim \frac{(\gamma - 1)M^2}{2\left(1 + \frac{\gamma - 1}{2} M^2\right)} T_0$$

i.e., approximately 7 per cent of absolute stagnation temperature at a Mach number of 0.6. Perturbations of such a stratum result in temperature fluctuations roughly proportional to the above increment ΔT, so that we may expect spottiness σ' on the order of $0.01\Delta T$ to $0.10\ \Delta T$ for the fluid lumps which had been in this boundary layer. (*c*) Finally, the mixing between the core of the

[1] By L. W. Lassiter, published in September, 1957, issue of the JOURNAL OF APPLIED MECHANICS, TRANS. ASME, vol. 79, pp. 349–354.

The work on which this note is based was supported by the United States Air Force through the Air Force Office of Scientific Research and Development Command under Contract AF 18(600)-1121.

[2] Research Scientist, Department of Aeronautics, The Johns Hopkins University, Baltimore, Md. Mem. ASME.

[3] "Fluctuations and Hot-Wire Anemometry in Compressible Flows," by M. V. Morkovin, AGARDograph No. 24, NATO, Paris, November, 1956.

[4] "Heat Loss Characteristics of Hot-Wire Anemometers at Various Densities in Transonic and Supersonic Flow," by W. G. Spangenberg, NACA Tech. Note No. 3381, May, 1955.

[5] Here Δe_τ is the rms voltage response to a velocity fluctuation u' of 1 per cent of local mean velocity U and $\bar{e}$ is the corresponding mean voltage across the wire. Similarly, Δe_σ is the response to entropy fluctuations of 1 per cent of the specific heat at constant pressure, C_p, or more conveniently, to 1 per cent nonisentropic rms changes in temperature or density relative to their absolute values. Finally, Δe_π represents the rms voltage response to plane sound waves, with 1 per cent isentropic density fluctuation, oriented at an angle $\cos^{-1}(n_x)$ relative to the local velocity vector (see reference 3, section 3).

[6] To appreciate this fully, we note that 1 per cent sound fluctuation as defined here corresponds to sound level of 157 decibels, while 1 per cent entropy fluctuation to 2.93 deg C rms fluctuation.

[7] "Thoughts on Supersonic Wind Tunnels With Low Free-Stream Disturbances," by M. V. Morkovin, Johns Hopkins Univ. Rept., Nov., 1957; AFOSR Tech. Note TN 56-540, ASTIA Document No. AD 110-359.

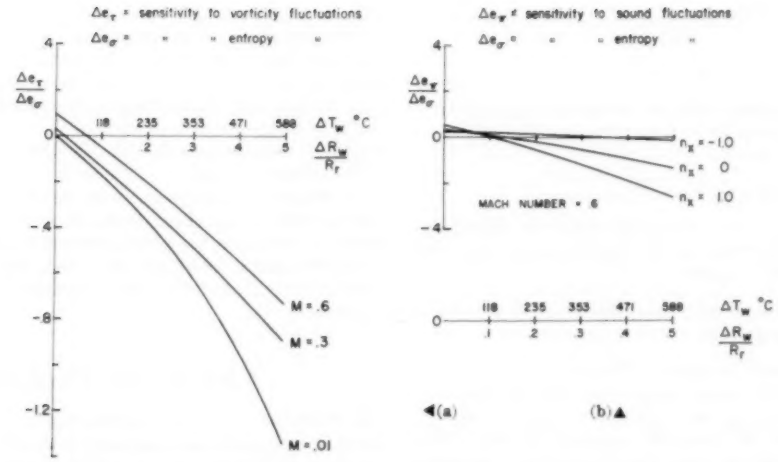

Fig. 1 Relative sensitivities to flow fluctuations in a jet in free atmosphere of a 0.0003-in. platinum-20 per cent iridium hot wire. (ΔT_w = overheat in deg C based on temperature coefficient of resistivity of 0.00085 and a recovery temperature T_r = 293 deg K.)

jet and the ambient air will result in entropy-temperature fluctuations roughly proportional to the difference of the static temperature between the two media (here unknown). In many cases, this mixing constitutes the most important source of temperature spottiness as schlieren and shadowgraph pictures of jets indicate.

The conditions at $x/D = 7$ where the peak of velocity fluctuations (i.e., $u'/U(x) \sim 0.165$) occurred—see author's Figs. 4(*a*) and 2(*a*)—were considered. With a wire heated to twice its cold temperature, i.e., $\Delta R_w/R_r \sim 0.25$, an error on the order of 10 per cent would have been committed if a temperature spottiness $\Delta T'/T(x)$ of 0.0045 were present and were neglected. That would have corresponded to an absolute temperature fluctuation of approximately 1.35 deg C. Temperature fluctuations of this magnitude are likely to occur in jets at $\mathbf{M} \sim 0.6$, judging from shadowgraphs and schlieren pictures.

Besides the errors arising from the disregard of temperature fluctuations as above, errors due to changes in sensitivities with Mach number might have been present. Thus the vorticity sensitivity at $\Delta R_w/R_r = 0.25$ decreased by nearly 40 per cent between $\mathbf{M} = 0.01$ and $\mathbf{M} = 0.6$. If then, the "incompressible" sensitivity were used[8] (and no entropy-temperature sensitivity), an underestimate of the vorticity fluctuation of nearly 40 per cent would result. At lower $\Delta R_w/R_r$ values, this overestimate would have been worse. In particular, at $\Delta R_w/R_r \sim 0.07$ ($\Delta T_w \sim 82$ deg C) the sensitivity to vorticity vanishes[9] and measurement at this overheat alone would be meaningless.

Summing up, we have reason to believe that the interpretation of the anemometer data may have caused changes comparable in magnitude to those which were ascribed to the true high-speed effect. It is unfortunate that the author's careful efforts should have been made less meaningful by previously accepted erroneous procedures of interpretation.

[8] At the time the author's work was in progress, reference[3] was not in existence and the NACA hot-wire research in the subsonic region was generally based on the analysis of Appendix F of NACA Tech. Note No. 2843 by J. C. Laurence and L. G. Landes. This analysis disregarded the observed variation of the heat-loss law with Mach number and the presence of stagnation temperature fluctuations (due to velocity or temperature changes). Furthermore, it used no-flow conditions for calibration, thus incurring errors from free-convection anomalies.

[9] The corresponding conditions of *zero* vorticity sensitivity for a platinum-10 per cent rhodium wire or a tungsten wire at $\mathbf{M} = 0.6$ occur at higher values of $\Delta R_w/R_r$; namely, from 0.25 to 0.55, depending upon the Reynolds number of the wire. Hence the choice of platinum-20 per cent iridium wire in this case was fortunate on this account at least.

Superharmonic Oscillations as Solutions to Duffing's Equation as Solved by an Electronic Differential Analyzer[1]

T. K. Caughey.[2] The author is to be congratulated on a most interesting paper which should provide a stimulus to further analysis of Duffing's equation.

Despite the amount of analysis of Duffing's equation, it is only within recent years that studies have been made of superharmonics. Hayashi (1948) (4)[3] and Young and Hess (1954) (2) pointed out that the harmonic solution of Duffing's equation is unstable in the vicinity of $\Omega = 1/n$, $n = 2, 3, 4 \ldots$. Both Dr. Burgess (1) and the writer (9) have analyzed the superharmonic of order 3, but to the best of the writer's knowledge, no analysis has yet been presented for superharmonics of other orders.

The writer is presently engaged in a study of superharmonic of orders other than the third, and finds that in a Duffing system with cubic nonlinearity:

1 For small enough damping superharmonics always exhibit jumps.

2 Superharmonics of orders other than the third cannot be described by a two-term approximation if damping is present.

[1] By C. P. Atkinson, published in the December, 1957, issue of the JOURNAL OF APPLIED MECHANICS, TRANS. ASME, vol. 79, pp. 520–525.

[2] California Institute of Technology, Pasadena, Cal.

[3] Numbers in parentheses refer to Bibliography in original paper.

For example, the superharmonic of order five can be represented by

$$X = A \cos rt + B \cos (3rt + a) + C \cos (5rt + b)$$

3 Even-order superharmonics are always accompanied by a nonperiodic term. For example, the superharmonic of order two can be represented by

$$X = A \cos rt + B \cos (2rt + b) + C$$

As will be appreciated readily, the complexity of the analysis increases rapidly with the order of the superharmonic, the third order being the notable exception.

With specific reference to the paper, the writer would like to make the following comments:

1 In Fig. 3, the arrows indicating jumps are not parallel to the $|Q_3|$-axis. The writer is greatly surprised at this and can only suppose that the frequency was varied rather rapidly, so that, during the duration of the jump the frequency changed appreciably. If this is indeed the case, then it is not too surprising that the results do not agree with Dr. Burgess' results, since his analysis was for constant frequency.

2 In Fig. 7, $q_{max} = Q_1 + Q_n$ is plotted against frequency and the results appear to support the author's hypothesis concerning the "harmonic backbone." From the point of analysis, however, it would appear to be difficult to justify this particular choice for q_{max}, except in the case where $Q_n > Q_1$.

3 The writer takes exception to the description of superharmonics as being sustained free oscillation, since sustained free oscillations are impossible in a system with dissipation. Superharmonics are forced oscillation maintained by the cross-modulation products arising out of the nonlinearity.

Author's Closure

The author thanks Dr. Caughey for his discussion and welcomes the excellent, though necessarily brief, summary of Dr. Caughey's present investigations into the field of nonlinear resonance.

The author must admit that the term "sustained free vibrations" is self-contradictory. Dr. Caughey is certainly right in calling these superharmonic oscillations "forced oscillations." The fact that these superharmonics have a frequency which is the frequency of the free vibrations of the system led the author to use the expression "sustained free vibrations."

Dr. Caughey suggests that the mechanism for maintaining superharmonics in forced oscillations is "cross-modulation products arising out of the nonlinearity." That is the best explanation the author has seen for the generation of superharmonics. It suggests a study of Duffing's equation with different types of forcing functions, such as forcing the system with an elliptic sine or cosine in order to cancel the cross-modulation products arising out of the nonlinearity. The author still insists, however, that a study of the free oscillations of a nonlinear system is the key to an understanding of nonlinear resonance.

The author considers $Q_{max} = Q_1 + Q_n$ when there is a strong superharmonic of order n associated with the fundamental, but only if the two components peak at the same time (called "in phase" in the article).

If the superharmonic peak subtracts from the fundamental peak, q_{max} is not equal to $Q_1 + Q_n$. For example, q_{max} is larger than Q_1 for order 3 superharmonic only if $Q_3 > 0.41\ Q_1$. Since the computer solutions show the value of q_{max} for any configuration of harmonics, q_{max} was gotten from the computer solutions.

The frequency of the forcing function was not varied rapidly in the computer solutions. At each value of Ω the solution was allowed to reach a steady state; then the Ω was incremented by a $\Delta\Omega$ of 0.005 to 0.02. The author does not believe this affected the position of the resonant peaks with respect to the axis. A recent study by the author[4] shows that the resonance region for the third harmonic for the amplitude of the forcing function specified in Fig. 3 of the paper extends from $\Omega = 0.47$ to 0.53, thus extending the resonance region in question beyond that given by the computer solutions.

Dr. Caughey's statement concerning the nonperiodic term associated with even-order harmonics is borne out by the computer records of even-order harmonics shown in Fig. 8*a*, *c*, which indicate a bias from the zero-voltage axis. Kats [8] presents a response curve for this nonperiodic term associated with a second-order harmonic.

The Sector Problem[1]

B. Friedman.[2] The self-equilibrating polynomials $f_k(r)$ introduced in this paper are connected with the well-known Jacobi polynomials. In fact, the polynomials $p_k(r) = r^{-2}(1 - r)^{-2}f_{k+2}(r)$ are Jacobi polynomials satisfying the differential equation

$$r(1 - r)p_k'' + (2 - 7r)p_k' + k(6 + k)p_k = 0$$

A basic assumption of the paper is the near orthogonality of the $f_k'(r)$ functions (see after Table 4). This does not seem justified because

$$\int_0^1 r^{-1}f_2'^2 dr = 2 \qquad \int_0^1 r^{-1}f'^2 dr = 5.8$$

and

$$\int_0^1 r^{-1}f_2'f_3' dr = 0.894$$

therefore, if ψ is the angle between the f_2' and the f_3' vector, we have $\cos \psi = 0.27$, which is not too close to zero.

M. L. Williams.[3] In this interesting paper, the approximate solution to the finite-sector plane-stress problem is divided into two parts, a radial one and a circumferential one. Whereas in the latter the possibility of stress singularities has been shown to exist as the radial distance r tends to zero, such singularities appear to be precluded for the radial problem by the initial requirement for "finite stresses at $r = 0$". It has occurred to the writer that some additional freedom and generalization in the solution may be available to the authors if they were to introduce in place of $r^2(1 - r)^2$, the weighting factor $r^p(1 - r)^q$, with the restriction that both exponents p and q merely exceed unity.

As a conjecture, it may be that the exponents approach the values for the circumferential problem for the respective local angles involved at $r \to 0$ and $r \to 1$, $\Theta = \pm\omega$. This type of product factor, which essentially amounts to multiplying the $r = 0$ and $r = 1$ singularities, has proved fairly accurate considering its simplicity.[4]

---

[4] "The Solution of Duffing's Equation by a Three-Term Approximation Using the Ritz-Galerkin Method," by Atkinson and Bourne, I. E. R. Report Series 106, No. 1, University of California, Berkeley, Calif., Sept., 1957.

[1] By G. Horvay and K. L. Hanson, published in the December, 1957, issue of the JOURNAL OF APPLIED MECHANICS, TRANS. ASME, vol. 79, pp. 574–581.

[2] AEC Computing Facility, Institute of Mathematical Sciences, New York University, New York, N. Y.

[3] Associate Professor, California Institute of Technology, Pasadena, Calif.

[4] "The Plate Problem for a Cantilever Sector of Uniform Thickness," by M. L. Williams, Air Force Technical Rep. 5761, Part VI, November, 1950, pp. 38–41.

In any event, on a physical basis some dependence of the local radial-stress variation near the origin upon the opening angle 2ω might be expected, e.g., $p(\omega)$ and $q(\omega)$, although the additional mathematical complications may prove to be too involved to warrant their inclusion in an approximate analysis.

I. K. Silverman.[5] The requirement of satisfying prescribed stress conditions on all three faces $\Theta = \pm\omega$ and $r = 1$ of a sector differs from the problem of satisfying a mixed set of boundary conditions which consist of stress conditions on the two faces $\Theta = \pm\omega$ and a condition with regard to displacements on the third, $r = 1$. This is the case with which the writer attempted to deal in his paper[6] to which the authors referred. This mixed-boundary condition is found when studying the stresses in a triangular wedge (sector) which may represent a gravity dam connected to a rigid or elastic foundation. The same problem is furnished by the gear tooth and cutting tool. It would hardly seem likely that Poisson's ratio would be immaterial in a problem of this type.

Solutions for an infinite wedge (sector) were first given by Lévy and Michell. The Lévy and Michell regimes would exist in a triangular dam, cutting tool, or gear tooth if the base were allowed to deform in the manner called for by such solutions. Since this is not always possible, the effect of the restraint of the base is required. Since the solutions of Lévy and Michell are in equilibrium with the external forces, any corrective stresses must furnish zero loads on the upstream and downstream faces of the sector, and also must furnish a set of forces on the base which are self-equilibrating and have such values that, when combined with the Lévy or Michell stresses, furnish zero displacements if the foundation is assumed to be perfectly rigid as a first approximation. This specification for the corrective function is the same as that for the authors' F_kH_k except for the displacement condition.

The writer has shown[6] that an Airy function satisfying $\nabla^4\Phi = 0$ and which furnishes zero stresses on the radial faces of a sector (wedge) is given by the following set of eigenfunctions

$$\Phi = \sum_n r^{n+1} f(\theta)$$

$$= \sum_n K_n r^{n+1} [n \cos n\theta \sin\theta - m \sin n\theta \sin\theta - \sin n\theta \cos\theta] \quad \ldots\ldots [1]$$

in which

$$n^2 \sin^2 2\omega = \sin^2 2n\omega \quad \ldots\ldots [2]$$

and

$$m = \cot 2\omega - n \cot 2n\omega$$

There is an infinite number of roots to Equation [2] and accordingly an infinite number of constants K_n which may be determined by satisfying displacement conditions at selected points along the base. The constants K_n also may be determined from the least-work principle or by least squares.

In his paper[6] the writer used an approximate stress function which satisfied the same boundary conditions as Equation [1] but which was not a solution of $\nabla^4\Phi = 0$. The variational principle applied to the strain energy was used to determine a function which would describe the effect of restraint at the base.

Authors' Closure

The authors are much indebted to the three discussers for their interesting comments. Particularly valuable is Professor Friedman's observation that self-equilibrating polynomials are, apart from weight factors, hypergeometric polynomials.[7] As was pointed out by the authors in their paper, by choosing rigorously orthogonal variational eigenfunctions f_kg_k for a problem (which is governed by a fourth-order elliptic differential operator), one hopes to obtain nearly orthogonal first and second derivatives f_k', f_k''. The skewness of these derivatives is a measure of the skewness of the original problem. If f_k', f_k'' are found to be rigorously orthogonal, then the original problem is rigorously separable (i.e., the eigenfunction may be written as a product of, say, an x-function and a y-function). If the skewness is substantial, then the product solution furnished by the variational method gives a rather poor approximation to the true (nonseparable) solution.[8]

What constitutes moderate skewness? Let us consider the polynomials of the more familiar rectangle problem (the arc polynomials of the sector coincide with these)

$$f_2(y) = (1 - y^2)^2, \qquad f_4(y) = (1 - y^2)^2 (1 - 11y^2)$$

Denoting $\langle\,(\,)\,\rangle \equiv \int_{-1}^{1} (\,)\,dy$, one finds

$$\frac{\langle f_2' f_4' \rangle}{[\langle f_2'^2 \rangle \langle f_4'^2 \rangle]^{1/2}} = -0.288, \quad \frac{\langle f_2'' f_4'' \rangle}{[\langle f_2''^2 \rangle \langle f_4'' \rangle]^{1/2}} = 0.141$$

[5] Denver, Colo.

[6] "Approximate Stress Functions for Triangular Wedges," by I. K. Silverman, JOURNAL OF APPLIED MECHANICS, TRANS. ASME, vol. 77, 1955, p. 401.

[7] For further applications of this idea, see "Thermal Stresses in a Sector Prism," by K. L. Hanson and G. Horvay, to be published in *Proceedings, Third U. S. National Congress of Applied Mechanics.*

[8] One may, of course, subject the variational eigenfunctions to a systematic improvement scheme—along the lines of the discussion on "The End Problem of Rectangular Strips," by G. Horvay, JOURNAL OF APPLIED MECHANICS, vol. 20, TRANS. ASME, vol. 75, 1953, p. 576—but the labor required may be more than can be justified.

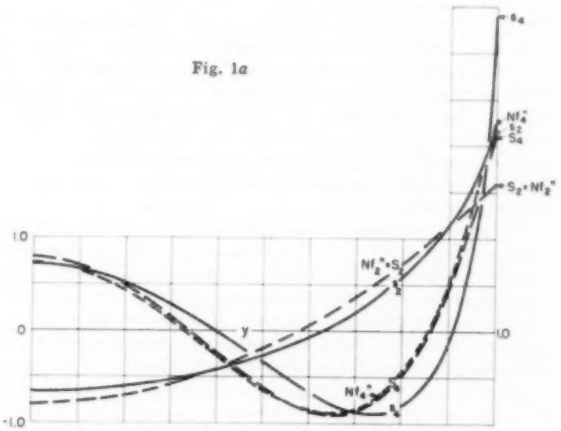

Fig. 1*a*

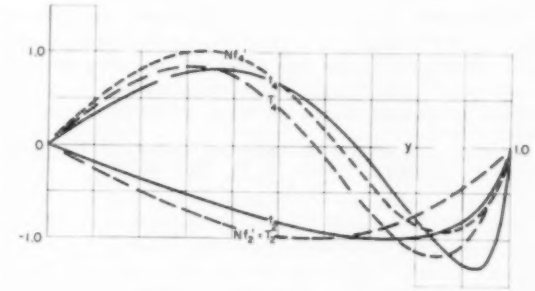

Fig. 1*b*

Are 17 deg and 8 deg deviations from orthogonality bad or moderate? We believe these deviations to be moderate. In Fig. 1*a* we plot the second derivatives Nf_2'', Nf_4'', where N are normalization factors. We also plot the rigorously orthogonal Legendre polynomials

$$S_2 = N(-1 + 3y^2), \qquad S_4 = N\left(1 - 10y^2 + \frac{35}{3}y^4\right)$$

($S_2 \equiv Nf_2''$.) The distinction between S_4 and Nf_4'' is almost imperceptible. In Fig. 1*b* we plot the first derivatives Nf_2', Nf_4', and the polynomials

$$T_2 = N(y - y^3), \qquad T_4 = N(y - 4y^3 + 3y^5)$$

obtained by constructing the orthogonal family T_k of Nf_2'. The disagreement between T_4 and Nf_4' is pronounced, but still not alarming. In the two figures we show, for comparison, also the $x = 0$ boundary values

$$t_2(y) = b_{22}K^\circ{}_{2,xy}, \qquad t_4(y) = b_{44}K^\circ{}_{4,xy} + b_{42}K^\circ{}_{2,xy}$$

$$s_2(y) = a_{22}J^\circ{}_{2,yy}, \qquad s_4(y) = a_{44}J^\circ{}_{4,yy} + a_{42}J^\circ{}_{2,yy}$$

of the orthonormalized derivatives of the rigorous eigenfunctions ($K^\circ \equiv K(0, y)$, $\Re \equiv$ real part)

$$K_2(x, y) = 4\Re \sum z_k^{-2}[2 + \cos^2 z_k]\Phi_k$$

$$K_4(x, y) = 8\Re \sum z_k^{-4}[42(3 + 2\cos^2 z_k) - z_k^2(34 + 3\cos^2 z_k)]\Phi_k$$

$$J_2(x, y) = 6\Re \sum z_k^{-1}(\sin^2 z_k/\cos^3 z_k)\,\Phi_k$$

$$J_4(x, y) = -30\Re \sum z_k^{-3}(\sin^2 z_k/\cos^3 z_k)[14 + 7\cos^2 z_k - 3z_k^2]\Phi$$

$$\Phi_k(x, y) \equiv e^{-z_k x}(\cos z_k y - y \cot z_k \sin z_k y)$$

which were established in an earlier paper.[9] The summation is carried out over the first quadrant roots z_k of $\sin 2z_k + 2z_k = 0$.

Professor Williams' comment about the nonuniqueness of the weight factor of the radial polynomials is very timely. In the reference[7] mentioned earlier the authors did encounter a difficulty with the choice of the r exponent, $p = 2$. They found that $p = 2 + \epsilon$ is a preferable choice, where $\epsilon > 0$ may be arbitrarily small. But in the lack of a specific rule for determining ϵ they retained their original choice, $\epsilon = 0$.

The authors are also in agreement with the comments of Dr. Silverman. Clearly, for problems involving displacement boundary conditions the results will depend on Poisson's ratio. The authors have not attempted to extend their method to mixed boundary-value problems, but such an extension may well require a switch from stress functions to displacement functions. (See, e.g., Equation [11] of reference in footnote 8.)

Cylindrical Shells Under Line Load[1]

Yi-Yuan Yu.[2] A re-examination of the problem of a cylindrical shell under line load on the basis of equations including the effect of transverse shear deformation, as is given in the present paper, is important as well as interesting. However, it should be pointed out that, from the standpoint of the theory of the cylindrical shell (not necessarily shallow), an operator of the form

$$\left(1 - \frac{1 - \nu}{2}\frac{h^2}{12\kappa_1}\nabla^2\right)$$

which should be operating on the left-hand member of Equation [3*a*] appears to be missing. A similar operator is missing from the corresponding dynamic equation given as Equation [5*a*] in reference (6) of the paper, by P. M. Naghdi and the author. As a consequence, Equation [3*a*] and its dynamic counterpart are of the eighth instead of tenth order, and they are thus not quite equivalent to the originally coupled equations from which the latter was and the former also could have been deduced. That these equations are somewhat incomplete may be seen from the fact that only four branches of the dispersion curve for the propagation of waves in cylindrical shells are obtainable from the dynamic counterpart of Equation [3*a*], although five are predicted by the theory which includes the effects of transverse-shear deformation and rotational inertia. A more appropriate form of the Donnell dynamic equations as well as another still more complete set of Donnell-type dynamic equations, both of which include the shear and rotation effects, have been derived by the writer in a forthcoming paper,[3] and the latter equations have been applied to the vibration problems of cylindrical shells.[4]

Author's Closure

The author wishes to thank Professor Yu for his interest in the paper. The following remarks are in order:

First, the system of Equations [3] of this paper are uncoupled from the five original displacement equations of equilibrium to the extent that homogeneous solutions are required for only two equations ([3*a*] and the second-order partial differential equation to which [3*d*] and [3*e*] can be reduced). Thus the complete solution depends on the solution of the *system* of Equations [3] and, as Professor Yu has observed, Equation [3*a*] is not the single (tenth-order) partial differential equation to which the original displacement equations can be reduced (even though w is the only dependent variable in [3*a*]). That is, the system of Equations [3] is not completely uncoupled in the sense to which Professor Yu is alluding when describing the equations which he has derived using the Donnell type approximations. However, it should be noted that such a single tenth-order equation can be obtained from the product of the factors operating on the two homogeneous equations which must be solved in obtaining the complete solution of Equations [3]. The dynamical counterpart of such an equation has been given in a recent paper[5] (the equation preceding [IIE] where a similar situation is evident.

[9] G. Horvay, "Biharmonic Eigenvalue Problem of the Semiinfinite Strip," *Quarterly of Applied Mathematics*, vol. 15, 1957, p. 65.

[1] By R. M. Cooper, published in the December, 1957, issue of the JOURNAL OF APPLIED MECHANICS, TRANS. ASME, vol. 79, pp. 553–558.

[2] Professor, Department of Mechanical Engineering, Polytechnic Institute of Brooklyn, Brooklyn, N. Y. Mem. ASME.

[3] "On the Donnell Equations and Donnell-Type Equations of Thin Cylindrical Shells," by Yi-Yuan Yu, to be presented at the Third U. S. National Congress of Applied Mechanics.

[4] "Vibrations of Thin Cylindrical Shells Analyzed by Means of Donnell-Type Equations," by Yi-Yuan Yu, presented at the Twenty-Sixth Annual Meeting of the Institute of the Aeronautical Sciences, New York, N. Y., January, 1958.

[5] "Propagation of Nonaxially Symmetric Waves in Elastic Cylindrical Shells," by R. M. Cooper and P. M. Naghdi, *Journal of the Acoustical Society of America*, vol. 29, 1957, pp. 1365–1373.

Book Reviews

Jets and Wakes

Jets, Wakes, and Cavities. By G. Birkhoff and E. H. Zarantonello, Academic Press, Inc., New York, N. Y., 1957. Cloth, 9¼ × 6¼ in., xii and 353 pp., illus. $10.

Reviewed by Lipman Bers[1]

THIS is an unusual book. Written by two mathematicians, it is directed primarily at "readers whose scientific curiosity spans all fields just mentioned" (pure and applied mathematics, experimental physics, hydraulics, and aeronautics). There are, probably, not too many such readers in our age of scientific overspecialization, and this reviewer regrets not to belong to this select group. He can only marvel at the catholic learning and the wide spread of interests of the authors who discuss, with equal enthusiasm, subtle points of sophisticated existence proofs, details of numerical computations, results of experiments, and semi-empirical theories.

Jets and wakes have intrigued scientists and engineers for a very long time. Today jets occur in such widely separated fields of technology as aircraft propulsion and dental drilling. The list of mathematicians who struggled to obtain a rational explanation of these fascinating phenomena reads like a "Who's Who" of mathematical analysis. But the readers of this monograph are never allowed to forget that, despite spectacular advances, the mathematical theory accounts for only a minute fraction of observed facts.

The book may be roughly divided into two parts. The first, comprising the first ten chapters, is a treatise on the mathematical theory of "free boundary-value problems" for steady potential flows. The bulk of the text in these chapters deals with two-dimensional flow of an incompressible fluid not subject to gravity. The authors explain, quite rightly, that this division of material merely reflects the present state of knowledge. After Chapter 10 the approach changes. Now one deals with physically more realistic and mathematically much less understood situations: unsteady flows (Chapter 11), viscosity (12), periodic wakes (13), turbulence (14), and miscellaneous experimental facts (15). In the authors' own words: "What theory there is involves little more than interpretation of momentum conservation, combined with similarity assumptions about asymptotic behavior." The reviewer is in complete sympathy with the authors when they express the hope that "those who find the analysis of Chapters 12 to 15 unpalatable will try to improve on it." It should be stated, however, that as the approach becomes more and more empirical the book reads more and more like a guide to the literature written for experts. For instance, in Chapter 13, dealing with vortex streets, von Karman's stability analysis is omitted, "since it can be found in many places."

The mathematical discussion in Chapters 1 to 10 is complete, though rather compressed, and presupposes a certain degree of mathematical sophistication. Of course, everything is precisely defined, all theorems used are clearly stated, and proper references are given for proofs. The research worker will be grateful to the authors for their precision, for many explicit formulas, and for an almost exhaustive bibliography. A student may find many pages rather tough going. But this monograph does not pretend to be a textbook.

A steady, two-dimensional, incompressible potential flow may be described by three complex variables: the position vector z, the complex velocity w, and the complex potential W, which are analytic functions of each other and are connected by the relation $dW = wdz$. This fact had important consequences for the development of both complex function theory and hydrodynamics. In particular, it allowed one to construct many important examples of free boundary flows by means of "elementary" conformal mappings, and the authors give an exhaustive treatment of this classical method in Chapters 2 and 5, supplementing it by a careful theoretical justification of Chapter 4. The theory becomes very far from elementary once one permits curved fixed boundaries and once one asks for general existence and uniqueness theorems. Attempts to answer these questions stimulated the creation of some of the subtlest and most powerful tools of modern analysis (for instance, various comparison theorems, or the concept of topological degree for transformations in function space). A highly competent discussion of these methods, including important developments of recent years, is given in Chapters 4, 6, and 7. In this case the reviewer is able to confirm that the authors fully redeemed their promise "to overlook no really important ideas, and at least to include an appropriate reference to every significant paper published prior to 1955."

Complex variable methods for treating free boundary-value problems can be generalized, to some extent, to the case of plane subsonic gas flows, by using Chaplygin's hodograph method. This work is presented in Chapter 8, which contains also a discussion of supersonic jets and a very brief (4 pages) presentation of the theory of potential incompressible flows with gravity. In connection with supersonic jets, the reviewer regrets that Frankl's work has been relegated to a footnote and that the theory of partial differential equations of mixed type is not even mentioned.

The theory of incompressible, axially symmetric, free boundary flows is much less developed than the corresponding two-dimensional theory. While some of the methods discussed in the previous chapters (variational approach, comparison theorems) are still applicable, the powerful tool of complex numbers is missing so that even the construction of examples becomes a formidable task. Chapter 10 is therefore less mathematical than the preceding ones, and approximate methods, as well as the comparison of approximate theories with experimental data, come to the forefront, thus providing a natural transition to the subsequent chapters of a more physical nature.

In their own research Birkhoff and Zarantonello were much concerned with numerical work and they report on this in the chapter on effective computation (Chapter 9). The results of computations are presented in several diagrams (pp. 339–350). Recent literature on the numerical solution of boundary-value problems emphasizes almost exclusively finite difference schemes. These, as well as the use of analog device, are, of course, mentioned here. But it is refreshing to see the attention focused on the effective calculation of quantities given by explicit though complicated formulas, and on the numerical solution of nonlinear integral equations. The integral equations in question are, by the way, rather similar to those occurring in the computation of incompressible and slow compressible flows past profiles, a sub-

[1] Professor, New York University Institute of Mathematical Sciences, New York, N. Y.

ject which lies outside of the very wide field this book is intended to cover. High-speed computing techniques are now in the process of rapid development, and the reviewer does not know whether all of this chapter is still up to date; the price quoted for using an electronic computer ($6 per hour) is certainly not.

The book, Volume 3 of a new series published under the auspices of the Applied Physics Laboratory, The Johns Hopkins University, is attractively printed and the numerous photographs and drawings are excellent. While the bibliography lists 91 titles, many more papers and books are listed in numerous footnotes. The amount of work required for completing this task must have been staggering. The authors may be rewarded by the knowledge that their monograph is certain to become indispensable to all workers in this field.

Physics of Flow

The Physics of Flow Through Porous Media. By A. E. Scheidegger. The Macmillan Company, New York, N. Y., 1957. Cloth, $9^1/_2 \times 6^1/_4$ in., xii and 236 pp., illus. $14.

Reviewed by J. S. Aronofsky[2]

THE study of the physics of flow through porous media has become basic for many scientific and engineering applications. Such diversified fields as soil mechanics, ground-water hydrology, petroleum engineering, water purification, industrial filtration, ceramic engineering, powder metallurgy, and the study of gas masks all rely heavily upon it as fundamental to their individual problems. It is not surprising that all of these branches of science and engineering have contributed a vast amount of literature, some of which is not readily accessible. Since the literature on porous media has been scattered over a multitude of journals, the author of the book felt the need to collect and coordinate the basic articles into a book form. Scheidegger states in the preface that he examined over two thousand references in carrying out this task.

However, this monograph by Scheidegger is much more than a simple bibliography. It is a highly interesting review of many of the controversial topics in flow through porous media, and, indeed, a generous number of references are provided. The author states in the preface that the material was selected and organized based on the following guiding principles: (*a*) Emphasis was laid on the general physical aspects of the phenomena rather than on particular cases applicable, say, to special engineering problems. (*b*) Of the many solutions available for some of the differential equations, only one was chosen for presentation in each case. The theory of differential equations is a well-established discipline of mathematics and has been considered of interest in the present context only if pertinent physical concepts were revealed. (*c*) The theoretical aspects have perhaps been stressed somewhat more than the experimental ones. However, descriptions of such procedures which enable one to determine theoretical "constants" have always been supplied in order to establish the proper logical sequence.

The afore-mentioned principles have led to an unusual monograph. It serves as an excellent guide through the literature, and it provides the research worker with an idea of the present state of knowledge about the physical principles of hydrodynamics in porous media. Most of the information presented is collected from original articles in the journal and the manner of presentation often follows closely the presentation employed in the original sources. The author has done a commendable job of overcoming the lack of uniformity in symbols and writing styles that exists in articles that come from many sources.

The book is organized into eight parts: Porous Media, Fluids, Hydrostatics in Porous Media, Darcy's Law, Solutions of Darcy's Law, Physical Aspects of Permeability, General Flow Equations, and Multiple Phase Flow. This organization is quite satisfactory, but the reader should know that it is not easy reading. The reader should be prepared to go to the original articles and existing treatises to fill in the many gaps. The basic theory is developed very rapidly and in concise terms. In some cases Scheidegger offers his own personal opinions and criticisms where controversial issues are involved.

[2] Manager, Electronic Computer Center, Socony Mobil Oil Company, Inc., New York, N. Y.

Digital Computer Programming

Digital Computer Programming. By D. D. McCracken. John Wiley & Sons, Inc., New York, N. Y., 1957. Cloth, $9^1/_4 \times 6$ inn vii and 253 pp., illus. $7.75.

Reviewed by Robin Esch[3]

THIS book is the first general introduction to digital computer programming in book form. The author is currently manager of training at the General Electric Computer Department, at Phoenix, Ariz. His background qualifies him to treat the problems and techniques peculiar to scientific computing, as well as those relevant both to scientific and business applications. In this reviewer's opinion he has succeeded admirably. The book is well written. Each point is made clear, yet seldom is an obvious statement labored. There are no obvious omissions.

The book is suitable as an introduction to programming, either by itself or together with the instruction manual of a specific machine with which the reader intends to work. A fair indication of the contents is given by the chapter headings: Computing Fundamentals; Coding Fundamentals; Binary and Octal Number Systems; Decimal Point Location Methods; Address Computation; Loops in Computing; Flow Charting; Index Registers; Subroutines; Floating Decimal Methods; Input-Output Methods; Magnetic Tape Programming; Program Checkout; Relative Programming Methods; Interpretive Programming Methods; Double Precision Arithmetic; Miscellaneous Programming Techniques; Automatic Coding.

This reviewer was gratified to find that adequate treatment is given to many problems that are ducked in manufacturers' programming manuals. For example, programming manuals often do not mention that many different methods of representing numbers (one and two register floating point, fixed point with various decimal point locations, double precision, etc.) are necessary in various problems; and moreover, that the execution of arithmetic operations on these representations involves the use of subroutines. Nor is the importance of coding reusable subroutines in relative address notation, so that they may be easily located in any segment of memory, ordinarily mentioned. Important practical matters such as methods of checkout and debugging and methods of coding a program so that it can be conveniently debugged are customarily soft-pedaled. McCracken explains such points clearly and describes many of the techniques, tricks, and trade secrets which heretofore have had to be learned by word of mouth or by trial and error.

The author illustrates the text by programs for a mythical computer, which he calls TYDAC (Typical Digital Automatic Computer). It is well that he has given such specific examples, which clarify the text much better than would generalized statements. Since TYDAC was designed to incorporate most of the im-

[3] Instructor in Applied Mathematics, Harvard University, Cambridge, Mass.

portant features of contemporary digital computers, this approach well suits the needs of one not committed to the use of a particular computer, or one who does not intend to program at all but wishes to know how to formulate his problems so they can be efficiently programmed by others. However, if one is committed to the use of a specific computer, it might be felt wasteful to learn TYDAC coding. This is not a serious objection, in this reviewer's opinion, since learning machine code is so small a part of the total effort of learning to program.

Process Instrumentation

Process Instruments and Controls Handbook. Douglas M. Considine, Editor. McGraw-Hill Book Company, Inc., New York, N. Y. 1957. Cloth, 9¼ × 6¼ in., xxiii and 1383 pp., illus. $19.50.

Reviewed by B. H. Sage[4]

This handbook has been assembled, as a result of the efforts of several persons, in a most satisfactory fashion and contains a wealth of information concerning process instrumentation presently in use. The style seems clear and the description adequate. The copious use of illustrations adds greatly to the interest in and the rapidity of reference to special instruments. Ten sections are devoted to descriptive material and one section to the principles of automatic control which can be followed without a great deal of mathematical background. Another section contains a limited amount of reference data, and a rather extensive glossary of terms makes up the final section. The book is a useful addition to the field of process instruments and controls.

Thermal Stresses

Thermal Stresses by B. E. Gatewood. McGraw-Hill Book Company, Inc., New York, N. Y., 1957. Cloth, 9¼ × 6¼ in., xv and 232 pp., illus. $7.50.

Reviewed by D. C. Drucker[5]

The author has combined into a rather brief volume the essentials of a textbook, of a reference work with an extensive bibliography, and an instruction manual on a high level for the designer of aircraft and missiles. Starting with the one-dimensional elastic thermal-stress problem of elementary strength of materials, there is a steady progression to the last chapter which deals with variational methods and complex variable approach.

As stated in the preface, "The book is not restricted to the classical thermal-stress problem of finding the elastic thermal stresses for a given temperature distribution in a structure with no buckling, but touches on all phases of the structural-design problem—the temperature distribution, the elastic and inelastic thermal stresses in various structures, the combined elastic and inelastic applied and thermal stresses, the allowable stresses for various materials and loading conditions, the buckling, deflection, stiffness, fatigue, shock, and flutter effects of elevated temperatures."

Although the properties of materials at high temperature are examined and creep is studied in detail, true plastic behavior is analyzed only through limiting allowable stresses.

[4] Professor of Chemical Engineering, California Institute of Technology, Pasadena, Calif.

[5] Professor and Chairman, Division of Engineering, Brown University, Providence, R. I.

Heat Transfer

Heat Transfer. Volume II. By the late Max Jakob. John Wiley & Sons, Inc., New York, N. Y., 1957. Cloth, 6¼ × 9¼ in., xxxii and 652 pp., illus. $15.

Reviewed by R. A. Seban[6]

This volume, together with Volume I of the same title, is the legacy of a half century of active participation in heat-transfer research, beginning almost at its inception and ending at a period of relative maturity. The substantial completion of this volume before his death in 1955, at the age of 76, is a tribute to the mental acuity and discipline that enabled Dr. Jakob to maintain a dynamic interest in the heat-transfer field during a period which most devote to retirement. Evident also throughout this book is the sympathetic and generous treatment that he always accorded to the work of his contemporaries. Completed in draft form in 1955, the book has emerged in final form through the care of Dr. S. P. Kezios, under whose hand the book attained the high standards of accuracy and careful presentation characteristic of the first volume.

As a continuation of Volume I, the book contains Part F, dealing with the engineering calculation of radiant energy interchange; Part G, on selected fields of application; Part H, supplements to Volume I.

The section on the calculation of radiant heat transfer contains the details of methods therefore to an extent far greater than available in any current book. Calculations for net interchange are given in detail, together with an exposition for many techniques for the determination of the necessary geometrical factors. The "net radiation" or "network" method of interchange calculation, which has been the subject of numerous recent papers, is interestingly enough presented in terms of a Russian reference of much earlier date, which had apparently escaped many contemporary workers on this subject.

Part G, on selected fields of application, actually contains such subjects to a lesser extent, in favor of chapters dealing with phases of heat transfer more fundamental in nature. The chapters relate to thermometry and related branches of measurement, on ordinary heat exchangers, regenerators, cooling towers, falling liquid films, cooling of surfaces exposed to hot gases, laminar boundary layers, turbulent boundary layers, liquid metals, and heat transfer in packed columns. Of these, the chapters on heat exchangers and on regenerators are the first presentation in English of a relatively comprehensive review of the analysis of such systems, paralleling somewhat, but with less detail, the treatment given by Hausen in his book on heat exchangers. Those on boundary layers are a reasonable review, beginning with the elementary solutions and progressing to the cases of variable free stream velocity, of variable properties, and of the inclusion of dissipative effects. A further presentation of the theory of the laminar boundary layer with transpiration cooling is contained in the chapter on the cooling of surfaces.

Part H, a section of 30 pages, contains supplementary material to various items of Volume I, for clarification or the provision of additional references. In addition, further problems are included; there is a detailed section on nomenclature as also a bibliography and author index, in the manner of Volume I.

It is hardly possible to appraise so monumental a work, containing 652 pages in this volume, which must be considered together with the 758 pages in Volume I. Certainly in so vast a structure there are parts which may be criticized, but such comments cannot ignore the existence and certain utility of the complete work. Encyclopedic in nature, there is substantial inde-

[6] Professor of Mechanical Engineering, University of California, Berkeley, Calif.

pendence among the various chapters, a merit in a reference but an objection even in an advanced text. Dispassionate in its presentation of material, which is primarily in terms of almost direct quotation from the references, it lacks the vitality and cohesiveness which would have been afforded by a reinterpretation of the material. But with the vast amount of material, this could hardly be expected of any author. Comprehensive in its treatment of the individual subjects, there is laudable attention to both analysis and experiment, the latter often subject to valuable appraisal by the author who himself was an outstandnig experimenter.

This treatise will endure as a primary reference on heat-transfer subjects in the same manner as Volume I has proved to be.

Strength of Materials

Strength of Materials. By F. R. Shanley. McGraw-Hill Book Company, Inc., New York, N. Y., 1957. Cloth, 6½ × 9¼ in., xxii and 783 pp., illus. $8.50.

Reviewed by R. M. Haythornthwaite[7]

THIS introductory text will probably exert a considerable influence on the teaching of elementary Strength of Materials. The author has made a deliberate attempt to deal with inelastic behavior as an integral part of the subject and to relate his analysis to the practical requirements of design, based on actual carrying capacity. Against such comprehensive objectives the book may well stir up some controversies, but if critics disagree on details, it is then up to them to do better themselves—and that may prove difficult.

The book is in three parts, headed: I. Forces and Deflections, Stress and Strain; II. Analysis of Structural Elements; III. Strength of Structural Elements; followed by Appendixes on Mechanical Properties and Section Properties. The part headings are clearly not intended as descriptions of exclusive content and there is considerable overlap, but they reflect the trend of the book, from a consideration of basic mechanics and test results, through analysis to estimation of carrying capacities of structural components under various loads. Many teachers will prefer not to follow the order of the book in detail, in particular to delay treating three-dimensional stress and strain (in Part I) until quite late. The book appears to have been written with such flexibility in mind and this increases its potentialities.

The book is quite long (783 pages) and there are many topics which are not generally introduced in a starting text. Notable among these are chapters on plastic strain (combined loading), inelastic torsion, local and lateral buckling, and the empirical treatment of strength under combined loading (using interaction curves). The chapters mentioned are there presumably to provide the student with background, for they will hardly lead him to develop facility in the topics covered. This is admitted in the chapter on local and lateral buckling where it is stated (p. 601): "No attempt will be made to derive the various equations that will be presented except to indicate their physical significance." Some case can be made for presenting material in this way if the object were to give training in routine design procedures. For engineers it might be better to leave the topics for more advanced texts in which the analysis itself could be presented.

The emphasis throughout is on developing clear pictures of the mechanical action, and in this the author is highly successful. The explanations and the figures are both exceptionally convincing. A possible exception is the treatment of virtual work, the reciprocal theorem, and Castigliano's second theorem. These topics are covered in eight pages, almost at the beginning of the book (pp. 25–32), and the treatment is backed up by only three worked examples and two examples suggested for the student. The author makes use of the reciprocal theorem on several occasions and later uses virtual work as an alternative method for computing beam deflection, but the average student is not given a reasonable chance to grasp these principles firmly at the beginning.

The book contains a great amount of lucid writing which is likely to be of considerable help to some students. Many of the obvious faults can be easily remedied in a second edition, which the reviewer is convinced the response will justify.

[7] Associate Professor of Engineering, Brown University, Providence, R. I.

Brittle Fracture

Brittle Behavior of Engineering Structures. By Earl R. Parker John Wiley & Sons, Inc., New York, N. Y., 1957. Cloth, 9¼ × 6 in., xv and 323 pp., illus. $6.

Reviewed by C. Mylonas[8]

THE problem of the brittle fracture of steels which under favorable conditions appear to have a normal ductility, is far from solved or even completely understood. As is usual in such instances, a colossal amount of incompletely correlated information exists in the literature. Its collection and intelligent classification are already great feats, and its presentation and discussion in the clear and systematic way of the author are worthy of every praise.

Chapters 1–3 contain the usually accepted concepts and theories of fracture. They deal with shear and cleavage fracture as well as with plastic deformation preceding fracture and their relation to brittle fracture; with the notch effect; with the necessity of judging steel brittleness by the indirect means of the brittle transition temperature as determined by fracture appearance or by ductility (energy); with Ludwik's theory and its modification for two modes of fracture, three-dimensional stress, and strain hardening; with energy theories of fracture as generalized by Orowan and Irwin (though Irwin's work is incompletely acknowledged); and with tests under combined stresses. The influence of temperature and strain rate is also discussed. These chapters are clear but incompletely up to date so far as plasticity, strain-hardening (anisotropic), and nonlinear loading paths are considered, and also without sufficient emphasis on the substantially different conditions of dynamic elastoplastic crack propagation as compared to static crack initiation. It would have also been desirable to express in even stronger terms the shortcomings of the current theories and the need of newer methods of attack.

All this may be due to the limitation of the book to the period essentially ending early in 1954. Nevertheless, the discussions are far-sighted and often provide elements which may show paths to possible solutions. Thus it is explained (Chapters 9, 13) that the problem of the initiation of brittle fracture is as yet unsolved. It is shown that brittle fracture, once started, may propagate at lower stress levels than often exist in structures, and that static central loading of undamaged plates with symmetrical notches even at temperatures below the brittle transition range does not cause a crack to grow, no matter how deep or sharp it may be, unless the average stress over the net section reaches the flow limit. These far-reaching observations are contrary to the usually proposed theories, and recently have led to new ideas on the mechanics

[8] Associate Professor of Engineering, Brown University, Providence, R. I.

of brittle fracture. Thus it is known that contained (small) plastic deformation occurs at the notch roots even at small loads and increases considerably only when the load approaches the section flow limit. Thus even the worst structural steel under the most unfavorable conditions has enough ductility to avoid fracture initiation at low average net static stress. Since brittle fractures nevertheless start at low stresses, it appears that the ductility at the notch roots may be exhausted or lowered below the extent demanded at low stress levels. In effect, recent tests have simulated real brittle fractures at low loads in the laboratory by local ductility reduction, which thus appears as a major factor in fracture.

The great interest and importance of the book lie mainly in the subsequent chapters. Chapters 4 to 9 deal with the determination, interpretation, and correlation of brittle transition temperatures, and with the factors affecting them. Here is collected a wealth of information on the independent and intercorrelated effects of C, Mn, Si, P, S, N, O, A, Ni, of grain size, of cold work and strain aging; on the effects and behavior of welds with or without stress relief; and on residual stresses. Chapter 10 discusses the influence of design and workmanship, shows the results of various hatch corner tests, and presents evidence of the cause of the initiation of brittle fractures in actual service failures. Faulty welding and its detection are also discussed. Chapter 11 describes and documents 21 brittle fractures of structures other than ships, of which 14 were welded and 7 riveted. Chapter 12 mainly contains a concise presentation of a statistical study of fracture occurrence in welded ships in relation with their type, design, region of failure, conditions at time of failure, origin of fracture, point of arrest, and steel properties. Chapter 13 is a general summary with some very interesting observations and conclusions, one of which was discussed above. Another is on the preference of the ductility criterion (energy of fracture) rather than the fracture appearance for the determination of transition temperature. The two methods have been assessed throughout the book, and this preference is based both on the physical correspondence to plastic deformation preceding fracture and on the better statistical correlation with actual in-service fractures.

The book is recommended as an excellent documented presentation of the problem of brittle fracture of steel mostly in relation to brittle transition temperature and the factors affecting it, and with extensive consideration of design and fabrication. Designer and researcher will find it of invaluable help.

Automation

Automation in Business and Industry. Edited by Eugene M. Grabbe. John Wiley & Sons, Inc., New York, N. Y., 1957. Cloth, 6¼ × 9¼ in., xix and 611 pp., illus. $10.

Reviewed by John A. Hrones[9]

This is a book which puts under a single cover a series of lectures given at the University of California by twenty-one engineers and scientists. The material is conveniently surveyed when considered in the following categories: (*a*) General background, history, and predictions. (*b*) Descriptive material pertaining to a variety of automatic systems now in existence. (*c*) Fundamental theory and concepts.

Five of the chapters and the introduction concern themselves with definitions, history, predictions for the future, and some indications as to how such predictions may be fulfilled. Five different writers have produced some overlapping material with a range of thought and competency of expression from poor to good. Taken as a whole, however, the material will be helpful to many readers. One has the impression that the discussions concerning how systems engineering at its highest level should be carried out are heavily weighted by experience in missile systems design.

A second group of chapters are largely devoted to the description of a number of automatically controlled systems including: Aircraft flight; electronic component production; petroleum and chemical processes; and machine-tool operation.

A third group of chapters are devoted to basic theory and concepts of feedback control, measurement, machine computation, and data handling. This material is handled rather well as a whole. Important material is clearly but briefly presented. Existing equipment is described. Some important references are included.

Most of the nineteen authors have succeeded in presenting difficult subject matter in a clear manner. The editor has done a good job in bringing a certain amount of continuity to the presentation. Yet, nothing that does not exist in print elsewhere is included. As a review, its success must depend on how well it is gaged to meet the needs of the interested engineers and managers. For those who have a strong training in science and engineering and have had some contact with the control field and are willing to really dig, this is a good book, particularly for those whose background and judgment result in the fast flipping of pages in the few portions of the book where such action is called for.

[9] Vice-President for Academic Affairs, Case Institute of Technology, Cleveland, Ohio.

Flame Spectroscopy

The Spectroscopy of Flames. By A. G. Gaydon. John Wiley & Sons, Inc., New York, N. Y., 1957. Cloth, 9½ × 6¼ in., ix and 279 pp., illus. $9.

Reviewed by S. S. Penner[10]

In his preface to the book the author stresses two objectives of the work; namely, that the treatment is designed to be intelligible to the beginner, and that the book is a "personal monograph" based largely on experimental work done at Imperial College. The author has succeeded in writing a readable text covering particularly his own work and the studies of his collaborators.

After some preliminary remarks relating to the value of flame spectroscopy in elucidating fundamental processes in combustion, the author presents a brief discussion of experimental methods. This is followed by a simple introduction to the theory of line spectra. Next we find surveys of spectroscopic studies on selected flames (e.g., hydrogen, carbon monoxide, and organic flames). The only excursion into quantitative spectroscopy involves flame temperature determinations from *relative* intensity measurements. This discussion would have profited greatly from a careful examination of measurement principles, distortions, and the like. Gaydon's work on translational temperature measurements is not definitive; careful recent experimental studies by several authors, which will be published shortly in the Journal of the Optical Society of America, cast serious doubts on the anomalous translational temperatures of electronically excited CH. In the discussion of rotational temperatures of OH, some of the pertinent literature is not cited.

A brief, qualitative survey of infrared flame spectroscopy is fol-

[10] Professor of Jet Propulsion, California Institute of Technology, Pasadena, Calif.

lowed by remarks on the very difficult and, unfortunately, never unambiguous interpretation of flame spectra in terms of flame structure and reaction processes. The last two chapters of the book deal with industrial flames and flames containing nitrogen, halogens, sulfur, and other inorganic substances.

A valuable feature of the book is a compilation of flame emission and absorption bands for selected chemical species.

The most obvious deficiency of Gaydon's book is the nearly complete absence of discussion of the principles of quantitative spectroscopy, including such topics as absolute intensities, spectral line widths and profiles, instrumental distortions during observations, and so on. The book is not designed for research workers who are primarily interested in using spectroscopic techniques for quantitative studies. On the other hand, Gaydon's book does provide a well-written, elementary introduction to the field of qualitative flame spectroscopy and identification of flame spectra.

Behavior of Metals

Behavior of Metals at Elevated Temperatures. The Institution of Metallurgists. The Philosophical Library, Inc., New York, N. Y., 1957. Cloth, $5^3/_4 \times 8^3/_4$ in., vii and 122 pp., illus. $6.

Reviewed by D. C. Drucker[11]

THE book contains the four lectures delivered at the tenth Institution of Metallurgists refresher course held in October, 1956. Emphasis is placed on engineering properties by each of the authors: N. P. Allen, G. Meikle, L. B. Pfeil, and W. E. Bardgett.

A survey and brief introduction to physical theory are provided which should prove helpful in beginning the study of this very important subject.

[11] Professor and Chairman, Division of Engineering, Brown University, Providence, R. I.

Information for Authors

• Manuscripts should be submitted in final form to the Technical Editors. Each manuscript must be accompanied by a statement that it has not been published elsewhere nor has it been submitted for publication elsewhere. A paper which would occupy more than five pages of the Journal may be returned to the author for abridgment.

• The author should state his business connection, the title of his position, and his mailing address. A short abstract (50 to 100 words) should be included on the first page immediately preceding the introductory paragraph of the paper.

• Three copies of the manuscript are required. One of these must be a carefully prepared printer's copy, typed in double spacing, on one side of the page only, with wide margins, on 8½ by 11-in. opaque white paper. Mimeographed manuscripts, if prepared with exceptional care, can be accepted provided they are completely edited.

• As far as possible, all mathematical expressions should be typewritten. Greek letters and other symbols not available on the typewriter should be carefully inserted in ink. Care should be taken to distinguish between capital and lower-case letters, between zero (0) and the letter (*O*), between the numeral (1) and the letter (*l*), etc. A letter representing a vector cannot be printed with an arrow above or below it. The letter should be underscored with a single wavy line, wherever it appears in the text, to designate boldface type. A list of symbols carefully marked for the use of the editor (thus: κ, Greek l.c. kappa), if it has not been included in the body of the paper, should accompany the manuscript on a separate page.

• Before preparing a manuscript the author should study printed articles in the Journal, with special attention to the form and style of mathematical expressions, tables, footnotes, references, and abstract. Numbers that identify mathematical expressions should be enclosed in parentheses. Numbers that identify references at the end of the paper should be enclosed in brackets. Care should be taken to arrange all tables and mathematical expressions in such a way that they will fit into a single column when set in type. Equations that might extend beyond the width of one column (fractions that should not be broken or long expressions enclosed in parentheses) should be rephrased to go on two or more lines within column width. Fractional powers are preferred to root signs and should always be used in more elaborate formulas. The solidus should be used instead of the horizontal line for fraction wherever possible.

• A normal paper should not exceed five pages in the Journal. It is about 6000 words or twenty to twenty-five double-spaced typewritten pages inclusive of drawings. A Brief Note should not exceed 750 words or about one column in the Journal inclusive of drawings.

• Originals and two copies of figures must accompany the manuscript. Line drawings should not be larger than 8½ × 11 inches and should be planned for reduction to column width. Lettering should be large enough to be clearly legible when the illustration is reduced. The originals of line drawings must be in India ink on white or pale blue tracing paper or tracing cloth. Photographs of equipment or test specimens must be glossy prints and should be used sparingly. Captions for figures should be typed double-spaced and included as the last page of the manuscript. The figure number and author's name should be written in the margin or on the back of each illustration.

• Titles of papers should be brief. If an adequate description of the subject requires a title which, along with the authors' names, would occupy more than one line on the cover of the Journal, a separate shorter title should be submitted.

• Authors can obtain copies of the ASME Manual MS-4, "An ASME Paper," from the Technical Editors and are urged to do so before drafting their papers in final form.

• Papers published in the Journal of Applied Mechanics must be presented at a Meeting, either in person or by title. Scheduling of papers is in the hands of the Secretary of the Applied Mechanics Division. Authors should indicate their preference in this respect to the Technical Editors when submitting a paper.

• An author is entitled to 25 preprints free of charge (in the case of two authors, 15 each, three or more authors, 10 each). Larger quantities of preprints or reprints can be ordered from Editorial Department, The American Society of Mechanical Engineers, 29 West 59th Street, New York 18, N. Y. Quotations will be sent on request.

D. C. Drucker and J. Kestin, *Technical Editors*

Please address all communications to:

Technical Editors
Journal of Applied Mechanics, ASME
Division of Engineering
Brown University
Providence 12, R. I.

REFERENCE TOOLS THAT REFLECT THE BEST THINKING AND PRACTICE OF SPECIALISTS

APPLIED MECHANICS REVIEWS

A unique, authoritative engineering reviewing service

Published monthly

$25 annually to nonmembers
$10 annually to ASME members

Engineers in all parts of the world rely on Applied Mechanics Reviews, for with its help they are able to survey world-wide advances in applied mechanics and engineering science in a relatively short time, pinpoint any major development in their fields in seconds, keep abreast of rapidly expanding scientific frontiers, and have a constant flow of new ideas, some of which have evolved into money-makers for them and their employers.

To provide this service, the most significant findings are culled from over a thousand sources including 750 engineering periodicals of thirty countries, new books in all languages, and reports of industrial specialists everywhere, which are then appraised and evaluated by engineers who are recognized specialists in the fields involved. Each review bears the signature of the reviewer, thus attesting to the authority of the opinion advanced.

Over 300 reviews are published monthly, highlighted by an article written exclusively for AMR by an established authority in one of the many phases of engineering to apprise readers of progress in a specialized area. In a year's issue AMR publishes 4000 digest reviews on approximately 600 subjects conveniently grouped under the following thirty-five headings: GENERAL: Theoretical and experimental methods, and mechanics. MECHANICS OF SOLIDS: Servomechanisms, governors, gyroscopics; Vibrations, balancing; Wave motion in solids, impact; Elasticity theory; Experimental stress analysis; Rods, beams, cables, membrane elements; Plates, disks, shells, anisotropy; Buckling problems; Joints and joining methods; Structures; Rheology; Failure, mechanics of solid state; Material test techniques; Mechanical properties of specific materials; Plasticity, forming and cutting. MECHANICS OF FLUIDS: Hydraulics, cavitation, transport; Incompressible flow; Compressible flow, gas dynamics; Wave motion in fluids; Turbulence, boundary layer; Aerodynamics of flight, wind forces; Aeroelasticity; Propellers, fans, turbines, pumps; Flow and flight test techniques. HEAT: Thermodynamics, heat and mass transfer, combustion. MISCELLANEOUS: Acoustics; Ballistics; Soil mechanics, seepage; Micromeritics; Geophysics, meteorology, oceanography; Lubrication, bearings; Marine engineering problems; Biomechanics.

TRANSACTIONS of the ASME for 1957

Published 1958

$15 to nonmembers
$7.50 to ASME members

Whether you wish to keep abreast of advances and trends throughout the mechanical-engineering field, obtain information that will help you develop a broad background, or have at your finger tips a unique collection of procedures and solutions that can be utilized when needed, you can look to the 2852-page volume for the help needed. Its 124 papers are classified under three major subject divisions.

Aerodynamics. Aircraft. Aluminum and Aluminum Alloys. Automatic Control. Bearings. Building. Combustion. Cooling Systems. Cooling Towers. Diesel Engines. Elasticity. Flow of Fluids. Friction. Fluid Meters. Gas Turbines. Heat Exchange Equipment. Heat Transfer. Hydraulics. Hydrostatic Testing. Impact. Impellers. Instruments. Lubricants and Lubrication. Machine Design. Management. Mathematics. Mechanisms. Metal Creep. Metal Cutting. Metal Finishing. Metal Rolling. Metal Testing. Nonlinear Systems. Nozzles. Photoelasticity. Pipe and Piping Systems. Plasticity. Plows. Nuclear, Steam, and Solar Power Plants. Power Systems. Rotors. Shells. Steam Turbines and Turbine Testing. Steam Superheaters. Stresses and Strains. Structures. Thermal Stresses. Thermodynamics. Valves. Vibration. Wave Mechanics.

SHOCK AND VIBRATION INSTRUMENTATION

Published 1956

$6 to nonmembers
$4 to ASME members

This book provides a fund of useful information on recent advances and new concepts in the technology of shock and vibration. Among the subjects discussed are random vibration, effect of nonrigid structures on vibration isolation, hysteresis and slip damping, vibration and shock testing, design approaches and scaling methods.

CONTENTS: Evaluation of Mounts Isolating Nonrigid Machines From Nonrigid Foundations. Experimental Study of the Effects of Foundation Resilience on Vibration Isolation. Effect of Material and Slip Damping on Resonance Behavior. Shock and Vibration Instruments. Mechanical Design for Random Vibration and Shock. Influence of Electrical and Mechanical Impedance on the Control and Performance of Some Vibration Machines. Shock Testing Machines and Procedures. Damaging Potential of Shock and Vibration. High-Speed Computing Methods for Shock and Vibration Problems.

DESIGN DATA AND METHODS, APPLIED MECHANICS

Published 1955

$4 to nonmembers
$3.20 to ASME members

Included in this collection of original and practical contributions are stress and deflection methods applied to circular and rectangular plates; analysis of circular beams; information on hydrostatic testing and variable-station column problems; design data for piping; data on stress concentrations, torsion, helical compression and tension springs, thermal stresses, stresses in pressure vessels, shrink-fitted assemblies, and thick-walled cylinders. There are also numerical solutions of gas-flow problems, information on two-dimensional supersonic flow; a chart for oblique shock waves under water; accurate bearing calculations; and methods of treating and solving problems of vibration and of balancing rotating appliances.

METALS ENGINEERING PROCESSES

Published 1958

$12.50 to nonmembers
$10.00 to ASME members

Composed of a wealth of practical, day-to-day engineering help, this handbook covers such areas as the heat-treatment of steel, all forms of casting, hot and cold working, powder metallurgy, welding, machining, and electroforming.

For each of the manufacturing methods there is a compilation of the basic physical characteristics to be considered and the general advantages and limitations usually encountered. Concise, parallel data concerning the suitability of various metals for each process, and the natural tolerances as also and surface finish obtainable, assist in evolving designs that meet all functional requirements consistent with economical production techniques.

Published by

THE AMERICAN SOCIETY OF MECHANICAL ENGINEERS
29 W. 39th St., New York 18, N. Y.